JUN 2 1982

NAS 1.55: 2201

NASA Conference Publication 2201

COMPLETED

Numerical Boundary Condition Procedures

ORIGINAL

Proceedings of a symposium held at
NASA Ames Research Center
Moffett Field, California
October 19-20, 1981

NASA

NASA Conference Publication 2201

Numerical Boundary Condition Procedures

Proceedings of a symposium held at
NASA Ames Research Center
Moffett Field, California
October 19-20, 1981

NASA
National Aeronautics
and Space Administration

**Scientific and Technical
Information Branch**

1982

Blank Page

Blank Page

PREFACE

This volume is a collection of papers presented at the Symposium on Numerical Boundary Condition Procedures held at Ames Research Center, NASA, October 19-20, 1981. The purpose of this symposium was to provide a forum for the presentation and interchange of recent technical findings in the field of numerical boundary approximations. The symposium was held in conjunction with the Symposium on Multigrid Methods, and both were sponsored by the Applied Computational Aerodynamics and Computational Fluid Dynamics Branches at Ames.

Probably, the single most important aspect in the successful application of any numerical technique in solving gas dynamic problems is the proper treatment of the impermeable and permeable boundaries that encompass the computational line, plane, or volume. Papers were solicited in this research area which utilized new or existing numerical boundary condition procedures for various types of boundaries and governing equations.

It is apparent from the contributed papers that computational fluid dynamicists as well as numerical analysts are quite active in this discipline. The papers cover a wide spectrum of research on topics that include numerical procedures for treating inflow and outflow boundaries, steady and unsteady discontinuous surfaces such as shock waves and slip surfaces, far field boundary conditions, and multiblock grids. In addition, papers were presented which consider the effects of numerical boundary approximations on stability, accuracy, and convergence rate of the numerical solution.

The symposium presented 3 invited and 21 contributed papers. The invited speakers were Dr. A. Bayliss, Prof. G. Moretti, and Prof. B. Gustafsson.

Paul Kutler

CONFERENCE COMMITTEE

General Ch	Paul Kutler
Program Com	Helen M. C. Yee Robert F. Warming John V. Rakich John D. Murphy Denny S. Chaussee
Administrative Chairman:	Walter A. Reinhardt
Publications Chairman:	Mamoru Inouye
Secretary:	Betty Beyerly

TABLE OF CONTENTS

Page

PREFACE iii

1. FAR FIELD BOUNDARY CONDITIONS FOR COMPRESSIBLE FLOWS (Invited paper) 1
Alvin Bayliss and Eli Turkel

2. A COMPARATIVE STUDY OF NONREFLECTING FAR-FIELD BOUNDARY CONDITION PROCEDURES FOR UNSTEADY TRANSONIC FLOW COMPUTATION 21
Dochan Kwak

3. IMPLEMENTATION OF NONREFLECTIVE BOUNDARY CONDITION AT THE OUTFLOW BOUNDARY 45
D. R. Hall and S. M. Yen

4. RAPID, HIGH-ORDER ACCURATE CALCULATION OF FLOWS DUE TO FREE SOURCE OR VORTEX DISTRIBUTIONS 61
Douglas Halsey

5. A PHYSICAL APPROACH TO THE NUMERICAL TREATMENT OF BOUNDARIES IN GAS DYNAMICS (Invited paper) 73
Gino Moretti

6. THREE DIMENSIONAL BOUNDARY CONDITIONS IN SUPERSONIC FLOW 97
S. Rudman and F. Marconi

7. ON VARIOUS TREATMENTS OF POTENTIAL EQUATIONS AT SHOCKS 121
Lee-Tzong Chen and D. A. Caughey

8. FULLY IMPLICIT SHOCK TRACKING 139
J. B. Bell, G. R. Shubin, and J. M. Solomon

9. CHARACTERISTIC BOUNDARY CONDITIONS FOR THE EULER EQUATIONS 165
T. H. Pulliam

10. NUMERICAL BOUNDARY CONDITION PROCEDURE FOR THE TRANSONIC AXISYMMETRIC INVERSE PROBLEM 183
Vijaya Shankar

11. STABILITY OF TWO-DIMENSIONAL HYPERBOLIC INITIAL BOUNDARY VALUE PROBLEMS FOR EXPLICIT AND IMPLICIT SCHEMES 199
Saul S. Abarbanel and Earll M. Murman

12. THE CHOICE OF NUMERICAL BOUNDARY CONDITIONS FOR HYPERBOLIC SYSTEMS (Invited paper) 209
Bertil Gustafsson

13. INFLUENCE OF BOUNDARY APPROXIMATIONS AND CONDITIONS ON FINITE-DIFFERENCE SOLUTIONS 227
F. G. Blottner

14. STABILITY ANALYSIS FOR NUMERICAL BOUNDARY CONDITIONS AND IMPLICIT DIFFERENCE APPROXIMATIONS OF HYPERBOLIC EQUATIONS 257
R. M. Beam, R. F. Warming, and H. C. Yee

15. STABILITY THEORY OF DIFFERENCE APPROXIMATIONS FOR MULTIDIMENSIONAL INITIAL-BOUNDARY VALUE PROBLEMS 283
Daniel Michelson

16. SOME EXPERIMENTS ON EXPLICIT BOUNDARY ALGORITHMS 287
K. Förster

17. PSEUDOSPECTRAL METHOD FOR PROBLEMS WITH NON-PERIODIC BOUNDARY CONDITIONS 313
H. N. Lee

18. UNCONDITIONAL INSTABILITY OF INFLOW-DEPENDENT BOUNDARY CONDITIONS IN DIFFERENCE APPROXIMATIONS TO HYPERBOLIC SYSTEMS 323
Eitan Tadmor

19. IMPLICIT BOUNDARY CONDITIONS FOR THE SOLUTION OF THE PARABOLIZED NAVIER-STOKES EQUATIONS FOR SUPERSONIC FLOWS 333
M. Barnett, R. T. Davis, and J. V. Rakich

20. BOUNDARY TREATMENTS FOR IMPLICIT SOLUTIONS TO EULER AND NAVIER-STOKES EQUATIONS 353
W. T. Thompkins, Jr., and R. H. Bush

21. RIGOROUS NUMERICAL TREATMENT OF THE NO-SLIP CONDITIONS IN A VORTICITY FORMULATION 367
J. Gazdag, Y. Takao, and J. Fromm

22. NUMERICAL TREATMENT OF NON-LINEAR LATENT HEAT BOUNDARY CONDITIONS AT MOVING INTERFACES IN GENUINE TWO-DIMENSIONAL SOLIDIFICATION PROBLEMS 379
P. M. Beckett

23. SHOCK-POINT OPERATORS IN CONSERVATIVE DIFFERENCING 389
C. P. Kentzer

24. A MESH EMBEDDING APPROACH FOR PREDICTION OF TRANSONIC WING/BODY/STORE FLOW FIELDS 403
D. S. Thompson

CONFEREES AT NUMERICAL BOUNDARY CONDITION PROCEDURES AND MULTIGRID METHODS SYMPOSIA 428

(Invited paper)

FAR FIELD BOUNDARY CONDITIONS FOR COMPRESSIBLE FLOWS

Alvin Bayliss
Courant Institute of Mathematical Sciences, New York University

Eli Turkel
Tel-Aviv University
Institute for Computer Applications in Science and Engineering

INTRODUCTION

An important goal of computational fluid dynamics is the computation of steady state flows exterior to a body, such as an airfoil. This is frequently accomplished by integrating the time dependent Navier-Stokes or Euler equations until a steady state is achieved. This raises two (related) computational problems:

a) How to compute in an exterior region;
b) How to accelerate convergence to the steady state.

The numerical treatment of exterior regions requires a method to convert the problem to one in a bounded region. One method is to map the exterior region into a finite region. However, many equations have oscillatory solutions near infinity. For these cases, the mappings can create substantial errors since waves in the vicinity of infinity cannot be resolved (see, e.g., Grosch and Orszag (ref. 1)). An alternative approach is to truncate the unbounded region at some finite, artificial surface. This creates a finite computational region at the expense of imposing boundary conditions at the artificial boundary.

If the problem has wave-like solutions near infinity, then these boundary conditions must simulate the radiation of energy out of the computational domain and towards infinity. Incorrect specification of these radiation boundary conditions can cause spurious reflected waves to be generated at the artificial boundary. These waves represent energy propagating into the computational domain from infinity. Since they are not part of the desired solution, they can substantially degrade the accuracy of the computed solution. If the time dependent equations are only an intermediate step towards computing a steady state, then a flow of energy into the computational domain can delay convergence. Conversely, the correct specification of radiation boundary conditions can accelerate convergence. Thus, the two questions raised in the first paragraph are related through the concept of radiation boundary conditions.

This work was partially supported under NASA Contracts No. NAS1-14472 and NAS1-16394 while the authors were in residence at ICASE, NASA Langley Research Center, Hampton, VA 23665. Additional support for the first author was provided by Air Force Contract No. AFOSR-76-2881.

In order to minimize the effect of spurious reflections, the computational region can be enlarged so that the artificial boundaries are far from the region of interest. This will increase both the memory requirements and the running time of the computer program. It is preferable to specify boundary conditions that allow the computational region to be constructed as much as possible.

Our goal is therefore to construct radiation boundary conditions which have the following properties:

(a) To accurately simulate the radiation of energy out of the computational domain;

(b) To accomplish (a) with an accuracy which improves as fast as feasible as the artificial surface is moved outward. Equivalently, the boundary conditions will be accurate when the computational domain is constricted;

(c) To accelerate convergence to the steady state (by minimizing spurious reflections).

The approach taken here is similar to that of references 2, 3 and 4. We assume that in the far field the (possibly nonlinear) equations reduce to some simple form, e.g. a wave equation, Poisson's equation or the reduced wave equation. An asymptotic solution to the model equation is then constructed. This solution is usually based on a general functional form which specifies the behavior of the solution near infinity. In the problems considered here, the desired behavior is that the solution be composed of outgoing waves. We wish to stress that the expansion depends on the geometrical properties of the computational domain. For example, the asymptotic expansion will differ in duct-like geometries (infinite in only one dimension) from that in fully exterior regions (infinite in all dimensions). Thus, the expansion is based on global properties of the solution. The asymptotic expansions will usually be in terms of a reciprocal radius, i.e. in terms of distances, but can also be in terms of frequencies.

Once the functional form of the asymptotic expansion is known, we can derive differential relations that are exactly satisfied by any function having the given functional form. These differential relations, when used as boundary conditions, effectively match the solution to the asymptotic expansion valid near infinity. These radiation boundary conditions become increasingly accurate as they match the solution to more terms of the asymptotic expansion.

This procedure of matching the solution to an expansion valid near infinity requires some knowledge of the solution in a neighborhood of infinity. Gustaffson and Kreiss (ref. 5) have shown that problems in an exterior domain can in general be restricted to a bounded domain only when the dependent variables (and coefficients) approach constants at infinity. This suggests that radiation boundary conditions, to be applied at some artificial finite boundary, can work only by conveying information about the behavior of the solution near infinity.

In this lecture we will concentrate on applications to fluid dynamics. Viscous effects are important, in aerodynamics, only in the vicinity of bodies. nce the far field behavior is governed by the Euler equations. A consequence of this is that solutions in the far field have a wave-like behavior. Hence, a steady state can be achieved only by allowing the radiation of energy outside the computational domain. Therefore, a more accurate simulation of the outward radiation of energy can accelerate the convergence to a steady state.

In the far field the solution is relatively constant. Hence, to derive the boundary conditions, we linearize the Euler equations about this constant solution. The resultant system is equivalent to a convective wave equation. A family of radiation conditions for the standard wave equation was developed in reference 2. This family was based on an expansion that was asymptotic in the distance from an arbitrary origin. A family of differential operators, B_m, was derived which annhilated the first m terms in the asymptotic expansion. An á priori estimate was obtained that showed that the error due to the use of an artificial surface coupled with the use of the boundary condition $B_m u = 0$ was $O(r^{-m})$.

The first member of this family was generalized to the convective wave equation in reference 3. As stated above, this allows the construction of boundary conditions for the full time dependent compressible Navier-Stokes equations. This condition will be discussed in more detail in this paper. In reference 4 these operators were generalized to elliptic equations such as the exterior Poisson and exterior Helmholtz equation.

Other approaches to the construction of outflow boundary conditions were developed by Rudy and Strikwerda (ref. 6 and 7) and Engquist and Majda (ref. 8 and 9). Rudy and Strikwerda analyzed a one-dimensional model problem. A boundary condition was developed which accelerated the convergence to a steady state. This condition depended on a free parameter, which was chosen, in the one-dimensional case to maximize the convergence rate. In references 6 and 7 this boundary condition was applied to some two-dimensional problems where the free parameter was chosen by computational experimentation. This boundary condition was shown to substantially accelerate convergence to the steady state.

A different philosophy was adopted by Engquist and Majda (refs. 8 and 9). Their approach was to construct a pseudo-differential operator which exactly annhilated outgoing waves. This pseudo-differential operator was a global boundary operator. In order to derive local (i.e., differential boundary operators) they expanded the pseudo-differential operators in the deviation of the wave direction from some preferred direction of propagation. In this manner they constructed a family of local boundary conditions which absorbed waves in a progressively larger band around a given propagation direction.

These boundary conditions were tested by Kwak (ref. 10) on the time dependent small disturbance equation. It was found that the first order condition significantly improved the standard condition ($\phi = 0$); where ϕ is the potential. The second order condition was found to offer no significant advantages. (This was an accuracy study and not a steady state problem.) In this case, as in other cases with circular or spherical symmetry the first order Engquist and Majda condition and the first order condition in reference 2 coincide.

We have so far concentrated on the use of radiation boundary conditions to accelerate convergence to steady state. There are also a great variety of problems which are inherently time dependent. These problems include the problem of acoustic radiation in a jet (ref. 11), problems in duct acoustics (ref. 12) and problems involving oscillations in the position of shocks (ref. 13). In these types of problems it is necessary to simulate the condition of outgoing radiation in order to obtain a correct numerical solution for the time scale of interest.

The theory to be presented here will be equally valid for these time dependent (or time harmonic) problems provided there is some knowledge of the functional form of the solution near infinity. In section 2 we will derive a family of boundary conditions designed to simulate outgoing radiation for the wave equation. This will lead to a radiation boundary condition applicable in the presence of a mean flow. This boundary condition shows great promise in accelerating flows to steady state. Numerical results illustrating this will be presented in section 3. In section 4 we will present extensions of this theory.

DEVELOPMENT OF RADIATION BOUNDARY CONDITIONS

Consider the wave equation in three space dimensions

$$p_{tt} = \Delta p. \tag{1}$$

In a general inviscid flow, if p is the deviation of the pressure from the far field pressure p_∞, then p will satisfy equation (1) provided the free stream velocities are zero. (Throughout this paper we will use the subscript "∞" to indicate free stream values.)

A spherical wave solution to equation (1) has the functional form

$$p = \frac{f(t-r)}{r}. \tag{2}$$

Here f is an arbitrary function and r is the distance from some fixed origin from which the spherical wave emanates. A boundary condition designed to simulate outgoing radiation should be exact at least for waves of the form (2). Suppose the artificial boundary is the sphere $r = r_1$. A boundary condition which is exactly satisfied by all waves of the form (2) is

$$B_1 p = 0, \tag{3}$$

where the operator B_1 is given by

$$B_1 = \frac{\partial}{\partial t} + \frac{\partial}{\partial r} + \frac{1}{r}. \tag{4}$$

Condition (3) can be regarded as matching the solution p to the functional form (2).

In general the waves impinging on the artificial surface are not exactly spherical. As an example, dipoles and quadrupoles often arise in aero-acoustics. In general, an outwardly radiating solution to equation (1) will have the asymptotic expansion

$$p \simeq \sum_{j=1}^{\infty} \frac{f_j(t-r,\theta,\phi)}{r^j}. \tag{5}$$

Here θ and ϕ are the angular variables associated with a spherical coordinate system centered at $r = 0$ while the functions f are arbitrary functions. (In principle f_j for $j > 1$ can be determined from the radiation pattern f_1, however for numerical purposes they should be treated as arbitrary functions.) The argument $t - r$ determines that the wave is outgoing, while the θ, ϕ dependence allows for a skewing from spherically symmetric waves.

The series (5) has been studied by many authors (see, e.g., Friedlander (ref. 14)). We are not concerned here with conditions for convergence, but merely require that this series represents the behavior of the solution in a neighborhood of infinity.

Applying the operator B_1 to the representation (5) we see that

$$B_1 p \Big|_{r = r_1} = O\left(\frac{1}{r_1^3}\right). \tag{6}$$

It therefore follows that the radiation boundary condition

$$B_1 p = 0, \tag{7}$$

will be increasingly accurate as the position of the artificial boundary, e.g. the sphere $r = r_1$, approaches infinity. The condition (7) is exact only for the first term in the expansion (5). It can be regarded as matching the solution to the first term in the expansion (5) with the error in (6) depending on the amount of skewing expressed in the next order term f_2.

Based on this motivation, a natural procedure to improve the condition (7) is to derive boundary conditions which match the solution to the first two terms in (5). Such a condition is

$$B_2 p \Big|_{r = r_1} = 0, \tag{8}$$

where the operator B_2 is given by

$$B_2 = \left(\frac{\partial}{\partial t} + \frac{\partial}{\partial r} + \frac{3}{r}\right)\left(\frac{\partial}{\partial t} + \frac{\partial}{\partial r} + \frac{1}{r}\right) = \frac{\partial^2}{\partial t^2} + \frac{\partial^2}{\partial r^2} + \frac{2\partial^2}{\partial t \partial r} + \frac{4}{r}\left(\frac{\partial}{\partial t} + \frac{\partial}{\partial r}\right) - \frac{2}{r^2}\,. \tag{9}$$

It can easily be verified that (8) is exactly satisfied by the first two terms in the expansion (5). Applying the operator B_2 to (5) we obtain

$$B_2 p \Big|_{r = r_1} = O\left(\frac{1}{r_1^5}\right). \tag{10}$$

Thus, the boundary condition (8) is more accurate in the vicinity of infinity because it matches the solution to the first two terms in (5). Consequently, the boundary condition (8) can be expected to be more accurate at near distances. Alternatively if the solution is, for example a pulse, (8) would be expected to accelerate convergence to the steady state value because the reflected waves generated at the boundary will be smaller.

The procedure which led to the operator (9) can obviously be extended to boundary operators which annhilate any number of terms in (5). The well-posedness of the resulting boundary conditions together with rigorous error bounds are discussed in reference 2. Some numerical results, for acoustic radiation problems will be presented in the next section.

In order to derive boundary conditions for more general fluid dynamics problems, we next consider the effect of a constant free stream flow. For simplicity we consider the two-dimensional Cartesian case. Let x and y denote the coordinate directions and u and v the corresponding velocity components. In addition, we let p be the pressure and ρ the density. We assume that in the far field the resulting steady state is given by

$$\begin{aligned} u &= u_\infty \\ v &= 0 \\ p &= p_\infty \\ \rho &= \rho_\infty \quad . \end{aligned} \tag{11}$$

(This can always be arranged by a rotation of the coordinate system.)

In the far field, away from bodies and boundary layers, viscosity and entropy changes can be neglected. If we therefore introduce the deviations from steady state

$$\begin{aligned} \hat{u} &= u - u_\infty \\ \hat{v} &= v - v_\infty \\ \hat{p} &= p - p_\infty \\ \hat{\rho} &= \rho - \rho_\infty \ , \end{aligned} \tag{12}$$

and assume that quadratic terms in these variables can be neglected, we obtain the linearized Euler equations

$$\begin{aligned} \hat{u}_t + u_\infty \hat{u}_x + \frac{\hat{p}_x}{\rho_\infty} &= 0 \\ \hat{v}_t + u_\infty \hat{v}_x + \frac{\hat{p}_y}{\rho_\infty} &= 0 \\ \hat{p}_t + u_\infty \hat{p}_x + \rho_\infty c_\infty^2 (\hat{u}_x + \hat{v}_y) &= 0. \end{aligned} \tag{13}$$

(Here c_∞ is the far field sound speed.)

By straight forward manipulation (13) can be reduced to a convective wave equation for $\hat{p}$,

$$\hat{p}_{tt} + 2u_\infty \hat{p}_{xt} - (c_\infty^2 - u_\infty^2)\hat{p}_{xx} - c_\infty^2 \hat{p}_{yy} = 0. \tag{14}$$

Assuming that the steady state is subsonic in the far field, i.e. $u_\infty < c_\infty$, we can derive radiation boundary conditions for (14) in the same manner as for the standard wave equation (1). At a subsonic boundary one boundary condition must be imposed, either for (14) or the system (13) (see ref. 15). Choosing a radiation boundary condition can be expected to accelerate the convergence to a steady state.

At a supersonic outflow boundary all of the characteristics go out of the domain. No extra boundary condition can be imposed in this case, instead the solution should be obtained by a numerical procedure such as extrapolation.

We next proceed to derive a radiation boundary condition based on the convective wave equation (14). The most convenient way to proceed is to introduce new coordinates which transform (14) into the standard wave equation. Let M_∞ be the free stream Mach number,

$$M_\infty = \frac{u_\infty}{c_\infty} . \tag{15}$$

($M_\infty < 1$ is the condition for a subsonic boundary.) Introducing new coordinates

$$\xi = (1-M_\infty^2)^{\frac{1}{2}}x, \qquad \tau = c_\infty(1-M_\infty^2)^{\frac{1}{2}}t + M_\infty\xi, \tag{16}$$

(14) is transformed into

$$\hat{p}_{\tau\tau} = \hat{p}_{\xi\xi} + \hat{p}_{yy}. \tag{17}$$

Equation (17) is the two-dimensional version of (1) and will therefore have outgoing circular waves, which in the two-dimensional case are asymptotic solutions. Introducing polar coordinates

$$d^2 = \xi^2 + y^2; \quad \tan\theta = y/\xi, \tag{18}$$

then for large values of t and d, p will have the asymptotic form

$$\hat{p} \approx f(\tau - d, \theta)/d^{\frac{1}{2}}. \tag{19}$$

(This was shown, for example, by Lax and Phillips in reference 16.)

In the same way as the boundary operator (4) was derived, it can be shown that the boundary condition

$$\hat{p}_\tau + \hat{p}_d + \frac{\hat{p}}{2d} = 0, \tag{20}$$

is exact for all functions having the functional form (19). We next express (20) in the physical coordinates t, x and y. For clarity we will write it in terms of the total pressure $p = \hat{p} + p_\infty$. We obtain the condition

$$\frac{1}{c_\infty\sqrt{1-M_\infty^2}}\left[1 - \frac{x}{d}\ \frac{M_\infty}{\sqrt{(1-M_\infty^2}}\right]p_t + \frac{x}{d}\,p_y + \frac{(p-p_\infty)}{2d} = 0, \tag{21}$$

where in physical coordinates

$$d^2 = \frac{x^2}{1-M_\infty^2} + y^2. \tag{22}$$

(The factor of 2 in the last term in (21) is due to the $d^{\frac{1}{2}}$ decay in equation (19) which is characteristic of two-dimensional problems.) We finally use the linearized Euler equation (13) to eliminate the spatial derivatives of p. The result is

$$(23)\quad \frac{1}{(c_\infty^2 - u_\infty^2)^{\frac{1}{2}}} p_t - \frac{\rho_\infty c_\infty^2}{c_\infty^2 - u_\infty^2} \frac{x}{d} [u_t - u_\infty v_y] - \rho_\infty \frac{y}{d} [v_t + u \ v_x] + \frac{p - p_\infty}{2d} = 0.$$

In the steady state (23) does not strictly enforce $p = p_\infty$, i.e. $p = p_\infty$ only when the gradient of v vanishes. Based on the functional form (19) any steady state must satisfy $p - p_\infty = 0(d^{-\frac{1}{2}})$ and it can then be seen that at the steady state (23) enforces $p = p_\infty$ to within $0(d^{-\frac{3}{2}})$ which is the accuracy of the boundary condition. In practice the gradients of v are negligible and in fact u and v are often obtained from zeroth order extrapolation which is a consistent approximation to $v_x = 0$ and hence $v_y = 0$ (from eqn. (13)). The numerical results presented in section 3 were generally obtained by neglecting the spatial derivatives of v in equation (23).

$$(24)\qquad \frac{1}{(c_\infty^2 - u_\infty^2)^{\frac{1}{2}}} p_t - \frac{\rho_\infty c_\infty^2}{c_\infty^2 - u_\infty^2} \frac{x}{d} u_t - \rho_\infty \frac{y}{d} v_t + \frac{p - p_\infty}{2d} = 0.$$

The coefficients in (23) require knowledge of $\rho_\infty, u_\infty, c_\infty$ which are not generally known á priori at the boundaries. We have used the values at the preceeding time step and have found no difficulties from this.

The boundary condition (24) is an outflow boundary condition which simulates outgoing radiation. When coupled with some numerical procedure for the other variables (typically zeroeth order extrapolation) it permits a boundary treatment which substantially accelerates convergence to the steady state. Our numerical experiments indicate that this acceleration is relatively insensitive to the choice of origin. From the nature of its construction, it is also applicable to truly time dependent problems, where there is a continuing radiation of energy across the outflow boundary.

Another application of this theory is at characteristic boundaries. These boundaries are tangent to the free stream velocities and arise even in supersonic flow. For example, in flow past a flat plate, with free stream velocity u_∞, $v_\infty = 0$, the boundary $y = \text{constant}$ (i.e. the top of a computational rectangle) is characteristic. At these boundaries one frequently extrapolates all the dependent variables. This can cause oscillations which delay convergence to a steady state. In addition, these oscillations require that the top boundary be sufficiently far away so that the oscillations will not degrade the accuracy of the steady state (see, e.g. reference 7).

We have applied condition (24) at characteristic boundaries with success. Since no condition (other than $v = 0$) should be imposed at a characteristic boundary, better results were obtained by replacing p_∞ by p at the proceeding time step. An alternative is simply to impose the one-dimensional characteristic condition

$$p_t - \rho_\infty c_\infty v_t = 0, \tag{25}$$

which is valid even if the basic flow is supersonic. The use of equation (25) can also dramatically improve convergence. The numerical results to be presented in the next section show the improvements that can be obtained by correctly treating the characteristic boundaries.

NUMERICAL EXAMPLES

To validate the boundary condition (24) we have studied several test problems. The first set of problems is designed to study the rate of convergence to a steady state.

In the first problem a compressible vortex is superimposed on a uniform flow $u = 1$, $v = 0$ in a rectangular domain $0 \leq x \leq 1$, $0 \leq y \leq 1$. The vortex is modelled by

$$d^2 = R^2 + (x - \tfrac{1}{2})^2 + (y - \tfrac{1}{2})^2 \quad , \quad R = 0.15$$

$$\begin{aligned} u &= \frac{\Gamma}{\pi}\,(y - \tfrac{1}{2})/d^2 \\ v &= -\frac{\Gamma}{\pi}\,(x - \tfrac{1}{2})d^2 \end{aligned} \tag{26}$$

$$\Gamma = \text{circulation} = 2\pi\ R(v_\theta)_{\max}$$

The Mach number is found by assuming that the temperature is a fixed constant while the pressure is calculated from the total pressure by assuming isentropic flow. Analytically the vortex convects downstream and out of the computational domain. The steady state is then just the free stream flow. Hence, the number of iterations required for convergence is directly related to the ability of the downstream boundary condition to allow the vortex to pass out of the domain without reflections.

This problem (which was suggested by David Rudy of NASA Langley) is a model for both steady state problems and time dependent compressible Navier-Stokes equations. MacCormack's method is used to numerically solve the equations. The free stream Mach number is 0.4 and the Reynolds number is approximately 2100.

In Table I the number of iterations required for convergence is shown for different choices of the origin. The boundary condition (24) is compared with that suggested by Rudy and Strikwerda (see ref. 6) and also the boundary condition $p = p_\infty$. The steady state is assumed to occur when the change in all the dependent variables is less than 10^{-7}.

The results show that (24) provides a significant acceleration to the steady state and that the number of iterations is relatively insensitive to the choice of origin. Similar results are obtained when the disturbance is a region of high pressure instead of a vortex (see refs. 3 and 6).

TABLE I. NUMBER OF ITERATIONS TO ACHIEVE A STEADY STATE FOR A MODEL PROBLEM CONTAINING A COMPRESSIBLE VORTEX.

Boundary Conditions	Origin	Number of Iterations
(24)	(0., 0.5)	2251
(24)	(0.5, 0.5)	2878
(24)	(0., 1.0)	2503
(24)	(0., 0.)	2530
Ref 6	-	7860
$p = p_\infty$	-	> 20,000

As a more realistic test case we consider the development of a subsonic boundary layer over a flat plate. This problem was used in reference 7 to compare a wide range of outflow boundary conditions. The computational domain is a rectangle with the bottom corresponding to the plate. The top of the computational rectangle is a characteristic boundary. A standard boundary treatment at this upper surface is to extrapolate all of the variables. We also consider the effect of constricting this upper boundary. In Table II the number of iterations required for convergence is shown for both different boundary treatments and for different positions of the upper boundary. Results are also presented for the radiation boundary condition of ref. 7 with the free parameter, α, chosen to be equal to 0.3. Distances are measured in boundary layer thicknesses with the x coordinate varying between 0.0 and 2.0 and the maximum upper boundary chosen as 1.0.

TABLE II. RESULTS FOR BOUNDARY LAYER OVER A FLAT PLATE
(Extrapolation on upper boundary)

Position of upper boundary	Boundary Condition	Origin	Iterations
1.0	(24)	(1.,0.)	12,500
1.0	(24)	(0.,0.)	14,000
1.0	Ref. 7	-	12,800
1.0	$p = p_\infty$	-	> 20,000
0.6	(24)	(1.,0.)	13,950*
0.4	(24)	(1,,0.)	> 14,000*

*Inaccurate steady state

The results presented in Table II demonstrate that all of the radiation conditions, i.e. (24) and those in refernce 7 provide a substantial improvement over the condition $p = p_\infty$. The effectiveness of (24) is still relatively insensitive to the choice of origin. Constricting the upper boundary and using extrapolation, led to oscillations which delayed the attainment of the steady state. The final steady state in this case also differed significantly from the steady state obtained by integrating the equations in the larger region.

The use of a larger computational domain substantially increases the cost of the computation. This is particularly true because, in many cases, only the solution near the surface (in this case the plate) is of interest. In order to test the possibility of constricting the upper boundary we applied the radiation condition (24), at the upper boundary. In this case, we replace p_∞ by p at the previous time step, as the condition $p = p_\infty$ in the steady state is not valid when the upper boundary is reduced. In Table III the results of applying (24) at the upper boundary are shown.

TABLE III. THE EFFECT OF THE RADIATION CONDITION AT THE UPPER BOUNDARY

Position of Upper Boundary	Outflow Boundary Condition	Top Boundary Condition	Iterations
1.0	(24)	(24)	8800
1.0	Ref. 7	(24)	12850
0.6	(24)	(24)	8800
0.4	(24)	(24)	9400

The data show that a substantial acceleration of convergence can be obtained by using a radiation condition at a characteristic boundary. We note that in all cases the steady states in Table III were virtually identical to the steady states obtained on the larger regions. Thus, a substantial savings in computer time can be achieved by a correct choice of the boundary condition at the characteristic boundary. We have found similar improvements by using a characteristic condition such as (25) which can be used for supersonic flow as well. The reason that the boundary condition of reference 7 is not accelerated by a radiation condition at the characteristic boundary is not presently clear.

As another example we consider inviscid flow in a quasi-one-dimensional nozzle with variable area $A(x)$. The equations are

$$
\begin{aligned}
&(A\rho)_t + (A\rho u)_x = 0 \\
(27)\qquad &(A\rho u)_t + [A(\rho u^2 + p)]_x = A_x p \\
&(AE)_t + [Au(E+p]_x = 0,
\end{aligned}
$$

where E is the total energy. At the (subsonic) inflow both u and E are specified. We will only consider the case of a subsonic outflow so that one boundary condition should be specified. By properly adjusting this outflow pressure both shocked and shock-free solutions can be obtained.

We consider the effect of different radiation conditions on convergence to a steady state for the system (27). In this case, the condition $p = p_\infty$ is valid during the temporal evolution of the flow. The use of a radiation condition is therefore a physically inconsistent artifice to accelerate the convergence to a steady state.

Since the system (27) is one-dimensional, traveling waves have no spatial decay in constrast to (2) or (19). Therefore, the appropriate generalization of (24) is the characteristic condition

$$\frac{\partial p}{\partial t} - \rho c \frac{\partial u}{\partial t} = 0. \tag{28}$$

This condition was tested along with the generalized radiation condition (see ref. 6)

$$\frac{\partial p}{\partial t} - \rho c \frac{\partial u}{\partial t} + \alpha(p - p_\infty) = 0. \tag{29}$$

The solution method used was a linearized, implicit Euler method (see refs. 7 and 8). Boundary conditions on the pressure are computed by using an equation for $\partial p/\partial t$ and using a linearization technique similar to the basic difference scheme. In Table IV we present results for several different choices of α. Both the number of iterations required for convergence and the steady state L_2 error are presented.

TABLE IV. STEADY STATE RESULTS FOR THE ONE-DIMENSIONAL NOZZLE FLOW

Boundary Condition	L_2 Steady State Error	Iterations
$\alpha = \infty$ (i.e. $p = p_\infty$)	11.4	153
$\alpha =$ 0.0	8.11	52
$\alpha =$ 0.278	9.33	118
$\alpha =$ 1.0	8.40	182
$\alpha =$ 10.0	11.16	158

The results show that the radiation condition at the outflow can substantially accelerate convergence. In this case it is not necessary to have a boundary condition which enforces $p = p_\infty$ in the steady state (i.e., $\alpha = 0$). The steady state condition $p = p_\infty$ is a consequence of the initial conditions. Similar results can be obtained by using the MacCormack explicit scheme (see ref. 3).

As an additional example we consider the use of the higher order boundary condition (10) in a time harmonic problem. In this case we compute the acoustic due to a quadrupole source in a medium at rest. Quadrupole sources are important in the theory of jet noise and an effective computation requires boundary conditions which will not allow spurious reflections. The first order condition (3) is inaccurate in this case because the leading term in the expansion (5) becomes very small at 90°.

In Table V the phase change between 0° and 90° is presented for the two boundary conditions (3) and (10). The analytic solution should exhibit a phase change of $\pi/2$ (i.e. from a cosine to a sine dependence as the angle changes from 0° to 90°. It can be seen that the second order boundary condition (10) gives an accurate phase change while (3) gives a completely wrong phase change. This result clearly indicates the crucial importance of radiation boundary conditions in simulating fluctuating flows such as those occurring in aeroacoustics.

TABLE V. PHASE CHANGE FOR QUADRUPOLE SOURCE

Boundary Condition	Phase Change
(3)	0.77 ± 0.08
(10)	1.64 ± 0.08

EXTENSIONS TO TIME-INDEPENDENT EQUATIONS

In the previous sections we have concentrated on developing boundary conditions for time dependent equations. These conditions were used even in cases where the time dependence was only a mechanism for achieving the steady state solution. There are many applications, however, when one solves the time independent equations directly. Generally in those cases a time harmonic solution is sought. Some examples of such aerodynamic problems are the small disturbance equation about a fluctuating airfoil (ref. 19), acoustic propagation in a duct (ref. 20) and the scattering of acoustic waves by a body such as an airplane fuselage (ref. 21). In this section we will consider the problem of deriving radiation boundary conditions for such problems.

As a model equation we consider the Helmholtz equation

$$\Delta\phi + k^2\phi = 0. \tag{30}$$

(In applications ϕ can be a velocity potential or a fluctuating quantity such as the pressure.) When (30) is considered exterior to a body it describes the scattering of waves by the body. When (30) is integrated in a duct it describes the propagation of acoustic (or electromagnetic) waves in the duct.

In each case, (30) must be supplemented by appropriate boundary conditions on the physical surfaces and a radiation condition enforcing outgoing radiation at infinity.

The appropriate radiation boundary condition is different in fully exterior geometry and in the duct geometry. This occurs since in the duct geometry there can exist a finite number of propagating modes each with a different wave number. In fully exterior regions, on the other hand, radiation propagates radially (with some angular skewing), and there is essentially only one wave number.

In the fully exterior region the appropriate boundary condition at infinity is the Sommerfeld radiation condition

$$\phi_r - ik\phi + \frac{\phi}{r} = o\left(\frac{1}{r}\right) \quad (r \to \infty). \tag{31}$$

This condition can be derived by formally differentiating the expansion

$$\phi = e^{-ikr} \sum_{j=1}^{\infty} \frac{f_j(\theta,\phi)}{r^j}, \tag{32}$$

which is the direct analog of (5) for the case of a harmonic time dependence. Higher order boundary conditions can be obtained by matching the solution to more terms in the expansion (32). For example, a second order boundary operator, analogous to (9) is

$$B_2 = \left(-ik+\frac{\partial}{\partial r}+\frac{3}{r}\right)\left(-ik+\frac{\partial}{\partial r}+\frac{1}{r}\right) = -k^2+\frac{\partial^2\phi}{\partial r^2} - \left(2ik-\frac{4}{r}\right)\frac{\partial\phi}{\partial r} - \left(\frac{4ik}{r}-\frac{3}{r^2}\right)\phi . \tag{33}$$

The properties of these boundary conditions are discussed in detail in reference 4.

A different situation occurs in the duct Helmholtz equation. For simplicity, we consider the Helmholtz equation in the rectangular region $0 \le x < \infty$, $0 \le y \le \pi$. The equations are

$$\text{(a)} \quad \phi_{xx} + \phi_{yy} + k^2\phi = 0$$

$$\text{(b)} \quad \frac{\partial\phi}{\partial y} = 0 \quad \text{at} \quad y = 0,\pi$$

$$\text{(c)} \quad \phi\Big|_{x=0} = f .$$

It is easy to see that the general solution is

$$\phi = \sum A_j \cos(jy)\left[e^{i\sigma_j x} a_j + b_j\, e^{-i\sigma_j x}\right]; \text{where } \sigma_j = \sqrt{k^2 - j^2}. \tag{35}$$

We see that for $j \le k$ the outgoing solution is obtained by choosing

$$\phi \sim e^{+i\sigma_j x}. \tag{36}$$

The modes with $j \geq k$ are evanescent (i.e. exponentially decaying) and the correct solution is obtained by requiring exponential decay as $y \to \infty$, i.e.

(37)
$$\phi \sim e^{-\sqrt{(j^2 - k^2)}x} .$$

Thus, the wave numbers of the solution at infinity vary with the mode.

A boundary operator which is exact for the propagating modes is

(38)
$$B\phi = \prod_{j=1}^{[k]} (\frac{\partial}{\partial x} - i\sigma_j)\phi.$$

It can be shown that imposition of the boundary condition

(39)
$$B\phi \Big|_{x=x_1} = 0,$$

accurately simulates the outgoing solution with an error that decreases exponentially as $x \to \infty$.

If the problem (34) is formulated in cylindrical geometry, it will describe waves propagating in a hard walled duct. Introducing cylindrical coordinates r and z, where r is normal to the duct centerline and z is distance along the axis, the problem becomes (the duct diameter is scaled to unity)

(40)

(a) $$\phi_{zz} + \frac{1}{r}(r\phi_r) + k^2\phi = 0$$

(b) $$\phi_r = 0, \text{ at } r = 0, \text{ and } r = \tfrac{1}{2}$$

(c) $$\phi\Big|_{z=-L} = f.$$

The solution is

(41)
$$\phi = \sum A_j J_0(\sigma_j r)e^{+i\sigma_j z},$$

where J_0 is the zero order Bessel function and λ_j is twice the j^{th} zero of J_0' also

(42)
$$\sigma_j = \sqrt{k^2 - \lambda^2} .$$

It can be seen that the boundary condition (39) is equally valid in this case. There is no need for the ducts to have straight walls except in the vicinity of infinity.

Similar boundary conditions can be developed for computing spin modes, ducts with flow, or for computing in ducts with liners where condition (40c) is replaced by an impedence boundary condition. The second order boundary condition can be implemented in finite element codes in a manner similar to that described in reference 4.

This theory has also been applied to underwater acoustics. A typical problem here is

$$
(43)\qquad
\begin{aligned}
&\text{(a)}\quad \phi_{zz} + \frac{(r\phi_r)_r}{r} + k^2\phi = 0\\
&\text{(b)}\quad \phi = 0 \quad \text{on} \quad z = 0\\
&\text{(c)}\quad \phi_z = 0 \quad \text{on} \quad z = \pi\\
&\text{(d)}\quad \phi = f \quad \text{on} \quad r = r_c .
\end{aligned}
$$

This problem differs from (40) in that the computational domain is infinite in the r direction. The outwardly radiating solution is

$$
(44)\qquad \phi = \sum_{j=1}^{\infty} A_j \sin(\lambda_j z) H_0^+(\sigma_j r); \quad \lambda_j = j - \tfrac{1}{2}\,, \quad \sigma_j = \sqrt{k^2 - \lambda_j^2}\ .
$$

(See for example, Fix and Marin, ref. 22.) Here H_0^+ is the Hankel function of zero order and of the first kind. By using the asymptotic expansion

$$
(45)\qquad H_0^+(z) \simeq \sqrt{2/\pi}\; e^{i(2-\pi/4)}\left[\frac{1}{\sqrt{z}} + O(z^{-3/2})\right],
$$

and the definition of σ_j we see that the solution is composed of a finite number of propagating modes $(\lambda_j < k)$ and an infinite number of evanescent modes $(\lambda_j > k)$.

Fix and Marin have developed an exact, global radiation condition for problem (43). This condition, can be applied at any artificial boundary $r = r_1$. Local approximations can be developed using the ideas presented here. If there are m propagating modes, we can use the boundary condition

$$
(46)\qquad B_m(r_1)\phi = 0,
$$

where B_m is the unique, m^{th} order differential operator which has as its fundamental set of solutions $\{H_0^+(\sigma_j r);\ j=1,\ldots,m\}$. Such an operator can easily be constructed using the theory of ordinary differential equations.

Simpler boundary conditions can be constructed by accepting an error of $r^{-3/2}$ and using the leading order term in the expansion (45). In this case, we take as the operator B_m the operator which has the fundamental set of solutions $\{e^{i\sigma_j r}/\sqrt{r},\ j=1,\ldots m\}$. For the case $m = 2$ we get

$$B_2(r) = \left(\frac{\partial}{\partial r} - i\sigma_2 + \frac{1}{2r}\right)\left(\frac{\partial}{\partial r} - i\sigma_1 + \frac{1}{2r}\right). \quad (47)$$

This second order boundary condition has been applied to various problems.

The theory presented here is also valid in the case of a variable sound speed or varying topography of the ocean bottom. The second order boundary condition can be easily implemented in variational principles as described in reference 4. An efficient implementation of the higher order boundary conditions must still be developed. Similar boundary conditions have been proposed by Kriegsmann (ref. 23) for wave guide problems in a cartesian coordinate system.

CONCLUSION

We have derived boundary conditions which can be used on the artificial boundaries that arise when an unbounded region is truncated for computational purposes. These boundary conditions are based on matching the solution to a known functional form valid near infinity.

These boundary conditions have been applied to the nonlinear compressible Navier-Stokes and Euler equations. They have been shown to yield a substantial acceleration of convergence to the steady state. Over or under specification can lead to oscillations which degrade the accuracy of the steady state. The radiation boundary conditions can be used at both subsonic outflow boundaries and at characteristic boundaries where the normal velocity is zero.

The radiation boundary conditions can also be developed directly for the steady state equations. For subsonic flows the equations are elliptic. Thus we are led to the development of Sommerfeld-type radiation conditions for elliptic equations. As before these allow for the constriction of the domain of integration without loss of accuracy. It is also seen that the appropriate boundary conditions depend on the geometry of the region. Hence, even though the boundary conditions are local they depend on global properties of the solution. This occurs since the boundary conditions are developed based on asymptotic solutions valid in the vicinity of infinity. These asymptotic expansions depend on global properties of the solution. In particular, the geometry of the region in the far field strongly affects the proper choice of boundary conditions. This is true for both the steady state and time dependent problems.

The boundary conditions developed are all local, i.e. differential boundary conditions. It is also possible to incorporate the asymptotic expansion directly in a finite difference scheme. This will lead to a relationship between the outermost grid points. This relationship is just the finite difference analog of the differential boundary conditions.

Numerical results have been presented here and in references 2, 3, 4, 11 and 24 which verify the usefulness of the proposed boundlary conditions.

REFERENCES

1. Grosch, C. E. and Orszag, S. A.: Numerical Solution of Problems in Unbounded Regions: Coordinate Transformations, J. Computational Phys., Vol. 25, 1977, pp. 273-295.

2. Bayliss, A. and Turkel, E.: Radiation Boundary Conditions for Wave-like Equations, Comm. Pure Appl. Math., Vol. 33, 1980, pp. 707-725.

3. Bayliss, A. and Turkel, E.: Outflow Boundary Conditions for Fluid Dynamics, to appear in SIAM J. Scientific and Statistical Computing.

4. Bayliss, A., Gunzburger, M. D., and Turkel, E.: Boundary Conditions for the Numerical Solution of Elliptic Equations in Exterior Regions, to appear in SIAM J. of Appl. Math.

5. Gustafsson, B. and Kreiss, H.-O.: Boundary Conditions for Time Dependent Problems with an Artificial Boundary, J. Computational Phys., Vol. 30, 1979, pp. 333-351.

6. Rudy, D. and Strikwerda, J. C.: A Non-reflecting Outflow Boundary Condition for Subsonic Navier-Stokes Calculations, J. Computational Phys., Vol. 36, 1980, pp. 55-70.

7. Rudy, D. and Strikwerda, J. C.: Boundary Conditions for Subsonic Compressible Navier-Stokes Calculations, Computers and Fluids, Vol. 9, 1981, pp. 327-338.

8. Engquist, B. and Majda, A.: Absorbing Boundary Conditions for the Numerical Simulation of Waves, Math. Comput., Vol. 31, 1977, pp. 629-651.

9. Engquist, B. and Majda, A.: Radiation Boundary Conditions for Acoustic and Elastic Wave Calculations, Comm. Pure Appl. Math., Vol. 32, 1979, pp. 312-358.

10. Kwak, D.: Non-reflecting Far Field Boundary Conditions for Unsteady Transonic Flow. AIAA Paper No. 80-1393, 1980.

11. Maestrello, L., Bayliss, A., and Turkel, E.: On the Interaction of a Sound Pulse with the Shear Layer of an Axisymmetric Jet, J. Sound and Vibration, Vol. 74, 1981, pp. 281-301.

12. Baumeister, K. J. and Rice, E. J.: A Difference Theory for Noise Propagation in Acoustically Lined Ducts with Mean Flow. AIAA Paper No. 73-1006, 1973.

13. Ballhaus, W. F. and Goorjian, P. M.: Implicit Finite Difference Computations of Unsteady Transonic Flows about Airfoils, Including the Treatment of Irregular Shock Wave Motions. AIAA Paper No. 77-205, 1977.

14. Friedlander, F. G.: On the Radiation Field of Pulse Soluitons of the Wave Equation, Proc. of the Royal Society of London, Ser. A 269, 1962, pp. 53-65.

15. Oliger, J. and Sundstrom, A.: Theoretical and Practical Aspects of Some Initial Boundary Value Problems in Fluid Dynamics, SIAM J. Appl. Math., Vol. 35, 1978, pp. 419-446.

16. Lax, P. D. and Phillips, R. S.: Decaying Modes for the Wave Equation in the Exterior of an Obstacle, Comm. Pure Appl. Math., Vol. 22, 1969, pp. 737-787.

17. Beam, R. W. and Warming, R. F.: An Implicit Finite Difference Algorithm for Hyperbolic Systems in Conservation-Law Form, J. Computational Phys., Vol. 22, 1976, pp. 87-110.

18. Briley, W. R. and McDonald, H.: Solution of the Multi-dimensional Compressible Navier-Stokes Equations by a Generalized Implicit Method, J. Computational Phys., Vol. 24, 1977, pp. 372-397.

19. Ehlers, F. E.: A Finite Difference Method for the Solution of the Transonic Flow Around Harmonically Oscillating Wings. NASA CR-2257, 1974.

20. Abrahamson, A. L.: A Finite Element Algorithm for Sound Propagation in Axisymmetric Ducts Containing Compressible Mean Flow. NASA CR-45209, 1977.

21. Bayliss, A. and Maestrello, L.: Measurements and Analysis of Far Field Scattering from a Prolate Spheroid, J. Acoust. Soc. America, Vol. 64, 1978, pp. 896-900.

22. Fix, G. J. and Marin, S.: Variational Methods for Underwater Acoustic Problems, J. Computational Phys., Vol. 28, 1978, pp. 253-270.

23. Kriegsmann, G.: Radiation Conditions for Wave Guide Problems. Technical Report 8007, Department of Engineering Sciences and Applied Mathematics, Northwestern University, November 1980.

24. Kriegsmann, G. and Morawetz, C. S.: Numerical Solutions of Exterior Problems with the Reduced Wave Equation, J. Computational Phys., Vol. 28, 1978, pp. 181-197.

Blank Page

A COMPARATIVE STUDY OF NONREFLECTING FAR-FIELD BOUNDARY CONDITION PROCEDURES FOR UNSTEADY TRANSONIC FLOW COMPUTATION

Dochan Kwak

Ames Research Center

SUMMARY

Various nonreflecting far-field boundary condition procedures are compared by implementing them in the computer code LTRAN2. This code solves the implicit finite-difference representation of the small-disturbance equations for transonic flows about airfoils. The first- and second-approximate nonreflecting conditions, as proposed by Engquist and Majda, are compared with the condition derived from the full-characteristic equation. The far-field boundary conditions and the description of the algorithm for implementing these conditions in LTRAN2 are discussed. Various cases are computed and compared with results from the older, more conventional procedures. One concludes that the full-characteristic equation produces the most effective results, thus allowing the far-field boundary to be located closer to the airfoil; this decreases the computer time required to obtain the solution because fewer mesh points are required.

INTRODUCTION

To compute time-dependent flows over an infinite region using finite-difference procedures requires that either the problem be reduced to one in a finite domain via a coordinate transformation, or that boundaries be placed at a finite distance from the body and the boundary conditions modified along them. However, for many practical problems the coordinate transformation method is not applicable. In such cases, computational simulations of unsteady flows in an unbounded region are performed on grids with finite dimensions. The artificial wall effect created by these grid far-field boundaries must therefore be minimized so as not to degrade the resulting numerical solution.

Various approaches have been developed to reduce this spurious influence of far-field boundaries on interior solutions (refs. 1-9) (a brief review of these methods is given in ref. 10). Among those approaches, the first- and the second-approximate local-condition procedures by Engquist and Majda (ref. 4) were selected to be compared with the procedure derived from the full-characteristic equation. All three procedures require a modest change in the existing computer code; however, these conditions result in an improvement in the computational efficiency of that code. In particular, there was marked improvement by the full-characteristic condition.

Unsteady transonic regions are encountered in many existing flight vehicles. Typical examples include a fluttering airfoil and spinning helicopter rotors (ref. 11). For unsteady small-disturbance transonic flows, Ballhaus and Goorjian (ref. 12) have developed a time-accurate, implicit finite-difference computer code, LTRAN2. Their boundary conditions at the top, bottom, and upstream boundaries (see fig. 1) are perfectly reflecting conditions and are permissible for boundaries placed far away. In the present work, approximate nonreflecting boundary conditions are employed in this code to bring the far-field boundaries closer to the airfoil. As illustrated in figure 1, waves originating from the airfoil propagate to the far-field boundaries. The old boundaries, which are placed at a large distance from the airfoil, leave the near-field solution unaffected by reflective waves from the outer boundary. With nonreflecting conditions, the new boundary can be located closer to the airfoil, thus reducing the area of computation.

In the following sections, the governing equation and the boundary condition procedures are presented; the finite-difference scheme for implementing these conditions in LTRAN2 is described; and computed results, using the old reflecting far-field boundary conditions and those using the new nonreflecting conditions, are compared with large-grid solutions.

GOVERNING EQUATION AND FAR-FIELD BOUNDARY CONDITIONS

Governing Equation

The unsteady, transonic small-disturbance equation for low reduced frequencies can be written as

$$A\phi_{xt} = B\phi_{xx} + \phi_{yy} \tag{1a}$$

where

$$\left.\begin{aligned} A &= 2kM_\infty^{\;2}/\delta^{2/3} \\ B &= (1 - M_\infty^{\;2})/\delta^{2/3} - (\gamma + 1)M_\infty^{\;m}\phi_x \end{aligned}\right\} \tag{1b}$$

Here, ϕ is the disturbance velocity potential, δ is the airfoil thickness-to-chord ratio, and M_∞ is the free-stream Mach number. The reduced frequency is defined as $k \equiv \omega c/U_\infty$ for an airfoil of chord length c executing some unsteady oscillatory motion of frequency ω. The choices of the exponent m are somewhat arbitrary and are made to extend the Mach number range of the small-disturbance theory (a fairly complete review is given in ref. 11). The quantities x, y, t, and ϕ have been scaled by c, $c/\delta^{1/3}$, ω^{-1}, and $c\delta^{2/3}U_\infty$, respectively. In deriving equation (1a), it is assumed that

$$k \sim \delta^{2/3} \sim (1 - M_\infty^{\;2}) << 1 \tag{2}$$

Far-Field Boundary Conditions

In LTRAN2, equation (1a) is solved for the flow about airfoils by an alternating-direction implicit (ADI) finite-difference algorithm. The existing far-field boundary conditions imposed in LTRAN2 are

$$\left.\begin{array}{ll} \text{upstream:} & \phi = \phi_o \\ \text{downstream:} & \phi_x = 0 \\ \text{top and bottom:} & \phi_y = 0 \end{array}\right\} \qquad (3)$$

Here ϕ_o is the steady-state solution. These conditions are perfectly reflecting. In other words, all the waves originating from the airfoil for unsteady problems are reflected back into the computational domain from the boundaries. Hence, the outer boundaries must be placed far enough from the airfoil in the original version of LTRAN2.

Following Engquist and Majda (ref. 4), conditions are introduced to absorb at least a portion of the waves incident on the outer boundaries. For the upstream condition, B in equation (1b) is assumed to be locally constant; therefore, the analysis is performed on a linear equation. This approximation assumes that the flow field is governed by a linear equation in the vicinity of a far-field boundary. By considering waves traveling left from the interior to the upstream boundary for subsonic free stream, a perfectly nonreflecting condition is derived. Since this condition requires information from the mathematical domain of dependence of that boundary, approximations are made to get the following local conditions.

$$\text{upstream}\left\{\begin{array}{lll} \text{1st approximation:} & \phi_t - \frac{B}{A}\phi_x = 0 & (4) \\ \text{2nd approximation:} & \phi_{xt} - \frac{A}{B}\phi_{tt} + \frac{1}{A}\phi_{yy} = 0 & (5) \end{array}\right.$$

The first approximate condition absorbs waves normally incident on the boundary, and higher approximations absorb portions of obliquely incident waves.

Since waves travel infinitely fast in the downstream direction, the following consistency conditions seem appropriate (ref. 9):

$$\text{downstream}\left\{\begin{array}{ll} \phi_x = 0 & (6) \\ \text{or } \phi_{xx} = 0 & (7) \end{array}\right.$$

Considering waves traveling to the top and bottom boundaries, a nonreflecting condition is developed. Subsequently, local approximations to it are made, resulting in

$$\text{top and bottom}\quad\begin{cases}\text{1st approximation:} & \phi_y \pm \sqrt{|\beta|}\,\phi_x = 0 \qquad (8)\\[2ex] \text{2nd approximation:} & \phi_{ty} + r_2\phi_{xy} \pm r_1\phi_{xt} = 0 \qquad (9)\end{cases}$$

Here, ± corresponds to the top and bottom boundaries, and r_1, r_2 governs the absorption of waves obliquely incident to the boundaries. The values r_1, r_2 are discussed in more detail by Engquist and Majda. Following one of their strategies, r_1 and r_2 are chosen for the present study as

$$r_1 = 6.4641\sqrt{B}$$

$$r_2 = 5.4641(2B/A)$$

Alternatively, a nonreflecting far-field condition can be designed by considering characteristic equations. Assuming $B = \text{constant}$ in equation (1b) at a large distance from the airfoil, the characteristic equation can be written as

$$B\xi_x\xi_x + \xi_y\xi_y - A\xi_x\xi_t = 0 \tag{10}$$

This equation is satisfied by the characteristic plane

$$\xi(x,y,t) = r - (x/\sqrt{B} + 2\sqrt{B}\,t/A) = \text{constant} \tag{11a}$$

where

$$\vec{r} = (x/\sqrt{B},\ y)$$

and

$$\phi = f(\xi) \qquad \text{[illegible]}$$

is a solution to equation (1a) that represents a traveling plane wave. From these, the following equation is derived (Goorjian, P. M.: unpublished note) by forcing linear combinations of the derivatives of ϕ to be zero:

$$\frac{x}{r}\phi_x + \frac{y}{r}\phi_y + \frac{1}{2}\left(-\frac{A}{B}\frac{x}{r} + \frac{A}{\sqrt{B}}\right)\phi_t = 0 \tag{12a}$$

To use this as an approximate nonreflecting condition on boundaries far away, a further simplification is made. In the upstream region, $x \to -\infty$ with $|y|$ finite, so that equation (12a) becomes

$$\phi_t - \frac{B}{A}\phi_x = 0 \tag{12b}$$

For the top and bottom boundaries, $y \to \pm\infty$ with $|x|$ finite, so that equation (12a) becomes

$$\phi_y \pm \frac{1}{2}\frac{A}{\sqrt{B}}\phi_t = 0$$

Replacing ϕ_t by ϕ_x using equation (11b), this equation can be written equivalently as

$$\phi_y \pm \sqrt{B}\,\phi_x = 0 \tag{12c}$$

These are the first-approximate relations obtained by Engquist and Majda. Therefore, we may interpret equations (4) and (8) as special forms of a far-field characteristic relation.

As will be shown later, equation (12b) is quite efficient at upstream boundary and easier to implement in LTRAN2 than equation (5) or (12a). Since, for the problems we are solving, the influence of y-boundary is more pronounced, an improvement is attempted using equation (12a) to absorb waves incident on the top and bottom boundaries. First, the stability properties of this equation are examined, using the energy method, as done by Enquist and Majda (ref. 4). Taking the total x-component of the kinetic energy as a measure of stability, we require the time rate of change of this quantity to satisfy

$$\frac{\partial}{\partial t}\,(ke) = \frac{\partial}{\partial t}\int_{-b}^{b}\int_{-a}^{a} (\phi_x)^2\,dx\,dy \le 0 \tag{13a}$$

Integrating this by parts using equation (1a),

$$\begin{aligned}\frac{\partial}{\partial t}\,(ke) = {} & \underset{x=a}{\int_{-b}^{b}\left(\frac{B}{A}\,\phi_x{}^2 - \frac{1}{A}\,\phi_y{}^2\right)dy} - \underset{x=-a}{\int_{-b}^{b}\left(\frac{B}{A}\,\phi_x{}^2 - \frac{1}{A}\,\phi_y{}^2\right)dy} \\ & + \underset{y=b}{\int_{-a}^{a}\left(\frac{2}{A}\,\phi_x\phi_y\right)dx} - \underset{y=-b}{\int_{-a}^{a}\left(\frac{2}{A}\,\phi_x\phi_y\right)dx} \le 0\end{aligned} \tag{13b}$$

Substituting equation (12a) into equation (13b) and then using equations (11a) and (11b), we can show that the inequality in equation (13b) is satisfied.

For stability, we need at the top boundary ($y = b$),

$$\phi_x\phi_y \le 0 \tag{14}$$

Substituting equation (12a) into (14),

$$\phi_x\phi_y = \underbrace{-\left(\frac{x}{b}\,\phi_x{}^2\right)}_{(I)}\ \underbrace{-\ \frac{r}{b}\,\frac{1}{2}\left(-\,\frac{A}{B}\,\frac{x}{r} + \frac{A}{\sqrt{B}}\right)\phi_t\phi_x}_{(II)}$$

From equations (11a) and (11b), we can show that $(I) + (II) \leq 0$. However, the first term $(I) \geq 0$ for $x \leq 0$. This causes some difficulty in obtaining stable results. To avoid this difficulty, a new nonreflecting condition for the top and bottom boundaries is chosen as follows:

$$\beta \frac{x}{r} \phi_x + \frac{y}{r} \phi_y + \frac{1}{2}\left(- \frac{A}{B}\frac{x}{r} + \frac{A}{\sqrt{B}}\right)\phi_t = 0 \tag{15}$$

where $\beta = 1$ when $x \geq 0$ and 0 when $x < 0$. This is equivalent to imposing the first approximation on the upstream side while using the full-characteristic equation on the downstream side of the airfoil at the top and bottom boundaries.

FINITE-DIFFERENCE SCHEME

In LTRAN 2 (ref. 1), equation (1a) is solved by a two-step procedure to advance from time-step n to n + 1.

$$\text{x-sweep:}\quad A(\Delta t)^{-1}\,\delta_x\left(\tilde{\phi}^{n+1}_{j,\ell} - \phi^{n}_{j,\ell}\right) = D_x f_{j,\ell} + \delta_{yy}\phi^{n}_{j,\ell} \tag{16}$$

$$\text{y-sweep:}\quad A(\Delta t)^{-1}\,\delta_x\left(\phi^{n+1}_{j,\ell} - \tilde{\phi}^{n+1}_{j,\ell}\right) = \frac{1}{2}\,\delta_{yy}\left(\phi^{n+1}_{j,\ell} - \phi^{n}_{j,\ell}\right) \tag{17}$$

The operators in equations (16) and (17) are defined by the following equations:

$$\delta_x \phi_{j,\ell} = 2(\phi_{j,\ell} - \phi_{j-1,\ell})(x_{j+1} - x_{j-1})^{-1} \qquad \text{(first order)}$$

$$= (3\phi_{j,\ell} - 4\phi_{j-1,\ell} + \phi_{j-2,\ell})(x_{j+1} - x_{j-1})^{-1} \quad \text{(second order)}$$

$$\delta_{yy}\phi_{j,\ell} = 2[(\phi_{j,\ell+1} - \phi_{j,\ell})(y_{\ell+1} - y_{\ell})^{-1}$$

$$- (\phi_{j,\ell} - \phi_{j,\ell-1})(y_{\ell} - y_{\ell-1})^{-1}](y_{\ell+1} - y_{\ell-1})^{-1}$$

$$f_{j,\ell} = \frac{1}{2}\left[B^{n}_{j,\ell}\phi^{n+1}_{x_{j,\ell}} + (1 - M_\infty{}^2)\phi^{n}_{x_{j,\ell}}/\delta^{2/3}\right]$$

$$B^{n}_{j,\ell} = (1 - M_\infty{}^2)/\delta^{2/3} - (\gamma + 1)M_\infty{}^m\phi^{n}_{x_{j,\ell}}$$

$$\phi_{x_{j+1/2,\ell}} = (\phi_{j+1,\ell} - \phi_{j,\ell})(x_{j+1} - x_j)^{-1}$$

$$D_x f_{j,\ell} = 2(x_{j+1} - x_{j-1})^{-1}[(1 - \varepsilon_j)(f_{j+1/2,\ell} - f_{j-1/2,\ell}) + \varepsilon_{j-1}(f_{j-1/2,\ell} - f_{j-3/2,\ell})]$$

$$\varepsilon_j = \left[\begin{smallmatrix}0\\1\end{smallmatrix}\right] \quad \text{for} \quad \left(B^n_{j+1/2,\ell} + B^n_{j-1/2,\ell}\right)\left[\begin{smallmatrix}>\\<\end{smallmatrix}\right]0$$

Here, Δt is the time-step and j, ℓ are the grid-point indices in the x and y directions.

The first-approximate nonreflecting far-field boundary conditions are readily incorporated into the above two-dimensional sweep procedure. For the x-sweep, the upstream boundary condition (12b) becomes

$$(\Delta t)^{-1}\left(\tilde{\phi}^{n+1}_{j+1/2,\ell} - \phi^n_{j+1/2,\ell}\right) - \frac{1}{2} B_{j+1/2,\ell}A^{-1}(\Delta x)^{-1}\left[\left(\tilde{\phi}^{n+1}_{j+1,\ell} - \tilde{\phi}^{n+1}_{j,\ell}\right) + \left(\phi^n_{j+1,\ell} - \phi^n_{j,\ell}\right)\right] = 0 , \quad j = 1,\ \ell = 1, \ldots, \ell\text{max} \tag{18}$$

Here,

$$B_{j+1/2,\ell} = [(1 - M_\infty^{\ 2})/\delta^{2/3}] - \left[(\gamma + 1)M_\infty^{\ m}\left(\phi^n_{j+1,\ell} - \phi^n_{j,\ell}\right)/(x_{j+1} - x_j)\right], \quad j = 1$$

The downstream boundary condition is

$$\tilde{\phi}^{n+1}_{j\text{max},\ell} + \phi^n_{j\text{max},\ell} - \tilde{\phi}^{n+1}_{j\text{max}-1,\ell} - \phi^n_{j\text{max}-1,\ell} = 0 \tag{19a}$$

or equivalently, since $\phi^n_{j\text{max},\ell} - \phi^n_{j\text{max}-1,\ell} = 0$, from the previous iteration

$$\tilde{\phi}^{n+1}_{j\text{max},\ell} = \tilde{\phi}^{n+1}_{j\text{max}-1,\ell} , \quad \ell = 1, \ldots, \ell\text{max} \tag{19b}$$

Here, jmax and ℓmax are maximum indices in x and y directions and represent downstream and top boundaries, respectively.

Similarly, for the y-sweep, the top and bottom boundary conditions become

$$\left(\phi^{n+1/2}_{j-1/2,\ell} - \phi^{n+1/2}_{j-1/2,\ell-1}\right)/(y_\ell - y_{\ell-1}) \pm \left|B_{j-1/2,\ell-1/2}\right|^{1/2}\left(\phi^{n+1/2}_{j,\ell-1/2} - \phi^{n+1/2}_{j-1,\ell-1/2}\right)/(x_j - x_{j-1}) = 0 , \quad j = 2, \ldots, j\text{max} \tag{20}$$

where

$$\phi_{j\pm1/2,\ell} = \frac{1}{2}\left(\phi_{j,\ell} + \phi_{j\pm1,\ell}\right)$$

$$\phi^{n+1/2} = \frac{1}{2}\left(\phi^{n+1} + \phi^{n}\right)$$

When $j = 2$, equation (20) requires ϕ at $j = 1$. Therefore, for $j = 2$ we use equation (12b) also. Here, the upstream condition, equation (18), is changed to

$$(\Delta t)^{-1}\left(\phi^{n+1}_{j+1/2,\ell} - \phi^{n}_{j+1/2,\ell}\right) - \frac{1}{2} B_{j+1/2,\ell}A^{-1}(\Delta x)^{-1}\left[\left(\phi^{n+1}_{j+1,\ell} - \phi^{n+1}_{j,\ell}\right) + \left(\phi^{n}_{j+1,\ell} - \phi^{n}_{j,\ell}\right)\right] = 0 , \qquad j = 1,\ \ell = 1, \text{ or } \ell\text{max} \qquad (21)$$

Then, equations (20) and (21) are solved simultaneously.

The second approximation (9) and the characteristic condition (15) are discretized in a similar manner. For the y-sweep, the top boundary conditions become

Second approximation:

$$\delta_{yt}\phi^{n+1}_{j-1/2,\ell} + r_1\delta_{xt}\phi^{n+1}_{j,\ell-1/2} + r_2\delta_{xy}\phi^{n+1/2}_{j,\ell} = 0 \qquad (22)$$

Characteristic condition:

$$\beta\,\frac{x}{r}\,(\Delta x)^{-1}(1 - E_x^{-1})\phi^{n+1/2}_{j,\ell-1/2} + \frac{y}{r}\,(\Delta y)^{-1}(1 - E_y^{-1})\phi^{n+1/2}_{j-1/2,\ell} + \frac{1}{2}\left(-\,\frac{A}{B}\,\frac{x}{r} + \frac{A}{\sqrt{B}}\right)(\Delta t)^{-1}(1 - E_t^{-1})\phi^{n+1}_{j-1/2,\ell-1/2} = 0 \qquad (23)$$

where

$$\delta_{yt} = (\Delta y\ \Delta t)^{-1}(1 - E_t^{-1})(1 - E_y^{-1})$$

$$\delta_{xy} = (\Delta x\ \Delta y)^{-1}(1 - E_x^{-1})(1 - E_y^{-1})$$

$$E_t^{-1}\phi^{n}_{j,\ell} = \phi^{n-1}_{j,\ell} , \qquad E_x^{-1}\phi^{n}_{j,\ell} = \phi^{n}_{j-1,\ell} , \quad \text{etc.}$$

The bottom boundary conditions are applied in the same way.

COMPUTED RESULTS FOR VARIOUS TEST CASES

In the production version of LTRAN2, the default grid boundaries are located 857 chords from the airfoil in the y-direction, and 200 chords from the leading edge, with smoothly stretched grid spacings in both directions (113, 97 mesh in x, y-directions). The large-grid solutions in figures 2-10 are obtained using this grid. However, depending on the particular problem, equivalent results can be obtained with smaller grids; the minimum number of mesh points required is shown in the figures. Therefore, identical solutions are obtained when far-field boundaries are placed farther away than the minimum required.

In computing the large-grid solutions, two different sets of far-field boundary conditions are imposed independently, namely:

1. Perfectly reflecting conditions, as given by equation (3)

2. The first-approximate conditions, as given by equations (4), (6), and (8)

These boundary conditions yield essentially identical results, that is, within plottable accuracy. Since the large-grid results can be duplicated using different combinations of grids and boundary conditions, it is reasonable to assume that these are solutions of equation (1) with far-field boundaries at infinity.

In a previous study (ref. 10), the first-approximate conditions were shown to be very effective in bringing the upstream boundary close to the airfoil, that is, 3.8 chord lengths away from the leading edge for the cases tested. On the other hand, the y-boundary had to be placed relatively farther away, for example, 61 chord lengths away for the case of a step change in angle of attack at $M_\infty = 0.85$. Therefore, in the present study, four different far-field conditions (described in the previous section, Finite-Difference Scheme) are compared by implementing them on the top and bottom boundaries, namely:

1. Perfectly reflecting condition — equation (3)

2. The first-approximate nonreflecting condition — equation (8)

3. The second-approximate nonreflecting condition — equation (9)

4. The nonreflecting approximation from the full-characteristic equation — equation (15)

Step Change in Angle of Attack

An impulsively started airfoil in plunging motion creates a pressure pulse. This is simulated numerically by a step change in the angle of attack. Owing to the low-frequency nature of the governing equation, the lift and moment coefficients gradually increase after the initial change in the angle of attack. A problem such as this provides a good test case for investigating the influence of the computational far-field distances on the flow solution near the airfoil.

Starting from the standard large grid, the far-field boundary distances are reduced by removing outer grid lines in the y-directions. Both the old reflecting boundary conditions (eq. (3)) and the new ones (eqs. (8), (9), and (15)) are tested with these reduced grids. In figures 2 and 3, the lift and moment coefficients for an NACA 64A006 airfoil are plotted on a time scale in units of chord lengths (c) of airfoil traveled. The indicial responses to a unit change in the angle of attack, α, are C_{ℓ_α} and C_{m_α}, as described in reference 12, and can be regarded as $C_{\ell/\alpha}$ and $C_{m/\alpha}$ in this case. By using the old conditions, the computed results start to deviate from the large-grid solutions when the y-boundary distance, Y_{max}, gets smaller than 80 c at $M_\infty = 0.85$. Applying the first approximate condition, Y_{max} can be reduced to 61 c without significant deviations from the large-grid results. Using the characteristic equation, Y_{max} can be further reduced to 10 c. However, there was no improvement using the second approximation over the results obtained by implementing the first approximation. It may be possible to adjust the two parameters r_1 and r_2 to produce better results. Since adjusting the parameters for different problems may not be practical, r_1 and r_2 are chosen by a fixed strategy in the present study. The sonic line extends to 1.04 c at time t = 170, as shown in figure 4. Therefore, the far-field boundary remained in the subsonic region throughout the computation. In table 1, the minimum mesh in the y-direction (ℓmax) and the y-boundary distance (Y_{max}) required to use the old or the new boundary conditions are shown. When the characteristic condition is used at the top and bottom boundaries, the gain in computational efficiency is about 18%. (Because the second approximation is not better than the first, the results for the second are not shown in table 1.)

Oscillating Flap Case

Another test of the nonreflecting boundary conditions was performed for the case of an oscillating trailing-edge flap. The configuration consisted of an NACA 64A006 airfoil with a sinusoidally oscillating flap. Two of the three types of possible shock-wave motions are shown in figures 5-8: (1) type A, sinusoidal shock-wave motion, and (2) type B, interrupted shock wave motion. In both cases, large-grid results can be obtained with a grid as small as 93 × 77 ($X_{max} = 3.8$, $Y_{max} = 47$). As expected, the minimum x-boundary distance, X_{max}, is very small, and the influence of y-boundary is very pronounced. By reducing the y-boundary distance, Y_{max}, further to 2 chords from the airfoil, the old reflecting conditions cause significant deviation of the lift and the moment coefficient from the large-grid solution. The reflecting boundary conditions on the top and bottom, $\phi_y = 0$, model solid-wall boundaries.

Hence, imposition of the y-boundary at this close position restricts the flow and produces stronger shocks (ref. 13).

However, it is expected that by applying nonreflecting conditions at the top and bottom boundaries, waves incident on the far-field y-boundaries will be absorbed. In figures 5-8, results after implementing various approximate nonreflecting conditions at the top and bottom boundaries are compared. For type-B shock, the characteristic condition (15) produces somewhat better results than the first approximation (8) as shown in figure 7. For type-A shock, the characteristic condition was marginally better than the first approximation, as shown in figure 5. However, in this case ($Y_{max} = 2$), a smaller time-step was required to use the first approximation. Therefore, the minimum CPU time to obtain solutions using the first-approximate condition was based on a larger grid ($Y_{max} = 2.9$) where a larger time-step was allowed for stability. The gains in computational efficiency are listed in table 1.

Impulsively Started Airfoil

To visualize the behavior of waves originating from the airfoil and then propagating throughout the computational domain, an NACA 64A006 airfoil is impulsively started from rest at time zero with $M_\infty = 0.85$. This is equivalently done in LTRAN2 by turning on the free stream from rest. To see the reflection more clearly, the far-field boundaries are placed very close to the airfoil ($X_{max} = 1.22$ c, $Y_{max} = 1.08$ c). The propagation of disturbances is demonstrated by the pressure contour of the upper half plane of the computational domain. In figure 6, the results are shown at three sequential times measured by chord lengths of airfoil traveled.

Figure 9(a) is obtained from the large-grid solution by looking through the window of 1.22 c × 1.08 c. In this sequence, taken from a movie produced from the calculation, waves from the airfoil propagate outwardly only during the time observed, as though the domain were infinite. In figure 9(b), the old reflecting conditions are used. Physically, this is equivalent to placing solid walls on the boundaries. As time increases, the influence of the boundaries, especially the y-boundary, becomes more apparent, and at $t = 7.1$, the flow is shown to be choked. This illustrates a possible influence that a solid wind-tunnel wall can have on experimental results. When the first approximate nonreflecting conditions are used (fig. 9(c)), the pressure-contour map more closely resembles the large-grid solution. As shown by the upper-surface pressure-coefficient plot in figure 10, the reflecting conditions contaminate the near-field solution much faster. Since the nonreflecting conditions used are simple approximations to perfectly absorbing conditions, some reflections still exist.

CONCLUDING REMARKS

The first- and the second-approximate nonreflecting boundary condition procedures of Engquist and Majda and the one derived from the full-characteristic equation have been compared by implementing them in solving various practical problems, using the unsteady small-disturbance transonic flow code, LTRAN2. It has been demonstrated successfully that the computational domain can be reduced significantly using the characteristic condition and to a somewhat less extent using the first-approximate condition; that is, for the most severe case of the indicial response, the far-field y-boundary distance could be brought from 80 c to 10 c using the characteristic condition and to 61 c using the first-approximate condition. However, since the mesh system is stretched in LTRAN2, the number of computational grid points is not linearly proportional to the distance of the boundary from the airfoil. The gain in computer time, after implementing the new conditions at the top and bottom boundaries, is problem-dependent; for the cases tested, the time saved ranged from 18 to 58% when the characteristic condition was used and from 0 to 41% when the first-approximate condition was used. For the particular set of r_1 and r_2 chosen for the present study, the second-approximate condition was not as effective as the first one. The boundary conditions applied here are all local in space and time and, therefore, should be applicable to any type of unsteady motion. In conclusion, the simplicity of the characteristic condition and the computational efficiency gained are difficult to surpass for applications in the design process.

REFERENCES

1. Ballhaus, W. F.; and Goorjian, P. M.: Implicit Finite-Difference Computations of Unsteady Transonic Flows About Airfoils. AIAA J., vol. 15, no. 12, Dec. 1977, pp. 1728-1735.

2. Engquist, B.; and Majda, A.: Absorbing Boundary Conditions for the Numerical Simulation of Waves. Math. Comput., vol. 31, no. 139, July 1977, pp. 629-651.

3. Engquist, B.; and Majda, A.: Radiation Boundary Conditions for Acoustic and Elastic Wave Calculations. Comm. Pure Appl. Math., vol. 32, May 1979, pp. 313-356.

4. Engquist, B.; and Majda, A.: Numerical Radiation Boundary Conditions for Unsteady Transonic Flow. J. Comput. Phys., vol. 40, 1981, pp. 91-103.

5. Bayliss, A.; and Turkel, E.: Radiation Boundary Conditions for Wave-like Equations. ICASE Report 79-26, Langley Research Center, NASA, Oct. 1979.

6. Fung, K.-Y.: Far-Field Boundary Conditions for Unsteady Transonic Flows. AIAA J., vol. 19, no. 2, Feb. 1981, pp. 180-183.

7. Bushby, F. H.; and Timpson, M. S.: A 10-level Atmospheric Model and Frontal Rain. Quart. J. R. Met. Soc., vol. 93, 1967, pp. 1-17.

8. Guderly, K. G.: Far Fields Conditions for Subsonic Flows with Small Superimposed Harmonic Oscillations. AFFDL-TR-79-3109, Wright-Patterson Air Force Base, July 1979.

9. Krupp, J. A.; and Cole, J. D.: Studies in Transonic Flow IV, Unsteady Transonic Flow. UCLA-ENG-76104, Oct. 1976.

10. Kwak, D.: Non-Reflecting Far-Field Boundary Conditions for Unsteady Transonic Flow Computation. AIAA Paper 80-1393, Snowmass, Colo., 1980.

11. Ballhaus, W. F.: Some Recent Progress in Transonic Flow Computations. VKI Lecture Series: Computational Fluid Dynamics, von Karman Institute for Fluid Dynamics, Rhode-St-Genese, Belgium, Mar. 15-19, 1976.

12. Ballhaus, W. F.; and Goorjian, P. M.: Computation of Unsteady Transonic Flows by the Indicial Method. AIAA J., vol. 16, no. 2, Feb. 1978, pp. 117-124.

13. Ballhaus, W. F.; and Goorjian, P. M.: Efficient Solution of Unsteady Transonic Flows About Airfoils. AGARD Paper No. 14, AGARD Conference Proceedings No. 226, AGARD Specialists Meeting on Unsteady Airloads in Separated and Transonic Flow, Lisbon, Portugal, Apr. 1977.

TABLE 1.- COMPUTATIONAL EFFICIENCY OF VARIOUS FAR-FIELD BOUNDARY CONDITIONS: NACA 64A006 (Y_{max} IN UNITS OF CHORD)

		Reflecting condition, eq. (3)	First-approximation condition, eq. (8)	Characteristic condition, eq. (15)
Case 1[a]	Y_{max}	80	61	10
	ℓ_{max}	81	79	63
	CPU[b]	1.18	1.21	1
Case 2[c]	Y_{max}	47	2.9	2
	ℓ_{max}	77	51	47
	CPU[b]	1.58	1.12	1
Case 3[d]	Y_{max}	47	7.6	2
	ℓ_{max}	77	61	47
	CPU[b]	1.48	1.23	1

[a] Case 1: Indicial response to a step change in angle of attack $\alpha = 1°$, $M_\infty = 0.85$.

[b] CPU time is normalized by the characteristic condition case.

[c] Case 2: Sinusoidally oscillating trailing-edge flap: Type-A shock, $M_\infty = 0.875$, $k = 0.468$.

[d] Case 3: Sinusoidally oscillating trailing-edge flap: Type-B shock, $M_\infty = 0.854$, $k = 0.358$.

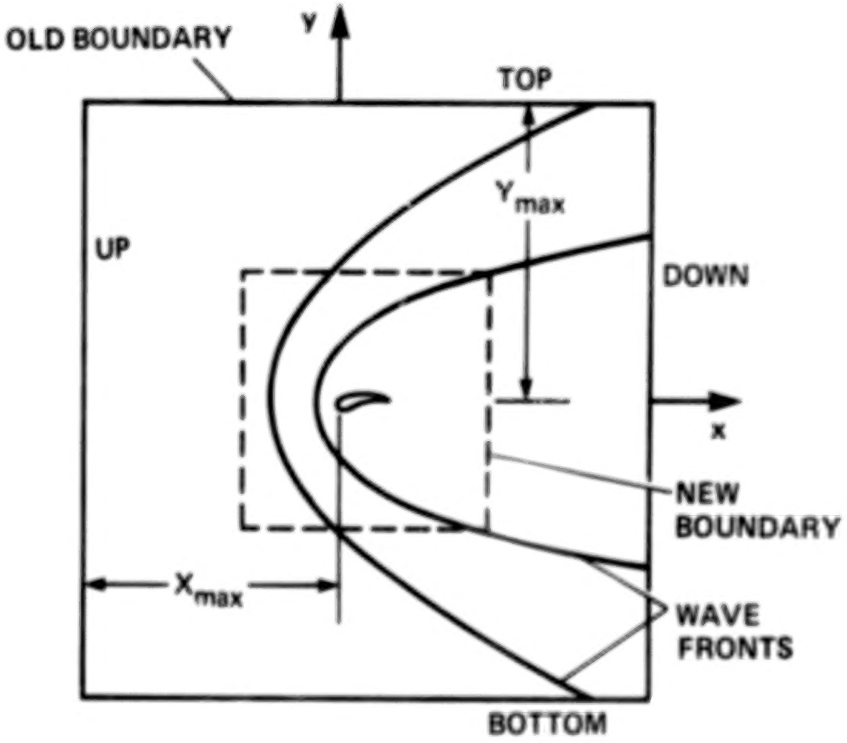
OLD BOUNDARY
y
TOP
Y_{max}
UP
DOWN
x
NEW BOUNDARY
X_{max}
WAVE FRONTS
BOTTOM

Figure 1.- Schematic of computational domain: old reflecting boundary vs new nonreflecting boundary.

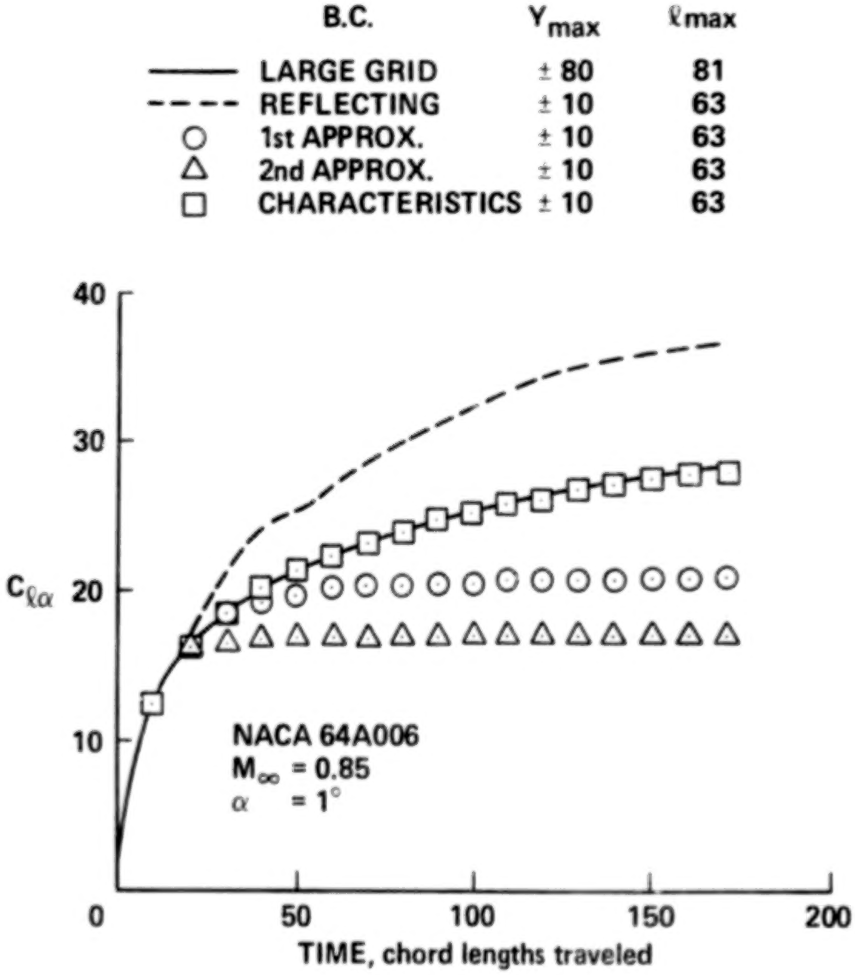

Figure 2.- Effect of far-field boundary distance on C_ℓ for step change in angle of attack.

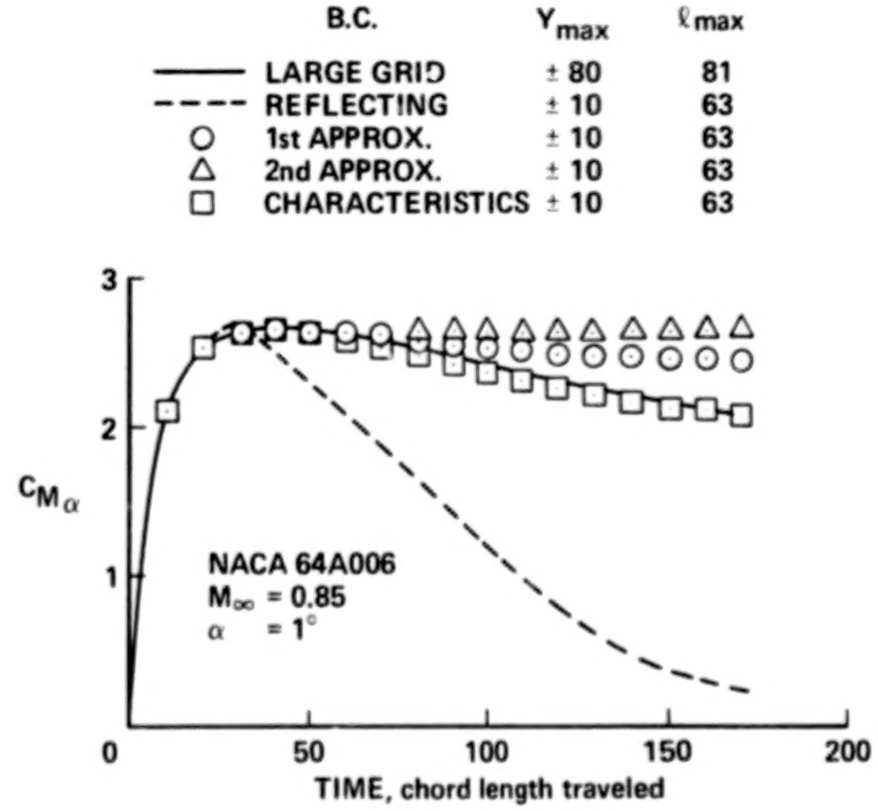

Figure 3.- Effect of far-field distance on C_M for step change in angle of attack.

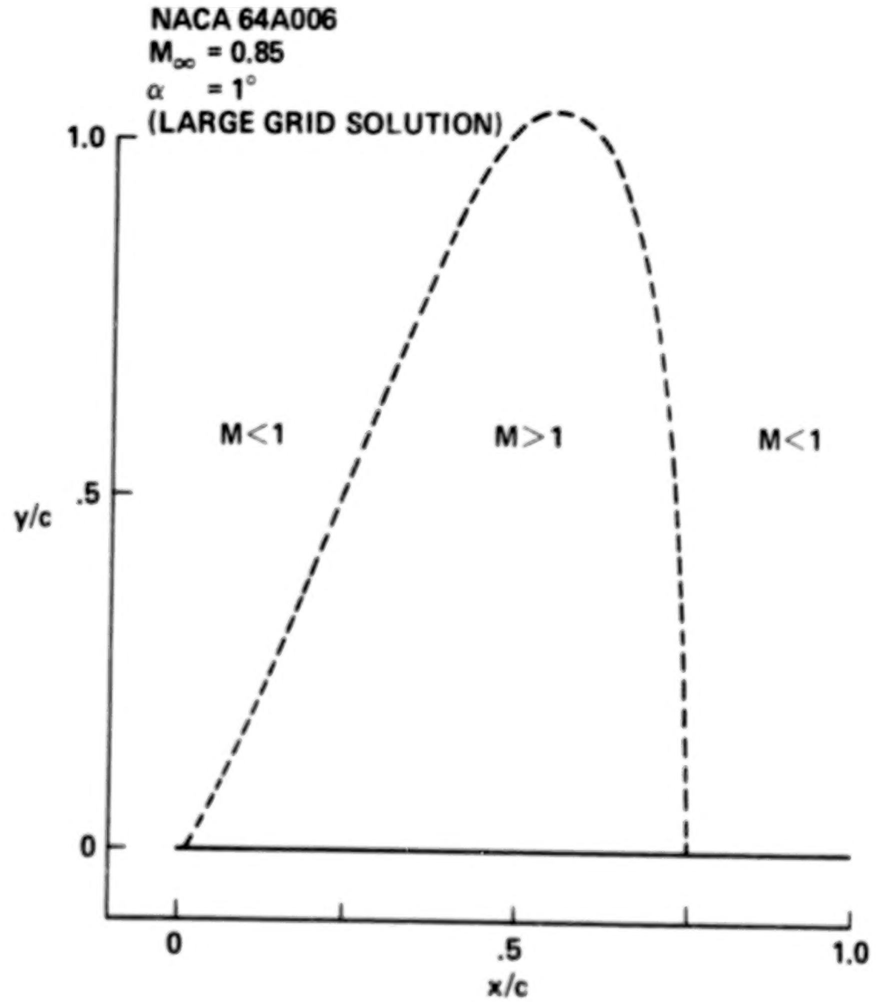

Figure 4.- Supersonic region above airfoil for step change in angle of attack (t - 170).

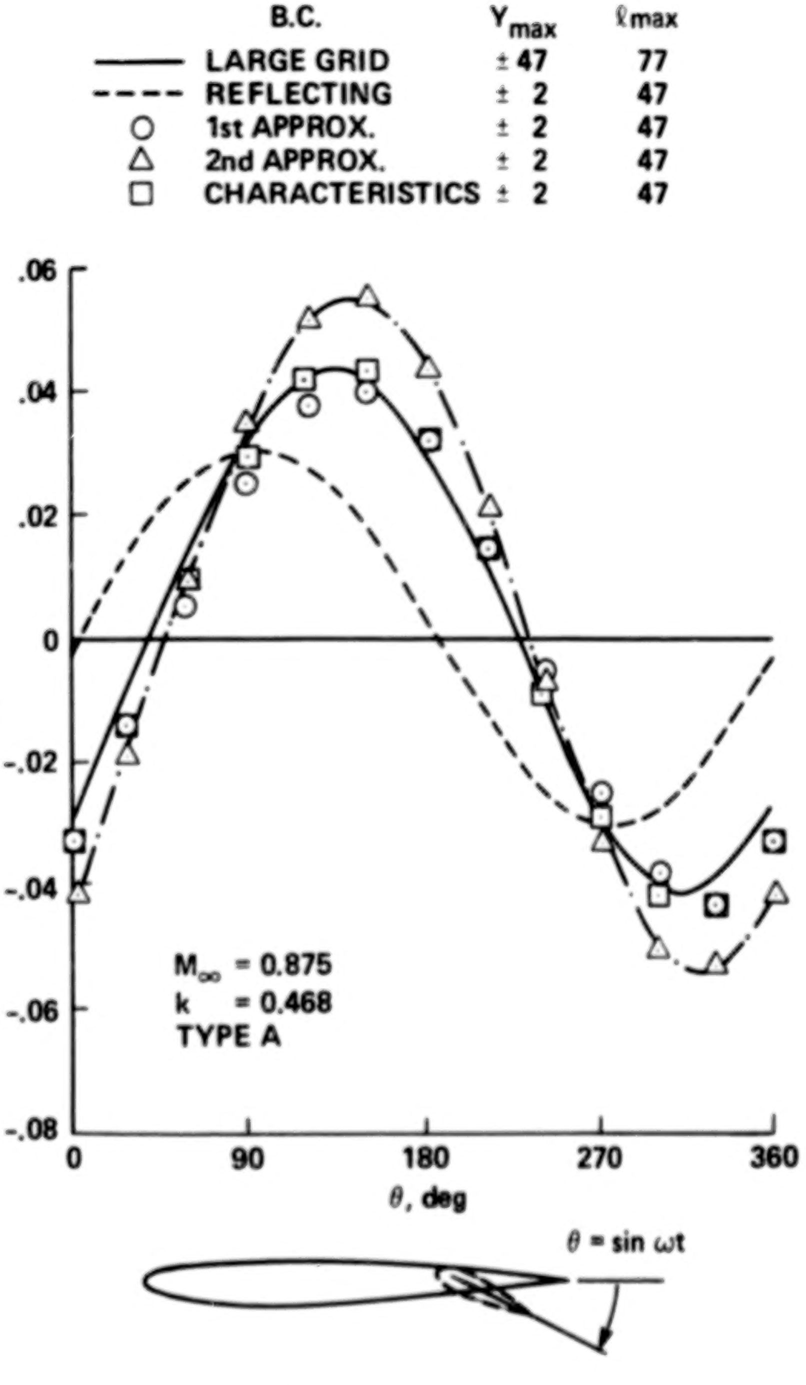

Figure 5.- Effect of far-field distance on C_ℓ for an NACA 64A006 airfoil with oscillating trailing-edge flap: type-A shock-wave motion.

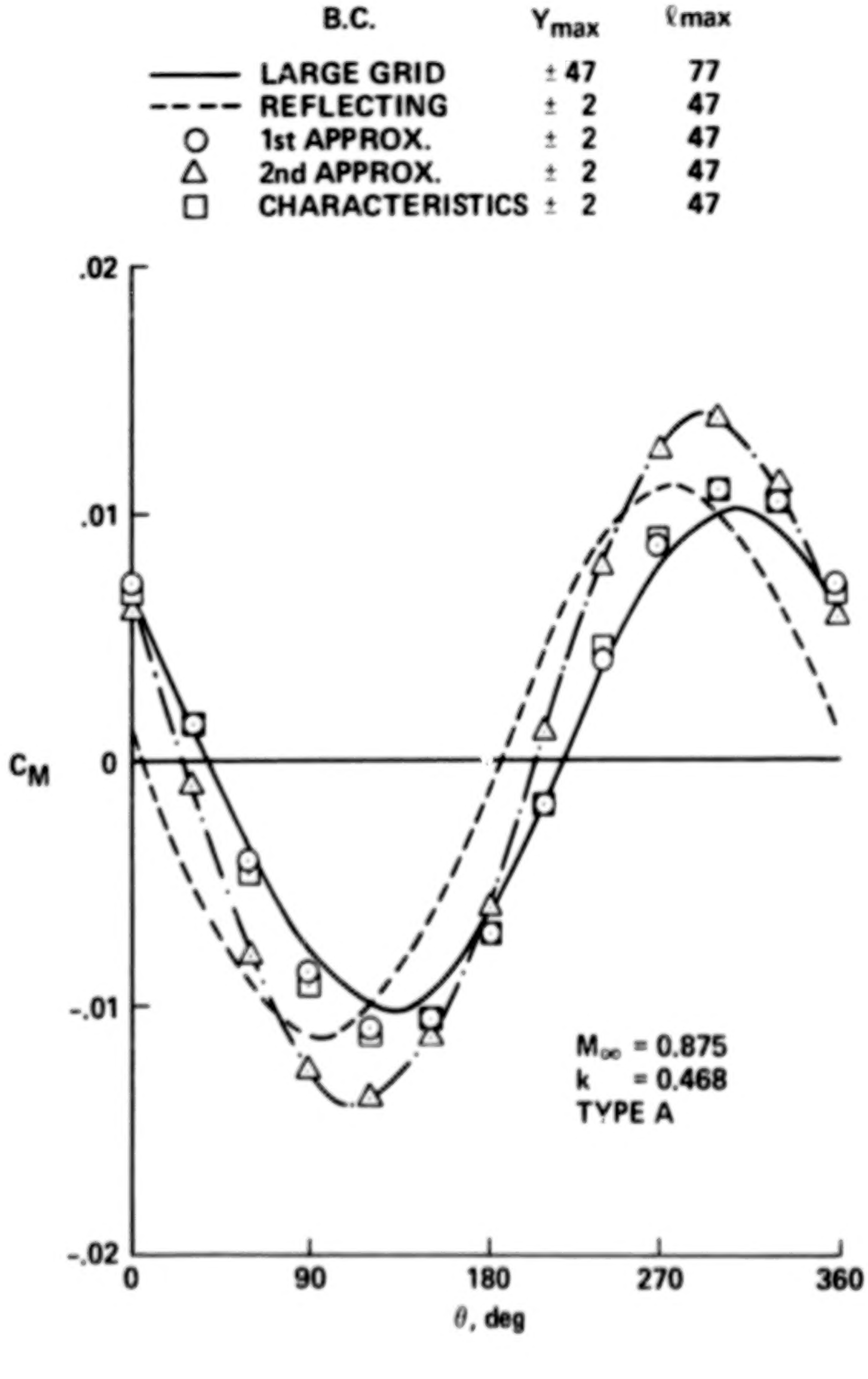

Figure 6.- Effect of far-field distance on C_M for an NACA 64A006 airfoil with oscillating trailing-edge flap: type-A shock-wave motion.

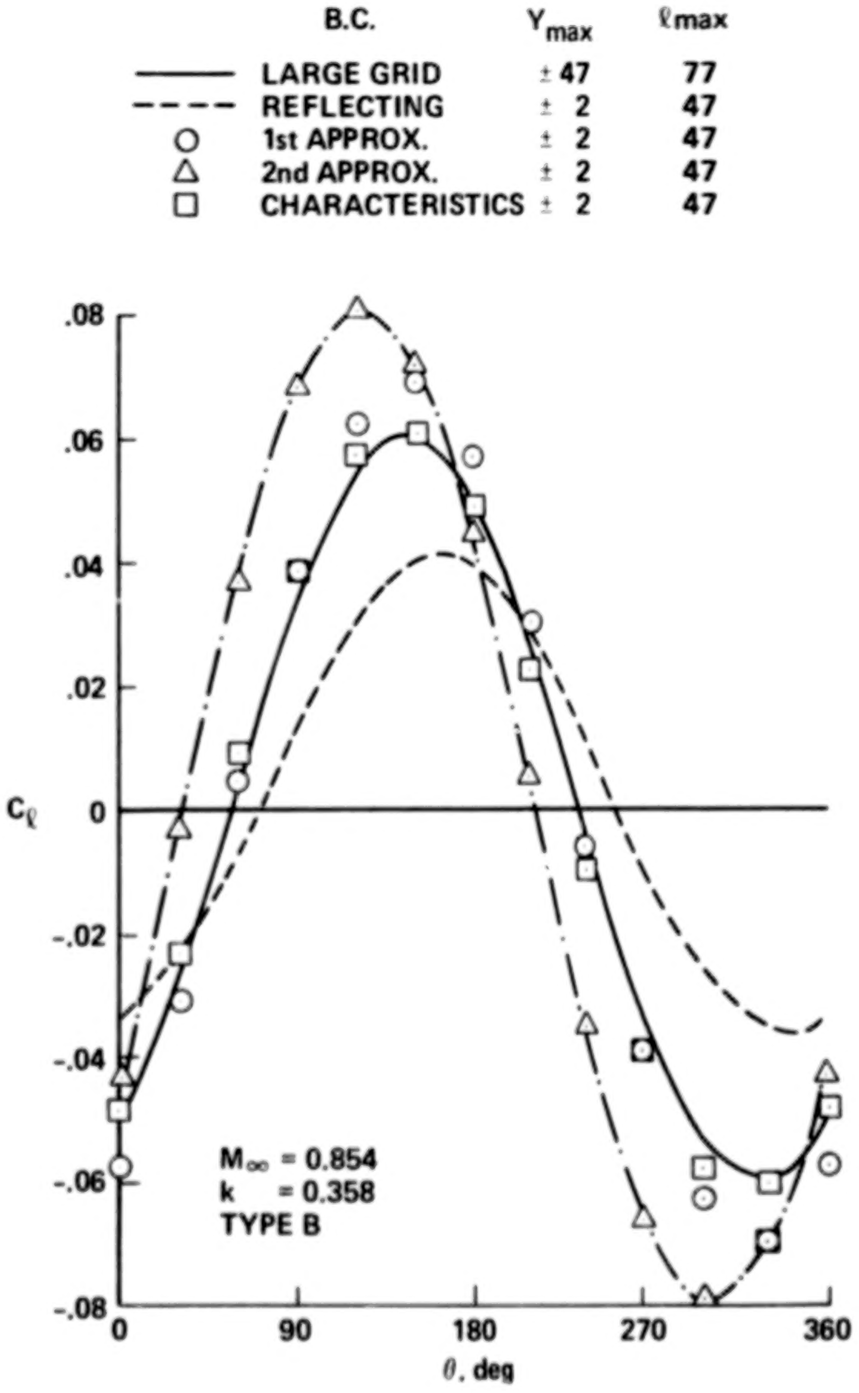

Figure 7.- Effect of far-field distance on C_ℓ for an NACA 64A006 airfoil with oscillating trailing-edge flap: type-B shock-wave motion.

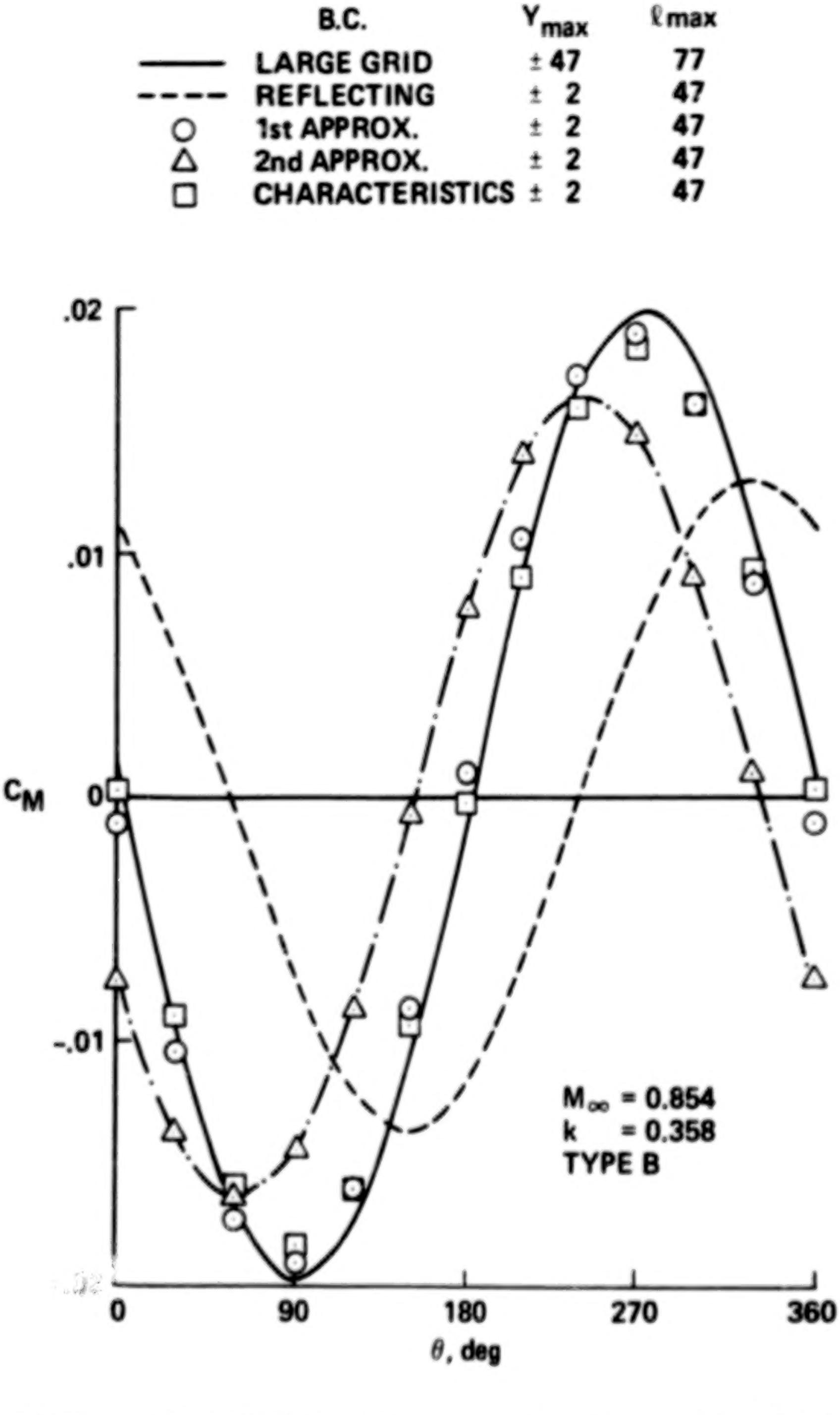

Figure 8.- Effect of far-field distance on C_M for an NACA 64A006 airfoil with oscillating trailing-edge flap: type-B shock-wave motion.

BLANK

PAGE

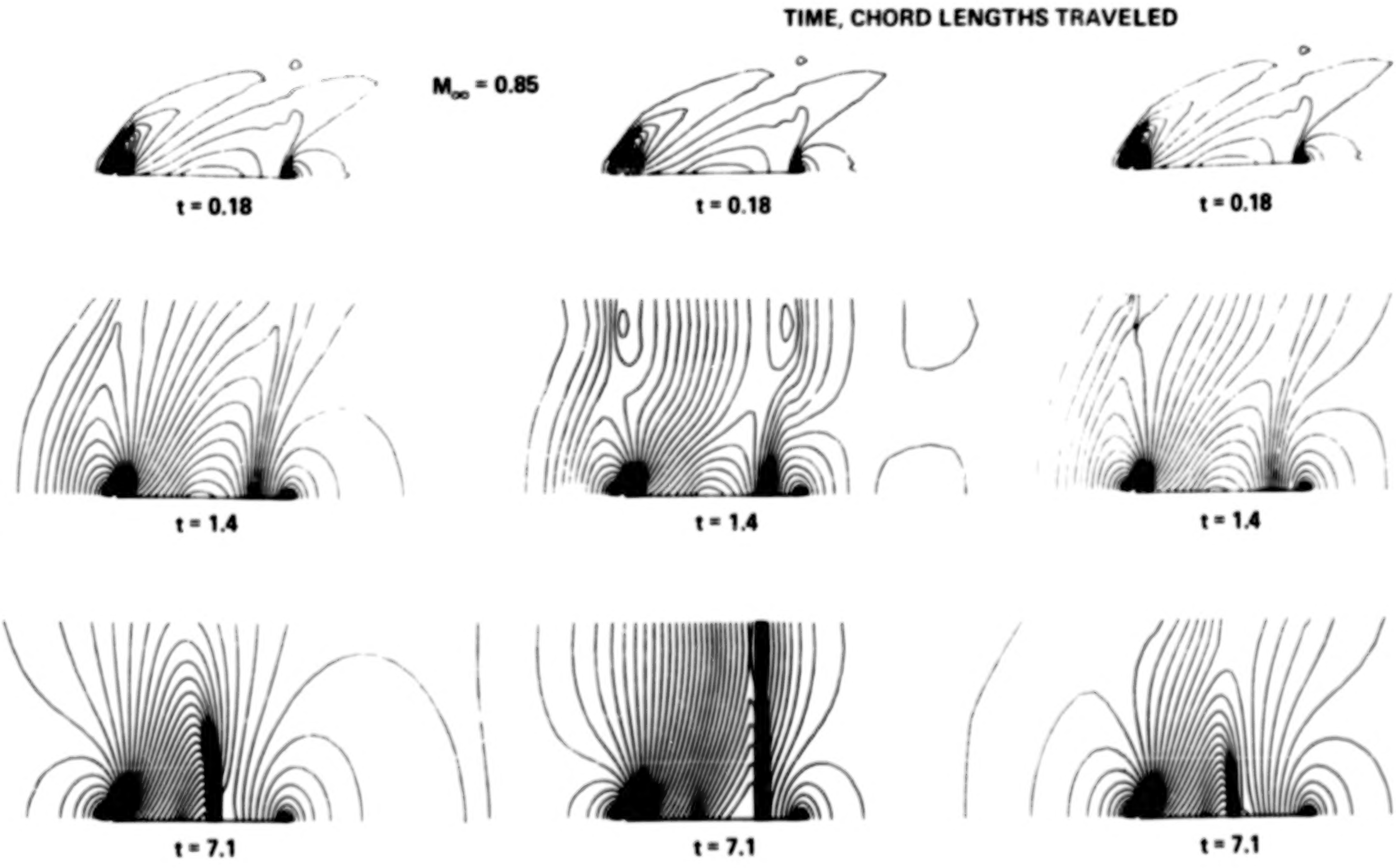

(a) LARGE GRID SOLUTION

(b) REFLECTING B. C.

(c) NONREFLECTING B. C. (1st APPROX.)

Figure 9.- Pressure contour for an impulsively started NACA 64A006 airfoil from rest.

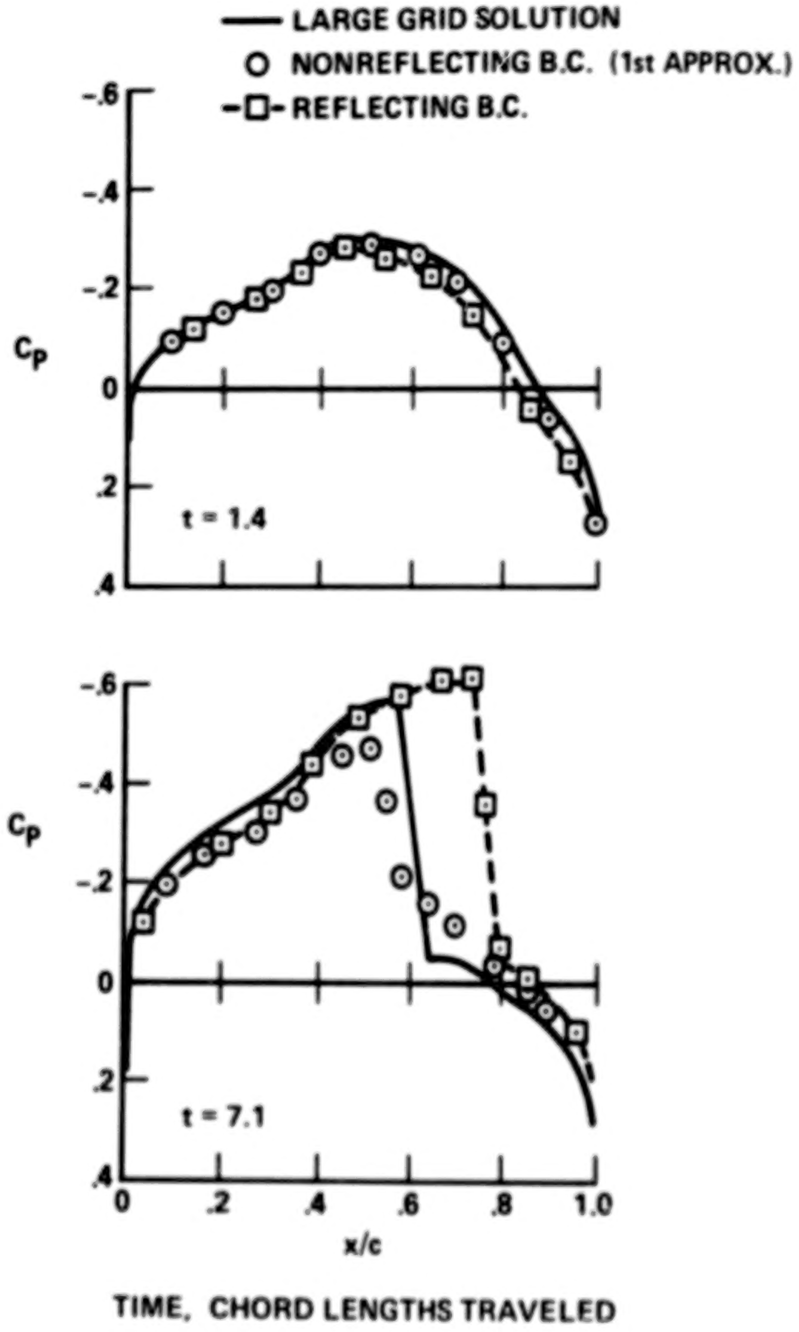

Figure 10.- Upper-surface pressure coefficient for an impulsively started NACA 64A006 airfoil.

IMPLEMENTATION OF NONREFLECTIVE BOUNDARY CONDITION AT THE OUTFLOW BOUNDARY*

D. R. Hall and S. M. Yen
University of Illinois

INTRODUCTION

The purpose of our work is to develop numerical techniques for the solution of free surface flows about a disturbance on or near a free surface. Any disturbance moving on or near a liquid surface generates surface waves that propagate away from the disturbance. We shall consider the potential flow problems in which the evolution of free surface waves is the principal phenomenon of interest. The distinct feature of these problems is that the position of the surface is also unknown and is to be determined as part of the solution. Two boundary conditions are required at the free surface since there are two unknown functions there, the free surface height and the potential function. The required boundary conditions are satisfied by the kinematic condition which states that no flow can cross the surface and the dynamic condition which matches the fluid pressure to the pressure acting on the surface through Bernoulli's equation. These boundary conditions introduce the nonlinearity that makes their solution difficult.

We have developed two computational schemes (ref. 1) designed to deal with the computational difficulties encountered in these problems. In one scheme, we use the finite element method to make the field calculation of the velocity potential and the finite difference method is used for the time evolution. The feasibility of this scheme was demonstrated by numerical solutions obtained for the two-dimensional problems of the pressure distribution and the submerged body. In the other scheme, a finite difference method that couples an explicit, single stage, second order time integration scheme with the solution of the Laplace equation for the velocity potential is used. The feasibility of this scheme has been demonstrated by numerical solutions obtained for a two-dimensional pressure distribution problem and a three-dimensional accelerating strut problem.

In both schemes, the computational domain is expanded downstream periodically during the computation as the disturbance on the free surface is propagated close to the downstream boundary. Therefore, the undisturbed condition is applied on the cut-off downstream boundary.

In order to obtain the longer time and steady state solution, we have studied the case of a fixed downstream boundary set close to the disturbance.

---

*This research was supported by the National Science Foundation under Grant NSF ENG 77-20436 and the Office of Naval Research under Contract N00014-80-C-0740.

Thus, we can increase the computation efficiency by using a small computational domain. We have focused this study on the application of our numerical schemes to the nonlinear free surface problems with a fixed and small computational domain. There are two major tasks involved in this study: (1) investigate the implementation of the open boundary condition at the outflow boundary to allow the waves to pass through it and (2) improve our numerical schemes so that accurate numerical solutions can be obtained using the open boundary condition at the outflow boundary.

We have studied in detail the method to implement the open boundary condition used by Chan (ref. 2). It is based on Orlanski's scheme (ref. 3) in which the Sommerfeld radiation condition is applied at the outflow boundary and the phase velocity is calculated numerically. We have conducted numerical experiments to study systematically the errors of Chan's numerical scheme to implement the advection equation and to study ways to minimize these errors.

Transient solutions have been obtained for the pressure distribution problem and have been compared with those obtained for expanding domain in order to establish their accuracy. These accuracy studies have led to the development of accurate time-dependent methods. Using these methods, we have obtained accurate transient and steady state solutions for the pressure distribution problem.

We have been studying an alternative method to implement the open boundary condition. In this method, we use directly the governing free surface equation instead of the advection equation at the outflow boundary. This method does have a problem of slow instability which can be dealt with.

The detailed results of our study have been presented at two international symposiums on numerical ship hydrodynamics (refs. 1 and 4). In this paper, we shall focus our presentation on the aspects of our study on the application of non-reflective boundary conditions at the outflow boundary to obtain steady state solutions of the pressure distribution problem. We shall first review briefly the nonlinear free surface problems under study and our numerical schemes to solve these problems using an expanding domain. Then, we will present the results of our study of the numerical scheme to implement Orlanski's method, our numerical schemes to solve nonlinear free surface wave problems using a fixed and small computational domain, and numerical solutions obtained.

FREE SURFACE PROBLEMS

We consider the potential flow produced by a disturbance moving forward on or near a free surface. The flow is governed by the potential equation, free surface boundary conditions and conditions at other boundaries. The free surface is characterized by two distinct conditions, kinematic and dynamic conditions. The kinematic condition comes from the fact that the free surface is a streamline so that the normal component of velocity vanishes on the free surface. If the free surface is given by the equation

$$\zeta(x,y,z;t) = 0, \tag{1}$$

the kinematic condition becomes

$$\frac{D\zeta}{Dt} = 0 \quad \text{on } \zeta = 0 \ . \tag{2}$$

Hence, by defining the free surface height as

$$y = \eta(x,z;t), \tag{3}$$

the free surface is given by

$$\zeta(x,y,z;t) = y - \eta(x,z;t) = 0 \ . \tag{4}$$

The kinematic condition yields

$$\eta_t + \Phi_x \eta_x - \Phi_y + \Phi_z \eta_z = 0 \qquad \text{on } y = \eta \ . \tag{5}$$

If the pressure P is given on the free surface, the dynamic condition can be derived from the Bernoulli's equation

$$\Phi_t + \tfrac{1}{2} (\nabla \Phi)^2 + gh + \frac{P}{\rho} = H(t) \tag{6}$$

where the time function H(t) is an integration "constant".

We shall summarize below the basic equations and the boundary conditions for the domain bounded by the free surface and three cut-off boundaries approximating boundaries at infinity. We show the pressure distribution problem in figure 1. The coordinate system (x,y,z) is attached to the disturbance with negative y oriented toward the acceleration of the gravity. The flow variables are the potential function Φ, the velocity $V(V_x,V_y,V_z)$, and the pressure P. All the variables in the basic equations and boundary conditions are nondimensionalized with respect to U, L, and P_0 which are the reference values of velocity, length and pressure respectively. We introduce two flow parameters:

$$Fr = \frac{U}{\sqrt{gL}} \tag{7}$$

and

$$\sigma = \frac{P_0}{\rho g L} \ . \tag{8}$$

The free surface height is defined as

$$y = \eta(x,z;t) \ . \tag{9}$$

A two-dimensional problem of a moving disturbance can be defined as follows:

$$\begin{aligned}
&\Phi_{xx} + \Phi_{yy} = 0 && \text{in } \mathcal{D}. \\
&\eta_t = \Phi_y - \Phi_x \eta_x && \text{on } y = \eta. \\
&\Phi_t = \tfrac{1}{2} - \tfrac{1}{2}(\Phi_x^2 + \Phi_y^2) - \frac{1}{Fr^2}\eta - \frac{\sigma}{Fr^2}P && \text{on } y = \eta. \qquad (10) \\
&\Phi = x && \text{on cut-off boundaries.} \\
&\frac{\partial \Phi}{\partial n} = 0 && \text{on solid boundary.} \\
&\Phi = 0, \quad \eta = -\sigma P && \text{at } t = 0 \text{ in } \mathcal{D}.
\end{aligned}$$

Here P is the applied pressure on the free surface.

For this paper the pressure distribution problem serves to illustrate our technique. In this problem, we consider the distribution

$$P = f(x) = \begin{cases} \dfrac{P_0}{2}\left(1 - \cos \dfrac{2\pi x}{L}\right) & 0 \leq x \leq 1 \\ 0 & \text{elsewhere} \end{cases} \qquad (11)$$

where P_0 is the maximum pressure in the surface distribution. The pressure distribution is initially at rest and starts to move with the uniform speed U in the negative direction on the x-axis. The span of the applied pressure is chosen as the length unit. The computational domain is bordered by the free surface and three cut-off boundaries. The downstream boundary is expanded periodically to contain the entire region of disturbance within the computational domain. The domain is initially divided into regular triangular elements with $\Delta x = \Delta y = 0.05$ for the case of finite element method.

NUMERICAL METHODS FOR EXPANDING COMPUTATIONAL DOMAIN

We shall describe here the numerical methods used for solving our free surface problems with an expanding computation domain.

Finite Element Method

In this method, the finite element method is used for the field calculation of the velocity potential while the time evolution is updated by using the finite difference method. The finite element method for field calculation is given in detail in reference 1.

The time advancement of the free surface boundary conditions is carried out using a predictor-corrector method. Let the free surface boundary conditions be expressed by

$$\eta_t = F(x,y;t)$$

and (12)

$$\Phi_t = G(x,y;t) \ .$$

The Euler method predicts the values at a particular x position at the new time step by

$$\eta_{\overline{n+1}} = \eta_n + \Delta t \; F_n$$

and (13)

$$\Phi^*_{\overline{n+1}} = \Phi^*_n + \Delta t \; G_n$$

where Φ^* denotes Φ on the free surface, the subscript n refers to the time level, and Δt is the time increment. The values at the new time-step are obtained from the corrector step by

$$\eta_{n+1} = \eta_n + \frac{\Delta t}{2} \left(F_n + F_{\overline{n+1}}\right)$$

and (14)

$$\Phi^*_{n+1} = \Phi^*_n + \frac{\Delta t}{2} \left(G_n + G_{\overline{n+1}}\right) \ .$$

In computing F and G, the spatial derivatives can be computed from the finite element algorithms. However, when the triangular mesh is used, the derivatives have comparably larger errors. In this case, the spatial derivatives are obtained from polynomial approximations after the iterative solutions converge at each time step.

The successive overrelaxation method is used to solve the Laplace equation iteratively with the specified values of Φ^* on the given boundary η. The updating of η and Φ^* is carried out by the predictor-corrector method after the iterative solutions converge within a required limit. The predictor-corrector method has less stringent conditions for stability and converges even in nonlinear problems; however, it does require two solutions for each time-step.

Finite element solutions were obtained for the pressure distribution problem and the problem of submerged bodies.

Finite Difference Method

Our finite difference method is to couple an explicit, single stage, second order time integration scheme with the solution of the Laplace equation for the potential function. In this method, the free surface conditions are integrated to provide a Dirichlet condition at the surface for the Laplace equation, the Laplace equation is solved, and the solution is used together with the free surface conditions to determine the derivatives needed for another time integration.

The time integration scheme is expressed by

$$\eta_{n+1} = \eta_n + \Delta t(\eta_t)_n + (\Delta t^2/2)(\eta_{tt})_n \tag{15}$$

and

$$\Phi^*_{n+1} = \Phi^*_n + \Delta t(\Phi^*_t)_n + (\Delta t^2/2)(\Phi^*_{tt})_n + \Delta\eta[(\Phi^*_y)_n + (\Delta\eta/2)(\Phi^*_{yy})_n + \Delta t(\Phi^*_{yt})_n]. \tag{16}$$

The subscript n denotes values at time $t = t_n$, Φ^* denotes Φ at $y = \eta$,

$$\Delta t = t_{n+1} - t_n$$

and

$$\Delta\eta = \eta_{n+1} - \eta_n \quad .$$

The Dirichlet condition at the new surface provided by the application of equations (15) and (16) and the other boundary conditions for the problem are used to solve the Laplace equation.

The final step of the method is to compute the derivatives appearing on the right hand side of equations (15) and (16).

Finite difference solutions were obtained for the pressure distribution problem and the surface piercing strut problem.

NUMERICAL SCHEME FOR A FINITE, SMALL COMPUTATIONAL DOMAIN

The fixed outflow boundary, as shown schematically for the pressure distribution problem in figure 2, requires special and careful treatment in order to prevent wave reflections that may impair the accuracy of solutions, or even destroy the calculations. Chan (ref. 2) used Orlanski's method (ref. 3) to implement boundary conditions at the open boundary. This method consists of imposing the Sommerfeld radiation condition at the outflow boundary and numerically evaluating the phase velocity of the boundary. We shall describe below our method of implementation of Orlanski's method.

The Sommerfeld radiation condition can be written as

$$Q_t + CQ_x = 0 \tag{17}$$

where Q is any perturbed variable and C is the phase velocity of the wave. In the free surface problem, we have the perturbed variable η and the potential function Φ. Therefore, we have to implement the following two equations at the outflow boundary:

$$\eta_t + C_\eta \eta_x = 0 \tag{18}$$

and

$$\Phi_t + C_\Phi(\Phi_x - 1) = 0 \quad . \tag{19}$$

Using Chan's (ref. 2) method to difference the derivatives, the open boundary condition for Φ can be written as follows:

$$\Phi_{IB}^{n+1} = \Phi_{IB-1}^{n-1} + [1-2\,\frac{C_\Phi(\Delta t^n)'}{\Delta x}][\Phi_{IB}^{n} - \Phi_{IB-1}^{n}] + 2\,C_\Phi(\Delta t^n)' \ , \qquad (20)$$

in which $(\Delta t^n)' = (\Delta t^n + \Delta t^{n-1})/2$,

$(\Delta t^{n-1})' = (\Delta t^{n-1} + \Delta t^{n-2})/2$,

Δt^n = nth time step,

$t^{n+1} = t^n + \Delta t^n$,

C_Φ = phase velocity for potential function Φ.

For the wave height,

$$\eta_{IB}^{n+1} = \eta_{IB-1}^{n-1} + [1-2\,\frac{C_\eta(\Delta t^n)'}{\Delta x}][\eta_{IB}^{n} - \eta_{IB-1}^{n}] \ , \qquad (21)$$

in which C_η = phase velocity for wave height η.

The phase velocities C_Φ and C_η are evaluated from equations (20) and (21):

$$C_\Phi = \frac{\Delta x}{2(\Delta t^{n-1})'}\ \frac{\Phi_{IB-1}^{n} + \Phi_{IB-2}^{n-1} - \Phi_{IB-1}^{n-1} - \Phi_{IB-2}^{n-2}}{(\Phi_{IB-2}^{n-1} - \Phi_{IB-1}^{n-1} + \Delta x)} \ , \qquad (22)$$

$$C_\eta = \frac{\Delta x}{2(\Delta t^{n-1})'} \cdot \frac{\eta_{IB-1}^{n} + \eta_{IB-2}^{n-1} - \eta_{IB-1}^{n-1} - \eta_{IB-2}^{n-2}}{(\eta_{IB-2}^{n-1} - \eta_{IB-1}^{n-1})} \ . \qquad (23)$$

We also take into account the wave crest or trough passing out of the downstream boundary. When this phenomenon happens, the denominators of equations (22) and (23) get very small. Thus, when

$$|\Phi_{IB-2}^{n-1} - \Phi_{IB-1}^{n-1} + \Delta x| \le 10^{-7}, \qquad (24)$$

we set

$$\Phi_{IB}^{n+1} = \Phi_{IB}^{n} \ ,$$

when

$$|\eta_{IB-2}^{n-1} - \eta_{IB-1}^{n-1}| \le 10^{-9} \ , \qquad (25)$$

we set

$$\eta_{IB}^{n+1} = \eta_{IB}^{n} \ .$$

We constrained the range of the values of C_ϕ and C_η could take. Letting C_ϕ^* be the right hand side of equation (22),

$$C_\phi = \begin{cases} 0 & , \text{ if } C_\phi^* < 0. \\ C_\phi^* & , \text{ if } 0 \le C_\phi^* \le \Delta x/\Delta t. \\ \Delta x/\Delta t & , \text{ if } C_\phi^* > \Delta x/\Delta t. \end{cases} \tag{26}$$

Similarly, letting C_η^* be the right hand side of equation (23),

$$C_\eta = \begin{cases} 0 & , \text{ if } C_\eta^* < 0 \text{ .} \\ C_\eta^* & , \text{ if } 0 \le C_\eta^* \le \Delta x/\Delta t. \\ \Delta x/\Delta t & , \text{ if } C_\eta^* > \Delta x/\Delta t. \end{cases} \tag{27}$$

As to be discussed later, we have found an alternative method to evaluate C_ϕ and C_η that leads to more accurate implementation of the open boundary condition. In this method, we use the derivatives of ϕ and η that have already been calculated on the free surface at nodes upstream of the outflow boundary. The expression for C_ϕ and C_η using this method are

$$C_\phi = - \frac{\phi_t}{\phi_x - 1} = - \frac{\left[(\phi_t)^{n-1}_{IB-2} + (\phi_t)^{n-1}_{IB-1}\right]}{\left[(\phi_x)^{n-1}_{IB-2} + (\phi_x)^{n-1}_{IB-1} - 2\right]} \quad , \tag{28}$$

and

$$C_\eta = - \frac{\eta_t}{\eta_x} = - \frac{\left[(\eta_t)^{n-1}_{IB-2} + (\eta_t)^{n-1}_{IB-1}\right]}{\left[(\eta_x)^{n-1}_{IB-2} + (\eta_x)^{n-1}_{IB-1}\right]} \quad . \tag{29}$$

In numerically implementing equation (19) for the potential ϕ, the spatial derivative ϕ_x is better represented by

$$(\phi_x)_{i+\frac{1}{2}} = \frac{\phi_{i+1} - \phi_i}{\Delta x} - \frac{\eta_{i+1} - \eta_i}{\Delta x} (\phi_y)_{i+\frac{1}{2}} \ . \tag{30}$$

The second term in this expression is to correct for error due to any significant change in wave height η at the outflow boundary.

As to be discussed later, we have found that, for long time solutions, the wave height at the outflow boundary becomes unstable. We are able to insure stability by setting the lower limit of C_η to be the free stream velocity. The new limits of C_η becomes

$$
C_\eta = \begin{cases} 1 & , \text{ if } C_\eta^* < 1. \\ C_\eta^* & , \text{ if } 1 \le C_\eta^* \le \Delta x/\Delta t. \\ \Delta x/\Delta t & , \text{ if } C_\eta^* > \Delta x/\Delta t. \end{cases} \tag{31}
$$

For our time integration scheme, we used the following predictor-corrector formula:

$$
\begin{aligned}
\overline{Q}^{n+1} &= Q^n + \Delta t(Q_t^n) \\
\overline{\overline{Q}}^{n+1} &= Q^n + (\Delta t/2)(Q_t^n + \overline{Q}_t^n) \\
Q^{n+1} &= Q^n + (\Delta t/2)(Q_t^n + \overline{\overline{Q}}_t^n) \ .
\end{aligned} \tag{32}
$$

NUMERICAL SOLUTION

Our first effort in using a fixed, small computational domain was to solve the pressure distribution problem and to compare the solutions to those obtained with the expanding computational domain. We set the outflow boundary $x_{IB} = 1.5$. Transient solutions have been obtained for $Fr = 1/\sqrt{2\pi}$ and $\sigma = 0.01$. It was found that two-grid interval ($2\Delta x$) waves of appreciable magnitude start to appear at $t = 0.8$ near the outflow boundary, spread quickly upstream and eventually cause the calculation to stop at $t = 5$. The appearance of $2\Delta x$ waves over the solution of the wave height at $t = 1$ is shown in figure 3.

The contamination of the solution by $2\Delta x$ waves discussed above led to our effort to conduct "advection experiments" to evaluate the performance of schemes that could be used to implement accurately the Sommerfeld advection equation at the open boundary. We wanted to compare Chan's scheme with other numerical schemes.

A series of experiments was tried for a simple problem. We were trying to reproduce the results we were getting in the free surface problem in the simpler problem. There are two experiments. In one experiment, a sine wave of several combinations of parameters (amplitude, wave length and advection velocity) is advected through a boundary. In another, a $2\Delta x$ wave is superposed on the advecting sine wave. In each experiment, we find the solution of the Sommerfeld advection equation using the chosen numerical schemes at the boundary. Each solution will yield boundary values of amplitude, phase, and phase velocity from which we may evaluate the performance of the schemes. The performance characteristics evaluated include amplitude and phase errors and stability.

In the first experiment, Chan's scheme proved to be superior to the other schemes. In the second experiment, we tested the performances of numerical schemes not only with 2Δx wave error but also with (and without) phase velocity error. It was found that: (1) all the schemes tested perform poorly with 2Δx waves present, (2) the effect of the phase velocity error without 2Δx waves present is not as significant; however, it becomes large in the presence of 2Δx waves. These findings are significant in that the 2Δx waves were present in the solution of free surface wave calculations (as shown in figure 3); therefore, some means has to be used to eliminate them.

These numerical experiments have helped us to identify two problems in numerically implementing the open boundary condition: high frequency errors in the free surface wave solution and phase velocity error in the calculation of the boundary condition.

On the basis of the results of the numerical experiments, we have formulated the following requirements for numerical schemes that could be used for free surface wave problems for a finite, small computational domain (1) some means should be used to minimize the 2Δx waves in the solution, (2) the open boundary condition should be implemented so that the phase velocity at the free surface should be calculated independent of the open boundary condition to insure the accuracy of its calculation and (3) a correction is necessary in implementing the open boundary condition for the potential function at the free surface. We have developed numerical methods to meet these requirements.

We wanted to eliminate the 2Δx waves by using damping in the numerical schemes. We modified our time marching integration schemes so that the high frequency wave errors are damped by the dissipation and dispersion. First we modified our schemes so that they would be dissipative. For the second order Taylor's series, we changed it to third order with the third term as the damping term. From the basic predictor-corrector scheme (equations (12) and (13)) we developed three dissipative predictor-corrector schemes. The one we chose was given in equation (32). Secondly we changed from center differencing of the spatial derivatives for equations (18) and (19) to upwind differencing.

We have found that the schemes become effective in damping the 2Δx waves when we use upwind differencing. Figure 4 shows the effectiveness of this method in minimizing the high frequency errors in the wave height solution for the pressure distribution problem at $t = 2$. The second and third requirements have been fulfilled respectively by equations (28) and (29), and equation (30).

We have obtained transient solutions for the pressure distribution and the accelerating strut problems and the steady state linear and nonlinear solutions for the pressure distribution problem. Figure 5 shows a comparison of the expanding domain solution with the corresponding solution for the fixed domain. The solutions are virtually the same except near the open boundary. Figures 6 and 7 show the wave height of the two steady state solutions for the following parameters: $Fr = 1/\sqrt{4\pi}$ and $\sigma = 0.01$. The outflow boundary is set at $x = 2$. The linear calculation by Haussling (ref. 5), using a spectral method, is also shown for comparison. As can be seen in figure 7, our linear solution agrees with Haussling results only in the region of the pressure distribution.

ALTERNATIVE METHOD OF IMPLEMENTATION OF OPEN BOUNDARY CONDITION

An alternative method of implementing the open boundary condition at the free surface is being studied. In this method, we used the wave height free surface boundary conditions at the outflow boundary. We feel that the use of the free surface boundary should be physically more comparable to the condition near the outflow boundary. The problem with using this technique is that it is unstable for the wave height solution under some conditions. Since the instability develops slowly, we use our experience with filtering to the following second order smoother to smooth the wave height at IB and IB-1:

$$\eta^{+}_{IB} = (9\eta_{IB-4} - 20\eta_{IB-3} + 6\eta_{IB-2} + 12\eta_{IB-1} + 6\eta_{IB})/13 \qquad (33)$$

$$\eta^{+}_{IB-1} = (-2\eta_{IB-4} + 3\eta_{IB-3} + 3\eta_{IB-2} + 6\eta_{IB-1} + 3\eta_{IB})/13 \qquad (34)$$

in which η^{+} is the smoothed wave height. These expressions have been developed on the basis of a combination of a second order interpolation formula with a $2\Delta x$ wave smoother. In practice, our smoother is used to detect the onset of the instability and is then applied to the wave height solution at the boundary. Comparing the wave height solution using both open boundary techniques, we found that the free surface boundary condition gives slightly better results near the outflow boundary. Figure 8 shows two solutions for the pressure distribution problem at $t = 4$ using the two techniques.

CONCLUDING REMARKS

1. To implement accurately the open boundary condition at the outflow boundary using Orlanski's method, we have found that (a) an accurate numerical scheme should be used to solve the advection equation at the boundary, (b) the numerical calculation of the phase velocity should be decoupled from the open boundary condition, (c) the evaluation of spatial derivative of the potential at the free surface (needed in the calculation of phase velocity) should take into consideration the change in wave height and (d) limiting values of the phase velocity should be set properly to insure stability of calculations at the boundary.

2. The most important task in developing method to solve free surface problems using a fixed and small computational domain is to find ways to eliminate the two-grid interval ($2\Delta x$) waves that appear in the solution and that inhibit the accurate implementation of the open boundary condition. We have used damping in our time marching schemes to control the high frequency errors. However, careful studies should be made to ascertain its influence on the accuracy of solutions.

REFERENCES

1. Yen, S. M., Lee, K. D. and Akai, T. J., "Finite Element and Finite Differences Solutions of Nonlinear Free Surface Wave Problems," Proceedings of the Second International Conference on Numerical Ship Hydrodynamics, Berkeley, CA, pp. 305-318, (1977).

2. Chan, Robert K. C., "Finite Difference Simulation of the Planar Motion of a Ship," Proceedings of the Second International Conference on Numerical Ship Hydrodynamics, Berkeley, CA, pp. 39-52, (1977).

3. Orlanski, L., "A Simple Boundary Condition for Unbounded Hyperbolic Flows," Journal of Computational Physics, 21, 1976.

4. Yen, S. M. and Hall, D. R., "Implementation of Open Boundary Conditions for Nonlinear Free Surface Wave Problems," Proceedings of the Third International Conference on Numerical Ship Hydrodynamics, Paris, France, pp. III-2-1 to III-2-14, (1981).

5. Haussling, H. J. and Van Eseltine, R. T., "Finite Difference Methods for Transient Potential Flows with Free Surfaces," Proceedings of the First International Conference on Numerical Ship Hydrodynamics, p. 295, (1975).

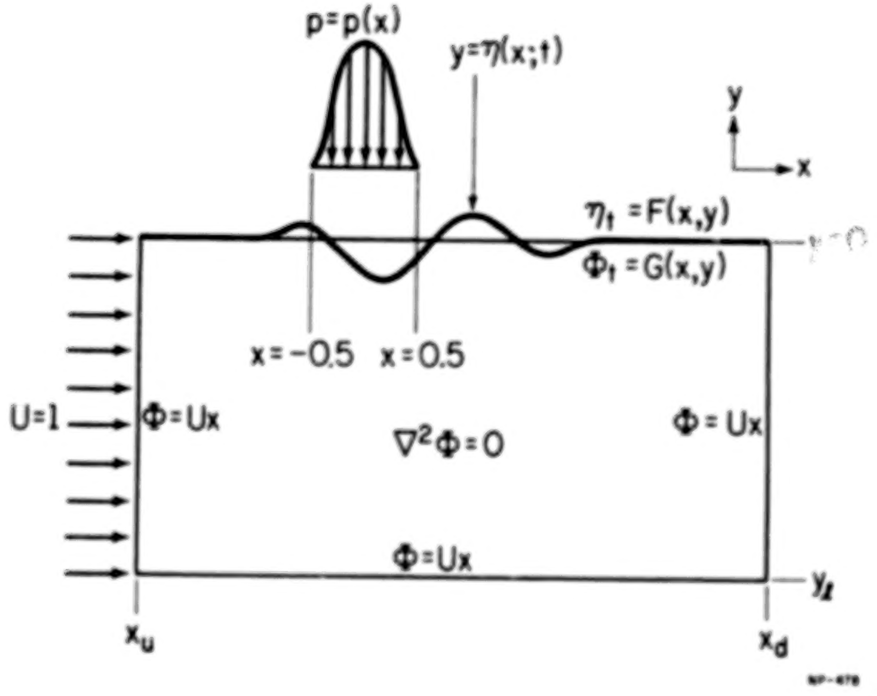
p=p(x)
y=η(x;t)
y
x
η_t =F(x,y)
y=0
Φ_t =G(x,y)
x=-0.5
x=0.5
U=1
Φ=Ux
∇²Φ=0
Φ=Ux
Φ=Ux
y_ℓ
x_u
x_d

Figure 1. Schematic of the two-dimensional pressure distribution problem.

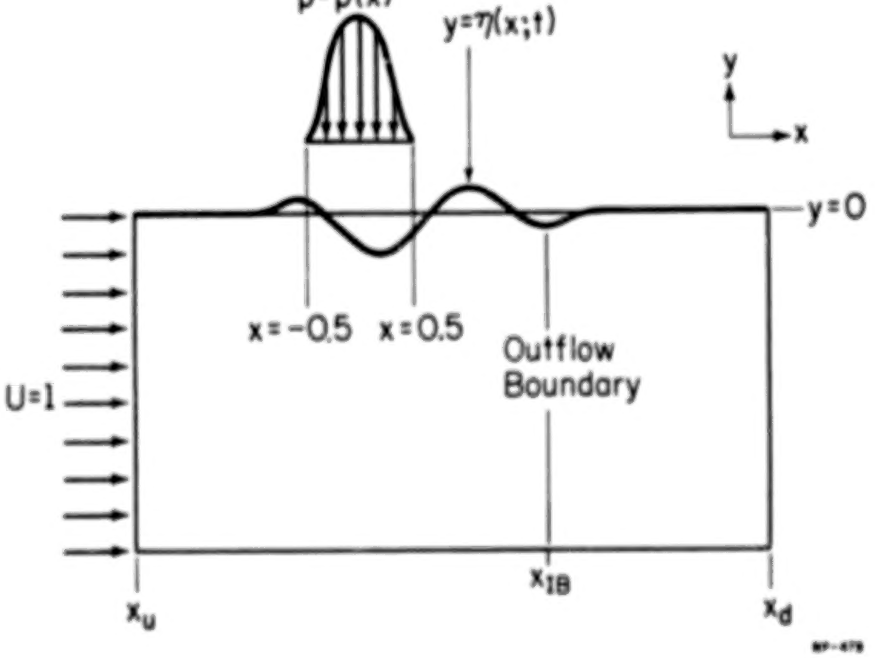
p=p(x)
y=η(x;t)
y
x
y=0
x=-0.5
x=0.5
Outflow Boundary
U=1
x_IB
x_u
x_d

Figure 2. Computational domain with fixed outflow boundary (x_{IB}).

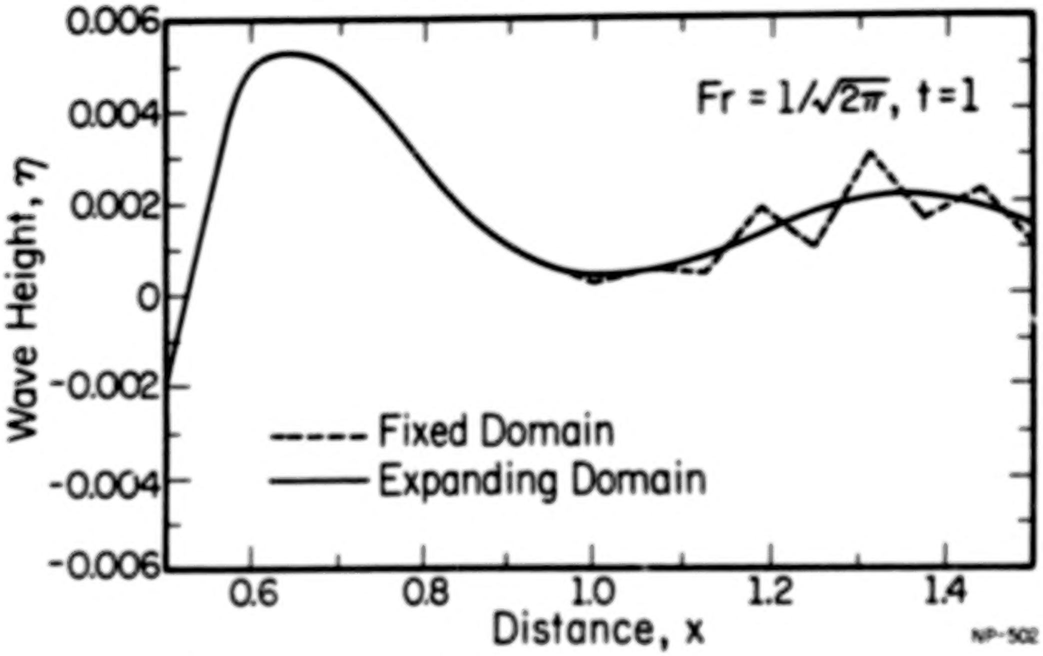

Figure 3. Appearance of two-grid interval ($2\Delta x$) wave in the solution of the pressure distribution problem for $Fr = 1/\sqrt{2\pi}$ and $\sigma = 0.01$.

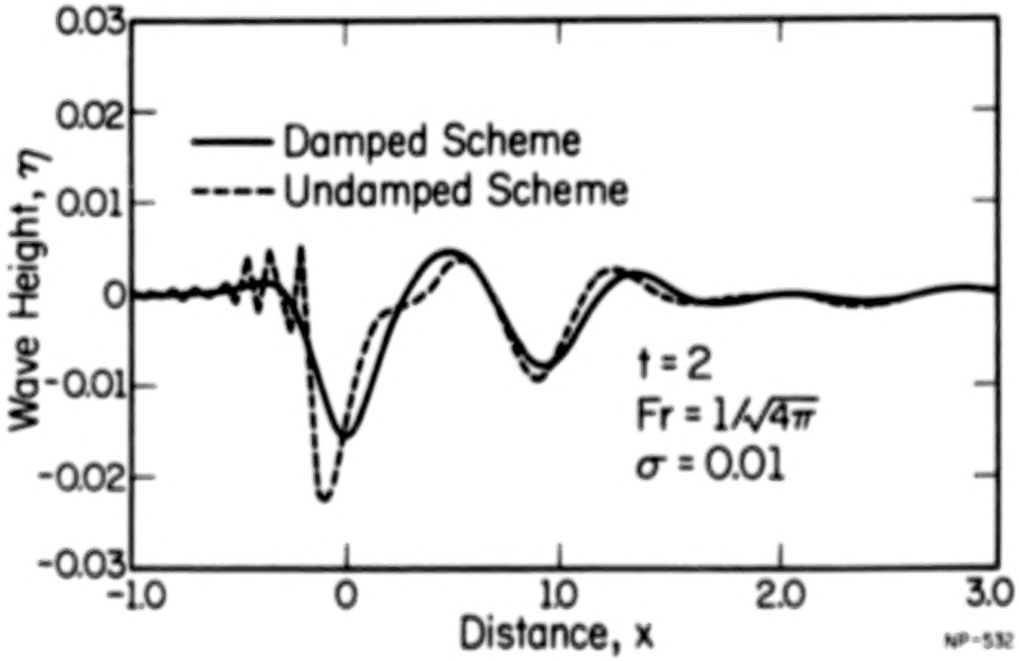

Figure 4. Solution of the pressure distribution problem by using damping in the time-integration scheme.

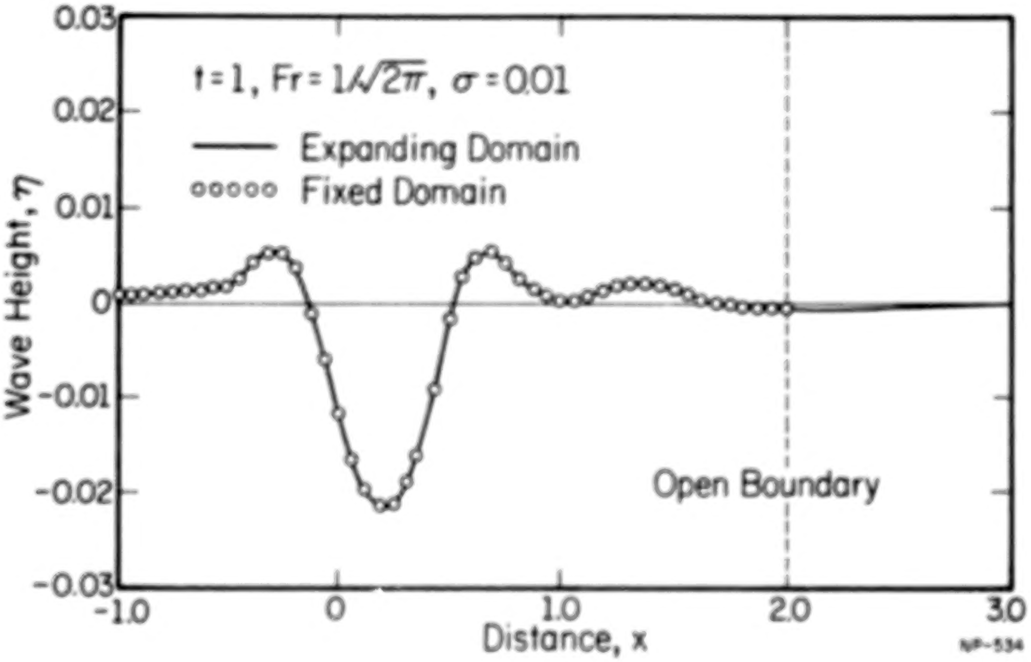

Figure 5. Comparison of solutions at t = 1 of the pressure distribution problem for $Fr = 1/\sqrt{2\pi}$ and $\sigma = 0.01$. Expanding computational domain vs. fixed computational domain.

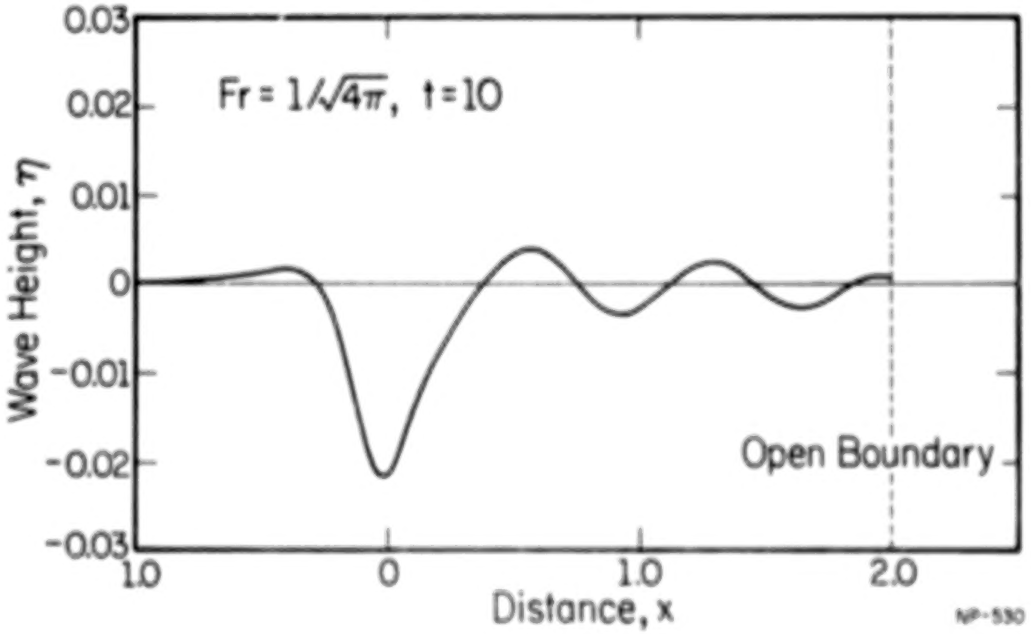

Figure 6. Nonlinear, steady state wave height solution of the pressure distribution problem for $Fr = 1/\sqrt{4\pi}$ obtained by using a fixed and small computational domain.

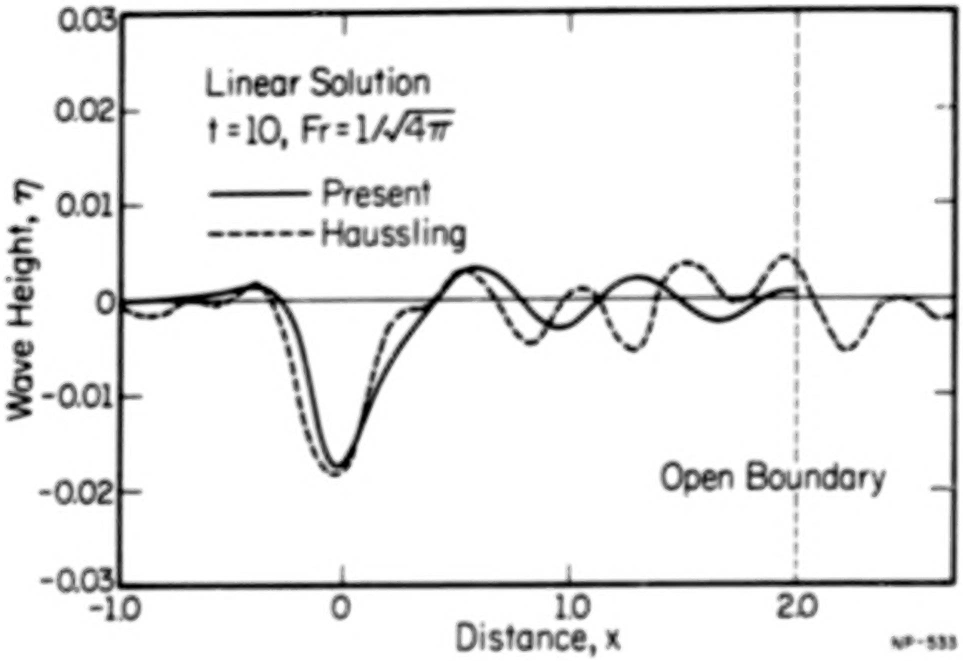

Figure 7. Linear, steady state wave height solution of the pressure distribution problem for Fr = $1/\sqrt{4\pi}$ obtained by using a fixed and small computational domain. Comparison with Haussling's solution.

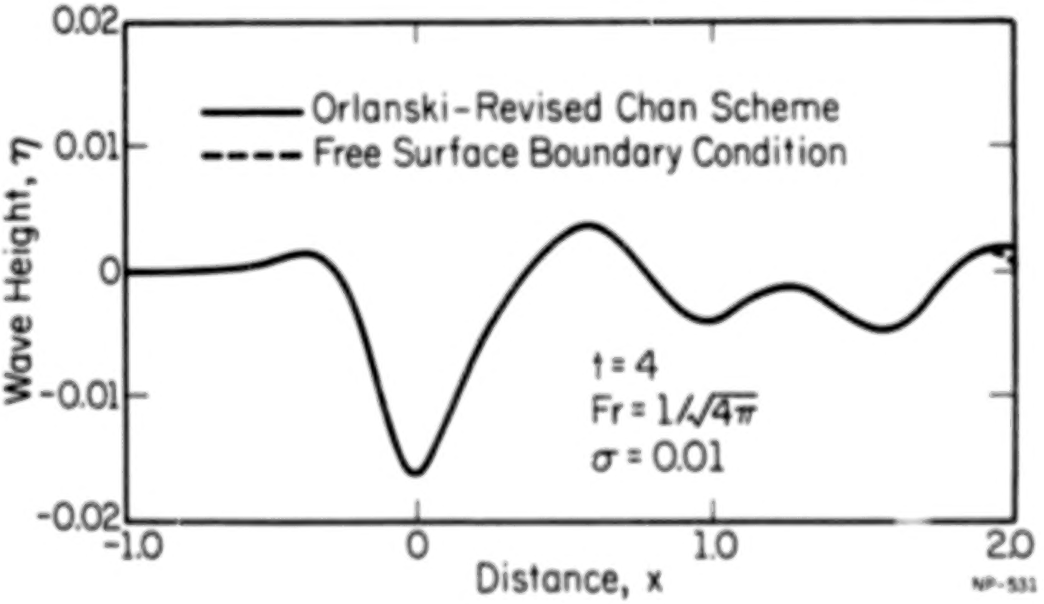

Figure 8. Nonlinear free surface wave height solutions obtained by using two different treatments of the open boundary conditions at the outflow boundary.

RAPID, HIGH-ORDER ACCURATE CALCULATION OF FLOWS DUE TO FREE SOURCE OR VORTEX DISTRIBUTIONS*

Douglas Halsey
Douglas Aircraft Company

ABSTRACT

Fast Fourier Transform (FFT) techniques are applied to the problem of finding the flow due to source or vortex distributions in the field outside an airfoil or other two-dimensional body. Either the complex potential or the complex velocity may be obtained to a high order of accuracy, with computational effort similar to that required by second-order fast Poisson solvers. These techniques are applicable to general flow problems with compressibility and rotation. An example is given of their use for inviscid compressible flow.

INTRODUCTION

Although distributed singularities (sources and vortices) arise most frequently in the study of inviscid, incompressible flows, they can also be useful for calculating much more general flows. Compressible potential flow is equivalent to an incompressible flow with distributed sources (or sinks) in the external field. Viscous incompressible flow is equivalent to an inviscid flow with distributed vorticity in the external field. General flows are equivalent to inviscid incompressible flows with distributed source and vortex singularities superimposed.

A number of investigators have developed flow calculation methods which make use of distributed singularities in the external field. Because they generally discretize the field distributions into panels over which the singularities vary in a simple manner (such as constant or bi-linear), these are referred to as field-panel methods (as opposed to finite-difference or finite-element methods). They are also sometimes referred to as integral representation methods. A source field-panel method for calculating compressible subsonic flow and shock-free transonic flow about two-dimensional airfoils or cascades has been developed by Luu and Coulmy (ref. 1). Extension to cases with shocks has been accomplished by Piers and Sloof (ref. 2). A vortex field-panel method for calculating incompressible viscous flow about two-dimensional bodies was developed by Wu and Thompson (ref. 3). Wu and his coworkers have subsequently made a number of improvements and extensions, reported in a series of papers, such as reference 4. The present author has also developed a source field-panel method for two-dimensional airfoils and is working to extend it to multielement airfoil cases.

---

*This research was sponsored by the Independent Research and Development program of the McDonnell-Douglas Corporation.

Some flow calculation methods using finite differences are closely related to the field-panel methods. Martin and Lomax (ref. 5) proposed a calculation strategy for transonic flows in which the field equations are arranged in the form $\nabla^2\phi = f(x,y)$, where the left-hand side is the Laplacian of the velocity potential and the right-hand side contains all the other terms in the field equation. Each iteration, the right-hand is frozen and a Poisson equation is solved using one of the fast elliptic solvers such as Buneman's (ref. 6). This is equivalent to finding the flow due to a source distribution with density proportional to the value of the right-hand side. Jameson (ref. 7) has used this approach to accelerate the convergence of a transonic flow calculation method.

The main computational difficulty in a field-panel method concerns the calculation of the influence of the distributed singularities on the velocity potential and/or its derivatives. Since each panel has an effect on each other panel, the amount of data storage and the number of arithmetical calculations both vary as the square of the total number of panels. For cases with large numbers of panels, it is therefore not feasible to apply a direct summation of all panel influences. Recognizing this, Wu (ref. 4) developed a relatively complicated flow-field segmentation procedure and has since (ref. 8) employed various hybrid flow calculation techniques.

The present author has adopted a procedure for the efficient calculation of the flow due to the distributed singularities. The influence is expressed in terms of Poisson's equation [$\nabla^2\phi = 4\pi\sigma(x,y)$, where σ is the local source density] and the velocity potential is found using a fast solver. The main difficulty of this approach (and the matter which makes this paper of relevance to this symposium) concerns the boundary conditions to be specified for the fast solver. A direct application of the fast solver given in reference 6 requires that the values of the potential at the boundary points be specified (Dirichlet conditions). Since these are not initially known, an alternative procedure to find them must be used. A direct summation of panel influences could be applied, but for large panel numbers the amount of data storage and arithmetical operations would still be excessive. This could lead to a situation in which the determination of the boundary conditions required several orders of magnitude more computational expense than the solution of the differential equations. Various approximate methods (ref. 9) could be employed to calculate the boundary conditions, but these could seriously affect the solution accuracy.

The remainder of this paper describes a method for determining the boundary conditions which combines the features of high-order accuracy and low computational cost. Accuracy should be of higher order than the fast solvers (which are generally second-order) and cost is of the same order. An extension to the procedure is also described which allows the direct calculation of the entire flow field and eliminates the need to apply a fast solver.

COMPUTATIONAL PLANE AND GRID TRANSFORMATIONS

The present method determines the complex potential $(\phi + i\psi)$ or the complex velocity $(u - iv)$ at a discrete set of points on the inner and outer boundaries of a two-dimensional polar-coordinate grid, given the source or vortex densities (σ or γ) at discrete points within the grid and on the boundaries. In the extended version of the method, it also determines the complex potential or complex velocity at the same interior grid points where the singularity densities are given. Both versions also determine the coefficients of series expansions for the flow outside the grid.

Since the method makes use of Fourier transforms in the circumferential direction, there are some restrictions on the number and spacing of the points. It is presently assumed that the function representing the singularity density at any fixed value of the radial coordinate is continuous and is defined by specifying 2^n values (where n is a small integer) at equally-spaced intervals. Some of these assumptions can undoubtedly be removed, but to date they have not proven to be overly restrictive.

There are generally no restrictions on the number and spacing of points in the radial direction. In some applications, however, it may be desirable for grid points to correspond directly to points in a rectangular grid (as used in most fast solvers). Since polar and rectangular grids are related by a logarithmic mapping, this condition would require that the radial grid coordinates vary in proportion to the exponential of the radial point index.

The present method may be applied to singularity distributions in the field surrounding an airfoil or other two-dimensional body of arbitrary shape by the application of a conformal transformation which maps the given body to a unit circle. Figure 1 shows a typical grid (65 x 21) for a modern airfoil and the corresponding grid in the polar computational plane. It is shown in elementary texts (ref. 10) that a conformal transformation does not alter the form of Poisson's equation, though the magnitude of the right-hand side is changed. Therefore, to calculate the influence of the singularity distributions in the physical plane, it is sufficient to be able to find the influence in the polar computational plane and to be able to perform the mapping between the two planes.

RELATIONSHIP BETWEEN SOURCE AND VORTEX FLOWS

It is well known that the velocity vector in a flow produced by a point vortex is identical to the velocity vector in a flow produced by a point source, except for a rotation through 90 degrees. The flow produced by a vortex distribution is related to the flow produced by a source distribution in the same way. Since a method to calculate source flows can be used directly to compute vortex flows, only source distributions will be discussed in the remainder of this paper. Flows due to vortex distributions (with vorticity positive clockwise) can be obtained by replacing the quantities $(\sigma, \phi, \psi, u, v)$ by $(\gamma, -\psi, \phi, -v, u)$.

SOURCE INFLUENCE ON THE REGION BOUNDARIES

In a polar grid, the exact expression for the complex velocity due to a source distribution is given by

$$[u(\zeta) - iv(\zeta)] = 2 \int_{r_i}^{r_o} \int_{0}^{2\pi} \sigma(r,\omega)[\zeta - \zeta_s(r,\omega)]^{-1} r\,dr\,d\omega \tag{1}$$

where r is the radial coordinate, r_i and r_o are the inner and outer limits of r, ω is the angular coordinate (measured clockwise from the positive horizontal axis), ζ is the complex coordinate of the point at which the velocity components (u and v) are found, and ζ_s is the complex coordinate of an elemental area of source density (σ). Separating the integrations in the radial and circumferential directions allows this equation to be represented by

$$[u(\zeta) - iv(\zeta)] = 2 \int_{r_i}^{r_o} rI(\zeta,r)\,dr \tag{2}$$

where

$$I(\zeta,r) = \int_{0}^{2\pi} \sigma(r,\omega)[\zeta - \zeta_s(r,\omega)]^{-1} d\omega \tag{3}$$

The basic idea of the present method is to find series expansions for the integrand of equation (3), and to integrate analytically in the circumferential direction and numerically in the radial direction. This gives a series expansion for the complex velocity, from which another series for the complex potential is easily obtained. Due to differing regions of convergence, separate series must be found for the inner and outer boundaries.

The integrand of equation (3) is expanded by multiplying the series expansions of its two factors. In order to facilitate the multiplication, a complex form of the series for $\sigma(r,\omega)$ is used. For a given value of r, $\sigma(r,\omega)$ can be represented by

$$\sigma(r,\omega) = a_0(r) + \sum_{j=1}^{\infty} [a_j(r)\zeta_s^j + a_{-j}(r)\zeta_s^{-j}] \tag{4}$$

where each coefficient is generally complex. Making use of the requirement that $\sigma(r,\omega)$ be purely real, a relationship can be derived between values of the coefficients with positive and negative indices. This allows the function to be expressed as

$$\sigma(r,\omega) = a_0(r) + \sum_{j=1}^{\infty} [2a_j(r)r^j]e^{+ij\omega} \tag{5}$$

In this form it is clear that a finite number of the series coefficients can be found very efficiently with one application of the FFT algorithm.

The other factor of the integrand can be expanded analytically. For points on the inner boundary (or at smaller values of the radial coordinate), the expansion

$$[\zeta - \zeta_s(r,\omega)]^{-1} = \frac{-1}{\zeta s} [1 + (\zeta/\zeta_s) + (\zeta/\zeta_s)^2 + \ldots] \tag{6}$$

is applicable, while for points on the outer boundary (or at larger values of the radial coordinate), the expansion

$$[\zeta - \zeta_s(r,\omega)]^{-1} = \frac{1}{\zeta} [1 + (\zeta_s/\zeta) + (\zeta_s/\zeta)^2 + \ldots] \tag{7}$$

is applicable. Each expansion is evidently divergent at the point $\zeta = \zeta_s$, but it will be shown below that this does not compromise the validity of the final results. After multiplying the series in equation (4) by the series in either equation (6) or equation (7), the integrand of equation (3) takes the form

$$\sigma(r,\omega)[\zeta - \zeta_s(r,\omega)]^{-1} = b_0(r) + \sum_{j=1}^{\infty} [b_j(r)\zeta_s^j + b_{-j}(r)\zeta_s^{-j}] \tag{8}$$

where each b_j coefficient may be found by summing a series involving the a_j coefficients and the complex coordinate ζ.

Integrating equation (8) term by term, it is found that all terms drop out except the zeroeth term. Equation (3) therefore reduces to

$$I(\zeta,r) = 2\pi b_0(r) \tag{9}$$

For points on the inner boundary, it is found that

$$b_0(r) = -[a_1(r) + a_2(r)\zeta + a_3(r)\zeta^2 + \ldots] \tag{10}$$

while for points on the outer boundary, it is found that

$$b_0(r) = 1/\zeta[a_0(r) + a_{-1}(r)/\zeta + a_{-2}(r)/\zeta^2 + \ldots] \tag{11}$$

These series will be absolutely convergent on their respective domains of application, provided the sequence of values of $[2a_j(r)r^j]$ in equation (5) is convergent. Since the convergence of this sequence depends only on the function $\sigma(r,\omega)$, the possible divergence of the series in equations (6) and (7) is of no consequence. This is consistent with the classical result that a continuous source distribution produces a finite flow solution, even though its influence is expressed in terms of singular integrals.

An expression for the complex velocity at points on the inner boundary is obtained by substituting equations (9) and (10) into equation (2):

$$[u(\zeta) - iv(\zeta)] = c_0 + c_1\zeta + c_2\zeta^2 + \ldots \tag{12}$$

where

$$c_j = -4\pi \int_{r_i}^{r_o} a_{j+1}(r)r\,dr$$

An expression for the complex velocity at points on the outer boundary is obtained in a similar manner (using equation (11) instead of equation (10))

$$[u(\zeta) - iv(\zeta)] = d_1/\zeta + d_2/\zeta^2 + \ldots \tag{13}$$

where

$$d_j = 4\pi \int_{r_i}^{r_o} a_{-j}(r)r\,dr$$

The integrals in the radial direction may be evaluated using a numerical method of any desired order of accuracy. In the present application, the trapezoidal rule is used.

Given the series for the complex velocity, the corresponding series for the complex potential are determined by analytic integration. For points on the inner boundary, it is found that

$$[\phi(\zeta) + i\psi(\zeta)] = c_0\zeta + \frac{1}{2}c_1\zeta^2 + \frac{1}{3}c_2\zeta^3 + \ldots \quad (14)$$

while for points on the outer boundary, it is found that

$$[\phi(\zeta) + i\psi(\zeta)] = d_1 \log\zeta - d_2/\zeta - \frac{1}{2}d_3/\zeta^2 - \ldots \quad (15)$$

The determination of all series coefficients is accomplished with N applications of the FFT algorithm, where N is the number of grid points in the radial direction, plus a small number of additional arithmetic operations. Each of these Fourier transforms involves a purely real function and therefore requires a number of additions and multiplications approximately equal to $M \log_2 M$, where M is the number of grid points in the circumferential direction. The evaluation of the series on the grid boundaries requires two additional general Fourier transforms, each requiring approximately $2M \log_2 M$ additions and multiplications. The total number of addition and multiplication operations is thus approximately $(N+4)M \log_2 M$. This compares to $2MN \log_2 N$ multiplications and several times that many additions for the fast Poisson solver of reference 6. The determination of source influences at all grid points (on both the boundary and interior of the grid) can thus be performed without seriously compromising the computational efficiency of the fast Poisson solver.

EXTENSION OF THE METHOD TO THE REGION INTERIOR

In addition to providing boundary conditions for a fast Poisson solver, this method can be extended to give the flow directly at all points in the region interior. This eliminates the need for the fast Poisson solver or any other use of finite-difference techniques. The procedure is very similar to that discussed above. At any given radial coordinate, the flow due to the source distribution is broken into two parts; the flow due to portions of the source distribution at smaller radial coordinate is computed using the method for points on the outer boundary, and the flow due to portions at larger radial coordinate is computed using the method for points on the inner boundary. To calculate the complex potential or the complex velocity at all grid points requires N applications of the Fourier transform algorithm for real functions and N applications of the general Fourier transform algorithm. The total number of addition and multiplication operations is approximately $3MN \log_2 M$. It is thus comparable in computational expense to the basic method (including the fast solver), but is probably of a higher order of accuracy.

SAMPLE CALCULATION

The method described above has been incorporated into a computer program to calculate the compressible potential flow about two-dimensional airfoils using a source field-panel method and iteration scheme similar to those described in the Introduction. Although the ultimate application of this computer program will be to multielement airfoils, it is currently operational only for single-element cases. It has proven to be very accurate and efficient for all cases run to date, provided the flow is entirely subsonic. A typical result is shown in figure 2, which compares the calculated pressure distribution about a modern supercritical airfoil at a high subsonic Mach number with the result calculated using a finite-difference technique (ref. 11). The grid used in the present method is shown in figure 1. The grid used in the finite-difference method is the default grid for that method. The good agreement between the results of the two methods is evidence of the accuracy of the present method. The fact that the present method required less than two seconds of CPU time on an IBM 370 computer (compared to 10 seconds for the finite-difference method) is evidence of its efficiency. Each calculation of the influence of the field source distributions required only 0.16 CPU seconds.

REFERENCES

1. Luu, Thoai-Sum; and Coulmy, Genevieve: Method of Calculating the Compressible Flow Round an Aerofoil or a Cascade up to the Shockfree Transonic Range. Computers and Fluids, Vol. 5, no. 4, 1977, pp. 261-275.

2. Piers, W.J.; and Slooff, J.W.: Calculation of Transonic Flow by Means of a Shock-Capturing Field Panel Method. AIAA Paper No. 79-1459, 1979.

3. Wu, J.C.; and Thompson, J.F.: Numerical Solutions of Time-Dependent Incompressible Navier-Stokes Equations Using an Integro-Differential Formulation. Computers and Fluids, Vol. 1, no. 2, 1973, pp. 197-215.

4. Wu, J.C.; Spring, A.H.; and Sankar, N.L.: A Flowfield Segmentation Method for the Numerical Solution of Viscous Flow Problems. Lecture Notes in Physics - Proceedings of the Fourth International Conference on Numerical Methods in Fluid Dynamics, Vol. 35, 1975, pp. 452-457.

5. Martin, E. Dale; and Lomax, Harvard: Rapid Finite-Difference Computation of Subsonic and Transonic Aerodynamic Flows. AIAA Paper No. 74-11, 1974.

6. Buneman, O.: A Compact Non-Iterative Poisson Solver. SUIPR Rept. 294, Stanford University, 1969.

7. Jameson, Antony: Accelerated Iteration Schemes for Transonic Flow Calculations Using Fast Poisson Solvers. ERDA COO-3077-82, New York University, 1975.

8. Wu, J.C.: Hybrid Procedures for Computing General Viscous Flows. Symposium on Numerical and Physical Aspects of Aerodynamic Flows, Long Beach, California, 1981.

9. James, R.A.: The Solution of Poisson's Equation for Isolated Source Distributions. J. of Comp. Phy., Vol. 25, no. 2, 1977, pp. 71-93.

10. Churchill, Ruel V.: Complex Variables and Applications. McGraw-Hill Book Co., 1960.

11. Dougherty, F. Carroll; Holst, Terry L.; Gundy, Karen L.; and Thomas, Scott D.: TAIR - A Transonic Airfoil Analysis Computer Code. NASA TM 81296, 1981.

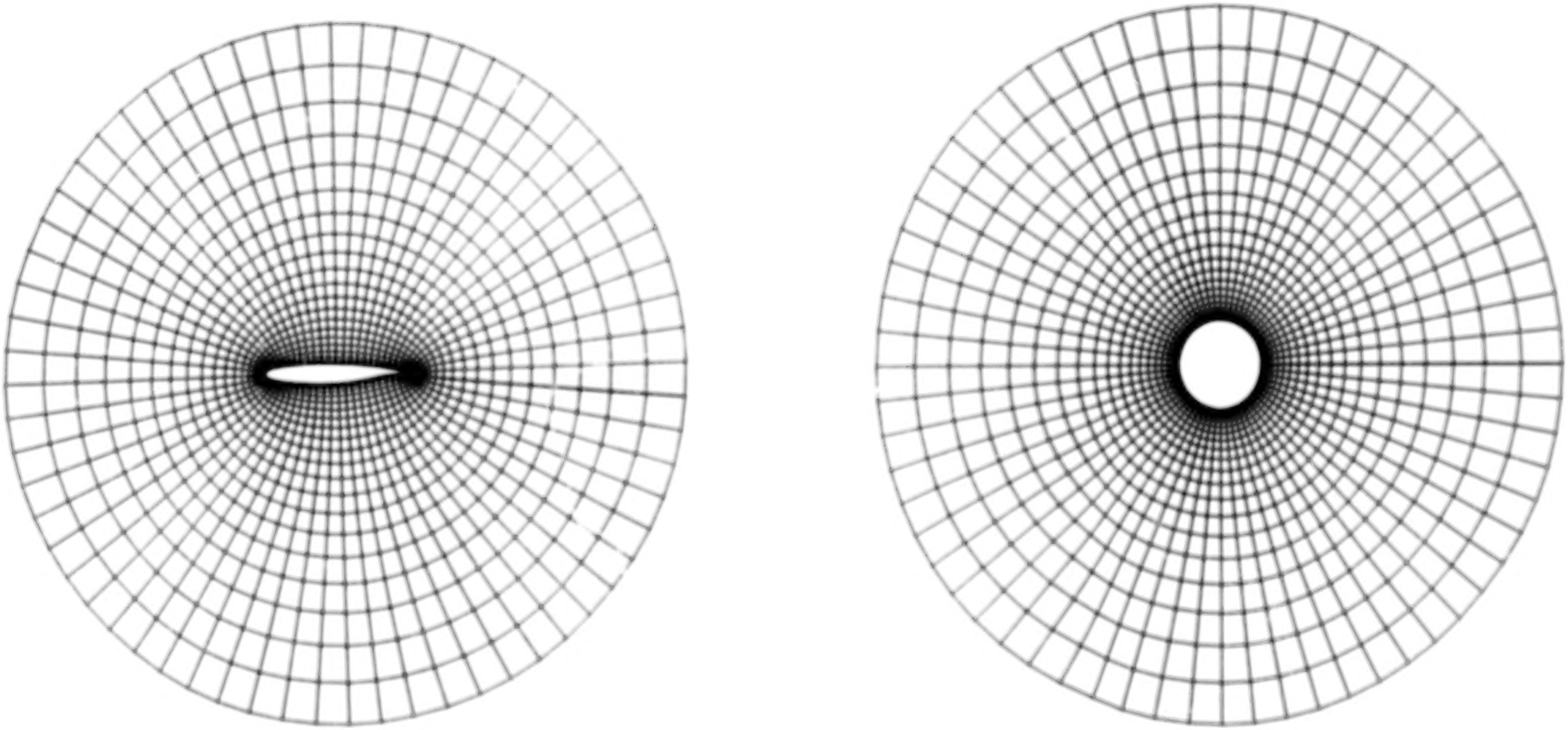

(a) PHYSICAL PLANE

(b) POLAR COMPUTATIONAL PLANE

Figure 1.- Typical grids for field singularity calculations.

BLANK

PAGE

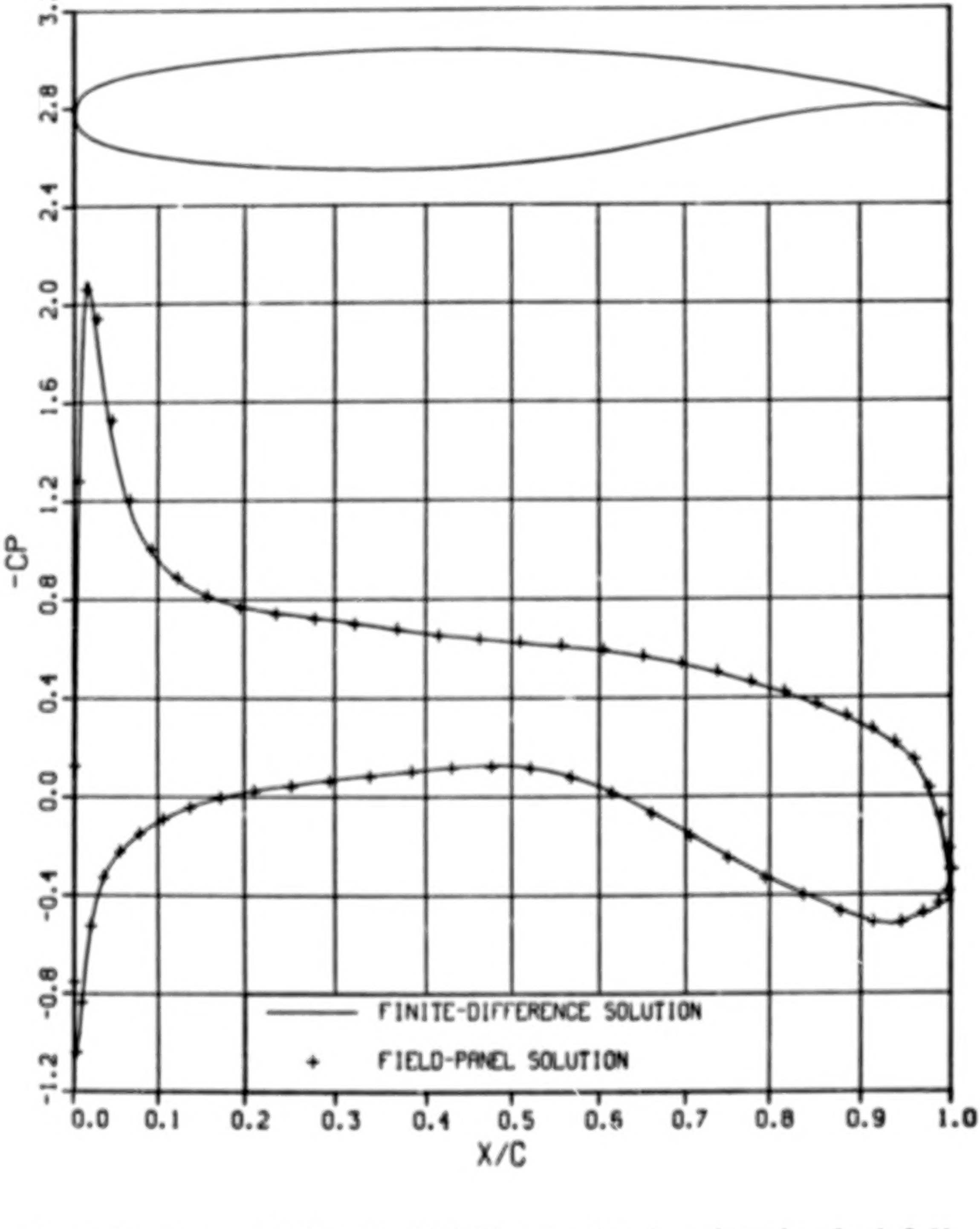

Figure 2.- Compressible potential flow about a two-dimensional airfoil - comparison of field-panel and finite-difference solutions ($M_\infty = 0.4$, $\alpha = 2.0$).

Blank Page

(Invited paper)

A PHYSICAL APPROACH TO THE NUMERICAL TREATMENT OF BOUNDARIES IN GAS DYNAMICS

Gino Moretti
G.M.A.F., Inc.

INTRODUCTION

I intend to discuss the numerical treatment of boundaries for hyperbolic problems in gas dynamics. I will consider only two types of boundaries: rigid walls, and artificial ("open") boundaries which have been arbitrarily drawn somewhere across a wider flow field.

A set of partial differential equations (typically, the Euler equations) has an infinite number of solutions, each one defined by a set of initial and boundary conditions. The initial conditions remaining the same, any change in the boundary conditions will produce a new solution. To pose the problem well, a necessary and sufficient number of boundary conditions must be prescribed.

Physical arguments, which can easily be formulated mathematically, show how many and which boundary conditions are needed. In fact, Euler's equations describe the propagation of signals. There are signals which reach the boundary from inside and signals which travel along the boundary. There are also signals which reach the boundary from outside or (in the case of rigid walls) which can be imagined to reach the boundary from outside to produce the same effect as the boundary itself. The latter signals must be equal in number to the available boundary conditions, and must be defined by them. In ref. 1 these concepts are expressed in mathematical form, and the reader may easily see that the vectors u^{I} and u^{II} of ref. 1 correspond to our incoming and outgoing signals, respectively.

When the solution is sought through numerical analysis, one chooses a necessary and sufficient number of unknowns and discretizes the equations of motion in order to update the unknowns approximately at each interior point. Naturally, for a numerical scheme to be reliable, it must be proven to be stable under any small perturbation generated by the discretization.

At boundary points, not all the unknowns can be updated using the same discretized scheme as at interior points. Indeed, if the unknowns are recombined to form all terms u^{I} and u^{II}, it is clear that all combinations of the u^{I}-type must be defined by boundary conditions. Such a partition is necessary, regardless of the original choice of unknowns for interior points. I will, therefore, introduce the following

RULE. At boundary points, only quantities of the u^{II}- type, and all of them, must be evaluated using interior information; and all quantities of the u^{I}- type must be evaluated using the boundary conditions. If the rule is violated, arbitrary elements are introduced.

How not to violate the rule is the main subject of this paper. In addition, I will introduce some guidelines for the modeling of boundary conditions on open boundaries (the choices are not as numerous as commonly believed, and each choice expresses a different problem). These are necessary premises for the building of a numerical technique, consistent with the physics of the problem as a whole.

With the preparatory work properly done, is there any chance of failure? Certainly, if instabilities develop. This may occur, even when the integration scheme for interior points is stable, as a result of the interaction between such a scheme and the procedure used at the boundaries. Methods exist for testing this kind of stability; when the test is satisfied, the numerical initial-boundary-value problem is said to be well-posed. The most efficient method is the "normal mode analysis" developed by Kreiss (see, for example, refs. 1, 2, 3).

I recommend testing the well-posedness of a code according to such formal rules, although I expect well-posedness to follow automatically if the advice given in this paper is followed.

By the same token, I anticipate trouble if the advice is not followed. In this respect, I believe that a word of warning must be given to inexperienced readers who may work in a formal way, missing the main points. The mathematical style, unfortunately, does not facilitate communication with the majority of people who have to set up a computational code in practice. Misreading can be particularly dangerous when a procedure is accepted as usable but it was, instead, only mentioned, perhaps negatively, in the course of an academic exercise. For example, most of the time, the complex analysis of ref. 3 deals with techniques which violate the Rule, that is, with techniques which should not be used in practice; but no word of warning is given. I will begin my discussion with one-dimensional considerations, for the sake of clarity.

ONE-DIMENSIONAL PROBLEMS

Some of the basic concepts can be examined in the framework of one-dimensional problems (x, t are the space and time coordinates, respectively). Euler's equations for one-dimensional or quasi-one-dimensional problems are quasi-linear and hyperbolic. At each point, they possess three characteristics, a "right-running" characteristic, defined by $dx/dt=u+a$, a "left-running" characteristic, defined by $dx/dt=u-a$, and the particle path, defined by $dx/dt=u$ (u and a are the particle velocity and the speed of sound, respectively). The Riemann quantities, $a/\delta+u$ and $a/\delta-u$ (where $\delta=(\gamma-1)/2$ and γ is the ratio of specific heats), are propagated along right-running and left-running characteristics, respectively; if the flow is strictly one-dimensional and homentropic, they are actually constant along such lines (whence their name of "invariants"). Entropy is always convected, unchanged, along a particle path.

For the sake of simplicity, let us consider first a strictly one-dimensional, homentropic problem. It can be formulated in divergence form:

$$\begin{aligned} \rho_t + (\rho u)_x &= 0 \\ (\rho u)_t + (p + \rho u^2)_x &= 0 \end{aligned} \qquad (1)$$

or in non-conservative form:

$$\begin{aligned} P_t + uP_x + \gamma u_x &= 0 \\ u_t + uu_x + TP_x &= 0 \end{aligned} \qquad (2)$$

In the first set, ρ is the density and p is the pressure, obtained from ρ via the isentropic relation; in the second, P is the logarithm of pressure and T is the temperature, obtained from P, similarly. Neither set is as good for numerical analysis as the following, equivalent set:

$$R_{it} + \lambda_i R_{ix} = 0 \qquad (i=1,2) \qquad (3)$$

where

$$R_1 = a/\delta - u, \qquad R_2 = a/\delta + u \tag{4}$$

$$\lambda_1 = u - a, \qquad \lambda_2 = u + a \tag{5}$$

Set (3) suggests a numerical procedure in which the domains of dependence of R_1 and R_2 are clearly defined; therefore, signals proceeding from one side can be approximated using information from that side only, without introducing spurious information. Such a technique can easily be extended to non-homentropic flows. Its origin may be traced to a paper by Courant, Isaacson and Rees (ref. 4). The technique has been recently exploited by the numerous schemes of the λ-family (refs. 5,6,7,8).

Interaction of techniques for interior and boundary points

Now, let us interpret some passages of ref. 3. The system of partial differential equations studied in that paper,

$$u_t = A\,u_x + B\,u + F$$

is in the form of eqs. (3) above. Nevertheless, the authors decided to investigate numerical techniques which are formulated in a different way (a natural consequence of the computational style of the sixties). Instead of one-sided derivatives, as naturally suggested by eqs. (3) for the λ-schemes, other schemes such as Lax-Wendroff and leap-frog are considered. These schemes use centered derivatives. Therefore, they violate the law of forbidden signals, which is consistent with the partition of the vectors u^I and u^{II} (which, in the present instance, are the R_i). Such an inconsistency of the integration scheme with the physics of the flow appears in all its ugliness in transonic regions. In subsonic regions the schemes may work reasonably well. It should be clear, though, that special care has to be applied at the boundaries, if an integration technique for interior points is used, which is unfit to handle the boundary.

Let us see first the consequences of starting from eqs. (3) and using a λ-scheme, in which (for subsonic flows) R_1 is computed using only forward information and R_2 only backward information. If the problem is to be solved to the right of x=0, at the boundary itself R_2 cannot be computed directly; it must, therefore, be determined by a boundary condition. Not considering open, supersonic boundaries which, obviously, present no difficulties, we examine six cases:

(a) The boundary is a rigid, fixed wall. R_1 is determined as at any interior point and, since $u = 0$ at the wall, a and R_2 become known from eqs. (4).

(b) The boundary is a wall, moving with a velocity V. By letting

$$\xi = x - V\,t, \qquad \tau = t, \qquad \Lambda_i = \lambda_i - V \tag{6}$$

eqs. (3) are replaced by

$$R_{i\tau} + \Lambda_i R_{i\xi} = 0 \qquad (i=1,2) \tag{7}$$

and the same arguments as in (a) hold, except that $u=V$ at the boundary.

(c) The boundary is traversed by an incoming flow, strictly one-dimensional and subsonic, and all perturbations have been produced in the computational region. In this case,the flow crossing the boundary can only be a left-running simple wave, through which R_2 is a constant. The boundary condition, then, is

$$R_{2t} = 0 \qquad \text{at } x=0 \tag{8}$$

This equation and the one defining R_{1t} from the interior, as above, solve the problem.

(d) The boundary is traversed by an incoming flow, which is subsonic, but right-running waves may cross the boundary. Such a situation occurs, for example, in quasi-one-dimensional problems, where the geometry of the duct varies up to the boundary, and no simple wave concept can be applied. In this case, a physical model of the outside must be provided and the choice of it depends on the nature of the problem. In many cases in which a steady state is asymptotically reached (for example, in problems involving nozzle design), a good model consists of assuming that the flow proceeds from an infinite capacity where the total temperature is prescribed. The boundary condition:

$$a_t = - \delta \frac{u}{a}\, u_t \qquad \text{at } x=0 \tag{9}$$

obviously follows. From eqs. (4) we get

$$R_{2t} = \frac{u - a}{u + a} R_{1t} \qquad \text{at } x=0 \tag{10}$$

(e) The boundary is traversed by an outgoing flow (to be computed on the left of $x=0$), strictly one-dimensional and subsonic, and all perturbations have been produced in the computational region. The flow crossing the boundary can only be a right-running simple wave, through which R_2 is a constant. The boundary condition, then, is

$$R_{1t} = 0 \qquad \text{at } x=0 \tag{11}$$

This equation and the one defining R_{2t} from the interior solve the problem.

(f) The boundary is traversed by an outgoing flow, which is subsonic, but left-running waves may cross the boundary. Only one boundary condition can be imposed. Note that, in establishing a boundary, we declare our ignorance of all details of the external world and we are forced to replace it with a model. A good one consists of assuming that the gas flows into an infinite capacity where the pressure, p_∞, is prescribed. We consider the boundary as a partition, on the inner side of which R_2 can be determined whereas, on the outer side, $P_{\infty t}$ is given and the velocity, u_∞, is yet unknown. The continuity equation, written between the two sides of the boundary, reads:

$$\frac{a_t}{\delta a} + \frac{u_t}{u} = \frac{P_{\infty t}}{\gamma} + \frac{u_{\infty t}}{u_\infty} \tag{12}$$

The total energy must be conserved in the boundary crossing, as well as the entropy. Therefore, the energy equation can be written in the form:

$$a a_t + \delta u u_t = \frac{\delta}{\gamma} a_\infty^2 P_{\infty t} + \delta u_\infty u_{\infty t} \tag{13}$$

The unknown $u_{\infty t}$ can be eliminated between eq. (12) and eq. (13); the equation thus obtained:

$$(a^2 - u_\infty^2)\, a_t/a + \delta(u^2 - u_\infty^2)\, u_t/u = \delta(a_\infty^2 - u_\infty^2)\, P_{\infty t}/\gamma \tag{14}$$

together with the definition of R_{2t} determine a and u. Obviously, a simple relation between R_{2t} and R_{1t} can be obtained in this case as well as in the previous ones:

$$R_{1t} = \frac{a+u}{a-u} R_{2t} - \frac{2ua}{a-u} \frac{a_\infty^2-u_\infty^2}{\gamma(a^2-u_\infty^2)} P_{\infty t} \qquad (15)$$

The sample of cases is not exhaustive but similar arguments can always be used, and it can always be shown that, if a discretization of eqs. (3) is used which emphasizes the role of the domains of dependence, the boundary conditions can be enforced without introducing physical arbitrarinesses and/or new procedures at the boundary points. In ref. 9, some results have been presented, the accuracy and stability of which are evident.

One may start appreciating how important the choice of a good integration scheme for interior points is for a proper handling of the boundary conditions. If any scheme, other than those of the λ-family, is used for interior points, some special treatment of the boundaries must be introduced, in order to isolate the Riemann variable which is defined from the interior. This happens if the discretization is applied to the equations in the form of eqs. (1) or (2), which was common, but not necessarily correct practice in the past. In building up the boundary point scheme, though, one should only define R_1 from the interior, not other variables or combinations thereof. When evaluating R_1 alone, one is naturally brought to use one equation, based on the concept of characteristics and, again, the procedure does not introduce arbitrary elements. In all my work prior to 1978, when I was integrating eqs. (2), mostly using the two-level MacCormack scheme, at the (x=0) left boundary, I always evaluated the combination:

$$P - \frac{a}{\gamma} u$$

(which is equivalent to R_1 for isentropic flows) instead of P and u separately. The procedure satisfies the Rule. It is, however, not as direct as the ones discussed above in connection with the use of eqs. (3); it requires additional coding and, obviously, the boundary point procedure is so different from the procedure for interior points that differences in truncation errors may occur and continuously be fed back into the region of interest. Nevertheless, results were always stable and, as far as we could compare with reliable benchmarks, accurate.

In the following section, I will show what is physically wrong with prescribing one of the variables, either P or u, at the inlet. If one attempts, instead, to evaluate P and u separately from the interior, then one needs two equations and, of course, the calculation becomes redundant and the Rule is violated. With these simple considerations in mind, one does not feel an urgent need for a large part of the existing literature.

Let us go back, for example, to ref. 3 and browse through its 37 pages as an inexperienced mathematician, looking for practical advice, would do. At page 661 we find three ways to compute R_1 at a boundary, using interior point information, prior to applying the boundary conditions to get R_2 (eqs. (6.3)). The second and, in a more complicated way, the third, use the correct method of characteristics, but the first is simply an extrapolation. The fact that the Lax-Wendroff method is stable when extrapolations at the boundaries are used tends to legitimate rudimentary methods for the treatment of boundaries which were found unacceptable fifteen years ago (ref. 10). The fact that the Lax-Wendroff method, which is dissipative, can stand the test whereas the leap-frog method, which is nondissipative, cannot, tends to suggest a need for dissipative mechanisms, which is totally unnecessary if a technique is used which is physically consistent.

The ultimate confusion is produced when the leap-frog method, which carries information to the right, without dissipation, is used to integrate (to the right of $x=0$) the equation

$$u_t - u_x = 0$$

which has a single family of characteristics, running to the left (ref. 11). Obviously, in this problem no boundary conditions are needed, because the line $x=0$ is not traversed by any signal proceeding from the left. Therefore, all values must be computed from the interior, but in a physically consistent way, that is, by stating that signals are carried to the boundary along left-running characteristics. If the boundary is treated accordingly, the amount of perturbation is minimized and the calculation proceeds as well as the leap-frog scheme permits elsewhere. This boundary treatment (not a boundary condition) is mentioned as acceptable at the very end of ref. 11, after a lengthy discussion of other obviously unacceptable techniques.

In addition to misinterpreting these early papers, many authors have shown a total lack of constructive curiosity, in not inquiring whether numerical methods, which should interpret the physics of a problem, really require more boundary conditions than the physics itself. The answer to the question, of course, should be an unqualified No. We find, instead, a large number of recent papers which keep dealing with the subject, making the same mistakes as pointed out above and even amplifying them. See, among the most recent contributions to confusion,† ref. 12 and, particularly, ref. 13, page

---

†See note added in print on page 94.

328 (which are mentioned as a random sample, not meaning to single them out).

I feel obliged to repeat what I said in 1968 (ref. 10):

Any extrapolation, being an act of arbitrariness, is wrong by definition.

Overspecification is also wrong.

And, as I am going to show in the next section, *using conditions which are mathematically acceptable does not mean that the problem is physically correct* (for example, because the boundary generates entropy when it is not supposed to do so).

Practical problems

Perplexity, to put it mildly, stems from lack of understanding of the physical role of the boundary conditions and of the physical consistency of their numerical treatment. In addition, one should never forget that a problem must be examined as a whole, so that the flow evolution depends not only on the events at one boundary but on the interaction of the two boundaries and of the interior as well.

For the following discussion, let us consider a duct with a variable cross-sectional area and lift the restriction of homentropic flow. Eqs. (3) must be replaced by

$$S_t = - u\, S_x \tag{16}$$

$$R_{it} = aS_t - \lambda_i(R_{ix} - a\, S_x) - au\alpha \qquad (i=1,2) \tag{17}$$

where S is the entropy divided by the gas constant and by γ, and α is the logarithmic derivative of the cross-sectional area of the duct. In the spirit of the λ-scheme, for subsonic, positive u, the x-derivative of S in eq. (16) is approximated by backward differences, and the x-derivatives of R_i and S in eqs. (17) are approximated by forward and backward differences for i=1 and 2, respectively.

Going back to page 426 of ref. 1, and interpreting it in the context of one-dimensional flows, we see four combinations of parameters mentioned as acceptable, when prescribed at an inflow (left) boundary. In our notation, they are:

(1) total temperature, T_o, and R_2,

(2) T_o and u,

(3) T_o and p,

(4) u and ρ.

To these, we add the combination which we consider most appropriate for asymptotically steady flows:

(5) T_o and S.

Our choice (5) is again justified by the model of a flow proceeding from an infinite capacity, where the gas is stored with a prescribed total energy, and which flows to the inlet without changing entropy, or increasing it by a prescribed amount. The interaction between outgoing perturbations and incoming flow does not produce entropy waves and does not produce work. Therefore, according to eq. (16), the entire flow in the duct tends to become homentropic, even if it was not so initially.

If choice (1) is made (a rather difficult one to be given a practical interpretation), eq. (9) and the definition of R_2 tie a_t and u_t, while eq. (17) with $i=1$ ties a_t, u_t and S_t. The entropy at the inlet is thus determined as a consequence of the imposed conditions. Physically, this amounts to describing a mechanism which produces or destroys entropy without altering the total energy. Without discussing the practical merits of a model of this kind, let us only see what consequences it may have on the calculation. At this stage, we must consider the outlet boundary as well, and let us assume that model (f), prescribing the pressure, is used. Entropy waves, produced at the inlet, will be convected along the duct. At the exit, where the pressure is prescribed, the changing entropy will produce changing values of a and u. These values will be carried back along the left-running characteristics, reach the inlet and interact again with the boundary conditions to produce a new change in entropy. These changes may produce instabilities, or periodical oscillations, or a steady state of a sort, according to the value of the exit pressure and the geometry of the duct. Generally, a convergent duct tends to stabilize a subsonic flow, and a divergent duct tends to amplify perturbations produced at the inlet and destabilize the flow.

Similar considerations can be made for choices (2) and (3). In case (4), ρ provides a relation between a and S which, together with eq. (17) for $i=1$, determines a; and R_2 follows, since u is prescribed. Nevertheless, neither S nor T_o maintain a constant value, because S is again determined by the interaction between left-running waves and a prescribed ρ, and eq. (9) is generally not satisfied. The mass flow is the only quantity which remains constant at the inlet, if ρ and u are constant; but this does not prevent the flow in the duct from becoming unstable.

In conclusion, the analysis of mathematically acceptable conditions for one single boundary does not guide to the choice of a proper set of conditions, which has to be made on the study of the problem as a whole.

TWO-DIMENSIONAL PROBLEMS

Increasing the number of space-like dimensions by one not only increases the amount of computations to perform but changes the nature of the problem and makes it extremely more difficult to solve. In one-dimensional problems, the characteristics define the directions along which signals propagate and the signals themselves (the Riemann variables and the entropy) are clearly defined. Mathematically, this is expressed by saying that the matrix A in the equations of motion, written in vector form as

$$u_t + A\,u_x + C = 0 \tag{18}$$

can be diagonalized. The equations of motion become ordinary differential equations along the characteristics. Each family of signals is, as much as possible, uncoupled from each other family.

With one more space dimension, signals are propagated along surfaces (typically, the Mach conoids). The two-dimensional counterpart of eq. (18) is

$$u_t + A\,u_x + B\,u_y + C = 0 \tag{19}$$

No matter how the basic variables are defined, and how integration paths on the conoids are chosen, the equations of motion cannot be reduced to ordinary equations so that the integration of any variable along a generator of a conoid depends on derivatives taken in a perpendicular direction. This is because the matrices A and B in eq. (19) cannot be diagonalized simultaneously. At first sight, it seems that there is no proper way to discriminate among domains of dependence of different signals, and that all advantages shown by equations such as eqs. (3) are lost. Consequently, it may seem that integration schemes not based on the concept of characteristics, although clearly unsatisfactory from a physical point of view, should be adopted, for lack of better procedures. The boundary conditions seem to be similarly affected. The closest one can get to the one-dimensional analysis is by recasting the equations of motion in such a way that the normal to the boundary is evidenced, and the velocity vector is decomposed into a normal and a tangential component. Considerations may be made along the normal which are very similar to the ones made for one-dimensional problems.

We will show that the boundaries can be treated without introducing arbitrary procedures. First, we will determine which conditions must be used and give examples of proper ways to use them. Then, we will introduce an integration scheme which naturally blends with the procedure used at the boundaries.

Rigid walls

Let us consider the rigid boundary and the open boundaries separately. For the rigid boundary the condition of vanishing of the normal velocity is sufficient. When integration schemes such as Lax-Wendroff, MacCormack or leap-frog are used for interior points, one easily slips into redundancy if one attempts to compute each variable separately and then impose the boundary condition (ref. 10). There is only one sequence of steps which avoids redundancy and is physically acceptable:

(1) Integrate S along the wall,

(2) Integrate the velocity along the wall,

(3) Integrate a generalized Riemann variable, containing the velocity component normal to the wall, using the boundary condition,

(4) Determine the velocity components in the given frame of reference by using the modulus of the velocity and the boundary condition again.

The first two steps are justified because the wall is a streamline; the energy equation and the relevant momentum equation can be written in the form:

$$S_t + q\, S_X = 0 \tag{20}$$

$$q_t + q\, q_X + \frac{a}{\delta} a_X - a^2 S_X = 0 \tag{21}$$

where q is the modulus of the velocity and X is the arc length along the wall. Therefore, S and q are obtained using only information from the wall. The third step is in line with the one-dimensional analysis. The normal velocity component vanishes at the wall, so that the third step provides a, or P. The fourth step is simply a redistribution of the velocity components according to the given frame.

Inflow boundaries

At an inflow boundary with subsonic flow, the tangential velocity component, or the slope of the velocity vector, as well as the entropy, depend on outside information. Another condition must be written along the normal; considerations similar to the ones presented in the one-dimensional case can be made. Once more, certain combinations of prescribed quantities produce entropy or unaccountable work, and should be avoided.

Typically, open boundaries occur in two categories of problems. The first contains flows in channels, with an inflow and an outflow boundary across the channel. Cascade flows can also be ascribed to this category, with some rigid walls replaced by a periodicity condition. Whatever crosses the inflow boundary, it comes from a more or less distant region where the physical state is assumed as known but about which, most of the times, one possesses only an imperfect description. For example, one can imagine the gas coming from an infinite capacity with gas practically at rest, or from a combustion chamber where energy is globally added according to a certain law, perhaps as a function of time, or, finally, from a supersonic intake in front of which the gas may pulsate and produce strongly irrotational flows, etc. Models of this kind suggest the use of T_o and S as parameters to be prescribed outside the inflow boundary. In addition, something has to be prescribed, related to the tangential velocity component, v which, as we said above, cannot be evaluated on the basis of interior information. Nevertheless, prescribing v itself is not advisable; in fact, the modulus of the velocity is already made to depend on T_o and S so that not v, but the slope of the velocity, $\sigma = v/u$, is a better choice. In a channel flow, σ is obviously known on the walls; in between, it must be guessed. A simple distribution of σ between the walls can be prescribed; for example, a linear distribution of σ between its values at the lower and upper wall. Physically, we can always justify it by thinking of a series of vanes, distributed along the inlet, to guide the flow without producing work. In addition to its practicality and to its closeness to an experimental setup, the model is safe because minor changes in σ at the inlet do not affect the flow at a relatively short distance.

Outflow boundaries

At the exit, one can follow the trend established by the one-dimensional analysis. The model of the outside world, however, is not complete without a specification of the flow direction at infinity. We are, thus, brought to imagining a series of vanes, located astride the boundary, which deflect the flow into a region where the pressure is prescribed. As in the one-dimensional case, the continuity equation must be written between the two sides of the boundary, together with the conservation of total energy and the non-restrictive condition of isentropy at the boundary crossing.

Denoting by an index, ∞, the values of P, u and σ outside the boundary, the continuity equation, eq. (12), remains unchanged and the energy equation can be written in the form:

$$aa_t + \delta uu_t + \delta vv_t = \frac{\delta}{\gamma} a_\infty^2 P_{\infty t} + \delta u_\infty u_{\infty t}(1+\sigma_\infty^2) + \delta u_\infty^2 \sigma_\infty \sigma_{\infty t} \tag{22}$$

In these two equations, $P_{\infty t}$, $\sigma_{\infty t}$ and v_t are known (v depends only on inside information); therefore, three unknowns remain, a_t, u_t and $u_{\infty t}$. The system is closed by a compatibility equation along a line reaching the boundary from the interior (a two-dimensional counterpart of a right-running characteristic compatibility equation in our previous one-dimensional analysis).

It is worth noting that in the preceding considerations there is no requirement for any boundary to be only an inflow boundary or an outflow boundary. The boundary can allow the flow to proceed in both directions in any of its portions, provided that the code switches automatically from inflow to outflow calculations wherever and whenever the normal velocity changes in sign. A pretty example of a calculation of this type has been given in ref. 14. By the same token, there are no restrictions in having the flow partly subsonic and partly supersonic along the same boundary.

Flows extending to infinity

The second type of problems is related to the analysis of flows surrounding finite bodies and extending to infinity. Such flows are usually considered as steady and uniform at infinity and one generally expects to find a steady flow in the vicinity of the body as well. The inner boundary of the flow is the wall of the body and there is no outer boundary, in principle. In practice, however, the calculation must be confined to a finite region and an artificial boundary must be introduced.

There is, indeed, a way to avoid considering an artificial boundary if the problem is started with the body at rest and the gas around it at rest. The body is then accelerated to a cruising speed, equal and opposite to the preceding velocity at infinity. The flow is then to be computed within a growing perturbation front, along which the boundary conditions are clearly defined (ref. 15). Since a steady state sets in very rapidly near the body, as soon as the cruising speed is reached, the computational region does not necessarily grow beyond unacceptable limits.

If one prefers to use a smaller region, with a fixed outer boundary, once more one has to choose a model for the inflow portion and a model for the outflow portion of it.

Now, the incoming flow at infinity is undoubtedly homentropic and homenergic; therefore, the assumptions of $^{-}_{o}$ and S constant in space and time along the inflow boundary are correct. At the outflow boundary, the assumptions that the pressure at infinity is constant and the flow is not deflected are acceptable and not inconsistent with part of the outgoing flow having a different entropy (if shocks occur inside the computed region). The model is thus clearly stated, as above for the channel flow, again with the exception of the inflow values of σ. Here too a reasonable guess on the distribution of σ along the inflow boundary must be made.

Improved methods
for two-dimensional flows

The current trend to solve eq. (19) is towards methods which emphasize the concept of characteristics as much as possible. Embryonically, the idea is applied in the original two-dimensional λ-scheme (ref. 5) but a much better physical interpretation of it is given in ref. 6, and can be explained with the help of fig. 1, which is suggested by that paper. Here we assume that the computational grid is orthogonal, and that the flow is homentropic. Let P be the point to be computed, and $\vec{V}$ the velocity vector. The circle represents the base of the Mach conoid having its apex at P. All signals affecting P travel along generators of the cone. If the four generators shown in the figure and numbered 1,2,4,5 are chosen, four compatibility equations can be written along them. Each equation contains generalized Riemann variables of the type

$$R_i = \frac{a}{\delta} \pm u \qquad (i=2,1)$$

$$R_i = \frac{a}{\delta} \pm v \qquad (i=5,4) \qquad (23)$$

and the directions of the generators are defined by corresponding values:

$$\begin{aligned} \lambda_i &= u \pm a \qquad (i=2,1) \\ \lambda_i &= v \pm a \qquad (i=5,4) \end{aligned} \tag{24}$$

In addition, we define the auxiliary symbols:

$$R_3 = v, \quad R_6 = u, \quad \lambda_3 = u, \quad \lambda_6 = v \tag{25}$$

Actually, only three unknowns (a,u,v) must be computed at P, so that one equation is redundant. Nevertheless, following Butler (ref. 16), we take advantage of the redundancy to eliminate the cross-derivatives which appear in all compatibility equations. When discretizing, the position of the generators with respect to the grid in fig. 1 will determine how derivatives have to be approximated. For example, R_{2x} will be approximated by backward differences, R_{2y} by backward differences too; R_{4x} by backward differences again but R_{4y} by forward differences.

A second-order accurate, two-level scheme can be devised (ref. 17) which integrates the equations of motion, written in the form:

$$\begin{aligned} a_t &= \frac{\delta}{2} (f_1 + f_2 + f_4 + f_5) \\ u_t &= \frac{1}{2} (f_2 - f_1) + f_6 \\ v_t &= \frac{1}{2} (f_5 - f_4) + f_3 \end{aligned} \tag{26}$$

(for the sake of simplicity, we have omitted additional terms which do not contain derivatives of the unknowns and are produced by non-Cartesian, but orthogonal frames of reference). Here,

$$\begin{aligned} f_i &= - \lambda_i R_{ix} \qquad (i=1,2,3) \\ f_i &= - \lambda_i R_{iy} \qquad (i=4,5,6) \end{aligned} \tag{27}$$

The splitting (which is almost identical with the one obtained by the original λ-scheme) is convenient to update the variables at the corrector level, when information has to be taken from different directions according to the index of f_i, that is, according to the sign of λ_i.

Suppose now that a rigid boundary has to be computed, defined by $y=1$, with the flow in the region defined by $y<1$. The boundary condition is:

$$v = 0 \qquad (28)$$

and fig. 1 should be replaced by fig. 2. Information necessary to evaluate f_1 and f_2 is available along the wall; f_3 and f_6 vanish identically because of eq.(28), and f_5 can be computed from the interior of the flow. Only f_4 remains unknown, and it can obviously be defined using the last of eqs. (26) with v_t=0:

$$f_4 = f_5 \qquad (29)$$

The problem is solved.

Consider now an inflow subsonic boundary, along the x=0 line (fig. 3). Let us assume that the slope of the velocity vector,

$$\sigma = v/u \qquad (30)$$

is given as a function of y but, for simplicity, constant in time. It follows that

$$v_t = \sigma\, u_t \qquad (31)$$

Let us also assume that the total temperature is considered constant in space and time. Therefore, an equation similar to eq. (9) follows:

$$a_t = - \delta(1 + \sigma^2)\, \frac{u}{a}\, u_t \qquad (32)$$

An inspection of fig. 3 shows that f_1 can be determined from the interior of the flow, f_4, f_5 and f_6 are computed using only information along the boundary, whereas f_2 and f_3 must be evaluated using the two boundary conditions, eqs. (31) and (32). Once more, the problem is physically well posed, there is no redundancy in the numerical procedure, and the scheme is consistent with the scheme for interior points.

The application of eqs. (31) and (32) is indeed straightforward. From eq. (32) and the first two equations (26), one obtains:

$$f_2 = \frac{(A-1)f_1 - (f_4 + f_5 + 2Af_6)}{A + 1} \qquad (33)$$

where

$$A = (1 + \sigma^2)\,\frac{u}{a}$$

and from eq. (31) and the last two equations (26), one obtains

$$f_3 = \frac{1}{2}\left[f_4 - f_5 + \sigma(f_2 - f_1 + 2f_6)\right] \tag{34}$$

At an outflow boundary, the same fig. 3, considered as having the interior of the computational region to the left of the y-axis, shows that only one condition must be imposed. Sometimes it is sufficient, for example, to impose a, which provides f_1 through the first eq. (26), or M, which again yields f_1 but through a combination of the first two eqs. (26). The value of v_t is totally determined from the interior. In a more sophisticated way, one can eliminate $u_{\infty t}$ between eq.(12) and eq. (22) and use eqs. (26) to get

$$f_1 = \frac{C - (A+B)f_2 - (a-v)f_4 - (a+v)f_5 - 2vf_3 - 2Bf_6}{A - B} \tag{35}$$

where

$$A = [a^2 - u_\infty^2(1+\sigma_\infty^2)]/a, \quad B = [u^2 - u_\infty^2(1+\sigma_\infty^2)]/u$$

$$C = u_\infty^2\sigma_\infty\sigma_{\infty t} + P_{\infty t}\,[a_\infty^2 - u_\infty^2(1+\sigma_\infty^2)]/\gamma$$

Boundary points which belong to two boundaries can be treated in a similar way. Consider, for example, point P in fig. 4, which belongs to a wall ($y=0$) and to an inflow boundary ($x=0$). As we said before, f_3 and f_6 vanish identically, because $v=0$. Two quantities cannot be determined from the interior: f_2 and f_4. Two conditions are also available at P, one given by eq. (32) and the other either by eq. (28) or by eq. (30), which are equivalent. Eq. (29) follows, and then f_2 is determined from eq. (33) with $f_4 = f_5$; the vanishing of f_3 is identically satisfied by eq. (34).

Non-orthogonal meshes

It remains to discuss the case when non-orthogonal meshes are used. To show how the method works, without complicating the algebra unnecessarily, let us assume that a non-orthogonal mesh is obtained from a basic Cartesian mesh by the affine transformation:

$$X = x, \qquad Y = y/\alpha x \tag{36}$$

The mesh is convenient for the analysis of the flow in a duct with a straight wall along the x-axis and another straight wall defined by $y = \alpha x$, so that $Y = 0$ and $Y = 1$ at the two walls, respectively. Since for any function, ϕ:

$$\phi_x = \phi_X + \phi_Y Y_x, \quad \phi_y = \phi_Y Y_y \tag{37}$$

the equations of motion, eqs. (26), must be replaced by the more complicated equations:

$$\begin{aligned} a_t &= \frac{\delta}{2} (f_1 + f_2 + f_4 + f_5 + f_7 + f_8) \\ u_t &= \frac{1}{2} (f_2 - f_1 + 2f_6 + f_8 - f_7) \\ v_t &= \frac{1}{2} (f_5 - f_4 + 2f_3) \end{aligned} \tag{38}$$

with

$$\begin{gathered} B = u\, Y_x + v\, Y_y \\ \lambda_4 = B - aY_y, \quad \lambda_5 = B + aY_y, \quad \lambda_6 = B \\ \lambda_7 = - aY_x, \quad \lambda_8 = aY_x \\ f_7 = - \lambda_7\, R_{1Y}, \quad f_8 = - \lambda_8\, R_{2Y} \end{gathered} \tag{39}$$

and the other definitions in eqs. (24),(25) and (27) unchanged, except for replacing x and y with X and Y, respectively.

Since $Y_x = - Y/x < 0$, the domains of dependence of f_7 and f_8 at the upper wall are as shown in fig. 5. At the upper wall, the boundary condition is

$$v = \alpha\, u \tag{40}$$

It is clear, thus, that B vanishes identically, so that $f_6 = 0$ as well. The X-related terms, f_1, f_2 and f_3 are computed along the wall. Of the remaining terms, f_5 and f_7 are computed from inside, but f_4 and f_8 must be determined otherwise. It seems here that, since we have only one boundary condition, eq. (40), at our disposal, and two unknowns to determine, we have fallen again into a problem of redundancy. This is not true, however, because the physics of the flow on the boundary provides us with an additional piece of information. The wall is a streamline, along which the relevant momentum equation can be written in the form shown in eq. (21), containing no Y-derivatives. If we express q_t in terms of u and v, using the last two eqs. (38) and eq. (40), we obtain

$$q \lfloor f_2 - f_1 + f_8 - f_7 + \alpha(f_5 - f_4 + 2f_3) \rfloor \tag{41}$$

Therefore, the sum of terms in eq. (40) containing Y-derivatives must vanish; this yields the needed additional condition:

$$f_8 - f_5 = \alpha\ (f_4 - f_5) \tag{42}$$

CONCLUDING REMARKS

Techniq[illegible] handling of boundary conditions must be devised keeping in mind that

(1) No numerical arbitrariness is allowed; the numerical technique should use all the boundary conditions which are prescribed physically and no other conditions,

(2) A physically consistent model of the outside world must be provided, when the boundary is open; such a model is not necessarily equivalent to common assumptions of steady state theoretical analyses, such as a uniform flow at infinity.

I have shown how the first requirement can be satisfied. The second is completely independent from the first; I have given some examples of proper choices of models.

Recent applications of the concepts discussed in this paper can be found in refs. 9, 14, and 17 through 21.

REFERENCES

1. Oliger, Joseph and Sundström, Arne, Theoretical and practical aspects of some initial boundary value problems in fluid dynamics, SIAM Appl. Math. 35, 1978, pp. 419-446.

2. Kreiss, Heinz-O., Initial boundary value problems for hyperbolic equations, Comm. Pure Appl. Math., 23, 1970, pp. 277-298.

3. Gustafsson, Bertil, Kreiss, Heinz-O. and Sundström, Arne, Stability theory of difference approximations for mixed initial boundary value prob-

lems, II, Math. Comp. 26, 1972, pp. 649-686.

4. Courant, Richard, Isaacson, E. and Rees, M., On the solution of nonlinear hyperbolic differential equations by finite differences, Comm. Pure Appl. Math. 5, 1952, pp. 243-249.

5. Moretti, Gino, The λ-scheme, Comp. and Fluids 7, 1979, pp. 191-205.

6. Zannetti, Luca and Colasurdo, Guido, Unsteady compressible flow: a computational method consistent with the physical phenomena, AIAA J. 19, 1981, pp. 852-856.

7. Zhu, You-lan and Chen, Bing-mu, Difference methods for initial-boundary-value problems and computations of flows around bodies, Comp. and Fluids 9, 1981, pp. 339-363.

8. Chakravarthy, Sukumar, Anderson, Dale and Salas, Manuel D., The split coefficient matrix method for hyperbolic systems of gasdynamic equations, AIAA Paper No. 80-0268, 1980.

9. Moretti, Gino, Towards a closer cooperation between theoretical and numerical analysis in gas dynamics, Proc. Symp. on transonic, shock and multidimensional flows, Univ. of Wisconsin, Madison, Wisc., May 1981 (to appear).

10. Moretti, Gino, Importance of boundary conditions in the numerical treatment of hyperbolic equations, Phys. of Fluids, 12, Suppl. II, 1969, pp.II-13-20.

11. Kreiss, Heinz-O., Difference approximations for initial boundary-value problems, Proc. Roy. Soc. London A 323, 1971, pp. 255-261.

12. Yee, H.C., Beam, R.M. and Warming, R.F., Stable boundary approximations for a class of implicit schemes for the one-dimensional inviscid equations of gas dynamics, Proc. 5th AIAA Comp. Fluid Dyn. Conf., 1981, pp. 125-135.

13. Rudy, David H. and Strikwerda, John C., Boundary conditions for subsonic compressible Navier-Stokes calculations, Comp. and Fluids 9, 1981, pp. 327-338.

14. Zannetti, Luca and Pandolfi, Maurizio, Two-dimensional unsteady flow in shallow waters. Numerical analysis, Atti III Congresso Naz. AIMETA, vol IV, 1976, pp. 5.1-9.

15. Moretti, Gino, Transient and asympotically steady flow of an inviscid, compressible gas past a circular cylinder, AGARD Lecture series No. 48, 1972, pp 9(1-17).

16. Butler, D.S., The numerical solution of hyperbolic systems of partial differential equations in three independent variables, Proc. Roy. Soc. London A255, 1960, pp. 232-252.

17. Moretti, Gino, A new, improved computational technique for two-dimensional unsteady compressible flows (submitted to the AIAA Journal).

18. Moretti, Gino and Pandolfi, Maurizio, Critical study of calculations

of subsonic flows in ducts, AIAA J. 19, 1981, pp. 449-457.

19. Moretti, Gino, Experiments on initial and boundary conditions, Proc. Symp. on Num. and Phys. Aspects of Aerodyn. Flows, Long Beach, Cal. Jan. 1981 (in print).

20. Zannetti, Luca and Moretti, Gino, Numerical experiments on the leading edge flow field, Proc. 5th AIAA Comp. Fluid Dyn. Conf., 1981, pp. 149-155.

21. Pandolfi, Maurizio and Zannetti, Luca, Some permeable boundaries in multidimendional unsteady flows, Lect. Notes in Phys. 90 (Proc. 6th Int. Conf. on Numer. Meth. in Fluid Dynam.), 1978, pp. 439-446.

NOTE ADDED IN PRINT

At a recent ICASE workshop, the subject of treatment of boundary conditions was extensively debated. My discussions with Robert Warming and Saul Abarbanel brought us to conclude that the confusion mentioned above (page 8) depends on semantics. What are called numerical boundary conditions and, even worse, additional numerical boundary conditions in refs. 12, 13 and elsewhere, should actually be called numerical treatments of boundaries. My ideas on how to handle boundaries, as exposed in the present paper, are not necessarily in conflict with some of the treatments suggested in refs. 12 and 13.

Another semantic problem arises form the use of the word "extrapolation". Many people apply it to embrace all calculations of boundary points on the basis of inside information. In this paper, I meant to limit the word to all formulas which cannot be interpreted as representing physical propagation or convection.

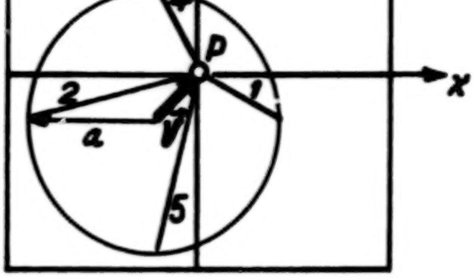

Fig. 1

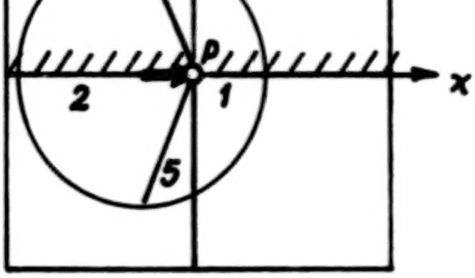

Fig. 2

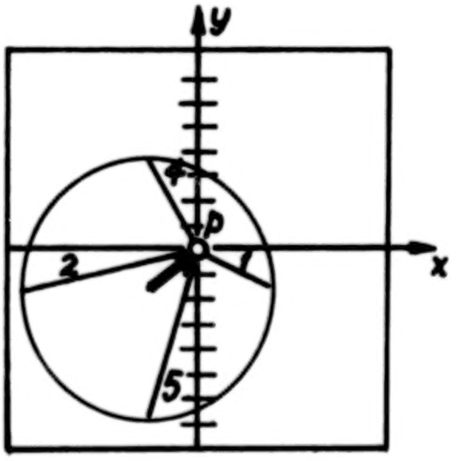

Fig. 3

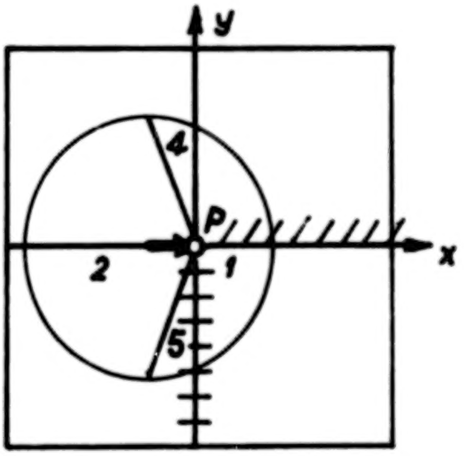

Fig. 4

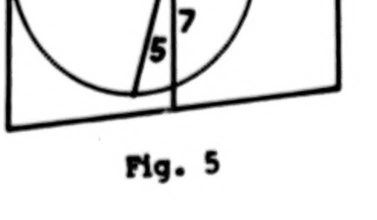

Fig. 5

Blank Page

THREE DIMENSIONAL BOUNDARY CONDITIONS IN SUPERSONIC FLOW

S. Rudman[†] and F. Marconi[†]

Grumman Aerospace Corporation
Research Department
Bethpage, New York 11714

ABSTRACT

A theoretical analysis of the flow pattern at a solid surface in three dimensional supersonic flow is presented. The purpose of the study is to develop the additional information necessary to overcome the nonuniqueness associated with the body tangency condition in three dimensions. The analysis is based on the fact that three dimensional waves propagate locally exactly as they do in axisymmetric flow when viewed in the osculating plane to the streamline. The supersonic flow over an infinite swept corner is examined by both the classical solution and the three dimensional solution in the osculating plane and the results are shown to be identical. A simple numerical algorithm is proposed which accounts for the three wave surfaces that interact at a solid boundary.

INTRODUCTION

Future success in the prediction of complex three dimensional supersonic flow fields will require increased theoretical understanding of such phenomena. In particular, the key to accurate and reliable numerical computations lies in the proper imposition of boundary conditions. A variety of three dimensional boundary point algorithms have been developed which are based on method of characteristic type analysis of the governing equations. The techniques reported in references 1-5 rely on the reduction of the full equations to a reference plane system in two space dimensions. The reference plane is employed in the vicinity of the boundary point in which the calculation is performed. The orientation of this plane relative to the boundary surface has been chosen, in the past, based on intuitive and ad hoc reasoning. Velocity components and gradients normal to the reference plane appear as forcing terms in the charactertistic equations. Theoretical analysis of the full three dimensional Euler equations (ref. 6) indicates that there is a unique plane in which the flow is equivalent to an axisymmetric (a two space dimension) flow. There is no velocity component normal to this plane and the only term appearing in the equations beyond the pure planar two dimensional expressions is a velocity gradient term analogous to that appearing in the axisymmetric equations. It is the object of this paper to study the implications of employing these concepts in the boundary point calculations involved in three dimensional supersonic flows.

[†] Senior Staff Scientist

The complexities of three dimensional flow calculations as compared to their two dimensional counterparts are manifest in the application of the boundary conditions. In two dimensional supersonic flow there is a well developed theoretical basis (c.f. refs. 7-9) upon which to model the numerical simulation of the boundary surface/flow interactions. Moretti (c.f. refs. 10,11) was the first to recognize that the standard finite difference algorithms employed for interior point calculations had to be replaced by a local solution based on the method of characteristics at solid boundary points as well as at shock points. Later, Abbett (ref. 5), showed how to combine finite difference calculations with a local Prandtl-Meyer solution at a solid boundary and thus greatly reduce the complexity of the boundary point calculation. DeNeff (ref. 12) and Rudman (ref. 13) extended this method to shock surface and contact surface boundary point calculations. The central new feature that arises in the three dimensional calculation is the nonunique nature of the boundary conditions. At a solid surface, for example, the boundary condition that the velocity vector be tangent to the surface is a single condition for the two unknown cross flow angles. In two dimensions a single flow angularity unambiguously determines the ratio of the two velocity components. In three dimension the surface tangency condition only determines a single linear relationship between the two cross flow velocities. This paper addresses the resolution of this ambiguity.

The boundary point algorithm under consideration employs first a finite difference calculation and then a "correction" to satisfy the surface tangency requirement. That is, the flow properties at the unknown point are computed using a variation of the finite difference scheme at the interior points. A modified interior point calculation is necessary because no mesh points are computed interior to the body. Either one sided differences away from the body are employed to model the cross derivatives or a reflection plane is used to define hypothetical flow properties at a plane one mesh width interior to the body. The flow properties so computed at the unknown point (fig. 1) do not in general satisfy the body tangency condition, and are denoted FD (finite difference). Following the methods of references 5,8 or 9 a wave is added to the solution at the boundary point (the correction) to bring the velocity in line with the desired direction. In two dimensional flow this is a simple Prandtl-Meyer wave. In three dimensional flow the orientation of the "correction" wave is not known a priori. Any rotation into the tangency plane satisfies the boundary condition. In the notation used in figure 1 the value of ϕ is unknown and must be determined from a detailed analysis of the flow.

The first step in developing the required information is recognizing that three dimensional supersonic flow is locally directly analogous to a two space dimension (axisymmetric) flow (ref. 6) when viewed in the osculating plane to the streamline. In supersonic flow all changes in flow properties are brought about by wave surfaces. Each wave surface in three dimensional flow when viewed locally is a plane wave moving at the local speed of sound relative to the fluid. The component of velocity normal to the wave front is sonic. Beyond that the orientation for the wave front is arbitrary so that it can rotate the oncoming velocity both vertically and horizontally depending on its strength and direction. In two dimensional flow, by contrast, the waves rotate the flow either upward or downward (first or second family waves) about an axis perpendicular to the plane of motion. In three dimensional flow the rotation takes place about the binormal vector to the local streamline direction. The direction of the local binormal vector is determined by the wave orientation.

In the following sections further discussion of the role of the osculating plane in three dimensional flow will be presented. These concepts identify two main bicharacteristics in the fore Mach cone (the intersection of the cone and the osculating plane) that determine the solution at any point. This description of the flow is then reconciled with the classical solution for flow over an infinite swept expansion (or compression) corner which is the prototype model for plane wave solutions. It is shown that the classical solution which is achieved by examining the flow in a plane normal to the sweep line is identical with the solution employing the osculating plane. For infinitesimal rotations the flow over the corner is a Prandtl-Meyer expansion (compression) for the total velocity vector. The rotation is about the binormal vector defined by $\nabla p \times \vec{q}$. At the body surface three wave fronts determine the solution; an incident wave, a reflected wave and a wave emitted by the body. In general, the sweep angle of the incident/reflected waves is different from that of the emitted wave. This is another manifestation of the three dimensionality of the flow. Each of the three waves has a binormal vector associated with it. In the context of numerical calculations these waves are considered infinitesimal, i.e. the body slope and the flow properties change in proportion to the step size. Because infinitesimal rotations can be added the rotations of each wave can be combined to yield a single binormal vector which defines the interaction at the body surface. A three dimensional boundary point calculation procedure is set forth based on these ideas. In the procedure the incident wave and reflected waves are computed as part of the finite difference calculation substantially simplifying the algorithm. The final rotation (correction) accounts for the emitted wave about the binormal vector associated with the change in body shape.

THREE DIMENSIONAL WAVES

A streamline in three dimensional space has the general properties of any line in space. Figure 2 shows the unit vector triad defined by the tangent, normal and binormal vectors at point 0. At 0 the velocity vector is parallel to the tangent vector. The streamline has a principal curvature in the normal direction. The acceleration of the fluid element at point 0 is in the t-n plane and the streamline remains in the t-n plane to second order. The streamline has a torsion in the binormal direction but this results in a higher order displacement. The Euler equations written using as local Cartesian coordinates t, n, b with velocity components, U, V, W are (ref. 6)

$$(\rho U)_t + (\rho V)_n + \rho W_b = 0 \quad (1)$$

$$\rho U U_t + \rho V U_n + p_t = 0 \quad (2)$$

$$\rho U V_t + \rho V V_n + p_n = 0 \quad (3)$$

$$p_b = 0 \quad (4)$$

$$\frac{1}{2}(U^2+V^2) + \gamma p/(\gamma-1)\rho = h_o \quad (5)$$

The fact that $W = 0$ at point 0 has been employed throughout. The momentum equation in the b direction (equation (4)) expresses mathematically the fact that there are no accelerations (or forces) in the b direction. Equations (1) - (3) and (5) are the familiar Euler equations in two space dimensions with the single additional term W_b in the continuity equation. This term is analogous to the forcing term in axisymmetric flow and produces intensification or decay as the wave progresses. Based on our understanding of axisymmetric flow this term does not produce qualitative changes in the wave nature of the solution.

The local solution to the flow is defined by two space dimension problem exactly like axisymmetric flow. Figure 3 is a schematic of the wave pattern near point 0. The intersection of the Mach cone through 0 and the osculating (t-n) plane are two bicharacteristics. These two lines carry the same characteristic information as first and second family waves in axisymmetric flow. The full three dimensional equations defined the Mach cones as possible characteristic surfaces as an expression of the fact that wave fronts can propagate at any arbitrary orientation to the local velocity vector. The local analysis presented in reference 6 and sketched out here shows that when the flow is not singular at point 0 only two bicharacteristics are at work. These bicharacteristics are in the osculating plane containing ∇p the only force on the fluid element.

In order to develop further confidence in these ideas and get quantitative results we examine the model problem of an infinite swept expansion using the classical solution and then the osculating plane analysis. The solution is examined at the point where the deflection occurs so that no wave intensification or decay is considered. Figure 4 is a sketch of flow which is infinite in the y or chord direction. A uniform flow parallel to a flat surface expands about a corner (true angle normal to the sweep line δ) which is swept relative to the oncoming velocity vector by the angle Λ. In the classical solution the oncoming velocity vector is decomposed into components normal and tangential to the sweep line. The tangential velocity vector is unchanged by the corner while the normal component undergoes a two dimensional expansion through the angle δ. Denoting downstream conditions by 2 and oncoming conditions by 1

$$\vec{q}_1 = q_{1n}\hat{N}_1 + q_{1t}\hat{T} \quad (6)$$

$$\vec{q}_2 = q_{2n}\hat{N}_2 + q_{2t}\hat{T} \tag{7}$$

where $\hat{N}$ is the unit vector normal to the sweep line lying on the surface and $\hat{T}$ is the unit vector tangential to the sweep line. Furthermore,

$$q_{2n} - q_{1n} = q_{1n}\delta/\sqrt{M_n^2-1} = q_{1n}\,\delta\tan\mu_n \tag{8}$$

$$q_{2t} = q_{1t} \tag{9}$$

$$M_n = M_1 \cos\Lambda \tag{10}$$

where equation (8) is the Prandtl-Meyer relationship for an infinitesimal wave which turns a flow at Mach number M_n an angle δ. Combining (8) and (9) with (7) and using

$$\hat{N}_2 = (\cos\Lambda\cos\delta,\ \sin\Lambda\cos\delta,\ -\sin\delta\ )$$

$$\hat{T} = (\sin\Lambda,\ -\cos\Lambda,\ 0)$$

and retaining only first order terms

$$\vec{q}_2 = q_1(1 + \delta\cos^2\Lambda\tan\mu_n,\ \delta\sin\Lambda\cos\Lambda\tan\mu_n,\ -\ \delta\cos\Lambda\ ) \tag{11}$$

where q_1 is the magnitude of the upstream velocity.

The change in the magnitude of the velocity vector is given by

$$\frac{\Delta q}{q_1} = \frac{q_2-q_1}{q_1} = \sqrt{(1+\delta\cos^2\Lambda\tan\mu_n)^2 + (\delta\sin\Lambda\cos\Lambda\tan\mu_n)^2 + \delta^2\cos^2\Lambda} - 1$$

retaining only the highest order terms

$$\frac{\Delta q}{q_1} = \delta\cos^2\Lambda\tan\mu_n \tag{12}$$

A sketch of the wave pattern is shown in figure 5. A plane wave is emitted by the sweep line at a true angle μ_n given by the expression

$$\sin\mu_n = \frac{1}{M_n} = \frac{1}{M_1\cos\Lambda} = \frac{\sin\mu_1}{\cos\Lambda}$$

The flow is turned by this wave front about a vector

$$\vec{R} = \frac{\vec{q}_1 \times \vec{q}_2}{q_1^2} = (0,\ \delta\cos\Lambda,\ \delta\sin\Lambda\cos\Lambda\tan\mu_n) \tag{13}$$

It is interesting to note that the rotation line is not parallel to the sweep line, in fact it has no x component. It is inclined to the x-y plane by the angle β

$$\tan\beta = z/y = \cot\mu_n\sin\Lambda \tag{14}$$

The direction of the initial and final velocity vectors can be related by a simple rotation about the vector $\vec{R}$. The angle between these two directions (in the plane normal to $\vec{R}$) is (see Appendix)

$$\delta' = \frac{\delta \cos\Lambda \cos\mu_1}{\cos \mu_n} = \frac{\delta \cos^2\Lambda \cos \mu_1}{\sqrt{\cos^2\Lambda - \sin^2\mu_1}} \qquad (15)$$

In the following paragraphs it will be shown that this exact solution can be achieved by solving the three dimensional flow problem using the osculating plane. The bicharacteristic in the osculating plane is first located as the line of tangency of the wave front leaving the swept leading edge and the Mach cone. The osculating plane is then shown to be perpendicular to the rotation vector $\vec{R}$ from the classical solution. There the $\vec{b}$ vector and the $\vec{R}$ vector are parallel and the required deflection is exactly that given by equation (15). Then it is shown that the final velocity achieved by expanding (or compressing) the total velocity q_1 through the rotation δ' results in the same magnitude of the final velocity as the classical solution. Thus since the rotation direction, magnitude of rotation and final velocities are identical the two solutions are identical.

Refering to figure 6 at any point on the sweep line a Mach cone is emitted with half angle $\mu_1 = \sin^{-1}(1/M_1)$. The Mach cone at the origin is shown on the figure but all are similar. The wave front attached to the sweep line rests on the Mach cones. The intersection (tangency line) of this wave front and the Mach cone occurs along a line (bicharacteristic) which can be easily found geometrically using vector analysis. In the cross section view (fig. 6(b)) the angle ξ locating this line is given by

$$\cos\xi = \tan \mu_1 \tan\Lambda \qquad (16)$$

the tangent of this angle can be found by standard trigonometric relationships and related to μ_n (see Appendix)

$$\tan\xi = \frac{1}{\tan \mu_n \sin\Lambda} \qquad (17)$$

A vector tangent to the plane containing the intersection line and the axis of the Mach cone (streamline direction) is therefore

$$\vec{T} = (0, -1, \tan \xi)$$

A vector parallel to the rotation vector $\vec{R}$ (equation (13)) is

$$\vec{R}_1 = (0, 1, \sin\Lambda \tan \mu_n)$$

The dot product of $\vec{R}_1$ and $\vec{T}$ is always zero.

$$\vec{T} \cdot \vec{R} = -1 + \tan\xi \sin\Lambda \tan \mu_n = -1 + 1 = 0 \qquad (18)$$

Therefore the $\hat{b}$ vector which is normal to the osculating plane and the $\vec{R}$ vector are parallel.

The $\hat{b}$ vector and $\vec{R}$ are parallel and the same turning angle δ' is specified by equation 15 in both solutions. All that remains is to show that expanding the total velocity q_1 an amount δ' changes its magnitude to the same value as the classical solution. The change in velocity is given by the Prandtl-Meyer expression (This is the same expression used in equation 8)

$$\frac{\Delta q}{q_1} = -\Delta\theta \tan \mu_1$$

In this case $\Delta\theta = -\delta'$

$$\frac{\Delta q}{q_1} = \delta' \tan \mu_1$$

Using the value of δ' given by equation 15

$$\frac{\Delta q}{q_1} = \frac{\delta \cos\Lambda \sin\mu_1}{\cos \mu_n} \qquad (19)$$

$M_n = M_1 \cos \Lambda$, therefore

$$\sin \mu_1 = \frac{\sin \mu_n}{\cos \Lambda}$$

Substituting this in equation 19 yields

$$\frac{\Delta q}{q_1} = \delta \cos^2 \Lambda \tan \mu_n \qquad (20)$$

Comparing this to equation 12 the results are identical.

The conclusion is summarized in figure 7. The flow over the swept expansion (or compression) corner can be evaluated by using the bicharacteristics in the osculating plane. The orientation of the osculating plane is determined by the relative orientation of the sweep line and the oncoming velocity. In the osculating plane figure 7b the flow is two dimensional and the incoming wave is oriented at the free stream Mach angle μ_1.

THE BOUNDARY CONDITIONS AT A SOLID WALL

The purpose of the previous discussion was to demonstrate that the wave processes in three dimensional flow are in fact locally equivalent to the familiar two dimensional wave process. The passing of an infinitesimal strength wave front in three dimensinal flow produces a change in flow direction, magnitude of velocity and hence pressure and density given by the Prandtl-Meyer relationship. The orientation of the deflection is given by a rotation about the binormal vector whose direction is determined by the relative orientation of the oncoming velocity and the wave front. In general in a three dimensional flow there can be an arbitrary number of wave fronts passing a given point. Each wave front has a given strength and associated binormal vector. Because the waves under discussion are infinitesimal in strength the rotations they produce are additive as well as are the increments in velocity. Therefore at any given point the effect of all wave fronts can be added to produce one binormal vector associated with all the changes in the flow properties at that point.

The wave pattern at a solid surface is shown schematically in figure 8. In general there are three wave fronts that must be considered: an incident wave and its reflected wave and an emitted wave. The incident wave originates in the flow and strikes the boundary. Upstream of this wave the flow is parallel to the surface. A reflected wave front originates at the body surface to bring the flow back parallel to the surface. These two waves intersect the body along line BB in figure 8. In addition at point O the body surface changes orientation. This results in a wave front moving away from the surface which originates on the body along line AA. This wave front rotates the velocity vector to make it parallel to the new body direction. The lines AA and BB are swept at different angles to the oncoming flow. This is one reason that the three dimensional boundary condition is more complex than the two dimensional counterpart. In two dimensional flow AA and BB are coincident as are the emitted and reflected waves. In that case there is no need to distinguish between the reflected wave and the emitted wave.

With this theoretical background it is now possible to suggest an algorithm for the correct imposition of the boundary condition at a solid surface in three dimensional flow. Figure 9 shows a portion of the computational mesh. At station Z all flow properties are known at the interior points and the boundary points. The boundary point denoted N at station $Z + \Delta Z$ is to be computed. Using a grid that is orthogonal to the body surface an additional line of mesh points interior to the body is defined using reflection conditions (more discussion later on these values). The standard interior point calculation is performed at point O to compute values at N. The values so computed at point N account for the incident and reflected waves by virtue of the construction of the reflected points. The emitted wave is now added by expanding (or compressing) the flow to the new body slope. This can be achieved by either of the two methods discussed in the previous paragraphs. The sweep line of this expansion is determined by taking the cross product of the new body normal at N and the normal at O (fig. 10).

The one question that remains is the specification of the flow properties on the reflection plane. The flow properties required on the reflection plane have the property that they cancel the incident wave. In the following discussion it will be shown that the values of the flow variables on the reflection plane are computed by the usual formulas despite the fact that there is wave intensification due to the velocity gradient normal to the osculating plane. Scalar variable and velocity components parallel to the plate are reflected using symmetry conditions while the velocity component normal to the plane is reflected using antisymmetry. Figure 11a shows a schematic of the osculating plane at the boundary point N for the incident/reflected wave process. Figure 11b is the wave pattern in the osculating plane. The characteristic starting at B reaches the body surface at N and propagates into the flow as the reflected wave. In the osculating plane the wave propagation process is equivalent to an axisymmetric flow (ref. 6). The characteristic equations governing axisymmetric waves are (ref. 7)

$$d\nu + d\theta = Kds \qquad \text{along AN} \tag{21}$$

$$d\nu - d\theta = Kds \qquad \text{along BN} \tag{22}$$

where ν is the Prandtl-Meyer function, S is distance along the characteristic and K is the forcing term due to the velocity gradient normal to the characteristics.

These equations are integrated in the usual manner.

$$\nu_N - \nu_A + \theta_N - \theta_A = \frac{1}{2}(K_A + K_N)\Delta s \tag{23}$$

$$\nu_N - \nu_B - \theta_N - \theta_B = \frac{1}{2}(K_B + K_N)\Delta s \tag{24}$$

The construction of the flow properties at point B by reflection relates the values at A and B by

$$\nu_B = \nu_A = \nu_o + (\nu_A - \nu_o) = \nu_o + \Delta\nu \tag{25}$$

$$\theta_B = \theta_o - (\theta_A - \theta_o) = \theta_o - \Delta\theta \tag{26}$$

$$K_A = K_o + K_{no}n_A + K_{nno}n_A^2/2 \tag{27}$$

$$K_B = K_o + K_{no}n_B + K_{nno}n_B^2/2 \tag{28}$$

$$n_B = -n_A = -\Delta s \sin\mu \tag{29}$$

Substituting equations 25-29 into the solution (eqs. 23 and 24) and solving for the values at N yields

$$\nu_N = \nu_o + (\Delta\nu - \Delta\theta) + \frac{1}{2}(K_o + K_N + K_{nno}\sin^2\mu(\Delta s)^2/2) \tag{30}$$

$$\theta_N = -((\Delta s)^2/2)\,K_{no}\sin\mu \tag{31}$$

The result sought is equation 31. To lowest order the reflected wave constructed by reflection produces no change in flow direction. This is a direct result of the fact that the nonhomogeneous terms in the characteristic equations 21 and 22 have the same sign.

CONCLUSIONS

An algorithm for the boundary point calculation at a solid surface in three dimensional flow has been proposed. It is based on an analysis of the three dimensional wave pattern that occurs at the surface. In three dimensional flow the body tangency condition does not uniquely determine the velocity direction at the boundary. The additional information necessary to complete the solution is contained in the wave pattern at the boundary point.

For a solid surface an incident and reflected wave and a wave emitted by the body represent the interaction of the flow with the boundary. The alogrithm proposed accounts for these processes in a relatively simple manner and is in fact a combination of two widely used techniques.

In the process of studying the boundary point algorithm several important concepts in three dimensional supersonic flow were developed. A. Frohn (ref. 6) showed that in the osculating plane to the streamline the wave propagation is locally exactly equivalent to an axisymmetric flow. Using this concept the model problem of the infinite swept expansion or compression corner was analyzed by classical methods and the three dimensional osculating plane analysis. The solutions were shown to be identical. The relative orientation of the wave front to the oncoming velocity defines the binormal direction or rotation ($\vec{b}$) vector associated with the wave. The intersection of the osculating plane and the Mach cone defines the two bicharacteristics which determine the solution. At a point in a three dimensional flow there are an arbitrary number of wave fronts each with an associated $\vec{b}$ vector. For infinitesimal strength waves a resultant $\vec{b}$ vector can be defined because infinitesimal rotations are additive.

The boundary condition at a contact surface discontinuity is the next logical problem to study. The wave analysis presented here can be used to examine that problem where there are six wave fronts at work. On each side of the contact surface an incident wave gives rise to a reflected wave and a transmitted wave on the other side of the contact surface.

REFERENCES

1. Moretti, G., Grossman, B., Marconi, F.: A Complete Technique for the Calculation of Three Dimensional Inviscid Supersonic Flows, AIAA Paper No. 72-192, 1972.

2. Marconi, F., Salas, M., Yaeger, L.: Development of a Computer Code for Calculating the Steady Super/Hypersonic Inviscid Flow Around Real Configuration, Vol. 1 Computational Technique NASA CR-2675, April 1976.

3. Dash, S., Del Guidice, P.: Numerical Methods for the Calculation of Three Dimensional Nozzle Exhaust Flow Fields, NASA SP 347, pp 659-702, March 1975.

4. Rudman, S.: Numerical Study of Highly Underexpanded Three Dimensional Plumes, ATL TR 184, General Applied Science Labs, Westbury, N.Y., June 1973.

5. Abbett, M.: Boundary Condition Calculational Procedures for Inviscid Supersonic Flow Fields, AIAA Computational Fluid Dynamics Conference Proceedings, July 1973.

6. Frohn, A.: An Analytic Characteristic Method for Steady Three Dimensional Isentropic Flow, Journal of Fluid Mechanics Vol 63, Part 1 pp 81-96, 1974.

7. Ferri, A.: Elements of Aerodynamics of Supersonic Flows, Macmillan Co., New York, 1949.

8. Courant, R. and Friedricks, K.O.: Supersonic Flow and Shock Waves, Interscience Publishers Ltd., New York, 1948.

9. Von Mises, R.: Mathematical Theory of Compressible Flow, Academic Press, 1958.

10. Moretti, G and Abbett, M.: A Time Dependent Computational Method for Blunt Body Flows, AIAA Journal, Vol. 4, No. 12, December 1966.

11. Moretti, G.: The Importance of Boundary Conditions in the Numerical Treatment of Hyperbolic Equations, Polytechnic Inst. of N.Y. PIBAL Rept. No. 68-34, Nov. 1968.

12. deNeff, T.: Treatment of Boundaries in Unsteady Inviscid Flow Computations, Rept. LR 262, Delft University of Technology, 1978.

13. Rudman, S.: Multinozzle Plume Flow Fields - Structure and Numerical Calculation, AIAA 10th Fluid & Plasma Dynamics Conference June 27-29 Paper No. 77-710.

APPENDIX

I. Evaluation of δ'

The unit vectors $\hat{q}_1$ and $\hat{q}_2$ are parallel to the initial and final velocity vectors and are related by the formula

$$\hat{q}_2 = \hat{q}_1 + \hat{R}\delta' \times \hat{q}_1 \tag{A1}$$

where $\hat{R}$ is the unit vector parallel to the rotation vector and δ' is the angular rotation between $\hat{q}_2$ and $\hat{q}_1$.

$$\hat{R} = (0,\ \cos\mu_n/\cos\mu,\ \sin\Lambda\sin\mu_n/\cos\mu)$$

Using

$$\hat{q}_1 = (1,0,0)$$

in equation (A1)

$$\hat{q}_2 = (1, \delta'\sin\Lambda\sin\mu_n/\cos\mu,\ -\delta'\ \cos\mu_n/\cos\mu) \tag{A2}$$

$\hat{q}_2$ is parallel to the surface whose normal is

$$\vec{n}_2 = (\delta\cos\Lambda,\ \delta\sin\Lambda,\ 1)$$

$$\hat{q}_2 \cdot \vec{n}_2 = 0 \tag{A3}$$

Substituting equation (A2) in equation (A3) and solving for δ'

$$\delta' = \delta\cos\Lambda\cos\mu/\cos\mu_n \tag{A4}$$

$\cos\ \mu_n$ can be eliminated by

$$\sin\mu_n = \sin\mu/\cos\Lambda \tag{A5}$$

$$\cos\mu_n = \sqrt{1-\sin^2\mu_n} = \sqrt{1-\frac{\sin^2\mu}{\cos^2\Lambda}} = \sqrt{\frac{\cos^2\Lambda-\sin^2\mu}{\cos\Lambda}} \tag{A6}$$

$$\delta' = \frac{\delta\cos^2\Lambda\cos\mu}{\sqrt{\cos^2\Lambda-\sin^2\mu}} \tag{A7}$$

II Evaluation of tan ξ

Using the value of cos ξ given in equation (16)

$$\tan\xi = \frac{\sin\xi}{\cos\xi} = \frac{\sqrt{1-\cos^2\xi}}{\cos\xi} = \frac{\sqrt{1-\tan^2\mu\tan^2\Lambda}}{\tan\mu\tan\Lambda}$$

$$\tan\xi = \frac{\sqrt{\cos^2\mu\cos^2\Lambda - \sin^2\mu\sin^2\Lambda}}{\sin\mu\sin\Lambda}$$

$$\tan\xi = \frac{\sqrt{(1-\sin^2\mu)\cos^2\Lambda-\sin^2\mu(1-\cos^2\Lambda)}}{\sin\mu\sin\Lambda} = \frac{\sqrt{\cos^2\Lambda-\sin^2\mu}}{\sin\mu\sin\Lambda}$$

Using equations (A5) and (A6)

$$\tan\xi = \frac{1}{\tan\mu_n\sin\Lambda}$$

Note: The subscript 1 has been suppressed on μ in the Appendix. Wherever μ appears without a subscript it refers to $\mu = \sin^{-1}(1/M_1)$.

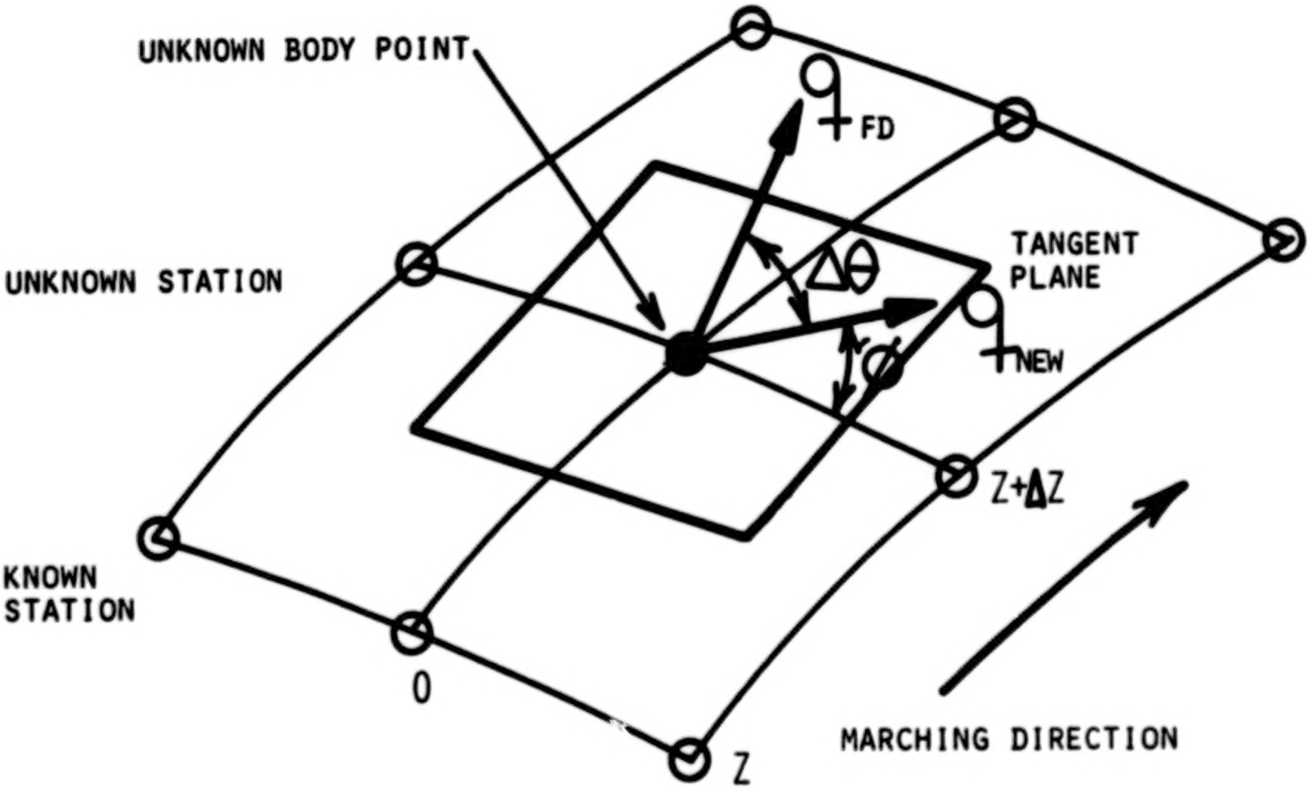
UNKNOWN BODY POINT
UNKNOWN STATION
KNOWN STATION
TANGENT PLANE
q_{FD}
q_{NEW}
$\Delta\theta$
ϕ
0
Z
Z+ΔZ
MARCHING DIRECTION

Figure 1.-Schematic of the computational mesh at a solid boundary point.

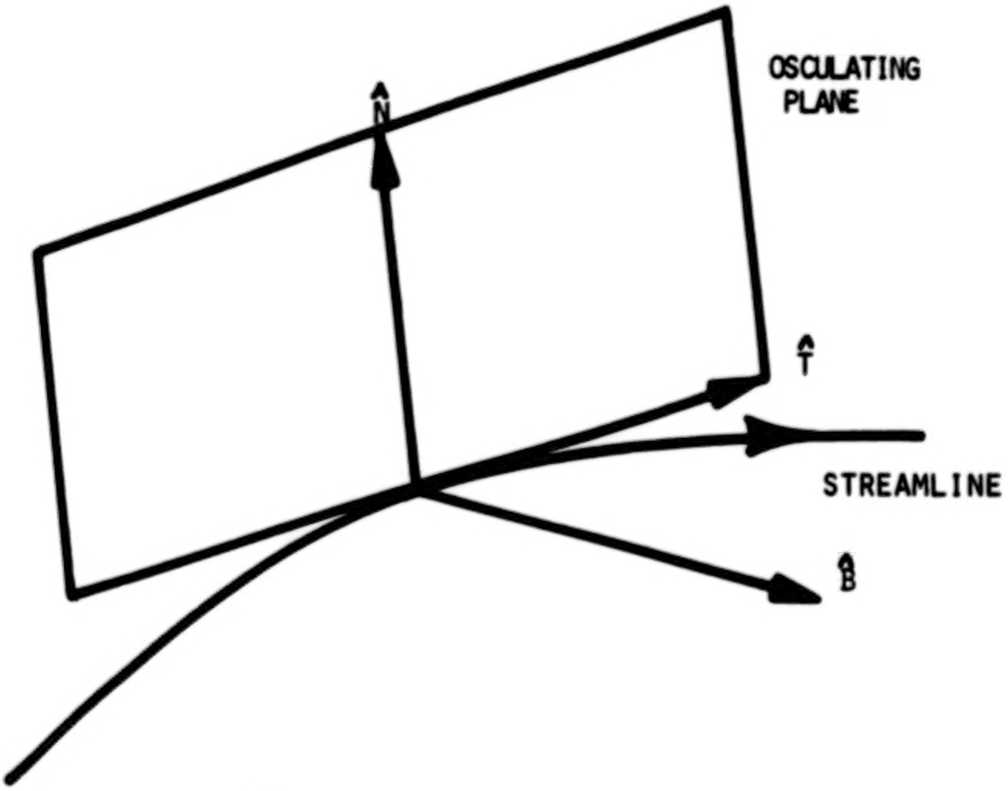
OSCULATING PLANE
$\hat{N}$
$\hat{T}$
STREAMLINE
$\hat{B}$

$\hat{T}$ = UNIT TANGENT VECTOR

$\hat{N}$ = UNIT NORMAL VECTOR

$\hat{B}$ = UNIT BINORMAL VECTOR

Figure 2.-The osculating plane to a streamline.

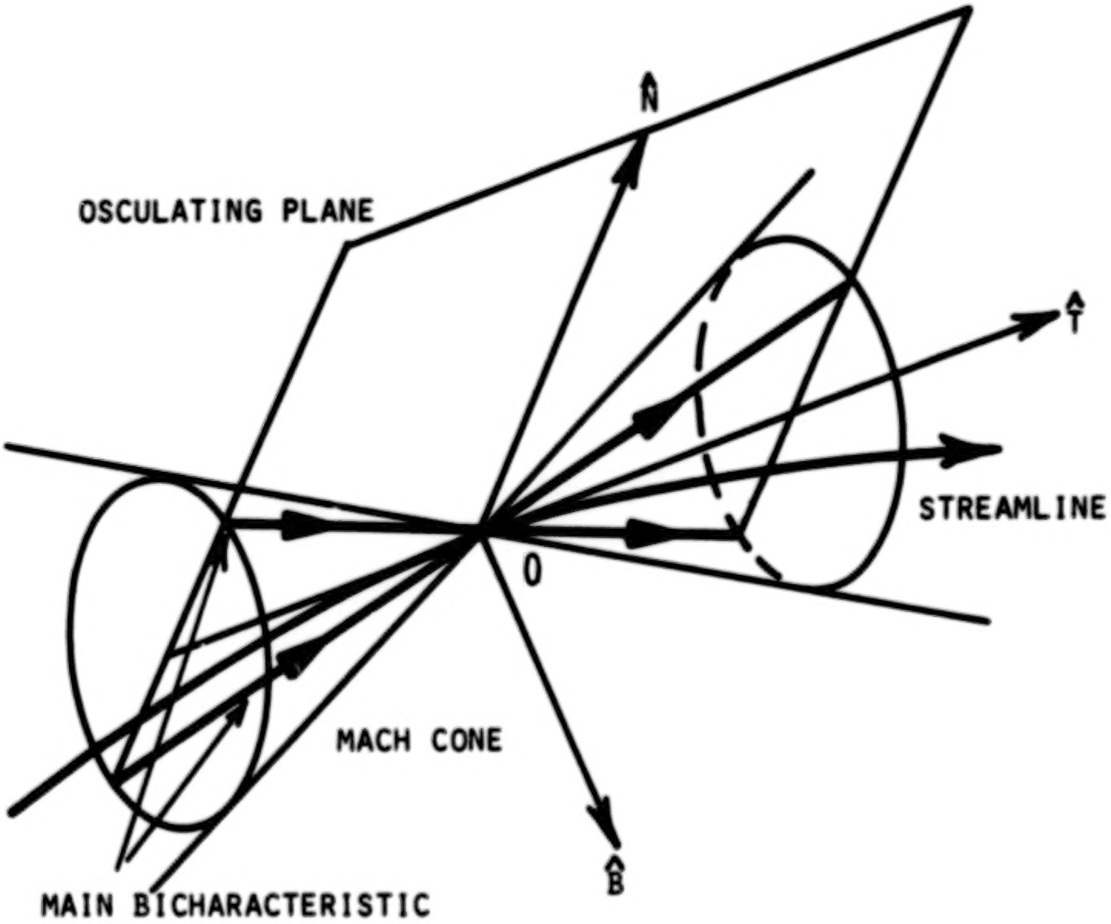
OSCULATING PLANE
$\hat{N}$
$\hat{T}$
STREAMLINE
0
MACH CONE
$\hat{B}$
MAIN BICHARACTERISTIC

Figure 3.-The mach cone and the main bicharacteristics.

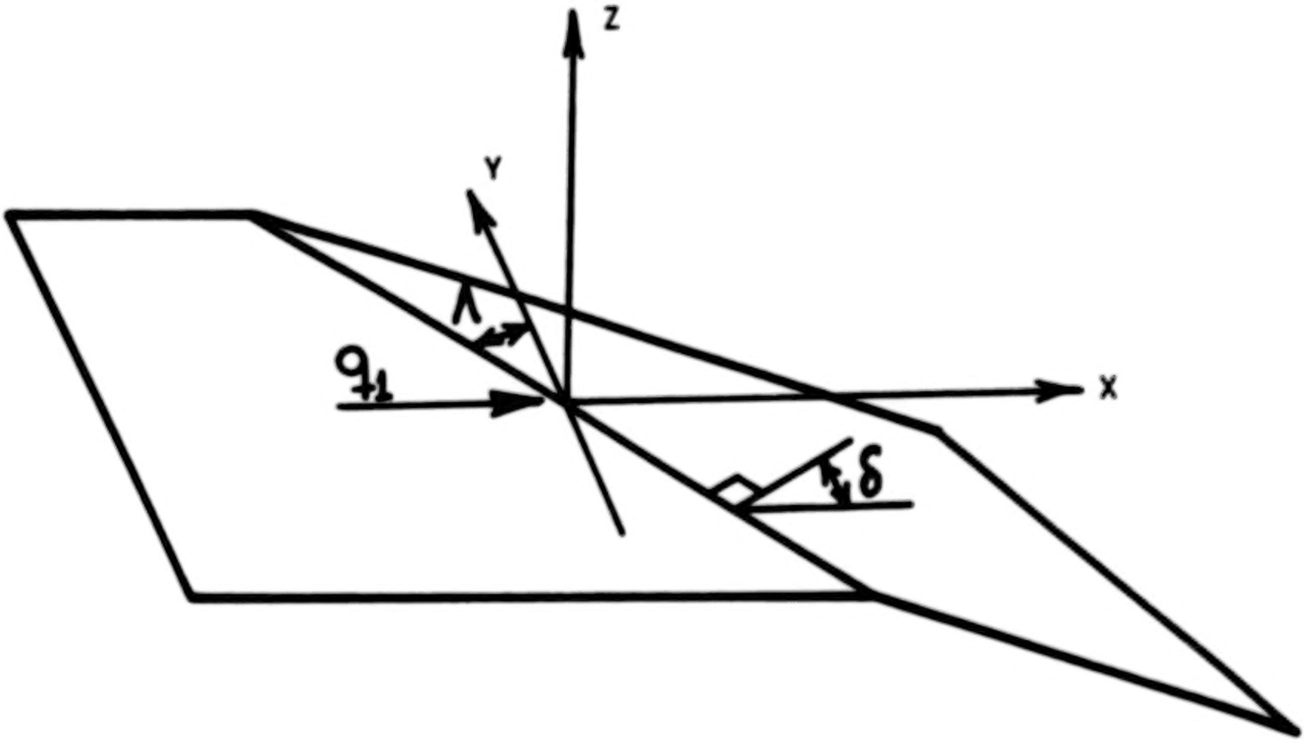
Z
Y
X
Λ
q_1
δ

Figure 4.-Schematic of the geometry for the infinite swept expansion corner.

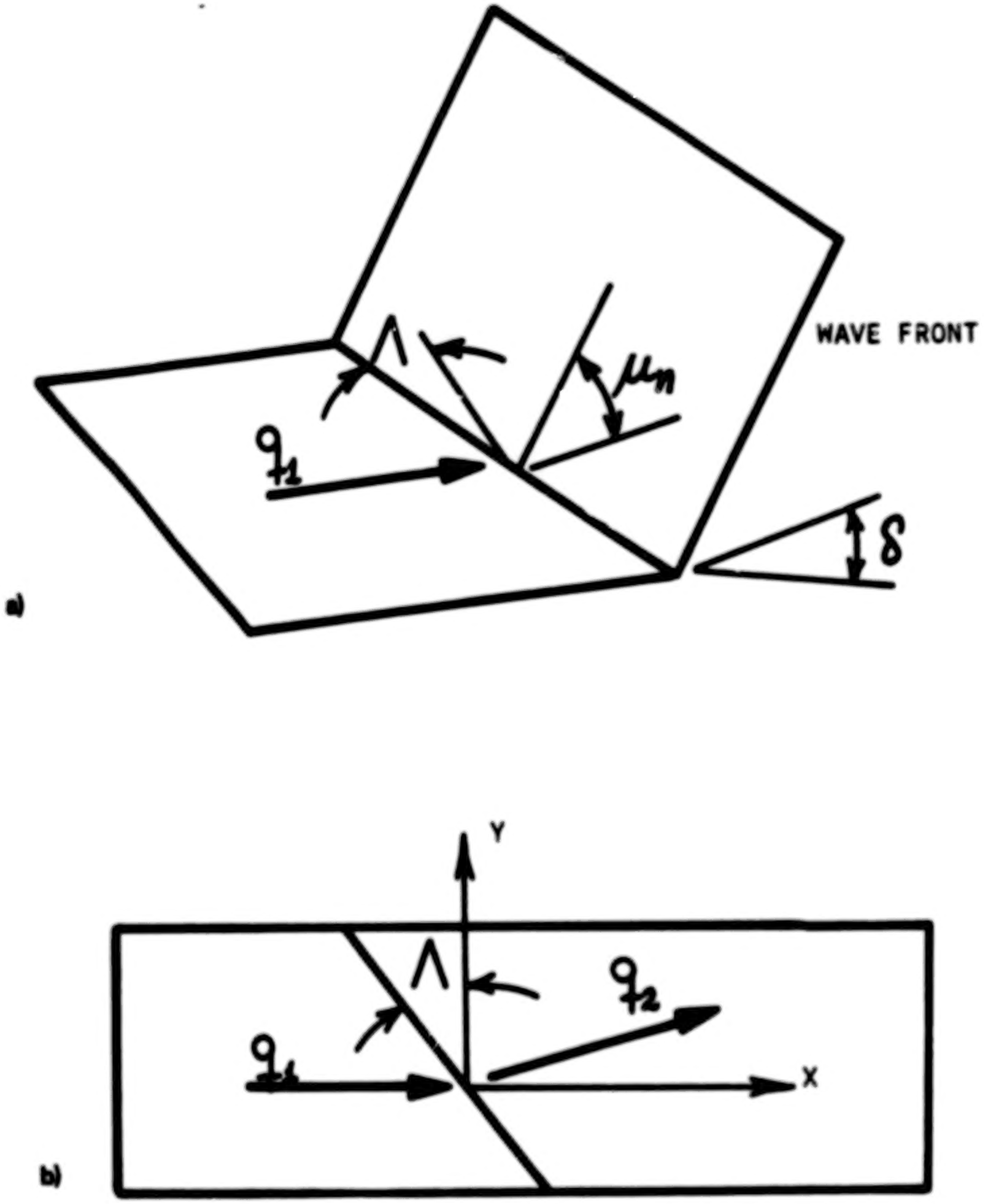
WAVE FRONT
Λ
μ_n
q_1
δ
a)
Y
Λ
q_2
q_1
X
b)

Figure 5.-Wave pattern at swept leading edge.

(a) Wave front plane.

(b) Top view.

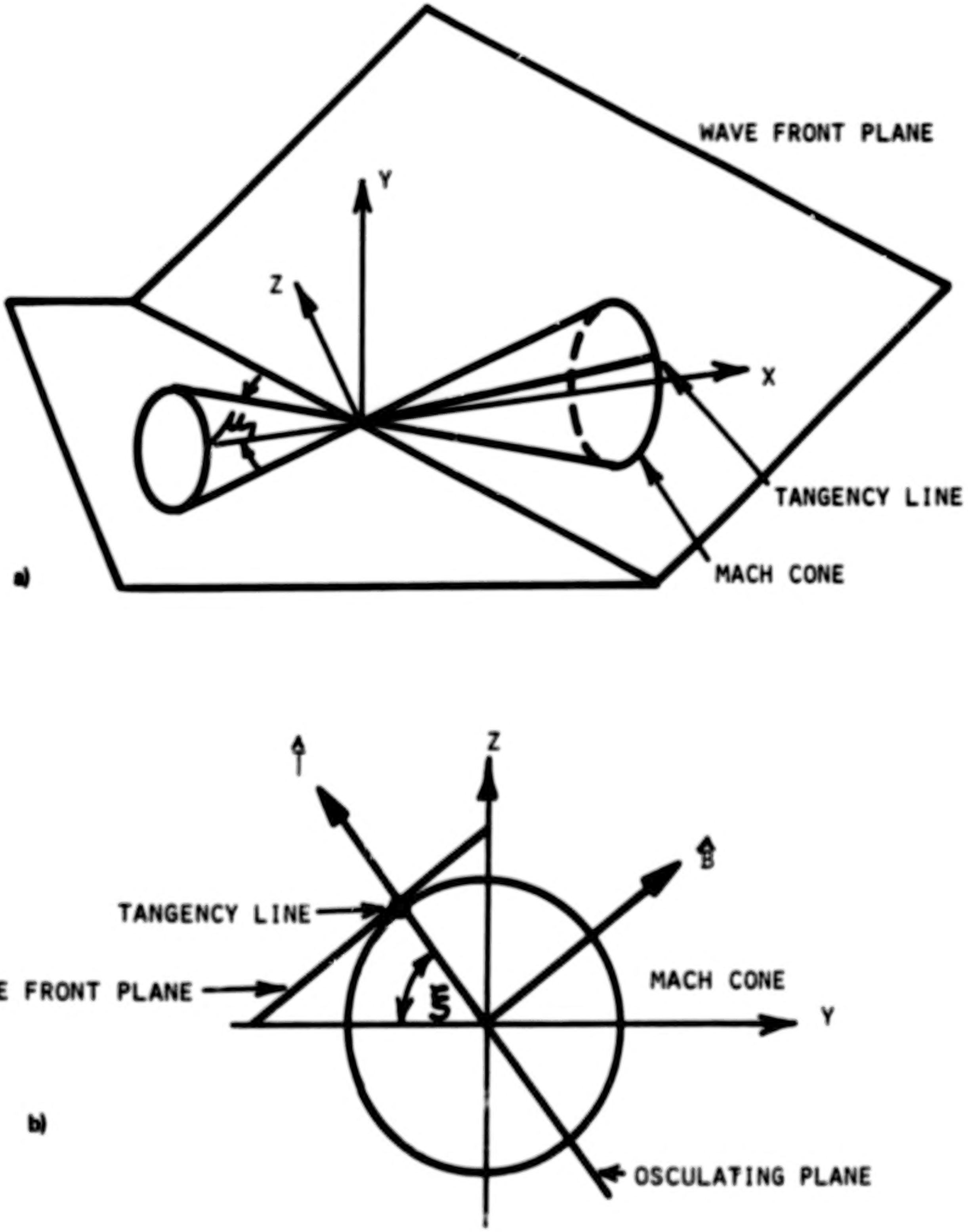
WAVE FRONT PLANE
Y
Z
μ
X
TANGENCY LINE
MACH CONE
a)
$\hat{T}$
Z
$\hat{B}$
TANGENCY LINE
WAVE FRONT PLANE
ξ
MACH CONE
Y
b)
OSCULATING PLANE

Figure 6.-The mach cone, osculating plane and wave front plane for the swept expansion.

(a) Three dimensional view.

(b) Cross section in yz plane.

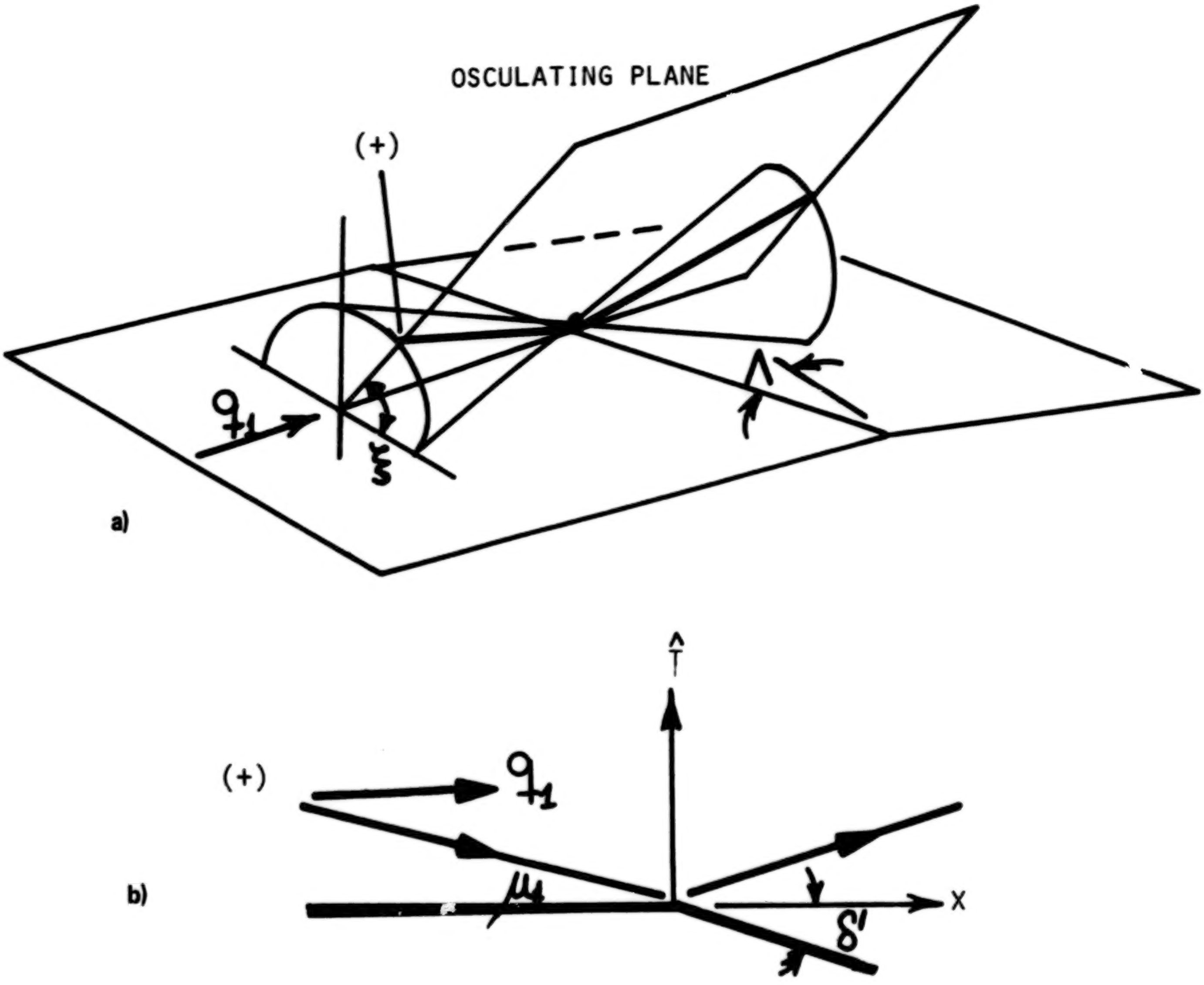
OSCULATING PLANE
(+)
q1
ξ
Λ
a)
T̂
(+)
q1
μ1
X
δ'
b)

Figure 7.-Three dimensional representation of swept expansion corner.

(a) The main bicharacteristics for the swept corner.

(b) Characteristics in the osculating plane.

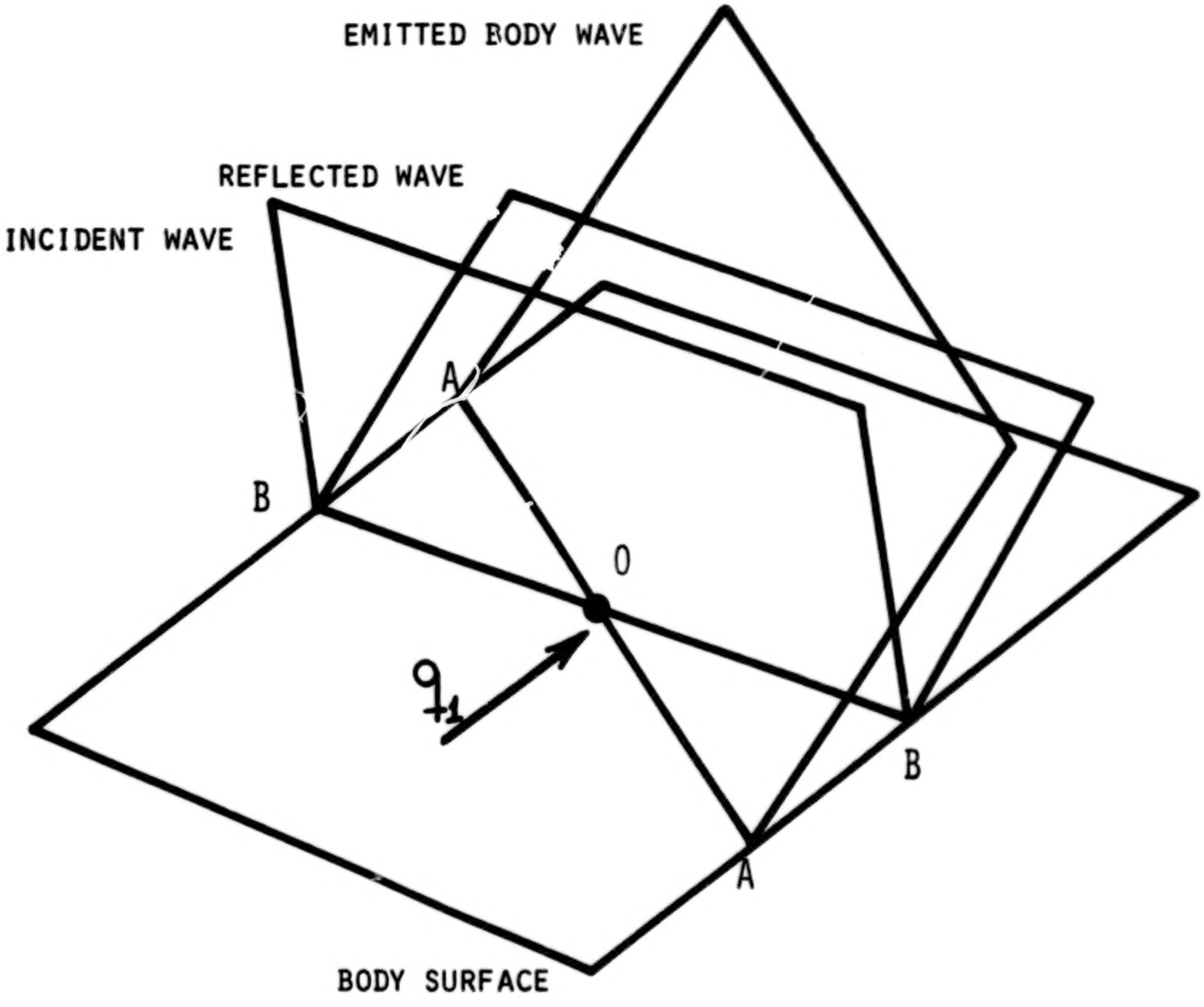
EMITTED BODY WAVE
REFLECTED WAVE
INCIDENT WAVE
A
B
O
q_1
B
A
BODY SURFACE

Figure 8.-Wave pattern at a solid surface.

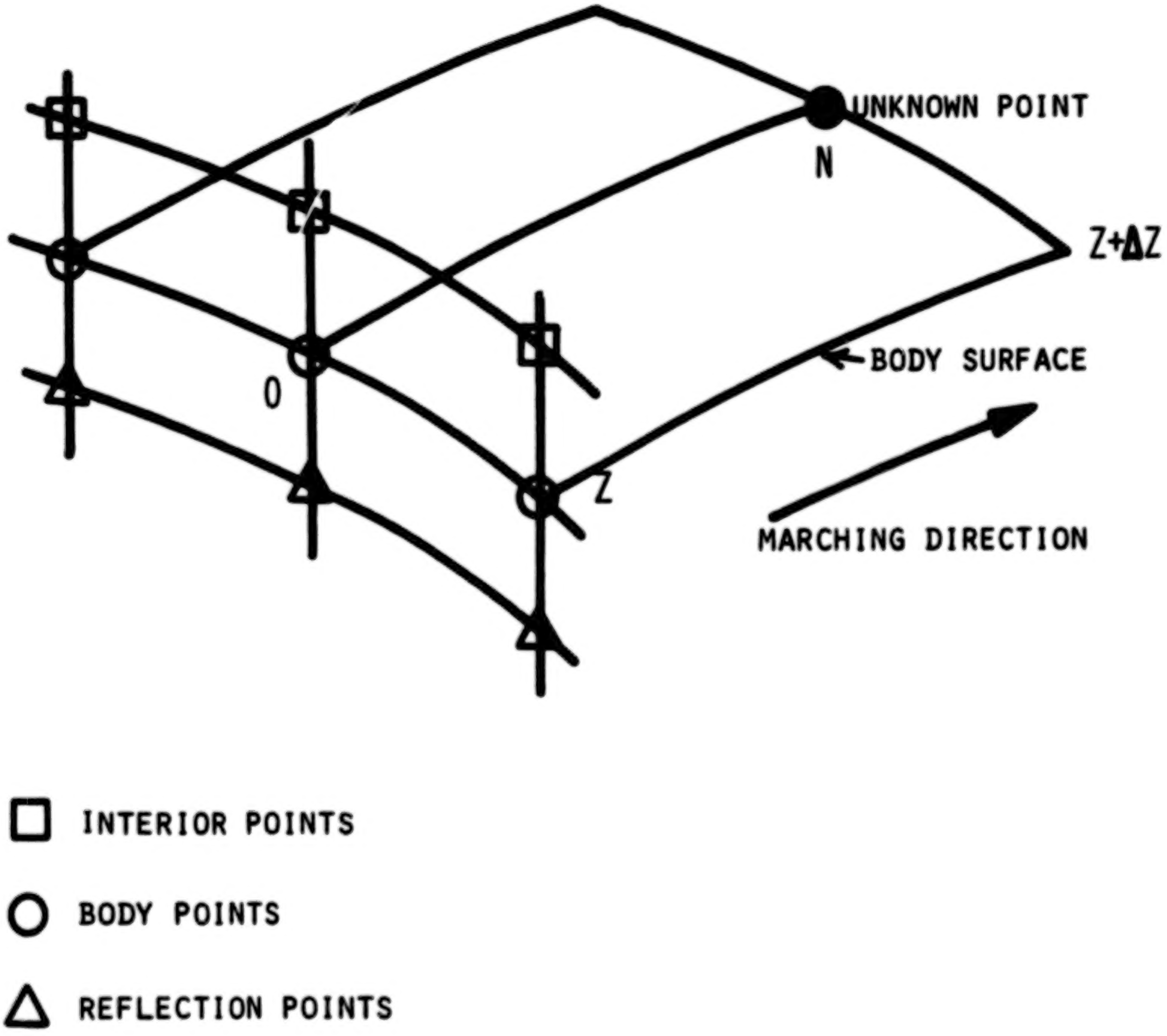
UNKNOWN POINT
N
Z+ΔZ
O
BODY SURFACE
Z
MARCHING DIRECTION
□ INTERIOR POINTS
○ BODY POINTS
△ REFLECTION POINTS

Figure 9.-Computational mesh for boundary point calculation.

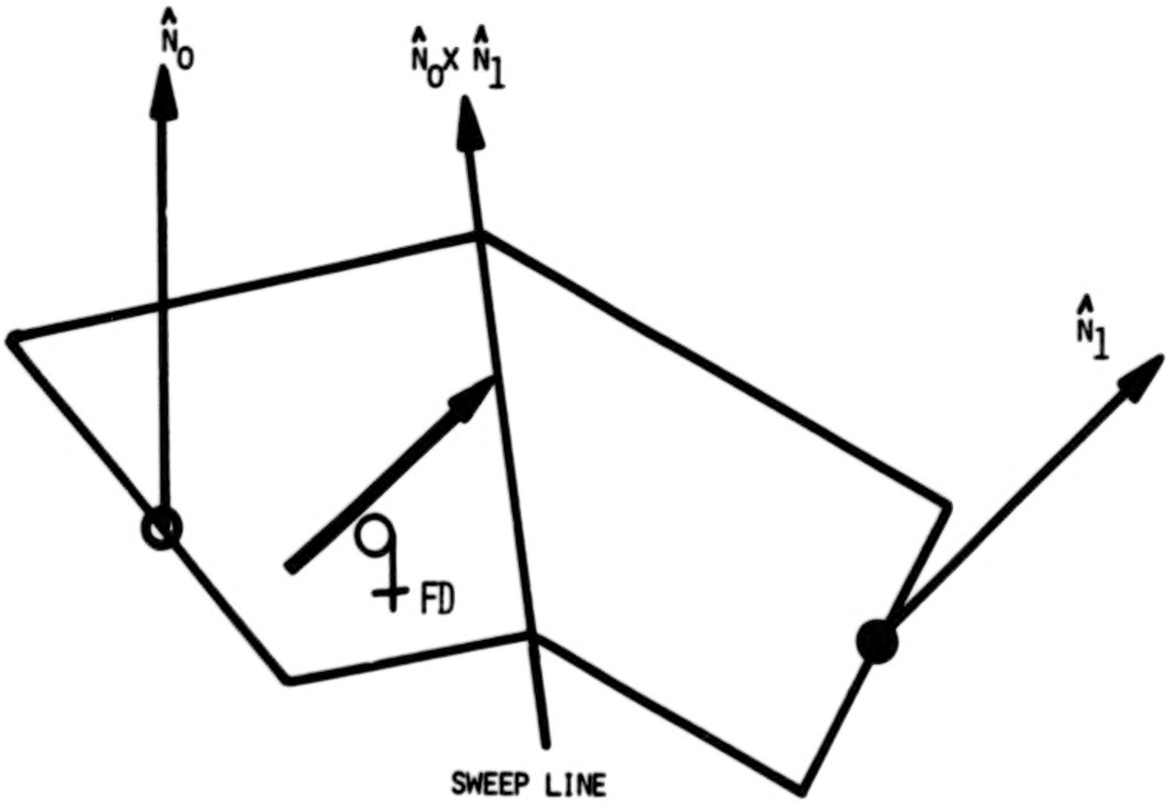
$\hat{N}_0$
$\hat{N}_0 \times \hat{N}_1$
$\hat{N}_1$
FD
SWEEP LINE

Figure 10.-Geometry for emitted body wave.

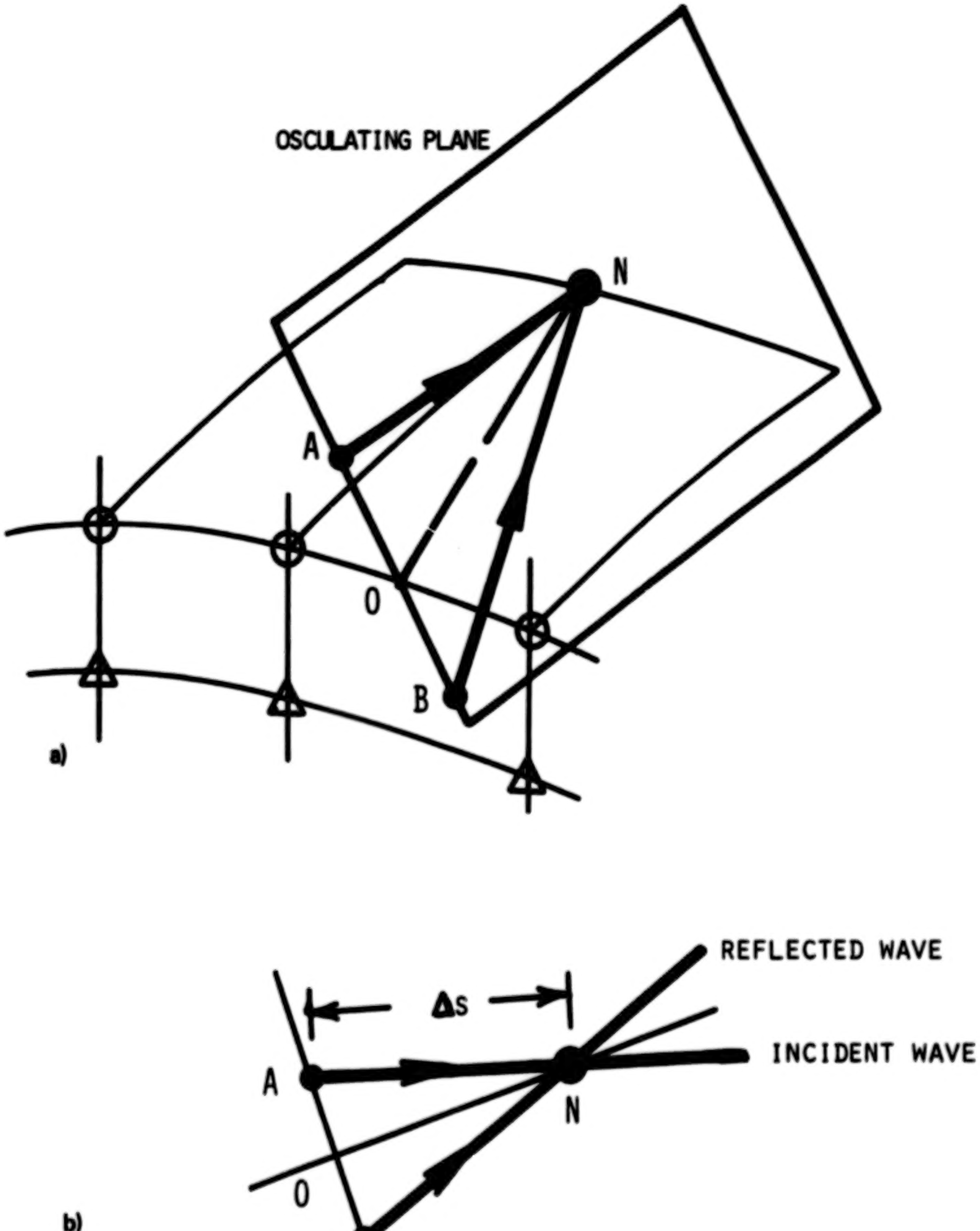
OSCULATING PLANE
N
A
O
B
a)
REFLECTED WAVE
Δs
INCIDENT WAVE
A
N
O
B
b)

Figure 11.-Schematic showing the osculating plane for the incident and reflected waves.

(a) Computational mesh.

(b) Osculating plane

ON VARIOUS TREATMENTS OF POTENTIAL EQUATIONS AT SHOCKS*

Lee-Tzong Chen**
and
D. A. Caughey†

McDonnell Douglas Corporation
St. Louis, MO 63166

INTRODUCTION

The potential equation that governs transonic inviscid flowfields is elliptic in subsonic regions and hyperbolic in supersonic regions. The transition from supersonic to subsonic flow may occur either continuously or across a surface of discontinuity known as a shock. Because of the changing type of governing equation and the presence of the surfaces of discontinuity, special treatments of the governing equations are needed at shocks to preserve mass conservation and to ensure satisfaction of the governing equation. In the so-called shock-capturing techniques, shocks are captured by smearing the discontinuity over several mesh cells in the computational domain. Most existing conservative schemes conserve mass flux throughout the flowfield, including shock boundaries; however, they also introduce zero-order errors in the approximation to the governing equation. It will be shown in this paper that the zero-order errors, which do not diminish as the mesh spacing approaches zero, can cause discrepancies in the prediction of shock strength and location. These parameters are extremely sensitive features of transonic inviscid flowfield calculations. It also will be shown that the zero-order errors can be avoided by developing higher-order schemes that properly model the governing equation at shocks.

The original Murman and Cole scheme (ref. 1) is nonconservative; it was modified later by Murman (ref. 2) to yield fully conservative solutions to the small disturbance equation by introducing a special shock-point operator. Unfortunately, the shock-point operator introduces a zero-order error term in the approximation to the governing equation at shocks. Jameson (ref. 3) generalized Murman's conservative scheme to treat the full potential equation and showed how to introduce a second-order artificial density to construct second-order-accurate fully conservative schemes. Jameson's second-order schemes also introduce zero-order errors in the approximation to the governing equation at shocks. Chen (ref. 4) developed a second-order-accurate quasi-conservative scheme which similarly introduces a zero-order error term in the approximation to the full potential equation at shocks. He found that both second-order fully conservative and quasi-conservative schemes tend to overpredict the shock strengths for cases with strong shocks because of the zero-order terms. In order to improve the second-order quasi-conservative scheme, special treatments of the governing equation at shocks will be introduced. To further improve the order of accuracy of supersonic-flow solutions, a new third-order quasi-conservative scheme will be presented. To the author's knowledge, this is the first demonstration of a fully consistent finite-difference representation of the governing potential equation at a shock and also of a successful third-order scheme for transonic potential flow calculations.

Studies of various finite-difference schemes and shock-point operators will be presented. Fundamental differences between the quasi-conservative and fully conservative schemes can be illustrated by analyzing a one-dimensional potential equation. However, to account for two-dimensional and surface-curvature effects, it is necessary to perform a more general numerical experiment. A series of numerical

---

This work was supported by the McDonnell Douglas Independent Research and Development program.

****Research Scientist, McDonnell Douglas Research Laboratories**

†Consultant, McDonnell Douglas Research Laboratories; Associate Professor, Sibley School of Mechanical and Aerospace Engineering, Cornell University, Ithaca, New York

results is obtained using first- and second-order nonconservative and first-, second-, and third-order quasi-conservative schemes for transonic flows inside a converging-diverging nozzle. The results are compared with Rankine-Hugoniot solutions in the diverging section where flows become nearly one-dimensional.

Finally, the numerical solutions obtained using the fully consistent second- and third-order quasi-conservative schemes for the transonic flow past several airfoils will be presented and compared with earlier second-order quasi-conservative and fully conservative solutions for which the governing finite-difference equation solved at shock points introduced a zero-order error term.

THE FULL POTENTIAL EQUATION

The full potential equation for two-dimensional transonic inviscid potential flow is given as

$$(a^2 - u^2)\phi_{xx} + (a^2 - v^2)\phi_{yy} - 2uv\phi_{xy} = 0, \tag{1}$$

where u and v are the velocity components in the x and y directions, respectively, and a is the local speed of sound determined from the energy equation

$$a^2 = a_o^2 - (\gamma - 1)(u^2 + v^2)/2, \tag{2}$$

where a_o is the stagnation speed of sound and γ is the ratio of specific heats for the assumed, calorically perfect gas.

In the computational plane, equation (1) is rewritten as (ref. 4)

$$C_1\phi_{XX} + C_2\phi_{YY} + C_3\phi_{XY} + C_4\phi_X + C_5\phi_Y = 0, \tag{3}$$

where

$$C_1 = \left[a^2(x_Y^2 + y_Y^2) - (uy_Y - vx_Y)^2\right]/D^2 \tag{4}$$

$$C_2 = \left[a^2(x_X^2 + y_X^2) - (uy_X - vx_X)^2\right]/D^2 \tag{5}$$

$$C_3 = -2\left[a^2(x_Xx_Y + y_Xy_Y) - (uy_Y - vx_Y)(uy_X - vx_X)\right]/D^2 \tag{6}$$

$$C_4 = \left[(C_1y_{XX} + C_2y_{YY} + C_3Y_{XY})x_Y - (C_1x_{XX} + C_2x_{YY} + C_3x_{XY})y_Y\right]/D \tag{7}$$

$$C_5 = \left[(C_1x_{XX} + C_2x_{YY} + C_3x_{XY})y_X - (C_1y_{XX} + C_2y_{YY} + C_3y_{XY})x_X\right]/D \tag{8}$$

and

$$u = (y_Y\phi_X - y_X\phi_Y)/D \tag{9}$$

$$v = (x_X\phi_Y - x_Y\phi_X)/D \tag{10}$$

$$D = x_Xy_Y - x_Yy_X \tag{11}$$

The transformation derivatives x_X, y_X, x_Y, y_Y, x_{XX}, x_{YY}, x_{XY}, ..., can be computed analytically if an analytical coordinate transformation can be found, or numerically through finite-difference approximations. In order to uncouple the grid generation from the flow equation solver, the transformation coefficients are computed numerically by using a second-order (figure 1) or third-order (figure 2) isoparametric element. The derivatives of the potential function, ϕ_X, ϕ_Y, ϕ_{XX}, ϕ_{YY}, and ϕ_{XY} in equations (3), (9), and (10) are similarly computed. A finite-difference representation of equation (3) can thus be obtained and solved at control points in the computational domain.

The required boundary conditions to be satisfied include the impermeability condition on solid surfaces, the Kutta condition at the airfoil trailing edges, and a compressible vortex flow representation of the potential on the far-field boundary for airfoil flows. Consistent finite-difference approximations of the boundary conditions can be obtained for the second-order or third-order isoparametric element, as discussed in reference 4.

ARTIFICIAL VISCOSITIES

The finite-difference representation of the full potential equation thus far described needs to be augmented by the addition of a proper artificial viscosity or density to reflect the directional bias of supersonic flows. The addition of the artificial viscosity or density can reduce the solution accuracy in supersonic regions. Earlier first-order quasi-conservative schemes (refs. 5, 6, 7) have been found to produce results which are virtually indistinguishable from those of first-order fully conservative schemes, although the differencing of the potential equation in the quasi-conservative schemes is in a nonconservative form, while the differencing of the artificial viscosity is in a conservative form. Several second-

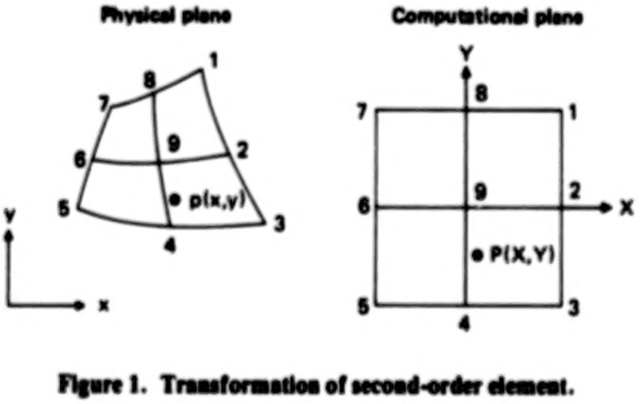

Figure 1. Transformation of second-order element.

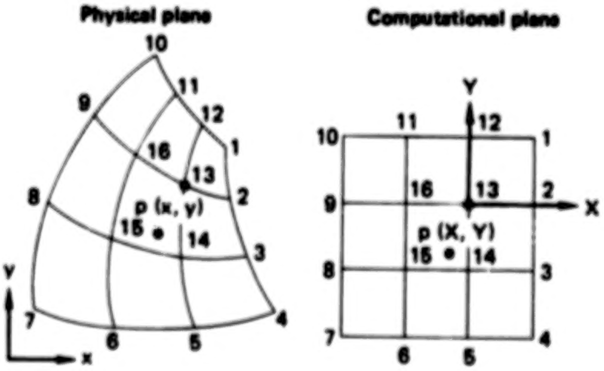

Figure 2. Transformation of third-order element.

order schemes have been developed, and their unique capabilities for predicting double shock structures have been demonstrated. Most first- and second-order, quasi- and fully-conservative schemes conserve mass flux across shocks, but generally introduce zero-order error terms in the governing finite-difference equations solved at shocks.

The best form of the potential equation to use at shocks is debatable. The potential equation holds everywhere in the flowfield except at shocks where the velocities are discontinous. However, as long as the equation is in conservation form, it is believed that solving the full potential equation at shocks as well as elsewhere is probably the most reasonable choice. It will be shown later that by eliminating the above mentioned zero-order error terms, more-consistent shock solutions can be obtained.

The second streamwise derivative of the potential function can be written as

$$\phi_{ss} = p_1\phi_{XX} + p_2\phi_{YY} + p_3\phi_{XY} + p_4\phi_X + p_5\phi_Y , \tag{12}$$

where p_1, ... p_5 are functions of the transformation derivatives. To simplify, further assume the streamwise direction to be approximately the X-direction; then the principal part of ϕ_{ss} is approximated by

$$\phi_{ss} \approx p_1\,\phi_{XX} . \tag{13}$$

The second-order artifical viscosity of reference 4 added to the finite-difference approximation of the full potential equation at supersonic points is

$$H = (\Delta X)^2\,(\mu p_1\phi_{XX})_{XX} = (\mu p_1\phi_{XX})_{i-2} - 2\,(\mu p_1\phi_{XX})_{i-1} + (\mu p_1\phi_{XX})_i , \tag{14}$$

where

$$\mu = \mathrm{Max}\left(1 - \frac{a^2}{q^2}, 0\right) . \tag{15}$$

Although this viscosity introduces only a second-order error at supersonic points, it results in a zero-order error at two points just downstream of a shock, i.e., the governing equation solved at these two points does not reduce to the full potential equation as the mesh size goes to zero. At the first subsonic point downstream of a shock $\mu_{i-1}, \mu_{i-2} \neq 0$ and $\mu_i = 0$, and at the second subsonic point, $\mu_{i-2} \neq 0$ and $\mu_{i-1} = \mu_i = 0$; therefore H becomes a zero-order term. To eliminate this zero-order error, the following first-order artificial viscosity was used at the first subsonic point downstream of a shock:

$$H = H_s = -\,(\Delta X)\,(\mu p_1\phi_{XX})_X = (\mu p_1\phi_{XX})_{i-2} - (\mu p_1\phi_{XX})_{i-1} . \tag{16}$$

It can be verified that the quantity $\mu p_1\phi_{XX}$ is conserved along Y = constant as in the earlier scheme, implying that mass flux is conserved. A stable, finite-difference relaxation scheme can be developed, incorporating a second- or third-order coordinate transformation to provide flowfield solutions that are at least second-order accurate at both subsonic and supersonic points and first-order accurate at shock points.

To improve further the order of accuracy of flowfield solutions at supersonic and shock points, a new third-order quasi-conservative scheme can be developed by adding the following third-order artificial viscosity.

$$H = (\Delta X)^3\,(\mu p_1\phi_{XX})_{XXX} = (\mu p_1\phi_{XX})_i - 3\,(\mu p_1\phi_{XX})_{i-1} + 3\,(\mu p_1\phi_{XX})_{i-2} - (\mu p_1\phi_{XX})_{i-3} \tag{17}$$

at supersonic points and adding a second-order artificial viscosity

$$H = H_s = -(\Delta X)^2 \left(\mu p_1 \phi_{XX}\right)_{XX} = -\left(\mu p_1 \phi_{XX}\right)_{i-3} + 2\left(\mu p_{XX}\right)_{i-2} - \left(\mu p_1 \phi_{XX}\right)_{i-1} \qquad (18)$$

at the first downstream sub-sonic point after shocks. It can again be verified that the quantity $\mu p_1 \phi_{XX}$ is conserved. A similar, stable, finite-difference relaxation scheme has been developed which incorporates a second- or third-order coordinate transformation and provides flowfield solutions that are at least second-order accurate at both subsonic and supersonic points and second-order accurate at shock points.

A summary of approximations of the full potential equation solved at subsonic, shock, and supersonic points by adding the various forms of artificial viscosity is presented in table 1. The shock point is defined as the first subsonic point downstream of a shock. In the original second-order quasi-conservative scheme, the artificial viscosity continues to be added to the second subsonic point downstream of the shock in order to maintain the flux balance. In the other schemes, no artificial viscosities are added after the shock point. From the table it is obvious that the approximation at shock points is always at least one order lower than the approximation to the equation at supersonic points.

ONE-DIMENSIONAL SHOCK JUMP ANALYSIS

The solution procedure suggested previously does not correspond to shock fitting where the shock jump relation is explicity enforced during iterations. It is therefore necessary to know how the predicted shocks compare with Rankine-Hugoniot shocks. The following one-dimensional analysis suggested by Caughey and Jameson (ref. 5) ignores the surface curvature effect as well, but can provide upper and lower bounds for normal shock jumps predicted by quasi-conservative schemes. Two-dimensional effects on shock predictions are important, especially on a curved surface, and the shock location and strength become undefined in nonconservative schemes in one-dimensional analysis; this aspect will be discussed separately in subsequent sections.

The one-dimensional potential equation,

$$\left(a^2 - u^2\right)\phi_{XX} = 0 \qquad (19)$$

can be rewritten as (ref. 5)

$$\left(1 - M^{*2}\right)\hat{\phi}_{XX} = 0, \qquad (20)$$

where the normalized Mach number $M^* = u/a^*$ is the dimensionless ratio of the fluid velocity $u = a^*\hat{\phi}_x = \phi_x$ to the sonic speed of sound a^* and is related to local Mach number, M, as

$$M^* = \sqrt{\frac{1.2\,M^2}{1 + 0.2\,M^2}} \qquad (21)$$

if $\gamma = 1.4$ is assumed.

In the second-order quasi-conservative scheme, the following finite-difference approximation to equation (20)

$$\left(1 - M_i^{*2}\right)\left(\hat{\phi}_{i-1} - 2\hat{\phi}_i + \hat{\phi}_{i-1}\right) + H_{i-2} - 2H_{i-1} + H_i = 0 \qquad (22)$$

is solved at supersonic and subsonic points, and

$$\left(1 - M_i^{*2}\right)\left(\hat{\phi}_{i-1} - 2\hat{\phi}_i + \hat{\phi}_{i+1}\right) + H_{i-2} - H_{i-1} = 0 \qquad (23)$$

TABLE 1. APPROXIMATIONS OF FULL POTENTIAL EQUATIONS.

$$L(\phi) = \left(\frac{a^2}{q^2} - 1\right) \phi_{ss} + \frac{a^2}{q^2} \phi_{nn}$$

$$\phi_{ss} = p_1 \phi_{XX} + p_2 \phi_{YY} + p_3 \phi_{XY} + p_4 \phi_X + p_5 \phi_Y$$

$$\phi_{nn} = {}^2\phi - \phi_{ss} \; ; \; \mu = \text{Max}\left(1 - \frac{a^2}{q^2} , 0\right)$$

$$\widehat{p}_1 = p_1 \phi_{XX} \approx \phi_{ss}$$

H	Supersonic	Shock	Subsonic
First order	$L(\phi) + \left(\mu\widehat{p}_1\right)_i - \left(\mu\widehat{p}_1\right)_{i-1} = 0$	$L(\phi) - \left(\mu\widehat{p}_1\right)_{i-1} = 0$	$L(\phi) = 0$
Second order (ref.4)	$L(\phi) + \left(\mu\widehat{p}_1\right)_i - 2\left(\mu\widehat{p}_1\right)_{i-1} + \left(\mu\widehat{p}_1\right)_{i-2} = 0$	$L(\phi) - 2\left(\mu\widehat{p}_1\right)_{i-1} + \left(\mu\widehat{p}_1\right)_{i-2} = 0$	$L(\phi) = 0$
Second order (present)	$L(\phi) + \left(\mu\widehat{p}_1\right)_i - 2\left(\mu\widehat{p}_1\right)_{i-1} + \left(\mu\widehat{p}_1\right)_{i-2} = 0$	$L(\phi) - \left(\mu\widehat{p}_1\right)_{i-1} + \left(\mu\widehat{p}_1\right)_{i-2} = 0$	$L(\phi) = 0$
Third order	$L(\phi) + \left(\mu\widehat{p}_1\right)_i - 3\left(\mu\widehat{p}_1\right)_{i-1} + 3\left(\mu\widehat{p}_1\right)_{i-2} - \left(\mu\widehat{p}_1\right)_{i-3} = 0$	$L(\phi) - \left(\mu\widehat{p}_1\right)_{i-1} + 2\left(\mu\widehat{p}_1\right)_{i-2} - \left(\mu\widehat{p}_1\right)_{i-3} = 0$	$L(\phi) = 0$

BLANK
PAGE

is solved at shock points, where

$$H_i = \mu_i \left(\hat{\phi}_{i+1} - 2\hat{\phi}_i + \hat{\phi}_{i-1} \right) \tag{24}$$

and

$$\mu_i = \text{Max} \left(M_i^{*2} - 1, 0 \right) . \tag{25}$$

The normalized Mach number M_i^* is determined by

$$M_i^* = \left(\hat{\phi}_{i+1} - \hat{\phi}_{i-1} \right) / 2(\Delta X) \tag{26}$$

if the second-order element is used and by

$$M_i^* = \left(2\hat{\phi}_{i+1} + 3\hat{\phi}_i - 6\hat{\phi}_{i-1} + \hat{\phi}_{i-2} \right) / 6(\Delta X) \tag{27}$$

if the third-order element is used. When using the second-order element, equation (22) satisfies a piecewise linear condition, i.e., the solution for $\hat{\phi}$ is a piecewise linear function of X in both subsonic and supersonic regions. However, if the third-order element is used, the piecewise linear behavior can be maintained only if equation (26) is used at two subsonic points downstream of the shock and equation (27) is used elsewhere. At the discontinuity point that divides the solution into two piecewise linear solutions, equation (23) is used to determine the shock jump condition, depending on the relative location of the discontinuity point to the nearest neighboring mesh point.

Following the analysis in reference 5, assume the shock to be located at a fraction, α, of the distance between the (i – 1)-th and i-th mesh points. A lower bound of the shock jump relation can be found, by setting $\alpha = 0$, to be

$$M_2^* = 2 - M_1^* , \tag{28}$$

where M_1^* and M_2^* represent the normalized Mach numbers upstream and downstream of the shock. An upper bound can be found by setting $\alpha = 0.5(\Delta X)$, as

$$M_2^* = -0.6 M_1^* + 0.8 \left(5 - M_1^* \right)^{1/2} \tag{29}$$

for the second-order element. Equations (28) and (29) are the same as the solutions derived for the first-order quasi-conservative scheme. The same upper- and lower-bound solutions for the second-order element can be found for the third-order quasi-conservative scheme, described by equations (17) and (18).

For the third-order element, a similar analysis can be carried out for first-, second-, and third-order quasi-conservative schemes. The upper- and lower-bound solutions are the same for all the quasi-conservative schemes. A lower-bound solution found for the third-order element by setting $\alpha = 0$ is identical to the one found for the second-order element, i.e., equation (28); by setting $\alpha = \Delta X$, the upper-bound solution is found to be

$$M_2^* = 3 - 2 M_1^* . \tag{30}$$

Shock jump results thus obtained in equations (28), (29), and (30) are presented in figure 3. The band between the upper- and lower-bound solutions for the third-order element is much wider than the band for the second-order element. The third-order element analysis also shows that as the location of the discontinuity point changes from $+ \epsilon(\Delta X)$ to $- \epsilon(\Delta X)$, where ϵ is an infinitesimal number, the solution changes suddenly from the lower bound to upper bound. These undesirable features are due to the

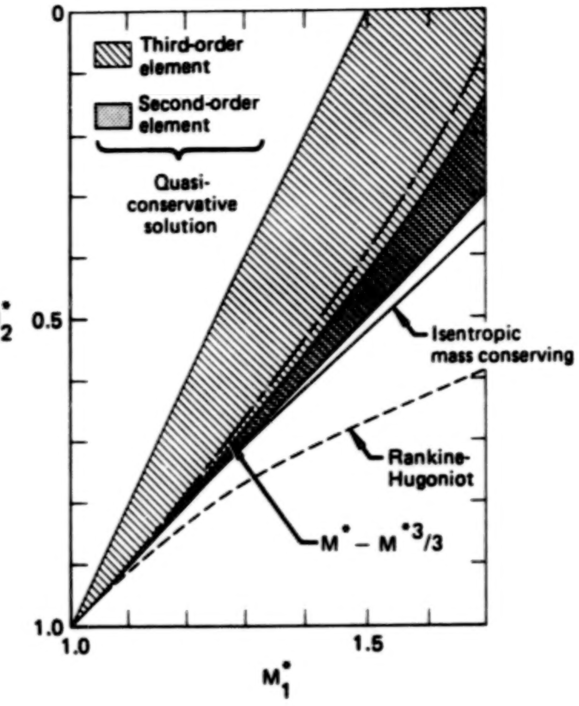

Figure 3. Shock relations for quasi-conservative solutions obtained by applying a second- and a third-order element.

asymmetry of the third-order element which tends to introduce additional asymmetric errors that generally cancel each other for the second-order element. A simple one-dimensional computer code was written to verify the above analysis. By specifying Cauchy data at the upstream supersonic boundary point and a Dirichlet condition at the downstream subsonic boundary point, and by adjusting the initial solutions and the number of mesh points between the two boundary points, various shock jumps corresponding to various values of α can be obtained and are found to be within the band predicted in the above analysis.

Three other shock jump relations are shown in figure 3. The lower curve represents the Rankine-Hugoniot shock relation. The middle curve represents the shock relation obtained by conserving mass flux across the shock isentropically, i.e., the exact fully conservative solution. The upper curve represents the shock relation obtained by conserving the quantity, $M^* - M^{*3}/3$, across the shock, or by solving

$$\left[\hat{\phi}_X - \frac{1}{3}\left(\hat{\phi}_X\right)^3\right]_X = 0\,. \qquad (31)$$

The shock relation is found to be

$$M_2^* = -\,0.5\,M_1^* + 0.5\left(12 - 3\,M_1^{*2}\right)^{1/2}. \qquad (32)$$

Equation (31) is obtained by rewriting the one-dimensional quasi-linear potential equation in divergence form. The exact, fully conservative solution lies closest to the Rankine-Hugoniot shock relation. Applying the third-order element at shock points in the quasi-conservative schemes can introduce large errors in the prediction of shock jumps. However, two-dimensional effects resulting from surface curvatures which are absent from the one-dimensional analysis, seem to provide relief from the overprediction of shock strength in many cases and will be discussed later.

TWO-DIMENSIONAL NOZZLE FLOWS

The precise strength of the shock wave is difficult to determine when it intersects a curved solid boundary because of the large gradients in the flow immediately downstream of the shock. These gradients result from the incompatibility of the normal momentum equation with the jump relations. The normal momentum equation that relates streamline curvature to the pressure (or velocity) gradient requires a negative normal pressure gradient in both subsonic and supersonic regions if there is a positive streamwise curvature; the shock jump relation that relates the flow properties on either side of the shock requires that the normal pressure gradient change sign crossing the shock. In fact, a logarithmic singularity must exist in the flow immediately downstream of the intersection of a normal shock with a wall of continuous, finite curvature (ref. 8). The inability of the numerical scheme to accurately resolve the flow in the region immediately downstream of the shock leads to an inaccurate prediction of the local Mach number, and, hence, to an imprecise estimate of the shock strength. For this reason, the shock strength can be more precisely determined in the special case of the intersection of a normal shock with a plane wall. A model problem which considers a choked flow inside a converging-diverging nozzle with a conical diverging section will be studied here.

A previously developed inlet program (refs. 9, 10) was modified to compute transonic flows about a planar symmetric inlet by incorporating the first-, second-, and third-order quasi-conservative schemes described earlier and the first- and second-order nonconservative schemes described in references 9 and 4, respectively. The transformed full potential equation is approximated within a local second- or third-order element, and a finite-difference solution is obtained by an extrapolated relaxation scheme. The prediction of shocks and the conservation of mass flux across shocks in the solutions obtained by various schemes will be scrutinized. The boundary conditions are adjusted so that the shocks occur in the diverging nozzle section where the surface slope is constant so that no surface curvature effects are present.

Figure 4 shows the contour and the grid system of the inlet considered for this study. The highlight of the inlet is located at $\hat{x}/D = 0$, where D is the outer height of the inlet. A converging section extends from the highlight to a minimum cross-section which is located at $\hat{x}/D = 0.5675$ or $x = 0$ and has a height equal to 0.3D. A diverging section extends from the minimum cross-section to $\hat{x}/D = 1.4675$ or $x = 1.0$ where the height is equal to 0.345D. Two meshes are used in the calculation: a coarse mesh having 40 cells from the upstream infinity to the nozzle exit and 12 mesh cells from the axis of symmetry to the nozzle surface, and a fine mesh having twice as many mesh cells in each direction. The converged solution obtained on the coarse mesh is used as an initial estimate for the iterative solution on the fine mesh. For all the results presented here, the freestream Mach number is arbitrarily set to be 0.700. A constant and sufficiently large flow rate is required at the nozzle exit as a boundary condition such that the flow is choked at the throat cross-section during iterations in the coarse mesh and during the first few hundred relaxation iterations in the fine mesh. Then the potential function at the nozzle exit is frozen for subsequent relaxation steps until a converged solution is reached, i.e., the total number of supersonic points ceases to change and the maximum residual has been reduced to less than 10^{-6}. Freezing the potential function at the nozzle exit boundary changes a Neumann boundary condition to a Dirichlet boundary condition, which not only improves the convergence rate but also ensures a well-defined shock. The flowfield inside the diverging nozzle is nearly one-dimensional. However, since the grid is not conical in the diverging section, the flowfield is effectively two-dimensional. Several sets of solutions obtained using the various schemes with the second-order element are summarized in table 2. H represents the order of artificial viscosity, M_e is the average Mach number at the nozzle exit, x_s represents the average shock location, M_{1w} and M_{2w} are the Mach numbers upstream and downstream of the shock at the nozzle wall, M_{1a} and M_{2a} are the Mach numbers upstream and downstream of the shock at the axis of symmetry, $\dot{m}_1$ and $\dot{m}_2$ are the mass flow rates per unit width at cross-sections upstream and downstream of

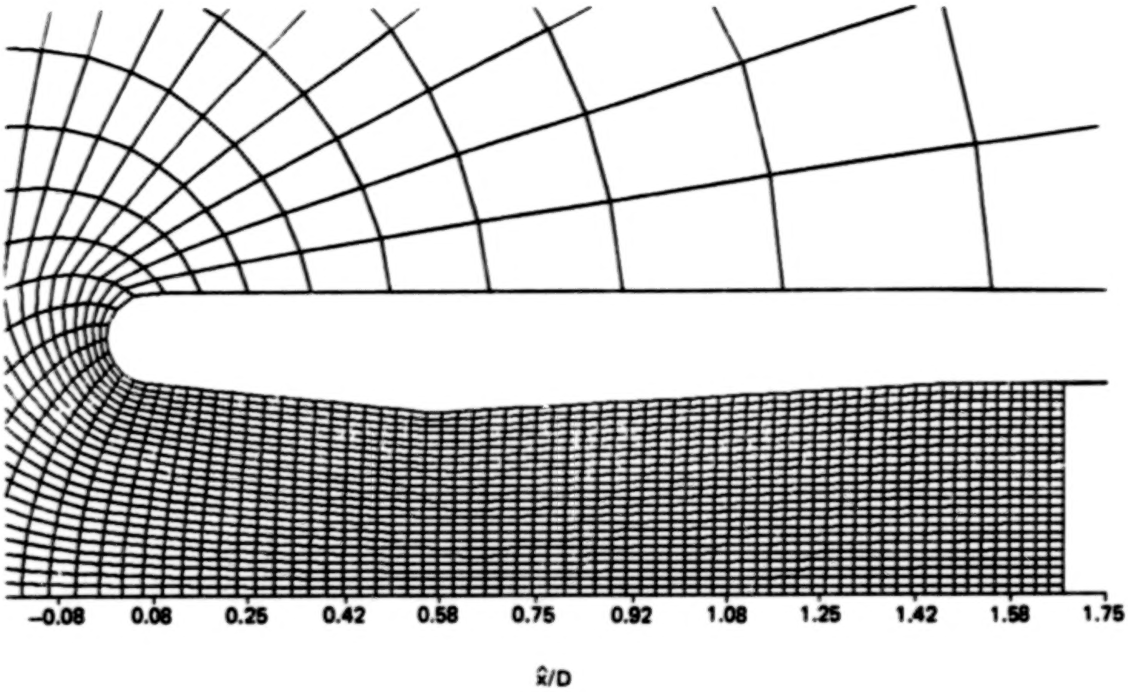

Figure 4. Contour and grid system for a converging-diverging nozzle.

TABLE 2. SUMMARY OF SHOCK SOLUTIONS IN A CONICAL DIVERGING NOZZLE.

	Case	H	M_e	X_s	M_{1w}	M_{2w}	M_{1A}	M_{2A}	$\dot{m}_1$	$\dot{m}_2$	ϵ (%)
Nonconservative	1	1	0.665	0.190	1.142	0.912	1.139	0.906	0.2766	0.2849	3.0
	2	1	0.695	0.395	1.210	0.844	1.269	0.897	0.2639	0.2781	5.4
	3	1	0.715	0.555	1.295	0.804	1.301	0.857	0.2639	0.2815	6.7
	4	2	0.665	0.190	1.214	0.889	1.139	0.932	0.2764	0.2849	3.1
	5	2	0.684	0.325	1.180	0.881	1.306	0.907	0.2638	0.2757	4.5
	6	2	0.712	0.640	1.387	0.760	1.318	0.826	0.2638	0.2810	6.5
Quasi-conservative	7	1	0.629	0.335	1.221	0.754	1.294	0.732	0.2645	0.2638	–0.3
	8	1	0.623	0.490	1.297	0.696	1.317	0.709	0.2646	0.2624	–0.8
	9	1	0.618	0.695	1.384	0.636	1.364	0.681	0.2650	0.2613	–1.4
	10	2	0.625	0.490	1.278	0.698	1.334	0.710	0.2645	0.2628	–0.7
	11	2	0.620	0.640	1.371	0.640	1.308	0.698	0.2644	0.2616	–1.2
	12	2	0.605	0.915	1.408	0.593	1.451	0.597	0.2486	0.2425	–2.5
	13	3	0.629	0.325	1.184	0.773	1.328	0.707	0.2644	0.2638	–0.2
	14	3	0.633	0.425	1.229	0.733	1.362	0.709	0.2648	0.2647	–0.04
	15	3	0.627	0.490	1.289	0.699	1.238	0.742	0.2645	0.2632	–0.5

the shock, and ϵ is the percentage change of mass flow rate across the shock, i.e., $(\dot{m}_2 - \dot{m}_1)\ \dot{m}_1$, where $\dot{m}$ is defined as

$$\dot{m} = \frac{1}{\rho_t U_\infty} \int \rho u dy\,, \tag{33}$$

ρ_t is the stagnation density upstream of the shock, and U_∞ is the freestream velocity. For isentropic flow, $\dot{m}$ can be expressed as

$$\frac{\left(1 + 0.2\,M_\infty{}^2\right)^{0.5}}{M_\infty} \int M_x \left(1 + 0.2\,M^2\right)^{-3} dy\,,$$

where M_x is the axial Mach number. Applying equation (34), the percentage changes of $\dot{m}$ can be computed and are listed in table 2; the nonconservative solutions are consistently shown to predict an increase of $\dot{m}$ while the quasi-conservative solutions consistently predict a decrease of $\dot{m}$. This result is consistent with the observed underpredictions and overpredictions of shock strengths in the nonconservative and quasi-conservative solutions, respectively, as shown in figures 5 to 10. Mach number distributions obtained by the various finite-difference schemes are plotted versus x in figures 5–10, for the diverging wall and along the axis of symmetry, and are compared with predictions of one-dimensional isentropic flow theory combined with Rankine-Hugoniot shocks. In the one-dimensional calculations, the throat Mach number was set equal to unity, and the shock location was matched to the shock location predicted by the finite-difference scheme. In supersonic regions, the average of the Mach number distributions on the wall and along the axis of symmetry agrees with the one-dimensional Mach number distribution; however, Mach numbers immediately downstream of shocks and throughout the subsonic regions are overpredicted for nonconservative solutions and underpredicted for quasi-conservative solutions.

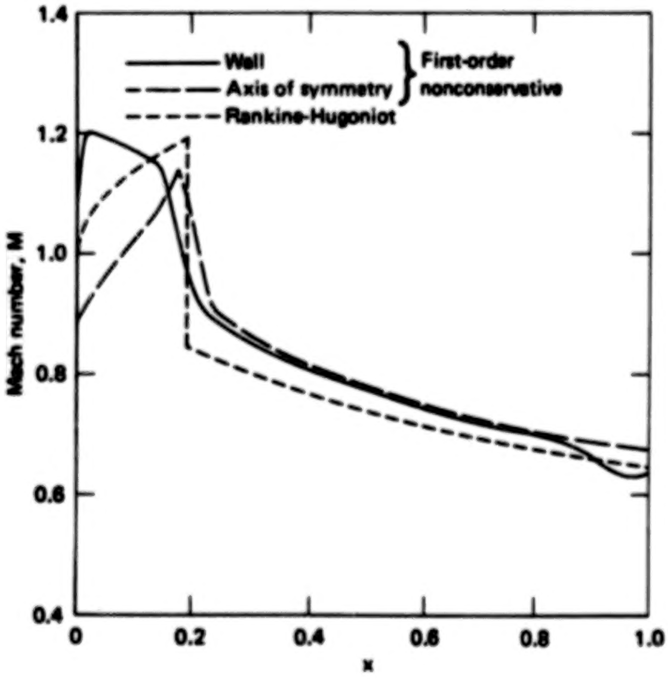

Figure 5. Mach number distributions for Case 1.

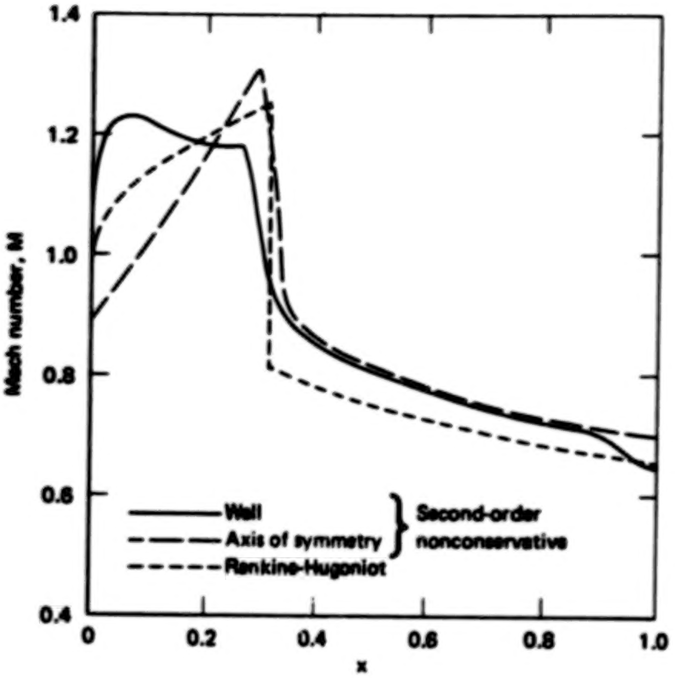

Figure 6. Mach number distributions for Case 5.

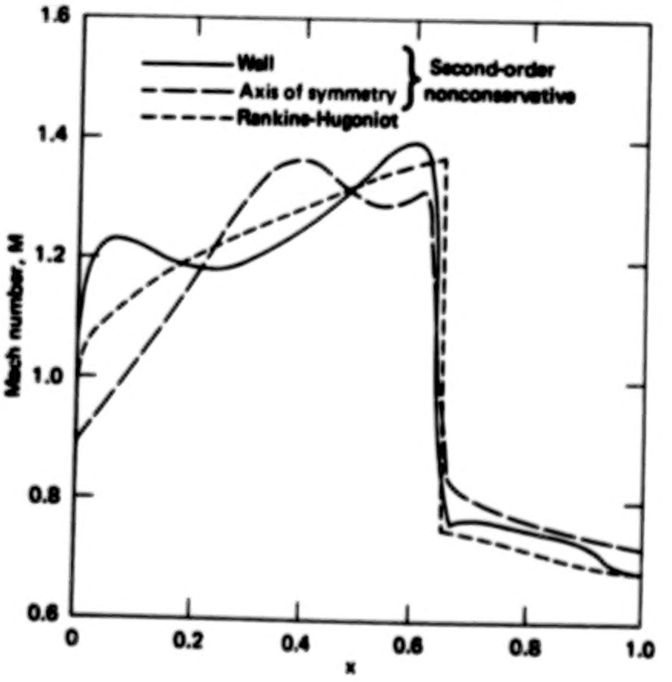

Figure 7. Mach number distributions for Case 6.

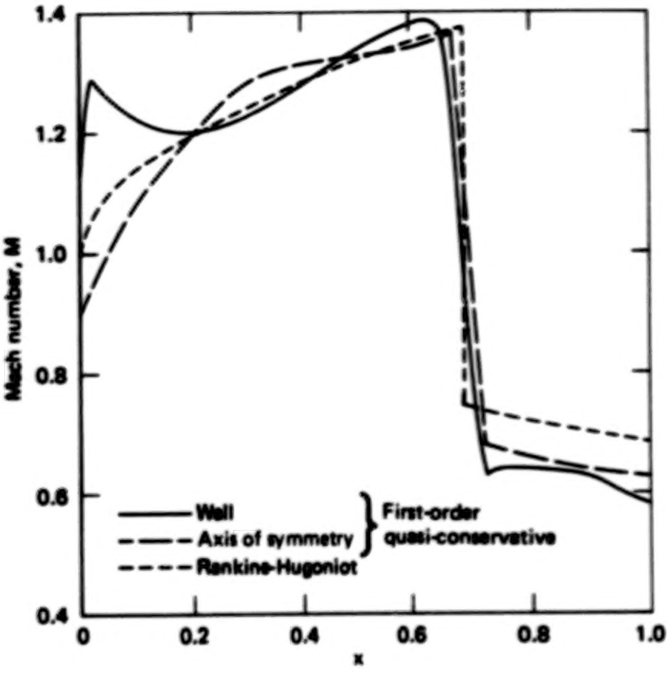

Figure 8. Mach number distributions for Case 9.

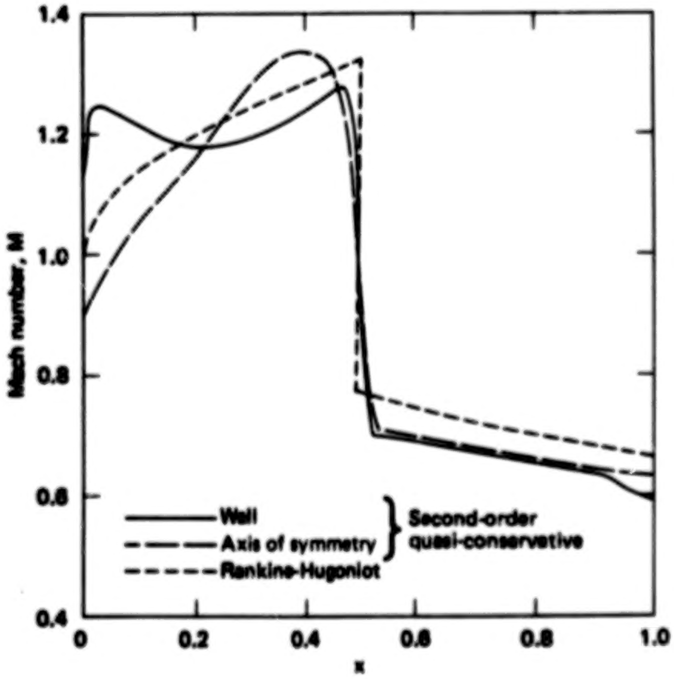

Figure 9. Mach number distributions for Case 10.

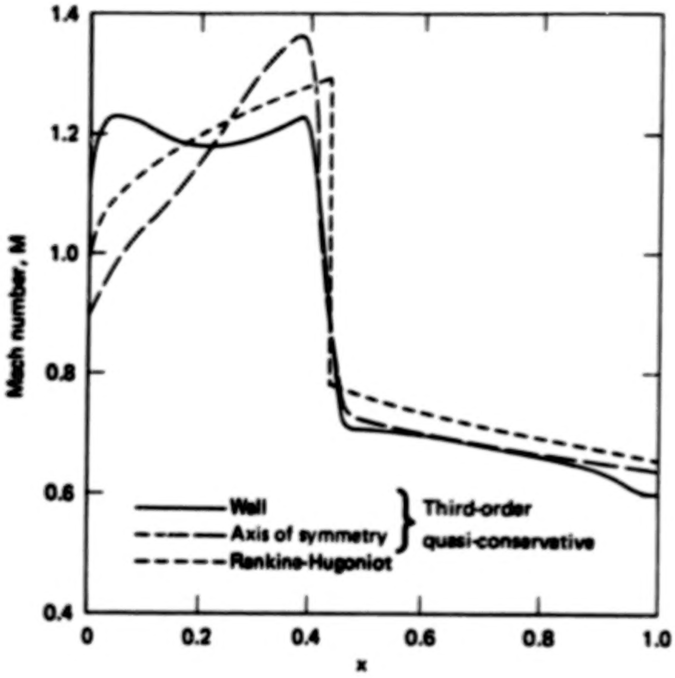

Figure 10. Mach number distributions for Case 14.

Even the nonconservative schemes provide well-defined shock locations in this nearly one-dimensional case. If the flow were exactly one-dimensional, the nonconservative schemes would admit any solution having a shock located upstream of the position given by the quasi-conservative schemes, which can be verified easily by analyzing equation (20). It is apparent that the two-dimensionality of transonic flows provides well-defined shock location in the nonconservative schemes.

AIRFOIL FLOWS

As mentioned in the previous sections, surface curvature may cause a logarithmic singularity in the flow solutions near the shock, which can result in an inaccurate prediction of the local Mach number distribution immediately downstream of the shock. Proper treatment of the potential equation at a shock can be made to eliminate the zero-order term. Solutions obtained by the improved second-order scheme and a new third-order quasi-conservative scheme will be shown and compared with earlier solutions.

Typical results obtained by the various treatments at shock and supersonic points are presented in figures 11 to 13. In figure 11, solutions obtained by the original and improved second-order quasi-conservative schemes are compared for a NACA 64A410 airfoil at a freestream Mach number $M_\infty = 0.72$ and angle of attack $\alpha = 0$. N is the total number of grid points on the airfoil surface, and M is the number of grid points in the surface normal direction. The original scheme has a zero-order H term added to the governing equation at shock points and results in a stronger shock than the consistent scheme. In figure 12, solutions obtained by using different artificial viscosities are compared for the same airfoil. The pressure jumps across the shock predicted by the solutions are shown, and the percentage differences between the jumps and the ones predicted by the Rankine-Hugoniot shock jump relation are listed in parentheses. The present solutions obtained by the second-order and third-order artificial viscosities agree within plotting accuracy and predict shock jumps almost identical to those calculated from the Rankine-Hugoniot shock jump relation. This conclusion is in contradiction to the one-dimensional shock jump analysis which predicts that the shock jump obtained from a quasi-conservative scheme should always be stronger than the mass-conserving isentropic shock jump, which is also stronger than the Rankine-Hugoniot shock jump, as shown in figure 3. This contradiction can be explained by the failure of the numerical scheme to resolve the large gradient which will be present near the logarithmic singularity downstream of the shock.

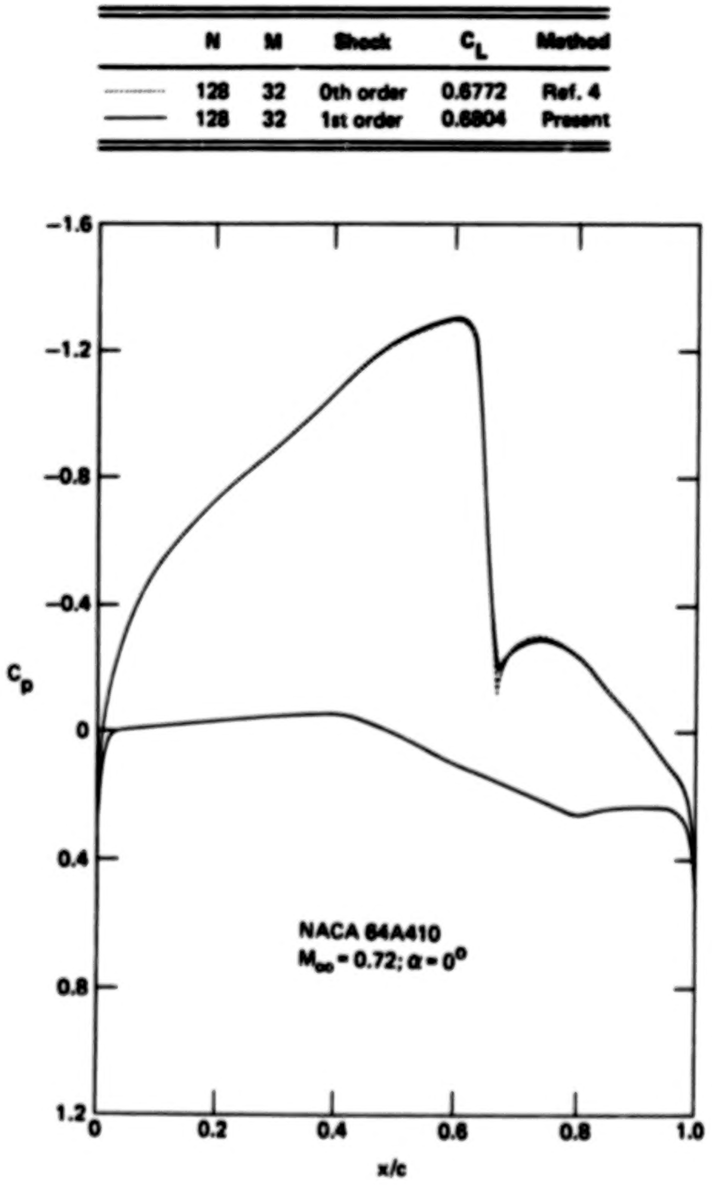

Figure 11. Comparison of second-order solutions obtained by the original and consistent second-order quasi-conservative solutions.

It has been shown in reference 4 that second-order quasi-conservative solutions generally avoid numerical shock smearing better than Jameson's second-order fully conservative solutions. The improved second-order and new third-order quasi-conservative solutions are compared with Jameson's first-order and second-order fully conservative solutions in figure 13 for a Korn airfoil at $M_\infty = 0.74$ and $\alpha = 0$. The present quasi-conservative solutions obtained by using second- and third-order artificial viscosities agree, except for a slight discrepancy near the first shock. The first-order solution cannot capture the first

	N	M	H	Shock	C_L	Method
----	192	32	1st order	0th order	0.6664	FLO-36
········	256	48	1st order	0th order	0.6662	FLO-36
——	128	32	3rd order	2nd order	0.6804	Present

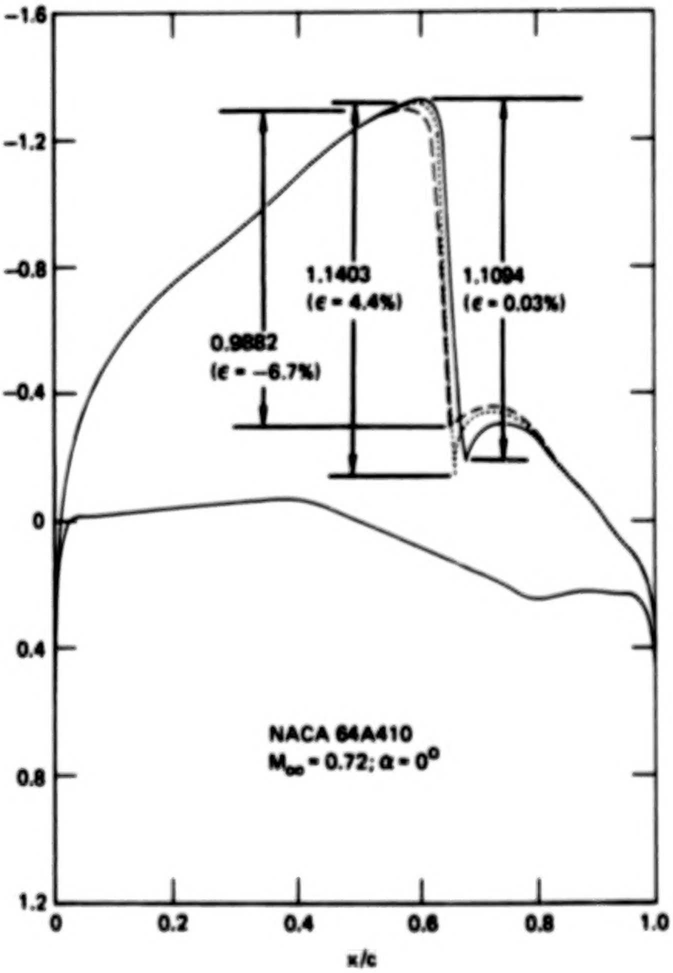

Figure 12. Comparison of first-order and third-order solutions for a NACA 64A410 airfoil.

shock. The second-order fully conservative solution predicts a first-shock location further downstream, which has been shown to move upstream as the mesh size becomes smaller (ref. 4), and also predicts an unrealistic pressure oscillation after the second shock, which also exists in the original second-order quasi-conservation solution (ref. 4). Again these discrepancies are believed to be caused by the zero-order error at shocks.

	N	M	H	Shock	C_L	Method
- - - -	256	48	1st order	0th order	0.5955	FLO-36
....	256	48	2nd order	0th order	0.6005	Fully conservative
— —	128	32	2nd order	1st order	0.6039	Present
——	128	32	3rd order	2nd order	0.6043	Quasi-conservative

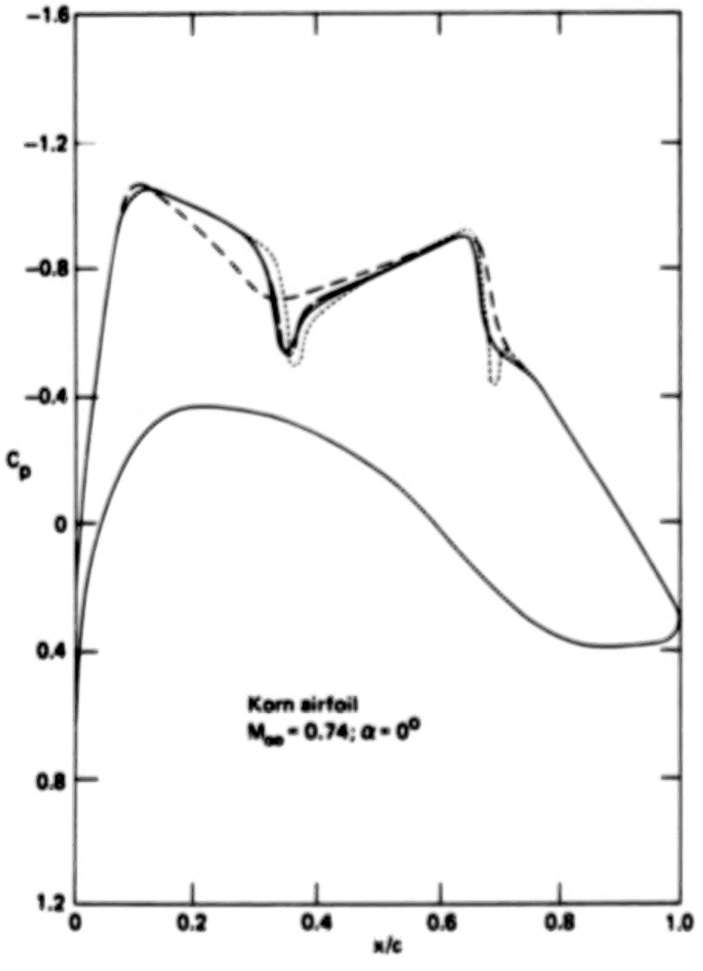

Figure 13. Comparison of first-, second-, and third-order solution for a Korn airfoil.

CONCLUSION

A new, third-order, quasi-conservative algorithm has been successfully developed for two-dimensional transonic flowfield calculations. Various treatments of the potential equation at shocks have been introduced that satisfy the conservation rule and the full potential equation at shocks as the mesh size is decreased. An extensive study of a nearly one-dimensional transonic flow inside a converging-diverging nozzle was conducted by applying various finite-difference schemes and comparing solutions with the Rankine-Hugoniot relation. Nonconservative solutions consistently underpredict the shock strength, while quasi-conservative solutions consistently overpredict the shock strength for this nearly one-dimensional flow case. Proper treatments of the governing equation at shocks have been shown to eliminate pressure oscillations which otherwise occur downstream of the shock for airfoil applications. Two-dimensionality has been shown to have a significant effect on obtaining a well-defined shock for nonconservative schemes.

ACKNOWLEDGEMENT

Helpful discussions on the nozzle problem with P. A. Henne of Douglas Aircraft Company and F. W. Spaid of McDonnell Douglas Research Laboratories are gratefully acknowledged.

REFERENCES

1. *Murman, E. M.; and Cole, J. D.: Calculations of Plane Steady Transonic Flows. AIAA Journal, vol. 9, no. 1, Jan. 1971, pp. 114–121.*

2. *Murman, E. M.: Analysis of Embedded Shock Waves Calculated by Relaxation Method. AIAA Journal, vol. 12, no. 5, May 1974, pp. 616–633.*

3. *Jameson, A.: Transonic Potential Flow Calculations Using Conservation Form. Proceedings of AIAA 2nd Computational Fluid Dynamics Conference, June 1975, pp. 148–161.*

4. *Chen, L. T.: Higher Accuracy Finite Difference Schemes for Transonic Airfoil Flowfield Calculations. AIAA paper 81-381, Jan. 1981; AIAA Journal, in press.*

5. *Caughey, D. A.; and Jameson, A.: Progress in Finite-Volume Calculations for Wing-Fuselage Combinations. AIAA Journal, vol. 18, no. 11, Nov. 1980, pp. 1281–1288.*

6. *Bauer, F.; and Korn, D. G.: Computer Simulation of Transonic Flow Past Airfoils with Boundary Layer Correction. Proceedings of AIAA 2nd Computational Fluid Dynamics Conference, June 1975, pp. 184–189.*

7. *Bauer, F.; Garabedian, D. R.; Korn, D. G.; and Jameson, A.:* **Supercritical Wing Sections II**, *Springer, New York, 1975.*

8. *Oswatitsch, K.; and Zierep, J.: Das Problem des senkrechten Stosses an einen gekrümmten Wand. Zeit. ang. Math. u. Mech. vol. 40, no. 143, 1960.*

9. *Chen, L. T.; and Caughey, D. A.: Calculation of Transonic Inlet Flowfields Using Generalized Coordinates. Journal of Aircraft, vol. 17, no. 3, March 1981, pp. 167–174.*

10. *Chen, L. T.; and Caughey, D. A.: Transonic Inlet Flow Calculations Using a General Grid-Generation Scheme. Journal of Fluid Engineering, vol. 102, no. 3, Sept. 1980, pp. 309–315.*

11. *Jameson, A.: Acceleration of Transonic Potential Flow Calculations on Arbitrary meshes by the Multiple Grid Method. Proceedings of AIAA 4th Computational Fluid Dynamics Conference, July 1979, pp. 122–146.*

FULLY IMPLICIT SHOCK TRACKING

J. B. BELL, G. R. SHUBIN, AND J. M. SOLOMON
Naval Surface Weapons Center/White Oak Lab
Silver Spring, Maryland 20910

Abstract

We present a fully implicit shock tracking method for solving hyperbolic free boundary problems arising in fluid dynamics. The new method is based on the noniterative implicit methods developed by Beam and Warming and others. The principal feature of the new approach is that the implicit form is used to simultaneously treat both interior points and boundary conditions. In particular, the location of the free boundary (shock) surface is treated implicitly and coupled with all other unknowns. The method is presented here in the context of unsteady one-dimensional flow in a variable area duct with an internal shock wave. The fully implicit method and other strategies for advancing the shock are compared for computing a steady solution via a time asymptotic approach. Issues regarding extension of the method to multiple dimensions are also discussed.

1. Introduction.

In this paper we develop a fully implicit shock tracking (or fitting) method for one dimensional flow in a variable area duct. The method is based on the noniterative implicit methods described, for example, in Beam and Warming [1]. Implicit methods have recently become popular for fluid dynamics problems, especially when using a time asymptotic approach to obtain steady state solutions (see e.g., [2]-[4]). The reason for this popularity is that implicit methods (based on von Neumann stability properties) allow a larger time step than is possible for explicit methods and consequently reduce the number of steps needed to reach a steady solution. However, in practical problems such as the supersonic blunt body problem we can often improve the accuracy and efficiency of computations by tracking at least some of the shockwaves present in the problem. This entails using the tracked shock as a computational boundary, the geometry of which is unknown and is to be determined. Existing applications of implicit methods to such problems treat the shock geometry explicitly (eg. [4]). It then becomes questionable whether the large time steps allowed at interior points can in fact be taken since the explicit advancement of the shock could impose restrictive bounds on step size.

The fully implicit method presented here (see section 3) addresses this issue by treating both the interior flow equations and the boundary conditions in an implicit, fully coupled, time accurate manner. This approach is rather complicated and requires more work per step than is needed when treating boundaries explicitly. However, the allowable time step also increases, in some cases quite dramatically. For comparison purposes, we also consider a method which explicitly advances the shock. In addition, we develop an implicit but uncoupled approach which enjoys some of the advantages of the fully implicit method without the attendant increase in work per step (see section 3).

Section 4 contains a detailed study of the computational efficiency of three methods for computing steady state solutions. It should be noted that to some extent the dramatic results for the fully implicit method are related to the one-dimensionality of the model problem. In the limit as time step size goes to infinity the fully implicit method reduces to Newton's method [5], which provides an extremely efficient technique for computing steady solutions when a good initial guess is available [6]. Unfortunately, in multidimensional problems, the associated matrix problem becomes prohibitively large and operator splitting or approximate factorization is generally used. In this case the reduction to Newton's method will not occur and splitting error will limit the allowable size of time steps. Issues relating to the extension of implicit shock tracking methods to several dimensions will be discussed more fully in section 5.

2. Analytic Formulation

In this section we formulate a model problem on which to illustrate the fully implicit method. We wish to compute the steady one-dimensional flow in a duct of variable cross-sectional area A(x) using a time asymptotic approach. The unsteady duct flow is described in physical space $0 \leq x \leq x_{max}$ by

$$\frac{\partial(A\mathcal{U})}{\partial t} + \frac{\partial}{\partial x}(A\mathcal{F}) - \mathcal{H} = 0 \qquad (1)$$

where

$$\mathcal{U} = \begin{pmatrix} \rho \\ \rho u \\ \rho E \end{pmatrix}, \quad \mathcal{F} = \begin{pmatrix} \rho u \\ \rho u^2 + p \\ (\rho E + p)u \end{pmatrix}, \quad \mathcal{H} = \frac{dA}{dx}\begin{pmatrix} 0 \\ p \\ 0 \end{pmatrix}$$

and ρ is density, u is velocity, $E = e + \frac{u^2}{2}$ where e is specific internal energy, and p is pressure. For simplicity the equation of state is chosen to be that of a perfect gas, $p = (\gamma-1)\,\rho e$.

For certain duct shapes $A(x)$ and boundary specifications (discussed later), a steady solution exists in which a shock stands at some location in the duct. For numerical solution we will not treat the problem in the form of (1) because of the difficulties associated with resolving the shock. Instead, we will use a tracking procedure in which the shock location is treated as a dependent variable. This is accomplished by tranforming the problem to a computational space (ξ,τ) in which the physical shock location $s(t)$ is forced to be at a fixed location. An example of a transformation which does this is given by the mapping to computational space

$$\tau = t$$
$$\xi = \xi(x,t) = \begin{cases} x/s(t) \;, & 0 \le x \le s(t) \\ 1 + (K-1)\left[\dfrac{x-s(t)}{x_{max} - s(t)}\right], & s(t) \le x \le x_{max} \end{cases} \qquad (2)$$

so that the physical shock location s is mapped into the internal computational boundary $\xi = 1$. Likewise the inflow location $x = 0$ and the outflow location $x = x_{max}$ are mapped into $\xi = 0$ and $\xi = K$ respectively (see Fig. 1).

Under transformation (2) the governing equations in computational space (ξ,τ) can be written in the weak conservation form [7]

$$\frac{\partial U}{\partial \tau} = -\frac{\partial F}{\partial \xi} + \frac{1}{J}\mathcal{H} \equiv R_1(\xi;\, U,\, s,\, s_t) \qquad (3)$$

where $U = A\mathcal{U}/J$, $F = \xi_t U + A\xi_x \mathcal{F}/J$ and $J = \xi_x$ is the Jacobian, for fixed τ, of the transformation (2).

It remains to specify the boundary conditions at inflow $(\xi = 0)$, outflow $(\xi = K)$ and at the shock $(\xi = 1)$. Appropriate boundary conditions can be

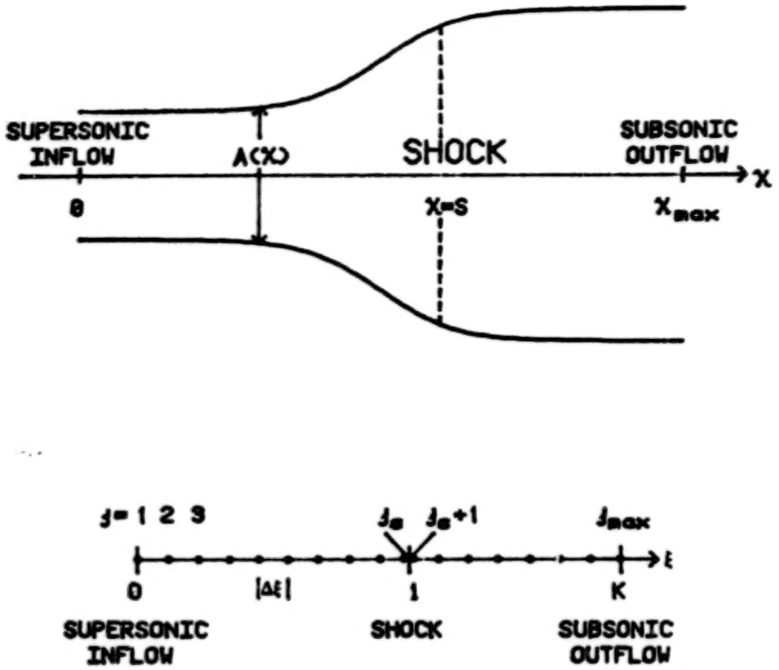
SUPERSONIC INFLOW
A(X)
SHOCK
SUBSONIC OUTFLOW
X
0
X=S
X_{max}
j=1 2 3
j_s j_s+1
j_{max}
ξ
0
|Δξ|
1
K
SUPERSONIC INFLOW
SHOCK
SUBSONIC OUTFLOW

Fig. 1 Physical and computational spaces for duct problem.

determined by a characteristic analysis of the system. Such an analysis is presented in detail in Appendix A for the case of supersonic inflow and subsonic outflow with an internal shock with flow crossing the shock from left to right.

At the supersonic inflow all flow quantities are specified so that

$$U\ (0,\tau) = sA(0) \begin{pmatrix} \rho_o \\ \rho_o\ u_o \\ \rho_o\ (e_c + u_o^2/2) \end{pmatrix} \tag{4}$$

where the subscripts "o" refers to the specified inflow quantities. At the subsonic outflow boundary ($\xi = K$), only the density ρ_e is specified; hence,

$$U_1\ (K,\tau) = A(x_{max}) \left(\frac{x_{max} - s}{K-1} \right) \rho_e . \tag{5a}$$

In addition, two compatibility conditions must be satisfied on $\xi = K$. These can be written in the form

$$\frac{\partial}{\partial \tau} \begin{pmatrix} U_2 \\ U_3 \end{pmatrix}_{\xi = K} = \mathbf{T} R_1\ (K;\ U,\ s,\ s_t) + \frac{A(x_{max})}{K-1} \left[\rho_e\ s_t - (x_{max} - s)\ \frac{d\rho_e}{dt} \right] B$$

$$\equiv R_2\ (U,\ s,\ s_t) \tag{5b}$$

where

$$B = -\begin{pmatrix} u_e - a_e \\ \\ \frac{a_e^2}{\gamma-1} - u_e \left(a_e - \frac{u_e}{2}\right) \end{pmatrix}, \quad \mathbf{T} = \left(B \;\middle|\; \begin{matrix} 1 & 0 \\ 0 & 1 \end{matrix} \right)$$

with the "e" subscript denoting quantities at the outflow boundary and "a" the sound speed $(\gamma\, p/\rho)^{\frac{1}{2}}$.

The shock $\xi = 1$ represents an internal boundary. Quantities at the left (the low pressure side) will be denoted with an "L" subscript and quantities at the right (the high pressure side) will be denoted with an "R" subscript. The flow quantities on both sides of the shock must satisfy the Rankine-Hugoniot relations. These can be written in the following form

$$U_R = \mathcal{R}(U_L,\ s,\ s_t). \tag{6}$$

The vector valued function $\mathcal{R}$ is given explicitly in Appendix B for a perfect gas with constant γ. On the left side of the shock, all of the original equations (3) hold with the ξ partial derivatives interpreted using only quantities on the left side (i.e., $0 < \xi \leq 1$). On the right side of the shock (the high pressure side), only one compatibility condition need be satisfied. This condition combined with the Rankine-Hugoniot relations differentiated with respect to τ gives the following equation for s_t:

$$\frac{\partial s_t}{\partial \tau} = \vec{\alpha}_1 \cdot \left[\frac{\partial(\xi_x\ U/A)}{\partial \xi}\right]_R - \vec{\alpha}_2 \cdot \left[\frac{\partial(\xi_x\ U/A)}{\partial \xi}\right]_L + \alpha_3 \left(\frac{1}{A}\ \frac{dA}{dX}\right)_{\xi=1} \equiv r_3(U,s,s_t)$$

where $\vec{\alpha}_1$, $\vec{\alpha}_2$ and α_3 are defined in Appendix A. Thus, the equations for s and s_t can be summarized in the form

$$\frac{\partial S}{\partial \tau} = \begin{pmatrix} s_t \\ r_3\ (U,\ s,\ s_t) \end{pmatrix} \equiv R_3\ (U,\ s,\ s_t);\ S = \begin{pmatrix} s \\ s_t \end{pmatrix} \tag{7}$$

The transformed form of the equation (3) and the boundary conditions (4), (5), (6) and (7) fully specify the problem to be discretized.

3. Numerical Methods.

The implicit methods considered here are based on generalized time differencing in delta form introduced by Warming and Beam [8]. Namely, for any vector of unknown W satisfying a system of equations of the form

$$\frac{\partial W}{\partial \tau} = R(\xi,\ \tau;\ W)$$

we have

$$\Delta W^n - c_1 h\ \Delta(R(\xi,\ \tau^n;\ W^n)) = c_2\ \Delta W^{n-1} + c_3 h\ R(\xi,\ \tau^n;\ W^n) + \left[2c_1-(1+\pi^2 c_2)\right] 0(h^2) + 0(h^3) \quad (8)$$

where $\Delta\ (\cdot)^n=(\cdot)^{n+1}-(\cdot)^n$, $h = \tau^{n+1}-\tau^n$, $\pi = (\tau^n-\tau^{n-1})/h$, $c_3 = 1-\pi c_2$, and c_1, c_2 are scalar parameters.

Fully Implicit Shock Tracking (FIST):

The FIST approach is to consider both the conservation variables U and the shock geometry S simultaneously in an implicit manner. Using (8), the FIST time discretization takes the form

$$\Delta U^n - c_1 h\Delta\ (R_1(U^n,\ S^n)) = c_2\ \Delta U^{n-1} + c_3 h\ R_1(U^n,\ S^n);\ 0<\xi\leq 1, 1<\xi<k \quad (9)$$

$$\Delta U^n{}_R = \Delta\ (\mathcal{R}(U^n{}_L,\ S^n));\ \xi = 1 \quad (10)$$

$$\Delta U^n - c_1 h\ \Delta\ (R_2(U^n,\ S^n)) = c_2\ \Delta U^n + c_3 h\ R_2\ (U^n,\ S^n);\ \xi = k \quad (11)$$

$$\Delta S^n - c_1 h\ \Delta\ (R_3(U^n,\ S^n)) = c_2\ \Delta\ S^{n-1} + c_3\ h\ R_3(U^n,\ S^n) \quad (12)$$

Here (9) represents the interior equations (3), (10) represents the shock relations (6), (11) represents the two outflow compatibility conditions (5b), and (12) represents (7). When ΔR_i (i=1,2,3) and $\Delta\mathcal{R}$ are linearized, the resulting equations remain fully coupled. More precisely, the linearizations involve both U and S; e.g.,

$$\Delta(R_i(U^n,\ S^n)) \approx \left[\frac{\partial R_i}{\partial U}\right]^n \Delta U^n + \left[\frac{\partial R_i}{\partial S}\right]^n \Delta S^n$$

where $\left[\frac{\partial R_i}{\partial U}\right]^n$ and $\left[\frac{\partial R_i}{\partial S}\right]^n$ represent the (unique) linear differential operators corresponding to the "derivatives" of R_i with respect to U and S, respectively, taken at (U^n, S^n). The evaluation of these linearizations will be discussed latter in this section.

The problem is discretized spatially using equally spaced points $j=1,\ldots,j_s$ to the left of the shock and $j=j_s+1,\ldots,j_{max}$ to the right of the shock (see Fig. 1) and replacing spatial derivatives by centered differences at interior points and appropriate one-sided differences at $\xi = 1$ and $\xi = K$. For convenience, the unknowns U at $\xi = 0$ are eliminated by substituting (4) into the discretized equations. The resulting discrete matrix problem for ΔU^n $(j=2,\ldots,j_{max})$, ΔS^n admits essentially a block tridiagonal solution when the equations and unknowns are suitably ordered. In particular, the linearized system is written with the following ordering

$$(I - c_1 h\left[\frac{\partial R_1}{\partial U}\right])\ \Delta U_j{}^n - c_1 h\left[\frac{\partial R_1}{\partial S}\right]\Delta S^n = c_2\ \Delta U_j{}^{n-1} + c_3 h\ R_1{}^n \qquad (j=2,\ldots,j_s)$$

$$\Delta U^n_{j_s+1} - \left[\frac{\partial \mathcal{R}}{\partial U_L}\right]\Delta U_{j_s}{}^n - \left[\frac{\partial \mathcal{R}}{\partial S}\right]\Delta S^n = 0$$

$$(I - c_1 h\left[\frac{\partial R_1}{\partial U}\right])\ \Delta U_j{}^n - c_1 h\left[\frac{\partial R_1}{\partial S}\right]\Delta S^n = c_2\ \Delta U_j{}^{n-1} + c_3 h\ R_1{}^n \qquad (j=j_s+1,\ldots,j_{max}-1)$$

$$\Delta U^n_{1,j_{max}} + \frac{A(x_{max})}{K-1}\ \rho_e\ \Delta S^n = 0$$

$$(I - c_1 h\left[\frac{\partial R_2}{\partial U}\right])\Delta U^n_{i,j_{max}} - c_1 h\left[\frac{\partial R_2}{\partial S}\right]\Delta S^n = c_2\ \Delta U^{n-1}_{i,j_{max}} + c_3 h\ R_2{}^n \qquad (i=2,3)$$

$$-c_1 h\left[\frac{\partial R_3}{\partial U}\right]\Delta U^n + (I - c_1 h\left[\frac{\partial R_3}{\partial S}\right])\ \Delta S^n = c_2\ \Delta S^{n-1} + c_3 h\ R_3{}^n.$$

Writing the system in this way yields an algebraic system of the form

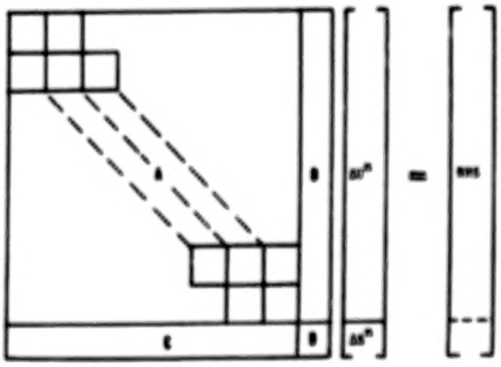

(13)

where $\mathbf{A}$ is a block tridiagonal matrix with $(j_{max} - 1)$ rows of blocks of size 3x3, $\mathbf{B}$ is $3(j_{max}-1) \times 2$, $\mathbf{C}$ is $2 \times 3(j_{max}-1)$, and $\mathbf{D}$ is 2x2. This system is solved using a block inversion procedure as found in ref. [9] (see Appendix C for details). After the solution of (13) is obtained, $U_{j_{s+1}}^{n+1}$ is redefined using (6) to insure that the Rankine-Hugoniot conditions are satisfied.

Explicit Shock Tracking (EST):

For comparison purposes, we consider an algorithm, EST, in which the shock quantities S are not treated implicitly. Preliminary experimentation with several ways of explicitly treating the unknowns S indicated that the following method showed the best convergence behavior. First, the conservation variables U are advanced implicitly using (9) - (11) linearized with S fixed at S^n, subject to the boundary conditions (4) and (5a) with $s = s^n$. The discrete algebraic system for $\Delta U^n (j=2,\ldots j_{max})$ is $\mathbf{A}\Delta U^n = RHS$ where the matrix $\mathbf{A}$ is the same as in (13). Next, S is advanced explicitly using

$$s_t^{\,n+1} = s_t^{\,n} + h\, r_3\, (U^{n+1},\, S^n),\; s^{n+1} = s^n + h s_t^{\,n+1}$$

The final step, as in FIST, is to redefine $U_{j_{s+1}}^{n+1}$ using (6) with $U_{j_s}^{n+1}$, S^{n+1}.

Alternating Unknown Implicit (AUI):

We also consider a compromise approach in which some of the implicit character of the shock advancement is maintained. In essence the method alternates the unknowns which are treated implicitly (AUI). First, the variables U are advanced implicitly keeping the shock fixed as in EST. Next, the shock variables S are advanced implicitly keeping U fixed at U^{n+1} using

$$(I - c_1 h \left[\frac{\partial R_3}{\partial S}\right])\Delta S^n = c_2\, \Delta S^{n-1} + h\left[c_1\, R_3(U^{n+1},\, S^n) + (c_3 - c_1)\, R_3\, (U^n, S^n)\right].$$

Finally, as in FIST and EST, $U_{j_{s+1}}^{n+1}$ is redefined using (6). As will be discussed in section 4, this method allows a larger time step than EST with no significant increase in computational time. For this reason AUI may be a valuable tool for multidimensional problems where operator splitting limits the time step.

Numerical Linearization:

Implementation of all the above methods require evaluations of various Jacobian matrices. Indeed, suppose we consider the differential operator $\frac{\partial G}{\partial \xi}$ where $G = G(V)$ and $V = V(\xi)$ are vector valued functions. Then the linearization of $\frac{\partial G}{\partial \xi}$ with respect to V is given by

$$\left[\frac{\partial}{\partial V}\left(\frac{\partial G}{\partial \xi}\right)\right]_j = \left(\frac{\partial}{\partial \xi}\left[\frac{\partial G}{\partial V}\right]\right)_j \approx \left(\left[\frac{\partial G}{\partial V}\right]_{j+1} - \left[\frac{\partial G}{\partial V}\right]_{j-1}\right)/(2\Delta\xi)$$

where $\left[\frac{\partial G}{\partial V}\right]$ is the Jacobian matrix of G with respect to V. In principle, for a perfect gas, analytic expressions can be obtained for the required Jacobian matrices. An alternative approach is to directly evaluate the Jacobians numerically (to order of the square root of machine error) by replacing the derivatives with respect to the components of V by appropriate first order forward differences. This direct numerical approach is used in the present study. It is simpler to program (especially for FIST) and appears to cause little or no difference in quality of results or execution time. Note that, using the direct numerical approach, the formation of the matrix for FIST requires essentially 6 evaluations of R_i $(i=1,2,3)$ and $\mathcal{R}$ (since U, S contain a total of 5 components). This is comparable to 4 evaluations for EST and AUI and 2 evaluations for an explicit predictor - corrector method.

4. Numerical Results

We now present our computational results for the duct flow problem, assessing first the accuracy of the steady state finite difference solution, and then the computational efficiencies of the various methods (FIST, EST, AUI). For the purposes of further comparison, we also compare with the explicit predictor-corrector method of Brailovskaya; see Appendix D. (For the present problem, this method converges faster than the second order accurate MacCormack scheme, and also enjoys the advantage that it reduces to the same steady state difference equations as do the other methods tested here.) In the numerical experiments, the duct shape was taken to be $A(x) = 1.398 + 0.347 (\tanh (0.8 x-4.))$, with $x_{max} = 10$

In all cases we take $K = 2$, $\gamma = 1.4$, $\rho_o = 0.502$, $u_o = 1.299$, $e_o = 1.897$, $\rho_e = .776$ and we use Euler implicit time differencing (i.e., $c_1 = c_3 = 1$, $c_2 = 0$). We use two different initial guesses, hereafter referred to as the "good guess" and "bad guess". The good guess is the exact steady state solution for a slightly perturbed duct shape, cf. ref.[6]. The bad guess is an exact solution for flow in the given duct $A(x)$ but with a different downstream density ρ_e specified. In our experiments, the outflow condition $\rho_e = .776$ was imposed impulsively at $t = 0$. Figures 2a and 2b illustrate the quality of the pressure profiles for the two guesses relative to the exact steady state solution. The steady state solution of the difference equations (obtained with any of the methods) is shown in Figures 3a and 3b for $j_{max} = 18$ and 34 respectively. In the latter case the numerical solution is virtually indistinguishable from the exact solution. We wish to emphasize that, in these results and all those that follow, no numerical dissipation was used.

In comparing the efficiencies of the various methods, we shall refer to runs made with time steps corresponding to various multiples of the CFL (Courant, Friedrichs, Levy) number, defined to be $\omega\Delta\tau/\Delta\xi$ where ω is the maximum over all j of the spectral radius of $\left[\frac{\partial F}{\partial U}\right]_j$. We first determine the approximate maximum value of CFL at which each of the methods will run with $j_{max} = 34$ and when started with the good or bad guess.

Method	Max CFL Good guess	Max CFL Bad guess	Time units per iteration
Brailovskaya	1	1	1
EST	9	6	3.4
AUI	10	10	3.5
FIST	10^{10}	175	4.8

We note that, as expected, FIST approaches Newton's method in the limit of large time steps. Indeed, with CFL $= 10^6$, FIST converged in 5 iterations to steady state tolerances within machine error (10^{-13}) when started with the good guess.

We next examine convergence behavior for the various methods. We plot maximum residual (value obtained by substituting the current difference solution into the steady state difference equations) versus either iterations or computer time. Computer time will be based on units where one unit is the time necessary for one step of the Brailovskaya method (see Table above). We note that in implementing FIST, EST, and AUI, the inversion of matrix $\mathbf{A}$ was actually obtained using a banded solver rather than a block tridiagonal solver. This was done because the block tridiagonal decomposition could become ill conditioned at large values of CFL.

We first look at runs made with FIST, EST, and AUI at various values of CFL (Figures 4a,4b,4c). In all cases, the bad guess was used and $j_{max} = 34$. As usually assumed, each method converges in fewer iterations as the CFL factor becomes larger. (It is interesting to note that starting with the good guess it is possible to find CFL values for which EST and AUI oscillate between two states instead of converging.) When compared with respect to computer time at fixed CFL = 3 and 6 (Figures 5a and 5b) we see that there is very little difference between EST and AUI, and that the extra work per iteration needed in FIST does not pay off in faster convergence. However when compared at their maximum allowable CFL values (Figure 5c), the FIST method is clearly superior.

5. Concluding Remarks

As demonstrated by the numerical results, for one-dimensional problems the FIST approach produces significant increases in computational efficiency when compared with purely explicit methods and with implicit methods using explicit shock tracking. In some sense, this comparison is unfair since for very large time steps FIST approaches Newtons method for solving the difference analog of the steady state equations, and thus exhibits quadratic convergence behavior. In fact, the FIST approach combines the advantages in computational efficiency of Newton's method with the robustness of time asymptotic methods.

The implications of the present study for multidimensional problems are difficult to assess. This is especially true if operator splitting or factorization is used. It is not clear how the various methods will compare with respect to computer time needed per iteration, or how large the maximum allowable CFL values will be. Two competing factors affect the computational time per iteration. Assuming a single shock, the fully coupled implicit shock treatment will occur in only one of the directional sweeps. However, the number of variables needed to specify the shock geometry and movement will increase. The maximum allowable CFL values for each method are problem dependent and will certainly be limited by splitting error. Since FIST will no longer reduce to Newton's method in this framework, the suitability of the various methods depends on the relation between the CFL restriction due to splitting and the CFL restriction due to explicit shock treatment. It is impossible to discern *a priori* which method will be best.

In closing we note that a split version of FIST is being developed for the supersonic blunt body problem. The results of this work will appear in a forthcoming paper.

References

[1] R. M. Beam and R. F. Warming, An Implicit Finite-Difference Algorithm for Hyperbolic Systems in Conservation-Law Form, J. Comp. Physics, v. 22, 1976, pp. 87-110.

[2] J. L. Steger, Implicit Finite Difference Simulation of Flow About Arbitrary Geometries with Application to Airfoils, AIAA Paper 77-665, Albuquerque, NM, June 27-29, 1977.

[3] T. H. Pulliam and D. S. Chaussee, A Diagonal Form of An Implicit Approximate - Factorization Algorithm, J. Comp. Physics, v. 39, 1981, pp. 347-363.

[4] P. Kutler, S. R. Chakravarthy, C. P. Lombard, Supersonic Flow Over Ablated Nosetips Using an Unsteady Implicit Numerical Procedure, AIAA Paper 78-213, Huntsville, Alabama, Jan. 16-18, 1978.

[5] W. R. Briley and H. McDonald, On the Structure and Use of Linearized Block Implicit Schemes, J. Comp. Physics, v. 34, 1980, pp. 54-73.

[6] G. R. Shubin, A. B. Stephens, and H. M. Glaz, Steady Shock Tracking and Newton's Method Applied to One-Dimensional Duct Flow, J. Comp. Physics, v. 39, 1981, pp. 364-374.

[7] H. Viviand, Conservative Forms of Gas Dynamics Equations, La Recherche Aerospatiale, v. 1, 1974, pp. 65-68.

[8] R. F. Warming and R. M. Beam, On the Construction and Application of Implicit Factored Schemes for Conservation Laws, Symposium on Computational Fluid Dynamics, New York, April 16-17, SIAM-AMS Proceedings, 1978.

[9] E. Isaacson and H. B. Keller, Analysis of Numerical Methods, Wiley, New York, 1966, pp. 58-61.

[10] R. Courant and D. Hilbert, Methods of Mathematical Physics, v. 2, Interscience, New York, 1962, pp. 599-605.

[11] C. P. Kentzer, Discretization of Boundary Conditions on Moving Discontinuities, Proceedings of Second Internat. Conf. on Numerical Methods in Fluid Dynamics, Univ. of Calif., Berkeley, 1970, Springer-Verlag, New York, 1971.

[12] Landau, L. D. and Lifshitz, E. M., Fluid Meahanics, Addison-Wesley, Reading, Mass., 1959, pp. 317-331.

[13] P. Roache, Computational Fluid Dynamics, Hermosa, Albuquerque, NM, 1972.

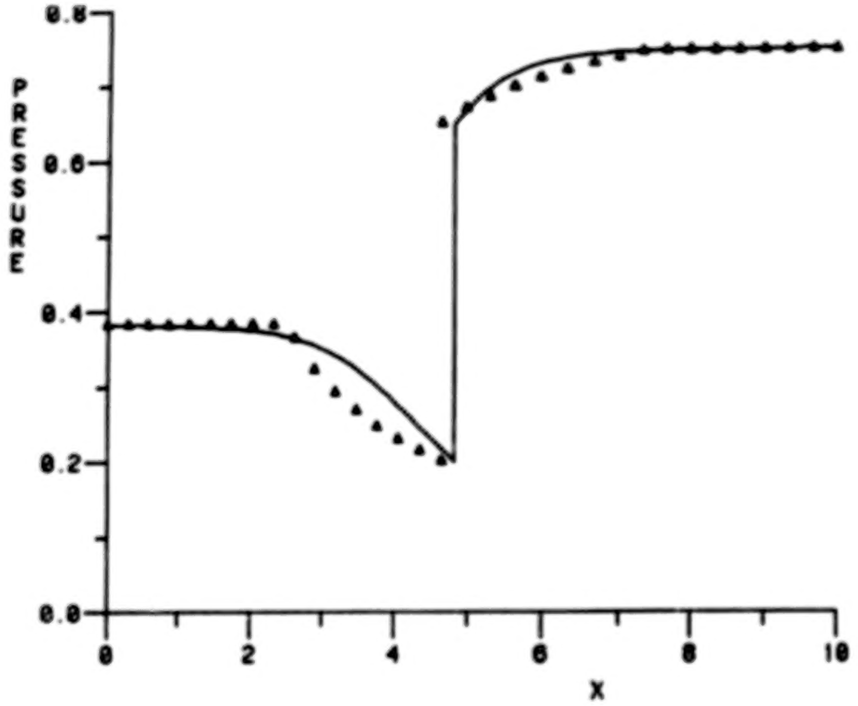

FIGURE 2a: Good guess (▲) vs. exact steady state solution.

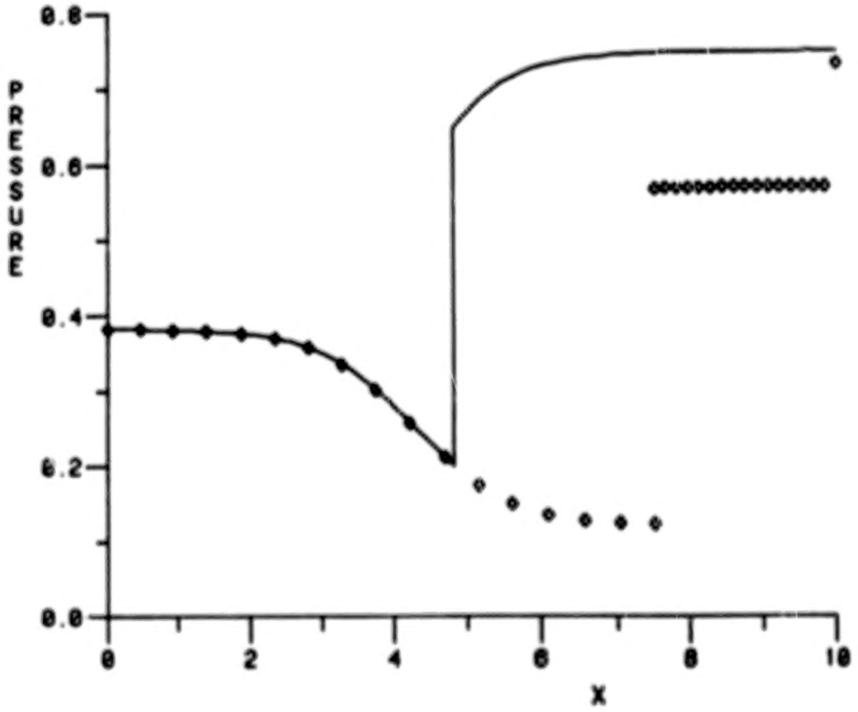

FIGURE 2b: Bad guess (◊) vs. exact steady state solution.

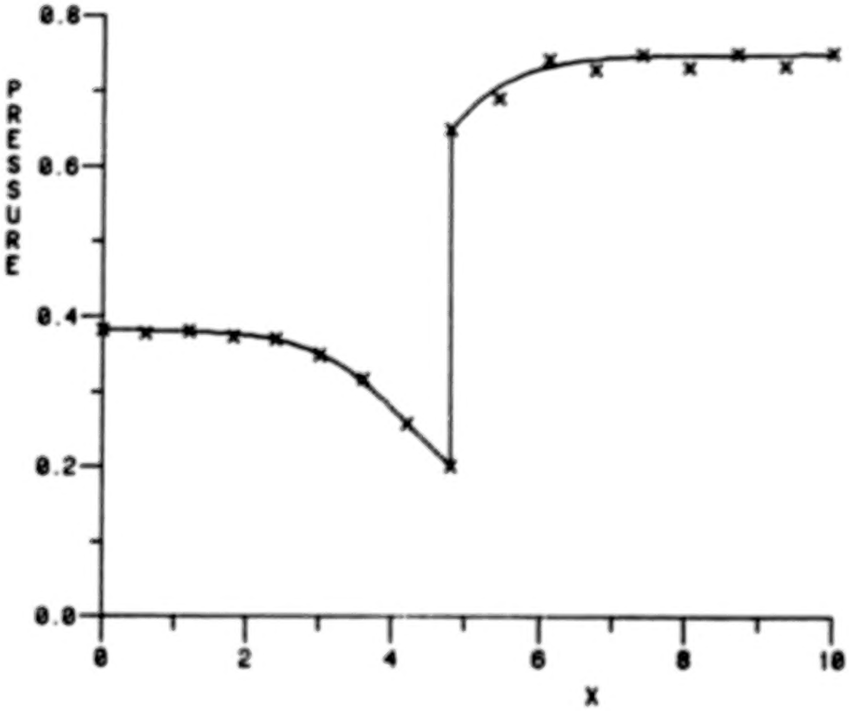

FIGURE 3a: Steady state difference solution (X) with j_{max} = 18 vs. exact solution.

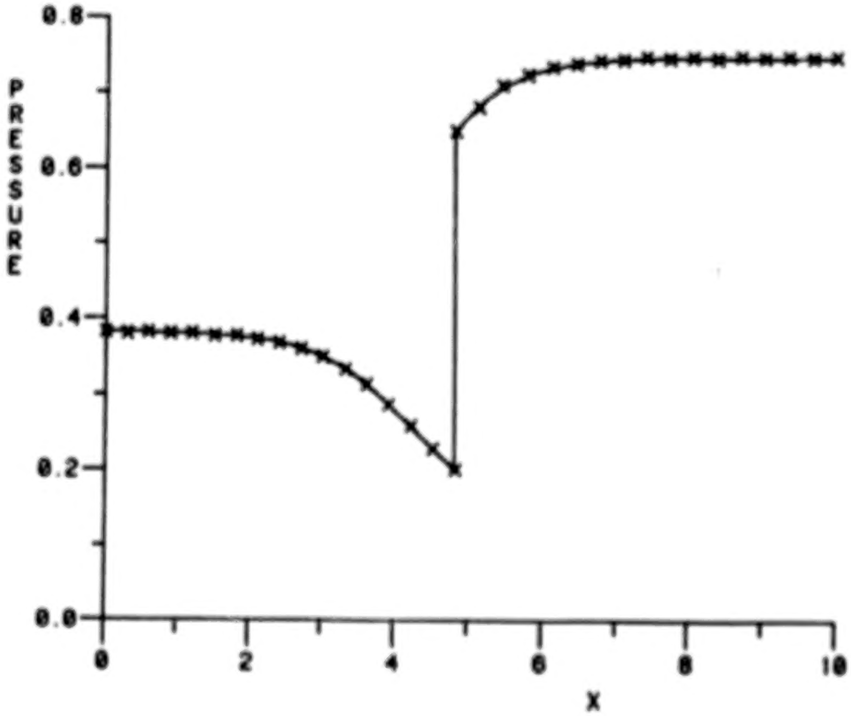

FIGURE 3b: Steady state difference solution (X) with j_{max} = 34 vs. exact solution.

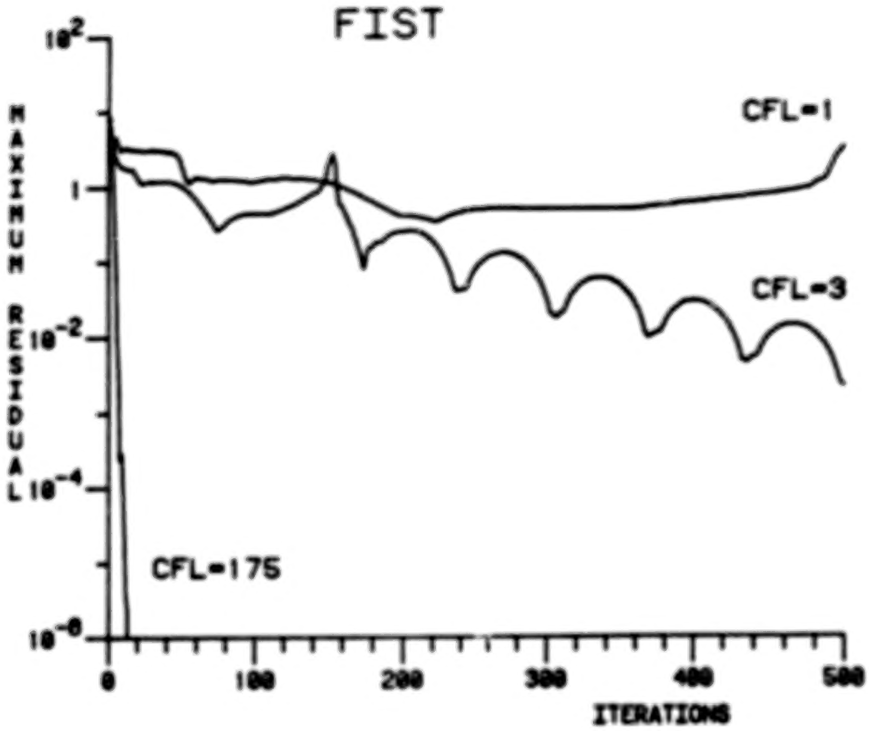

FIGURE 4a.

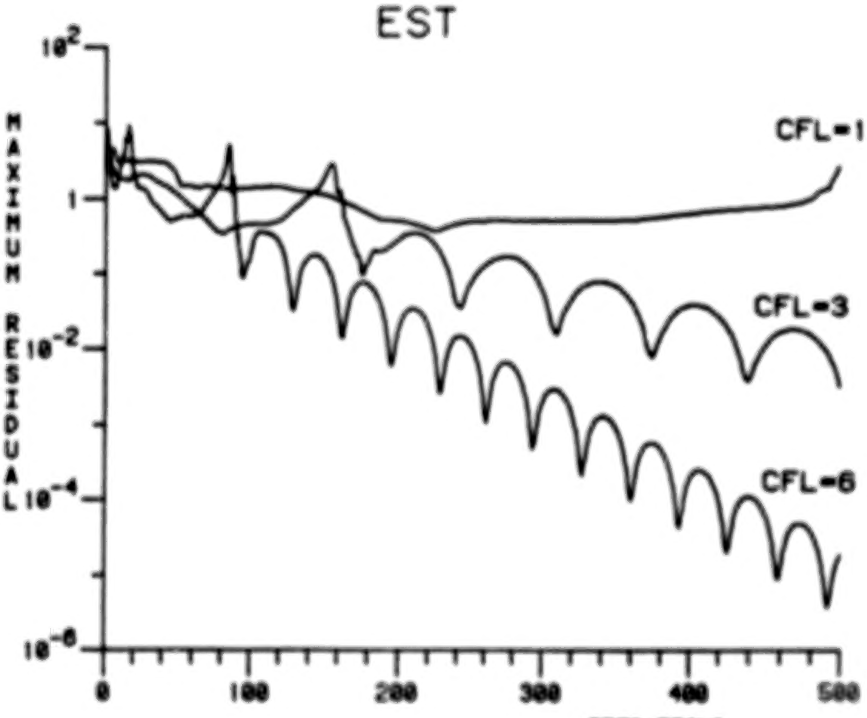

FIGURE 4b.

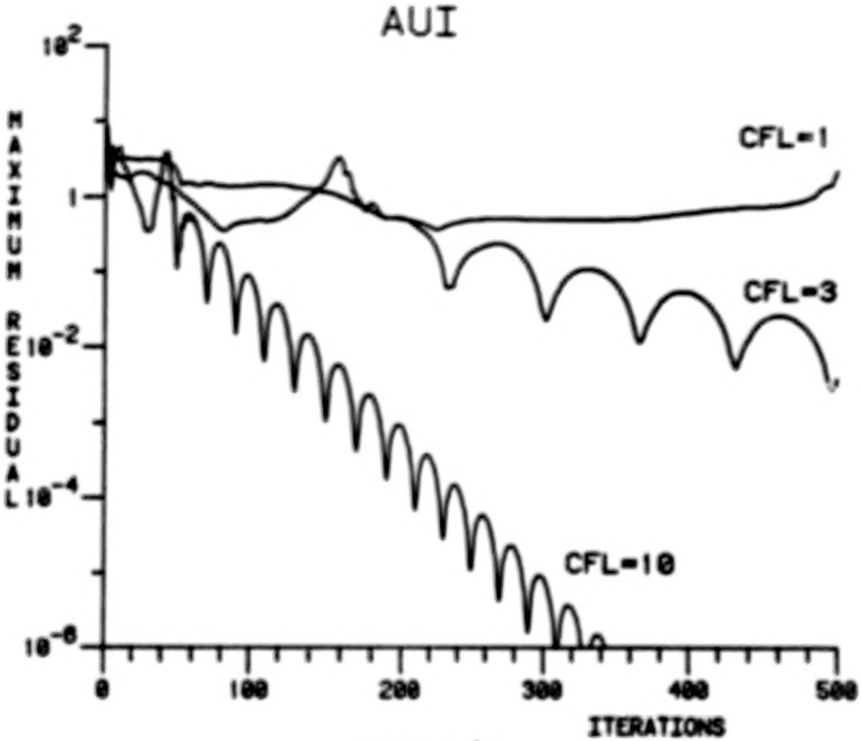

FIGURE 4c.

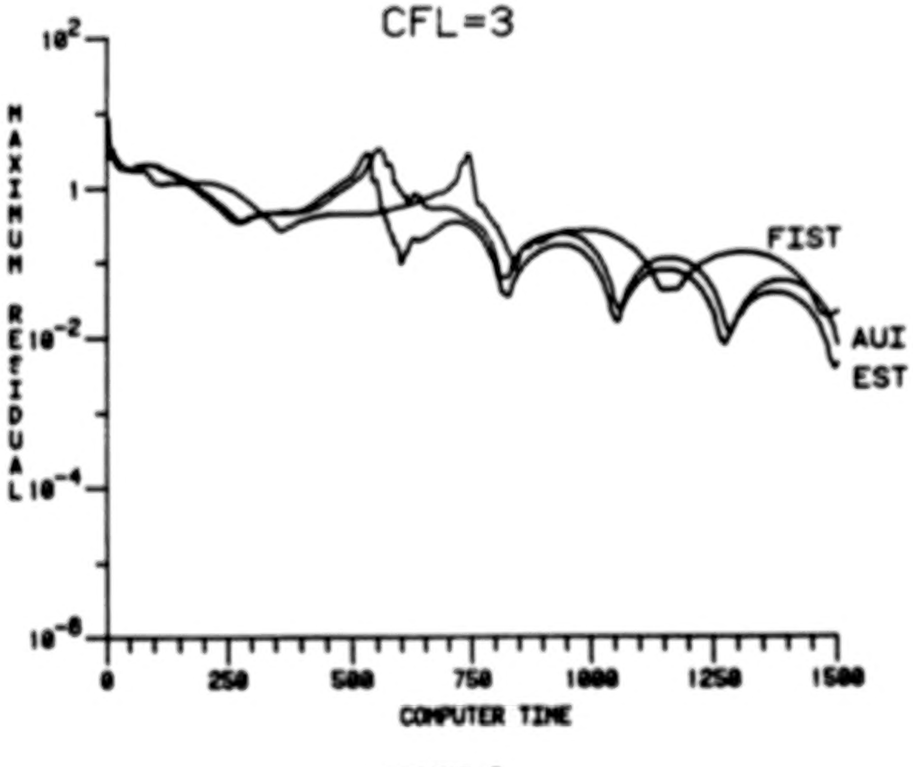

FIGURE 5a.

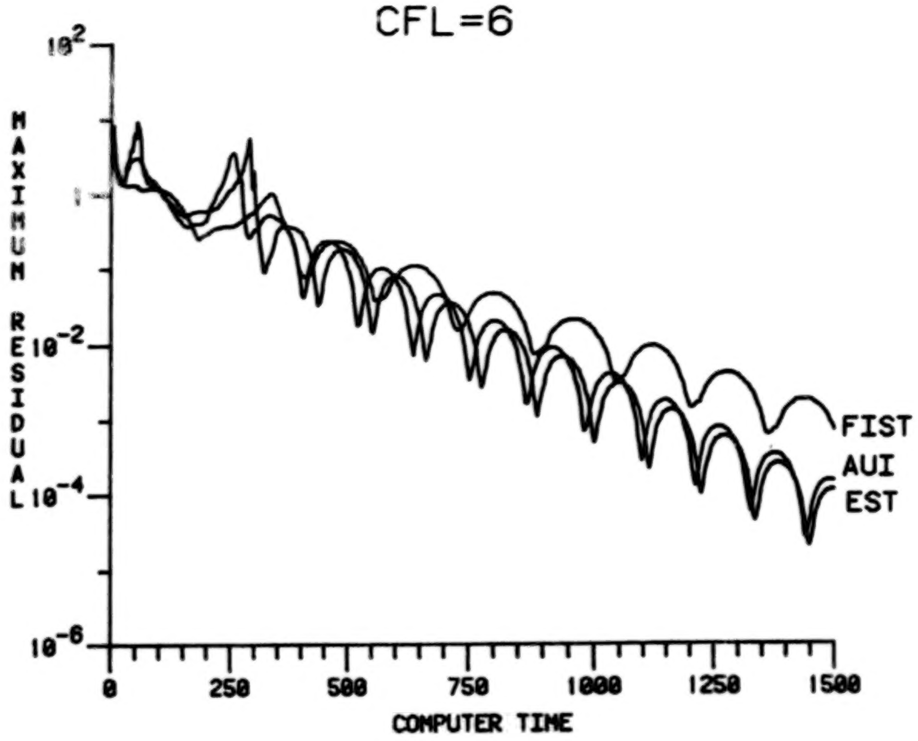

FIGURE 5b.

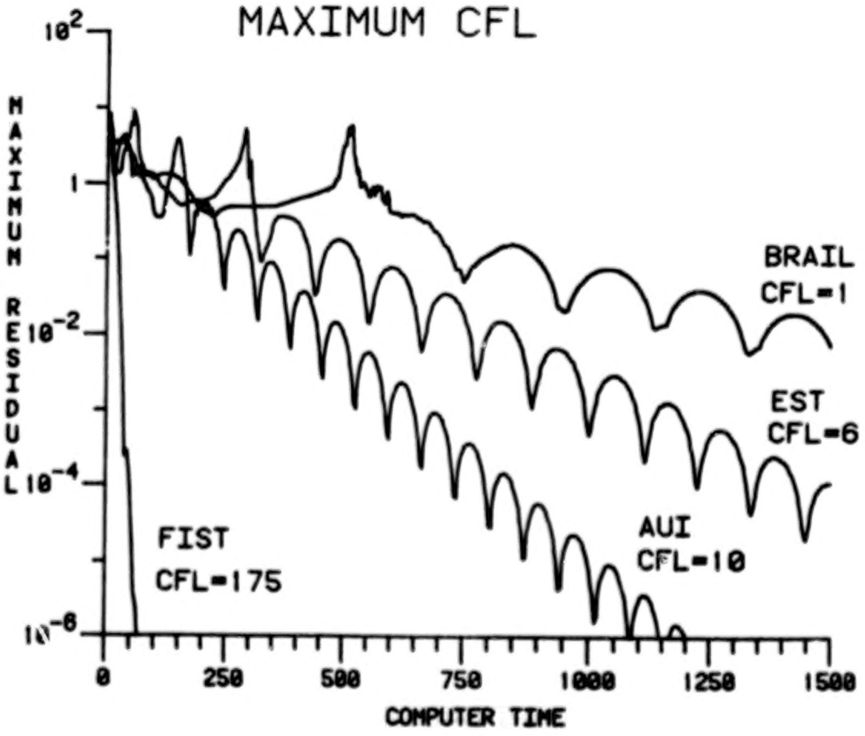

FIGURE 5c.

Appendix A: Characteristic analysis of the boundaries

The background on characteristic theory and characteristic compatibility conditions may be found in ref. [10]. For their application to the treatment of boundaries in fluid dynamics, see ref. [11]. We give here only an outline of the general approach and apply it to system (3).

Since system (3) is hyperbolic, it is equivalent to three characteristic compatibility conditions. These conditions take the form of ordinary differential equations which hold along characteristic curves in (τ,ξ) space. At a boundary of the computational domain, certain of these curves are "admissible" since they reach the boundary from inside the computational domain (when moving along them in the direction of increasing τ). The compatibility conditions associated with these admissible characteristics may be applied as computational boundary conditions. Other characteristic curves are "inadmissible" since they reach the boundary from outside the domain. The compatibility conditions corresponding to these curves must be replaced by specified boundary valves.

Specifically, (3) is equivalent to the quasilinear system.

$$\frac{J}{A} L\ (U) \equiv \frac{J}{A}\left(\frac{\partial U}{\partial \tau} - R_1\right) = \frac{\partial \mathfrak{U}}{\partial \tau} + \mathbb{B}\,\frac{\partial \mathfrak{U}}{\partial \xi} + \frac{1}{A}\left(\frac{dA}{dx}\,\mathfrak{F} - \mathfrak{H}\right) \equiv \mathfrak{L}(\mathfrak{U}) = 0 \qquad (A.1)$$

where $\mathbb{B} = \xi_t\, I + \xi_x \left[\frac{\partial \mathfrak{F}}{\partial \mathfrak{U}}\right]$, and $\left[\frac{\partial \mathfrak{F}}{\partial \mathfrak{U}}\right]$ is the Jacobian matrix of $\mathfrak{F}$ with respect to $\mathfrak{U}$. The characteristic matrix associated with (A-1) is

$$\begin{aligned}&\mathbf{C}(\lambda_o,\lambda_1)\\ &\quad \equiv \lambda_o\, I + \lambda_1\mathbb{B} = \begin{pmatrix} \Lambda_o & \Lambda_1 & 0 \\ \frac{\gamma-3}{2}\,\Lambda_1 u^2 & \Lambda_o - \Lambda_1(\gamma-3)u & \Lambda_1(\gamma-1) \\ -\Lambda_1 u\left(\frac{a^2}{\gamma-1} - \frac{\gamma-2}{2}\,u^2\right) & \Lambda_1\left[\frac{a^2}{\gamma-1} - \left(\gamma - \frac{3}{2}\right)u^2\right] & \Lambda_o + \gamma u \Lambda_1 \end{pmatrix}\end{aligned} \qquad (A.2)$$

where $\Lambda_o = \lambda_o + \lambda_1\, \xi_t$, $\Lambda_1 = \lambda_1\, \xi_x$, and a is the speed of sound. A characteristic curve $\Phi\ (\xi,\tau)$ = constant satisfies the characteristic condition

$$\det \mathbf{C} = \sigma\ (\sigma^2 - a^2\, \Lambda_1{}^2) = 0 \qquad (A.3)$$

where $\sigma = \Lambda_o + u\Lambda_1$, $\lambda_o = \Phi_\tau$, and $\lambda_1 = \Phi_\xi$. The slopes of the characteristic curves $\mathfrak{C}_o, \mathfrak{C}_{\pm}$ associated with the three distinct characteristic conditions

$\sigma_o = 0$, $\sigma_\pm = \pm a \Lambda_1$ are given, respectively, by

$$
\begin{aligned}
\mathfrak{C}_o &: \quad \frac{d\xi}{d\tau} = q \\
\mathfrak{C}_\pm &: \quad \frac{d\xi}{d\tau} = q \mp a\,\xi_x
\end{aligned}
\tag{A.4}
$$

where $q = \xi_t + u\xi_x$. The $\mathfrak{C}_o$ curve is a particle path and the $\mathfrak{C}_\pm$ curves represent Mach (or sound) waves. Corresponding to the three charateristic conditions are three independent left null vectors (defined by $\vec{\ell}\cdot\mathbf{C} = 0$) given by

$$
\begin{aligned}
\vec{\ell}_o &= \left(\frac{u^2}{2} - \frac{a^2}{\gamma-1} \,,\, -u \,,\, 1\right) \\
\vec{\ell}_\pm &= \left(\frac{\pm u^2}{2} + \frac{au}{\gamma-1} \,,\, \frac{-a}{\gamma-1} \mp u \,,\, \pm 1\right)
\end{aligned}
\tag{A.5}
$$

The three characteristic compatibility conditions holding along the characteristic curves are obtained by left multiplying (A.1) by $\vec{\ell}_o, \vec{\ell}_\pm$ in the form

$$
\vec{\ell}\cdot L(U) = 0 \text{ or } \vec{\ell}\cdot\mathfrak{L}(\mathfrak{U}) = 0. \tag{A.6}
$$

Inflow and Outflow Boundaries

At the inflow boundary $\xi = 0$, we assume the flow to be supersonic ($u>a$). Since $\xi_t = 0$ and $\xi_x > 0$ at $\xi = 0$, it follows from (A.4) that the characteristic slopes are as depicted in Fig. A-1. Hence, none of the characteristics are admissible and accordingly all the flow variables must be specified at $\xi = 0$.

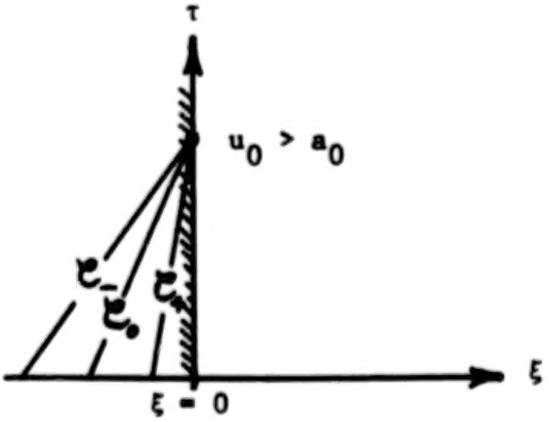

Fig. A-1. Characteristic slopes at $\xi = 0$ for supersonic inflow.

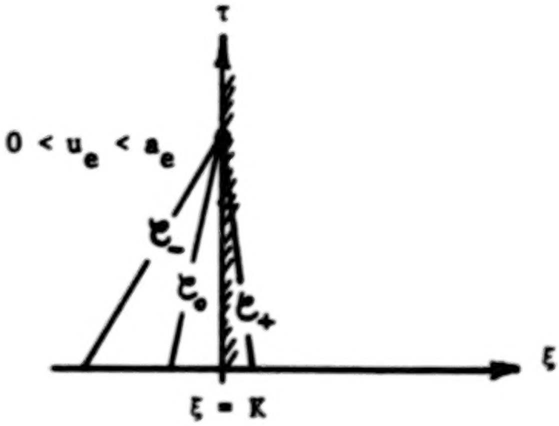

Fig. A-2. Characteristic slopes at $\xi = K$ for subsonic outflow.

At the outflow boundary $\xi = K$, we assume subsonic flow ($0 < u < a$). In this case, the characteristic slopes are depicted in Fig. A-2. Hence, at $\xi = K$, the compatibility conditions associated with the admissible characteristics $\mathcal{C}_0$ and $\mathcal{C}_-$ should be satisfied and one flow variable must be specified. Although several possibilities exist, we specify the density, ρ_e, at outflow. This leads to (5a) for the first component of U on $\xi = K$. The derivative of (5a) with respect to τ and the compatibility conditions (A.6) for $\mathcal{C}_0$ and $\mathcal{C}_-$ give the following system on $\xi = K$:

$$\mathbf{T}_0 \left(\frac{\partial U}{\partial \tau}\right)_{\xi=K} = - \mathbf{T}_1 \left(\frac{\partial F}{\partial \xi} - \frac{1}{J}\mathcal{H}\right)_{\xi = K} + \frac{A(x_{max})}{K-1}\left[\frac{d\rho_e}{dt}(x_{max} - s) - \rho_e \, s_t\right]\begin{pmatrix}1\\0\\0\end{pmatrix}$$

where

$$\mathbf{T}_0 = \begin{pmatrix} 1 & 0 & 0 \\ \frac{1}{2}u^2 - \frac{a^2}{\gamma-1} & -u & 1 \\ \left(\frac{a}{\gamma-1} - \frac{u}{2}\right)u & u - \frac{a}{\gamma-1} & -1 \end{pmatrix}_{\xi = K}, \quad \mathbf{T}_1 = \mathbf{T}_0 - \begin{pmatrix} 1 & 0 & 0 \\ 0 & 0 & 0 \\ 0 & 0 & 0 \end{pmatrix}$$

The above can be solved for $\left(\frac{\partial U_2}{\partial \tau}\right)_{\xi = K}$ and $\left(\frac{\partial U_3}{\partial \tau}\right)_{\xi = K}$. The result is given in (5b).

Shock Wave Boundaries

The shock wave $\xi = 1$ is an internal computational boundary. We first analyze each side separately and then combine the results appropriately. We assume that the flow crosses the shock from left (L) to right (R) which implies that the left side of $\xi = 1$ is the low pressure side. In addition we have that $w_L = u_L - s_t > a_L$ and $0 < w_R = u_R - s_t < a_R$ (see, for example, ref. [12]). Since on both sides of $\xi = 1$, $\xi_t = -\xi_x s_t$ and $\xi_x > 0$, it follows from (A.4) that the characteristic slopes on each side of $\xi = 1$ are as depicted in Fig. A-3.

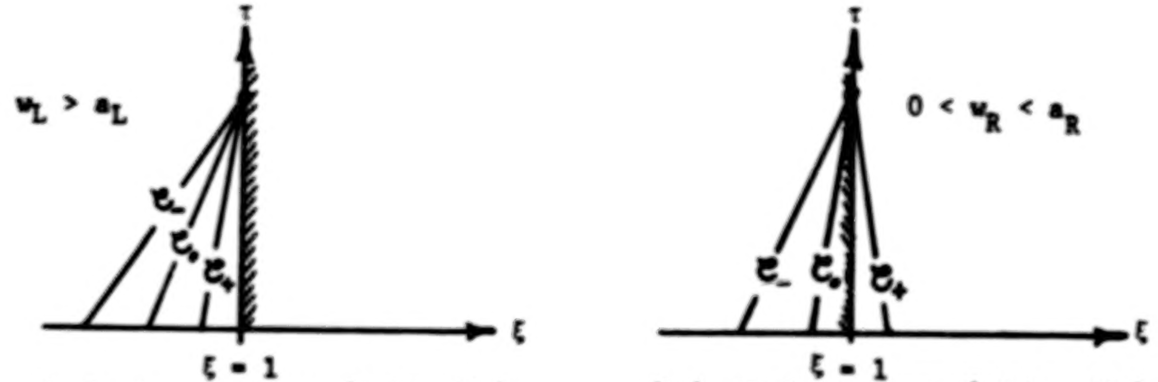

(a.) Low pressure (left side) (b.) High pressure (right side)

Fig. A-3. Characteristic slopes on each side of $\xi = 1$

For the left side of $\xi = 1$, all the compatibility conditions should be satisfied, c.f., Fig. A-3(a). This is equivalent to satisfying the full system (3) on the left side of $\xi = 1$ (with the ξ - derivatives interpreted using quantities only to the left side of $\xi = 1$).

For the right side of $\xi = 1$, only the compatibility condition corresponding to $\mathfrak{C}_+$ should be satisfied; c.f., Fig. A-3(b). The form of this compatibility condition used in this study is obtained from the second expression in (A.6). Noting that $(\lambda_0/\lambda_1)_R \vec{\ell}_+ = -\vec{\ell}_+ \cdot \mathbf{B}$ and that $(\lambda_0/\lambda_1)_R = -(\xi_x)_R (w_R - a_R)$, we obtain

$$\vec{\ell}_+ \cdot \left(\frac{\partial \mathfrak{U}}{\partial \tau}\right)_R = -(\xi_x)_R (w_R - a_R)\, \vec{\ell}_+ \cdot \left(\frac{\partial \mathfrak{U}}{\partial \xi}\right)_R - \frac{1}{A}\left[\ \vec{\ell}_+ \cdot \left(\frac{dA}{dx}\mathfrak{F} - \mathfrak{H}\right)\right]_R \quad (A.7)$$

Here $\vec{\ell}_+$ is evaluated at the right side of the shock. The left side of (A-7) can be written in terms of $Q = (p, u, \rho)^t$ as

$$\vec{\ell}_+ \cdot \left(\frac{\partial \mathfrak{U}}{\partial \tau}\right) \quad \vec{\ell}_+ \cdot \left[\frac{\partial \mathfrak{U}}{\partial Q}\right]_R^{-1} \frac{\partial Q_R}{\partial \tau} = \frac{1}{\gamma-1}\left[\frac{\partial p}{\partial \tau} - a\rho\,\frac{\partial u}{\partial \tau}\right]_R \quad (A.8)$$

where $\left[\frac{\partial \mathfrak{U}}{\partial Q}\right]$ is the Jacobian matrix of $\mathfrak{U}$ with respect to Q which, for a perfect gas, can be obtained by direct calculation. In (A.8), the derivatives of p_R and u_R can be eliminated using the Rankine-Hugoniot relations, (B.1) of Appendix B, differentiated with respect to τ. The result is

$$(\gamma-1)\ \vec{\zeta}_{+} \cdot \left(\frac{\partial \mathcal{U}}{\partial \tau}\right)_{R} = -c_o \frac{\partial s_t}{\partial \tau} + b_1 \frac{\partial p_L}{\partial \tau} + b_2 \frac{\partial \rho_L}{\partial \tau} + b_3 \frac{\partial u_L}{\partial \tau} \qquad (A.9)$$

where

$$c_o = \frac{\rho_R-\rho_L}{w_R-a_R}\left[(\gamma-1)\ w_R\ (w_L-w_R) - a_R\ (w_R + a_R)\right]$$

$$b_1 = \frac{\gamma(w_L - w_R)}{w_R - a_R} + 1$$

$$b_2 = \frac{1}{w_R-a_R}\left\{ a_R^2\ w_R - a_L{}^2\ w_L - (w_L - w_R)\left[(\gamma-1)w_L\ w_R + a_R(w_L-a_R)\right]\right\}$$

$$b_3 = c_o - a_R\rho_R.$$

An expression for the τ derivatives of p_L, u_L, ρ_L required in (A.9) can be obtained from the differential equations on the left side of $\xi = 1$ in the form

$$\frac{\partial Q_L}{\partial \tau} = -\left[\frac{\partial \mathcal{U}}{\partial Q}\right]_L^{-1}\left\{\mathbf{B}\frac{\partial \mathcal{U}}{\partial \xi} + \frac{1}{A}\left[\frac{dA}{dx}\ \mathcal{F} - \mathcal{H}\right]\right\}_L \qquad (A.10)$$

Substitution (A.10) and (A.9) gives, after some manipulation, the final result

$$\frac{\partial s_t}{\partial \tau} = \vec{\alpha}_1 \cdot \left(\frac{\partial \mathcal{U}}{\partial \xi}\right)_R - \vec{\alpha}_2 \cdot \left(\frac{\partial \mathcal{U}}{\partial \xi}\right)_L + \alpha_3\left(\frac{1}{A}\ \frac{dA}{dx}\right)_{\xi = 1}$$

where

$$\vec{\alpha}_1 = \frac{(\gamma-1)\ (\xi_x)_R\ (w_R-a_R)}{c_o}\left[\frac{u_R^2}{2} + \frac{a_R}{\gamma-2}\ u_R,\ -u_R - \frac{a_R}{\gamma-1}, 1\right]$$

$$\vec{\alpha}_2 = \frac{(\xi_x)_L}{c_o}\Bigg[u_L\ b_1\left(\frac{\gamma-1}{2}\ u_L\ w_L-a_L{}^2\right) + \frac{u_L}{\rho_L}\ b_3\left(\frac{\gamma-1}{2}\ u_L - w_L\right)+ b_2(w_L-u_L),$$

$$b_1\ (a_L{}^2 - (\gamma-1)u_L\ w_L) + \frac{b_3}{\rho_L}\ (w_L-(\gamma-1)u_L) + b_2\ ,$$

$$(\gamma-1)\ \left(w_L\ b_1 + \frac{b_3}{\rho_L}\right)\Bigg]$$

$$\alpha_3 = \frac{1}{c_o}\left[\gamma p_R\ u_R - u_L\ (\gamma\ \rho_L\ b_1 + \rho_L\ b_2)\right]$$

Appendix B: Rankine-Hugoniot Shock Relations

We give here the jump conditions across the shock in terms of the U variables and s, s_t. For a perfect gas, we have (cf., ref.[12])

$$Q_R \equiv \begin{pmatrix} p_R \\ u_R \\ \rho_R \end{pmatrix} = \begin{pmatrix} p_L(\gamma\beta M^2+1) \\ u_L - (u_L - s_t)\beta \\ \rho_L \,/\, (1-\beta) \end{pmatrix} \equiv \vec{f}(Q_L, s_t) \tag{B.1}$$

where

$$M^2 = (u_L - s_t)^2 \rho_L \,/(\gamma p_L) \text{ and } \beta = 2(M^2-1)/[(\gamma+1)M^2].$$

Since on the left side (subscript L) of the shock $\xi_x = 1/s$,

$$Q_L \equiv \begin{pmatrix} p_L \\ u_L \\ \rho_L \end{pmatrix} = \begin{pmatrix} \frac{(\gamma-1)}{sA(s)}\left(U_3 - \frac{U_2^2}{2U_1}\right)_L \\ (U_2/U_1)_L \\ (U_1)_L/[sA(s)] \end{pmatrix} \equiv \vec{g}(U_L, s). \tag{B.2}$$

On the right side (subscript R) of the shock $\xi_x = (K-1)/(x_{max}-s)$ which implies

$$U_R = \frac{(x_{max}-s)A(s)}{K-1} \begin{pmatrix} \rho_R \\ \rho_R u_R \\ p_R \,/(\gamma-1) + \rho_R u_R^2/2 \end{pmatrix} \equiv \vec{h}(Q_R, s) \tag{B.3}$$

We therefore have

$$U_R = \mathcal{A}(U_L, s, s_t) = \vec{h}(\vec{f}(\vec{g}(U_L, s), s_t), s).$$

Appendix C: Inversion Algorithm for Equation (13)

Here we give a 2×2 block matrix inversion algorithm for the system

$$\left[\begin{array}{c|c} \mathbf{A} & \mathbf{B} \\ \hline \mathbf{C} & \mathbf{D} \end{array}\right] \left[\begin{array}{c} y \\ \hline z \end{array}\right] \qquad \left[\begin{array}{c} f_1 \\ \hline f_2 \end{array}\right]$$

where $\mathbf{D}$ is a very small (in the present context 2×2) and $\mathbf{A}$ admits a convenient L-U factorization (in this case $\mathbb{A}$ is block tridiagonal).

Following ref.[9] observe that

$$\mathbb{A}y + \mathbb{B}z = f_1 \tag{C.1}$$

and

$$\mathbb{C}y + \mathbb{D}z = f_2. \tag{C.2}$$

Then from (C.1),

$$y = \mathbb{A}^{-1} f_1 - (\mathbb{A}^{-1}\mathbb{B})z. \tag{C.3}$$

Substitution of (C.3) into (C.2) yields

$$\mathbb{C}(\mathbb{A}^{-1} f_1) - \mathbb{C}(\mathbb{A}^{-1}\mathbb{B})z + \mathbb{D}z = f_2$$

or

$$z = (\mathbb{D} - \mathbb{C}\mathbb{A}^{-1}\mathbb{B})^{-1} (f_2 - \mathbb{C}\mathbb{A}^{-1} f_1). \tag{C.4}$$

Substitution of (C.4) into (C.3) yields

$$y = \mathbb{A}^{-1} f_1 - \mathbb{A}^{-1}\mathbb{B}(\mathbb{D} - \mathbb{C}\mathbb{A}^{-1}\mathbb{B})^{-1} (f_2 - \mathbb{C}\mathbb{A}^{-1} f_1) \tag{C.5}$$

Note that in the evaluation of (C.4) and (C.5), $\mathbb{A}^{-1} f_1$ and $\mathbb{A}^{-1}\mathbb{B}$ are obtained simultaneously; indeed, the evaluation of $\mathbb{A}^{-1} f_1$ is a standard inversion technique and the computation of $\mathbb{A}^{-1}\mathbb{B}$ requires only one extra backsolve for each column of $\mathbb{B}$. Theoretical work estimates indicate that (for the case when $\mathbb{D}$ is 2×2) the evaluation of $\mathbb{A}^{-1}\mathbb{B}$ increases the work by only 60% over that required for $\mathbb{A}^{-1} f_1$. By design, $\mathbb{D} - \mathbb{C}\mathbb{A}^{-1}\mathbb{B}$ is a small matrix and thus easily inverted.

Appendix D: The Brailovskaya Scheme

The Brailovskaya scheme [13](also known as the Matsuno scheme) for the system $U_\tau + F_\xi + H = 0$ is given by the following explicit predictor-corrector sequence:

(predictor) $\quad U_j^* = U_j^n - \Delta\tau[(F_{j+1}^n - F_{j-1}^n)/(2\Delta\xi) + H_j^n]$

(corrector) $\quad U_j^{n+1} = U_j^n - \Delta\tau[(F_{j+1}^* - F_{j-1}^*)/(2\Delta\xi) + H_j^*]$

where F_j^*, H_j^* are evaluated at τ^{n+1} using U_j^*. For the differential equations (5b),(7), the above scheme is used with appropriate one-sided ξ differences. The formal truncation error of this scheme is $O(\Delta\tau, \Delta\xi^2)$ and a sufficient stability (von Neumann) condition is CFL ≤ 1 (cf., Sec. 4).

Blank Page

CHARACTERISTIC BOUNDARY CONDITIONS FOR THE EULER EQUATIONS

T. H. Pulliam

Ames Research Center

SUMMARY

Stable and accurate numerical boundary conditions are applied to the Euler equations in terms of characteristic variables. The boundary conditions are demonstrated for the quasi-one-dimensional Euler equations with the extension to two and three dimensions being straightforward. In this application an implicit finite-difference scheme is employed with the boundary conditions being applied implicitly. The boundary application uses both characteristic extrapolations and evaluations which distinguishes it from other theories. Flow fields with shocks are calculated with inflow-outflow conditions of supersonic-subsonic and subsonic-subsonic flow.

I. INTRODUCTION

Formulation of boundary conditions (BC) in terms of characteristic variables and directions is an obvious and frequently explored area of research (refs. 1-7). It seems natural to express the transfer of information at boundaries in terms of characteristics. The characteristic directions (the eigenvalues of the system of equations) reveal the propagation directions of information. The characteristic variables (variables transformed by the eigenvectors of the system of equations) are the natural variables with which to work. In general, though, we cannot recast our equations in terms of the characteristic variables because the equations are usually nonlinear, for example, the Euler equations. We shall present here a way in which the characteristic directions and variables can be used in boundary condition applications.

Many forms of characteristic and noncharacteristic boundary condition applications for the Euler equations exist in the literature. In particular, Yee (ref. 1) and Yee et al. (ref. 2) provide a detailed discussion of various methods and an extensive literature reference on such boundary condition application. They provide a comprehensive study contrasting a number of different boundary conditions for this class of problems and also provide some rigorous stability and consistency arguments. The concepts presented here are similar to others and are actually suggested in form by Yee (ref. 1), but this particular derivation presents some novel concepts and observations which make it unique. It should be pointed out that this paper does not attempt to provide any rigorous stability, well-posedness or accuracy analysis. Rather, conditions are employed which are consistent with available analysis, and through numerical experiment we validated the techniques used here.

II. CHARACTERISTICS

It is quite obvious that characteristic formulation of boundary conditions is an appropriate way to approach the problem. Once the variables are transformed to their characteristic directions, the form of boundary condition application is easily chosen. For example, let us examine the coupled system of linear equations

$$Q_t + E_x = 0 \tag{1a}$$

where

$$E = A\ Q \tag{1b}$$

and A is an $m \times m$ constant coefficient matrix. The Euler equations can be put into a similar form and have the same property of equation (1b), called the homogeneous property.

Assuming that the matrix A has a complete set of eigenvectors and eigenvalues (this is also true for the Euler equations), then a similarity transformation exists,

$$A = X\ D\ X^{-1} \tag{2}$$

where X is the eigenvector matrix and D is a diagonal matrix of the eigenvalues of A.

Multiplying equation (1a) by [illegible] and using the identity $I = X\ X^{-1}$, we have

$$(X^{-1}\ Q)_t + (X^{-1}\ A\ X\ X^{-1}\ Q)_x = 0 \tag{3a}$$

or

$$W_t + (D\ W)_x = 0 \tag{3b}$$

with

$$W = X^{-1}\ Q$$

where since X^{-1} is a constant matrix it has been placed inside of the derivative expressions without creating any error.

The vector W is the characteristic vector and each of its elements w_i is a characteristic variable. The elements of the matrix D, d_i determine the direction of propagation of information. Notice that since D is diagonal, equation (3b) represents m uncoupled equations. The sign of the elements of D at a boundary tells us which variables w_i can be used from outside the boundary domain and which cannot. That is, which characteristic variables feed information into the domain of interest and which do not (and therefore should not be included in any boundary conditions).

Let us choose a boundary in space and talk of left- and right-hand domains where the left-hand domain is the region of interest and the right-hand domain is not, in a sense an outflow boundary (see fig. 1). In terms of the characteristic variables, if $d_i > 0$ at the boundary, information propagates from the left to the right and the corresponding w_i should not be specified, that is, a fixed value of w_i is not included in the boundary conditions for the left domain. It should be either calculated at the boundary or allowed to float, since it is information which is propagated out of the left domain into the right. For $d_i < 0$, information propagates into the left domain from the right, and therefore the w_i should be specified at the boundary and used as a boundary condition for the left domain.

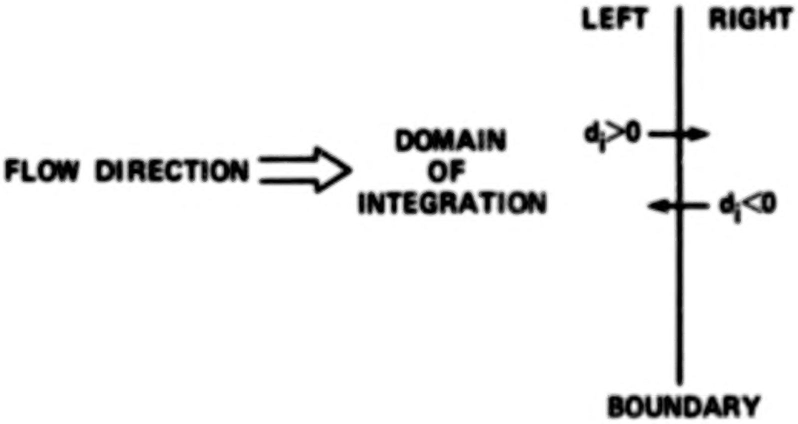

Figure 1.- Propagation of characteristic information at boundary.

These concepts will be used for the Euler equations where the eigenvalues of the system will be used to determine which variables are to be calculated and which must be specified. Also, the boundary conditions will be developed in terms of W, the characteristic variable, and any numerical application of conditions will be in terms of these variables.

III. EULER EQUATIONS

The quasi-one-dimensional Euler equations in nondimensional form transformed by a one-dimensional stretching are

$$[X_\xi a(\xi)Q]_t + E_\xi - H = 0 , \qquad X = X(\xi) \tag{4a}$$

where

$$Q = \left|\begin{matrix} \rho \\ \rho u \\ e \end{matrix}\right| \qquad E = a(\xi) \left|\begin{matrix} \rho u \\ \rho u^2 + p \\ (e + p)u \end{matrix}\right| \qquad H = a_\xi \left|\begin{matrix} 0 \\ p \\ 0 \end{matrix}\right| \tag{4b}$$

$$p = (\gamma - 1)(e - 0.5\,\rho u^2) \; ; \qquad a = a(\xi), \text{ the area ratio.}$$

Now E has a representation as

$$E = A\,Q \tag{5a}$$

where

$$A = \left(\frac{\partial E}{\partial Q}\right) =$$

$$a(\xi)\begin{bmatrix} 0 & 1 & 0 \\ (\gamma - 3)u^2/2 & -(\gamma - 3)u & \gamma - 1 \\ \left[-\gamma u(e/\rho) + (\gamma - 1)u^3\right] & \left[\gamma(e/\rho) - (3/2)(\gamma - 1)u^2\right] & \gamma u \end{bmatrix} \tag{5b}$$

and A has a complete set of eigenvalues and eigenvectors

$$D = X^{-1}\,A\,X \tag{5c}$$

with

$$D = a(\xi)\begin{bmatrix} u & 0 & 0 \\ 0 & u + c & 0 \\ 0 & 0 & u - c \end{bmatrix} \quad , \qquad c = \sqrt{\gamma p/\rho} \tag{5d}$$

and

$$X = \begin{bmatrix} 1 & \alpha & \alpha \\ u & \alpha(u + c) & \alpha(u - c) \\ \frac{u^2}{2} & \alpha\left[\frac{u^2}{2} + uc + \frac{c^2}{(\gamma - 1)}\right] & \alpha\left[\frac{u^2}{2} - uc + \frac{c^2}{(\gamma - 1)}\right] \end{bmatrix} \tag{5e}$$

$$\alpha = \rho/(\sqrt{2}c)$$

$$X^{-1} = \begin{bmatrix} 1 - \frac{u^2}{2}(\gamma - 1)c^{-2} & (\gamma - 1)uc^{-2} & -(\gamma - 1)c^{-2} \\ \beta\left[(\gamma - 1)\frac{u^2}{2} - uc\right] & \beta\left[c - (\gamma - 1)u\right] & \beta(\gamma - 1) \\ \beta\left[(\gamma - 1)\frac{u^2}{2} + uc\right] & -\beta\left[c + (\gamma - 1)u\right] & \beta(\gamma - 1) \end{bmatrix} \tag{5f}$$

$$\beta = 1/(\sqrt{2}\rho c)$$

In further discussions we will consider A to be held at some reference value, A^*. This will be convenient when a finite difference scheme is chosen and a local linearization will produce a similar representation.

We can now examine the form of the flux vector E and develop a representation of E in terms of characteristic variables. From the above relations

$$E = A^* Q = A^* X^* X^{*-1} Q = A^* X^* W \tag{6}$$

This form of E will be used at the boundaries, and the eigenvalues of A^* will be used to determine which variables are specified and which are calculated.

The vector W contains the three characteristic variables

$$W = \begin{vmatrix} w_1 \\ w_2 \\ w_3 \end{vmatrix} = X^{*-1} Q \ , \qquad Q = \begin{vmatrix} q_1 \\ q_2 \\ q_3 \end{vmatrix} = \begin{vmatrix} \rho \\ \rho u \\ e \end{vmatrix}$$

where

$$\left.\begin{aligned} & w_1 = q_1 - (\gamma - 1)(c^*)^{-2}\theta \ , \qquad \theta = q_3 + 0.5(q_2^*/q_1^*)^2 q_1 - (q_2^*/q_1^*)q_2 \\ & w_2 = \beta^*(\gamma - 1)\theta + \beta^* c^* \phi \quad , \qquad \phi = q_2 - (q_2^*/q_1^*)q_1 \\ & w_3 = \beta^*(\gamma - 1)\theta - \beta^* c^* \phi \end{aligned}\right\} \tag{7}$$

It is interesting to examine W at the reference values, that is, evaluate equations (7) at Q^*. Then we have

$$\left.\begin{aligned} & w_1^* = \frac{\gamma - 1}{\gamma} q_1^* = \frac{(\gamma - 1)}{\gamma} \rho^* \\ & w_2^* = \frac{\beta^* q_1^* c^*}{\gamma} = \frac{1}{\sqrt{2}\gamma} c^* \\ & w_3^* = \frac{\beta^* q_1^* c^*}{\gamma} = \frac{1}{\sqrt{2}\gamma} c^* \end{aligned}\right\} \tag{8}$$

We see that the characteristic variables at the reference values reduce to known simple variables with which we are more familiar.

IV. IMPLICIT NUMERICAL METHOD

An implicit finite difference scheme is chosen to demonstrate the boundary condition application. The conditions are applicable to any numerical scheme for the Euler equations. We have the first order in time implicit scheme

$$[X_\xi a(\xi)I - hB^n + h\delta_\xi A^n]\Delta Q = -h(\delta_\xi E^n - H^n)$$

$$B = a_\xi(\gamma - 1)\begin{vmatrix} 0 & 0 & 0 \\ \frac{u^2}{2} & -u & 1 \\ 0 & 0 & 0 \end{vmatrix}, \quad A\text{: eq. (5b)} \tag{9a}$$

with

$$\Delta Q^n = Q^{n+1} - Q^n , \qquad h = \Delta t \tag{9b}$$

where the second-order linearizations

$$\left.\begin{aligned} E^{n+1} &= E^n + A^n(Q^{n+1} - Q^n) + O(\Delta t^2) \\ H^{n+1} &= H^n + B^n(Q^{n+1} - Q^n) + O(\Delta t^2) \end{aligned}\right\} \tag{9c}$$

are used. Note that, due to the homogeneous property, $E^n = A^nQ^n$, and therefore equation (9c) reverts to

$$E^{n+1} = A^nQ^{n+1} + O(\Delta t)^2 \tag{9d}$$

Here, n refers to a reference level *. Second-order central differences are used for the spatial derivatives, where

$$\delta_\xi(Q)_j = (Q_{j+1} - Q_{j-1})/2\Delta\xi \tag{10}$$

The above implicit scheme is well-known and is unconditionally stable in the linear sense. The specific boundary conditions and their implicit application will be discussed below.

Introducing a discrete mesh (see fig. 2) with J points in the computational domain, equation (9a) has the general form

$$(X_\xi aI - hB^n)_j\ \Delta Q^n_j + \frac{h}{2\Delta\xi}\left(A^n_{j+1}\ \Delta Q^n_{j+1} - A^n_{j-1}\ \Delta Q^n_{j-1}\right) = -\frac{h}{2\Delta\xi}\left(E^n_{j+1} - E^n_{j-1}\right) + hH^n_j \tag{11a}$$

and the specific form at J, the last computational point,

$$(X_\xi aI - hB^n)_J\ \Delta Q^n_J + \frac{h}{2\Delta\xi}\left(A^n_{J+1}\ \Delta Q^n_{J+1} - A^n_{J-1}\ \Delta Q^n_{J-1}\right) = -\frac{h}{2\Delta\xi}\left(E^n_{J+1} - E^n_{J-1}\right) + hH^n_J \tag{11b}$$

(Here we will assume that $j = J$ is an outflow boundary and $j = 1$ is an inflow boundary.)

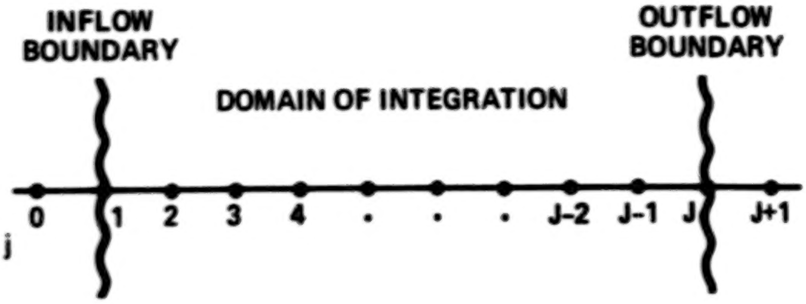

Figure 2.- Discrete computational mesh.

Now note that if $j = J$ is the last computational point, then we need to evaluate terms in equation (11b) at $J + 1$ which is outside the domain of integration. Given the previous discussion on characteristics, certain variables can be obtained from outside the domain of interest and others cannot. The form of the specific boundary conditions depends upon the type of flow conditions at the boundary (i.e., subsonic or supersonic). Similar arguments occur at the first computational point $j = 1$.

Below we present a derivation of the characteristic boundary conditions for subsonic outflow, and then point out the slight differences for other cases, such as subsonic inflow and supersonic inflow, and outflow. The present concepts are based on a flux splitting which is in some sense similar to ideas introduced by Steger and Warming (ref. 8). Instead of splitting the eigenvalues into two types (Steger and Warming (ref. 8) split the positive from the negative eigenvalues) and forming associated fluxes, we partition the eigenvector set into two parts, very much the same as employed by Yee (ref. 1). The eigenvector partitioning produces two characteristic vectors, one associated with incoming wave propagation of information at a boundary and one associated with outgoing propagation.

V. CHARACTERISTIC BOUNDARY CONDITIONS

V-a. Characteristic Boundary Application

To demonstrate the characteristic boundary conditions, we shall first choose the case of subsonic outflow. For subsonic outflow, the eigenvalues of A at the boundary are

$$\left.\begin{aligned} u &> 0 \\ u + c &> 0 \\ u - c &< 0 \end{aligned}\right\} \tag{12}$$

The propagation of information is therefore outside of the integration domain for two of the characteristic variables (w_1 and w_2) and into the domain for the one variable (w_3).

First, note that the characteristic vector W can be partitioned into two vectors

$$W = W_{in} + W_{out} \tag{13a}$$

where

$$W_{in} = \begin{vmatrix} 0 \\ 0 \\ w_3 \end{vmatrix} , \quad W_{out} = \begin{vmatrix} w_1 \\ w_2 \\ 0 \end{vmatrix} \tag{13b}$$

The subscript in refers to incoming characteristics (information) and the subscript out refers to outgoing characteristics.

Using the definition of W in equation (3b) and splitting the X^{-1} into two matrices, one containing the last row of X^{-1} and zero for the first two rows and the other containing the first two rows of X^{-1} and zero for the last row, we can rewrite W_{in} and W_{out} as

$$W_{in} = X_{in}\, Q , \quad W_{out} = X_{out}\, Q \tag{14a}$$

where

$$X_{in} = \begin{vmatrix} 0 & 0 & 0 \\ 0 & 0 & 0 \\ \beta\left[(\gamma - 1)\frac{u^2}{2} + uc\right] & -\beta[c + (\gamma - 1)u] & \beta(\gamma - 1) \end{vmatrix} \tag{14b}$$

and

$$X_{out} = \begin{vmatrix} 1 - \frac{u^2}{2}(\gamma - 1)c^{-2} & (\gamma - 1)uc^{-2} & -(\gamma - 1)c^{-2} \\ \beta\left[(\gamma - 1)\frac{u^2}{2} - uc\right] & \beta[c - (\gamma - 1)u] & \beta(\gamma - 1) \\ 0 & 0 & 0 \end{vmatrix} \tag{14c}$$

Examining equation (11b), we see that two quantities involve values outside the domain of integration. They are

$$A^n_{J+1}\, \Delta Q^n_{J+1} \quad \text{and} \quad E^n_{J+1} \tag{15}$$

Now we can rewrite the expressions in equation (15) in terms of W as

$$A^n_{J+1}\ X^n_{J+1}\ \Delta W^n_{J+1} \quad \text{and} \quad A^n_{J+1}\ X^n_{J+1}\ W^n_{J+1} \tag{16}$$

where equation (6) was used and an error of the same order as in equation (9c) was introduced in forming the first term as a function of ΔW. That is, we can move the eigenvector matrix X^{-1} inside the ΔQ expression, thereby producing an error of the same order as the linearization error. This process will later be reversed when we finally put the formulation back in terms of ΔQ.

The characteristic vector W is split as in equations (13) and (14), and we have

$$A^n_{J+1}\ X^n_{J+1}\ \Delta W^n_{in_{J+1}} + A^n_{J+1}\ X^n_{J+1}\ \Delta W^n_{out_{J+1}} \tag{17a}$$

for the first term of equation (16) and

$$A^n_{J+1}\ X^n_{J+1}\ W^n_{in_{J+1}} + A^n_{J+1}\ X^n_{J+1}\ W^n_{out_{J+1}} \tag{17b}$$

for the second term.

The values of W_{in} and W_{out} must be provided at $J + 1$ to complete the problem definition. The previous analysis shows that W_{in} must be specified, and from equation (8) we see that this reduces to specifying c, the speed of sound. For W_{out}, we will use a linear extrapolation of W_{out} from the interior points $J - 1$ and J. That is,

$$W_{out_{J+1}} = 2\ W_{out_J} - W_{out_{J-1}} \tag{18}$$

W_{in} is to be specified $\Delta W_{in} = 0$ and the same linear extrapolation is used for $(\Delta W_{out})_{J+1}$ as in equation (18). Equation (17a) then becomes

$$A^n_{J+1}\ X^n_{J+1}\ X^n_{in_{J+1}}\ \Delta Q^n_{J+1} + A^n_{J+1}\ X^n_{J+1}\left[2\left(X^n_{out_J}\ \Delta Q_J{}^n - X^n_{out_{J-1}}\ \Delta Q^n_{J-1}\right)\right] \tag{19}$$

where the same error as before is introduced when we extract X^{-1} from ΔW^n_{out}. A similar expression can be written for equation (17b).

Equation (11b) can now be rewritten as

$$\left[(X_\xi a)I - hB_J{}^n + \frac{h}{\Delta\xi}(AX)^n_{J+1}(X^n_{out})_J\right]\Delta Q_J{}^n - \frac{h}{2\Delta\xi}\left[A^n_{J-1} + (AX)^n_{J+1}(X^n_{out})_{J-1}\right]\Delta Q^n_{J-1} =$$

$$-\frac{h}{2\Delta\xi}\left\{(AX)^n_{J+1}\left[(W^*_{in})_{J+1} + 2(X_{out}Q)_J{}^n - (X_{out}Q)^n_{J-1}\right] - E^n_{J-1}\right\} + hH_J{}^n \tag{20}$$

The elements on the left-hand side of equation (11a) form a block tridiagonal matrix which must be inverted to obtain the solution. The corresponding elements of equation (20) show how the block tridiagonal matrix is modified to obtain the implicit characteristic boundary conditions. The right-hand sides of both equations are evaluated in the usual straightforward manner.

Examining equation (8), we see that for subsonic outflow the condition that (W^*_{in}) is specified, that is, equivalent to fixing the speed of sound at $j = J + 1$. We are therefore assuming that the flow variables at $j = J + 1$ reach some overall reference state, *, so that equation (7) collapses to equation (8). For steady-state problems this means that we need to know the steady-state value of c or in unsteady (forced at the boundary) problems we need to provide the unsteady value of c. Usually, one is used to having other variables specified, such as pressure, at boundaries and the speed of sound seems to be an unnatural variable. It is important to stress that the speed of sound is a consistent variable, since the characteristic formulation directly introduces it. Therefore, one should try to use the speed of sound when available and, if not, other boundary conditions such as those suggested by Yee (ref. 1) are adequate and work very well.

The characteristic conditions introduced here are applied implicitly and therefore do not degrade the unconditional stability of the implicit algorithm. They are also consistent with the physics of the flow, since they are based on the characteristic propagation of information, and they are consistent with the spatial and temporal accuracy of the main integration scheme.

V-b. Subsonic Inflow

In the subsonic inflow case the eigenvalues of A^n at the boundary point $j = 1$ are

$$\left.\begin{aligned} u &> 0 \\ u + c &> 0 \\ u - c &< 0 \end{aligned}\right\} \tag{21}$$

In this case, W_{in} is composed of w_1 and w_2 which implies that both density, ρ, and speed of sound c must be specified at $j = 0$. The characteristic vector W_{out} is only composed of w_3. The application of the characteristic boundary conditions are the same as above with equation (20) now having the form

$$\left[(X_\xi a)_1 I - hB_1{}^n - \frac{h}{\Delta\xi}(AX)_0{}^n(X_{out})_1{}^n\right]\Delta Q_1{}^n + \frac{h}{2\Delta\xi}\left[A_2{}^n + (AX)_0{}^n(X_{out})_2\right]\Delta Q_2{}^n = - \frac{h}{2\Delta\xi}\left\{E_2{}^n - (AX)_0\left[(W_{in}^*)_0 + 2(X_{out}Q)_1{}^n - (X_{out}Q)_2{}^n\right]\right\} + hH_1{}^n \tag{22}$$

V-c. Supersonic Inflow and Outflow

For supersonic inflow all the flow and characteristic variables are specified since all the eigenvalues of A are positive, that is, $W_{out} = 0$. At supersonic outflow, all information propagates out of the integration domain and therefore the conditions are that $W_{in} = 0$. Equation (20) then has the form

$$\left[(X_\xi a)_J I - hB_J{}^n + \frac{h}{\Delta\xi}A_{J+1}^n\right]\Delta Q_J{}^n - \frac{h}{2\Delta\xi}\left[A_{J-1}^n + A_{J+1}^n\right]\Delta Q_{J-1} = - \frac{h}{2\Delta\xi}\left[A_{J+1}^n\left(2Q_J{}^n - Q_{J-1}^n\right) - E_{J-1}^n\right] + hH_J{}^n \tag{23}$$

(Note that for $W_{in} = 0$, $X_{out} = X^{-1}$ and $XX^{-1} = I$.) For supersonic inflow, the central differencing naturally attaches the fixed flow variables.

V-d. Flow Variable Boundary Application

In the above derivation, nothing has been said about how to evaluate A_{J+1}^n and X_{J+1}^n in eqs. (20), (22), and (23). The flow variables at the previous time step, n, are used to form these terms, and they must be updated before the next time step can be taken. The only restriction on the value of Q_{J+1}^n is that it is consistent with W_{in} fixed. In the case of subsonic outflow, the variables ρ and u are extrapolated from the interior to the exterior, for example, at $j = J + 1$,

$$\left.\begin{aligned} \rho_{J+1}^n &= 2\rho_J{}^n - \rho_{J-1}^n \\ u_{J+1}^n &= 2u_J{}^n - u_{J-1}^n \end{aligned}\right\} \tag{24}$$

and pressure is calculated such that the speed of sound, c, is fixed, that is,

$$p_{J+1}^n = \left(\frac{c^2\rho}{\gamma}\right)_{J+1}^n = (2\gamma w_3{}^2\rho)_{J+1}^n\ , \qquad (w_3)_{J+1} \text{ is fixed.} \tag{25}$$

This insures that W_{in} is fixed at $j = J + 1$ for all n. In the subsonic inflow case only u is extrapolated, and fixed density and speed of sound are used to insure that W_{in} is fixed. For supersonic outflow all the flow variables are extrapolated since $W_{in} = 0$, and in supersonic inflow all the variables are held at fixed values.

V-f. Multidimensional Application

In two and three dimensions, the mechanics of the above scheme can be applied in a straightforward manner. The characteristic formulation only requires that each flux vector be handled in the appropriate way. That is, each flux vector produces a characteristic splitting. An examination of the characteristic directions at the boundary determines which variables are specified and which are extrapolated. Note that the scheme does not rely upon any commutative or simultaneous diagonalization properties of the multidimensional flux Jacobians (properties that the Euler equations do not possess). When curvilinear transformations are used in multidimensional flows (see refs. 9 and 10), the transformed fluxes, Jacobian matrices, and eigensystems are employed.

VI. RESULTS

Results are presented for two different nozzle shapes at different flow conditions. The first case is a diverging nozzle at either supersonic-supersonic or supersonic-subsonic conditions. The second case is for a converging-diverging nozzle at subsonic-subsonic conditions. For both cases the numerical solutions are compared with theoretical results taken from classical nozzle flow theory. The characteristic boundary conditions are shown, through numerical experiment, to be accurate and stable in both a physical and numerical sense. In all the cases to be shown, the numerical results compare quite well with theory.

VI-a. Diverging Nozzle for Supersonic-Subsonic Flow

The quasi-one-dimensional Euler equations are solved for a nozzle flow with supersonic inflow and subsonic outflow. With a specified outflow speed of sound, the conditions produce a shock which stands inside the nozzle. The nozzle shape used is one suggested by Shubin et al. (ref. 3) and also used by Yee (ref. 1). The area shape is

$$a(x) = 1.398 + 0.347 \tanh(0.8)(x - 4) \quad \text{for} \quad 0 < x < 10 \tag{26}$$

With this area ratio and an inflow Mach number of 1.26 and outflow speed of sound (nondimensionalized) of 1.127, a shock occurs at $x = 4.816$. The exact solution taken from the shock tables is compared in figure 3(a) with a converged result where the characteristic boundary conditions were used. Clustering in the region of the shock is used to produce a sharp shock jump. Figure 3(b) shows a result for a uniform grid with $dx = 0.169$. In the clustered case the minimum $dx = 0.075$. Every other numerical point is plotted in the figures for clarity.

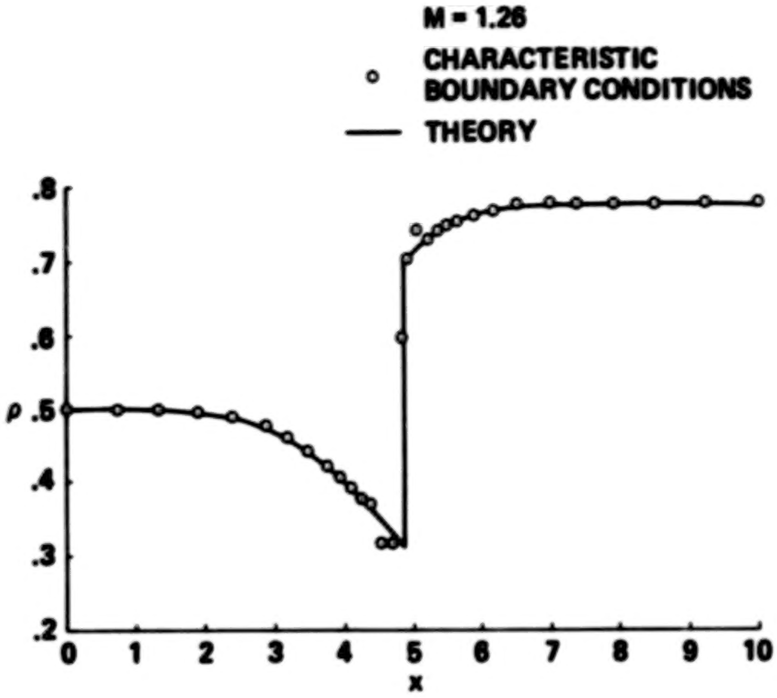

(a) Clustered grid.

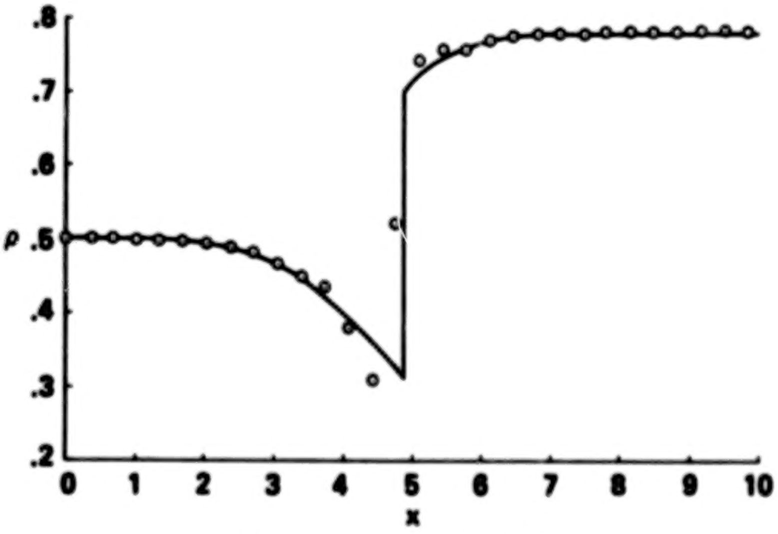

(b) Unclustered grid.

Figure 3.- Supersonic-subsonic flow through diverging nozzle.

Free-stream (at inflow conditions) initial conditions are used with no special treatment of the boundaries. The solution evolves naturally in time. A sequence of results taken at various stages in the solution process is shown in figure 4. These illustrate the fact that this application of characteristic boundary conditions allows for the physical development of the solution. Note that the outflow boundary variables are computed to their final steady-state values and the shock progresses across the solution domain in a time-accurate fashion.

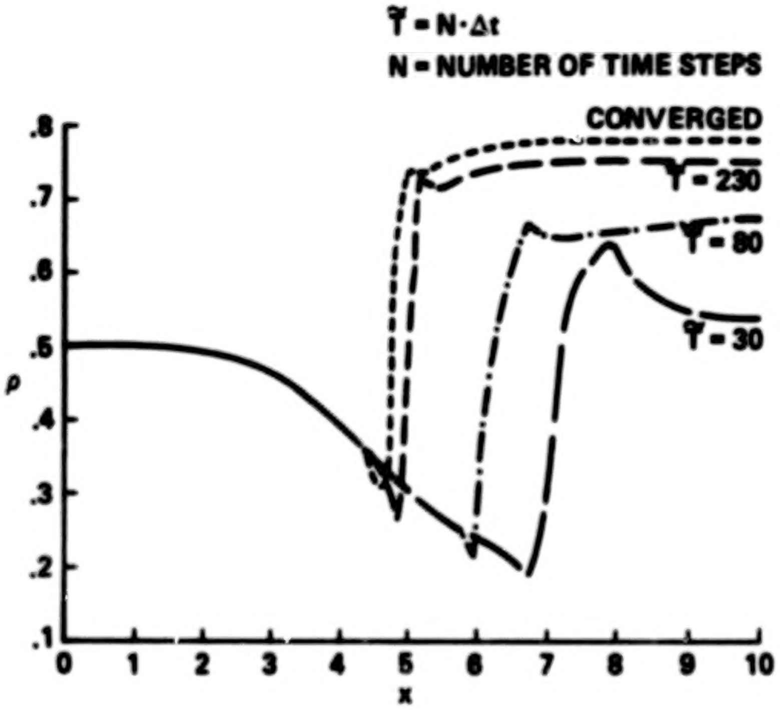

Figure 4.- Convergence development of supersonic-subsonic flow through diverging nozzle.

The numerical solution process was very stable with very large Courant numbers. Initially, the Courant number was kept low at about 5, for about 100 time steps, so that the shock could form physically and not be propagated too fast. Then the solutions converge in 300 more steps at a Courant number of 50. Courant numbers of up to 1 million were tried and were stable. If we want an unsteady time-accurate propagation of the shock, then a Courant number less than 1 should be used for time accuracy. These particular boundary conditions would then form a time-accurate calculation of the outflow values.

VI-b. Diverging Nozzle for Supersonic-Supersonic Flow

A pure supersonic case was solved for the diverging nozzle, and results are shown in figure 5. This is a very simple flow case with a smooth solution.

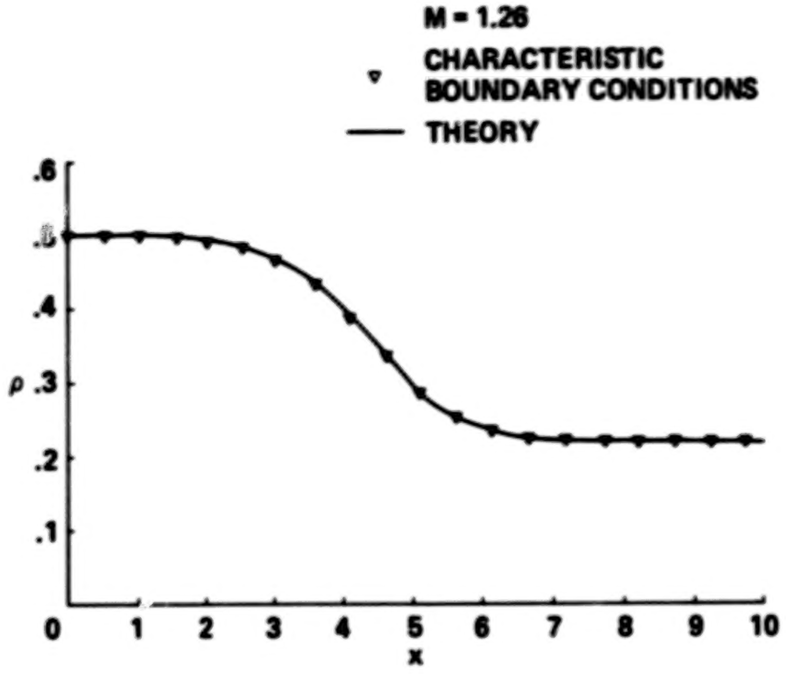

Figure 5.- Supersonic-supersonic flow through diverging nozzle.

VI-c. Converging-Diverging Nozzle for Subsonic-Subsonic Flow

Subsonic-subsonic flow is solved for flow through a converging-diverging nozzle with an inflow Mach number $M = 0.2395$. The nozzle shape is

$$\begin{aligned} a(x) &= 1 + 1.5[(5 - x)/5]^2 \quad , \qquad x < 5 \\ a(x) &= 1 + 0.5[(x - 5)/5]^2 \quad , \qquad x > 5 \end{aligned} \tag{27}$$

The boundary conditions are a nondimensional inflow density, $\rho = 1$, incoming speed of sound, $c = 1$, and an outflow speed of sound, $c = 0.98633$. Results are shown in figure 6 for a clustered one-dimensional grid. The initial conditions are set to the inflow conditions with the inflow Mach number $M = 0.2395$. Again, the solution evolves in a time-like fashion, and unconditional stability is achieved.

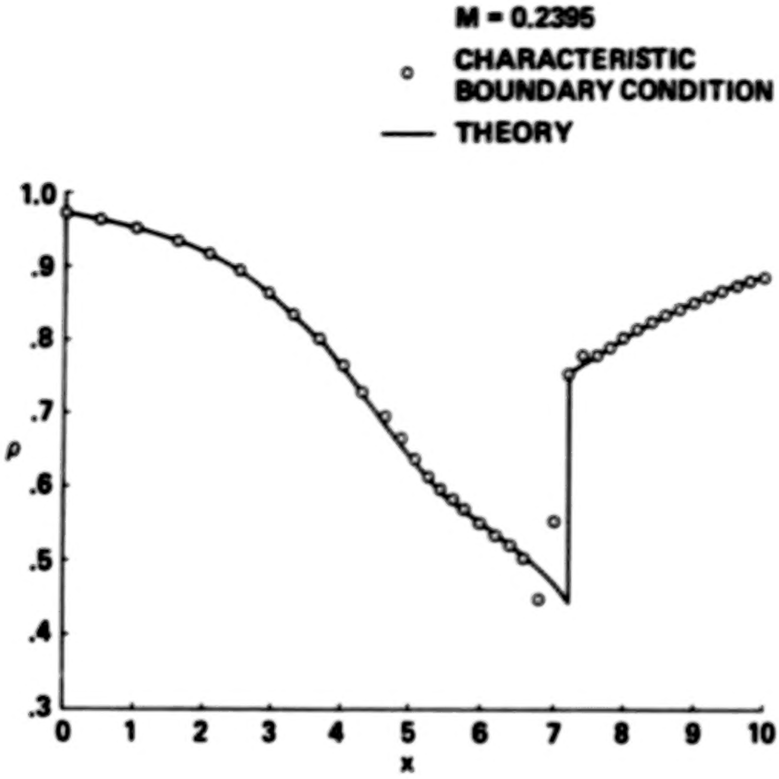

Figure 6.- Subsonic-subsonic flow through converging-diverging nozzle.

VII. SUMMARY

A boundary condition procedure for the Euler equations has been presented which employs characteristic conditions. They are applied to a conventional implicit numerical method and have been shown to be very stable, accurate, and consistent with the physics of the problem. The boundary conditions can be easily extended to two and three dimensions and other numerical methods.

Numerical results for an implicit finite difference scheme at a variety of inflow and outflow conditions demonstrate the consistency, stability, and accuracy of the characteristic boundary applications.

REFERENCES

1. Yee, H. C.: Numerical Approximations of Boundary Conditions with Application to Inviscid Equations of Gas Dynamics. NASA TM-81265, March 1981.

2. Yee, H. C.; Beam, R. M.; and Warming, R. F.: Stable Boundary Approximations for a Class of Implicit Schemes for the One-Dimensional Inviscid Equations of Gas Dynamics. AIAA Paper 81-1009, 1981.

3. Shubin, G. R.; Stephens, A. B.; and Glaz, H. M.: Steady Shock Tracking and Newton's Method. J. of Comp. Phys., vol. 39, no. 2, 1981, pp. 364-374.

4. Rudy, D.; and Strikwerda, J. C.: A Nonreflecting Outflow Boundary Condition for Subsonic Navier-Stokes Calculations. J. Comp. Phys., vol. 36, 1980, pp. 55-70.

5. Steger, J. L.; Pulliam, T. H.; and Chima, R. V.: An Implicit Finite Difference Code for Inviscid and Viscous Cascade Flow. AIAA Paper 80-1427, Snowmass, Colo., 1980.

6. Kentzer, C. P.: Discretization of Boundary Conditions on Moving Discontinuities. Second International Conference on Numerical Methods in Fluid Dynamics. Lecture Notes in Physics, Springer-Verlag, Berlin, 1971.

7. Oliger, J.; and Sundstrom, A.: Theoretical and Practical Aspects of Some Initial Boundary Value Problems in Fluid Dynamics. SIAM J. Appl. Math., vol. 35, no. 3, Nov. 1978.

8. Steger, J. L.; and Warming, R. F.: Flux Vector Splitting of the Inviscid Gas Dynamics Equations with Application to Finite Difference Methods. J. of Comp. Phys., vol. 40, no. 2, April 1981, pp. 263-293.

9. Steger, J. L.: Implicit Finite-Difference Simulation of Flow About Two-Dimensional Geometries. AIAA Journal, vol. 16, no. 4, July 1978, pp. 679-686.

10. Pulliam, T. H.; and Steger, J. L.: On Implicit Finite-Difference Simulations of Three Dimensional Flow. AIAA Journal, vol. 18, no. 2, Feb. 1980, pp. 159-167.

Blank Page

NUMERICAL BOUNDARY CONDITION PROCEDURE FOR THE TRANSONIC AXISYMMETRIC INVERSE PROBLEM*

Vijaya Shankar
Rockwell International Science Center

INTRODUCTION

Despite the advances made over the last ten years in the computational treatment of the transonic axisymmetric analysis problem[1] to compute pressure distributions over prescribed axisymmetric bodies, currently there exists no axisymmetric inverse methodology (aside from expensive optimization techniques[2]) to predict the body shape corresponding to a given favorable pressure loading. In this period of energy conservation, achievement of low drag shapes is of critical interest from the point of improving range, acceleration, and maximum speed characteristics and reducing fuel consumption. At transonic speeds, the wave drag rise is extremely sensitive to the area distribution along the axisymmetric body. Use of area ruling based on linear theory and concepts developed by Whitcomb[3] as well as Oswatitsch's equivalence area rule[4] to achieve low drag shapes usually results in nonoptimum configurations at transonic speeds due to lack of nonlinearity in the formulation. A strong need exists for the development of nonlinear transonic area ruling. The purpose of this paper is to provide an inverse methodology for predicting axisymmetric body shapes corresponding to prescribed pressures exhibiting low wave drag as a step towards the ultimate development of nonlinear area ruling concepts. The crux of the axisymmetric inverse problem is the proper implementation of the nonlinear pressure boundary condition involving the unknown body shape.

This paper describes two types of boundary condition procedures for the axisymmetric inverse problem. One is a Neumann type boundary condition (analogous to the analysis problem) and the other is a Dirichlet type boundary condition, both requiring special treatments to make the inverse scheme numerically stable. The dummy point (or ghost) concept[5] is utilized in implementing both the analysis and inverse boundary conditions. The results from this study indicate that the Dirichlet type inverse boundary condition is more robust and conceptually simpler to implement than the Neumann type procedure. The paper includes a few results demonstrating the powerful capability of this newly developed inverse method that can handle both shocked as well as shockless body design.

---

*Supported in full by AFOSR under contract F49620-80-C-0081.

of J we no longer have the condition $z = \kappa$ and must consider the more complicated relation (4.15). To simplify the investigation we seek only the asymptote (J large) of the P-stability bound.

First we rewrite the characteristic equation (A.3) and the boundary condition polynomial (4.15), i.e.,

$$\frac{z - 1}{\theta z + 1 - \theta} = \frac{1}{2}\,\nu\left(\kappa - \frac{1}{\kappa}\right) \tag{A.12}$$

and

$$z = \frac{(-1)^{J/q}\,\kappa^{-[(J/q)-1]} + \kappa^{(J/q)-1}}{(-1)^{J/q}\,\kappa^{-(J/q)} - \kappa^{J/q}} \tag{A.13}$$

and we will assume $J \gg q$. Next we assume $J \gg 1$ and eliminate κ from (A.12) and (A.13). For notational convenience let

$$\frac{z - 1}{\theta z + 1 - \theta} = \lambda^{*}\Delta t \tag{A.14}$$

From (A.12) we have

$$\kappa^2 - \frac{2\lambda^{*}\Delta t}{\nu}\,\kappa - 1 = 0$$

or

$$\kappa = \frac{\lambda^{*}\Delta t}{\nu} \pm \sqrt{\left(\frac{\lambda^{*}\Delta t}{\nu}\right)^2 + 1} \tag{A.15}$$

Recall

$$\nu = \frac{c\Delta t}{\Delta x} = \frac{c\Delta t}{\ell}\,J$$

therefore for large J, (A.15) becomes

$$\kappa = 1 + \frac{\ell\lambda^{*}}{c}\,\frac{1}{J} \tag{A.16}$$

Note that the choice of the sign before the radicand is arbitrary due to the special form of (A.12) and (A.13). We have chosen the positive sign. If we introduce κ from (A.16) into (A.13) and assume $J \gg 1$ we obtain

$$z = -\frac{e^{\ell\lambda^{*}/qc} + (-1)^{J/q}\,e^{-(\ell\lambda^{*}/qc)}}{e^{\ell\lambda^{*}/qc} - (-1)^{J/q}\,e^{-(\ell\lambda^{*}/qc)}}$$

or

$$e^{2\ell\lambda^*/qc} = \frac{(-1)^{J/q}(z - 1)}{z + 1} \tag{A.17}$$

Thus, we have replaced κ in (A.12) and (A.13) by λ^* in (A.14) and (A.17). At the stability boundary $|z| = 1$. We set $z = e^{i\psi}$ and substitute in the characteristic equation (A.14)

$$\lambda^* = \frac{2}{\Delta t}\left[\frac{(2\theta - 1)\tan\frac{\psi}{2} + i}{(2\theta - 1)^2 \tan\frac{\psi}{2} + \operatorname{ctn}\frac{\psi}{2}}\right] \tag{A.18}$$

and the boundary condition (A.17)

$$\lambda^* = \frac{cq}{2\ell}\, ln\left[i(-1)^{J/q} \tan\frac{\psi}{2}\right] \tag{A.19}$$

For example, if we choose zeroth- or first-order space-time extrapolation, $q = 1$ or 2, (A.19) becomes

$$\lambda^* = \frac{qc}{2\ell}\left[ln\left(\tan\frac{\psi}{2}\right) + i\left(\frac{\pi}{2} + 2m\pi\right)\right], \quad \frac{J}{q} = \text{even integer} \tag{A.20a}$$

$$= \frac{qc}{2\ell}\left[ln\left(\tan\frac{\psi}{2}\right) + i\left(\frac{3\pi}{2} + 2m\pi\right)\right], \quad \frac{J}{q} = \text{odd integer} \tag{A.20b}$$

$$= \frac{qc}{2\ell}\left[ln\left(\tan\frac{\psi}{2}\right) + i(\pi + 2m\pi)\right], \quad \frac{J}{q} = \text{even integer} + \frac{1}{2} \tag{A.20c}$$

$$= \frac{qc}{2\ell}\left[ln\left(\tan\frac{\psi}{2}\right) + i(2m\pi)\right], \quad \frac{J}{q} = \text{odd integer} + \frac{1}{2} \tag{A.20d}$$

where $m = 0, \pm 1, \pm 2, \ldots.$

Symbolically we can write (A.18) and (A.19)

$$\lambda^*_{CE} = \frac{1}{\Delta t} f(X) \tag{A.21a}$$

$$\lambda^*_{BC} = \frac{qc}{\ell} g(X) \tag{A.21b}$$

where $X = \tan(\psi/2)$ and f and g are complex functions of X. The subscripts CE and BC on λ^* have been added for notational convenience; of course, λ^*_{CE} must equal λ^*_{BC}.

We have found the following procedure to be convenient for solving (A.21). Choose θ. Equate the arguments of λ^*_{CE} and λ^*_{BC}, i.e.,

$$\mathrm{Arg}(\lambda^*_{BC}) = \mathrm{Arg}(\lambda^*_{CE})$$

or

$$\mathrm{Arg}(f(X)) = \mathrm{Arg}(g(X)) \tag{A.22}$$

where (A.22) is a nonlinear equation in X which can easily be solved by Newton's method. Next equate the absolute values of λ^*_{CE} and λ^*_{BC}, i.e.,

$$|\lambda^*_{CE}| = |\lambda^*_{BC}|$$

or

$$\frac{1}{\Delta t}\,|f(X)| = \frac{qc}{\ell}\,|g(X)|$$

or, since $\nu = c\Delta t/\Delta x$, $\Delta x = \ell/J$,

$$\nu = \frac{J}{q}\left|\frac{f(X)}{g(X)}\right| \tag{A.23}$$

which is an asymptote for the stability boundary, $|z| = 1$. In general, there can be more than one asymptote since $g(X)$ is a function of m, e.g., equation (A.20). The P-stability condition is the most restrictive condition (minimum ν) obtained from the set (A.23) and (4.13), (4.14). P-stability domains for typical methods with the space-time-extrapolation boundary scheme (J even, $q = 1$) are shown in figure A2.

For some values of θ and q there are no asymptotes (A.23). For example, let $q = 1$ and J be even. We have from (A.18)

$$f(X) = \frac{(2\theta - 1)X + i}{(2\theta^2 - 2\theta)X + \frac{1}{2}\left(X + \frac{1}{X}\right)}$$

and from (A.20a)

$$g(X) = \frac{1}{2}\left[\ln(X) + i\left(\frac{\pi}{2} + 2m\pi\right)\right]$$

therefore (A.22) becomes

$$\frac{1}{(2\theta - 1)X} = \frac{\frac{\pi}{2} + 2k\pi}{\ln(X)} \tag{A.24}$$

Equation (A.24) has no solution ($\theta > 1/2$) if

$$\theta > \frac{1}{2}\left[1 + \frac{1}{\pi e\left(\frac{1}{2} + 2m\right)}\right]$$

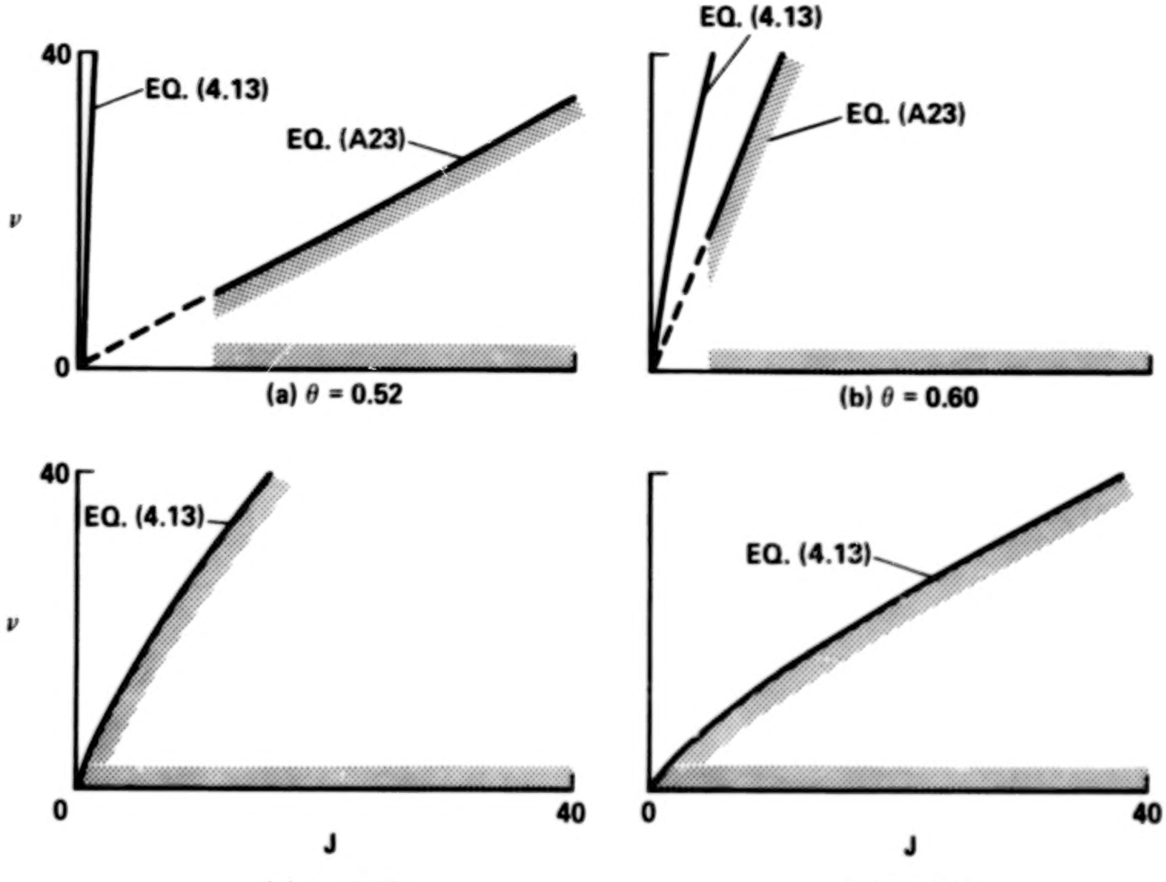

(a) $\theta = 0.52$ (b) $\theta = 0.60$

(c) $\theta = 0.75$ (d) $\theta = 1.0$

Figure A2.- P-stability domain (shaded region) for typical θ methods, space-time-extrapolation boundary condition, J even, $q = 1$.

Therefore, if

$$\theta > \frac{1}{2} + \frac{1}{\pi e} \approx 0.6171 \tag{A.25}$$

there are no asymptotes (A.23) and the P-stability bound is (4.13), (4.14). Similarly, if $q = 1$ and J is odd there are no asymptotes (A.23) if

$$\theta > \frac{1}{2} + \frac{1}{3\pi e} \approx 0.5390 \tag{A.26}$$

and the schemes are unconditionally P-stable. Note that the values (A.25) and (A.26) were derived for large J and may not apply for J near unity.

REFERENCES

1. Yee, H.; Beam, R.; and Warming, R.: Stable Boundary Approximations of a Class of Implicit Schemes for the One Dimensional Inviscid Equations of Gas Dynamics, AIAA-81-1009-CP, AIAA Computational Fluid Dynamics Conference, Palo Alto, CA, June 22-23, 1981.

2. Gustafsson, B.; Kreiss, H.-O.; and Sundström, A.: Stability Theory of Difference Approximations for Mixed Initial Boundary Value Problems. II, Mathematics of Computations, vol. 26, 1972, pp. 649-686.

3. Kreiss, H.-O.: Difference Approximations for the Initial-Boundary Value Problem for Hyperbolic Differential Equations, Numerical Solutions of Nonlinear Differential Equations, Proceedings of Advanced Symposium, Madison, Wis., 1966, pp. 141-166. Wiley, New York.

4. Gear, C.: Numerical Initial Value Problems in Ordinary Differential Equations. Prentice-Hall, Englewood Cliffs, N.J., 1971.

5. Dahlquist, G.: A Special Stability Property for Linear Multistep Methods, BIT, vol. 3, 1963, pp. 27-43.

6. Beam, R.; and Warming, R.: An Implicit Factored Scheme for the Compressible Navier-Stokes Equations II. The Numerical ODE Connection, Paper No. 79-1446, AIAA 4th Computational Fluid Dynamics Conference, Williamsburg, VA, July 1979.

7. Gustafsson, B.; and Oliger, J.: Stable Approximations for a Class of Time Discretizations of $u_t = AD_0u$, Uppsala University, Department of Computer Sciences, Report No. 87, 1980.

STABILITY THEORY OF DIFFERENCE APPROXIMATIONS FOR MULTIDIMENSIONAL INITIAL-BOUNDARY VALUE PROBLEMS

Daniel Michelson
University of California at Los Angeles

Consider a first order hyperbolic system of partial differential equations

$$\frac{\partial u}{\partial t} + \sum_{j=1}^{m} A_j(x,t)\,\frac{\partial u}{\partial x_j} = F(x,t) \tag{1}$$

which is solved in the domain

$$x_1 > 0, \quad t > 0, \quad x_- = (x_2, x_3, \dots, x_m) \in R^{m-1}$$

with zero initial condition

$$u(x,0) = 0 \tag{2}$$

and boundary condition

$$Su(0,x_-,t) = g(x_-) \ . \tag{3}$$

We assume that system (1) is strictly hyperbolic, i.e. the eigenvalues of the symbol $A(\omega) = \sum A_j\omega_j$ are real and distinct for real $\omega \neq 0$. We also assume that the boundary is not characteristic, i.e. A_1 is not singular. The well posedness of the problem in (1)-(3) is stated in terms of the a priori estimate

$$\eta\|u(x,t)e^{-\eta t}\|^2 + \|u(0,x_-,t)e^{-\eta t}\|^2 \le K\left(\frac{1}{\eta}\,\|F(x,t)e^{-\eta t}\|^2 + \|g(x_-,t)e^{-\eta t}\|^2\right) \tag{4}$$

which should hold for any $\eta > \eta_0 \geq 0$ and some constant K independently on the function $u(x,t)$. Here $\|\cdot\|$ denotes the L_2 norm over domains indicated by the arguments. The problem in (1)-(3) was investigated by H.-O. Kreiss in [1], where he shows that estimate (4) follows from so-called uniform Kreiss condition (referred farther as UKC) and in the cases of constant coefficients is equivalent to this condition.

Now suppose that equation (1) is approximated by a multistep difference scheme

$$L(E_x, E_t)u(x,t) = \Delta t \cdot F(x,t) \tag{5}$$

with corresponding zero initial condition and boundary condition

$$S(E_x, E_t)u(0,x_-,t) = g(x_-,t) \ . \tag{6}$$

Here $E_x = (E_{x_1}, \dots, E_{x_m})$, where E_{x_j}, E_t are the displacement operators in the directions x_j and t with the increments Δx_j and Δt respectively ($\Delta x_j/\Delta t$ are constant), and $L(E_x,E_t)$, $S(E_x,E_t)$ are difference operators consistent with equations (1) and (3). We assume also that the difference equations (5)-(6) are solvable in time, i.e. assumption 3.1 in [3]. Our goal is to obtain for the difference problem (5)-(6) the same estimate (4) with discrete L_2 norms. Insofar this problem was treated only in one-space dimensional case: for some dissipative schemes by Kreiss in [2] and for more general dissipative as well as strictly non-dissipative schemes by Gustafsson, Kreiss and Sundström in [3]. An attempt to generalize these results for arbitrary multi-dimensional difference schemes encounters severe obstacles. However for dissipative difference schemes the problem may be resolved. In fact we prove the following.

THEOREM 1. Let the difference operator $L(E_x,E_t)$ be uniformly dissipative, i.e. for $\xi \neq 0$ the eigenvalues z of the characteristic equation $\det L(e^{i\xi},z) = 0$, where

$$e^{i\xi} = (e^{i\xi_1}, e^{i\xi_2}, \ldots, e^{i\xi_m}) ,$$

are in the unit disc $|z| < 1$ and for small $|\xi|$ each eigenvalue z_j satisfies an inequality

$$1 - \delta_2|\xi|^{2n_j} \le |z_j| \le 1 - \delta_1|\xi|^{2n_j} .$$

Then UKC is sufficient and, in the case of constant coefficients, necessary for estimate (4) to hold.

The UKC is formulated as for the differential problem. However the verification of this condition in multidimensional case is very complicated. Applying to problem (5)-(6) Fourier transform in the tangential variables x_- with the dual variables $\xi_- = (\xi_2,\ldots,\xi_n)$ we arrive at the difference problem in x_1,t depending on the parameters ξ_-

$$L(E_{x_1}, e^{i\xi_-}, E_t)u(x_1,t) = \Delta t \cdot F(x_1,t) \tag{7}$$

$$S(E_{x_1}, e^{i\xi_-}, E_t)u(0,t) = g(t) \tag{8}$$

with zero initial condition.

We can prove the following result:

THEOREM 2. If (5)-(6) is a consistent approximation of a well-posed problem (1)-(3), then UKC for problem (5)-(6) is satisfied if and only if it is satisfied for (7)-(8) for any ξ_-. (I.e. we do not need uniformity in ξ_-.)

So the multidimensional problem is reduced to a set of one-space dimensional ones. It is still a difficult task to check well posedness of each one of the problems (7)-(8). However, by adding sufficient amount of dissipativity in the tangential variables, this problem may be further reduced to the single case of (7)-(8) with $\xi_- = 0$. Namely, introduce the difference operator $\Delta = \sum_{j=2}^{m}(E_{x_j} + E_{x_j}^{-1} - 2)$ and consider the difference problem

$$L(E_x, E_t(1 - K\Delta^k))u(x,t) = \Delta t \cdot F(x,t) \tag{9}$$

$$S(E_x, E_t(1 - K\Delta^k))u(0,x_-,t) = g(x_-,t) \tag{10}$$

with zero initial condition. Here K is a positive constant and k is a positive integer. We have the following result.

THEOREM 3. Let problem (5)-(6) satisfy the conditions:
(a) the Cauchy problem for (5) is well posed
(b) (5)-(6) is consistent with a well posed problem (1)-(3)
(c) (5)-(6) is solvable in time
(d) For $\xi_- = 0$ problem (7)-(8) is well posed and the operator in (7) is dissipative. (Note that we do not require the general dissipativity of L.)

Then for any positive integer k there exists a positive constant K such that problem (9)-(10) is well posed (in the sense of estimate (4)).

Theorem 1 is essentially proved in [4] for the more complicated but particular case of Burstein difference scheme applied to some characteristic boundary value problem. Theorems 2 and 3 follow easily from the proof of Theorem 1.

REFERENCES

[1] Kreiss, H.-O.: Initial boundary value problems for hyperbolic systems, Comm. Pure Appl. Math., Vol. 23, 1970, pp. 277-298.

[2] Kreiss, H.-O.: Stability theory for difference approximations of mixed initial boundary value problems I, Math. Comp., v. 22, 1968, pp. 703-714.

[3] Gustafsson, B.; Kreiss, H.-O. and Sundström, A.: Stability theory of difference approximation for mixed initial boundary value problems II, Math. Comp., v. 26, 1972, pp. 649-686.

[4] Michelson, D.: Initial-boundary value problems for hyperbolic equations and their difference approximation with uniformly characteristic boundary, Ph.D. Thesis, Dept. of Math. Sciences, Tel-Aviv University, June 1980.

Blank Page

Blank Page

SOME EXPERIMENTS ON EXPLICIT BOUNDARY ALGORITHMS

K. Förster
University of Stuttgart

Summary

This paper describes some experiments done with the aim of improving the accuracy and efficiency of explicit boundary algorithms for quasilinear hyperbolic systems of partial differential equations in matrix form.

The starting point

Some time ago we tested a number of finite difference schemes using an exact but non-trivial solution of the gasdynamic equations due to Ringleb /1/. This solution had been cast into some convenient subroutines for the purpose of a workshop held by the author in 1977 (see /2/) and further developed since then into a veritable "Ringleb machine" which is described in the appendix 1. The outcome of these tests was surprising: if we inserted the exact boundary values (fig.1a) instead of computing them numerically (fig.1b), the error level was decreased drastically, even by orders of magnitude. That means that the accuracy potential of the tested field algorithms is much higher than commonly anticipated but is deteriorated by common boundary algorithms to an astonishing degree.
The consequences are important. Should it be possible to cure the defect and to maintain reasonably similar accuracy levels for both, boundary and field, the number of grid points necessary for a certain accuracy would be substantially reduced resulting

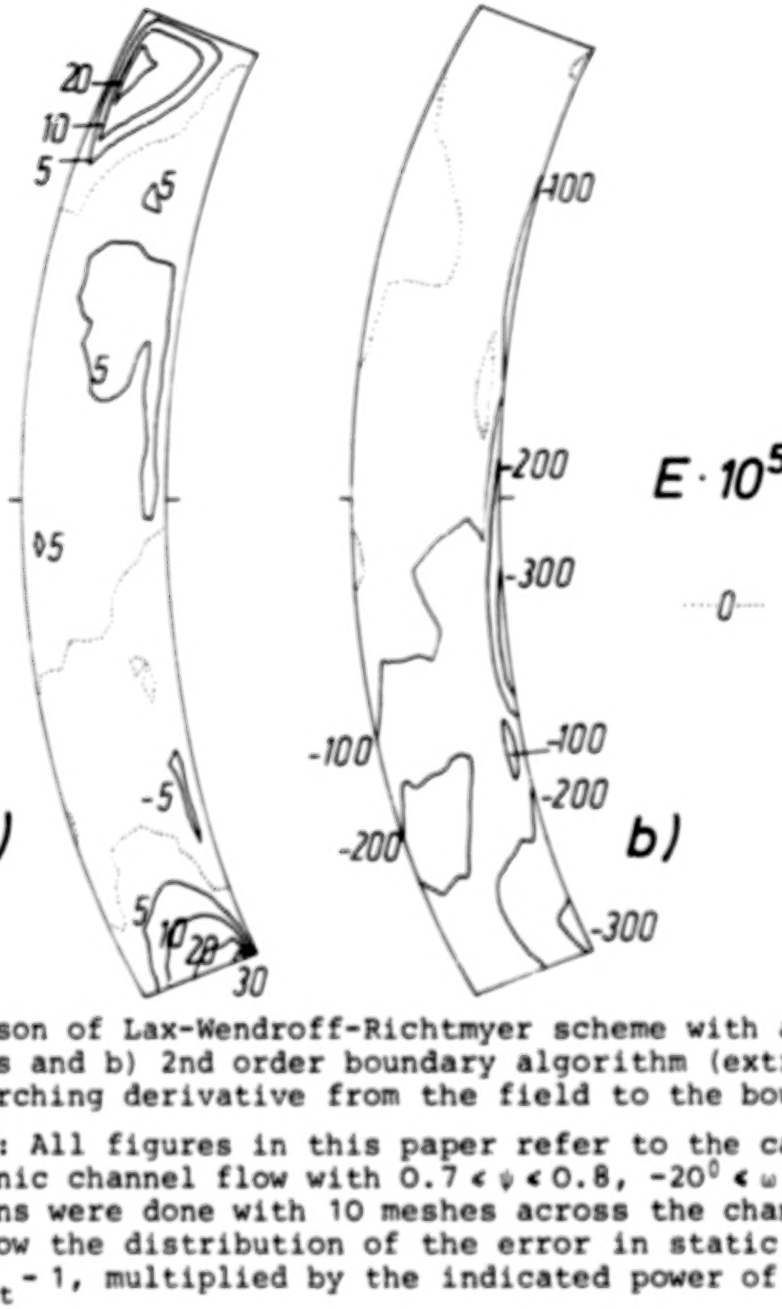

Fig.1 Comparison of Lax-Wendroff-Richtmyer scheme with a) exact boundary values and b) 2nd order boundary algorithm (extrapolation of the marching derivative from the field to the boundary).

General remark: All figures in this paper refer to the case of steady supersonic channel flow with $0.7 < \psi < 0.8$, $-20^0 < \omega = 20^0$. All computations were done with 10 meshes across the channel. The figures show the distribution of the error in static pressure $E = p/p_{exact} - 1$, multiplied by the indicated power of ten.

either in a decrease in cost or in the possibility to tackle more complex problems on smaller computers than before.

We tried two independent paths in the direction to this goal. The first one, already well trodden, consists in scrutinizing common boundary schemes by their Taylor expansions, testing whole groups of algorithms and trying to fit them together in some sense. The second one is a new approach based on a special handling of the differential equations at the boundary. Both ideas are still far from being in a final shape: we report on work in progress and give only some promising examples.

Error matching and restglied engineering

The following train of thought leading to possible improvements is simple enough: if the application of some algorithm at the boundary brings forth a distinct change, this algorithm must be different from that in the field. Provided that both are of pth order of accuracy, i.e. their Taylor expansions agree up to this order, the difference must be contained in the remaining part of the expansion which can be taken as an infinite series or represented by the (p+1)st order term at a different locus, the truncation error or restglied.
So our immediate concern should be to construct boundary algorithms inside their strongly asymmetric regime in such a manner as to match the Taylor expansion of the (typically symmetric) field algorithm as far as possible.
And a more general point of view were to concentrate not only upon the order of accuracy of an algorithm but also upon its truncation error, for instance to assimilate it to the expansion of the exact value as far as possible without too much coding expense - in other words: to exercise "restglied engineering" in the broadest sense.[0]

In practice this simple concept meets some technical difficulties. Especially if we use the differential system in matrix form

$$\vec{w}_t = A\,\vec{w}_x + \vec{f}\ ,\quad A = A(\vec{w})$$

there are usually many possible discretization variants with respect to A, so it is not adequate to expand the linear model (constant matrix) because it does not contain sufficient information. On the other hand, the labor of expanding the quasilinear system

---

[0] This is of course only one side of the triangle: we may not disregard the theory of characteristics (most important: the domain of dependence) and we must ask how far the assumption of strong solutions which is basic for the application of the Taylor expansion, is at all admissible in hyperbolic problems.

$$u_t = a(u,v)\,u_x + b(u,v)\,v_x + f(u,v)$$
$$v_t = c(u,v)\,u_x + d(u,v)\,v_x + g(u,v)$$

(which is only slightly more general than our test example, see appendix 1) is considerable even if one confines himself to second order only - the minimum for examining first order schemes in the above sense! Thus the aid of a formula handling compiler is nearly indispensable (we use the very comfortable MASYCA system by W.Degen /3/ installed in interactive form on a Cyber 174). Even then one may meet limits in the form of storage restrictions. Luckily, however, in many cases sufficient information can be gained already from the scalar model

$$u_t = a(u)\,u_x \quad ; \; a_t = a'u_t \;,\; a_x = a'u_x$$

which is much less involved. We start with applying it to the examination of some second order schemes.

Application to second order schemes

Execution of the above concept yields the table 1. Below the expansion of the exact value $\bar{u}_i^+ = u_{exact}(ih,(n+1)k)$, $h = \Delta x$, $k = \Delta t$,$^{0)}$ the two most common field algorithms are listed: Lax-Wendroff-Richtmyer and MacCormack (though results for the latter will not be presented in this paper). Then follow some boundary schemes, part of them known, others constructed ad hoc:

A) "Rusanov", given in its general form by Rusanov and Nazhestkina /4/ for the conservative form. From the two most practical discretization variants of the matrix form we have chosen

$$\tilde{u}_0^+ = u_0 + \frac{1}{2}\left[(A_{3/2} + A_{1/2})(u_{3/2} - u_{1/2}) + (A_1 + A_0)(u_1 - u_0) - (A_2 + A_1)(u_2 - u_1)\right]$$

because it can be coded very compactly together with the field

---

$^{0)}$ The indexing used is: $u_i = u(ih,nk)$, $u_{i+1/2} = u((i+\frac{1}{2})h, (n+\frac{1}{2})k)$,
$u_i^+ = u(ih,(n+1)k)$.

BLANK

PAGE

Table 1 Taylor expansion of $u_t = a(u)\,u_x$ and of some algorithms up to $O(h^3)$

1. Exact value:

$$\bar{u}_i^+ = u_i + hAu_x + \frac{h^2}{2}\left\{A^2 u_{xx} + 2AA' u_x^2\right\} + \frac{h^3}{6}\left\{A^3 u_{xxx} + 9A^2 A' u_x u_{xx} + \left[6A\,A'^2 + 3A^2 A''\right] u_x^3\right\}$$

with $A = \frac{k}{h} a$

2. Field point algorithms:

LWR $\quad u_i^+ = 2^{nd}$ order $+ \frac{h^3}{6}\left\{A\,u_{xxx} + \left(\frac{3}{2} + \frac{3A^2}{2}\right)A' u_x u_{xx} + \left[\frac{3A}{2}\,A'^2 + \left(\frac{3}{4} + \frac{3A^2}{4}\right)A''\right]u_x^3\right\}$

MC $\quad u_i^+ = 2^{nd}$ order $+ \frac{h^3}{6}\left\{A\,u_{xxx} + \left(\pm 3A + 3A^2\right)A' u_x u_{xx} + \left[3A\,A'^2 + \left(\pm\frac{3A}{2} + \frac{3A^2}{2}\right)A''\right]u_x^3\right\}$

+ for backw. predictor/forward corrector
− for forward predictor/backw. corrector

3. Boundary point algorithms: $(i = 0)$

A) Rusanov $\quad \tilde{u}_0^+ = 2^{nd}$ order $+ \frac{h^3}{6}\left\{(-2A + 3A^2)\,u_{xxx} + \left(-\frac{15}{2} + 18A + \frac{3A^2}{2}\right)A' u_x u_{xx} + \left[\left(6 + \frac{3A}{2}\right)A'^2 + \left(-\frac{9}{4} + 6A + \frac{3A^2}{4}\right)A''\right]u_x^3\right\}$

B) Extrapol. $\quad \tilde{u}_0^+ = 2^{nd}$ order $+ \frac{h^3}{6}\left\{-5A\,u_{xxx} + \left(-\frac{33}{2} + \frac{3A^2}{2}\right)A' u_x u_{xx} + \left[\frac{3A}{2}\,A'^2 + \left(-\frac{21}{4} + \frac{3A^2}{4}\right)A''\right]u_x^3\right\}$

C) Vers. II $\quad \tilde{u}_0^+ = 2^{nd}$ order $+ \frac{h^3}{6}\left\{-5A\,u_{xxx} + \left(\frac{3}{2} + \frac{3A^2}{2}\right)A' u_x u_{xx} + \left[\frac{3A}{2}\,A'^2 + \left(\frac{3}{4} + \frac{3A^2}{4}\right)A''\right]u_x^3\right\}$

D) Vers. II spez. $\quad \tilde{u}_0^+ = 2^{nd}$ order $+ \frac{h^3}{6}\left\{-5A\,u_{xxx} + \left(\frac{3}{2} + \frac{3A^2}{2}\right)A' u_x u_{xx} + \left[\frac{3A}{2}\,A'^2 + \left(-\frac{9}{4} + \frac{3A^2}{4}\right)A''\right]u_x^3\right\}$

E) Compact $\quad u_0^+ = 2^{nd}$ order $+ \frac{h^3}{6}\left\{(-2A + 3A^2)\,u_{xxx} + \left(\frac{3}{2} + \frac{3A^2}{2}\right)A' u_x u_{xx} + \left[\frac{3A}{2}\,A'^2 + \left(-\frac{3A}{2} + \frac{3A^2}{4}\right)A''\right]u_x^3\right\}$

algorithm using a statement function

$$DU_i = \tfrac{1}{2}(A_i + A_{i-1})(u_i - u_{i-1}),$$

symbolized in the computational molecule by the horizontal brackets. The computed value bears a tilde because in the sense of the characteristic correction approach (see appendix 2) it is only a provisional value.

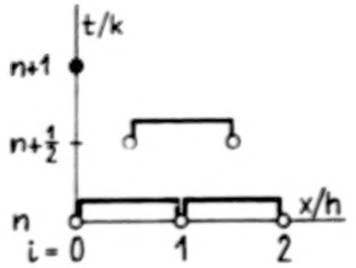

B) "Extrapolation" - already mentioned in the introductory fig.1 in its crudest form, but used in this context with characteristic correction - is based upon the very simple concept of extrapolating u_t at the level $(n+\frac{1}{2})k$ from inside the field to the boundary:
$$(u_t)_0 = 2(u_t)_1 - (u_t)_2$$
yielding for instance
$$\tilde{u}_0^+ = u_0 + (A_{3/2} + A_{1/2})(u_{3/2} - u_{1/2}) - \tfrac{1}{2}(A_{5/2} + A_{3/2})(u_{5/2} - u_{3/2}) \quad .$$

C) "Version II" is a multiparameter family of algorithms also using exclusively values at the intermediate level $(n+\frac{1}{2})k$, but derived via a general ansatz. Matching its h^3-term as far as possible with that of the LWR scheme gives the one-parameter family
$$\tilde{u}_0^+ = u_0 + \tfrac{\beta}{2}(3A_{1/2} - A_{3/2})(u_{3/2} - u_{1/2}) - \frac{(4-3\beta)A_{1/2} - (3-\beta)A_{3/2} + A_{5/2}}{2(1-\beta)}\left[(2-\beta)u_{1/2} - (3-\beta)u_{3/2} + u_{5/2}\right].$$

D) "Version IIspez" stems from the additional requirement (forbidden in Version II) that the last term be a second difference:
$$\tilde{u}_0^+ = u_0 + \tfrac{1}{2}(3A_{1/2} - A_{3/2})(u_{3/2} - u_{1/2}) - \left[(2+\alpha)A_{1/2} - (1+2\alpha)A_{3/2} + \alpha A_{5/2}\right](u_{5/2} - 2u_{3/2} + u_{1/2}) .$$
Other families of algorithms, mainly using values at both levels nk and $(n+\frac{1}{2})k$, have been tested but are omitted here.

For the test proper with the help of the Ringleb machine, all these algorithms had to be transduced to the forms appropriate for the quasilinear system and also for the other (righthand) boundary $x = 1$. The results were as follows.
Firstly, we could state that a variation of the family parameter in C) and D) introduced nearly no changes at all. Therefore one can venture that the truncation error is sufficiently well represented by the third order term and that similar relations might

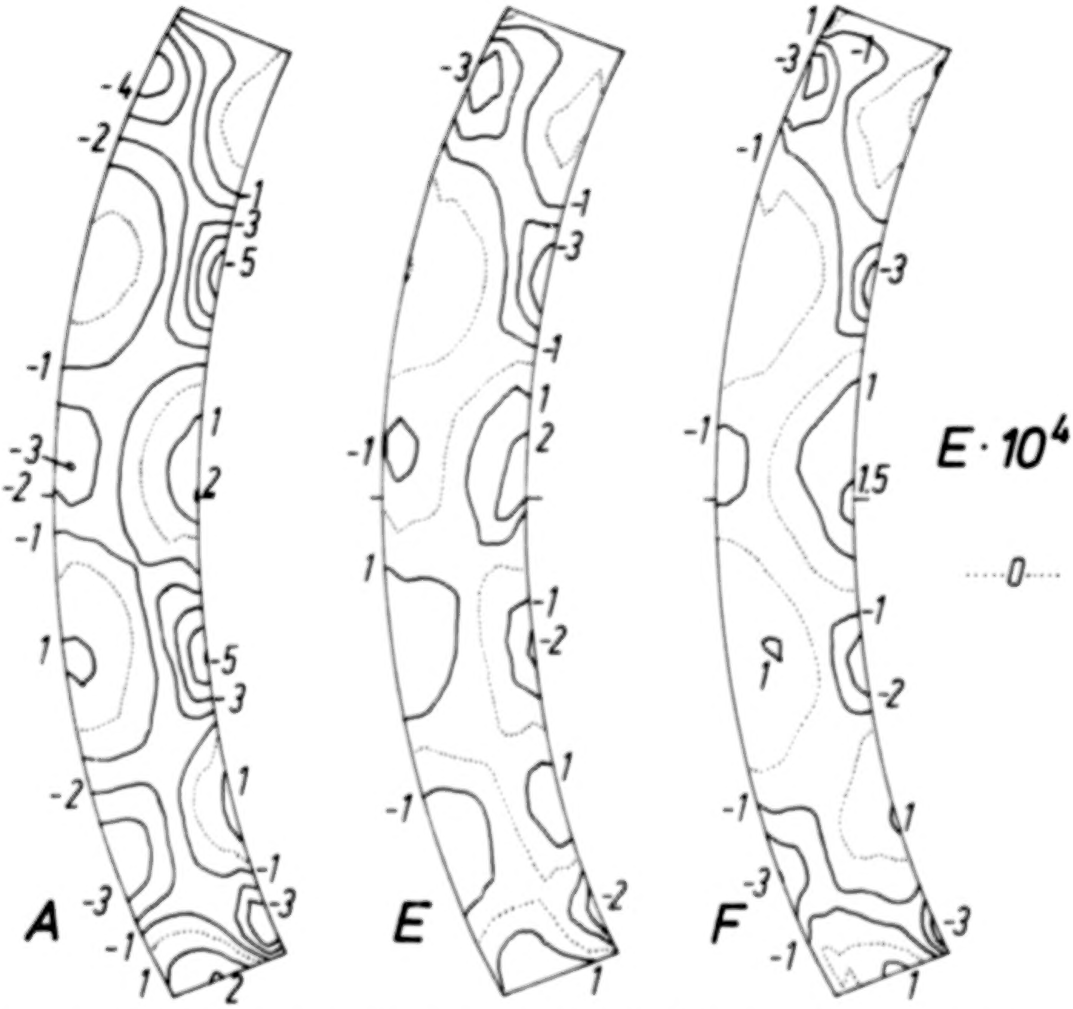

Fig.2 Error diagrams for the boundary schemes A), E) and F)

be true for higher order schemes.

Secondly, we found the following particular results also depicted in figure 2 and assembled in table 2:

Rusanov's scheme (fig.2 A) yields fair values compared with a computation using exact boundary values (fig.1 a) but the other three (fig.2 BO, CO, DO) fail, and they do so in a most insidious way: they are completely stable and the errors are large but not dramatic (of "technical quality" so to speak), so in a production run they might pass undetected.

A glance to table 1 raises the suspicion that the remarkable term $h^3/6\,(-5Au_{xxx} \cdots$ which is to be found in all three culprit expansions might be responsible for this behaviour, and in-

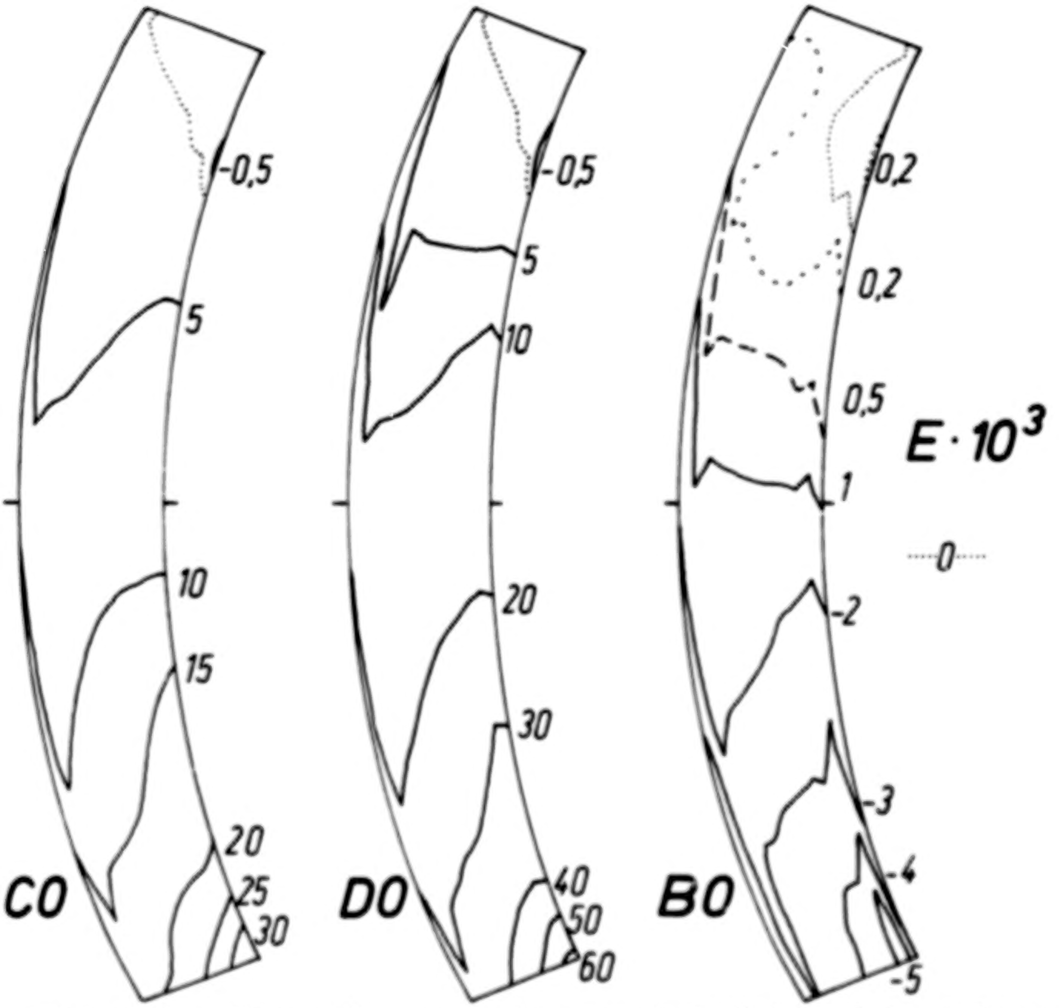

Fig.2(continued) Error diagrams for unmatched boundary schemes B, C and D

deed if we change this term into $h^3/6\ \{Au_{xxx} \cdots\}$ by simply adding

$$A_0(u_3 - 3u_2 + 3u_1 - u_0)$$

to the algorithms - and thus matching this term to the LWR scheme - the defect is completely cured (see fig.2 B1, C1, D1). Now the simple Extrapolation is tolerable, the more sophisticated Version II is nearly equal to Rusanov and Version IIspez is distinctly better in the mean square error

$$E_{msq} = \left(\frac{1}{N}\sum_{i=1}^{N} E_i^2\right)^{1/2} \quad , \text{N number of computed points}$$

which is a good measure for the overall quality of the solution. We have tried one more algorithm: E) in table 1, "Compact".

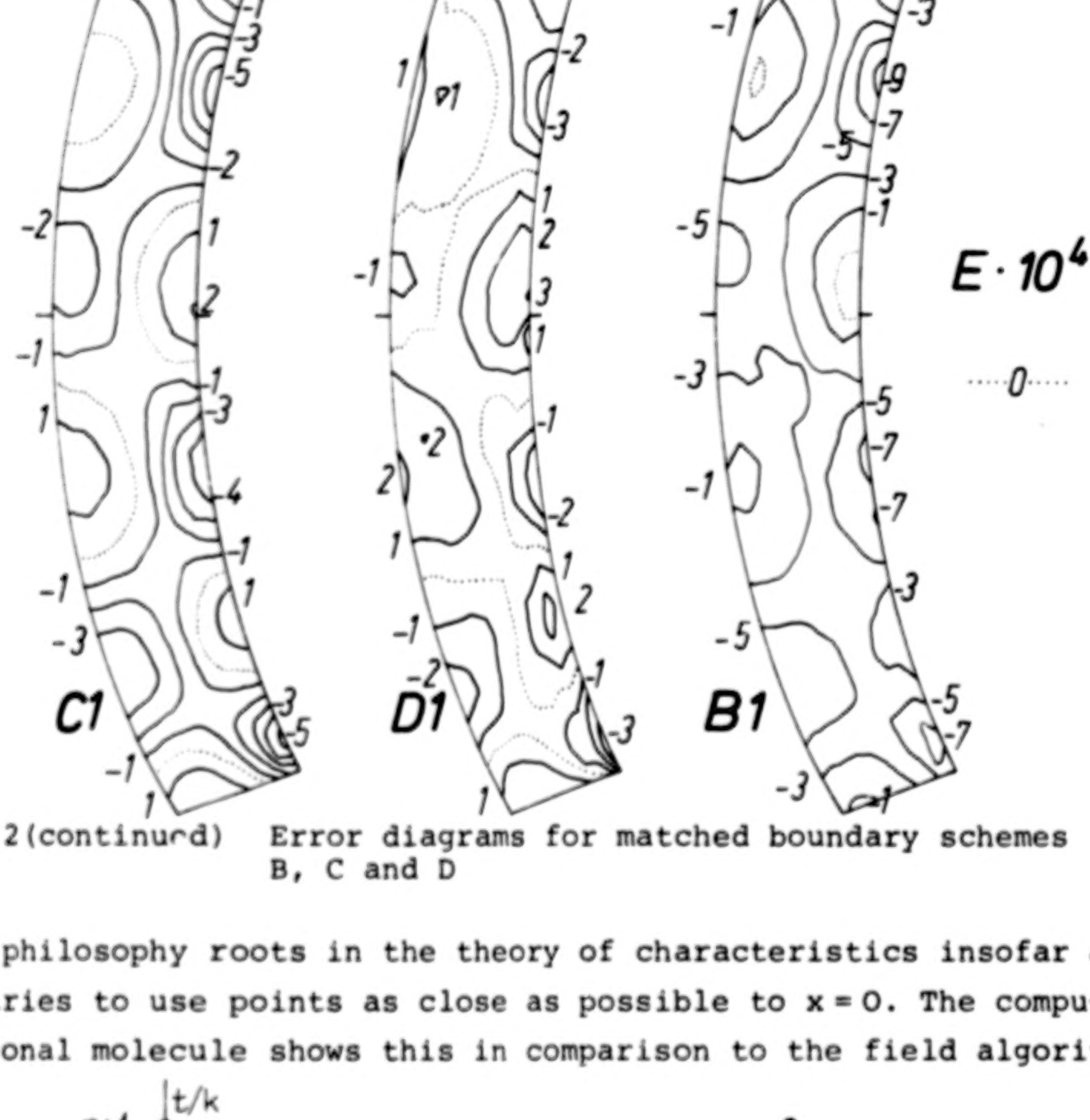

Fig.2(continued) Error diagrams for matched boundary schemes B, C and D

Its philosophy roots in the theory of characteristics insofar as it tries to use points as close as possible to x = 0. The computational molecule shows this in comparison to the field algorithm

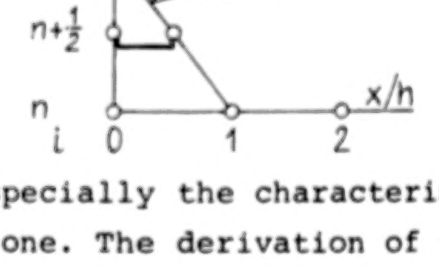

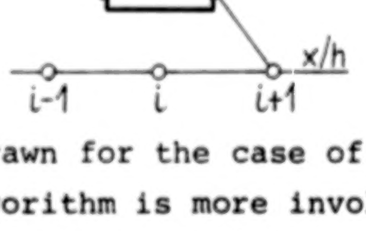

note especially the characteristic drawn for the case of Courant number one. The derivation of this algorithm is more involved than the usual Runge-Kutta procedure: $u_{0/2} = u(0,(n+\frac{1}{2})k)$ must be

Table 2 Figures of merit for second order schemes

	E_{min}	E_{max}	E_{msq}	$\cdot 10^5$
Field points only,				
6 meshes computed	-23	38	7.0	
8 meshes computed	-25	39	8.0	
A) Rusanov	-57	16	18.7	
without error-matching:				
BO) Extrapolation	-588	25	218.0	
CO) Version II	-57	3571	1219.0	
DO) Version IIspez	-91	6185	2261.0	
with error-matching:				
B1) Extrapolation	-97	14	37.6	
C1) Version II	-58	22	19.2	
D1) Version IIspez	-38	31	12.9	
E) Compact	-38	28	12.3	
F) Boundary Equation	-39	17	11.3	

computed such that

$$2(u_{1/2}-u_{0/2}) = u_{1/2}-u_{-1/2} + O(h^3)$$

where $u_{-1/2} = u(-\frac{h}{2},(n+\frac{1}{2})k)$ is a fictitious point outside the grid and used only for the purpose of derivation. The general ansatz yields a two-parameter family, and a sensible matching towards the LWR scheme gives

$$u_{0/2} = \frac{1}{4}(5u_0-2u_1+u_2)+\frac{1}{8}(3A_0-2A_1+A_2)(-3u_0+4u_1-u_2)$$

from which we can compute

$$\tilde{u}_0^+ = u_0 + 2A_{0/2}(u_{1/2}-u_{0/2}) \; .$$

Of course no characteristic correction is to be applied at the level $(n+\frac{1}{2})k$ as it would destroy the correct h^3-term.

This scheme is a bit better than Version IIspez in the smooth Ringleb flow (see fig.2 E and table 2) and we hope for good results in not-so-smooth flows too.

A new approach

For a system of differential equations all aforementioned algorithms are a little awkwardly to apply because they need the characteristic correction procedure for good accuracy. In our case that means that instead of computing the non-Dirichlet variable only, both variables must be computed and mingled according to the formula derived in appendix 2. Thus a lot of extra code is needed.

Based on a preliminary paper /5/ we will try a simpler way instead. If in addition to the system

$$\begin{aligned} u_t &= a u_x + b v_x + f \\ v_t &= c u_x + d v_x + g \end{aligned} \tag{1}$$

along the boundary $x = 0$ (we assume boundary fitted coordinates) a boundary condition is prescribed:

$$B(u,v,r(t)) = 0 \tag{2}$$

the whole system (1) + (2) is overdetermined. However, differentiation of eq.(2) with respect to the marching direction t yields

$$B_u u_t + B_v v_t + B_r r_t = 0$$

and now we have two possibilities:

1. We can use this equation to eliminate v_t from eqs.(1):

$$\begin{array}{rl} u_t & = a u_x + b v_x + f \\ -u_t B_u/B_v & = c u_x + d v_x + g + r_t B_r/B_v \end{array} \qquad \begin{array}{|l} +1 \\ -\frac{a}{c} \end{array} \quad \begin{array}{|l} +1 \\ -\frac{b}{d} \end{array}$$

   and by the two linear combinations indicated at the right we arrive at the two simple alternatives

$$u_t = \frac{B_v}{aB_u + cB_v}\left[(bc-ad)v_x + cf - ag - \frac{B_r}{B_v} a r_t\right] \tag{3}$$

   or

$$u_t = \frac{B_v}{bB_u + dB_v}\left[(ad-bc)u_x + df - bg - \frac{B_r}{B_v} b r_t\right] \tag{4}$$

   containing v_x or u_x but not both.
2. Eliminating u_t along the same tracks yields

$$v_t = \frac{B_u}{aB_u + cB_v}\left[(ad-bc)v_x - cf + ag - \frac{B_r}{B_u} c r_t\right] \tag{5}$$

or

$$v_t = \frac{B_u}{bB_u + dB_v}\left[(bc - ad)u_x - df + bg - \frac{B_r}{B_u}\,d\,r_t\right] \tag{6}$$

In principle, any of the equations (3) through (6) can, together with the equation (2), form the computational system at the boundary, so we call them "boundary equations". The selection among its different variants is usually simplified by the fact that the denominator may not vanish at the boundary or be unduly small there. Further the ease and/or the accuracy with which the remaining spatial derivative can be computed should be decisive.

A special case occurs if one of the dependent variables, say v, is a Dirichlet variable, i.e. its value is prescribed along the boundary so that for the calculation eqs. (5) and (6) are uninteresting. The boundary condition takes the special form

$$B(u,v,r) \equiv v(0,t) - v_0(t) = 0 \tag{2'}$$

so that $B_u = 0$, $B_v = 1$, $B_r = -1$ and we get instead of eqs. (3) and (4):

$$u_t = \left(b - \frac{ad}{c}\right)v_x + f - \frac{a}{c}g + \frac{a}{c}v_t \tag{3'}$$

or

$$u_t = \left(a - \frac{bc}{d}\right)u_x + f - \frac{b}{d}g + \frac{b}{d}v_t \tag{4'}$$

which now together with eq. (2') can form the computational system. For selection, again an eventual vanishing of c or d at the boundary must be considered. In our case which is simplified by $d = a$, $f = 0$, $g = g(v)$, a can be zero at the boundary so that finally

$$u_t = \frac{a}{c}v_t - \frac{a}{c}g + \left(b - \frac{a^2}{c}\right)v_x \quad .$$

Integration over t gives

$$u_0^+ = u_0 + \left\langle\frac{a}{c}\right\rangle\left(\bar{v}_0^+ - v_0\right) - k\left\langle\frac{a}{c}\right\rangle\bar{g} + k\left\langle\left\langle\left(b - \frac{a^2}{c}\right)v_x\right\rangle\right\rangle \quad .$$

Here the terms $(\bar{v}_0^+ - v_0)$ and $\bar{g}$ are exact Dirichlet values whereas the wedge brackets denote appropriate mean values in the sense of numerical integration. From linear analysis (the nonlinear case is not yet completed) we derived the following second order accurate discretization:

$$u_0^+ = u_0 + \frac{1}{2}\left[\left(\frac{a}{c}\right)_0 + \left(\frac{a}{c}\right)_0^+\right](\bar{v}_0^+ - v_0) - \frac{k}{2}\left[\left(\frac{a}{c}q\right)_0 + \left(\frac{a}{c}q\right)_0^+\right]$$
$$+\frac{k}{2h}\left[\left(b-\frac{a^2}{c}\right)_0 \left(v_1 - v_0 - (v_2 - 2v_1 + v_0)\right) + \left(b-\frac{a^2}{c}\right)_0^+ (v_1^+ - v_0^+)\right]$$

where the coefficients at lev 1 (n+1)k are linearly extrapolated, for instance $a_0^+ = 2a_1^+ - a_2^+$ etc.

The result is the best one in the examined series of second order algorithms (see figure 2 F and table 2).

Application to a third order scheme

For field points, a family of symmetric schemes of the Runge-Kutta type has been given by Rusanov /6/. We confine ourselves to its simplest member (also published by Burstein and Mirin /7/). Appropriate boundary and boundary neighbor algorithms have been developed by Rusanov and Nazhestkina /4/; summarizing, we have for the differential system in conservative form $\vec{w}_t = \vec{F}_x + \vec{f}$ the following computational sequences:

a) $w_{i+1/2} = \frac{1}{2}(w_{i+1} + w_i) + \frac{k}{3h}(F_{i+1} - F_i) + \frac{k}{3}\frac{1}{2}(f_{i+1} + f_i)$ 0)

b) $w^i = w_i + \frac{2}{3}\frac{k}{h}(F_{i+1/2} - F_{i-1/2}) + \frac{2k}{3}\frac{1}{2}(f_{i+1/2} + f_{i-1/2})$

c1) field points $w_i^+ = w_i + \frac{1}{4}\left\{\frac{k}{h}\left[\frac{7}{6}(F_{i+1} - F_{i-1}) - \frac{1}{3}(F_{i+2} - F_{i-2})\right] + k f_i\right\}$
$+ \frac{3}{4}\left\{\frac{k}{h}\frac{1}{2}(F^{i+1} - F^{i-1}) + k f^i\right\} + \gamma_i \delta^4 w_i$

c2) boundary neighbor $w_1^+ = w_1 + \frac{1}{4}\left\{\frac{k}{h}\left[\frac{1}{2}(F_2 - F_0) + \frac{5}{6}\delta^3 F_{3/2}\right] + k\left[f_1 - 3\delta f_{3/2}\right]\right\}$
$+ \frac{3}{4}\left\{\frac{k}{h}\left[F^2 - F^1 - \frac{1}{2}\delta^2 F^2\right] + k\left[f^1 + \delta f^{3/2}\right]\right\} + \gamma_1 \delta^4 w_2$

c3) boundary point $\tilde{w}_0^+ = w_0 + \frac{1}{4}\left\{\frac{k}{h}\left[F_1 - F_0 - \frac{1}{2}\delta^2 F_1 + \frac{35}{6}\delta^3 F_{3/2}\right] + k\left[f_0 + 3\delta^2 f_1\right]\right\}$
$+ \frac{3}{4}\left\{\frac{k}{h}\left[F^2 - F^1 - \frac{3}{2}\delta^2 F^2\right] + k\left[f^1 - \delta f^{3/2}\right]\right\} + \gamma_0 \delta^4 w_2$

with $\delta z_i = z_{i+1/2} - z_{i-1/2}$ and $\gamma_i = (4\sigma^2 + 1)(\sigma^2 - 4)/120$, $i > 2$
$\sigma = \max_j \left(\frac{k}{h}\lambda_j\right)$, λ eigenvalues of $\frac{d\vec{F}}{d\vec{w}}$

For the tested Ringleb flow, $\gamma_0 =$ [illegible] is allowable.

d) Upon the provisional boundary value $\tilde{w}_0^+$ the characteristic cor-

---

0) The indexing used is $u_i = u(ih, nk)$, $u_{i+1/2} = u((i+\frac{1}{2})h, (n+\frac{1}{3})k)$, $u^i = u(ih, (n+\frac{2}{3})k)$, $u_i^+ = u(ih, (n+1)k)$.

rection is to be inflicted as described for the second order schemes.

For the system in matrix form the discretization is based upon the identities $\delta^2 F = \delta(\delta F)$ and $\delta^3 F = \delta(\delta(\delta F))$

with $\delta F_i = \frac{1}{2}(A_{i+1/2} + A_{i-1/2})(u_{i+1/2} - u_{i-1/2})$.

It is helpful to sketch the computational molecules

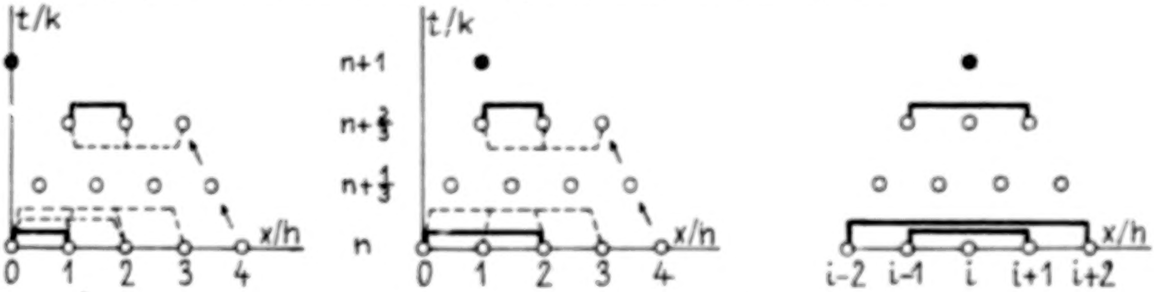

The solid brackets symbolize again first differences, the dotted ones stand for higher differences needed for third order accuracy. The field point algorithm (right) is quite symmetric whereas the other two exhibit asymmetries seemingly larger than necessary. One could think out less asymmetric schemes using the boundary points at the intermediate levels which could be computed readily by one of the boundary algorithms of first respectively second order. However, the Taylor expansion procedure shows that their incorporation is not compatible with third order accuracy; in a general ansatz their coefficients become identically zero, and one must live with the above asymmetries. Thus it is not surprising that in the Ringleb test the error level from the field point calculation alone (fig.3 left) is distinctly raised by computing the boundary neighbors numerically (fig.3 center), and still more, of course, by numerically calculated boundary points (fig.4 left).

We set out first to redevise the algorithm for the neighbor with the aim to achieve as much symmetry as possible, in spite of the above. Obviously we can use first differences $F_2 - F_0$ and $F^2 - F^0$ as in the field point algorithm if and only if u^0 is computed in such a way that its Taylor expansion is not only second order ac-

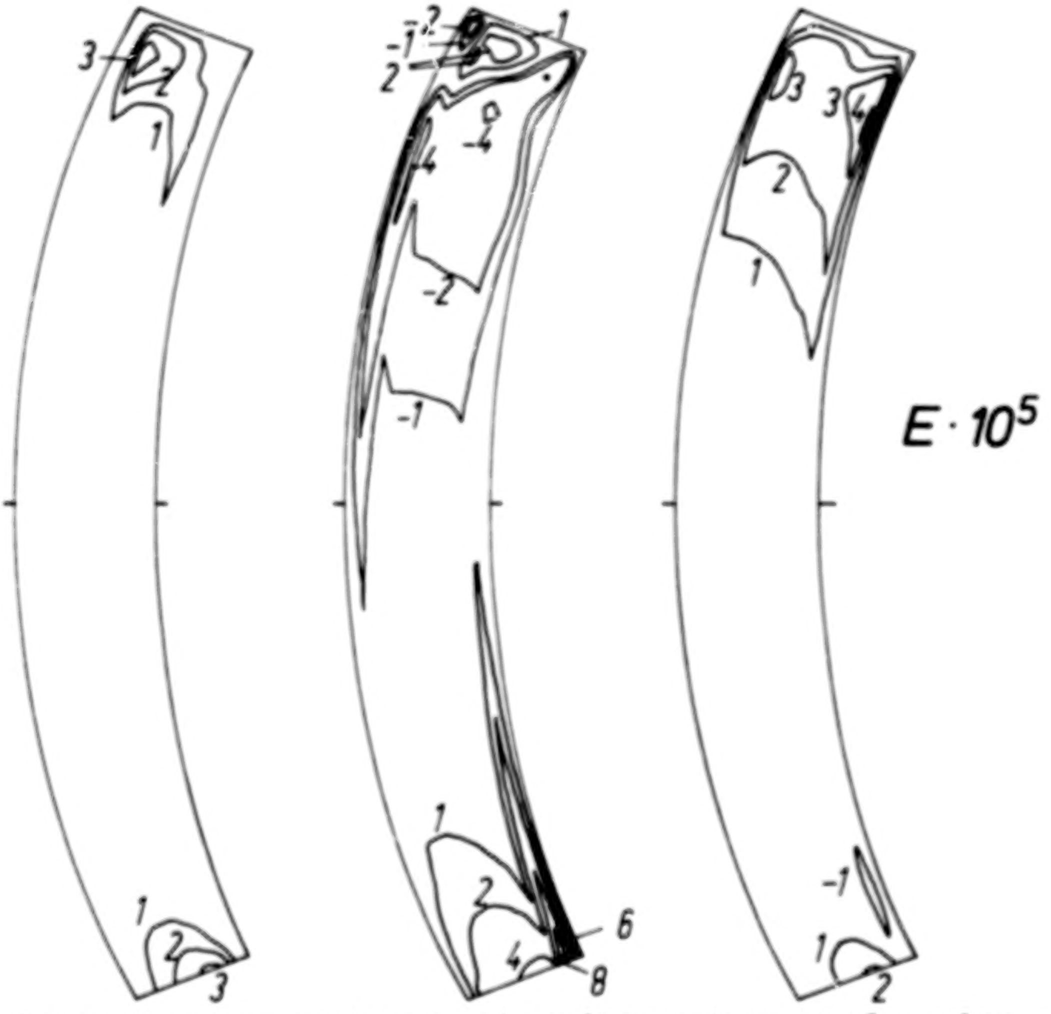

Fig.3 Error diagrams with exact boundary points. Left: also exact boundary neighbors. Center: neighbors calculated after Rusanov and Nazhestkina. Right: neighbors after the new formula.

curate but also matches the expansion of u^i in the field algorithm including terms of order h^3. To effect this (according to our flow problem in matrix form, and with $f = 0$) we make the extrapolating ansatz

$$u^0 = u_0 + \frac{2}{3}\frac{k}{h}\left[(1-\alpha_1-\alpha_2)A_{1/2} + \alpha_1 A_{3/2} + \alpha_2 A_{5/2}\right]\left[2(u_{3/2}-u_{1/2}) - (u_{5/2}-u_{3/2}) + \beta\,\delta^3 u_{3/2}\right]$$

and expand it. Matching it up to order h^3 with the expansion of the field point scheme using the fictitious point $x = -h$ yields the algorithm

$$u^0 = u_0 + \frac{2}{3}\frac{k}{h}\left(2A_{1/2} - \frac{3}{2}A_{3/2} + \frac{1}{2}A_{5/2}\right)\left[u_{3/2} - u_{1/2} - (u_{5/2} - 2u_{3/2} + u_{1/2}) + \delta^3 u_{3/2}\right] .$$

Using this value we can - along the usual tracks - derive a for-

Table 3 Figures of merit for the third order scheme

·	E_{min}	E_{max}	E_{msq} $\cdot 10^5$
Boundary and neighbor exact	-0.4	3.6	0.8
Boundary exact, neighbor: Rusan/Nazh.	-5.0	8.6	1.9
Boundary exact, neighbor: new formula	-1.4	4.2	1.2
Boundary and neighbor: Rusan/Nazh.	-17.2	8.5	9.3
Boundary: boundary equation, neighbor: Rusan/Nazh	-9.5	9.1	4.3
Boundary: boundary equation, neighbor: new formula	-3.2	6.1	2.4

mula for the boundary neighbor. A general ansatz produces a family of algorithms, their simplest member is

$$u_1^+ = u_1 + \frac{1}{4} A_1\left[\frac{1}{2}(u_2-u_0) - \frac{1}{6}(u_3-3u_2+3u_1-u_0)\right] + \frac{3}{4} A^1 \frac{1}{2}(u^2-u^0) .$$

The inclusion of f into the above schemes is straightforward.

The computational molecules show clearly that this algorithmical sequence has the advantage of being based only upon points i = 0...3, i.e. it stretches only 2h from i = 1 toward the inner field like the field point formula itself whereas the Rusanov/Nazhestkina algorithm extends 3h into this direction. The domain of dependence of the new formula is therefore closer to the theoretical one than that of Rusanov/Nazhestkina's:

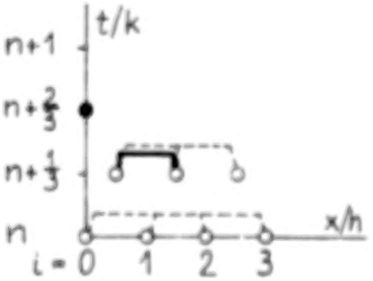

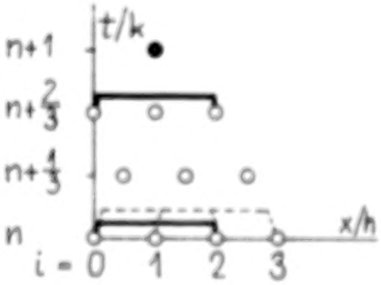

The Ringleb test (fig.3 right) consequently shows a considerable improvement against the corresponding fig.3 center and also the figures of merit are clearly better.

The incorporation of a boundary equation based algorithm for u_1^*

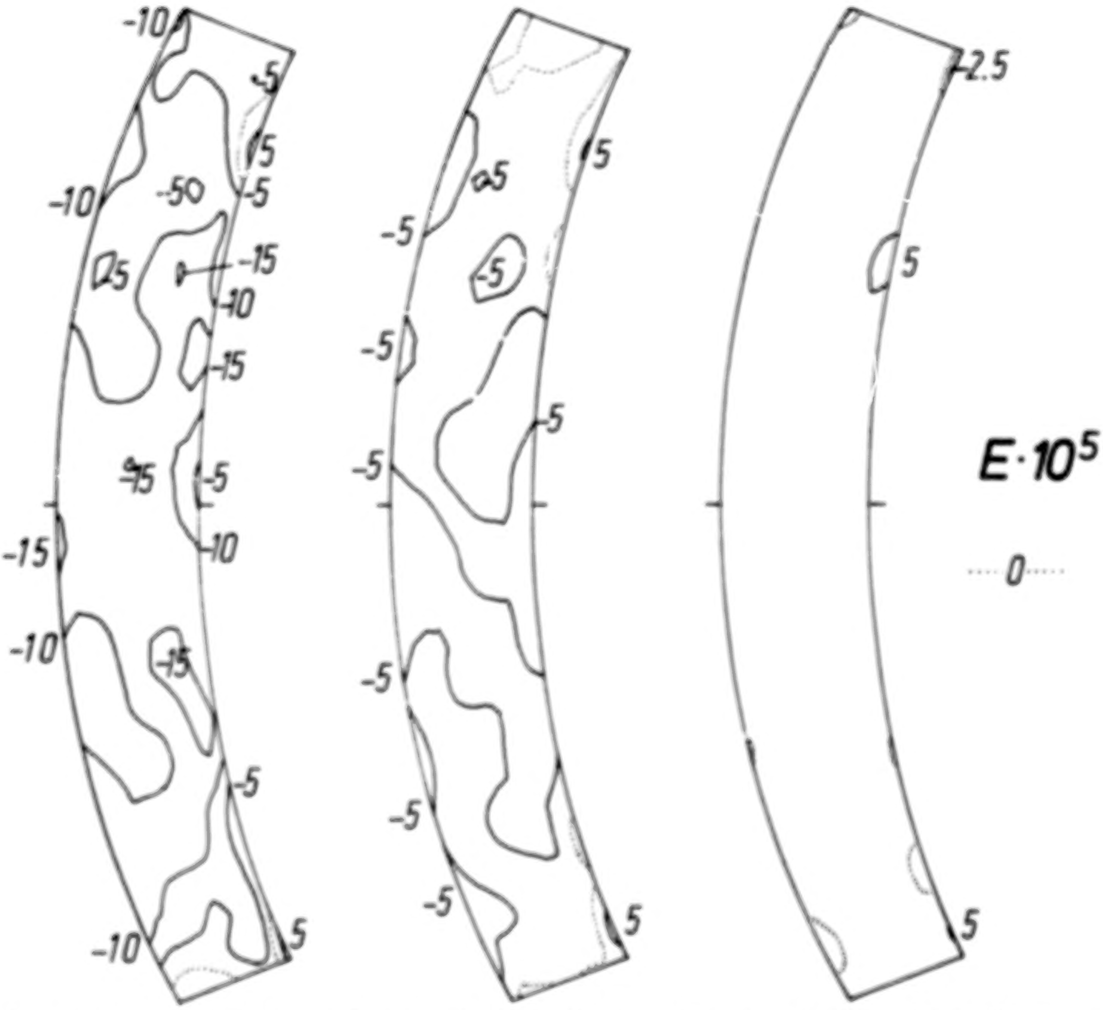

Fig.4 Error diagrams for third order scheme. Left: boundary and neighbor: Rusan/Nazh..Center: boundary equation, neighbor: Rusan/ Nazh.. Right: boundary equation, neighbor: new formula.

is the next and last step. The discretization becomes

$$u_0^* = u_0 + \frac{1}{4}\Big[\left(\frac{a}{c}\right)_0 \left(\bar{v}_0^* - v_0 - kg_0\right) + \frac{k}{h}\left(b - \frac{a^2}{c}\right)_0 \Big(v_1 - v_0 - \frac{1}{2}\left(v_2 - 2v_1 + v_0\right) + \frac{1}{3}\left(v_3 - 3v_2 + 3v_1 - v_0\right)\Big]$$
$$+ \frac{3}{4}\Big[\left(\frac{a}{c}\right)^0 \left(\bar{v}_0^* - v_0 - kg^0\right) + \frac{k}{h}\left(b - \frac{a^2}{c}\right)^0 \Big(v^1 - v^0 - \frac{1}{2}\left(v^2 - 2v^1 + v^0\right) + \frac{1}{3}\left(v^3 - 3v^2 + 3v^1 - v^0\right)\Big]$$

From the possible combinations we present here results for the boundary equation plus u_1^* after Rusanov/Nazhestkina (fig.4 center) and plus u_1^* after the new formula (fig.4 right). The latter displays a mean square error of only about one quarter of that of the original scheme (fig.4 left)(table 3).

References

/1/ Ringleb,F.: Exakte Lösungen der Differentialgleichungen einer adiabatischen Gasströmung.
ZAMM vol.20 no.4 (1940), pp.185-198

/2/ Förster,K.(ed.): Boundary algorithms for multidimensional inviscid hyperbolic flows.
Notes Num.Fluid Mech. vol.1, Vieweg (Braunschweig/Wiesbaden) 1978, ISBN 3-528-08075-2

/3/ Degen,W.: MASYCA - eine interaktive Kommandosprache zur symbolischen Manipulation mathematischer Formeln.
Angew.Informatik, 1/80, pp.18-26

/4/ Rusanov,V. and E.Nazhestkina: Boundary conditions in difference schemes for hyperbolic systems.
Notes Num.Fluid Mech. vol.2, Vieweg (Braunschweig/Wiesbaden) 1980, ISBN 3-528-08076-0, pp.251-268

/5/ Förster,K.: An accurate algorithm for Dirichlet boundary conditions in hyperbolic flows.
Arch.Mech. vol.32(1980), no.5, pp.655-661

/6/ Rusanov,V.: Difference schemes of third order of accuracy for continuous computation of discontinuous solutions.
Dokl.Akad.Nauk SSR vol.180 (1968)
also: On difference schemes of third order accuracy for nonlinear hyperbolic systems.
J.Comput.Phys. vol.5 no.3 (1970), pp.507-516

/7/ Burstein,S. and A.Mirin: Third order accurate difference methods in hydrodynamics.
Novosibirsk, 1969

/8/ Kentzer,C.: Discretization of boundary conditions on moving discontinuities.
Proc.2nd Int.Conf.Num.Meth.in Fluid Dyn., 1970

/9/ Moretti,G. and M.Pandolfi: Entropy layers.
Computers and Fluids vol.1 (1973)
also: see /2/ pp.68-88

/10/ Rusanov,V.: Advanced techniques for computation of supersonic flows.
AIAA-Paper 77-173 (15th Aerosp.Sci.Meeting, Los Angeles, Jan.24-26, 1977)

/11/ deNeef,T.: Treatment of boundaries in unsteady inviscid flow computations.
Delft Univ. of Technology, Dept.of Aerosp.Engin., Report LR-262, Febr. 1978

Appendix 1: The Ringleb machine

Ringleb's solution /1/ of Tchaplygin's equation consists of three Riemann surfaces from which only the first one makes practical sense: it describes the homentropic flow of a gas with a ratio of specific heats $\kappa = 1.4$ from, for instance, upper righthand infinity around a blunt body which is symmetric to the x axis to lower righthand infinity (fig.5). It contains subsonic and supersonic regimes and can thus be used as test solution for plane sub-, trans- and supersonic channel- or free jet- or Coanda flow, all steady or unsteady (transient flow with asymptotic steady state). Details, formulae and some applications are given in /2/.

The real computation is facilitated by two sets of subroutines, one for the description of the flow in cartesian, one for polar coordinates - see also /2/. In the high precision testing described in this paper the polar subroutine PWRING, if used on a common minicomputer with an effective (including hexadecimal normalization) mantissa of only 21 bits was too inaccurate around the line of symmetry and was therefore redevised (Geiger,A., internal report).

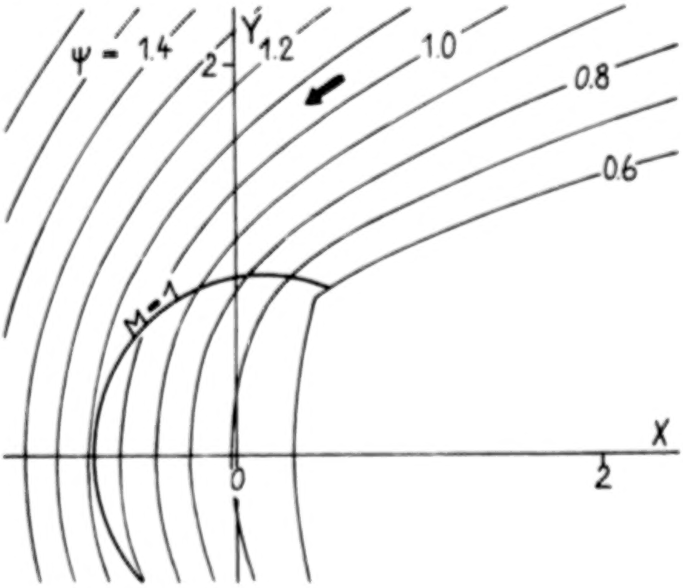

Fig.5
Ringleb flow, first Riemann surface.
$\psi = 0.6$ is the border streamline to this surface.

The Ringleb machine used in this paper is specialized for the following case:

a) The dependent variables are P - natural logarithm of the static pressure, and $T = \tan\theta$, θ - angle between streamline and circumferential direction (see fig.6). Thus the boundary conditions are always of the Dirichlet type: T given along solid walls and P along free jet boundaries.

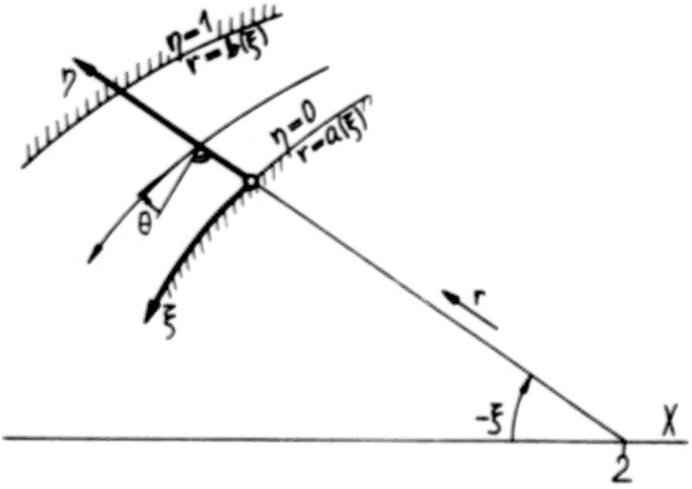

Fig.6
Boundary fitted, polar based coordinate system ξ, η.

b) The coordinate system is boundary fitted: the boundaries $\psi_u = \text{const}$ and $\psi_o = \text{const}$ are lines $\eta = 0$ and $\eta = 1$, respectively. ξ is the marching direction as long as one deals with steady supersonic flow. In this case the governing equations are:

$$P_\xi = pp\,P_\eta + pt\,T_\eta$$
$$T_\xi = tp\,P_\eta + pp\,T_\eta + (1 + T^2)$$

with $pp = [a_\xi + \eta(b_\xi - a_\xi) - r M^2 T/\mu^2]/(b-a)$, M - Mach number

$pt = -r \varkappa M^2/\mu^2/(b-a)$

$tp = -r(M^2-1)(1+T^2)^2/(\varkappa M^2 \mu^2)/(b-a)$

$r = a + \eta(b-a)$ and $a_\xi = a\,T(0,\xi)$

$\mu^2 = M^2 - (1 + T^2)$ $\quad b_\xi = b\,T(1,\xi)$.

This system appears sufficiently non trivial for a realistic test of smooth flows.

The following listing gives the complete FORTRAN program for testing a third order algorithm using the intermediate levels $(n+\frac{1}{3})k$ and $(n+\frac{2}{3})k$ which is to be substantiated in the subroutine called CP1130.

Listing of test program "Ringleb machine"

```
      COMMON/SV/P(11),T(11),CQ(11),DX,DE,X,XA,A0,B0,A1,B1,A2,B2,AN,BN
      COMMON/CV/ PP(34),PT(34),TP(34)
      DATA PSU,PSO,XAG,XEG,IO,NP /.7,.8,-20.,20.,10,2/
      LX=5
      XA=XAG*ATAN(1.)/45.
      XE=XEG*ATAN(1.)/45.
      X=XA
      I00=IO+1
      IOM=IO-2
      DE=1./FLOAT(IO)                             grid size Δη
      CALL RAND(X,PSU,PSO,A0,B0,P(1),P(I00),T(1),T(I00))
      DO 1 I=2,IO
    1 CALL VERTE(A0+(I-1)*DE*(B0-A0),X,P(I),T(I))
      CALL SAVE(I00,LX)
      DO 5 N=1,1000                               marching loop
      DX=1.
      DO 6 I=1,I00                                marching step Δξ (CFL-condition)
      CALL COEFF(P(I),T(I),(I-1)*DE,A0,B0,A0*T(1),B0*T(I00),
     1PP(I),PT(I),TP(I))
      CQ(I)=DE/(ABS(PP(I))+SQRT(PT(I)*TP(I)))
      IF(CQ(I).LT.DX) DX=CQ(I)
    6 CONTINUE
      DX=.8*DX
      DO 8 I=1,I00
    8 CQ(I)=DX*DX/CQ(I)/CQ(I)                     square of Courant Number
      CALL RAND(X+DX/3.,PSU,PSO,A1,B1,PU1,PO1,TU1,TO1)      ┐ special case
      CALL RAND(X+2.*DX/3.,PSU,PSO,A2,B2,PU2,PO2,TU2,TO2)   │
      X=X+DX                                                ├ of third or-
      CALL RAND(X,PSU,PSO,AN,BN,PU,PO,TU,TO)                │
      CALL CP1130(TU1,TO1,TU2,TO2,TU,TO)                    ┘ der scheme
      T(1)=TU
      T(I00)=TO
      A0=AN
      B0=BN
      GOTO 99
C FOR EXACT BOUNDARY POINT VALUES, INSERT
      P(1)=PU
      P(I00=PO
C FOR EXACT BOUNDARY NEIGHBOR VALUES, INSERT
      DO 9 I=2,IO,IOM
    9 CALL VERTE(AN+(I-1)*DE*(BN-AN),X,P(I),T(I))
   99 CONTINUE
      IF(MOD(N,NP*IO/10).NE.0) GOTO 4
      CALL SAVE(I00,LX)
    4 IF(X.GE.XE) GOTO 7
    5 CONTINUE
    7 CONTINUE
      X=10.
      CALL SAVE(I00,LX)
      STOP
      END
      SUBROUTINE RAND(X,PSU,PSO,A,B,PU,PO,TU,TO)
      XX=ABS(X)
      CALL PVRING(XX,PSU,2.,V,A,G7)
      CALL PVRING(XX,PSO,2.,V,B,G7)
      CALL VERTE(A,X,PU,TU)                      Computation of
      CALL VERTE(B,X,PO,TO)                      radii a,b and of
      IF(XX.GE..01) GOTO 1
      PR=100.*X                                  exact boundary
      CALL PVRING(.01,PSU,2.,V,AA,G7)
      CALL PVRING(.01,PSO,2.,V,BB,G7)            values
      CALL VERTE(AA,.01,V,TU)
      CALL VERTE(BB,.01,V,TO)
      TU=TU*PR
      TO=TO*PR
    1 RETURN
      END

      SUBROUTINE VERTE(RD,X,P,T)
      CALL PRINGL(RD,ABS(X),2.,V,G7,PSI)
      P=ALOG(G7)                                 Computation of
      S=SIN(X)
      C=SQRT(1.-S*S)                             P and T
      H=SQRT(1./(V*V*PSI*PSI)-1.)
      IF(X.GT.0.) H=-H
      IF(X.EQ.0.) H=0.
      T=(S+C*H)/(C-S*H)
      RETURN
      END

      SUBROUTINE COEFF(P,T,E,A,B,AX,BX,PP,PT,TP)
      TQ=1.+T*T
      QM=5./EXP(P/3.5)-5.                        Computation of
      H=(A+E*(B-A))/(QM-TQ)
      PP=(AX+E*(BX-AX)-H*T*QM)/(B-A)             coefficients
      PT=-1.4*H*QM/(B-A)                         pp, pt, tp
      TP=-H*TQ*T2*(QM-1.)/1.4/QM/(B-A)
      RETURN
      END

      SUBROUTINE SAVE(IOO,LX)
      COMMON/SV/P(11),T(11),CG(11),DX,DE,X,XA,A0,B0,A1,B1,A2,B2,AN,BN
      INTEGER F(11)
      DIMENSION H(3,11)                          Example of
      IF(X.GT.9.) H(1,1)=10.
      IF(X.GT.9.) GOTO 2                         output program
      DO 1 I=1,100
      J=100+1-I
      R=A0+FLOAT(I-1)*DE*(B0-A0)
      H(1,I)=2.-R*COS(-X)
      H(2,I)=R*SIN(-X)
      CALL PRINGL(R,-X,2.,V,G7,PSI)
      H(3,I)=EXP(P(I))/G7-1.
    1 F(J)=IFIX(H(3,I)*10.**LX)               ⎫ Integer part of
      OM=-X*57.2958                           ⎬ error for
      WRITE(6,20) OM,(F(I),I=1,100)           ⎪
   20 FORMAT(F10.4,11I5)                      ⎭ quick-look
    2 CONTINUE
      WRITE(7,21) X,A0,B0,(H(3,L),L=1,4)      ⎫ mass storage of
      WRITE(7,21) (H(3,L),L=5,11)             ⎭ grid and error
   21 FORMAT(7F11.7)
      RETURN
      END
```

```
  SUBROUTINE PWRING(O,PSI,XP,V,R,G7)
  DIMENSION VV(20),FF(20),Z(20)
  OM=ABS(O)
  V=.5/PSI-.175*PSI+.425+(.5/PSI+.175*PSI-.425)*COS(2.*OM)
  CALL FFS(OM,PSI,XP,V,F,FS,R,G7)
  FQ=ABS(F)
  IF(FQ.LT.1.E-6) GOTO 1                  &)
  VV(1)=V
  FF(1)=F
  DEC=F/FS                                   for CDC.
  IF(DEC.LT.1.E-6) DEC=1.E-6              &) Reduce for shorter
  V=V-DEC                                    machine word
  DO 2 I=2,20
  CALL FFS(OM,PSI,XP,V,F,FS,R,G7)
  VV(I)=V
  FF(I)=F
  FQ=ABS(F)
  IF(FQ.LT.1.E-6) GOTO 1                  &)
  V=AINE(VV,FF,Z,I,PSI)
2 CONTINUE
1 RETURN
  END
  SUBROUTINE FFS(OM,PSI,XP,V,F,FS,R,G7)
  PQ=PSI*PSI
  VQ=V*V                                  Auxiliary routine
  GQ=ABS(1.-.2*VQ)
  G=SQRT(GQ)                              for PWRING
  G3=GQ*G
  G5=GQ*G3
  XL=XP-(((.2/GQ+1./3.)/GQ+1.)/G-ALOG((1.+G)/(1.-G))/2.)/2.
  V=SQRT(AMAX1(0.,1./VQ-PQ))
  IF(V.LT.1.E-10) V=1.E-10
  A=PSI*V
  B=PQ-.5/VQ+G5*XL
  AS=-PSI/VQ/V/V
  BS=1./VQ/V-G3*V*(XL+3/10.*(1./(1.-GQ)+((1./GQ+1.)/GQ+1.)/GQ))
  AB=A/B
  IF(AB.LT.1.E-30) F=-OM
  IF(AB.GE.1.E-30) F=ATAN(AB)-OM
  FS=(B*AS-A*BS)/(A*A+B*B)
  R=SQRT(A*A+B*B)/G5
  G7=GQ*G5
  RETURN
  END
  FUNCTION AINE(X,Y,Z,N,PSI)
  DIMENSION X(N),Y(N),Z(N)
  DO 1 I=1,N                              Auxiliary routine
1 Z(I)=X(I)
  DO 2 I=2,N                              for PWRING
  IJI=I-1
  DO 3 J=1,IJI
  JII=I-J
  IIJ=JII+1
  YN=Y(JII)-Y(I)
  ZN=Y(JII)*Z(IIJ)-Y(I)*Z(JII)
  VGL=1.E-38
  IF(ABS(YN).LE.VGL) Z(JII)=1./PSI
  IF(ABS(YN).GT.VGL) Z(JII)=ZN/YN
3 CONTINUE
2 CONTINUE
  AINE=Z(1)
  RETURN
  END
```

```
      SUBROUTINE PRINGL(R,OM,XP,V,G7,PSI)
      X=XP-R*COS(OM)
      Y=R*SIN(OM)
      V=1.3
      RR=X*X+Y*Y
      IF(RR.GE..088) V=1./SQRT(2.*SQRT(RR))
      DEC=1.
      DO 1 N=1,100
      VQ=V*V
      GQ=1.-VQ/5.
      IF(GQ.LT.0.) GQ=0.
      G=SQRT(GQ)
      G3=G*GQ
      G5=GQ*G3
      XL=X-.5*((.2/GQ+1./3.)/GQ+1.)/G+.25*ALOG((1.+G)/(1.-G))
      IF(ABS(DEC).LT..2E-6) GOTO 2      &) for CDC. Reduce for
      Z2=(XL*XL+Y*Y)*4.                    shorter machine word
      XLS=1./(1.-GQ)+((1.+1./GQ)/GQ+1.)/GQ
      F=Z2*VQ*VQ*G5*G5-1.
      FS=2.*VQ*V*G5*G5*(Z2*(2.-VQ/GQ)-.4*VQ/G*XL*XLS)
      DEC=F/FS
      V=V-DEC
    1 CONTINUE
    2 PSI=SQRT(.5/VQ-G5*XL)
      G7=G5*GQ
      RETURN
      END
```

Appendix 2: Characteristic correction vs.boundary equation

As an heuristic approach to better boundary algorithms in finite difference methods people tried to switch at the boundary to the scholarly method of characteristics, i.e. in the two dimensional case the application of a compatibility condition along a characteristic inciding backwards from the new boundary point $x = 0$, $t = (n+1)k$ to the line $t = nk$. The results were in general much worse than to be expected from a method so theoretically sound, the reason being perhaps the necessary interpolations which do not fit into the basic concept of grid functions which are defined only in isolated points.

Work towards better methods, based on a suggestion by Kentzer /8/ was begun by Moretti and Pandolfi /9/ (see also /2/). The final shape is due to Rusanov /10/; an independent ad hoc deduction is by deNeef /11/. According to /4/ it is as follows:
We consider the m dimensional system

$$\vec{w}_t = A\,\vec{w}_x$$

where A has r positive and $(m - r)$ negative eigenvalues

$$\Lambda^+ = \begin{bmatrix} \lambda_1^+ & & \\ & \ddots & \\ & & \lambda_r^+ \end{bmatrix} \quad , \qquad \Lambda^- = \begin{bmatrix} \lambda_{r+1}^- & & \\ & \ddots & \\ & & \lambda_m^- \end{bmatrix} .$$

Further, there exists a matrix T reducing A to diagonal form:

$$TAT^{-1} = \left[\begin{array}{c:c} \Lambda^+ & 0 \\ \hdashline 0 & \Lambda^- \end{array}\right] \quad , \qquad T = \left[\begin{array}{ccc} t_{1,1} & \cdots & \\ \hdashline t_{r+1,1} & \cdots & \\ \vdots & & \end{array}\right] = \left[\begin{array}{c} T^+ \\ \hdashline T^- \end{array}\right] .$$

Then the compatibility conditions for the leftrunning characteristics (which are needed at the lefthand boundary) arise from

$$T^+\vec{w}_t = \Lambda^+ T^+ \vec{w}_x \quad .$$

The trick now is the following:
instead of applying the diagonal transformation to the differential equations one applies it to the chosen difference system

$$w_0^+ = w_0 + k\,\mathcal{L}(w_i) \quad , \quad i = 0,1,\ldots$$

giving
$$T^{+} w_0^{+} = T^{+}\left[w_0 + k\mathcal{L}\right]$$
and the computational system at the boundary is closed by the $m-r$ boundary conditions $\quad B(w_0, r(t)) = 0$.

In two dimensions simpler procedures can be applied. To get the compatibility condition the system is subjected to a linear combination
$$\left.\begin{array}{l} u_t = a u_x + b v_x \\ v_t = c u_x + d v_x \end{array}\right| \begin{array}{l} +1 \\ +\lambda^{+} \end{array} \quad , \quad \lambda^{+} = \left(\frac{dt}{dx}\right)_{-Ch} = \sqrt{\frac{b}{c}}$$
giving
$$u_t = (a + \sqrt{bc})\, u_x - \sqrt{\frac{b}{c}}\, v_t + \sqrt{\frac{b}{c}}\,(d + \sqrt{bc})\, v_x \qquad \text{(A)}$$

which together with the boundary condition forms the computational system in the method of characteristics proper, whereas for the inclusion into a finite difference method the same linear combination is applied to the difference equations
$$\left.\begin{array}{l} u_0^{+} = u_0 + k\,\mathcal{L}_u(u_i, v_i) \\ v_0^{+} = v_0 + k\,\mathcal{L}_v(u_i, v_i) \end{array}\right| \begin{array}{l} +1 \\ +\lambda^{+} \end{array}$$

giving - in the case of v being a Dirichlet variable -
$$u_0^{+} = \underbrace{(u_0 + k\mathcal{L}_u)}_{=\tilde{u}_0^{+}} + \sqrt{\frac{b}{c}}\left[\underbrace{(v_0 + k\mathcal{L}_v)}_{=\tilde{v}_0^{+}} - \bar{v}_0^{+}\right] \quad .$$
This is the characteristic correction formula as applied in this paper.

In contrast to the above method the boundary equation approach certainly uses a linear combination, too:
$$u_t = \qquad - \frac{a}{c} v_t \qquad + \left(b - \frac{ad}{c}\right) v_x \qquad \text{(B)}$$
but it is derived with a different purpose: that of obtaining a formula which is optimal with respect to accuracy and simplicity of discretization. A comparison of eqs. (A) and (B) shows the difference: (B) does not contain the difficult variable u but only the "easy" v.

PSEUDOSPECTRAL METHOD FOR PROBLEMS WITH NON-PERIODIC BOUNDARY CONDITIONS

H. N. Lee

Department of Meteorology
University of Utah
Salt Lake City, Utah 84112

1. INTRODUCTION

Numerical methods which are in general used are the spectral method, the finite element method and the finite difference method. The phase speed errors associated with finite difference methods have been recognized. Spectral methods generally have very small phase speed errors. The pseudospectral method is an approximation which is merely used to evaluate spatial derivatives on a grid in physical space in place of finite difference or finite element approximations. In a simple analysis of the advection equation with constant velocity, the pseudospectral method and spectral method give the same results. The pseudospectral method is as accurate as the spectral method and is more general, simpler and at least a factor of 2 or more faster than the spectral method [1].

The pseudospectral technique has been used by many researchers for solving the problems with periodic boundary conditions because the numerical error associated with it is minimized and the high accuracy is achieved. But it has not been widely applied in solving the problems which have non-periodic solutions subjected to non-periodic boundary conditions. This is because of the periodic boundary conditions which are necessary in the pseudospectral approximation. Hence, a technique for applying pseudospectral method to the problems with non-periodic boundary conditions will be discussed in this paper.

The techniques used for solving non-periodic problems via FFT (Fast Fourier Transform) procedures have been recommended by many authors. The technique used by Gazdag [2] was to add an additional data in the computational regime. Hence additional computational time is required for the FFT and the form of the data added is appropriate only for that particular problem (see [3]).

In order to apply pseudospectral technique in diffusion problem, Christensen and Prahm [4] added a sink term of the form $-\overline{C}(\overline{x},t)/\xi(\overline{x})$ to the diffusion equation, where $\overline{C}(\overline{x},t)$ is the pollutant concentration and $\xi(\overline{x})$ is the decay constant. The decay constant $\xi(\overline{x})$ was chosen so as to give no advection near the horizontal boundaries. Physically this means that a distribution $\overline{C}(\overline{x},t)$ which is not allowed to advect out over one boundary appears periodic characteristic satisfying the pseudospectral approximation. However, the problem is that the Fourier Transformation is made on a 32 x 32 grid point system while the real computational regime consists only of 17 x 23 grid points (see [5]). How to determine correctly the sink term is another difficulty. And the term chosen is also appropriate only for that particular diffusion problem studied.

Following the studies of Orszag [6], Lyness [7] and Gottleib and Orszag [8], Roache [3] introduced a "reduction-to-periodicity" technique which was more generally applicable. Essentially it is a polynomial subtraction technique. The idea is to express the solution as the sum of periodic function and a polynomial function in one direction at a time. The pseudospectral technique is applied only to the periodic function to obtain its derivatives. The finite difference methods are used to evaluate the high order derivatives at the boundaries in order to obtain the coefficients of the polynomial function. The technique has been used in solving the diffusion problems [9] and the results are encouraging.

In this work, a general and accurate technique which is constructed to obtain the coefficients of polynomial function, instead of using finite difference method, is discussed. An advection-diffusion equation is examined.

2. TECHNIQUE FOR NON-PERIODIC BOUNDARIES

Consider the advection-diffusion equation.

$$\frac{\partial \overline{C}}{\partial t} = - \overline{u} \frac{\partial \overline{C}}{\partial x} + K_y \frac{\partial^2 \overline{C}}{\partial y^2} + \text{source} \tag{1}$$

where $\overline{C}(x,y,t)$ is the solution of pollutant concentration, $\overline{u}$ the horizontal velocity in the x-direction and K_y the constant eddy diffusivity in the y-direction.

We express the solution to Eq. (1) as the sum of periodic function $\overline{C}_{px}$ and a polynomial function with degree N in x-direction at time t

$$\overline{C}(x,y,t) = \overline{C}_{px}(y,t) + \sum_{i=1}^{N} b_i(y,t)X^i \tag{2}$$

where b_i's are the polynomial coefficients. The constant coefficient b_o has been combined into periodic part. The b_i's are chosen such that

$$\overline{C}^{(m)}_{px_1} = \overline{C}^{(m)}_{px_n} \quad , \qquad 0 \le m \le N - 1 \tag{3}$$

where superscript (m) denotes the m-th derivative and subscripts X_1 and X_n denote the distances at the left and right boundaries in the x-direction, respectively. The general solutions for b_i are

$$b_N = \frac{1}{E}\left(\frac{1}{N!}\, D_{N-1}\right) \tag{4a}$$

$$b_k = \frac{1}{E}\left[\frac{1}{k!}\, D_{k-1} - \frac{1}{k}\sum_{i=k+1}^{N} \frac{i!}{(i-k+1)!(k-1)!}\, b_i\right], \quad 0 < k < N \tag{4b}$$

where

$$D_k = \overline{C}^{(k)}(X_n,y,t) - \overline{C}^{(k)}(X_1,y,t) \tag{4c}$$

$$E = X_n - X_1 \tag{4d}$$

In order to obtain the polynomial coefficients b_i in Eq. (4a) and (4b), the one-sided finite difference methods can be used to evaluate the high order derivatives for D_k in Eq. (4c) at the boundaries. However, there is shortcoming in the finite difference formula for evaluation of high order derivatives by one-sided formula (see [3]). Hence, the idea to avoid applying finite difference formula is to use periodic polynomial spline [10] satisfying the periodic boundary conditions Eq. (3) in order to get the solutions for b_i.

For the periodic quintic spline which is defined to be piecewise continuous with continuous first, second, third and fourth derivatives, a system of algebraic four equations can be obtained for the periodic boundary point. For instance, imposing the continuity condition at the boundary point for m=4 in Eq. (3) we have

$$\overline{C}^{(2)}_{px_{n-0.5}} - \overline{C}^{(2)}_{px_{2-0.5}} = -\frac{1}{\frac{h}{2}}\left(7\overline{C}^{(1)}_{px_{n-0.5}} + 16\overline{C}^{(1)}_{px_n} + 7\overline{C}^{(1)}_{px_{2-0.5}}\right) - \frac{15}{\left(\frac{h}{2}\right)^2}\left(\overline{C}_{px_{n-0.5}} - \overline{C}_{px_{2-0.5}}\right) \tag{5}$$

Note that $\overline{C}_{px} = \overline{C}^{(0)}_{px}$ and h is a equal grid point interval in x-direction. By assuming

$$\begin{aligned} \overline{C}^{(q)}_{px_{n-0.5}} &= \frac{1}{2}\left(\overline{C}^{(q)}_{px_{n-1}} + \overline{C}^{(q)}_{px_n}\right) \\ \overline{C}^{(q)}_{px_{2-0.5}} &= \frac{1}{2}\left(\overline{C}^{(q)}_{px_n} + \overline{C}^{(q)}_{px_2}\right) \end{aligned} \qquad 0 \le q \le 2 \tag{6}$$

Eq. (5) can be rewritten as

$$\bar{C}''_{px_{n-1}} - \bar{C}''_{px_2} = -\frac{2}{h}\left(7\bar{C}'_{px_{n-1}} + 46\bar{C}'_{px_n} + 7\bar{C}'_{px_2}\right) - \frac{60}{h^2}\left(\bar{C}_{px_{n-1}} - \bar{C}_{px_2}\right) \tag{7}$$

Similarly we can have for the continuity conditions

$$m=3; \qquad \bar{C}''_{px_{n-1}} - 10\bar{C}''_{px_n} + \bar{C}''_{px_2} = -\frac{16}{h}\left(\bar{C}'_{px_{n-1}} - \bar{C}'_{px_2}\right) - \frac{80}{h^2}\left(\bar{C}_{px_{n-1}} - 2\bar{C}_{px_n} + \bar{C}_{px_2}\right) \tag{8}$$

$$m=2; \qquad 3\bar{C}''_{px_{n-1}} - 3\bar{C}''_{px_2} = -\frac{8}{h}\left(4\bar{C}'_{px_{n-1}} + 52\bar{C}'_{px_n} + 4\bar{C}'_{px_2}\right) - \frac{240}{h^2}\left(\bar{C}_{px_{n-1}} - \bar{C}_{px_2}\right) \tag{9}$$

and

$$m=1; \qquad 9\bar{C}''_{px_{n-1}} + 22\bar{C}''_{px_n} + 9\bar{C}''_{px_2} = -\frac{160}{h}\left(\bar{C}'_{px_{n-1}} - \bar{C}'_{px_2}\right) - \frac{240}{h^2}\left(\bar{C}_{px_{n-1}} - 2\bar{C}_{px_n} + \bar{C}_{px_2}\right) \tag{10}$$

If N = 5 is chosen, the solutions for b_2, b_3, b_4 and b_5 can be obtained by solving Eqs. (7) - (10) with the use of Eq. (2). Since the functions in Eqs. (7) - (10) are periodic, the pseudospectral method is applied to obtain their first derivative $\bar{C}'_{px}$ and second derivative $\bar{C}''_{px}$. Once we have the solutions for b_2, b_3, b_4, and b_5, b_1 can be obtained by setting k=1 and N=5 in Eq. (4b). Similar procedures are applied to have the solutions for the polynomial coefficients in the y-direction.

3. TIME-INTEGRATION SCHEME

The time-integration schemes used were second-order Adams-Bashforth method and "partially-correct second-order Adams-Bashforth" method [11]. It has been shown that for pure advection problems the "partially-corrected second-order Adams-Bashforth" method is stable and appears in all ways to be preferable to the second-order Adams-Bashforth method. With a non-zero value of the diffusion term the partially-corrected Adams-Bashforth scheme for the advection term and the backward scheme for the diffusion term are suggested in this paper. Such a semi-implicit scheme can be written as

$$\begin{cases} \tilde{\overline{C}}^{n+1} = \overline{C}^{n} + (3\tilde{A}^{n} - \tilde{A}^{n-1})\,\Delta t/2 + \Delta t\,\tilde{F}^{n} & \text{(11a)} \\ \overline{C}^{n+1} = \overline{C}^{n} + (\tilde{A}^{n} + \tilde{A}^{n+1})\,\Delta t/2 + (\tilde{F}^{n} + F^{n+1})\,\Delta t/2 & \text{(11b)} \end{cases}$$

where $\overline{C}^n$ stands for $\overline{C}\,(x,y,\, n\Delta t)$, A stands for the advection term and F for the diffusion term. Quantities with "~" mean uncorrected values, for instance, $\tilde{A}^n$ which are not computed from the corrected values $\overline{C}^n$. Therefore, the partially-corrected second-order Adams-Bashforth scheme required about 1% more computation than the customary second-order Adams-Bashforth scheme [11].

4. NUMERICAL INTEGRATION OF THE ADVECTION-DIFFUSION EQUATION

The pseudospectral technique and the time-integration scheme described in the previous sections were tested by applying them to Eq. (1). In the test, $\overline{u} = 1.0$, $K_y = 0.1$, $\Delta x = \Delta y = 1.0$ and $\Delta t = 0.1$ on a 16 x 16 grid point system were chosen. Four continuous adjacent sources each of source = 250 were assumed and placed in grid points (4,8), (4,9), (5,8) and (5,9). The analytical solution and numerical steady state solutions are shown in Fig. 1. The numerical steady state solutions give the final concentration field which is approached after a long integration. Fig. 1.b is a numerical steady state result after t = 32 corresponding to advection of a point twice through the grid point system. For comparing the present numerical solutions with the published results using other numerical techniques under the same test conditions, Christensen and Prahm's [4] and Pepper and Baker's [12] numerical solutions are shown in Fig. 1.c and Fig. 1.d, respectively. The information from the two outmost column grid points is sacrificed in Christensen and Prahm's solutions because the sink term is applied in these grid points which act as the boundary. It is seen in Fig. 1 that the solutions using present method give very well agreement with the analytical solutions and the present method is superior to the other in technique.

5. CONCLUSIONS

The present paper demonstrates the capability of the pseudospectral technique and the time integration scheme for the time dependent non-periodic problem. Significant improvements have been shown in the accuracy for calculation of the two-dimensional time-dependent advection-diffusion equation. The pseudospectral method has emerged as a viable alternative to finite difference methods for the evaluation of the spatial derivatives.

References

1. Meriless, P. E. and Orszag, S. A.: Numerical Methods Used in Atmospheric Models, Vol. II; Chapter 4. The Pseudospectral Method, GARP Series No. 17, 1979.

2. Gazdag, J.: Numerical Convective Schemes Based on Accurate Computation of Space Derivatives, J. Comp. Phys., Vol. 13, 1973, 100-113.

3. Roache, P. J.: A Pseudospectral FFT Technique for Non-periodic Problems, J. Comp. Phys., Vol. 27, 1978, 204-220.

4. Christensen, O. and Prahm, L. P.: A Pseudospectral Model for Dispersion of Atmospheric Pollutants, J. Appl. Met., Vol. 18, 1976, 1287-1295.

5. Berkowicz R. and Prahm, L. P.: Pseudospectral Simulation of Dry Deposition from a Point Source, Atmos. Environ., Vol. 12, 1978, 379-387.

6. Orszag, S. A.: Numerical Simulation of Incompressible Flows Within Simple Boundaries, I. Galerkin (Spectral) Representation, in "Studies in Applied Mathematics" Vol. L., No. 4, 1971, 293-327.

7. Lyness, J. N.: Computational Techniques Based on the Lanczos Representation. Math. Comp. Vol. 28, 1974, 81-123.

8. Gottlieb, D. and Orszag, S. A.: Numerical Analysis of Spectral Methods: Theory and Application, 1977, SIAM 26.

9. Lee, H. N.: An Alternate Pseudospectral Model for Pollutant Transport, Diffusion and Deposition in the Atmosphere, Atmos. Environ., Vol. 15, 1981. 1017-1024.

10. Ahlberg, J. H., Nilson, E. N. and Walsh, J. L.: The Theory of Splines and their Applications. New York, Academic Press, 1967.

11. Gazdag, J.: Time-differencing Schemes and Transform Methods, J. Comp. Phys., Vol. 20, 1976, 196-207.

12. Pepper, D. W. and Baker, A. J.: Modeling Pollutant Dispersion Over Irregular Terrain With Second Moment and Cubic Splines, Fourth Symp. on Turb., Diff., and Air Pollution, Amer. Meteor. Soc., Reno, Nevada, 1979, 197-204.

a. Analytical solutions

									12	16	19	23
				14	24	34	43	51	58	64	69	74
	18	65	107	129	143	151	156	160	161	162	162	161
125	366	444	388	356	331	311	294	280	267	256	246	238
125	366	444	388	356	331	311	294	280	267	256	246	238
	18	65	107	129	143	151	156	160	161	162	162	161
				14	24	34	43	51	58	64	69	74
									12	16	19	23

b. Present numerical results

									12	16	20	23
				14	24	34	43	51	58	63	69	74
	33	78	109	129	142	151	156	159	160	161	161	161
124	389	432	380	356	329	311	293	279	266	255	246	242
124	389	432	380	356	329	311	293	279	266	255	246	242
	33	78	109	129	142	151	156	159	160	161	161	161
				14	24	34	43	51	58	63	69	74
									12	16	20	23

c. Christensen and Prahm's numerical results

								10	15	18
				17	27	37	46	55	57	70
	48	84	116	134	145	156	156	165	160	172
129	385	431	381	359	331	315	295	285	265	268
129	385	431	381	359	331	315	295	285	265	268
	48	84	116	134	145	156	156	165	160	172
				17	27	37	46	55	57	70
								10	15	18

d. Pepper and Baker's numerical results

								11	14	17
			12	19	27	35	43	49	56	61
	34	70	97	116	130	140	147	151	154	156
111	340	426	392	363	339	319	302	287	273	262
111	340	426	392	363	339	319	302	287	273	262
	34	70	97	116	130	140	147	151	154	156
			12	19	27	35	43	49	56	61
								11	14	17

Fig. 1 Steady-state solutions of advection-diffusion equation from four continuous sources placed within the heavily drawn square. (a) analytical solutions (b) present numerical solutions (c) Christensen and Prahm's numerical solutions based on pseudospectral technique (d) Pepper and Baker's numerical solutions using cubic spline approximation. Values numerically less than 10 have been suppressed.

Blank Page

UNCONDITIONAL INSTABILITY OF INFLOW-DEPENDENT BOUNDARY CONDITIONS IN DIFFERENCE APPROXIMATIONS TO HYPERBOLIC SYSTEMS[*]

Eitan Tadmor

Department of Applied Mathematics
California Institute of Technology
Pasadena, California 91125

ABSTRACT

In this paper we study the stability of finite difference approximations to initial-boundary hyperbolic systems. As is well-known, a proper specification of boundary conditions for such systems is essential for their solutions to be well-defined. We prove a discrete analogue of the above - if the numerical boundary conditions are consistent with an inflow part of the problem, they render the overall computation unstable. An example of the inviscid gasdynamics equations is considered.

1. INTRODUCTION - WELL DEFINED HYPERBOLIC SYSTEM

We consider the first order hyperbolic system

$$\frac{\partial u}{\partial t} + A(x)\frac{\partial u}{\partial x} = F(x,t), \qquad t > 0 , \tag{1.1a}$$

with initial data

$$u(x,0) = f(x), \qquad t = 0 , \tag{1.1b}$$

in the first quarter of the plane $0 \leq x < \infty$. Here $u \equiv u(x,t)$ is the N-dimensional vector of unknowns and by hyperbolicity we mean that the (nonsingular) coefficient matrix $A \equiv A(x)$ is similar to a real diagonal Λ

$$\begin{aligned} &TAT^{-1} = \Lambda \equiv \mathrm{diag}(\lambda_1,\ldots,\lambda_N), \\ &\lambda_1 > \cdots > \lambda_\ell > 0 > \lambda_{\ell+1} > \cdots > \lambda_N, \qquad \lambda_j \equiv \lambda_j(x) . \end{aligned} \tag{1.2}$$

---

[*] Sponsored in part by the United States Army under Contract No. DAAG29-80-C-0041.

The system (1.1a) - rewritten in its characteristic form

$$\frac{\partial \tilde{u}}{\partial t} + \Lambda \frac{\partial \tilde{u}}{\partial x} = \tilde{F} \tag{1.3}$$

($\tilde{\ }$ denotes multiplication by T on the left), asserts that the characteristic variables $\tilde{u}_j$ are uniquely determined by the forcing terms $\tilde{F}_j$ along the characteristic curves $\dot{x}_j(t) + \lambda_j(x_j) = 0$. The last $N - \ell$ of these curves are outgoing curves impinging on the boundary $x = 0$ from the right, each of which carries one piece of initial data; thus, exactly $N - \ell$ pieces of information flow toward the left boundary $x = 0$; these are the last $N - \ell$ outflow components of $\tilde{u}$ associated with $\dot{x}_j = -\lambda_j > 0_{|\ell < j < N}$. It therefore follows that for the system (1.1) to be uniquely solvable, exactly ℓ additional pieces of information must be provided at the boundary $x = 0$,

$$Bu_{|x=0} = G, \quad \text{rank } [B] = \ell \ . \tag{1.4a}$$

The requirement of these boundary conditions to be on top of the predetermined outflow components can be expressed as follows (Hersh [1]):

For all nontrivial ϕ in the eigenspace Φ^+ spanned by the eigenvectors $\{\phi_j\}_{j=1}^{\ell}$ associated with the positive eigenvalues $\{\lambda_j\}_{j=1}^{\ell}$, we have

$$B\phi \neq 0 \ . \tag{1.4b}$$

Had the system (1.1a) been given to us in its characteristic form (1.3), the boundary conditions (1.4) then can be reformulated as the standard reflection

$$\tilde{u}^+ = \tilde{B}\tilde{u}^- + \tilde{G} \tag{1.5}$$

where $\tilde{u} = (\tilde{u}^+, \tilde{u}^-)$ partitioned corresponding to its inflow and outflow parts. The first ℓ inflow characteristic variables $\tilde{u}^+$ are then everywhere determined via (1.5) and (1.1b) along the ingoing characteristics $\dot{x}_j = -\lambda_j < 0_{|1 < j < \ell}$, combined with the $N - \ell$ outflow pieces of data, the solution u is then well defined throughout the region of integration.

Example. The linearized inviscid 1 - D gasdynamics equations take the primitive form(1)

$$\frac{\partial u}{\partial t} + A \frac{\partial u}{\partial x} = F, \qquad 0 < x < \infty, \qquad t > 0 \tag{E.1a}$$

---

(1) Neglecting low order terms due to the linearization.

where $u \equiv (\rho,U,p)^t$ are the density velocity and pressure respectively, F stands for the external forces and

$$\text{(E.1b)} \qquad A = \begin{bmatrix} \eta & \xi & 0 \\ 0 & \eta & 1/\xi \\ 0 & \gamma\zeta & \eta \end{bmatrix} \qquad \gamma = \text{ratio of specific heats}$$

with $(\xi,\eta,\zeta)^t$ denoting the corresponding variables we linearize about. The system is hyperbolic since A is diagonalizable by

$$T = \begin{bmatrix} c^2 & 0 & -1 \\ 0 & \xi c & 1 \\ 0 & -\xi c & 1 \end{bmatrix}, \qquad c = \sqrt{\gamma\zeta/\xi}$$

$$TAT^{-1} \equiv \mathrm{diag}(\eta, \eta + c, \eta - c) .$$

We consider the subsonic inflow case $0 < \eta < c$; two boundary conditions are required at $x = 0$ to complement the only predetermined outflow variable $\tilde{u}_3 \equiv p - \xi cU$ associated with $\lambda_3 \equiv \eta - c < 0$. While prescribing the two conditions one should neither set boundary values for the predetermined $p - \xi cU_{|x=0}$, nor should he prescribe only $U_{|x=0}$ and $p_{|x=0}$ (or otherwise the two independent relations will again set values for $p - \xi cU_{|x=0}$). Failure to satisfy either one of the above constraints will either imply inconsistency, or at best, the consistent condition will give no new information and we will still be missing one piece of data at the boundary. Both cases are saved by requiring (1.4b) to hold:

For all $u \equiv (\rho,U,p)^t \neq 0$ in $\mathrm{span}\{\phi_1,\phi_2\}$ where $\phi_1 = (2\xi c,0,0)^t$, $\phi_2 = (\xi c, c^2, \xi c^3)^t$ corresponding to $\lambda_1 = \eta > 0$, $\lambda_2 = \eta + c > 0$ we should have $Bu \neq 0$. Indeed, requiring $B\phi_1 \neq 0$ amounts to the requirement of not imposing $U_{|x=0}$ and $p_{|x=0}$ alone (i.e, without involving $\rho_{|x=0}$), while $B\phi_2 \neq 0$ (or -- which is the same thing -- $B(2\phi_2 - \phi_1) \neq 0$) prevent us from prescribing $p - \xi cU_{|x=0}$. We are then assured that we have two genuinely additional boundary conditions complementing the third predetermined outflow one (for more details we refer to [2]).

In this paper we study difference approximations to the hyperbolic system (1.1). We show that when our numerical boundary conditions are zeroth-order accurate with an inflow part of the problem, they render the overall computation unstable -- a discrete analogue of the necessary condition (1.4b). In the next section we set the exact mathematical framework for our discussion, and proof of the main theorem is given in Section 3.

This paper was written while visiting the Mathematics Research Center, University of Wisconsin-Madison, Madison Wisconsin, and I thank the Center and its Director, J. Nohel for their hospitality.

2. WELL DEFINED DIFFERENCE APPROXIMATIONS-STATEMENT OF MAIN THEOREM

We would like to solve (1.1), (1.4) by difference approximations. In order to do so, we introduce a mesh size $\Delta x > 0$ and a time step $\Delta t > 0$ such that $\lambda \equiv \Delta t/\Delta x = \text{const}$. Using the notation $v_\nu(t) \equiv v(\nu\Delta x,t)$ we approximate (1.1) by a consistent two-step solvable basic scheme of the form

$$\text{(2.1a)} \qquad \sum_{j=-r}^{p} A_j(x_\nu)v_{\nu+j}(t + \Delta t) = \sum_{j=-r}^{p} A_j(x_\nu)v_{\nu+j}(t) + \Delta t H_\nu(t),$$

$$\nu = r, r + 1, \ldots .$$

Starting with the initial data

$$\text{(2.1b)} \qquad v_\nu(t = 0) = f_\nu, \qquad \nu = 0,1,\ldots ,$$

the scheme (2.1a) is then used to advance in time. To enable our calculation, the r boundary values $\{v_\nu(t + \Delta t)\}_{\nu=0}^{r-1}$ are required at each time step, and these are obtained from solvable boundary conditions of the form

$$\text{(2.1c)} \qquad \sum_{j=0}^{q} B_{j\nu}(x_\nu)v_j(t + \Delta t) = \sum_{j=0}^{q} B_{j\nu}(x_\nu)v_j(t) + \Delta t H_\nu(t),$$

$$\nu = 0,1,\ldots,r - 1 .$$

Usually for obtaining $v_0(t + \Delta t)$ one complements the $N - \ell$ inflow values taken from (1.4) by additional ℓ consistent outflow relations and in case of higher order basic scheme, $r > 1$, extra boundary conditions as in (2.1c) must be provided for both the outflow and inflow components of $\{v_\nu(t + \Delta t)\}_{\nu=1}^{r-1}$.

We now have an overall difference approximation consisting of interior scheme (2.1a) together with boundary conditions (2.1c) and the main property we would like our approximation to have is stability; that is, we want small initial perturbations not to excite our homogeneous computation but rather to have only a small comparable affect. For, it is the stability which guarantees the convergence of our results to the exact solution of (1.1), (1.4), as we refine the mesh $\Delta x, \Delta t \to 0$. In fact, lack of stability is most likely to cause our computation to diverge. We therefore make the natural

Assumption. The basic scheme (2.1a) is stable for the pure Cauchy problem $-\infty < \nu < \infty$ (1).

We are now left with the task of determining whether our boundary conditions (2.1c) maintain the assumed interior stability overall, or either our careless boundary treatment renders the overall computation unstable. During the last decade since the appearance of the works of Kreiss and his coworkers, [3]-[5], which introduce a stability theory for approximations to such mixed problems, many safe procedures to handle the outflow components were analyzed (e.g. [5]-[8]). Here however, we are interested in the inflow components whose boundary calculation is required when either the exact inflow conditions (1.4) are not known or when extra inflow values must be provided at $\{x_\nu\}_{\nu=1}^{r-1}$. Our main result is basically a negative one telling what one should not do.

Theorem. If the boundary conditions (2.1c) are zeroth-order accurate with an inflow component of system (1.1), i.e., there exists $\phi_*^+ \in \Phi^+$ such that

$$\sum_{j=0}^{q} [\mathcal{B}_{j\nu} - B_{j\nu}]\phi_*^+ \Big|_{x=0} = 0, \qquad \nu = 0,1,\ldots,r-1, \tag{2.2}$$

then the overall approximation (2.1) is unstable.

The above theorem is clearly the discrete analogue of the necessary requirement (1.4b) for well-posedness; both reflect the independence of the inflow boundary values on the differential equation. In the special case of explicit one-leveled boundary extrapolation it was first proved by Kreiss [9] for the scalar case, and extended substantially by Burns [10] for the vector case. Here we give a simplified version of her proof for the general two-leveled implicit approximation. The assumption made in [10, Assumption 3.2], that A_j, A_j are polynomials in A, is removed here so our result is also valid for multileveled multidimensional approximations, as can be shown using the standard devices which for simplicity are omitted. Finally we give a direct estimate of the unstable polynomial growth of the computed solution. Even though such growth by itself may be accepted as weak instability, it is rejected here due to the possible reflections at the other (right) boundary which will then result into the untolerable exponential instability [5].

As an example, consider any standard 5-point interior scheme approximating the system (E.1a) above. Two dimensional inflow eigenspace is to be determined at (x_1,t) and - in case the exact inflow conditions are not known - at (x_0,t) as well. According to the above theorem, any attempt to calculate the missing values in an inflow-dependent manner, that is using zeroth-order accurate conditions for either $\rho c^2 - p$, $\xi c U + p$ or any combination of them will result into instability.

---

(1) Local stability around $x = 0$ is in fact enough - see Section 3.

We close this section by finally noting that in general the boundary conditions (2.1c) are obtained using consistent discretizations of the two sources available to us - the differential system (1.1a) augmented by the inflow boundary conditions (1.4). By the above theorem, the approximated inflow boundary values cannot be calculated in an inflow-dependent manner by a consistent discretization of solely the inflow part of system (1.1a); one must take into account also the outflow data via conditions (1.4). A detailed procedure along these lines to achieve these values with any degree of accuracy is described in [8].

3. UNCONDITIONAL INSTABILITY-PROOF OF MAIN THEOREM

From the nature of our negative result it is sufficient to restrict attention to the case localized about $x = 0$, since it is the constant coefficient case $\mathcal{A}_j \equiv \mathcal{A}_j(0)$, $A_j \equiv A_j(0)$, $\mathcal{B}_{j\nu} \equiv \mathcal{B}_{j\nu}(0)$, $B_{j\nu} \equiv B_{j\nu}(0)$, which infers the instability of the general case.

The solution of the homogeneous approximation $(\underset{\sim}{2}.1)$ with vanishing interior initial data $f_\nu\big|_{\nu \geq r} = 0$ $(\underset{\sim}{f} \equiv (f_0,\ldots,f_{r-1})^t$ yet to be determined) is given by the Cauchy formula

$$(3.1) \qquad v_\nu(t) = \frac{1}{2\pi i}\int_\Gamma z^n \varphi_\nu(z)\,dz, \qquad t = n\cdot\Delta t\ .$$

Here Γ is any contour enclosing the spectrum of the underlying difference operator and $\{\varphi_\nu(z)\}_{\nu=0}^{\infty}$, $\sum_{\nu=0}^{\infty} |\varphi_\nu|^2 < \infty$ obeys the resolvent equation

$$(3.2a) \qquad \sum_{j=-r}^{p} (z\mathcal{A}_j - A_j)\varphi_{\nu+j}(z) = 0, \qquad \nu = r, r+1, \ldots\ ,$$

together with the side conditions

$$(3.2b) \qquad \sum_{j=0}^{q} (z\mathcal{B}_{j\nu} - B_{j\nu})\varphi_j(z) = f_\nu, \qquad \nu = 0,1,\ldots,r-1\ .$$

Equation (3.2a) is an ordinary difference equation with constant coefficient matrices; its most general $\underline{\ell_2\text{-bounded}}$ solution is given by [11]

$$(3.3) \qquad \varphi_k(z) = X(z)L^k(z)\underset{\sim}{\sigma}, \qquad k = 0,1,\ldots\ ,$$

where we employed the assumption of the Cauchy stability. Here $X(z)$

consists of Nr columns vectors - they are the N-dimensional Jordan chains $\{\phi_m(z)\}_{m=1}^{Nr}$ associated with the characteristic eigenvalue problem[1]

$$(3.4)\qquad \sum_{j=-r}^{p} (z\mathit{A}_j - \mathrm{A}_j)\kappa_m^j(z)\phi_m(z) = 0 \;;$$

$L(z)$ is an Nr-dimentional matrix consisting of the Jordan blocks associated with the eigenvalues $\kappa_m(z)$; and $\underset{\sim}{\sigma}$ is an Nr-dimensional free vector yet to be determined by Nr^m boundary conditions (3.2b):

$$(3.5a)\qquad D(z)\underset{\sim}{\sigma} = \underset{\sim}{f}, \qquad D(z) = [D_0(z),\ldots,D_{r-1}(z)]^t$$

where

$$(3.5b)\qquad D_\nu(z) = \sum_{j=0}^{q} (z\mathit{B}_{j\nu} - \mathrm{B}_{j\nu})X(z)L^j(z), \qquad \nu = 0,1,\ldots,r-1 \;.$$

The key of the instability proof lies in the study of the singular point $z = 1$; indeed in what follows we will show that $z = 1$ is an eigenvalue of the problem whose eigenprojection has a polynomial growth; this in turn implies the unstable polynomial growth of the whole difference operator. In order to do so, we are now going to use the consistency condition to gain more precise information about the behaviour near $z = 1$.

In [5] it was proved by the assumption of Cauchy stability, that the matrix $L(z)$ in the neighbourhood of $z = 1$ takes the form [5, Theorem 9.1]

$$(3.6a)\qquad L(z) = \begin{bmatrix} L_+(z) & 0 \\ 0 & L_0(z) \end{bmatrix} \;,$$

where using the consistency of the interior scheme it follows that the ℓ-dimensional $L_+(z)$ is of the form [5, Theorem 9.3]

$$(3.6b)\qquad L_+(z) = I - (\lambda\Lambda^+)^{-1}(z-1) + \mathcal{O}(z-1)^2$$

while the $(Nr - \ell) \times (Nr - \ell)$ $L_0(z)$ satisfies

$$(3.6c)\qquad L_0^*(z)L_0(z) \le (1-\delta)I, \qquad \delta > 0 \;.$$

Consider the first ℓ column vectors $\phi_m(z)_{|1\le m\le \ell}$ in $X(z)$ which we denote by $X_+(z)$. Inserting the corresponding eigenvalues of $L_+(z)$ from (3.6b), $\kappa_m(z) = 1 - (\lambda\lambda_m)^{-1}(z - 1) + \mathcal{O}(z - 1)^2$, into (3.4), and using the consistency of the basic scheme which amounts to the standard

---

[1] By consistency it is enough to consider only simple Jordan chains around $z = 1$ - see below.

$$\sum_{j=-r}^{p} [\mathcal{A}_j - A_j] = \sum_{j=-r}^{p} [j(\mathcal{A}_j - A_j) - \lambda A_j A] = 0 ,$$

we arrive to

$$(z - 1) \cdot \sum_{j=-r}^{p} \mathcal{A}_j [I - zA\lambda_m^{-1}] \phi_m(z) = \mathcal{O}(z - 1)^2 .$$

By the solvability $\sum_{j=-r}^{p} \mathcal{A}_j e^{ij\theta}|_{\theta=0} = \Sigma \mathcal{A}_j$ is nonsingular; dividing by $(z - 1)\Sigma \mathcal{A}_j$ we obtain that

$$(3.7) \qquad X_+(z) = X_+(1) + \mathcal{O}(z - 1), \quad X_+(1) \in \Phi^+ ,$$

where $X_+(1)$ consists of the ℓ column vectors $\phi_m(1) \equiv \phi_m$ - the eigenvectors of A corresponding to its positive eigenvalues $\lambda_m > 0$.

We now claim that $[D(z)]^{-1}$ is singular at $z = 1$. To see that we take $\underset{\sim}{\tau}$ to be an Nr-dimensional vector whose first ℓ scalar components, $\underset{\sim}{\tau}_+$, are uniquely determined as the solution of (see (2.2))

$$X_+(1)\underset{\sim}{\tau}_+ = \phi_+^+ ,$$

and the remaining $Nr - \ell$ components are taken to zero. Taking into account (3.6b) and (3.7) we then find by (2.2)

$$(3.8a) \qquad D(z)\underset{\sim}{\tau}_+ = \sum_{j=0}^{q} (\mathcal{B}_{j\nu} - B_{j\nu})X_+(1)\underset{\sim}{\tau}_+ + \mathcal{O}(z - 1) = \mathcal{O}(z - 1)$$

and hence for $d(z) \equiv \det[D(z)]$ we conclude that

$$(3.8b) \qquad d(z) = \mathcal{O}(z - 1)^s \qquad s > 1 .$$

The proof of the theorem is almost at our hands now; we consider that part of the solution corresponding to the eigenprojection associated with $z = 1$:

$$(3.9a) \qquad w_\nu(t) = \frac{1}{2\pi i} \int_{|z-1|=\epsilon} z^n \varphi_\nu(z)\,dz, \quad \nu = 0,1,\ldots, \quad t = n\cdot\Delta t ,$$

where by (3.3), (3.5), $\varphi_\nu(z)$ has the analytic representation ($[D(z)]^{-1} \equiv \mathcal{D}(z)/d(z)$)

(3.9b)
$$\varphi_\nu(z) = [X_+(z), X_0(z)] \begin{bmatrix} L_+(z) & 0 \\ 0 & L_0(z) \end{bmatrix}^\nu \mathcal{D}(z)\underline{f}/d(z) \ .$$

Taking (3.8b) into account, the residue theorem implies

(3.10)
$$w_\nu(t) = \sum_{k=0}^{s-1} \binom{n}{k} \cdot \mathrm{Res}\left[(z - 1)^k \varphi_\nu(z)\right]_{|z=1}$$

and since by (3.6b) $L_+(z = 1) = I$ we finally conclude

(3.11)
$$\|w(t)\| > \Big[\sum_{\nu=0}^{(n+1)\cdot r} |w_\nu(t)|^2\Big]^{1/2} \geq \text{const.}[t/\Delta t]^s \|\underline{f}\| \ .$$

REMARKS

(i) As in [10] one can show that also in our case, the resolvent condition $\|\Psi(z)\| < \text{const.}(|z| - 1)^{-1}$ is violated. Indeed using the representation (3.9b) and employing the equivalent H-norm,
$$\|\psi(z)\|_H = \Big[\sum_{\nu=0}^{\infty} \psi_\nu^*(z) H(z) \psi_\nu(z)\Big]^{1/2}, \quad \text{with} \quad H(z) \equiv [X_+(z) X_+^*(z)]^{-1}, \quad \text{one}$$
gets $\|\varphi(z)\| > \text{const.}|z - 1|^{-3/2}$.

(ii) Unlike the case of one-leveled boundary extrapolation [10, Section 5], it does not follow that the more accurate the boundary conditions with an inflow part of our problem, the worse is the singular behaviour at $z = 1$ - the R.H.S. of (3.8a) remains unaffected in the genuinely two-leveled case.

REFERENCES

[1] Hersh, R.: Mixed Problems in Several Variables. J. Math. Mech., vol. 12, 1963, pp. 317-334.

[2] Oliger, J; and Sundström, A.: Theoretical and Practical Aspects of some Initial Boundary Value Problems in Fluid Dynamics. SIAM J. Appl. Math., vol. 35, 1978, pp. 419-446.

[3] Kreiss, H.-O.: Difference Approximations for the Initial-Boundary Value Problem for Hyperbolic Differential Equations. Numerical Solutions of Nonlinear Differential Equations, Wiley, New York, 1966, pp. 141-166.

[4] Kreiss, H.-O.: Stability Theory for Difference Approximations of Mixed Initial Boundary Value Problems. I. Math. Comp., vol. 22, 1968, pp. 703-714.

[5] Gustafsson, B; Kreiss, H.-O.; and Sundström, A.: Stability Theory of Difference Approximations for Mixed Initial Boundary Value Problems. II. Math. Comp., vol. 26, 1972, pp. 649-686.

[6] Sköllermo, G.: How the Boundary Conditions Affect the Stability and Accuracy of some Implicit Methods for Hyperbolic Equations. Report no. 62, Dept. of Comp. Sci., Uppsala Univ., Sweden, 1975.

[7] Gottlieb, D.; Gunzburger, M.; and Turkel, E.: On Numerical Boundary Treatment for Hyperbolic Systems. ICASE Report no. 78-13, Sept. 1978.

[8] Goldberg, M.; Tadmor, E.: Scheme Independent Stability Criteria for Difference Approximations of Hyperbolic Initial Boundary Value Problems. II. Math. Comp., vol. 36, 1981, pp. 603-626.

[9] Kreiss, H.-O.: Difference Approximations for Mixed Initial Boundary Value Problems. Proc. Roy. Soc. London Ser. A, vol. 323, 1971, pp. 255-261.

[10] Burns, A.: A Necessary Condition for the Stability of a Difference Approximation to a Hyperbolic System of Partial Differential Equations. Math. Comp., vol. 32, 1978, pp. 707-724.

[11] Lancaster, P.: A Fundamental Theorem on Lamda-Matrices with Applications, II: Finite Difference Equations. Lin. Alg. Appl., vol. 18, 1977, pp. 213-222.

IMPLICIT BOUNDARY CONDITIONS FOR THE SOLUTION OF THE PARABOLIZED NAVIER-STOKES EQUATIONS FOR SUPERSONIC FLOWS†

by M. Barnett,* R.T. Davis* and J.V. Rakich**
*University of Cincinnati
**NASA Ames Research Center

ABSTRACT

A fully implicit set of boundary conditions is developed for the solution of the parabolized Navier-Stokes equations for supersonic flow in two dimensions. Shock fitting is employed at the shock and the body has no-slip and specified temperature conditions. A specified heat transfer condition at the wall can be handled in a similar manner. In addition, the shock location is advanced in space in a fully implicit manner by utilizing the Rankine-Hugoniot conditions along with global conservation of mass.

NOMENCLATURE

c_1, c_2, c_3, c_4	constants arising from linearized shock relations
e	specific internal energy
F, G	vectors in governing equations
i	index in streamwise (ξ) direction
j	index in stream-normal (η) direction
J	Jacobian of the coordinate transformation
M	Mach number
p	pressure
Q	vector of flow variables
u	velocity component in x-direction
v	velocity component in y-direction
x, y	Cartesian coordinates, physical plane
γ	ratio of specific heats, $\gamma = c_p/c_v$
δ	shock standoff distance
ξ, η	coordinates in transform plane
ρ	density

subscripts

b	body
s	shock
t	total

---

† This research was sponsored by NASA Ames Research Center under contracts numbers NCA2-OR130-901 and NCA2-OR130-101.

v	viscous
w	wall
x,y	partial derivatives with respect to x and y respectively
ξ,η	partial derivatives with respect to ξ and η respectively
∞	freestream value

INTRODUCTION

In reference 1 a parabolic form of the Navier-Stokes equations for supersonic compressible flow is solved using the Beam-Warming factored implicit algorithm (ref. 2). External flows over bodies at angle of attack were calculated for the domain bounded by the body surface and the enveloping shock wave. In that work, and most other works of a similar nature, the shock boundary conditions (the Rankine-Hugoniot jump conditions) are applied in an explicit manner. While adequate for small marching steps, (within the CFL condition at the shock), the explicit method has a stability imposed stepsize limitation. It is advantageous from the standpoint of computational efficiency to have fully implicit boundary conditions at both the shock and the body in order to remove this stability restriction on stepsize and allow the solution over a given domain to be obtained with less computational effort.

The earlier studies of Srivastava, Werle and Davis (ref. 3) and Lubard and Helliwell (ref. 4) are examples of viscous shock layer calculations utilizing the Rankine-Hugoniot relations at the shock. The study of Srivastava, et al. utilized a relaxation technique to obtain the overall solution and iterate on the shock shape. Lubard and Helliwell's study utilized space marching with iteration at each streamwise station. The solution scheme developed in the present study requires no iteration.

Although the problem is viscous, the shock boundary condition can, for most applications, be treated in an inviscid manner as viscous effects are mainly of interest near the solid boundary where a boundary layer exists. This implies that the Rankine-Hugoniot relations may be employed at the shock since the flow there is inviscid.

In the present study the equations are solved in block tridiagonal form by a matrix inverter tailored to solve four second order equations. The set of equations which is solved here consists of two first order and two second order equations. To achieve compatibility with the inversion scheme, an appropriate finite difference scheme must be applied to the inviscid type equations at the boundaries. This situation is illustrated through a simple model problem. The use of a difference scheme at the boundaries such as that developed here removes what may be the source of oscillations in many numerical solution techniques. In the present parabolized Navier-Stokes solver, smooth solutions are obtained without the use of numerical smoothing schemes for flows without imbedded discontinuities.

GOVERNING EQUATIONS AND THE SOLUTION SCHEME

The system of equations which is solved in this study is a parabolic form of the Navier-Stokes equations. The gas considered is laminar, perfect and compressible.

The development of the basic solution scheme and the transformation from the physical to the computational plane follows much the same line of reasoning as was employed in reference 1.

Parabolization of the full Navier-Stokes equations is accomplished by assuming steady flow and neglecting streamwise diffusion in comparison to diffusion normal to the body surface. With these approximations, the governing equations can be written in nondimensional form as

$$\frac{\partial \bar{F}}{\partial \xi} + \frac{\partial \bar{G}}{\partial \eta} = \frac{\partial \bar{G}_v}{\partial \eta} \quad . \tag{1}$$

These equations are in strong conservation form in the transform (ξ,η) plane where

$$\bar{F} = y_\eta F, \qquad \bar{G} = -\, y_\xi F + G \quad \text{and} \quad \bar{G}_v = -\, y_\xi F_v + G_v \tag{2a-c}$$

with

$$F = \begin{bmatrix} \rho u \\ \rho u^2 + p \\ \rho uv \\ (\rho e_t + p)u \end{bmatrix} \qquad G = \begin{bmatrix} \rho v \\ \rho uv \\ \rho v^2 + p \\ (\rho e_t + p)v \end{bmatrix} \tag{2d,e}$$

$$F_v = \begin{bmatrix} 0 \\ \sigma_{xx} \\ \tau_{xy} \\ u\sigma_{xx} + v\tau_{xy} + q_x \end{bmatrix} \quad \text{and} \quad G_v = \begin{bmatrix} 0 \\ \tau_{xy} \\ \sigma_{yy} \\ u\tau_{xy} + v\sigma_{yy} + q_y \end{bmatrix} \quad . \tag{2f,g}$$

The continuity, x-momentum, y-momentum and energy equations are represented in each vector.

The above equations are written in the present case for the coordinate transformation defined by

$$x = \xi \quad \text{and} \quad y(\xi,\eta) = y_b(\xi) + s(\eta)\delta(\xi) \tag{3a,b}$$

where $s(\eta)$ is the stretching function employed to cluster mesh points near the wall for proper boundary layer resolution and $\delta(\xi)$ is the shock standoff distance measured from body to shock along constant ξ. The corresponding Jacobian of the transformation is given by

$$J = \frac{1}{y_\eta} = \eta_y \quad . \tag{4}$$

The η coordinate is given by

$$\eta = (j-1)\,\Delta\eta \tag{5a}$$

with $\eta = 0$ at the shock and $\eta = 1$ at the body. The index in the ξ-direction is denoted by "i" so that

$$\xi = \xi_o + i\,\Delta\xi \tag{5b}$$

with ξ_o being the location of the initial data plane.

Typical physical and transformed planes and their nomenclature are given in figures 1a and 1b.

The elements of F, G, F_v and G_v can be written in terms of the elements of Q and their derivatives where

$$Q = \begin{bmatrix} \rho \\ \rho u \\ \rho v \\ \rho e_t \end{bmatrix} \tag{6a}$$

and

$$\bar{Q} = \frac{Q}{J} \quad . \tag{6b}$$

In the present formulation, the η-momentum equation is assumed inviscid; this is a consistent assumption with regard to the order of magnitude of the terms already neglected as long as the body slope is small. The more appropriate assumption would be that the momentum equation for the direction normal to the body surface is inviscid.

The streamwise pressure gradient term is treated in a manner similar to that of reference 1 in order to prevent the appearance of departure solutions.

The development of the implicit finite difference scheme and appropriate linearization are discussed in detail in reference 5. The finite difference scheme in incremental variable form is given by

$$\Delta^i\bar{F} + \Delta\xi\,\frac{\partial}{\partial\eta}\left(\Delta^i\bar{G} - \Delta^i\bar{G}_v\right) = \Delta\xi\,\frac{\partial}{\partial\eta}\left(-\bar{G}^i + \bar{G}^i_v\right) \tag{7}$$

where $\Delta^i z = z^{i+1} - z^i$ along η = constant. Equation (7) is first order accurate in ξ. Local linearization applied to (7) results in

$$\left[\frac{\partial\bar{F}}{\partial\bar{Q}} + \Delta\xi \frac{\partial}{\partial\eta}\left(\frac{\partial\bar{G}}{\partial\bar{Q}} - \frac{\partial\bar{G}_v}{\partial\bar{Q}}\right)\right]^i \Delta^i\bar{Q} = -\Delta\xi \frac{\partial}{\partial\eta}\left(\bar{G}^i - \bar{G}_v^i\right) \quad . \tag{8}$$

Discretization of equation (8) is performed later, after the boundary conditions have been developed.

DEVELOPMENT OF THE BOUNDARY CONDITIONS

Equation (8) describes a sixth order set of equations in the η-direction, two first order (continuity and η-momentum) and two second order (ξ-momentum and energy) equations. Hence six boundary conditions are required and they must be distributed between the shock boundary and wall boundary in an appropriate manner. For the present purposes, three boundary conditions are applied at each boundary.

Shock Boundary

The physical unknowns at the shock are the incremental variables given by

$$\Delta Q_s = \begin{bmatrix} \Delta\rho \\ \Delta\rho u \\ \Delta\rho v \\ \Delta\rho e_t \end{bmatrix}_s \tag{9}$$

which can be rewritten, utilizing the shock jump relations of reference 6, in the form

$$\Delta Q_s = \begin{bmatrix} c_1 \\ c_2 \\ c_3 \\ c_4 \end{bmatrix} \Delta p_s = \bar{C}\,\Delta p_s \tag{10}$$

where c_1 through c_4 are obtained by locally linearizing about the shock slope and corresponding values of the flow variables at the previous march station, hence the c_i's are all known. They are given by

$$c_1 = \frac{(\gamma+1)}{2\sin^2\theta}\,\rho_s\left[1 - \rho_s\frac{\gamma-1}{\gamma+1}\right] \quad , \tag{11a}$$

$$c_2 = c_1 u_s - \rho_s \quad , \tag{11b}$$

$$c_3 = \rho_s[\cot\theta - \frac{\gamma+1}{4\sin^3\theta \cos\theta} (1-u_s)] + c_1 v_s \tag{11c}$$

and

$$c_4 = \frac{1}{\gamma-1} + c_2 u_s + c_3 v_s - c_1 \frac{(u^2+v^2)_s}{2} \quad . \tag{11d}$$

The jump conditions providing the above relationships are derived from conservation of mass, momentum and energy at the shock. Through linearization they serve to reduce the four unknowns at the shock to one unknown parameter, Δp_s, hence providing three boundary conditions. The linearization performed here is consistent with the basic solution method, equation (8).

Because the strongly conservative form of the governing equations is used, an expression for $\Delta^i \bar{Q}$ is required where

$$\bar{Q} = \frac{Q}{J}$$

and

$$\Delta^i \bar{Q} = \frac{\Delta^i Q}{J} - \bar{Q}^i \frac{\Delta^i J}{J^i} \quad . \tag{12}$$

In order to have a fully implicit method, the term $\Delta^i J$ in equation (12) must be evaluated in terms of the solution vector $\Delta^i \bar{Q}$. This is accomplished in the following manner.

Based on the definitions of the Jacobian J and $y(\xi,\eta)$ the following relationship exists

$$J = \frac{1}{\delta(\xi)s(\eta)} \quad . \tag{13a}$$

Therefore, since ΔJ is taken along constant η, it follows that

$$\frac{\Delta^i J}{J^i} = - \frac{\Delta^i \delta}{\delta^i} \quad . \tag{13b}$$

An implicit means for finding $\Delta^i \delta$ can be developed through the principle of global mass conservation. For this purpose the continuity equation is utilized in the form of equation (7). Thus,

$$\Delta^i \bar{f} + \Delta\xi \frac{\partial \Delta^i \bar{g}}{\partial \eta} = - \Delta\xi \frac{\partial \bar{g}^i}{\partial \eta} \quad . \tag{14}$$

For the continuity equation, the appropriate variables are

$$\bar{f} = y_\eta \rho u = \overline{\rho u} \quad \text{and} \quad \bar{g} = -\,y_\xi \rho u + \rho v = -\frac{y_\xi}{y_\eta}\,\overline{\rho u} + \frac{1}{y_\eta}\,\overline{\rho v} \quad . \qquad (15a,b)$$

Equation (14) is next discretized across a box centered at i+½, j-½ to obtain

$$\frac{1}{2}\,(\Delta^i \bar{f}_j + \Delta^i \bar{f}_{j-1}) + \frac{\Delta\xi}{\Delta\eta}\,(\Delta^i \bar{g}_j - \Delta^i \bar{g}_{j-1}) = -\frac{\Delta\xi}{\Delta\eta}\,(\bar{g}^i_j - \bar{g}^i_{j-1}) \quad . \qquad (16a)$$

Equation (16a) is now summed from shock to body, which is effectively trapezoidal rule integration, giving

$$\sum_{j=2}^{NJ} \frac{1}{2}\,(\Delta^i \bar{f}_j + \Delta^i \bar{f}_{j-1})\Delta\eta + \frac{\Delta\xi}{\Delta\eta} \sum_{j=2}^{NJ} (\Delta^i \bar{g}_j - \Delta^i \bar{g}_{j-1})\,\Delta\eta$$

$$= -\frac{\Delta\xi}{\Delta\eta} \sum_{j=2}^{NJ} (\bar{g}^i_j - \bar{g}^i_{j-1})\,\Delta\eta \qquad (16b)$$

where j = NJ at the body. This is the appropriate integration for the present scheme. Performing the indicated summation and imposing the no-slip condition at the body results in

$$\frac{1}{2}\,(\Delta^i \bar{f}_1 + \Delta^i \bar{f}_2 + \ldots + \Delta^i \bar{f}_{NJ-1}) - \frac{\Delta\xi}{\Delta\eta}\,\Delta^i \bar{g}_1 = \frac{\Delta\xi}{\Delta\eta}\,\bar{g}^i_1 \quad . \qquad (17)$$

The first term on the left-hand side of equation (17) is $-\Delta^i y_s$, the change in shock position between i and i+1, as next shown. Integrating the mass flux through the inflow and outflow planes of two subsequent ξ-stations and setting the difference equal to the amount of mass admitted through the shock between those two stations (if no mass is injected at the body) leads to

$$\Delta^i y_s = -\int_0^1 \Delta^i\,(\rho u y_\eta)\,d\eta \quad . \qquad (18)$$

The right-hand side of equation (18) is the negative of the first term on the left-hand side of equation (17), giving

$$\Delta^i y_s = -\frac{\Delta\xi}{\Delta\eta}\,(\Delta^i \bar{g}_1 + \bar{g}^i_1) \quad . \qquad (19)$$

Now, since

$$y_s = y_b + \delta \qquad (20a)$$

it follows that

$$\Delta^i\delta = \Delta^i y_s - \Delta^i y_b \quad . \tag{20b}$$

Equation (19) is then substituted into equation (20b) giving us an expression for $\Delta^i\delta$ in terms of the prescribed $\Delta^i y_b$, known terms, and the unknown $\Delta^i\bar{g}_1$ of continuity. Using this expression for $\Delta^i\delta$ together with equation (10) in equation (12) gives us the desired expression for $\Delta^i\bar{Q}_s$ in terms of one unknown parameter, $\Delta^i p_s$. Performing the above described manipulations and rearranging terms to solve for $\Delta^i\bar{Q}_s$ we can write in compact notation

$$\Delta\bar{Q}_s = \bar{S}\,\frac{\Delta^i p_s}{J^i} + \bar{T} \tag{21}$$

where $\bar{S}$ and $\bar{T}$ are easily obtained.

Before proceeding to application of the boundary conditions at the shock using the finite difference scheme, we next turn to the body boundary conditions.

Wall Boundary

At the body the no slip conditions $(u = v = 0)$ are applied and the wall temperature is specified. This provides three boundary conditions.

We can write

$$\Delta Q_b = \begin{bmatrix} \Delta\rho \\ 0 \\ 0 \\ \Delta(\rho e_t) \end{bmatrix}_b \quad . \tag{22}$$

Since at the wall $e = e_t$ the equation of state yields

$$(\rho e_t)_b = e_w \rho_b \tag{23a}$$

thus

$$\Delta(\rho e_t)_b = e_w\,\Delta\rho_b \tag{23b}$$

where e_w is a constant given by

$$e_w = \frac{T_w}{\gamma(\gamma-1)M_\infty^2} \quad . \tag{23c}$$

Therefore we can write

$$\Delta Q_b = \begin{bmatrix} 1 \\ 0 \\ 0 \\ e_w \end{bmatrix} \Delta\rho_b \quad . \tag{24}$$

We wish now to consider the form of $\Delta\bar{Q}_b$. According to equation (12) we can write

$$\Delta\bar{\rho} = \frac{\Delta\rho}{J} - \bar{\rho}\,\frac{\Delta J}{J} \quad \text{and} \quad \Delta\overline{\rho e}_t = \frac{\Delta\rho e_t}{J} - \overline{\rho e}_t\,\frac{\Delta J}{J} \quad . \tag{25a,b}$$

Use of equations (23a) and (23b) permits us to write

$$\Delta(\overline{\rho e}_t)_b = e_w \Delta\bar{\rho}_b \quad . \tag{26}$$

Finally we can write at the wall

$$\Delta\bar{Q}_b = \begin{bmatrix} 1 \\ 0 \\ 0 \\ e_w \end{bmatrix} \Delta\bar{\rho}_b \quad . \tag{27}$$

As at the shock, one unknown parameter remains at the wall, $\Delta\bar{\rho}_b$.

DEVELOPMENT OF THE BOUNDARY POINT DIFFERENCE SCHEME

The boundary conditions and use of the continuity equation has allowed us to express the eight unknowns at the shock and wall boundaries in terms of two unknowns, $\Delta^i p_s$ and $\Delta^i \bar{\rho}_b$, respectively. With application of a suitable finite difference scheme at the boundaries the system of equations can be cast into block tridiagonal form, which results in a set of equations that is relatively easy to solve with existing methods, see reference 7, for example. We intend to show that there exists one particularly suitable finite difference scheme to use at the boundaries. Further, if the boundary point difference scheme can be developed directly from the interior point difference scheme, then the finite differencing will be completely compatible over the entire solution field. It will be demonstrated that incompatibility of the boundary point differencing with the interior point differencing can lead to oscillatory solutions.

Model Problem

A simple model problem is used to illustrate the above claims. It is desired to numerically integrate the equation

$$\frac{df}{dy} = \pi\cos\pi y \quad , \qquad f(0) = 0 \tag{28}$$

over the interval $0 \leq y \leq 1$.

One might discretize equation (28) as follows:

$$\frac{f_{i+1} - f_i}{\Delta y} = \frac{\pi}{2}\left(\cos\pi y_{i+1} + \cos\pi y_i\right) \quad . \tag{29a}$$

With a boundary condition on f at $i = 1$ ($f_1 = F$), the solution can be obtained at all points by stepping equation (29a) out from the boundary. If equation (29a) is written across $i-\frac{1}{2}$ by decrementing i by one and these two expressions are added together, one obtains the central difference form for constant Δy

$$\frac{f_{i+1} - f_{i-1}}{2\Delta y} = \frac{\pi}{4}\left(\cos\pi y_{i+1} + 2\cos\pi y_i + \cos\pi y_{i-1}\right) \quad . \tag{29b}$$

With equation (29b) the system of equations can be cast into tridiagonal form and solved by conventional methods using a tridiagonal inverter. This is how the model problem is solved in this study.

An alternative method of solution is the following. By stepping equation (29b) from $i = 1$, the solution can be obtained at all of the odd numbered mesh points. To obtain the solution at the even numbered mesh points, a difference expression relating f at i and i+1 must be employed. The obvious choice is equation (29a) which can be employed once, and then, with the solution at one even numbered mesh point, equation (29b) can be used to find the solution at all remaining even numbered mesh points. This technique will give precisely the same solution as when equation (29a) is used for all points or when the system is solved in tridiagonal form. Equation (29a) is not the only possible finite difference expression which can be used to transfer the solution to an even numbered mesh point when using equation (29b). However, it is the only compatible difference expression for this task, having been used to derive the interior point difference scheme. This model problem was solved for this study and the percent error in the solution is plotted for the compatible and an incompatible boundary point difference expression in which the derivative is written as a three point backward difference at the upper boundary. The incompatible expression was not chosen at random. It has formally the same order of accuracy at the boundary point as the interior point difference scheme for df/dy has at those points. The results (fig. 2) show that the incompatible boundary point differencing yields an oscillatory solution which reproduces the compatible differencing results only at the odd numbered mesh points. The solution has not been properly transferred to the even numbered mesh points.

If the solution method for this model problem utilizing equations (29b) and (29a) is written out in matrix form, it is found to be a tridiagonal system with all zero elements on the main diagonal except at the upper boundary where equation (29a) is applied. This system is clearly lacking diagonal dominance, yet we note that this poses no problem provided the boundary point differencing is treated properly.

The situation can be summarized as follows. A first order equation is integrated using a two point central difference written across three mesh points. In order to correctly recouple the solution points a "numerical boundary condition" is required which we shall call a "connection condition". Hence the first order equation with a two point central difference written across three mesh points requires one boundary condition and one connection condition. This is exactly analogous to the parabolic Navier-Stokes problem, which we recall was formulated with two inviscid equations.

We now proceed to develop the finite difference scheme for the solution of equation (8). Only the inviscid form of that equation is considered because the connection conditions are required only for the inviscid (first order) equations.

Equation (8) is discretized across the box centered at $i+\frac{1}{2}$, $j+\frac{1}{2}$ for an inviscid equation as

$$\left[\frac{1}{2}\left(\left.\frac{\partial\bar{f}}{\partial\bar{Q}}\right|_{j+1} + \left.\frac{\partial\bar{f}}{\partial\bar{Q}}\right|_{j}\right) + \frac{\Delta\xi}{\Delta\eta}\left(\left.\frac{\partial\bar{g}}{\partial\bar{Q}}\right|_{j+1} - \left.\frac{\partial\bar{g}}{\partial\bar{Q}}\right|_{j}\right)\right]^{i} \Delta^{i}\bar{Q}$$

$$= -\frac{\Delta\xi}{\Delta\eta}\left(\bar{g}_{j+1} - \bar{g}_{j}\right)^{i} \quad . \tag{30}$$

As for the model problem, decrement j by one to give the expression for the box centered at $i+\frac{1}{2}$, $j-\frac{1}{2}$, then add this and equation (30) to give

$$\left[\frac{1}{4}\left(\left.\frac{\partial\bar{f}}{\partial\bar{Q}}\right|_{j+1} + 2\left.\frac{\partial\bar{f}}{\partial\bar{Q}}\right|_{j} + \left.\frac{\partial\bar{f}}{\partial\bar{Q}}\right|_{j-1}\right) + \frac{\Delta\xi}{2\Delta\eta}\left(\left.\frac{\partial\bar{g}}{\partial\bar{Q}}\right|_{j+1} - \left.\frac{\partial\bar{g}}{\partial\bar{Q}}\right|_{j-1}\right)\right]^{i} \Delta^{i}\bar{Q}$$

$$= -\frac{\Delta\xi}{2\Delta\eta}\left(\bar{g}_{j+1} - \bar{g}_{j-1}\right)^{i} \quad . \tag{31}$$

This is the interior point difference scheme for the inviscid terms in all of the conservation equations. Note that as for the model problem the η-derivatives are two point centeral differences written across three mesh points. We should thus expect the same uncoupling of adjacent solution points in the inviscid equations as was observed in the model problem. This also occurs in the viscous equations in inviscid regions where the viscous terms die out. Hence we choose to employ equation (30) at the two boundaries on the inviscid equations, one at each boundary. This will allow us to apply the correct connection conditions while at the same time providing a relationship between the one remaining unknown at each boundary and the solution vector at the adjacent mesh point. Thus the boundary points are eliminated from the inversion of the system of equations and the desired block tridiagonal form is achieved. Note that the present algorithm could be used for computing totally inviscid flows by providing two more required connection conditions.

The application of the connection conditions for the viscous problem is detailed in the next section.

Application of Connection Conditions

The continuity equation written in the form of equation (30) is utilized at the shock boundary. Using compact notation the equation is rewritten as

$$A \, \Delta^i \bar{Q}_1 + B \, \Delta^i \bar{Q}_2 = R \quad . \tag{32a}$$

Noting that $\Delta\bar{Q}_s = \Delta\bar{Q}_1$, equation (21) is substituted into equation (32a) and $\Delta p_s/J$ solved for to yield

$$\frac{\Delta^i p_s}{J^i} = (A\bar{S})^{-1} \, [R - A\bar{T} - B \, \Delta^i \bar{Q}_2] \tag{32b}$$

expressing $\Delta p_s/J$ in terms of the unknown vector $\Delta\bar{Q}_2$ and known quantities. Next substituting equation (32b) into equation (21) gives $\Delta\bar{Q}_1$ in terms of $\Delta\bar{Q}_2$ and known quantities. The final step is to substitute for $\Delta\bar{Q}_1$ in terms of $\Delta\bar{Q}_2$ in the overall finite difference scheme written at $j = 2$ for all of the governing equations. This redefines the coefficient matrices and right-hand side term for $j = 2$ and eliminates the shock point from the direct inversion of the system of equations. Once $\Delta\bar{Q}_2$ is known, $\Delta\bar{Q}_1$ is obtained from the expression relating the two.

The procedure at the body is almost identical to that at the shock, therefore it will not be detailed here. The main difference is that at the body the connection condition is made on the η-momentum equation.

The boundary conditions in conjunction with the connection conditions have been developed in this study in a completely implicit manner. One other point must be discussed, namely, the method for advancing the shock shape in a fully implicit manner.

IMPLICIT ADVANCE OF THE SHOCK SHAPE

Some parabolized Navier-Stokes schemes which employ shock fitting have in the past not used implicit means to advance the shock shape, even though the rest of the scheme may have been implicit. In reference 1 the authors note that the use of Euler explicit integration to march the shock shape downstream leads to restrictions on the maximum allowable streamwise stepsize. It is found that an implicit method for advancing the shock can be developed straightforwardly based on global conservation of mass.

In reference 3, the shock shape is solved for implicitly by making the shock standoff one of the unknowns solved for when the equations are inverted. This is more costly than the present approach in terms of the computational effort required.

The integration indicated in equation (18) is all that is needed to implicitly advance the shock. Once the equations have been inverted at station i+1, the vector $\Delta^i\bar{Q}$ is known, hence $\Delta^i(\rho u y_\eta)$ is available. The integration of equation (18) is performed using the trapezoidal rule to find $\Delta^i y_s$. $\Delta^i\delta$ follows from equation (20b) with the prescribed $\Delta^i y_b$. Finally

$$\delta^{i+1} = \delta^i + \Delta^i\delta \quad . \tag{33}$$

Once δ^{i+1} is known, J^{i+1} is computed and $\bar{Q}^{i+1}$ is decoded to give Q^{i+1}, the physical variables.

RESULTS

In this study a fully implicit set of boundary conditions for the parabolized Navier-Stokes equations in strong conservation form has been developed. Figure 3 shows the surface pressure for the 10% parabolic arc airfoil at the conditions solved for in an earlier numerical study by Schiff and Steger (ref. 8). Agreement is good between the present code and their results. All profiles were found to be free of oscillations except for very small magnitude oscillations near the shock. No smoothing of any sort was applied in the present scheme.

The three-dimensional solution scheme of reference 1 was reduced to two dimensions and a stepsize study performed to compare the effect of the difference in the boundary conditions between the two schemes. The earlier scheme was found to be limited in stepsize to a condition which corresponds approximately to a CFL number of one at the shock. The present scheme permits shock CFL numbers up to approximately seven, although the accuracy of the results declines as expected at the higher CFL numbers. This is illustrated in figure 4 where wall shear profiles are plotted for various shock CFL numbers and compared to the results of self similar compressible boundary layer theory.

CONCLUSIONS

The importance of a carefully considered choice of the boundary point difference scheme has been indicated through a simple model problem.

Finally, an implicit method has been devised for advancing the shock based on the principle of global mass conservation. It was found that if the present scheme is used with the shock advanced by Euler explicit integration, the maximum stepsize is again curtailed to a shock CFL number of approximately one, independent of the fact that the boundary conditions are otherwise fully implicit.

Though the present analysis is for two dimensional flow, extension of the boundary conditions to three dimensions should be possible using the same principles.

REFERENCES

1. Vigneron, Y.C.; Rakich, J.V.; and Tannehill, J.C.: Calculation of Supersonic Viscous Flow over Delta Wings with Sharp Subsonic Leading Edges. AIAA paper 78-1137, Seattle, Washington, July 1978.

2. Warming, R.F.; and Beam, R.M.: On the Construction and Application of Implicit Factored Schemes for Conservation Laws. SIAM-AMS Proceedings, Vol. 11, pp. 85-129.

3. Srivastava, B.N.; Werle, M.J.; and Davis, R.T.: Viscous Shock-Layer Solutions for Hypersonic Sphere Cones. AIAA Journal, vol. 16, no. 2, February 1980, pp. 137-144.

4. Lubard, S.C.; and Helliwell, W.S.: Calculation of the Flow on a Cone at High Angle of Attack. AIAA Journal, vol. 12, no. 7, July 1974, pp. 965-974.

5. Barnett, M.: Solution of the Parabolized Navier-Stokes Equations by a Fully Implicit Method for Supersonic Flows with an Analysis of Departure Solution Behavior. M.S. Thesis, Dept. of Aerospace Engg. and Appl. Mech., Univ. of Cincinnati, August 1981.

6. Equations, Tables and Charts for Compressible Flow. NACA Rept. 1135, 1953.

7. Steger, J.L.: Implicit Finite Difference Simulation of Flow about Arbitrary Geometries with Application to Airfoils. AIAA paper 77-665, Albuquerque, NM, June 1977.

8. Schiff, L.B.; and Steger, J.L.: Numerical Simulation of Steady Supersonic Viscous Flow. AIAA Journal, vol. 18, no. 12, December 1980, pp. 1421-1430.

BLANK
PAGE

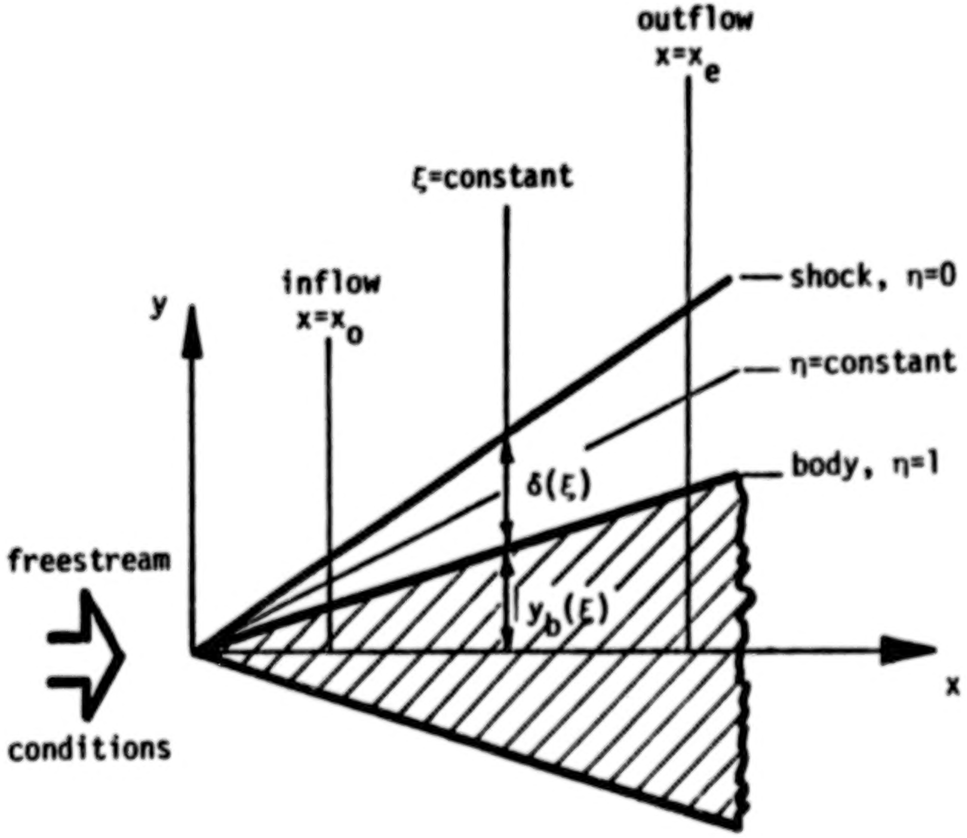
outflow
x=x_e
ξ=constant
inflow
x=x_o
y
shock, η=0
η=constant
body, η=1
δ(ξ)
y_b(ξ)
freestream
conditions
x

Figure 1.a Typical Physical Plane Geometry and Notation

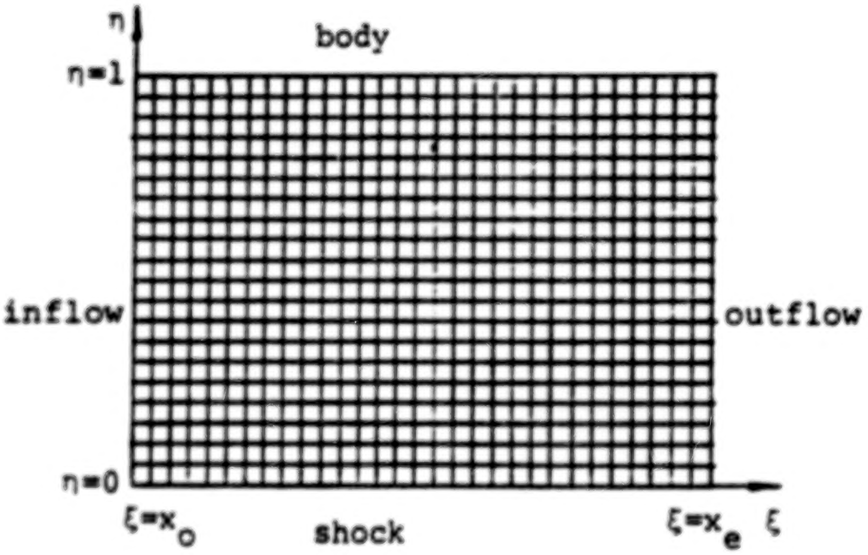
η
body
η=1
inflow
outflow
η=0
ξ=x$_o$
shock
ξ=x$_e$
ξ

Figure 1.b Typical Computational Plane

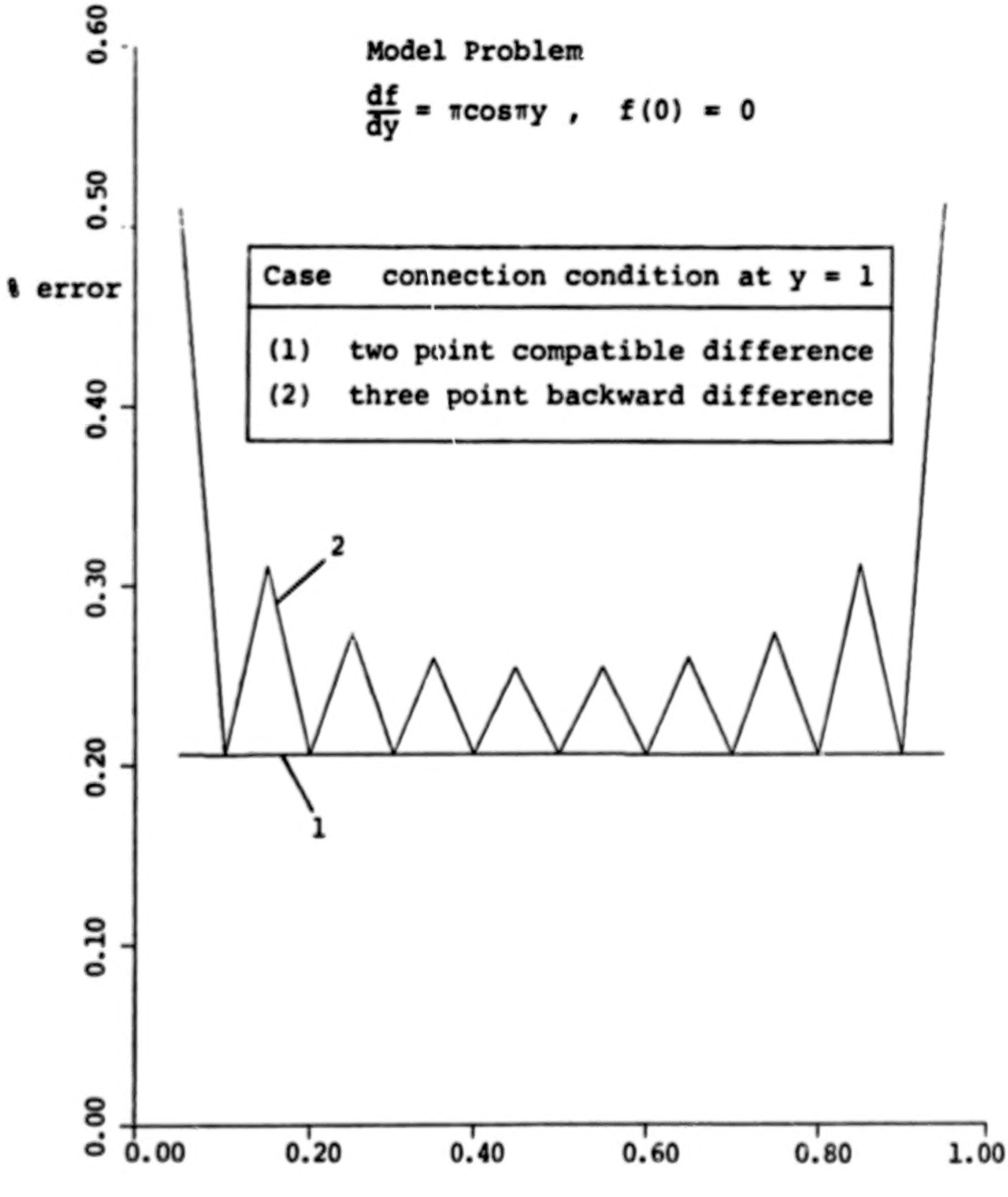

Figure 2 Model Problem: Percent Error vs. y at Interior Points

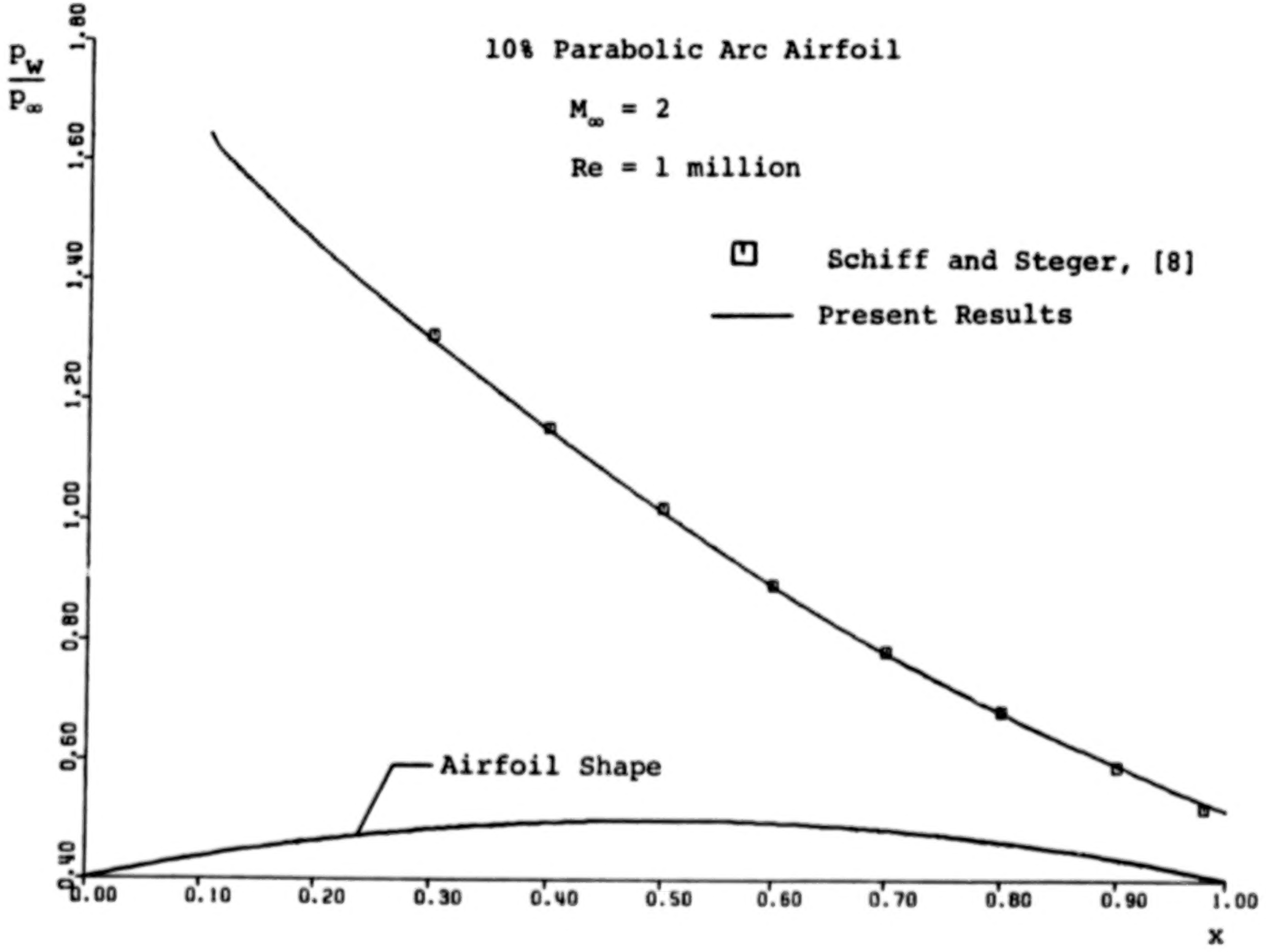

Figure 3 10% Parabolic Arc Airfoil, P_w/P_∞ vs. x

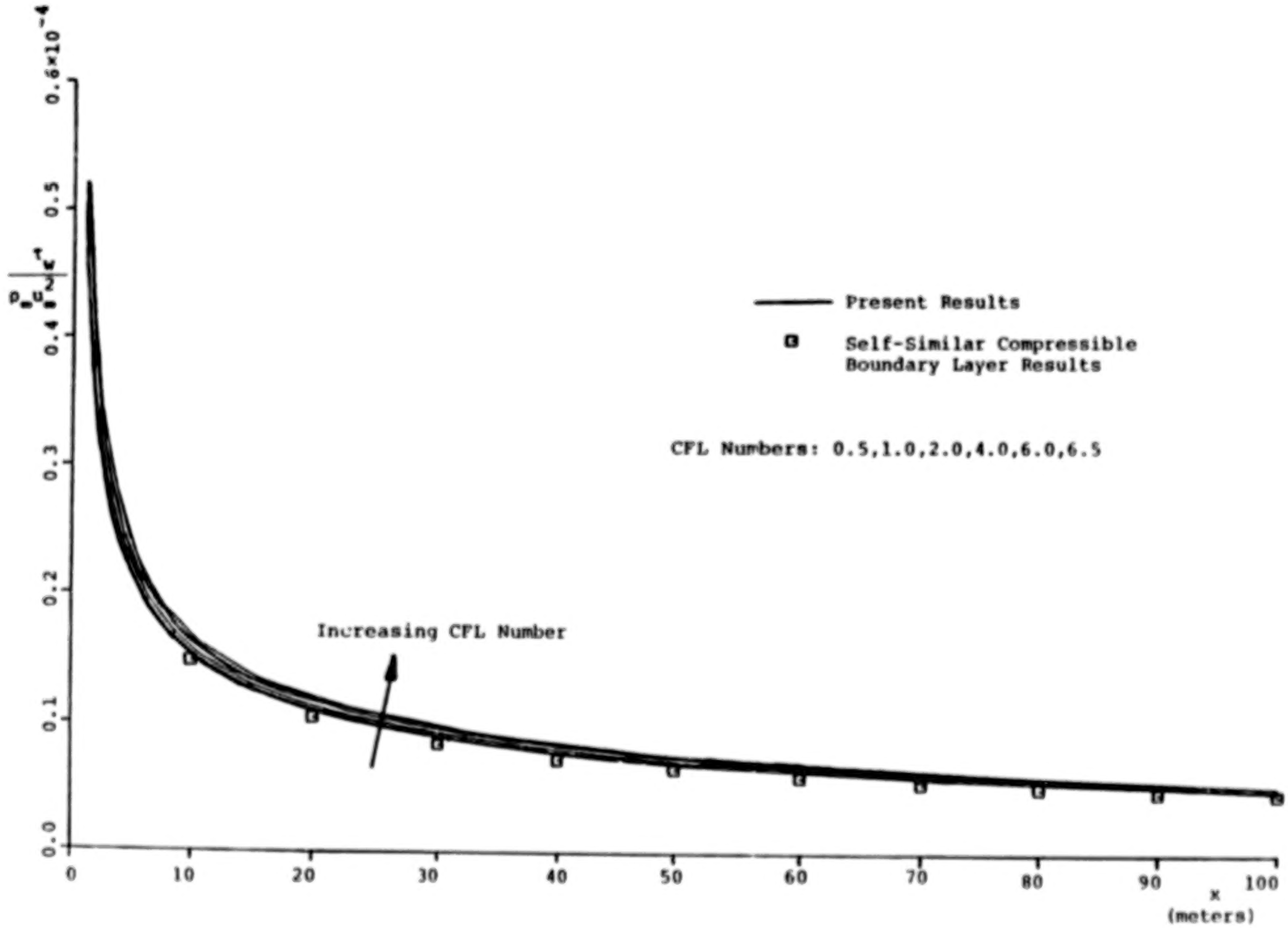

Figure 4 Wall Shear vs. x for Various CFL Numbers

Blank Page

BOUNDARY TREATMENTS FOR IMPLICIT SOLUTIONS TO EULER AND NAVIER-STOKES EQUATIONS*

W. T. Thompkins, Jr.
R. H. Bush
Massachusetts Institute of Technology

INTRODUCTION

Implicit time marching schemes like those of Beam and Warming [1], Briley and McDonald [2], and MacCormack (1980) [3] generally have not been as robust as would be expected from a stability analysis for the pure initial value problem. Recently, Yee, Beam and Warming [4] illustrated that a more general stability analysis, which includes the effect of boundary conditions, may explain some of the seemingly anomalous behavior of these schemes. The major theoretical basis for this type of modal stability analysis was established in a series of papers by Kriess [5,6], Osher [7,8] and Gustafsson et al [9].

Yee as well as Gustafsson and Oliger [10] considered the effect of inflow/outflow boundary condition formulations on the stability of a class of numerical schemes to solve the Euler equations in one-space dimension. The characteristic feature of a subsonic inflow/outflow boundary is that a priori boundary values may be specified for only some problem variables while remaining boundary values must be determined as part of the solution process. Yee demonstrated a rather large disparity in stability bounds between the use of explicit or implicit extrapolation procedures and in general demonstrated that implicit extrapolation procedures had the least restrictive stability bounds. The intent of this work is to explore computationally the implication of this work for several two-dimensional Euler and Navier-Stokes simulations. A parallel effort by Abarbanel and Murman [11] has begun the extension of the modal analysis to problems in two-space dimensions.

NUMERICAL PROCEDURES

The two-dimensional Navier-Stokes equations may be written in vector form as

$$\frac{\partial U}{\partial t} + \frac{\partial E}{\partial x} + \frac{\partial F}{\partial y} = \frac{\partial R}{\partial x} + \frac{\partial S}{\partial y} \quad . \tag{1}$$

---

*This work was partially supported by NASA Lewis Research Center under NASA Grant NAG 3-9.

where

$$U = \begin{pmatrix} \rho \\ \rho u \\ \rho v \\ E_t \end{pmatrix} \qquad E = \begin{pmatrix} \rho u \\ \rho u^2 + p \\ \rho uv \\ u(E_t + p) \end{pmatrix} \qquad F = \begin{pmatrix} \rho v \\ \rho uv \\ \rho v^2 + p \\ v(E_t + p) \end{pmatrix}$$

$$R = \begin{pmatrix} 0 \\ \tau_{xx} \\ \tau_{xy} \\ R_4 \end{pmatrix} \qquad S = \begin{pmatrix} 0 \\ \tau_{xy} \\ \tau_{yy} \\ S_4 \end{pmatrix}$$

and

$$E_t = \rho\left(e + \frac{1}{2}(u^2 + v^2)\right)$$

$$\tau_{xx} = (\lambda + 2\mu)\frac{\partial u}{\partial x} + \lambda\frac{\partial v}{\partial y}$$

$$\tau_{xy} = \mu\left(\frac{\partial u}{\partial y} + \frac{\partial v}{\partial x}\right)$$

$$\tau_{yy} = (\lambda + 2\mu)\frac{\partial v}{\partial y} + \lambda\frac{\partial u}{\partial x}$$

$$R_4 = u\,\tau_{xx} + v\,\tau_{xy} + k\,P_r^{-1}(\gamma - 1)^{-1}\frac{\partial a^2}{\partial x}$$

$$S_4 = u\,\tau_{xy} + v\,\tau_{yy} + k\,P_r^{-1}(\gamma - 1)^{-1}\frac{\partial a^2}{\partial y}$$

The strong conservation law form may be retained under a general coordinate mapping as illustrated in Viviand [12]. All computations to be described were conducted in a mapped computational domain but numerical and boundary condition procedures will be described in the simple two-dimensional geometry shown in figure 1 for simplicity.

A 1979 paper by Beam and Warming [13] outlined a solution scheme for systems of equations of the form (1) which includes most numerical schemes for which the modal boundary condition analysis has been conducted. This scheme uses the well developed methods for ordinary differential equations as a guide to developing numerical methods for partial differential equations. The scheme presented combines Linear Multistep Methods, local linearization, approximate factorization and One Leg methods. The scheme, a generalization of the scheme presented in reference [1], solves for a variable $\rho(E)U$ which is equivalent to ΔU^n in the class of schemes represented by the earlier paper. The earlier scheme is somewhat easier to understand as ΔU^n is just the change in the solution from time level n to level n+1, while $\rho(E)U$ is a more general time differencing formula.

The solution schemes chosen are implemented as:

$$(I + L_y^n)\,\Delta U^* = RHS^n \tag{2}$$

$$(I + L_x^n)\,\Delta U^n = \Delta U^* \tag{3}$$

$$U^{n+1} = U^n + \Delta U^n \tag{4}$$

where

RHS^n is very nearly the finite difference approximation to the steady state equations, and

L_x and L_y are linearized finite difference operators representing a particular time and spatial differencing scheme.

Full details of these operators are contained in Beam and Warming [1]. If the spatial differencing is taken to be centered, the computational form of either equation (2) or (3) appears at each interior point as:

$$A_i^n\,\Delta U_{i-1}^n + B_i^n\,\Delta U_i^n + C_i^n\,\Delta U_{i+1}^n = D_i^n \tag{5}$$

where A_i, B_i, and C_i are 4x4 matrices, known at time level n, and D_i is the right-hand side vector at node point i known at time level n and ΔU_i^n is the unknown vector at node point i. The boundary points will be assumed to involve only the nearest two points.

$$A_0^n\Delta U_0 + B_0^n\Delta U_1 + C_0^n\Delta U_2 = D_0^n \tag{6}$$

The full matrix equation appears as:

$$\left|\begin{array}{ccccccc} A_0 & B_0 & C_0 & 0 & 0 & \cdots & 0 \\ A_1 & B_1 & C_1 & 0 & 0 & \cdots & 0 \\ 0 & A_2 & B_2 & C_2 & 0 & \cdots & 0 \\ 0 & 0 & & & & & 0 \\ \vdots & \vdots & & A_{n-1} & & B_{n-1} & C_{n-1} \\ 0 & 0 & \cdots & A_n & & B_n & C_n \end{array}\right| \left|\begin{array}{c} \Delta U_0 \\ \Delta U_1 \\ \Delta U_2 \\ \vdots \\ \Delta U_{n-2} \\ \Delta U_{n-1} \\ \Delta U_n \end{array}\right| = \left|\begin{array}{c} D_0 \\ D_1 \\ D_2 \\ \vdots \\ D_{n-2} \\ D_{n-1} \\ D_n \end{array}\right| \tag{7}$$

and will reduce to tridiagonal form by substituting the first and nth equations into the second and the n-1th equations.

$$\begin{vmatrix} B_1' & C_1' & 0 & \cdots & 0 \\ A_2 & B_2 & C_2 & \cdots & 0 \\ 0 & & & & \vdots \\ \vdots & & & & 0 \\ & & A_{n-2} & B_{n-2} & C_{n-2} \\ 0 & \cdots & 0 & A_{n-1}' & B_{n-1}' \end{vmatrix} \begin{vmatrix} \Delta U_1 \\ \Delta U_2 \\ \vdots \\ \\ \Delta U_{n-2} \\ \Delta U_{n-1} \end{vmatrix} = \begin{vmatrix} D_1' \\ D_2 \\ \\ \\ D_{n-2} \\ D_{n-1}' \end{vmatrix} \tag{8}$$

where for example

$$B_1' = B_1 - A_1 A_0^{-1} B_0 \quad .$$

This cumbersome development allows us to show clearly how a large variety of explicit or implicit boundary forms can be included without difficulty.

BOUNDARY TREATMENTS

Inflow/Outflow Boundary

The finite difference algorithms studied usually require more boundary values than are required for the partial differential equations which they simulate. These extra numerical boundary conditions cannot be set arbitrarily and are usually determined through an extrapolation procedure. These extrapolation procedures may either be explicit, that is boundary values needed at a new time are determined uniquely from the old time level solution, or implicit, that is boundary values are determined as part of the new time level solution. The analytical boundary conditions or the extrapolation quantities are usually not conservation variables but primitive variables and a local linearization is usually required as part of defining the extrapolation procedure.

Consider, for example, an implicit, subsonic outflow boundary at which the local static pressure is specified as a boundary condition, and all other variables are to be determined by extrapolation. Figure 1 shows a typical computational grid and defines the subscripts used.

$$P_{i,j}^{n+1} = P_{i,j}^{n} \quad ; \quad \text{given} \tag{9}$$

$$\begin{pmatrix} \rho \\ \rho u \\ \rho v \end{pmatrix}_{i,j}^{n+1} = 2 \begin{pmatrix} \rho \\ \rho u \\ \rho v \end{pmatrix}_{i,j-1}^{n+1} - \begin{pmatrix} \rho \\ \rho u \\ \rho v \end{pmatrix}_{i,j-2}^{n+1} \quad \begin{array}{l} \text{implicit} \\ \text{space} \\ \text{extrapolation} \end{array} \tag{10}$$

In order to complete the boundary formulation, all equations must be expressed in delta form and in terms of conservation variables. For the total internal energy this may be done through its definition:

$$E_t = \frac{P}{(\gamma-1)} + \frac{1}{2}\left[\frac{(\rho u)^2}{\rho} + \frac{(\rho v)^2}{\rho}\right] \tag{11}$$

Since the relations between conservation variables are nonlinear, some linearization step will be necessary before the boundary condition formulation may be used. We choose to introduce our linearization step here as:

$$\Delta E_t = \left(E_t^{n+1} - E_t^{n}\right) = \frac{1}{(\gamma-1)}\,\Delta P - \frac{1}{2}\left(u^2 + v^2\right)^n \Delta\rho + u^n\Delta(\rho u)$$

$$+\ v^n\Delta(\rho v) + \quad (\Delta u\Delta v,\ \Delta u^2,\ \Delta v^2,\ \Delta\rho\Delta u,\ \Delta\rho\Delta v) \tag{12}$$

If terms of order $\Delta u\Delta v$ are neglected, the error is equivalent to the linearization error of the interior point scheme. We may express the transformation from boundary variables to conservation variables as:

$$\Delta U_{i,j} = \begin{pmatrix} \Delta\rho \\ \Delta\rho u \\ \Delta\rho v \\ E_t \end{pmatrix}_{i,j} \begin{pmatrix} 1 & 0 & 0 & 0 \\ 0 & 1 & 0 & 0 \\ 0 & 0 & 1 & 0 \\ \frac{-(u^2+v^2)^n}{2} & u^n & v^n & \frac{1}{(\gamma-1)} \end{pmatrix} \begin{pmatrix} \Delta\rho \\ \Delta\rho u \\ \Delta\rho v \\ \Delta P \end{pmatrix} = N_{i,j}\Delta W_{i,j} \tag{13}$$

We will in general denote transformation from conservative to primitive variables as

$$\Delta W_{i,j} = T_{i,j}\Delta U_{i,j} \tag{14}$$

The extrapolation conditions for $\Delta W_{i,j}$ are:

$$W_{i,J} = \begin{pmatrix} \Delta\rho \\ \Delta\rho u \\ \Delta\rho v \\ \Delta P \end{pmatrix}_{i,J} = \begin{pmatrix} 2 & 0 & 0 & 0 \\ 0 & 2 & 0 & 0 \\ 0 & 0 & 2 & 0 \\ 0 & 0 & 0 & 0 \end{pmatrix} \begin{pmatrix} \Delta\rho \\ \Delta\rho u \\ \Delta\rho v \\ \Delta P \end{pmatrix}_{i,J-1} + \begin{pmatrix} -1 & 0 & 0 & 0 \\ 0 & -1 & 0 & 0 \\ 0 & 0 & -1 & 0 \\ 0 & 0 & 0 & 0 \end{pmatrix} \begin{pmatrix} \Delta\rho \\ \Delta\rho u \\ \Delta\rho v \\ \Delta P \end{pmatrix}_{i,J-2} \tag{15}$$

or

$$\Delta W_{i,J} = P_{J-1}\Delta W_{i,J-1} + P_{J-2}\Delta W_{i,J-2} \tag{16}$$

The final equations relating the boundary conservation variables and the interior conservation variables are:

$$\Delta U_{i,J} = N^n_{i,J}\left(P_{J-1}T^n_{i,J-1}\Delta U_{i,J-1} + P_{J-2}T^n_{i,J-1}\Delta U_{i,J-2}\right) \tag{17}$$

or

$$\Delta U_{i,J} = G^n_{i,J-1}\Delta U_{i,J-1} + H^n_{i,J-2}\Delta U_{i,J-2} \tag{18}$$

With the definition of P_{J-1} and P_{J-2} given in equation (15), $T_{i,J-1}$ and $T_{i,J-2}$ are the identity matrix.

An explicit outflow boundary treatment was constructed using:

$$P^{n+1} = P^n \text{ ; given}$$

$$\begin{pmatrix} \rho \\ \rho u \\ \rho v \end{pmatrix}^{n+1}_{i,J} = \begin{pmatrix} \rho \\ \rho u \\ \rho v \end{pmatrix}^{n}_{i,J-1} \tag{19}$$

and setting $G_{i,J-1} = H_{i,J-2} = 0$.

Solid Wall Boundary Procedures

The boundary treatment procedures illustrated for inflow/outflow boundary are easily extended to cover solid walls in either inviscid or viscous flow situations. Here,

$$\Delta U_{0,j} = \begin{pmatrix} \Delta\rho \\ \Delta\rho u \\ \Delta\rho v \\ \Delta E_t \end{pmatrix} \begin{pmatrix} \gamma/T & \rho/T & 0 & \\ \gamma u/T & \rho u/T & 0 & \\ \gamma v/T & \rho v/T & 0 & Sq \\ \frac{1}{\gamma-1}+\frac{1}{2}\frac{\gamma v^2}{T} & -\frac{1}{2}\frac{\rho q}{T} & \rho q & 0 \end{pmatrix} \begin{pmatrix} \Delta P \\ \Delta T \\ \Delta q \\ \Delta u \end{pmatrix} \tag{20}$$

or

$$\Delta U_{0,j} = N^n_{0,j}\Delta W_{0,j} \tag{21}$$

where q is the velocity parallel to the wall and S is the wall slope. For the inviscid flow examples $\partial P/\partial y$, $\partial T/\partial y$ and $\partial U/\partial y$ are set equal to zero; while, for the viscous flow examples v, u, and $\partial T/\partial y$ are set equal to zero and $\partial P/\partial y$ is equal to $4/3\ \mu(\partial/\partial y^2)(v)$. All derivatives are evaluated by one-sided finite difference formulas.

As indicated by Buggeln, Briley and McDonald [14], an ADI type procedure requires boundary conditions for the intermediate step. Usually the intermediate step was in the "y" direction and the boundary conditions were applied as if the intermediate results were physical quantities; that is, the boundary conditions of equation (20) were applied to the quantities ΔU^* of equation (2).

Explicit wall boundary treatments are generated by applying the primitive variable form of equation (20) and forcing the correction matrices to be zero.

NUMERICAL RESULTS

Three geometries were selected for detailed study: an inviscid supersonic diffuser with weak oblique shock, supersonic in - supersonic out; an inviscid supersonic diffuser with a strong normal shock, supersonic in - subsonic out, and a viscous supersonic diffuser with weak oblique shock illustrating a shock-boundary layer interaction. Sketches of the geometries are shown in figures 2, 3 and 4. Solutions for each geometry were run to steady state for a range of time step size or CFL number. A typical convergence history is shown in figure 5 which shows the log of the value of the steady state residual

$$\frac{\partial E}{\partial x} - \frac{\partial R}{\partial x} + \frac{\partial F}{\partial y} - \frac{\partial S}{\partial y}$$

plotted against the iteration number. A solution was not termed stable unless the residual converged to the machine accuracy, about 1×10^{-6}.

Each geometry calculation was run with fully explicit extrapolations,

$\Delta U = 0$, and with fully implicit extrapolations, and the results summarized in Table 1.

The results for the strong shock diffuser can reasonably be compared to those of Yee, Beam and Warming [4]. They reported a CFL number stability limit between 10 and 20, while we found stability limits between 90 and 150. Thus the analysis in one-space dimension does appear to provide a sufficient condition for stability, but it may not provide a close approximation to the stability limit. However, it is essential to emphasize that the largest convergence rates were observed at time steps corresponding to CFL numbers of order 10 and that only a marginal advantage for the implicit boundary formulations was observed.

The results for the shock-boundary layer calculation are of somewhat more interest, but they demonstrate a substantial computational advantage for the implicit solid wall conditions, not for the inflow/outflow extrapolation. Here the stability boundary and the best convergence rates were observed at time step sizes corresponding to streamwise CFL numbers of 5 to 10. When using the implicit wall conditions, the algorithm stability appeared to be independent of grid spacing in the normal direction as might be hoped. When using the explicit wall condition, the algorithm stability was limited to a CFL number in the normal direction of about 500.

CONCLUSIONS

While it is difficult to generalize from only a few test examples, it does seem apparent that for inviscid calculations the differences between the explicit and implicit boundary formulations tested are far smaller than had been anticipated. In fact the most interesting result is that the time step size for maximum convergence rate is so small, CFL numbers of order 10. This also seems to be the limiting factor for viscous flow computations and new work should focus on understanding of how the convergence rate is limited or affected by boundary formulations. Since the inflow/outflow boundary treatments tested were simple extrapolations, it may easily be the case that treatments more closely representing the differential equations will prove to have superior convergence properties. However several such "improved" boundary treatments have been attempted with very disappointing results.

BLANK

PAGE

Table 1

	Weak Oblique Shock Diffuser			Strong Shock Diffuser			Shock Boundary Layer		
	CFL_x	CFL_y	Iterations to Convergence	CFL_x	CFL_y	Iterations to Convergence	CFL_x	CFL_y	Iterations to Convergence
Explicit Boundary Treatments	1.5	0.6	225	1.5	0.6	3000	1.5	125	1300
	6.0	2.4	130	6.0	2.4	1200	6.0	500	Unstable
	15.0	6.0	225	15.0	6.0	800	15.0	1250	Unstable
	45.0	18.0	500	45.0	18.0	800	45.0	3750	Unstable
	90.0	36.0	1000	90.0	36.0	1000	90.0	7500	Unstable
	150.0	60.0	3000	150.0	60.0	3000	150.0	12500	Unstable
Implicit Boundary Treatments	1.5	0.6	225	1.5	0.6	3000	1.5	125	1300
	6.0	2.4	130	6.0	2.4	950	6.0	6500	400
	15.0	6.0	225	15.0	6.0	400	15.0	1250	Unstable
	45.0	18.0	500	45.0	18.0	1000	45.0	3750	Unstable
	90.0	36.0	1000	90.0	36.0	1500	90.0	7500	Unstable
	150.0	60.0	Unstable	150.0	60.0	Unstable	150.0	12500	Unstable
	15.0	1250	250				15.0	600	Unstable

NOTE: Backward Euler Time Differencing used for all reported calculations.

REFERENCES

1. Beam, R.M. and Warming, R.F.: An Implicit Factored Scheme for the Compressible Navier-Stokes Equations. AIAA Journal, Vol 16, No. 4, April 1978, pp 393.

2. Briley, W.R. and McDonald, H.: Three Dimensional Supersonic Flow of a Viscous or Inviscid Gas. J.Comp.Phys., Vol. 19, 1975, pp 150.

3. MacCormack, R.W.: A Numerical Method for Solving the Equations of Compressible Viscous Flow. AIAA Paper 81-0110, 1980.

4. Yee, H.C., Beam, R.M. and Warming, R.M.: Stable Boundary Approximations for a Class of Implicit Schemes for the One-Dimensional Inviscid Equations of Gas Dynamics. Proc. of AIAA Computational Fluid Dynamics Conference, Paper No. 81-1009, June 1981.

5. Kreiss, H.O.: Stability Theory for Difference Approximations of Mixed Initial Boundary Value Problems. I. Mathematics of Computations. Vol. 22, 1968, pp 703-714.

6. Kreiss, H.O.: Difference Approximations for Initial Boundary Value Problems. Proceedings of the Royal Society of London, Series A, Vol. 323, 1971, pp 255-261.

7. Osher, Stanley: Systems of Difference Equations with General Homogeneous Boundary Conditions. Transactions of the American Mathematical Society, Vol. 137, 1969, pp 177-201.

8. Osher, Stanley: Stability of Difference Approximations of Dissipative Type for Mixed Initial Value Problems. I. Mathematics of Computations, Vol. 23, 1969, pp 335-340.

9. Gustafsson, B., Kreiss, H.O. and Sundstrom, A.: Stability Theory of Difference Approximations for Mixed Initial Boundary Value Problems. II. Mathematics of Computations, Vol. 26, 1972, pp 649-686.

10. Gustafsson, B. and Oliger, J.: Stable Boundary Approximations for a Class of Time Discretizations of $U_t=AD_0U$. Report No. 87, Dept. of Computer Science, Upsala U., Sweden, Sept. 1981.

11. Abarbanel, S.S. and Murman, E.M.: Stability of Two-Dimensional Hyperbolic Initial Boundary Value Problems for Explicit and Implicit Schemes. Symposium on Numerical Boundary Conditions, NASA Ames Rsch Ctr, Oct. 1981.

12. Viviand, H.: Conservation Forms of Gas Dynamic Equations. La Recherche Aerospatiale, No. 1, Jan. 1974, pp 65-68.

13. Beam, R.M. and Warming, R.F.: An Implicit Factor Scheme for the Compressible Navier-Stokes Equations. II: The Numerical ODE Connection. AIAA paper 79-1446, Williamsburg, VA, 1979.

14. Buggeln, R.C., Briely, W.R. and McDonald, H.: Solution of the Navier-Stokes Equations for Three-Dimensional Turbulent Flow with Viscous Sublayer Resolution. Proceedings of AIAA Computational Fluid Dynamics Conference, Paper No. 81-1023, June 1981.

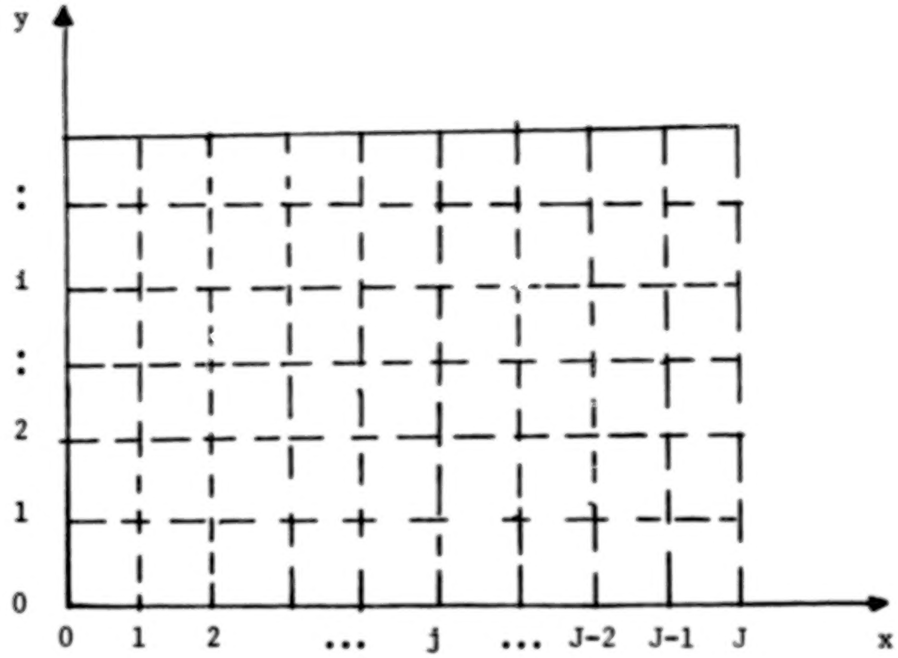
y
:
i
:
2
1
0
0
1
2
...
j
...
J-2
J-1
J
x

Figure 1. Grid Numbering Scheme for Boundary Condition Formulation

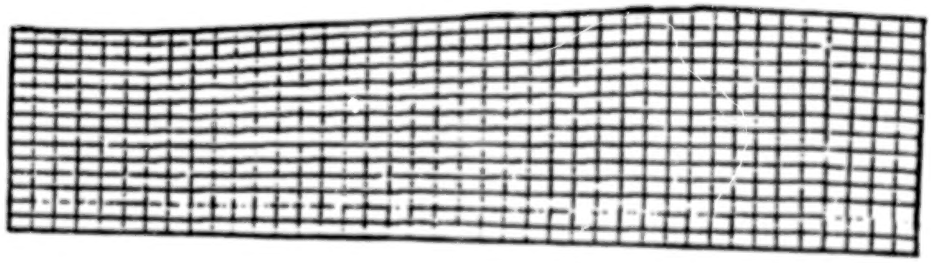

Figure 2. Computational Grid for Weak Shock Diffuser Calculations

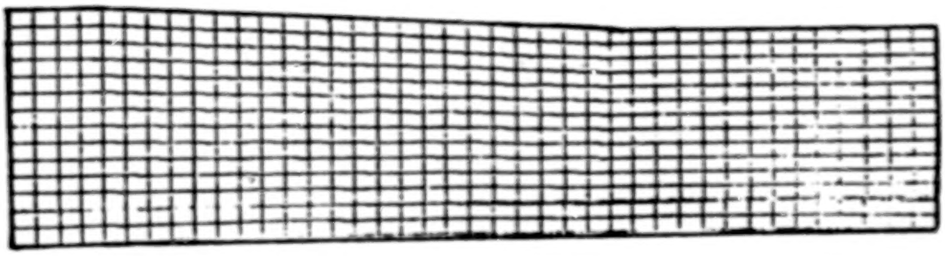

Figure 3. Computational Grid for Strong Shock Diffuser Calculations

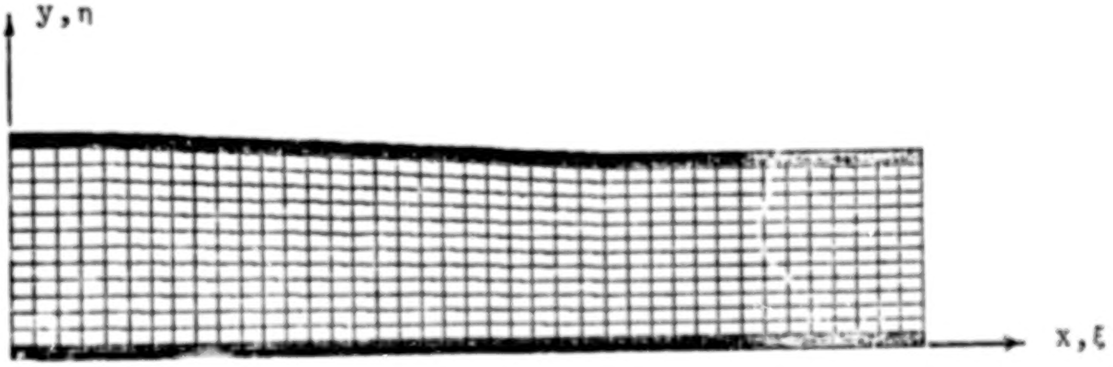

Figure 4. Computational Grid for Shock-Boundary Layer Computation

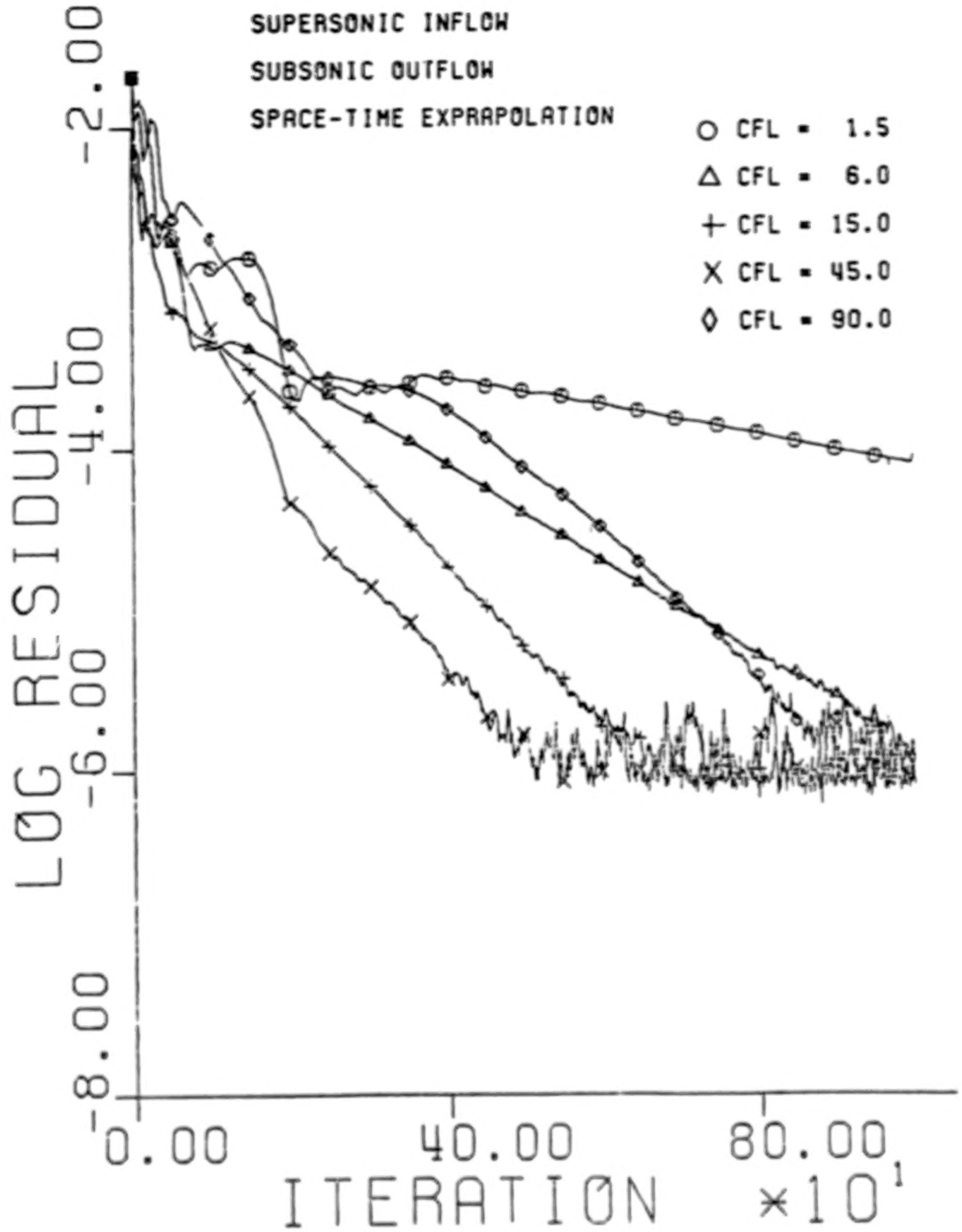

Figure 5. Convergence History for Strong Shock Diffuser Calculation

RIGOROUS NUMERICAL TREATMENT OF THE NO-SLIP CONDITION IN A VORTICITY FORMULATION

J. Gazdag
IBM Scientific Center
Palo Alto, California

Y. Takao
IBM Scientific Center
Tokyo, Japan

J. Fromm
IBM Research Laboratory
San Jose, California

Abstract

In this paper it is shown that a rigorous mathematical treatment of the boundary conditions for rigid no-slip surfaces requires, in general, that two passes be made in solving Poisson's equation. A Fourier solution procedure was the key to this realization. It is also shown that a corresponding method exists for finite differences and, for the same local approximation, the usual one step method gives the same result for the geometry considered here. The more fundamental two step method gives a new insight into the physical significance of boundary vorticity.

I. Introduction

Numerical solutions of the Navier-Stokes equations are often obtained using the so-called "primative equation" formulation. If the flow is incompressible, it is necessary to solve an elliptic equation as part of the system, and this implies some form of simultaneous solution of the entire flow region for any given time. In the primative equation case, this is usually a solution in terms of a pressure field with Neumann boundary conditions. An alternate formulation allowing Dirichlet boundary conditions is the "vorticity streamfunction" formulation. The latter has widespread use, particularly if the solution is restricted to two space dimensions.

Because the solutions are approximations, it is generally necessary to satisfy the conservation laws within the framework of the approximation and thereby provide constraints on error propagation which may lead to false solutions. Generally, but depending on the numerical method, better constraints are provided by the vorticity formulation, and hence better results are obtained.

Here we consider the mechanics of satisfying the physical conditions at a rigid surface in the vorticity formulation. Clearly the normal component of velocity much vanish at the surface, but in a Newtonian flow the tangential component likewise must vanish. The normal component condition is easily satisfied in the streamfunction solution and provides the necessary and sufficient condition for solution of Poisson's equation. In fact, the additional condition is too much, and the problem is overspecified. Thus one condition must reside with the inhomogeneous part of the equation, the vorticity. It seems natural for the no-slip condition to apply to the vorticity, and this is usual in numerical treatment. It turns out that reversed roles of the conditions are apparently more fundamental. That is, to associate the no-slip condition with the streamfunction and no wall penetration with the vorticity. This leads to an interesting insight.

This new approach came to light in the desire to obtain solutions using Fourier transforms. We consider a parallel flow problem in a rectangular reference frame with periodic lateral end boundaries. Assuming an arbitrary distribution of vorticity in the flow region and on parallel rigid boundaries, a first solution is obtained by an image calculation. The image vorticity values are of like sign to real interior values and symmetrically placed relative to a rigid boundary. This satisfies the no-slip condition at the rigid boundaries, and further the image provides an imposed periodicity. Appropriately, we thus have periodicity in both space dimensions for solution by Fourier transforms.

FORMULATION OF THE ANALYSIS-INVERSE PROBLEM

The axisymmetric transonic small disturbance equation is given by

$$\left[K - (\gamma+1)\phi_x\right]\phi_{xx} + \frac{1}{\tilde{r}}\left(\tilde{r}\phi_{\tilde{r}}\right)_{\tilde{r}} = 0 \tag{1}$$

where

$$K = (1 - M_\infty^2)/(M_\infty\tau)^2 \quad ; \quad \tilde{r} = \tau r \ .$$

The parameter τ is the thickness ratio of the body defined by $r_b(x) = \tau R_b(x)$ where $R_b(x)$ is the nondimensionalized body radius such that $R_{b,\max}(x) = 0.5$. The analysis and the inverse problem both use equation (1) and differ only in the way the boundary condition is applied at the body.

Analysis Problem

In the analysis problem the body shape $R_b(x)$ and τ are prescribed and equation (1) is solved subject to the slender body boundary condition

$$\lim_{\tilde{r}\to 0}(\tilde{r}\phi_{\tilde{r}}) = R_b R_b'(x) = S'(x) \doteq \varepsilon(\phi_{\tilde{r}})_{\tilde{r}=\varepsilon} \tag{2}$$

or

$$\lim_{\tilde{r}\to 0} \phi = S'(x)\ln(\tilde{r}) + g(x) \tag{3}$$

where $S(x) = R_b(x)^2/2$ is the nondimensional cross-sectional area divided by 2π and prime denotes differentiation with respect to x. For convenience, the boundary condition equation (2) is applied not at the actual body location (see figs. 1,2) but on a cylinder of finite small radius ε. The value of ε is chosen sufficiently away from the axis[1] to avoid the log singularity in ϕ represented by equation (3). Using a dummy point procedure as shown in figure 2 such that $(\tilde{r}_3 - \tilde{r}_2) = (\tilde{r}_2 - \tilde{r}_1)$, the finite differenced form of equation (2) at the cylinder point j=2 can be written as (the dummy point has to lie above the axis for numerical stability)

$$a\phi_3 + d\phi_2 + b\phi_1 = c \tag{4}$$

where $a = 1$, $b = -1$, $d = 0$, and $c = S'(\tilde{r}_3 - \tilde{r}_1)/\tilde{r}_2$. Similarly, the finite differenced form of equation (1) at the same cylinder point j=2 can be written as (using the transonic type dependent operator)

$$a_1\phi_3 + d_1\phi_2 + b_1\phi_1 = c_1 \ . \tag{5}$$

Combining equations (4) and (5) to eliminate the dummy point potential ϕ_1, the boundary discretization at j=2 is written as

$$\bar{a}\phi_3 + \bar{d}\phi_2 = \bar{c} \ . \tag{6}$$

In the successive line overrelaxation algorithm, equation (6) will be used to modify the coefficients of the tridiagonal matrix at the body point to bring in the analysis boundary condition. After the relaxation procedure converges the pressure coefficient $C_p(x)$ on the axisymmetric body is computed from the relation

$$(C_p)_{body} = -\tau^2\left[2S''(x)\ln(M_\infty\tau^2 R_b/\varepsilon) + 2(\phi_x)_{j=2} + (R_b')^2\right] \ . \tag{7}$$

Equation (7) has been derived by matching the outer transonic solution to an inner solution represented by equation (3). This formula includes the cross flow contribution $(R_b')^2$ which is significant near the body. The pressure coefficient at any point in the flow field (other than the body point) can be obtained from

$$C_p = -2\tau^2\phi_x \ . \tag{8}$$

This completes the analysis problem.

Inverse Problem

The main purpose of this paper is to illustrate the inverse procedure where the pressure coefficient equation (7) is prescribed and the corresponding body shape $R_b(x)$ is sought. It can be seen from equation (7) the $C_p(x)$ involves the unknown body information $S''(x)$, $R_b(x)$, and $R_b'(x)$, as well as the velocity potential ϕ. The objective here is to solve equations (1) and (7) at the cylinder point j=2 and compute the resulting body shape $R_b(x)$ by satisfying the body boundary condition, equation (2). There are two ways to implement equation (7) at the body point. One is a Neumann type treatment and the other is a Dirichlet formulation. Both will now be described.

Neumann boundary condition – In this formulation, equation (7) will be used to get an estimate for $(\phi_{\tilde{r}})$ at the cylinder point j=2 from the prescribed C_p distribution. Knowing this $\phi_{\tilde{r}}$ at j=2, the problem can be treated as an analysis boundary condition (just like eq. (2)). In the real analysis problem, $\phi_{\tilde{r}}$ at j=2 is given and held fixed during the calculation, but in this Neumann type inverse problem, $\phi_{\tilde{r}}$ at j=2 will be changing during the transient calculation and convergence critically depends on the representation of equation (7) as a pseudo-time dependent process.

First, the pressure relation given by equation (7) will be rewritten in terms of ϕ as much as possible in the following way by replacing S" and R_b' terms

$$S'(x) = R_b R_b' = \lim_{r \to 0}(\tilde{r}\phi_{\tilde{r}}) = \varepsilon(\phi_{\tilde{r}})_{\tilde{r}=\varepsilon} \ . \tag{9}$$

From equation (9), we can write

$$\left.\begin{aligned} S''(x) &= \varepsilon(\phi_{\tilde{r}x})_{\tilde{r}=\varepsilon} \\ R_b'(x) &= (\varepsilon/R_b)(\phi_{\tilde{r}})_{\tilde{r}=\varepsilon} \ . \end{aligned}\right\} \tag{10}$$

Substituting equation (10) into equation (7) we get

$$(C_p)_{body} = -\tau^2\Big[2\varepsilon\phi_{\tilde{r}x}\ \ln(M_\infty\tau^2R_b/\varepsilon) + 2\phi_x + (\varepsilon/R_b)^2(\phi_{\tilde{r}})^2\Big] \ . \tag{11}$$

In order to finite difference equation (11), the nonlinear square term $(\phi_{\tilde{r}})^2$ will first be linearized by considering each relaxation iteration cycle as a marching procedure in the pseudo time direction t as in Jameson's[6] analysis.

$$\begin{aligned} (\phi_{\tilde{r}}^2)^{n+1} &\doteq (\phi_{\tilde{r}}^2)^n + 2\phi_{\tilde{r}}\phi_{\tilde{r}t}\Delta t + \cdots \\ &\doteq (\phi_{\tilde{r}}^2)^n + 2\phi_{\tilde{r}}^n(\phi_{\tilde{r}}^{n+1} - \phi_{\tilde{r}}^n) + \cdots \\ &\doteq 2\phi_{\tilde{r}}^n\phi_{\tilde{r}}^{n+1} - (\phi_{\tilde{r}}^2)^n \ . \end{aligned} \tag{12}$$

Substituting equation (12) into equation (11) the prescribed C_p can be written in the form

$$(-C_p/\tau^2) = A\phi_{\tilde{r}x} + B\phi_{\tilde{r}t} + C\phi_x + D \tag{13}$$

where $A = 2\varepsilon\ \ln(M_\infty\tau^2R_b/\varepsilon)$, $B = 2(\varepsilon^2/R_b^2)\phi_{\tilde{r}}^n$, $C = 2$, $D = (\varepsilon^2/R_b^2)(\phi_{\tilde{r}}^n)^2$, and n represents the previous cycle value. Interpreting the difference scheme for equation (13) as a representation of a time-dependent process, for the evolution of $(\phi_{\tilde{r}})$, equation (13) has a solution of the form

$$(\phi_{\tilde{r}})^{n+1} \sim e^{-(A/B)t} \tag{14}$$

where $t = n\Delta t$. Whether this Neumann type (eq. (13)) treatment will converge or not depends on the sign and magnitude of (A/B) in equation (14). If (A/B) is negative at some point on the cylinder j=2, then $\phi_{\tilde{r}}$ will grow as the relaxation process continues and will diverge eventually. A stable iteration scheme for equation (13) can be devised by adding a temporal damping term $\beta\phi_{rt}$ to alter the form of the solution to

$$(\phi_{\tilde{r}})^{n+1} \sim e^{-[A/(B+\beta)]t} \ . \qquad (15)$$

The sign and magnitude of β can be chosen in such a way $[A/(B+\beta)]$ remains positive at all points on the cylinder j=2. Usually A and B vary along the cylinder and change signs and use of β is very critical to achieve a convergent solution for $\phi_{\tilde{r}}$. When β is set to zero, the inverse calculations usually diverged within 10 iteration cycles, but when an appropriate β value was chosen at each cylinder point under inverse mode, the calculations remained stable.

Dirichlet formulation – In the Dirichlet procedure, equation (7) is used to get an estimate for the velocity potential ϕ at the cylinder point j=2. This potential is then imposed as a Dirichlet boundary condition while solving equation (1) at the point above the cylinder (j=3 in fig. 2). From the given prescribed C_p distribution and assuming the previous body shape, a value for ϕ_x is first computed from equation (7) and then integrated to get ϕ at the cylinder point j=2. To ensure numerical stability, the quantity ϕ_x obtained from equation (7) was usually underrelaxed. The amount of underrelaxation was based on how often the body shape changes were updated in the C_p relation, equation (7).

Both the Neumann and Dirichlet inverse formulations as reported here proved to be successful. However, it was found that the Dirichlet method was more robust and always yielded converged results much sooner than the Neumann treatment. The inverse results to be reported here were obtained using the Dirichlet method.

RESULTS

The results presented here were performed using the LBL CDC 7600 machine and a (90 × 40) grid in the $(x,\tilde{r})$ plane. Analysis calculations typically required 500 iterations and the subsequent inverse calculations needed 300 iterations for a convergence level of 10^{-4} to 10^{-5} change in ϕ between any two consecutive iterations.

Figure 3 shows the pressure distribution over a parabolic arc of revolution at $M_\infty = 0.98$ and $\tau = 0.167$. The analysis calculation using a dummy point procedure (the cylinder point located at $\tilde{r} = 0.0075$ and the dummy point at $\tilde{r} = 0.006$) shows the pressure of a shock wave on the body at $x/\ell \sim 0.75$. The C_p on the body was computed using equation (7) while the pressure distributions in the flow field as shown in figure 3 were computed using equation (8). An estimate of the drag was made by computing the integral

$$\overline{C}_D = \int_0^1 S'(x/\ell)C_p d(x/\ell) \ . \tag{16}$$

When multiplied by an appropriate nondimensionalization factor, the quantity $\overline{C}_D$ would provide the actual inviscid drag coefficient. For the case shown in figure 3, the value of $\overline{C}_D$ came out to be 0.0462, representing a sizeable wave drag. The shocked pressured distribution of figure 3 was modified to a shockless pressure as shown in figure 4 and used as an input to the axisymmetric inverse code. The inverse calculations were started from the converged analysis results of figure 3 and after 300 inverse iterations the body shape and the flow field is converged to less than 10^{-4} accuracy. The resulting body shape is shown in figure 4 and indicates a flattening of the body surface to avoid the formation of a shock. The flow field pressure distributions as shown in figure 4 also indicate that specification of a shockless pressure on the body seems to eliminate the shock away from the body also. The associated $\overline{C}_D$ estimate for the new body is 0.0269 which is considerably less than that exhibited by the original body.

Figure 5 shows two design studies indicating a gradual flattening of the body due to increasingly mild specified shockless pressure distributions.

The real test of the inverse code comes when the designed body is run in an analysis mode to verify if the specified pressures are recovered. Figure 6 shows the performance of the designed shockless body of figure 4 in an analysis mode. The pressure distribution that came out of the analysis code did indeed check very well with the specified pressures in figure 4.

Shockless bodies at a given design point are usually very sensitive to off design conditions. This is illustrated in figure 7. When the shockless body of figure 4 was run at an off design Mach number of 0.99, the shock wave appeared at $x/\ell \sim 0.85$. However, the strength of the shock and the resulting $\overline{C}_D$ were smaller than that for the original body at the same off design Mach number.

Figure 8 shows another test case using the inverse code. First, an analysis calculation was performed on a parabolic arc-circular cylinder body of revolution (parabolic arc for $0 \leq x/\ell \leq 0.5$, and constant cylinder for $x/\ell \geq 0.5$) at $M_\infty = 0.98$ and $\tau = 0.167$. The resulting pressure distribution shows the presence of a weak shock near the shoulder region ($x/\ell \sim 0.5$). The pressure was modified to reflect a no shock situation. The resulting designed body is not appreciably different from the original body but those slight modifications are critical to eliminate the weak shock. Figure 8 also shows a table comparing the ordinates of the original body and the designed body. The drag estimate is considerably less for the modified body ($\overline{C}_D = 0.00115$) than the original body ($\overline{C}_D = 0.011$). The entire analysis-inverse calculation usually takes 25 seconds of CPU time on the CDC 7600 machine.

Sometimes, specification of an arbitrary pressure can lead to an unphysical or unacceptable base area. One can construct optimization type routines within this inverse methodology whereby the specified pressures can be altered systematically to achieve a more desirable base area. This idea will be pursued in the future, along with extensions of this work to design favorably interfering wing-body configurations using an equivalent body of revolution model.

REFERENCES

1. Krupp, J.A. and Murman, E.M., "Computation of Transonic Flows Past Lifting Airfoils and Slender Bodies," AIAA Journal, Vol. 10, No. 7, 1972.

2. Chan, Y.Y., Mundie, D.L., and Jones, D.J., "Transonic Axisymmetric Bodies with Minimal Wave Drag," Canadian Aeronautics and Space Journal, Vol. 26, No. 3, 1980.

3. Whitcomb, R.T., "A Study of the Zero Lift Drag Rise Characteristics of Wing Body Combinations Near the Speed of Sound," NACA Report 1273 (1956).

4. Oswatitsch, K. and Keune, F., "Ein Äquivalensatz fur Nichtangestellte Flugl Kleiner Spannweite in Schallnaher Strömung," Zeitschrift fur Flugwissenshaften 3 Jahrgung Heft 2, February 1955, S. 29-46.

5. Shankar, V., Malmuth, N.D., and Cole, J.D., "Computational Transonic Inverse Procedure for Wing Design," AIAA Paper 80-1390, presented at the AIAA 13th Fluid and Plasma Dynamics Conference, Snowmass, Colorado, July 14-16, 1980. Also to appear in AIAA Journal.

6. Jameson, A., "Iterative Solution of Transonic Flows over Airfoils and Wings Including Flows at Mach 1," Communications of Pure and Applied Mathematics, Vol. 27, 1974, pp. 283-309.

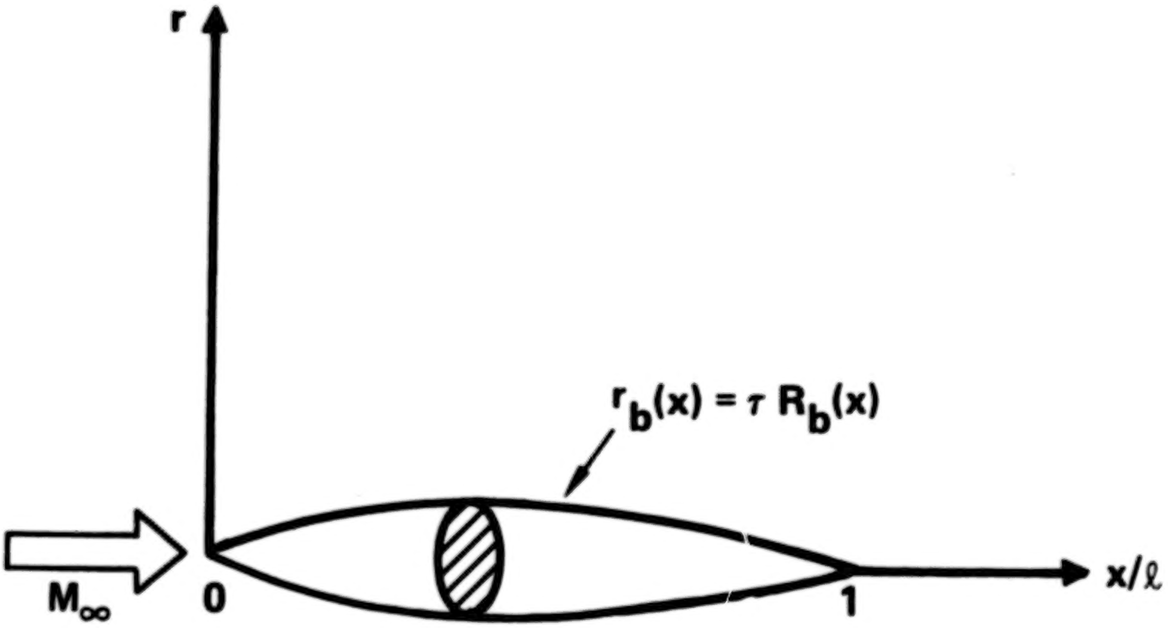
r
$r_b(x) = \tau R_b(x)$
M_∞
0
1
x/ℓ

Figure 1. — Axisymmetric body definition.

BLANK

PAGE

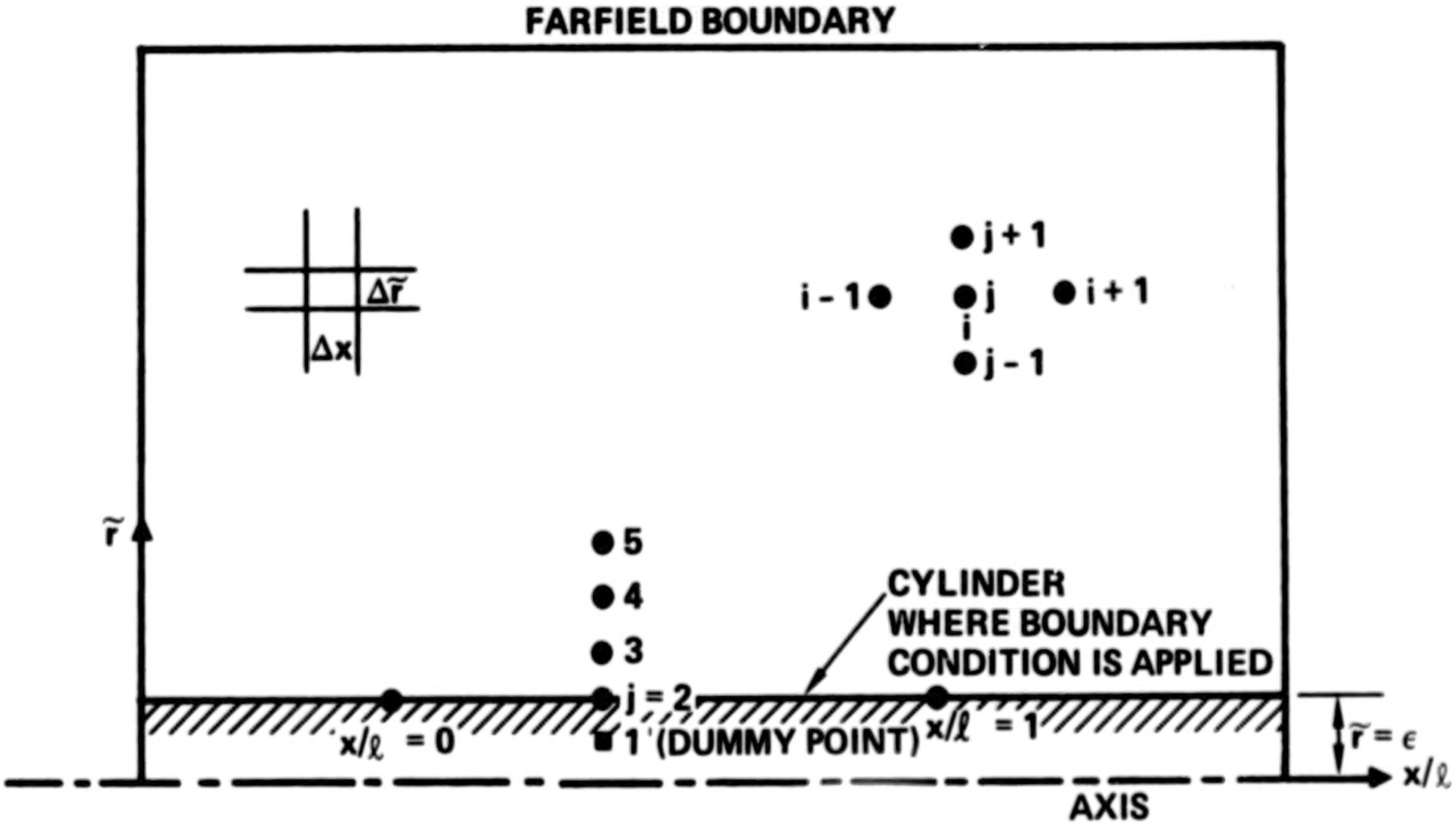
FARFIELD BOUNDARY
$\Delta\tilde{r}$
Δx
j + 1
i - 1
j
i + 1
i
j - 1
$\tilde{r}$
5
4
3
CYLINDER WHERE BOUNDARY CONDITION IS APPLIED
j = 2
x/ℓ = 0
1 (DUMMY POINT)
x/ℓ = 1
$\tilde{r} = \epsilon$
x/ℓ
AXIS

Figure 2. – Dummy point treatment for boundary condition procedure.

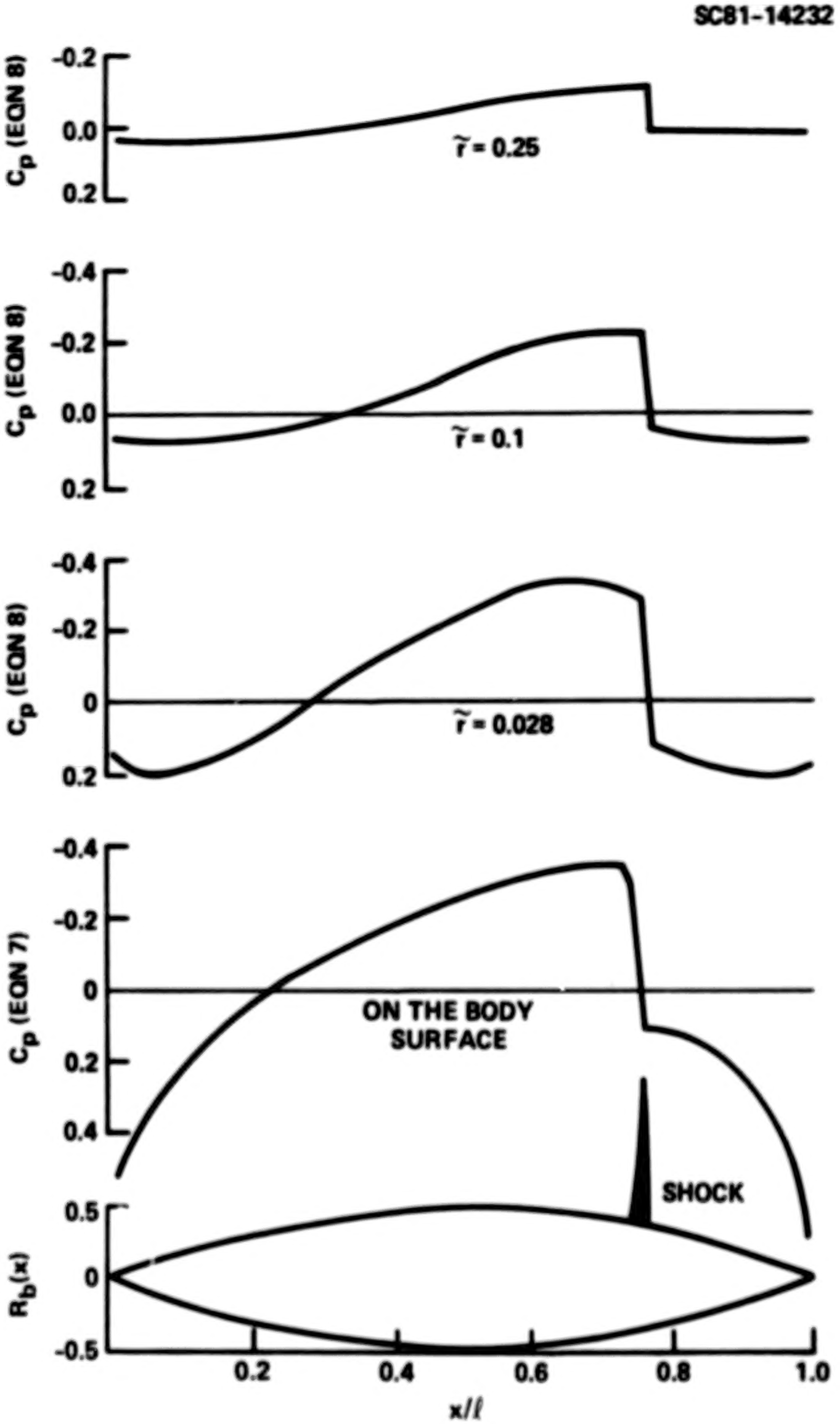

Figure 3. — Surface and flow field pressure distribution for parabolic arc of revolution, $M_\infty = 0.98$, $\tau = 0.167$, $\overline{C}_D = 0.0462$.

SC81-14234

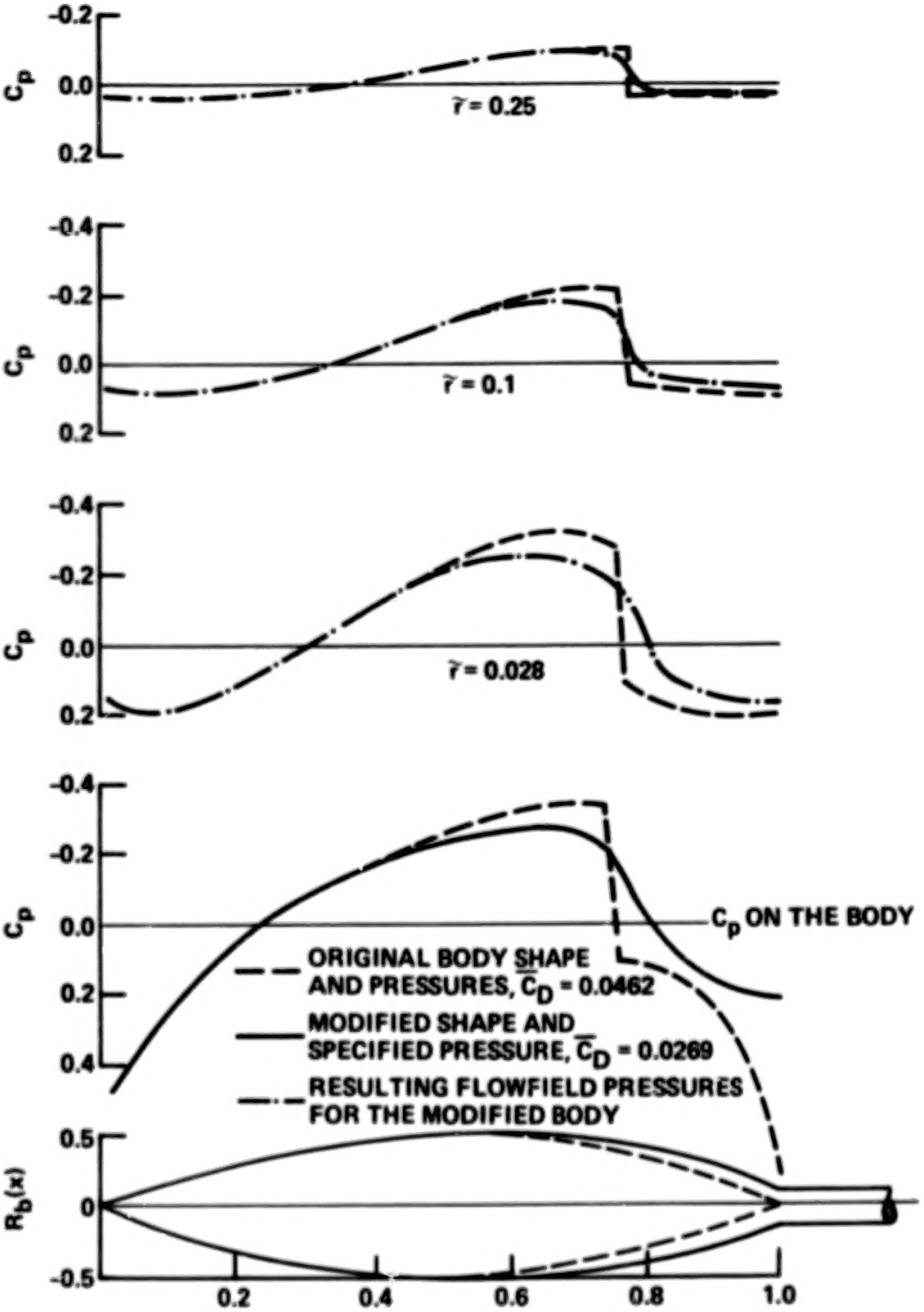

Figure 4. — Shockless modified pressure distribution specified and the resulting body shape, M_∞ = 0.98, τ = 0.1673.

SC81-14231

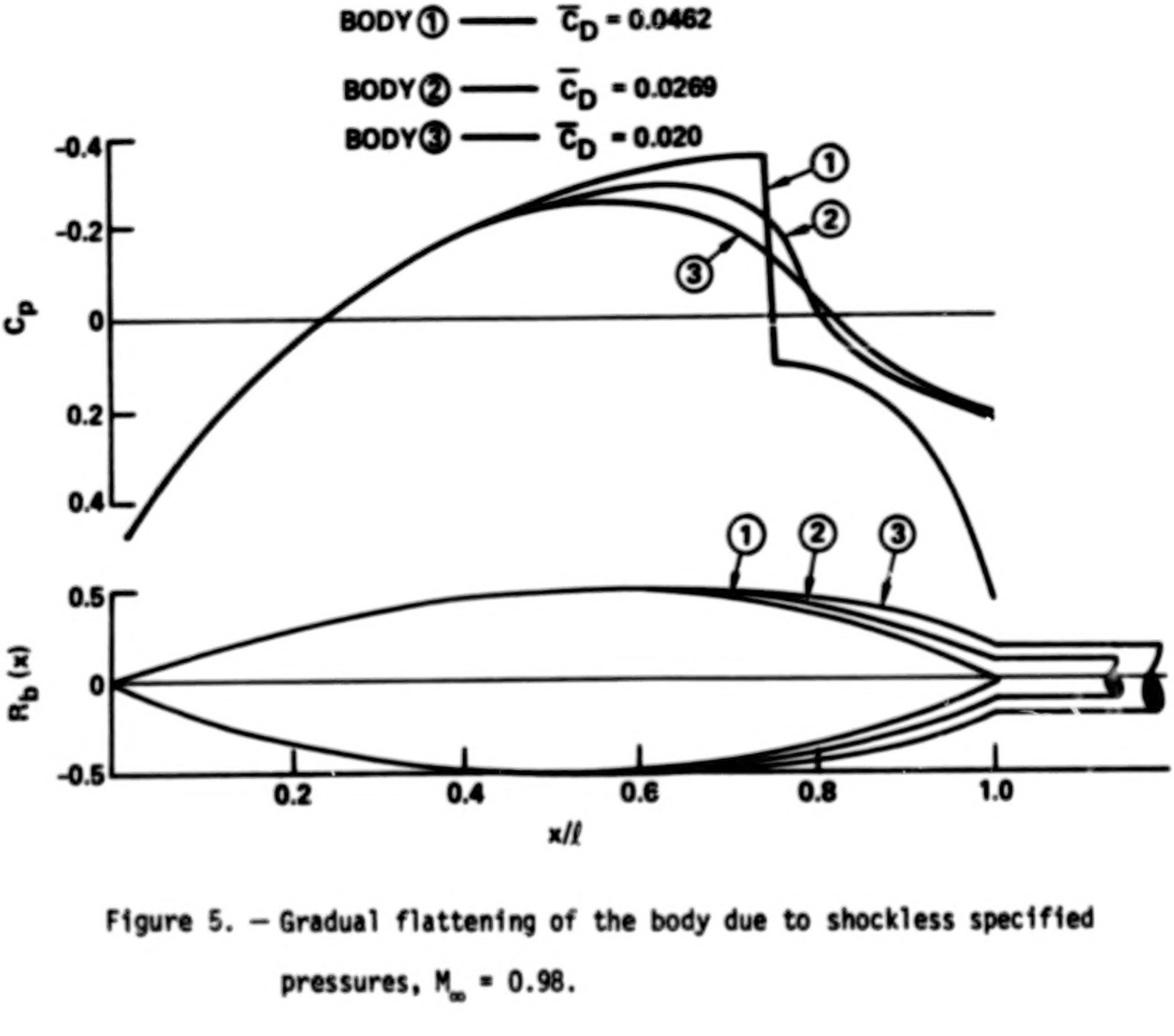

Figure 5. — Gradual flattening of the body due to shockless specified pressures, M_∞ = 0.98.

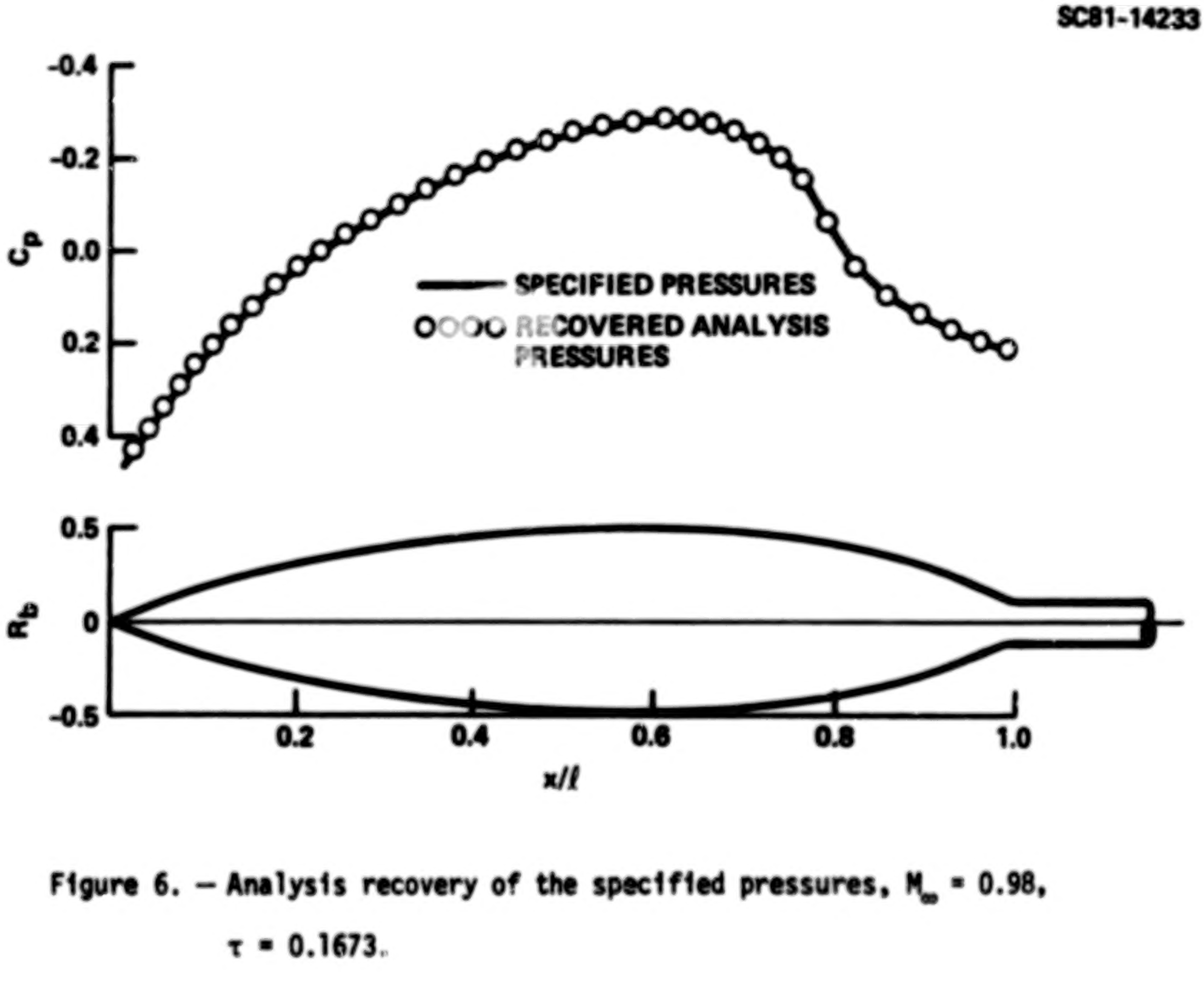

Figure 6. — Analysis recovery of the specified pressures, $M_\infty = 0.98$, $\tau = 0.1673$.

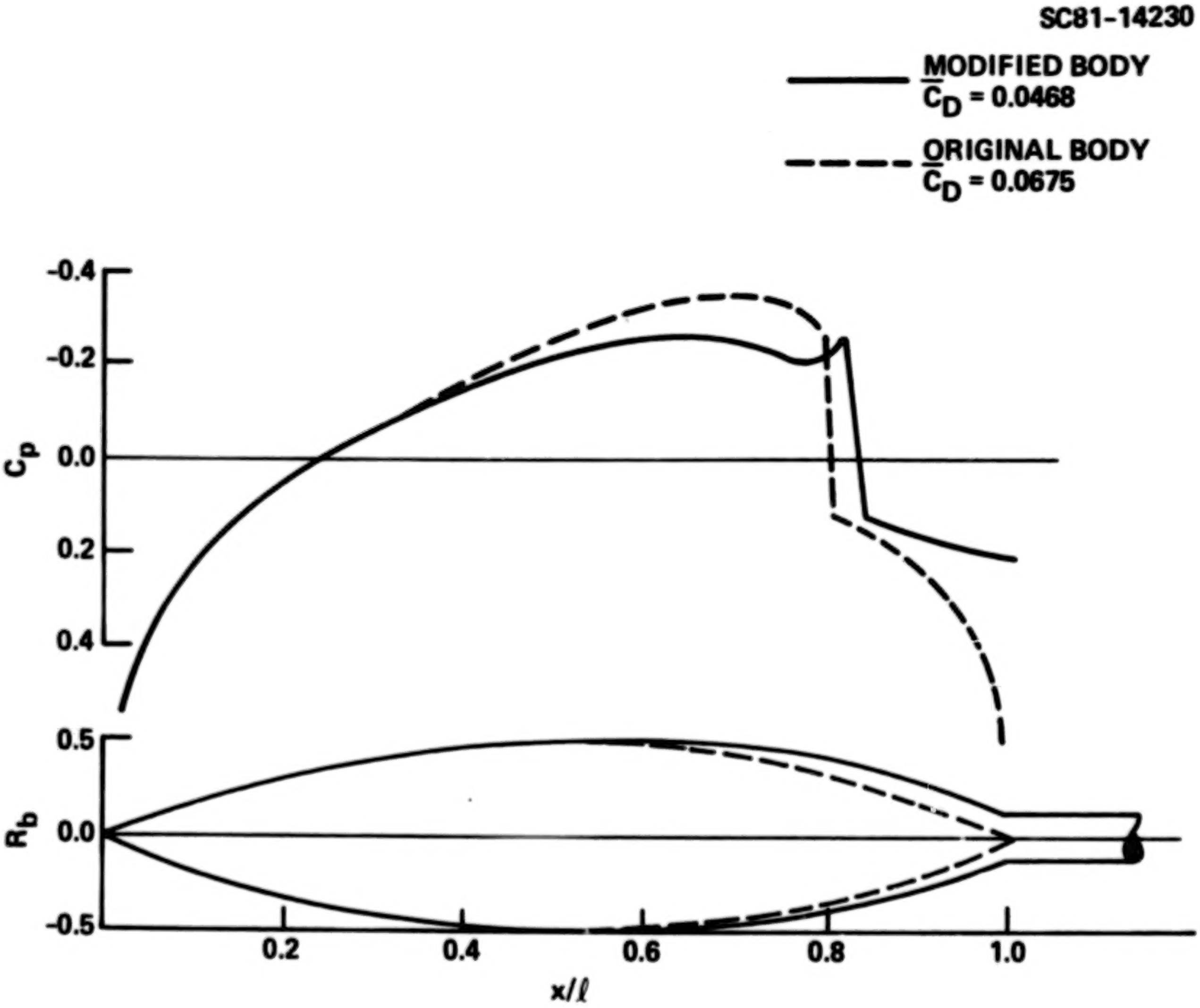

Figure 7. — Off design performance of the original and modified body, $M_\infty = 0.99$, $\tau = 0.167$.

SC81-14229

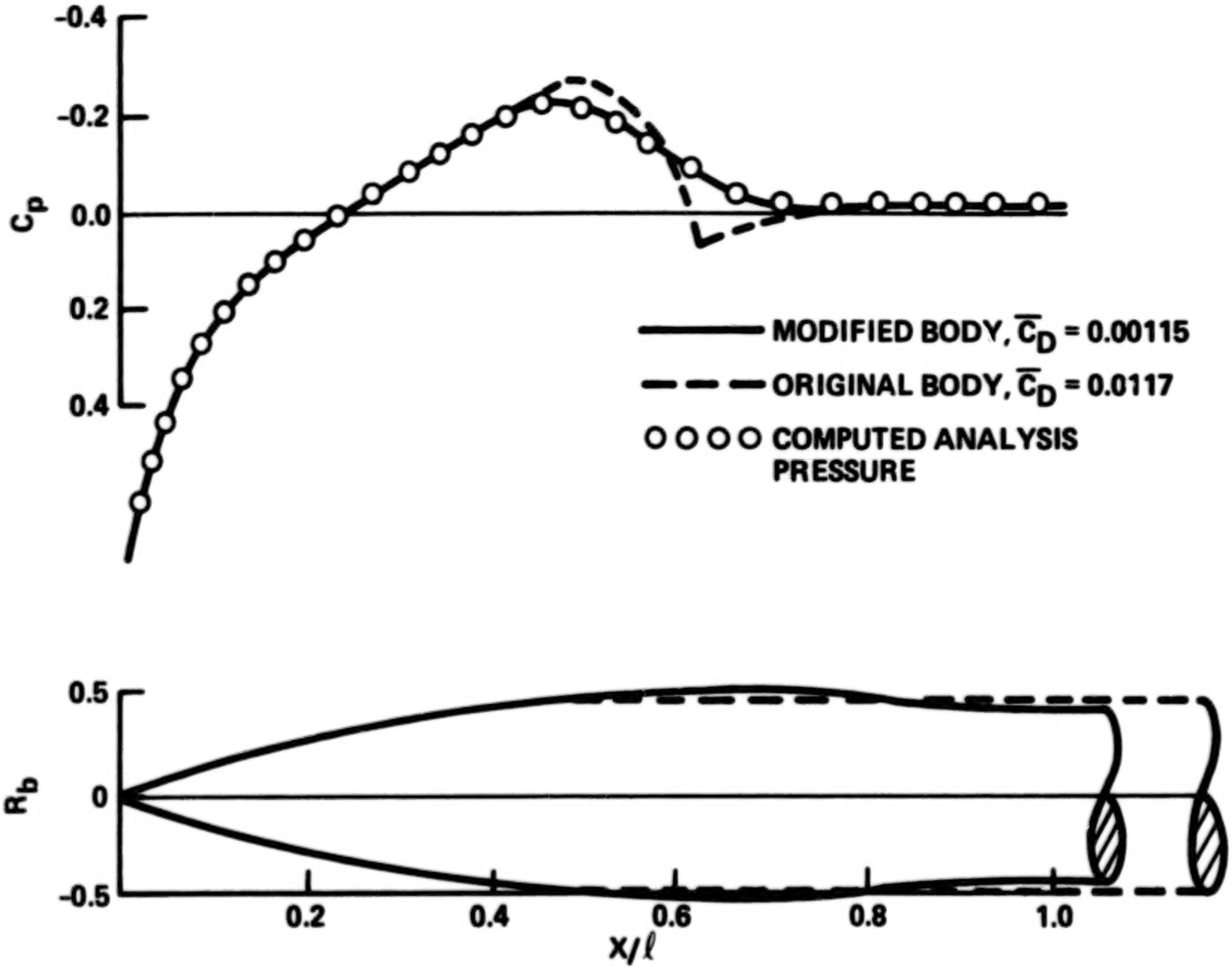

X/ℓ	$2R_b$ ORIGINAL	$2\ R_b$ NEW
0.391	0.9521	0.9517
0.545	1.000	1.0137
0.70	1.000	1.0218
0.859	1.000	0.9947
0.945	1.000	0.97984
0.96	1.000	0.9771
0.975	1.000	0.9742
0.990	1.000	0.9711
1.00	1.000	0.9694

Figure 8. — Drag reduction for a parabolic arc-cylinder body of revolution, $M_\infty = 0.98$, $\tau = 0.167$.

Blank Page

STABILITY OF TWO-DIMENSIONAL HYPERBOLIC INITIAL BOUNDARY VALUE PROBLEMS FOR EXPLICIT AND IMPLICIT SCHEMES*

Saul S. Abarbanel
Tel-Aviv University

Earll M. Murman
Massachusetts Institute of Technology

SUMMARY

The paper discusses stable and unstable boundary conditions for various explicit and implicit schemes for the linear two-dimensional wave equations. A modal analysis is used to analyze stability.

INTRODUCTION

Recently much more attention has been given to the effect of boundary conditions on the overall stability of finite-difference calculations employing schemes which are stable for the pure initial value problem. The basic theoretical approach was established in a series of papers by Kriess (refs 1, 2), Osher (ref 3,4), Gustafsson et al (ref 5) and others. Surveys of these and more recent developments can be found in Yee (ref 6) and Coughran (ref 7).

More recently Gustafsson and Oliger (ref 8) and Yee, Beam and Warming (ref 9) considered, among other things, the scalar-outflow boundary condition (i.e. the numerical boundary condition which cannot be specified for the original p.d.e. problem but must be given for the system of difference equations) in the case of a class of one-dimensional algorithms given by

$$\rho(E)U_j^n = \Delta t\sigma(E)\left(\frac{U_{j+1}^n - U_{j-1}^n}{2\Delta x}\right) \tag{1a}$$

where E is the shift operator defined by $EU_j^n = U_j^{n+1}$, and $\rho(E)$ and $\sigma(E)$ are defined by

$$\rho(E) = (1+\xi)E^2 - (1+2\xi)E + \xi \tag{1b}$$

$$\sigma(E) = \theta E^2 + (1-\theta+\phi)E - \phi. \tag{1c}$$

---

*This work was partially supported by the Air Force Office of Scientific Research (NAM), United States Air Force under Grant AFOSR-80-0249, and by NASA Cooperative Agreement NCC1-45, while the senior author was visiting MIT; partially by NASA Contracts NAS1-15810 and NAS1-14101 at ICASE, NASA Langley Research Center, Hampton, VA 23665; and by NASA Grant NGT 22-009-901.

This class of algorithms contains both explicit and implicit schemes. For example, $\xi = -1/2$, $\theta = \phi = 0$ yields the leap-frog method and $\xi = \phi = 0$, $\theta = 1$ yields the backward Euler schemes. One may find tables listing other combinations in references (8, 9). The methods defined by equations (1) solve numerically the linear partial differential equation

$$U_t = U_x \;. \tag{2}$$

The constant coefficient of U_x was absorbed, without loss of generality, by "stretching" the coordinate x.

For the present study we consider the p.d.e.

$$U_t = \frac{\partial}{\partial x} F(U) + \frac{\partial}{\partial y} G(U) \tag{3}$$

in the half space $0 \leq x < \infty$, $-\infty < y < \infty$, $(t>0)$, where for the purpose of the (linear) stability consideration we may set $F = G = U$, and $\lambda = \Delta t/\Delta x = \Delta t/\Delta y$. Within the limitation of linear stability analysis this assumption is not severe since by "stretching" the x, y and t coordinates one may account for different (constant) coefficients in the partial differential equation (3).

We investigate the effect of imposing at $x = 0$ the same type of extrapolations considered by Yee, Beam and Warming (ref 9) and Gustafsson and Oliger (ref 10). The analytical results are obtained for the 2-D explicit Burstein (ref 10, 11) and MacCormack (ref 12) schemes and for the implicit backward Euler and Crank-Nicolson schemes. The results are summarized in the following sections.

STABILITY OF TWO-DIMENSIONAL EXPLICIT SCHEMES

We first consider the two-step explicit algorithm due to Burstein (ref 10, 11). It is second order accurate both in time and space and is given by

$$U^{n+1/2}_{j,k} = \mu_x\mu_y U^n_{j,k} + \frac{\Delta t}{2}\left(\delta_x\mu_y U^n_{j,k} + \delta_y\mu_x U^n_{j,k}\right) \tag{4a}$$

$$U^{n+1}_{j,k} = U^n_{j,k} + \Delta t \left(\delta_x\mu_y U^{n+1/2}_{j,k} + \delta_y\mu_x U^{n+1/2}_{j,k}\right) \tag{4b}$$

The difference operators δ_x and δ_y are defined by
$\delta_x U^n_{j,k} = (U^n_{j+1/2,k} - U^n_{j-1/2,k})/\Delta x$ and $\delta_y U^n_{j,k} = (U^n_{j,k+1/2} - U^n_{j,k-1/2})/\Delta y$.
The averaging operators μ_x and μ_y are defined by
$\mu_x U^n_{j,k} = (U^n_{j+1/2,k} + U^n_{j-1/2,k})/2$ and $\mu_y U^n_{j,k} = (U^n_{j,k+1/2} + U^n_{j,k-1/2})/2$. For the pure initial value problem the stability condition is $\lambda \leq 1/\sqrt{2}$.

At this point we would like to describe briefly the procedure for checking stability for the initial-boundary value problem in the half-space. The analysis is based on assuming that the finite difference equations have solutions of the type

$$U_{j,k}^{n} = z^{n}\kappa^{j}e^{ik\eta} \qquad (5)$$

where the indices n,j,k are those appearing in the finite difference schemes and $i=\sqrt{-1}$. For $|\kappa| < 1$; $|z| > 1$ indicates instability and $|z| < 1$ establishes stability. If we get a solution such that $|z| = |\kappa| = 1$, we will check the origin of this solution, i.e. how does a perturbation in κ affect z.

Substituting equation (4a) into (4b) and using equation (5) one gets after some manipulations the following characteristic equation:

$$\kappa(z - 1) = \frac{\lambda}{4}(\kappa-1)(\kappa+1)(1+\cos\eta) + \frac{\lambda^2}{2}\left((\kappa^2+1)\cos\eta - 2\kappa\right)$$
$$+ i\,\frac{\lambda}{4}(\kappa+1)^2\sin\eta + i\,\frac{\lambda^2}{2}(\kappa-1)(\kappa+1)\sin\eta . \qquad (6)$$

Consider first the space extrapolation type of boundary condition:

$$U_{0,k}^{n+1} = 2U_{1,k}^{n+1} - U_{2,k}^{n+1} \qquad (7)$$

where $j = 0$ is the boundary point. Substituting equation (5) into equation (7) we obtain the resolvent equation:

$$(\kappa - 1)^2 = 0 \text{ , or } \kappa = 1 . \qquad (8)$$

Using equation (8) in equation (6) gives

$$z = 1 - \lambda^2(1 - \cos\eta) + i\lambda\sin\eta$$

or

$$|z|^2 = 1 - 2\lambda^2(1 - \cos\eta) + \lambda^4(1-\cos\eta)^2 + \lambda^2\sin^2\eta.$$

The "worst" case is for $\lambda = 1/\sqrt{2}$, leading to

$$|z|^2 = 1 - \frac{1}{4}(1 - \cos\eta)^2 \leq 1 . \qquad (9)$$

We thus get our
Result 1: The 2-D Burstein scheme (eq 4), under the implicit boundary condition (eq 7), is stable.

Note, however, that the boundary condition (eq 7) is not the only way to generalize the analogous 1-D condition.

$$U_{0}^{n+1} = 2U_{1}^{n+1} - U_{2}^{n+1} . \qquad (10)$$

Boundary condition (eq 7) is a generalization of equation (10) which is taken in a direction normal to the boundary $x = 0$. A more general analogy to equation (10) would be taken in a skewed direction, for example

$$U_{0,k}^{n+1} = 2U_{1,k+1}^{n+1} - U_{2,k+2}^{n+1} . \tag{11}$$

In fact, sometimes such "skewed" extrapolations are indeed used. For example, if a shock wave intersects the boundary at some angle, near the intersection skewed extrapolation is sometimes used to avoid differencing across the shock. We now ask what is the effect of equation (11) on the stability of the Burstein scheme (eq 4). Using equation (5) in equation (11) we get

$$(\kappa e^{i\eta} - 1)^2 = 0 \quad \text{or} \quad \kappa = e^{-i\eta} . \tag{12}$$

We will now show

Result 2: The 2-D Burstein scheme (eq 4) under the skewed boundary condition (eq 11) is unstable. It will suffice to provide a counter example to stability. Take $\eta = \pi$ i.e., from equation (12), $\kappa = -1$. Equation (6) becomes $z = 1$ since $\sin\eta = 0$ and $\cos\eta = -1$. We thus have to invoke the perturbation procedure around $\kappa = -1$, $z = 1$. Set

$$z = 1 + \varepsilon \quad , \quad \kappa = -1 - \delta$$

and substitute into equation (6). A simple calculation shows that $\delta = \pm(\sqrt{2}/\lambda)\sqrt{\varepsilon} + O(\varepsilon/\lambda^2)$, and we have instability.

Another type of boundary condition considered in references (8) and (9) was the space time extrapolation

$$U_0^{n+1} = 2U_1^n - U_2^{n-1} . \tag{13}$$

Its "normal" and "skewed" generalizations to the two-dimensional case are, respectively

$$U_{0,k}^{n+1} = 2U_{1,k}^n - U_{2,k}^{n-1} \tag{14}$$

and

$$U_{0,k}^{n+1} = 2U_{1,k+1}^n - U_{2,k+2}^{n-1} \tag{15}$$

leading to $\kappa = z$ and $\kappa = ze^{-i\eta}$ respectively. Computations analogous to those carried above yield similar results; namely

Result 3: The 2-D Burstein (eq 4) scheme under the boundary condition (eq 14) is stable.

Result 4: The 2-D Burstein (eq 4) scheme under the boundary condition (eq 15) is unstable.

Next we consider the 2 step 2-D MacCormack scheme (ref 12)

$$\begin{aligned}
U^{*}_{j,k} &= U^{n}_{j,k} + \lambda(U^{n}_{j+1,k} - U^{n}_{j,k}) + \lambda(U^{n}_{j,k+1} - U^{n}_{j,k}) \\
U^{**}_{j,k} &= U^{*}_{j,k} + \lambda(U^{*}_{j,k} - U^{*}_{j-1,k}) + \lambda(U^{*}_{j,k} - U^{*}_{j,k-1}) \\
U^{n+1/2}_{j,k} &= (1/2)(U^{n}_{j,k} + U^{**}_{j,k}) \\
U^{\dagger}_{j,k} &= U^{n+1/2}_{j,k} + \lambda(U^{n+1/2}_{j,k} - U^{n+1/2}_{j-1,k}) + \lambda(U^{n+1/2}_{j,k} - U^{n+1/2}_{j,k-1}) \qquad (16) \\
U^{\dagger\dagger}_{j,k} &= U^{\dagger}_{j,k} + \lambda(U^{\dagger}_{j+1,k} - U^{\dagger}_{j,k}) + \lambda(U^{\dagger}_{j,k+1} - U^{\dagger}_{j,k}) \\
U^{n+1}_{j,k} &= \frac{1}{2}(U^{n+1/2}_{j,k} + U^{\dagger\dagger}_{j,k})
\end{aligned}$$

which is stable for the pure initial value problem under the condition $\lambda \leq 1$.

Substituting equation (5) into equation (16) gives the characteristic equation

$$z = \left[1 + \frac{\lambda}{2}(\kappa - \frac{1}{\kappa}) + \frac{\lambda^2}{2}(\kappa + \frac{1}{\kappa} - 2)\right]\left[1 + i\lambda \sin\eta - \lambda^2(1 - \cos\eta)\right] \qquad (17)$$

Modal analysis carried out as above yields
Result 5: The MacCormack scheme (eq 16) is stable under all the above mentioned boundary conditions (eqs 7, 11, 14, and 15).

STABILITY OF THE TWO-DIMENSIONAL IMPLICIT SCHEMES

The 2-D implicit backward Euler scheme that solves equation (3) may be written as

$$U^{n+1}_{j,k} = U^{n}_{j,k} + \Delta t(\delta_x\mu_x + \delta_y\mu_y)U^{n+1}_{j,k} \ . \qquad (18)$$

Usually, however, it is put in a time-split, or approximate-factorization form*

$$(1 - \Delta t\delta_x\mu_x)(1 - \Delta t\delta_y\mu_y)U^{n+1}_{j,k} = U^{n}_{j,k} \ . \qquad (19)$$

---

*It may be shown that all forthcoming results hold also for the non-split form of the difference equations. Also, putting equation (19) in the delta-form will not change the linear-stability considerations.

Substituting equation (5) into equation (19) gives the characteristic equation

$$z\left[1 - \frac{\lambda}{2}\left(\kappa - \frac{1}{\kappa}\right)\right]\left[1 - i\lambda \sin\eta\right] = 1 \ . \tag{20}$$

We now consider equation (20) under the various boundary conditions (eqs 7, 11, 14 and 15). The computations for the case of equation (7) are trivial and we get from equation (20)

$$z(1 - i\lambda \sin\eta) = 1 \ . \tag{21}$$

For $\eta = 0$ equation (21) reduces to the 1-D case that was shown to be stable (see ref 8). For $0 < \eta < \pi$, the factor $(1 - i\lambda \sin\eta)$ is greater than 1 in magnitude and hence $|z| < 1$ for that case. There remains to examine the case $\eta = \pi$, in which case we get $z = \kappa = 1$. The perturbation procedure of putting $z = 1 + \varepsilon, \kappa = 1 + \delta$, $\eta = \pi$ into equation (20) leads directly to $\varepsilon = \lambda\delta$ and hence to our

Result 6: The 2-D backward Euler scheme (eq 18) under the boundary condition (eq 7) is stable.

Next consider the skewed extrapolation (eq 11), i.e. $\kappa = e^{-i\eta}$ and take $\eta = \pi$, i.e. $\kappa = -1$. We find again that $z = 1$. Now we have to perturb about $z = 1$, $\kappa = -1$, $\eta = \pi$. Substituting $z = 1 + \varepsilon$, $\kappa = -1 - \delta$ into equation (20) gives $\varepsilon = -\lambda\delta$ and thus,

Result 7: The 2-D backward Euler scheme (eq 18) under the boundary condition (eq 11) is unstable.

Next consider the space-time extrapolation (eq 14). Again, since the factor $(1 - i\lambda \sin\eta)$ is at most unity, the 1-D analysis holds and we have

Result 8: The 2-D backward Euler scheme (eq 18) under the boundary condition (eq 14) is stable.

For the skewed space time extrapolation (eq 15) we put (for $\eta = \pi$) $z = \kappa e^{-i\eta} = -\kappa$. Substitution into equation (20) yields a quadratic equation in z whose solutions are $z = 1$ and $z = -1 - (2/\lambda)$. Since $|\kappa| = |z|$ the second the second root is stable, but we also have to investigate once more the case $z = 1$, $\kappa = -1$. The calculation is identical to that which led to Result 7 and thus we have

Result 9: The 2-D backward Euler scheme (eq 18) under the boundary condition (eq 15) is unstable.

The 2-D implicit Crank-Nicolson scheme has the following time-split form

$$\left(1 - \frac{\Delta t}{2}\,\delta_x\mu_x\right)\left(1 - \frac{\Delta t}{2}\,\delta_y\mu_y\right)U^{n+1}_{j,k} = \left(1 + \frac{\Delta t}{2}\,\delta_x\mu_x\right)\left(1 + \frac{\Delta t}{2}\,\delta_y\mu_y\right)U^{n}_{j,k} \ . \tag{22}$$

Using equation (5) leads to the characteristic equation

$$z\left(1-\frac{\lambda}{4}\left(\kappa-\frac{1}{\kappa}\right)\right)\left(1-\frac{i\lambda}{2}\sin\eta\right)=\left(1+\frac{\lambda}{4}\left(\kappa-\frac{1}{\kappa}\right)\right)\left(1+\frac{i\lambda}{2}\sin\eta\right)\ . \qquad (23)$$

Analysis completely analogous to that carried in the preceding section gives also analogous results, namely:

Result 10: The 2-D Crank-Nicolson scheme (eq 22) under boundary condition (eq 7) is stable.

Result 11: The 2-D Crank-Nicolson scheme (eq 22) under boundary condition (eq 11) is unstable.

Result 12: The 2-D Crank-Nicolson scheme (eq 22) under boundary condition (eq 14) is stable.

Result 13: The 2-D Crank-Nicolson scheme (eq 22) under boundary condition (eq 15) is unstable.

SUMMARY

The present study applies modal analysis to the two-dimensional linear wave equation in half space in order to investigate the effect on numerical stability of outflow-type boundary conditions.

The boundary conditions under investigation may be considered as 2-D generalizations of 1-D ones which were studied by Gustafsson and Oliger (ref 8). This generalization is not unique. Thus, for example, the space-time extrapolation in 1-D, equation (13), may be considered as extrapolation along the characteristic. The true characteristic extrapolation in 2-D is the skewed boundary condition equation (15), but we also consider its projection on the x-t plane, equation (14).

We consider the boundary conditions for four typical algorithms. Two of them are explicit (Burstein and MacCormack) and two are implicit (backward Euler and Crank-Nicolson).

The major results may be summarized as follows:

(i) The boundary conditions equations (7) and (14) in which the extrapolation is taken normal to the y-t plane are stable for all cases. In this sense they seem to be the proper generalization from the 1-D case.

(ii) The boundary conditions equations (11) and (15) in which the extrapolation is taken along the characteristic, (eq 15), or its projection on the t-constant plane, (eq 11), are unstable for all schemes except the split MacCormack. This may be explained by noting that for the pure-initial value problem the Burstein, backward Euler and Crank-Nicolson algorithms are not dissipative at the point $\xi=\eta=\pi$; ξ,η being the dual Fourier variables. The MacCormack scheme however is strictly dissipative, i.e. its amplification factor, G, is less than unity for all $0<\xi,\eta\leq\pi$ (at $\xi=\eta=0$ consistency demands that $G=1$).

Gas dynamic computations require solving sets of nonlinear equations represented by equation (3). It is expected, however, that the results of the modal analysis of the linearized model equation will help in the selection of stable numerical boundary conditions. A parallel study at MIT by Thompkins and Bush (ref 13) is presented elsewhere in these proceedings. The study involves the solution of the 2-D Euler equations for cascade geometries using a backward Euler scheme which is unconditionally stable for the linear pure initial value problem. When some extrapolation boundary conditions are done explicitly the computations are unstable for Courant numbers exceeding about 2. However, when all extrapolation boundary conditions are done implicitly and normal to the boundary (i.e. not skewed), stability is improved to the point that the maximum practical Courant number is limited by other factors. In an unpublished study by Thompkins and Tong, calculations for the same geometry and equations but using the explicit MacCormack scheme have shown the characteristic extrapolation normal to the boundary [represented by equation (14) in the present study] is stable. These computational results in agreement with the modal analysis are encouraging.

REFERENCES

1. Kreiss, H.O.: Stability Theory for Difference Approximations of Mixed Initial Boundary Value Problems. I. Mathematics of Computations. Vol. 22, 1968, pp 703-714.

2. Kreiss, H.O.: Difference Approximations for Initial Boundary Value Problems. Proceedings of the Royal Society of London, Series A, Vol. 323, 1971, pp 255-261.

3. Osher, Stanley: Systems of Difference Equations with General Homogeneous Boundary Conditions. Transactions of the American Mathematical Society, Vol. 137, 1969, pp 177-201.

4. Osher, Stanley: Stability of Difference Approximations of Dissipative Type for Mixed Initial Value Problems. I. Mathematics of Computations, Vol. 23, 1969, pp 335-340.

5. Gustafsson, B., Kreiss, H.O. and Sundstrom, A.: Stability Theory of Difference Approximations for Mixed Initial Boundary Value Problems. II. Mathematics of Computations, Vol. 26, 1972, pp 649-686.

6. Yee, H.C.: Numerical Approximations of Boundary Conditions with Applications to Inviscid Equations of Gasdynamics. NASA TM-81265, 1981.

7. Coughran, W.M.: On the Approximate Solution of Hyperbolic Initial Boundary Value Problems. Thesis, Stanford U., Stanford, CA. June 1980.

8. Gustafsson, B. and Oliger, J.: Stable Boundary Approximations for a Class of Time Discretizations of $U_t=AD_0U$. Report No. 87, Dept. of Computer Science, Upsala U., Sweden, Sept. 1980.

9. Yee, H.C., Beam, R.M. and Warming, R.M.: Stable Boundary Approximations for a Class of Implicit Schemes for the One-Dimensional Inviscid Equations of Gas Dynamics. Proceedings of the AIAA Computational Fluid Dynamics Conference, Paper No. 81-1009, June 1981.

10. Burstein, S.Z.: Higher Order Accurate Difference Methods in Hydrodynamics. Nonlinear Partial Differential Equations. Ed. F. Ames. Academic Press, N.Y. 1967. pp 279-290.

11. Burstein, S.Z.: Finite Difference Calculations for Hydrodynamic Flows Containing Discontinuities. Journal of Computational Physics, Vol. 2, 1967, pp 198-222.

12. MacCormack, R.W. and Paulley, A.J.: Computational Efficiency Achieved by Time Splitting of Finite Difference Operators. AIAA Paper No. 72-154, 1972.

13. Thompkins, William T. Jr. and Bush, Robert H.: Boundary Treatments for Implicit Solutions to Euler and Navier-Stokes Equations. Symposium on Numerical Boundary Conditions, at NASA-Ames Research Center, Oct. 1981.

Blank Page

(Invited paper)

The choice of numerical boundary conditions for hyperbolic systems

by

Bertil Gustafsson
Uppsala University
Department of Computer Science

Abstract. In this paper we will discuss two fundamental problems for mixed initial-boundary-value problems with applications in fluid mechanics. First different stability properties are discussed, which are of importance for long time integrations and steady state calculations. Secondly we introduce a new numerical technique for problems with an artificial boundary.

1. Introduction

The general term stability for a difference approximation to a time dependent problem can be given many different intepretations. For ordinary differential equations there are presently so many different kinds of stability defined, that the alphabet seems to be too short for the one-letter type labeling starting with A-stability. For partial differential equations there are fewer definitions. All the different stability definitions for O.D.E.s can of course be applied to a P.D.E. once the discretization in space has been made. In fact, the procedure of semi-discretization followed by the use of a standard O.D.E. solver for the resulting time-dependent system

$$\frac{\partial u}{\partial t} = Pu \tag{1}$$

has gained popularity. For this so called "method of lines", the O.D.E.-stability theory is frequently used. However, one must be aware that system (1) depends on the step-size h, and the number of equations is unbounded when we consider arbitrary small h.

When one is interested in the solution over large time-intervals, or when a time dependent method is used for obtaining a steady-state solution, all methods which allow growing solutions are of course useless. On the other hand, a method which for a given fixed step-size gives solutions which converge to a steady state solution, might have very bad stability properties. Recently Yee, Beam and Warming [8] defined P-stability for initial-boundary-value problems, such that stability holds in the sense of Gustafsson, Kreiss and Sundström [4] (Definition 3.3) and furthermore such that (almost) no growing solutions are allowed. The last condition is made precise by requiring that the operator Q in the difference scheme written in one-step form

$$u^{n+1} = Qu^{n} \tag{2}$$

has no eigenvalues outside the unit circle.

In this paper we will analyze these matters further for general hyperbolic initial-boundary-value problems. Sufficient conditions are given such that all the eigenvalues to Q are all inside the unit circle.

If the equations are defined on a domain which is unbounded in space, the most common computational techniques are based on the introduction of an artificial boundary. If the hyperbolic system has characteristics pointing into the computational domain, then extrapolation-procedures do not work well as was shown in [5]. The construction of stable and convenient conditions at artificial boundaries has been considered by many authors. Engquist and Majda [2] designed absorbing boundary conditions, Hedstrom [6] constructed a similar type. Rudy and Strikwerda [7] considered the steady state problem for the Navier-Stokes equations, and managed to speed up the convergence rate by introducing a parameter in the boundary condition. Bayliss and Turkel [1] derived a down-stream boundary condition for the Euler equations using the acymptotic behaviour of the wave equation.

In Section 3 we will introduce a new numerical technique, which is based on the very natural requirement that the solution remains bounded on the infinite domain. It is applied to the down-stream boundary problem in fluid dynamics for the Euler equations. The full report on this latter work will be presented in a joint work with Lars Ferm [3].

2. Stability

It is well known that the numerical boundary conditions for a hyperbolic problem may introduce instabilities to a difference approximation which is stable for the Cauchy-problem. One reason to this sensitivity is that the energy of the true solution is almost conserved, the only dissipation is created through the boundary. As an example, consider the simple problem

$$(3) \qquad \left\{ \begin{array}{ll} u_t = u_x \quad , & 0 \le x \le 1 \quad , \quad 0 \le t \\ u(1,t) = 0 & \\ u(x,0) = f(x) & \end{array} \right.$$

With the norm defined by

$$||u||^2 = \int_0^1 u(x,t)^2 dx$$

we get immediately

$$(4) \qquad \frac{d}{dt}||u||^2 = -u(0,t)^2$$

A semi-discrete approximation is

$$(5) \qquad \left\{ \begin{array}{ll} \frac{\partial u_j}{\partial t} = D_0 u_j \quad , & j = 1,2,\ldots,N-1 \\ u_N(t) = 0 & \\ u_j(0) = f_j \quad , & j = 0,1,\ldots,N \end{array} \right.$$

where D_0 is the usual centered difference operator. An extra boundary condition is required at $j = 0$, and we use zero order extrapolation

(6) $$u_0(t) = u_1(t)$$

With the norm defined by

$$||u||^2 = \sum_{j=1}^{N-1} u_j(t)^2 h$$

a simple calculation shows

(7) $$\frac{d}{dt}||u||^2 = - u_1(t)u_0(t) = - u_0(t)^2$$

which is completely analogous to (4).
However, the accuracy of (6) is too low, and we may consider second order extrapolation

(8) $$u_0(t) = 2u_1(t) - u_2(t) \quad .$$

With the norm defined as above, we get

(9) $$\frac{d}{dt}||u||^2 = - u_1(t)^2 - u_1(t)(u_1(t) - u_2(t))$$

The last term destroys our estimate, and the sign of the right hand side is unknown. The extra boundary condition (8) has introduced the possibility of an increasing energy represented by the norm chosen. This does not mean that the difference scheme is unstable, it can be shown that with another choice of norm, we get the energy-dissipation back. The example only serves as an illustration of the sensitivity of the approximation to the choice of boundary conditions. The situation becomes even worse for the fully discretized problem. For example, if a centered difference operator is used also in time resulting in the Leap-frog scheme, it is well known that if the operator P in (1) has eigenvalues in the left half-plane, there is a growing mode in the solutions to (2). This again does not by itself necessarily mean that the scheme is unstable, but in this case it can be shown by the normal mode analysis that it really is.

Sometimes it is argued that a sufficient test would be to compute the eigenvalues μ of the matrix Q in (2) and make sure that there is none outside the unit circle and only simple ones on the unit circle. The following example shows the insufficiency of such a procedure.

The Lax-Wendroff scheme for the model equation $u_t = u_x$ is

$$u_j^{n+1} = (I + kD_0 + \frac{k^2}{2} D_+D_-)u_j^n \quad , \quad j = 1,2,\dots,N-1$$

where D_+ and D_- are the forward and backward difference operators respectively. Instead of specifying the value at $j = N$, we reverse the boundary conditions used above and obtain

$$\begin{cases} u_0^n = 0 \\ u_N^n = u_{N-1}^n \end{cases}$$

This simulates an extrapolation procedure at a subsonic down-stream boundary, and an overspecification at a subsonic inflow boundary, see [5]. The resulting matrix representation of the operator Q in (2) is

$$Q = \begin{bmatrix} 1-\lambda^2 & \frac{\lambda}{2}+\frac{\lambda^2}{2} & & & & 0 \\ -\frac{\lambda}{2}+\frac{\lambda^2}{2} & \ddots & \ddots & & & \\ & -\frac{\lambda}{2}+\frac{\lambda^2}{2} & 1-\lambda^2 & \frac{\lambda}{2}+\frac{\lambda^2}{2} & & \\ & & \ddots & \ddots & \ddots & \\ 0 & & & -\frac{\lambda}{2}+\frac{\lambda^2}{2} & 1-\lambda^2 & \frac{\lambda}{2}+\frac{\lambda^2}{2} \\ & & & & -\frac{\lambda}{2}+\frac{\lambda^2}{2} & 1+\frac{\lambda}{2}-\frac{\lambda^2}{2} \end{bmatrix}$$

where $\lambda \leq 1$ is the ratio between the timestep k and the space step h. The eigenvectors $(v_1,v_2,\ldots,v_{N-1})^T$ must satisfy the relations

$$\begin{cases} (-1+\lambda)\,\frac{\lambda}{2}\,v_{j-1} + (1-\lambda^2)v_j + (1+\lambda)\frac{\lambda}{2}\,v_{j+1} = \mu v_j \quad , \\ \qquad\qquad\qquad\qquad\qquad\qquad j=1,2,\ldots,N-1 \\ v_0 = 0 \\ v_N = v_{N-1} \end{cases}$$

The first equation is an ordinary difference equation which has the solution

$$v_j = \sigma_1\kappa_1{}^j + \sigma_2\kappa_2{}^j \quad , \quad \kappa_1 \neq \kappa_2 \tag{10}$$

where κ_1,κ_2 are the roots of

$$(-1+\lambda)\,\frac{\lambda}{2} + (1-\lambda^2)\kappa + (1+\lambda)\,\frac{\lambda}{2}\,\kappa^2 = \mu\kappa \tag{11}$$

The boundary conditions imply

$$(12) \qquad \begin{cases} \sigma_1 + \sigma_2 = 0 \\ (\kappa_1^N - \kappa_1^{N-1})\sigma_1 + (\kappa_2^N - \kappa_2^{N-1})\sigma_2 = 0 \end{cases}$$

An eigenvector and corresponding eigenvalue μ exists if and only if this system has a non-trivial solution, and the condition for this is

$$(13) \qquad \kappa_1^N - \kappa_1^{N-1} = \kappa_2^N - \kappa_2^{N-1}$$

A straightforward calculation using (11) shows that if N is odd, all the eigenvalues μ are strictly inside the unit circle. Therefore the solutions u^n will **eventually** die out as n goes to infinity, and there might be a temptation to consider the scheme as stable for odd N. However, if an inhomogenous term is introduced simulating rounding errors

$$(14) \qquad \tilde{u}_j^{n+1} = Q\tilde{u}_j^n + \varepsilon_j^n \quad ,$$

the scheme behaves very ill. The finer mesh that is used (of course keeping the mesh-ratio λ), the worse the solutions becomes, as can be seen in fig 1.

The reason is that the scheme is unstable which is easily shown by the normal mode analysis [5]. It is sufficient to study each boundary separately, and in order to analyze the effect of the second condition in (10), we can as well define the corresponding approximation for $u_t = - u_x$:

$$(15) \qquad \begin{cases} u_j^{n+1} = (I - kD_0 + \frac{k^2}{2} D_+D_-)\, u_j^n \quad , \quad j = 1,2,\ldots \\ u_0^n = u_1^n \\ \sum\limits_{j=0}^{\infty} (u_j^n)^2 h < \infty \end{cases}$$

The normal mode analysis is analogous

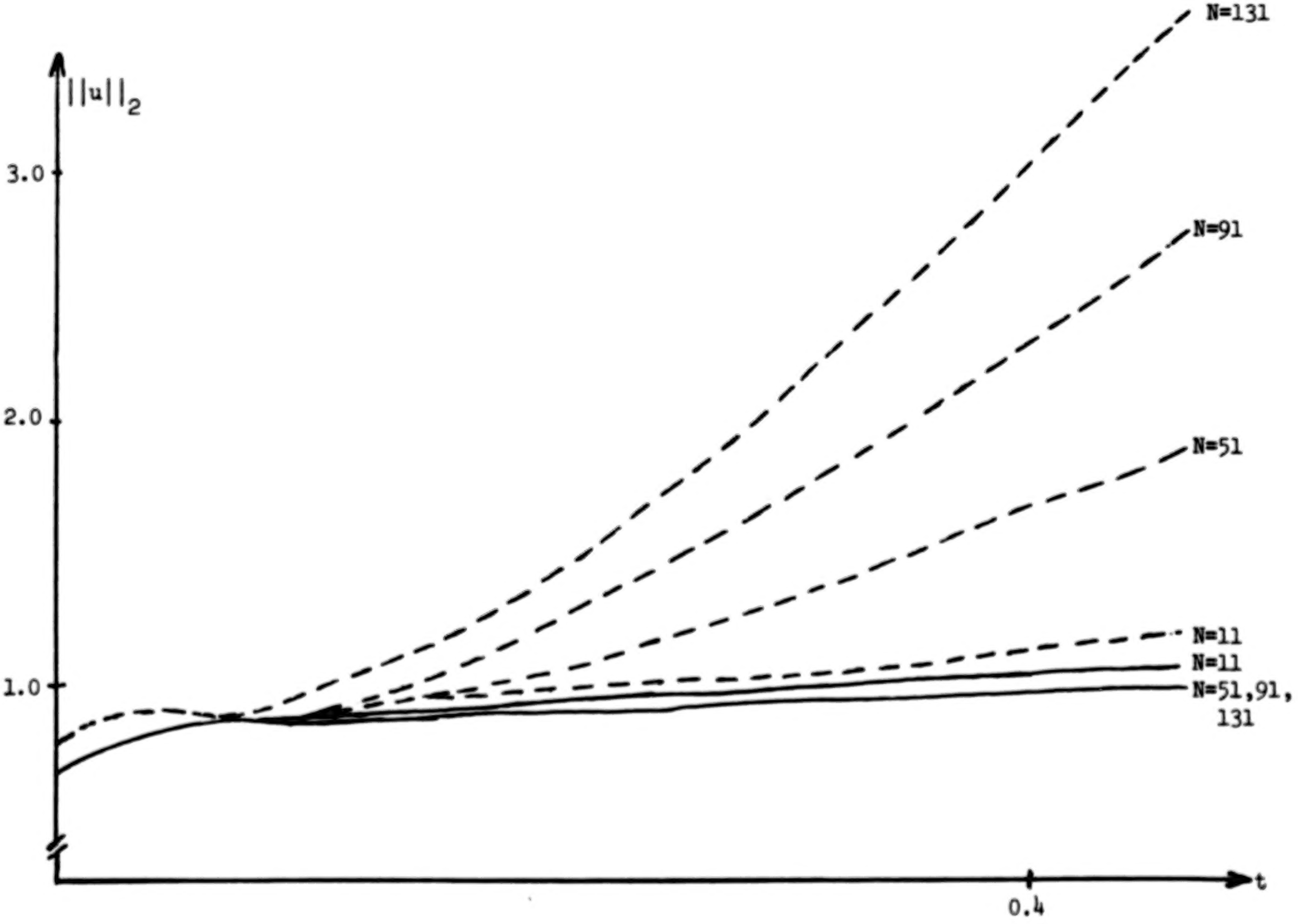

fig 1 Difference schemes with all eigenvalues $\mu(Q)$ inside the unit circle.
stable: solid line ————
unstable: dashed line --------

BLANK

PAGE

to the eigenvalue calculation above.
We look for non-trivial solutions to the resolvent equations

$$(16) \qquad \begin{cases} zv_j = (1-kD_0 + \frac{k^2}{2} D_+D_-)v_j \quad , \quad j = 1,2,\ldots \\ v_0 = v_1 \\ \sum_{j=0}^{\infty} v_j^2 h < \infty \end{cases}$$

For $|z| > 1$, one can show that the last condition implies that there is only one mode in the solution, i.e.

$$v_j = \sigma\kappa^j$$

where κ is the root of

$$z\kappa = (1+\lambda)\,\frac{\lambda}{2} + (1-\lambda^2)\kappa + (-1+\lambda)\,\frac{\lambda}{2}\,\kappa^2$$

satisfying $|\kappa| < 1$ for $|z| > 1$. Obviously, a non-trivial solution exists if and only if $\kappa = 1$, which happens when $z = 1$. One says that there is a generalized eigenvalue at $z = 1$, and the approximation is unstable.
If on the other hand the boundary conditions are posed in the more normal way such that we have for the original problem

$$(17) \qquad \begin{cases} u_0^{\,n} = u_1^{\,n} \\ u_N^{\,n} = 0 \end{cases} ,$$

then the scheme is stable. The numerical experiments for this approximation with an inhomogenous term introduced, is represented by the dotted line in fig 1. The norm is practically independent of the mesh size in this case.
As discussed in the introduction, for long time integrations no growing modes can be allowed in the solution. Therefore, it is natural to require that in addition to stability the operator Q in (2) has no eigenvalue outside the unit circle.

Since one may want to use the approximation for steady state calculations, it is actually desirable to require that all the eigenvalues of Q are strictly inside the unit circle. In that way convergence is guaranteed when the number of time steps tend to infinity. We say that the problem has only decreasing modes.

The normal mode analysis and the stability theory in [4] has the advantage that a problem defined on a domain with two boundaries can be divided in two quarter-space problems ($[0 \leq x] \times [0 \leq t]$ and $[x \leq 1] \times [0 \leq t]$) which are analyzed separately. We will investigate under what conditions any conclusions about decreasing modes for the two-boundary problem can be drawn from the analysis of the quarter-space problems. We take the view that it is good enough if one can show that only decreasing modes are present for N sufficiently large, provided the quarter space problems are stable. (From now on "stable" refers to Definition 3.3 in [4] .)

Let us consider the eigenvalues calculation for the Lax-Wendroff scheme in some more detail. The elements of the eigenvalues of the eigenvector v have the form (10), and the different modes κ_1, κ_2 satisfy (11). For $|\mu| > 1$ the two roots are separated by the unit circle, and we define the roots such that $|\kappa_1| < 1$, $|\kappa_2| > 1$. Since the condition

$$\kappa_1\kappa_2 = \frac{\lambda-1}{\lambda+1}$$

is always satisfied, there is a constant $\delta > 0$ independent of μ such that

$$(18) \qquad \begin{cases} |\kappa_1| \leq 1-\delta \quad , & |\mu| \geq 1 \\ |\kappa_2| \geq 1 \quad , & |\mu| \geq 1 \end{cases}$$

In fact one can prove that κ_2 approaches the unit circle only when μ approaches 1, and in this case $\kappa_2 = 1$. For the stable boundary conditions (17) the coefficients σ_1, σ_2 in (10) satisfy

$$(18) \qquad \begin{cases} (1-\kappa_1)\sigma_1 + (1-\kappa_2)\sigma_2 = 0 \\ \kappa_1{}^N\sigma_1 + \kappa_2{}^N\sigma_2 = 0 \end{cases}$$

and the condition for a non-trivial solution is

$$(19) \qquad 1 - \kappa_1 - r(N) = 0$$

where

$$(20) \qquad r(N) = \left(\frac{\kappa_1}{\kappa_2}\right)^N (1-\kappa_2)$$

The term $1 - \kappa_1$ is well separated from zero and $r(N)$ vanishes when N tends to infinity. Therefore the result is:

The operator Q for the problem with two boundaries has all its eigenvalues strictly inside the unit circle if N is sufficiently large.

We will now generalize these results to larger classes of equations and approximations. Consider the general hyperbolic system with constant coefficients

$$(21) \qquad u_t = Au_x$$

Without restriction it can be assumed that the $(m\times m)$-matrix A has diagonal form. The difference approximation is

$$(22) \qquad Q_{-1}u^{n+1} = \sum_{\nu=0}^{s} Q_\nu u^{n-\nu}$$

Where Q_ν are difference operators in space. Boundary conditions are specified at $x = 0$ and $x = 1$. The symbols $\hat{Q}_\nu(\theta)$, $0 \leq |\theta| \leq \pi$ are obtained after Fourier transformation. It is assumed that the von Neumann condition is fulfilled, i.e. the equation

$$[z\hat{Q}_{-1}(\theta) - \sum_{\nu=0}^{s} z^{-\nu}\,\hat{Q}_{\nu}(\theta)]\,v = 0 \quad , \quad v = (v^{(1)},v^{(2)},\dots v^{(m)})^T \tag{23}$$

has no non-trivial solution for $|z| > 1$.
The resolvent equation for (22) is

$$zQ_{-1}v = \sum_{\nu=0}^{s} z^{-\nu}\,Q_{\nu}v \tag{24}$$

This difference equation in space can be written in one-step form

$$w_{j+1} = Mw_j \tag{25}$$

It is shown in [4] that M can be transformed to block-diagonal form

$$T^{-1}(z)M(z)T(z) = \text{diag}\,(L_1,L_2,N_1,N_2) \tag{26}$$

The properties of the blocks when L_j,N_j when z approaches the unit circle are crucial for the stability theory. For a large class of approximations, class R, the following inequalities hold in the neighbourhood of any given point z_0 on the unit circle:

$$\begin{cases} L_1^*L_1 \leq (1-\delta)I \\ L_2^*L_2 \leq (1-\delta)(|z|-1)I \\ N_1^*N_1 \geq (1+\delta)I \\ N_2^*N_2 \geq (1+\delta)(|z|-1)I \qquad , \quad \delta > 0 \end{cases} \tag{27}$$

The eigenvalues of the different blocks are the roots κ_j to the characteristic equation derived for the Lax-Wendroff scheme above. In that case it was demonstrated that the block L_2 is empty near the whole unit circle, and that N_2 is empty except near $z = 1$, where N_1 is empty. We will prove the following general result for problems with two boundaries.

Theorem. Assume that both quarter-space problems are stable and that the inequalities (27) are fulfilled. If either L_2 or N_2 are empty, then there are only decreasing modes in the solutions to the two boundary problem for N sufficiently large.

Proof. Without restriction it can be assumed that M has the form (26). Assume first that L_2 is empty. w_j is partitioned correspondingly:

$$w_j = (v_j, y_j^{(1)}, y_j^{(2)})^T$$

The stability assumptions imply that without restriction the boundary conditions can be written in the form

$$\begin{cases} v_0 + D_1y_0^{(1)} + D_2y_0^{(2)} = 0 \\ E_1v_N + y_N^{(1)} = 0 \\ E_2v_N + y_N^{(2)} = 0 \end{cases}$$

or equivalently

$$\begin{cases} v_0 + D_1 y_0^{(1)} + D_2 y_0^{(2)} = 0 \\ -E_1 L_1^N (D_1 y_0^{(1)} + D_2 y_0^{(2)}) + N_1^N y_0^{(1)} = 0 \\ -E_2 L_1^N (D_1 y_0^{(1)} + D_2 y_0^{(2)}) + N_2^N y_0^{(2)} = 0 \end{cases}$$

Hence, the condition for a non-trivial solution is that the matrix

$$-E_2 L_1^N [D_1 (I - N_1^{-N} E_1 L_1^N D_1)^{-1} E_1 L_1^N D_2 + D_2] + N_2^N$$

is singular. Obviously the inequalities (27) makes this impossible for N sufficiently large.

The case that N_2 is empty is treated completely analogously, and the theorem is proved.

It was shown in [4] that the inequalities (27) are fulfilled for dissipative approximations.

The requirement of an empty L_2 or N_2 is normally fullfilled for systems (21) with all the eigenvalues of A having the same sign. This was proved for the Lax-Wendroff scheme above since (22) is a set of scalar equations. If the requirement is not fulfilled, the situation is still not too bad for dissipative approximations or "almost" dissipative approximations. The reason is that only those points where L_2 and N_2 are not empty requires an investigation. We illustrate by an example. Consider the problem

$$\begin{cases} w_t = A\, w_x \qquad , \quad A = \begin{bmatrix} 1 & 0 \\ 0 & -1 \end{bmatrix} \quad w = \begin{bmatrix} u \\ v \end{bmatrix} \\ v(0,t) = 0 \\ u(1,t) = v(1,t) \end{cases}$$

and the Lax-Wendroff approximation

$$w^{n+1} = (I + kAD_0 + \frac{k^2}{2} A^2 D_+ D_-) w^n$$

with the boundary conditions

$$\begin{cases} v_0^n = 0 \\ u_N^n = v_N^n \\ v_N^n = 2v_{N-1}^n - v_{N-2}^n \\ u_0^n = 2u_1^n - u_2^n \end{cases}$$

Both quarter space problems are easily shown to be stable.

Using the same notation for the variables in the resolvent equation we have

$$u_j = \sigma_1\kappa_1^j + \sigma_2\kappa_2^j$$
$$v_j = \tau_1\mu_1^j + \tau_2\mu_2^j$$

where κ_1, κ_2 and μ_1, μ_2 are roots to

$$z\kappa = \kappa + \frac{\lambda}{2}(\kappa^2-1) + \frac{\lambda^2}{2}(\kappa-1)^2$$

and

$$z\mu = \mu - \frac{\lambda}{2}(\mu^2-1) + \frac{\lambda^2}{2}(\mu-1)^2$$

respectively.
The only crucial point where the conditions in the theorem are not fulfilled is $z = 1$ where $|\kappa_1| \leq 1 - \delta$, $\kappa_2 = 1$, $\mu_1 = 1$, $\mu_2 \geq 1 + \delta$. (The identification with the general notation in (26) is obtained through the relations $L_2 = \kappa_1$, $L_2 = \mu_1$, $N_1 = \mu_2$, $N_2 = \kappa_2$.) However, the equation for v is independent of u and from the scalar result we know already that there is no eigenvalue z with $|z| \geq 1$ for N sufficiently large. The boundary conditions for u imply

$$\begin{cases} \kappa_1^N\sigma_1 + \kappa_2^N\sigma_2 = \mu_1^N\tau_1 + \mu_2^N\tau_2 \\ (\kappa_1-1)^2\sigma_1 + (\kappa_2-1)^2\sigma_2 = 0 \end{cases}$$

Since $\tau_1 = \tau_2 = 0$ for $|z| \geq 1$, the scalar result for u applies, and there are obviously only decreasing solutions for N sufficiently large.

Let us go back to the original model example $u_t = u_x$ and study the Backward Euler approximation

$$\begin{cases} (I-kD_0)u_n^{n+1} = u_j^n \quad , \quad j = 1,2,\ldots,N-1 \\ u_0^n = 2u_1^n - u_2^n \\ u_N^n = 0 \end{cases}$$

The characteristic equation is

$$z(\kappa - \frac{\lambda}{2}(\kappa^2-1)) = \kappa \tag{28}$$

For $\kappa = e^{i\theta}$ we have

$$z = \frac{1}{1-\lambda i \sin\theta} \quad ,$$

and z hits the unit circle at $z = 1$ not only or $\theta = 0$ but also for $\theta = \pi$. For $z = 1$ the two roots to (28) are $\kappa_1 = -1$, $\kappa_2 = 1$, which shows that L_2 and N_2 in (26) are non-empty. However, this point is easily investigated. The general solution to the resolvent equation for $z = 1$ is

$$v_j = \sigma_1(-1)^j + \sigma_2$$

with σ_1, σ_2 satisfying

$$\begin{cases} 4\sigma_1 = 0 \\ (-1)^N \sigma_1 + \sigma_2 = 0 \end{cases}$$

Obviously there is no non-trivial solution to this system, and therefore only decreasing solutions exist for N sufficiently large.

We end this section by making a comment about problems with non-constant coefficients. The analysis above gives no information about the behaviour of the solutions to problems with variable coefficients. In fact, it must be expected that in such cases there exist growing solutions even if the analysis above shows decreasing solutions for constant coefficients. We would like to emphasize that this is in general the correct behaviour. Consider the non-linear model problem

$$\begin{cases} u_t = uu_x \\ u(1,t) = 0 \\ u(x,0) = f(x) \end{cases}$$

with positive solutions u. The norm $||u||^2 = \int_0^1 u(x,t)^2 dx$ is decreasing, since

$$\frac{d}{dt} ||u||^2 = -\frac{2}{3} u(0,t)^3$$

The linearized problem is

$$\begin{cases} u_t = a(x,t)u_x \quad , \quad a(x,t) > 0 \\ u(1,t) = 0 \\ u(x,0) = f(x) \end{cases}$$

and for the same norm we obtain

$$\frac{d}{dt} ||u||^2 = \int_0^1 2auu_x dx = -a(0,t)u(0,t)^2 - \int_0^1 a_x^2 u^2 dx$$

Obviously there may be growing solutions to this problem. Therefore, if the full non-linear problem cannot be analyzed, it makes sense to "jump over" the variable coefficient case and analyze the problem with constant coefficients.

3. Unbounded domains

We will consider an ideal fluid in a channel according to fig. 2

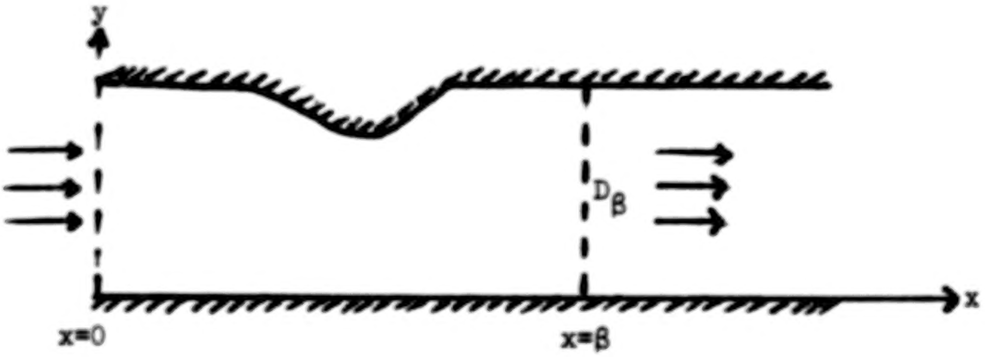

fig 2

The Euler equations are

(29) $$w_t + A(w)w_x + B(w)w_y = 0$$

where with the usual notation

$$w = \begin{bmatrix} \rho \\ u \\ v \end{bmatrix}, \quad A(w) = \begin{bmatrix} u & \rho & 0 \\ c^2/\rho & u & 0 \\ 0 & 0 & u \end{bmatrix}, \quad B(w) = \begin{bmatrix} v & 0 & \rho \\ 0 & v & 0 \\ c^2/\rho & 0 & v \end{bmatrix}$$

The flow is assumed to be subsonic, but no data are available at D_β.

Seeking the steady state solution, we will construct the down-stream conditions using the condition

(30) $$\sup_{x,y,t}|w| < \infty \quad , \quad |w|^2 = \rho^2 + u^2 + v^2$$

The solution still contain an undetermined constant, therefore we add a condition on the massflow:

(31) $$\int_0^1 \rho u \, dy = m$$

Since m does not depend on x, it can be measured at the inflow boundary. The question is how these conditions can be converted into something usable in a computational procedure.

For the derivation it is assumed that the matrices A and B in (29) are constant, and since $v = 0$ at the boundary we assume a zero diagonal in B, ρ and u are expanded in cosine-series in the y-direction, v is expanded in a sine-series.

$$\rho(x,y) = \sum_{=0}^{\infty} \hat{\rho}_w(x) \cos\pi\omega y$$

$$u(x,y) = \sum_{\omega=0}^{\infty} \hat{u}_w(x) \cos\pi\omega y$$

$$v(x,y) = \sum_{\omega=1}^{\infty} \hat{u}(x) \sin\pi\omega y$$

Introduction of these expansions into the steady state system gives the transformed equation

(32) $$\bar{A} \frac{\partial \hat{w}_\omega}{\partial x} + \pi\omega\bar{B}\hat{w}_\omega = 0 \quad , \quad w_\omega = \begin{bmatrix} \hat{\rho}_\omega \\ \hat{u}_\omega \\ \hat{u}_\omega \end{bmatrix}$$

The solution has the form

(33) $$\hat{w}_\omega = \sum_{j=1}^{3} \alpha_j q_j e^{\omega\pi\lambda_j(x-\beta)}$$

where the scalars λ_j and the vectors q_j satisfy the eigenvalue problem

(34) $$(\bar{A}\lambda_j + \bar{B})q_j = 0$$

λ_2 is positive, and the condition (30) therefore implies $\alpha_2 = 0$ for $\omega \neq 0$. A straight-forward calculation gives the final form of the solution

(35) $$\begin{bmatrix} \rho_\omega \\ u_\omega \\ v_\omega \end{bmatrix} = \alpha_1 \begin{bmatrix} 0 \\ 1 \\ 0 \end{bmatrix} + \alpha_3 \begin{bmatrix} -\bar{u}\bar{\rho}/\bar{c} \\ \bar{c} \\ s \end{bmatrix} e^{\frac{-\omega\pi\bar{c}}{\omega s}(x-\beta)} \quad , \quad \omega=1,2,\ldots$$

The quantities $\bar{u},\bar{p}$ represent the coefficients in $\bar{A},\bar{B}$, and s is defined by $\omega_s = \sqrt{\bar{c}^2 - \bar{u}^2}$. (35) immediately gives the desired conditions to be used at $x = \beta$:

(36) $$\hat{\rho}_\omega = -\frac{\bar{u}\bar{\rho}}{\bar{c}s}\hat{v}_\omega \quad , \quad \omega = 1,2,\ldots$$

The remaining condition for $\hat{\rho}_0$ is obtained form (31).

It can be shown by the energy-method that the system

(37) $$\frac{\partial\hat{w}_\omega}{\partial t} + \bar{A}\frac{\partial\hat{w}_\omega}{\partial x} + \pi w\bar{B}\hat{w}_\omega = 0 \quad , \quad \omega = 0,1,\ldots$$

is well posed with the boundary conditions derived above. Therefore methods for time-dependent problems can be used for computing the steady state solution.

In our numerical experiments we have used Newton's method for a difference approximation using centered differences in both directions.

For comparison two other boundary procedures have been used. In the first the conditions are based on the commonly used assumption that the solution has flattened out at $x = \beta$. If $w_t = w_x = 0$ in (29) it follows that $\rho_y = 0$. With the discretized version of this equation as the down-stream boundary condition (everything else the same as above) a method is defined which is denoted by RC in the figures below.

The second alternative used for comparison is the Bayliss-Turkel method mentioned in the introduction, which is denoted by BT in the figures.

The boundary D_β was placed at $x = 5/14$ and $x = 1/14$. The figures show the remarkably good agreement beetween the correct solution and the one obtained with the conditions (36) (denoted by FG).

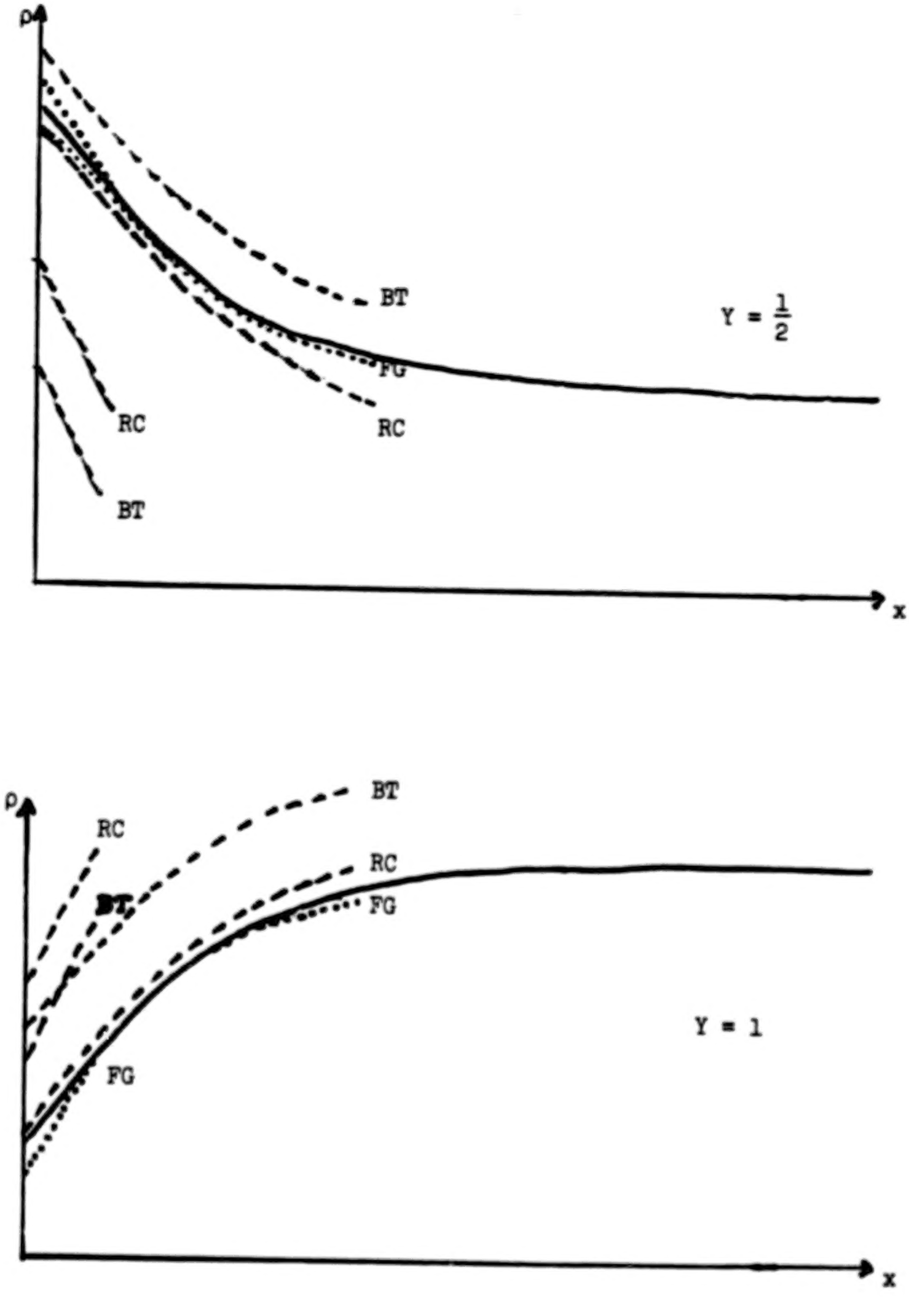

fig 3

ρ as a function of x

References

1. Bayliss A. and Turkel E.: Outflow boundary conditions for fluid dynamics. ICASE Report No 80-21, Hampton, Va. (1980).

2. Engquist B. and Majda A.: Absorbing boundary conditions for the numerical simulation of waves. Math. Comp. No 31 (1977), pp. 629-651.

3. Ferm L. and Gustafsson B.: A down-stram boundary procedure for the Euler equations. Uppsala University, Dept. of Computer Sciences, Report No 88, 1981.

4. Gustafsson B, Kreiss H.-O. and Sundström A.: Stability theory of difference approximations for mixed initial boundary value problems II. Math. Comp., vol 26 (1972), pp. 649-686.

5. Gustafsson B. and Kreiss H.-O.: Boundary conditions for time dependent problems with an artificial boundary. J.Comp. Phys., vol 30 (1979), pp. 333-351.

6. Hedström G.: Nonrefleeting boundary conditions for nonlinear hyperbolic systems. J. Comp. Phys., vol 30 (1979), pp. 202-237.

7. Rudy D. and Strikwerda J.C.: Boundary conditions for subsonic compressible Navier - Stokes calculations. Computers and Fluids, vol 9 (1981), pp. 327-338.

8. Yee H.C., Beam R.M. and Warming R.F.: Stable boundary approximations for a class of implicit schemes for the one-dimensional inviscid equations of gas dynamics. AIAA-81-1009-CP, AIAA Computational Fluid Dynamics Conference, Palo Alto, California, 1981.

Blank Page

INFLUENCE OF BOUNDARY APPROXIMATIONS AND CONDITIONS ON FINITE-DIFFERENCE SOLUTIONS*

F. G. Blottner
Sandia National Laboratories**
Albuquerque, New Mexico 87185

ABSTRACT

Numerical representations of boundary approximations and conditions for three problems are investigated to determine the resulting global accuracy of the steady-state solution. Numerical accuracy with various boundary approximations is determined for quasi-one-dimensional inviscid flow in a duct with the interior grid points evaluated using the MacCormack scheme. When an extrapolation approximation with first-order local truncation error is used, the global second-order accuracy of the difference scheme can be destroyed. For one-dimensional flow in a porous medium, an implicit midpoint difference scheme which is consistent with the boundary conditions is developed without the need of boundary approximations. A dissipative model problem is solved with the boundary conditions discretized with first- and second order accuracy. The overall second-order accuracy of the difference scheme is destroyed if first-order numerical representation of one of the boundary conditions is used. With a boundary approximation, the second-order global accuracy of the model problem is retained if either second-order extrapolation or first-order representation of the governing equation is used.

INTRODUCTION

Finite-difference schemes are usually developed for computing the interior points of the computational domain and then boundary conditions and special relations are used at and near boundaries. For a given set of governing equations, there are appropriate boundary conditions that result in a well posed problem with continuous solutions and provide relations which allow some of the dependent variables to be determined at the boundaries. These boundary conditions are usually obtained from the physics of the problem. The remaining relations required to determine the dependent variables at the boundaries must be determined from boundary approximations; such as extrapolation, characteristic compatibility relations or difference relations obtained from the governing equations. The boundary approximations can influence the stability of the overall scheme and can influence the global accuracy of the difference approximation. These properties of the boundary approximations must be investigated for each interior difference scheme and set of governing equations. A review of this problem has been given recently by Turkel (ref. 1). Gustafsson (ref. 2) indicates that boundary approximations for the transient solution of hyperbolic equations can be differenced with one-order lower accuracy than used for the interior difference scheme without decreasing the overall accuracy. This statement is perhaps misleading due to the accuracy definition.

---

* This work was supported by the U.S. Department of Energy under contract DE-AC04-76-DP00789.

** A U.S. Department of Energy facility.

Skollermo (ref. 3) restates this conclusion as "formally, the local truncation error in the boundary approximation should also be of the same order as the global error of the interior scheme." Bramble and Hubbard (ref. 4) have shown that the solution of Poisson's equation with Dirichlet boundary conditions on an irregular computational region can use first-order difference relations of the governing equation near the boundary and still provide an overall second-order scheme. In this case the boundary condition can be satisfied exactly but the governing equation has a local truncation error of order of the stepsize near the boundary due to non-uniform grid spacing. If the solution is interpreted in terms of a uniform grid with grid points exterior to the boundary, the boundary condition discretization uses quadratic extrapolation for the exterior grid points. Thomas (ref. 5) investigated the boundary approximations with implicit ADI techniques at various flow boundaries that occur in external and internal flow problems. The boundary approximations are conservatively differenced forms of the flow equations and have a local truncation error that is first order. The global truncation error in space is indicated to be second-order accurate but no numerical results are given to demonstrate this behavior.

The present study is concerned with obtaining a better understanding of the influence numerical representations of the boundary approximations and conditions have on the global accuracy of the finite-difference solution to steady-state problems. Quasi-one-dimensional flow in a duct is used as an illustration of the influence boundary approximations have on the global accuracy when the MacCormack explicit scheme is used for the interior grid points. The steady-state problem is obtained from the asymptotic time solution of the transient equations. The case of subsonic entry to supersonic exit flow has previously been investigated by Turkel (ref. 1) while the present study is concerned with this problem plus the case of complete subsonic flow where an exit boundary condition must be specified. The numerical treatment of computational boundaries for a limited region with subsonic flow is discussed by Moretti and Pandolfi (ref. 6). A physical model of the flow outside of the boundaries provides the boundary conditions which can interact with the interior flow.

The importance of the interior difference scheme is illustrated with the problem of compressible flow through a porous material where the governing equations are the same as the quasi-one-dimensional problem with a friction term added. The porosity of the material corresponds to the cross-sectional area of the duct and for low speed flows the friction factor is related to the permeability of the porous material. The problem considered is the steady-state subsonic flow resulting from a pressure drop across the porous material. The solution is obtained with an implicit, midpoint difference scheme which provides exactly the correct number of difference relations along with the boundary conditions needed to solve for the dependent variables at all of the grid points. Therefore, with this approach the interior difference relations are not supplemented with boundary approximations. With central differences, three boundary or extraneous approximations are required for this problem and the influence on the global error is investigated.

Finally, a dissipative model problem is studied to illustrate the effect of numerical discretization of the boundary conditions and boundary approximations on global error. For this case the global error is determined both numerically and analytically.

QUASI-ONE-DIMENSIONAL FLOW

The properties of the governing equations for transient flow in a duct are well understood from the point of view of the method of characteristics and are described by Shapiro (ref. 7). This relatively simple flow problem provides an excellent test case for studying the effects of boundary conditions and approximations as the exact steady-state solution for this flow is known. The quasi-one-dimensional flow problem is also of engineering interest to approximate more complex flows. The time-dependent approach is used in the present study to obtain the steady-state continuous solution to the flow in a duct with subsonic entry flow and with either subsonic or supersonic exit flow. The flow in a nozzle with supersonic flow has been investigated by Turkel (ref. 1) with both continuous flow and with a shock where a downstream pressure is specified. The handling of computational boundaries for subsonic flows has been investigated by Moretti and Pandolfi (ref. 6).

The quasi-one-dimensional inviscid flow equations are written as

$$\frac{\partial Q}{\partial t} + \frac{\partial F}{\partial x} = S \tag{1}$$

where

$$Q = \begin{bmatrix} \rho A \\ \rho u A \\ e A \end{bmatrix} \qquad F = \begin{bmatrix} \rho u A \\ (\rho u^2 + p)\ A \\ (e + p)\ uA \end{bmatrix} \qquad S = \begin{bmatrix} 0 \\ p\ \frac{dA}{dx} \\ 0 \end{bmatrix}$$

The variable A is the cross sectional area of the duct and the remaining variables have the usual meaning. The total energy is defined as

$$e = \rho(h + \frac{1}{2}\ u^2) - p \tag{2}$$

where the enthalpy for a perfect gas is

$$h = \left(\frac{\gamma}{\gamma - 1}\right)\ p/\rho \tag{3}$$

the characteristics of the governing equations (1) are

$$\begin{aligned} \frac{dx}{dt} &= u \pm c \quad \text{(Mach lines)} \\ \frac{dx}{dt} &= u \quad\quad\ \ \text{(Path lines)} \end{aligned} \tag{4}$$

where the speed of sound for a perfect gas is determined from $c = \sqrt{\gamma p/\rho}$. The compatibility relations along the characteristics are

$$\rho u \, du \pm dp \pm \frac{p u \gamma}{A} \frac{dA}{dx} dt = 0 \qquad \text{along } u \pm c$$

$$dp - c^2 \, d\rho = 0 \qquad \text{along } u \tag{5}$$

These relations can be written as finite-difference equations and used to determine the solution at the next time step from the appropriate initial and boundary conditions. A finite-difference approach for solving the governing equation (1) is used rather than the method of characteristics. The above relations are given to help understand the physical boundary conditions and to obtain computational relations at the boundaries.

The dependent variables at the interior grid points are advanced in time with the MacCormack explicit scheme. The variables are first predicted at time (n + 1) with first-order accuracy from the known conditions at time (n) and then a corrector is used to obtain the new results at time (n+1) with second-order accuracy. The difference relations for the governing equations (1) with the backward-forward difference version are

$$\bar{Q}_i = Q_i^{\,n} - \frac{\Delta t}{\Delta x}\left(F_i - F_{i-1}\right)^n + \Delta t \, S^n_{i-1/2} \qquad i = 2,3,\ldots,I$$

$$Q_i^{n+1} = \frac{1}{2}\left[Q_i^{\,n} + \bar{Q}_i - \frac{\Delta t}{\Delta x}\left(\bar{F}_{i+1} - \bar{F}_i\right) + \Delta t \, \bar{S}_{i+1/2}\right] \tag{6}$$

$$i = I-1, I-2, \ldots, 2$$

The MacCormack scheme requires the following Courant number restriction:

$$C = (|u| + c) \, \Delta t/\Delta x \leq 1 \tag{7}$$

When the steady-state solution is obtained with the MacCormack scheme, the governing equations (1) are effectively evaluated with a midpoint difference scheme, which is second-order accurate in space.

At the boundaries of the computational domain the MacCormack difference relations are not adequate and additional difference relations must be used along with the boundary conditions to complete the solution procedure for $\bar{Q}_1$ and Q_I^{n+1}. In addition, the variations of three dependent variables along the duct at the initial time is also required to start the solution.

For the case of subsonic entry flow, the u + c and u characteristics are entering the computational domain and the u-c characteristic is leaving the computational domain. Therefore, two conditions must be specified and the remaining dependent variable must be determined from the compatibility relation equation (5) along the u-c characteristic or from some other difference relation. Since in the present study only the steady-state solution is desired, the two physical boundary conditions utilize the steady-state isentropic relations for the entry pressure and density as a function of the entry Mach number, stagnation density and stagnation pressure

$$\rho_1 = \rho_0\left(1 + \frac{\gamma-1}{2} M_1^2\right)^{-1/(\gamma-1)}$$

$$P_1 = P_0(\rho_1/\rho_0)^\gamma \tag{8}$$

where

$$M_1^2 = u_1^2/\left[\gamma - \frac{1}{2}(\gamma-1)\, u_1^2\right]$$

The subscript 1 indicates the entry conditions while subscript 0 indicates the variables are stagnation conditions in an infinite reservoir. The above relations assume quasi-steady streamtube flow to determine the pressure and density from the entry velocity and become exact for the steady-state solution. For steady-state conditions the governing equations (1) are evaluated with a midpoint scheme where subscript 1 and 2 are the entry point and next grid point downstream. This gives three relations which are used to solve for the entry velocity at the new time level after the corrector step of the MacCormack difference scheme has been used to determine the dependent variables at grid point 2.

$$u_1 = (-b + \sqrt{b^2-4ac})/2a \tag{9}$$

where

$$a = 1 - \left(\frac{4\gamma}{\gamma-1}\right) A_1/(A_1 + A_2)$$

$$b = (1-a)\left[(\rho u^2 A)_2 + \frac{1}{2} P_2(A_1 + A_2)\right]/(\rho u A)_2$$

$$c = -2\left[(e+p)/\rho\right]_2$$

Equation (9) is second-order accurate and consistent with the MacCormack scheme when the steady-state solution is obtained and replaces the compatibility relation, equation (5). An extrapolation technique is often used to obtain a dependent variable at the boundary if a physical boundary condition does not specify the variable. The following linear extrapolation relation for the velocity at the entry has been investigated:

$$u_1 = 2u_2 - u_3 \tag{10}$$

where the velocities are at the (n + 1) time level.

For subsonic exit flow, there are two characteristics leaving the computational domain and one entering. For supersonic flow, all three characteristics leave the computational domain. Therefore, one physical boundary condition is required for subsonic flow at the exit while no boundary conditions can be specified for continuous supersonic exit flow. Three boundary relations have been investigated for subsonic exit flow and are applied to obtain the dependent variables at the (n + 1) time level.

The characteristic boundary relation method uses the compatibility conditions, equation (5), along the u + c and u characteristics to obtain the first-order, finite-difference relations

$$u_I^{n+1} = u_a - \left[p_I^{n+1} - p_a + \left(\frac{\rho u \gamma}{A}\frac{dA}{dx}\right)_I \Delta t\right] / (\rho c)_I \tag{11a}$$

$$\rho_I^{n+1} = \rho_b + \left(p_I^{n+1} - p_b\right) / {c_I}^2 \tag{11b}$$

For subsonic flow the exit pressure ${p_I}^{n+1}$ is specified. The dependent variables at the grid points a and b are at time n and are on the u + c and u characteristics respectively. Linear interpolation along with a first-order difference relation for the characteristic locations are used to determine these variables as follows:

$$\begin{aligned} W_a &= (1 - \alpha)\, W_I + \alpha\, W_{I-1} \qquad \text{where } W = u \text{ or } p \\ W_b &= (1 - \beta)\, W_I + \beta\, W_{I-1} \qquad \text{where } W = p \text{ or} \end{aligned} \tag{12}$$

and the coefficients are

$$\alpha = \Delta t\ (u_I + c_I)/\Delta x$$

$$\beta = \Delta t\ u_I/\Delta x$$

With the above relations, equation (12) used in equations (11), the right side of these equations are known and the exit velocity and density can be determined.

The unsteady midpoint boundary relations are developed from the continuity and momentum equations (1) using one-sided spatial differences and are written in the following finite-difference form:

$$\left(\frac{Q^{n+1} - Q^{n}}{\Delta t}\right)_I + \left(\frac{F_I - F_{I-1}}{\Delta x}\right)^{n+1} = \frac{1}{2}(S_I + S_{I-1})^{n+1} \tag{13}$$

The continuity equation becomes

$$(\rho A)_I^{n+1} = \left[(\rho A)_I^n + \frac{\Delta t}{\Delta x}\,(\rho u A)_{I-1}^{n+1}\right] \Big/ \left(1 + \frac{\Delta t}{\Delta x}\,u_I^{n+1}\right) \tag{14}$$

The momentum equation (13) and the above continuity equation (14) are combined to obtain the exit velocity

$$\begin{aligned} u_I^{n+1} = & \left\{(\rho u A)_I^n + \Delta t\left[(\rho u^2 A)_{I-1}^{n+1} - \frac{1}{2}\,(p_I - p_{I-1})^{n+1}(A_I + A_{I-1})\right]\Big/\Delta x\right\} \\ & \cdot \left\{(\rho A)_I^n + \Delta t\ (\rho u A)_{I-1}^{n+1}/\Delta x\right\}^{-1} \end{aligned} \tag{15}$$

With exit velocity determined from equation (15), the density is then evaluated from equation (14).

The extrapolation boundary relations for a uniform grid spacing use the following expressions to determine the exit density and velocity:

$$\left.\begin{aligned} &\text{First-order:} && W_I = W_{I-1} + O(\Delta x) && (16a) \\ &\text{Second-order:} && W_I = 2W_{I-1} - W_{I-2} + O(\Delta x^2) && (16b) \end{aligned}\right\} W = \rho \text{ or } u$$

According to Gustafsson's definition (ref. 2), equations (16a) and (16b) are zeroth and first-order accurate boundary approximations, respectively.

The flow in ducts with the geometries utilized by Griffin and Anderson (ref. 8) are used to illustrate the accuracy of the various boundary conditions. These geometries are of the Laval nozzle type with the throat height above the centerline used as the reference length L. With entry at $x = 0$, the throat at $x = x_T$ and the exit at $x = x_I$, the area variation of the duct is given as

$$\begin{aligned} A &= 1 + (A_1 - 1)\left[(x_T - x)/x_T\right]^2 && x \leq x_T \\ A &= 1 + (A_I - 1)\left[(x - x_T)/(x_I - x_T)\right] && x > x_T \end{aligned} \tag{17}$$

The entry area A_1 and the exit area A_I must be specified to complete the description of the duct.

The first example is a duct flow with $A_1 = 1.5$, $A_I = 2.0$, $x_I = 40$ and $x_T = 10$ with supersonic flow at the exit without any shock waves. The exact analytical solution for the isentropic flow is used as the initial conditions for the dependent variables along the duct. The numerical solution is obtained with $\Delta x = 1$ and Δt is chosen at each time step such that the maximum Courant number at any grid point is 0.9. The steady-state solution to the finite-difference equations is different than the initial conditions due to truncation error and will be the same only when $\Delta x \to 0$. The MacCormack finite-difference technique is used to obtain the steady-state solution for the duct configuration. The approach of the solution towards a steady-state is illustrated in Table I where the entry velocity is presented for the midpoint boundary relation, equation (9). With the number of decimal places shown in this table, a steady-state is obtained after 400 time steps for the midpoint boundary relation. The time shown is the nondimensional time $(t/L)\sqrt{\rho_0/p_0}$. The result of using the linear extrapolution relation, equation (10), for the entry velocity is shown in Table I. After 1000 time steps a steady-state is not obtained and this technique appears to give a solution that is drifting. When linear extrapolation is used to determine the dependent variables ρ, u and p at the exit, a steady-state solution is obtained and the entry velocity is the same as that given in Table I with the midpoint relation, equation (9). However, since the linear extrapolation relations are not consistent with the MacCormack finite-difference relations; the mass flux near the exit oscillates about the "correct" numerical value as shown in figure 1. The correct upstream numerical solution is used to judge the error of ρuA and this "correct" numerical solution has an error of 0.053% relative to the exact analytical solution. Although the oscillation shown in figure 1 is unpleasant, the error is about the same or less than the truncation error of the "correct" numerical solution with $\Delta x = 1$.

TABLE I

ENTRY VELOCITY FOR SUPERSONIC DUCT

Number of Time Steps	Time	Midpoint	Extrapolation
0	0	0.499922	0.499922
100	33.5	0.500244	0.498947
200	66.9	0.500247	0.498998
300	100.4	0.500246	0.499271
400	133.9	0.500247	0.499201
500	167.3	0.500247	0.499042
600	200.8	0.500247	0.498816
700	234.3	0.500247	0.498532
800	267.7	0.500247	0.498189
900	301.2	0.500247	0.497781
1000	334.7	0.500247	0.497306

The second example considered is subsonic duct flow with $A_1 = 6$, $A_I = 1$, $s_I = 20$ and $s_T = 20$. The pressure at the exit has a value of 0.93716250 p_0 and is held fixed as the known physical boundary condition. Steady-state solutions are obtained with $\Delta x = 2$, 1 and 0.5 with 1000, 2000 and 4000 time steps respectively. The exit velocity is used to judge the spatial accuracy of the steady-state solutions where the exact value of the exit velocity is $0.358610 \sqrt{\rho_o / p_o}$. The percent error of the steady-state exit velocity is given in figure 2 for the boundary relations given by the characteristic equation (11), finite difference equation (15) and the extrapolation equation (16). All of the methods have an error behavior that indicates that the spatial differencing is second-order. When the characteristic boundary relation is used, the mass flux wiggles at the grid points near the exit with behavior similar to that shown in figure 1.

The global second-order behavior with the first-order extrapolation boundary approximation cannot be expected to occur in general. The foregoing example has zero gradients of the dependent variables at the exit and the first-order extrapolation is appropriate. The solution was obtained for the same problem except the exit conditions are applied at $x_I = 10$ where the dependent variable gradients are non-zero. The results of this accuracy study are given in Figure 3, where the first-order extrapolation boundary approximation results in first-order global accuracy. The other boundary approximations result in global second-order accuracy. The characteristic approximation is based on first-order approximations to the governing equations and does not destroy the global second-order behavior. A boundary approximation which uses the governing equations can have a local truncation error of first order while extrapolation techniques must be second-order in order to avoid reduction of the global accuracy.

FLOW IN POROUS MEDIA

One-dimensional, high-speed, subsonic compressible flow thru a porous material is considered. The gas and porous material are allowed to have different temperatures but energy transport due to conduction and dispersion is neglected. The governing equations are of the same form as equations (1) except there are four dependent variables as follows and the flux vector is

$$Q = \begin{bmatrix} \rho\varepsilon \\ \rho u\varepsilon \\ e_f\varepsilon \\ e_s(1-\varepsilon) \end{bmatrix} = \begin{bmatrix} Q_1 \\ Q_2 \\ Q_3 \\ Q_4 \end{bmatrix} \qquad F = \begin{bmatrix} \rho u\varepsilon \\ (\rho u^2 + p)\varepsilon \\ (e_f + p)\, u\varepsilon \\ 0 \end{bmatrix} \tag{18}$$

where ρ = density of fluid
p = pressure of fluid
u = local or interstitial velocity of fluid
e_f = total fluid energy per unit fluid volume
e_s = total solid energy per unit solid volume = $\rho_s\, c_s\, T_s$
ε = porosity of solid material.

These relations are the same as the quasi-one-dimensional equation (1) except the cross sectional area is replaced by the porosity. The source term in equation (1) becomes

$$S = \begin{bmatrix} 0 \\ p(d\varepsilon/dx) - (\alpha\mu + \beta\rho u\varepsilon)\varepsilon^2 u \\ - h\ a_p\ (T - T_s) \\ h\ a_p\ (T - T_s) \end{bmatrix} \tag{19}$$

where α and β are dependent on the flow resistance model
h = heat transfer coefficient
a_p = particle surface area per unit volume of porous media
= $6\ (1-\varepsilon)/d_p$ for spherical particles of diameter d_p
T = temperature of fluid = $\overline{M}\ \varepsilon\ p/R\rho$
T_s = temperature of solid porous material.

The coefficients α and β are determined from the Ergun (ref. 9) equation for gas flow thru a packed bed of particles with effective diameter d_p

$$\begin{aligned} \alpha &= 150\ (1-\varepsilon)^2/(\varepsilon^3 d_p^{\ 2}) \\ \beta &= 1.75\ (1-\varepsilon)/(\varepsilon^3\ d_p) \end{aligned} \tag{20}$$

The foregoing momentum equation includes the usual Forchheimer equation which relates the pressure gradient to the flow resistance terms. In addition, the momentum equation includes the inertia term as suggested by Emanuel and Jones (ref. 10) and predicts choked flow if there is sufficient pressure drop. The energy equations are the Schumann (ref. 11) model for heat transfer in a bed of particles except the kinetic energy of the fluid and work done on the fluid by pressure forces are included.

The governing equations require two boundary conditions at the inflow locations ($x = 0$) and one boundary condition is needed at the outflow ($x = L$). The pressures p_{in} and p_{out} are assumed known at both locations while the gas temperature T_{in} is specified at the inflow. The initial variation of the dependent variables across the porous material is obtained from the steady-state, isothermal solution with the inertia term neglected in the momentum equation. The pressure variation has been determined by Morrison (ref. 12) and the result is

$$p = \left[p_{in}^2 + (p_{out}^2 - p_{in}^2)(x/L)\right]^{1/2} \tag{21}$$

The mass flux density is

$$\rho u \varepsilon = \left\{ - \alpha\mu + \left[(\alpha\mu)^2 + 2\beta (P_{in}^2 - P_{out}^2) \rho / pL \right]^{1/2} \right\} / 2\beta \tag{22}$$

The density is determined from the equation of state with the inflow temperature used along with the pressure obtained from equation (21).

This investigation is concerned with obtaining the steady-state solution where the solid and gas temperatures are the same at any location without heat transfer between the two phases. The adiabatic flow case has an exact solution but for the present formulation a difficult iteration process is required to determine the inflow Mach number. Therefore, even for the steady-state solution, an efficient numerical solution is needed. The initial approach considers the steady-state form of equation (1) and uses midpoint difference relations to obtain the difference equations

$$(F_{i+1} - F_i)/\Delta x_i = (S_{i+1} + S_i)/2 \tag{23}$$

where $\Delta x_i = x_{i+1} - x_i$. The quantities F and S are linearized about the previous known value which is indicated with a bar and the expansions are

$$\begin{aligned} F &= \bar{F} + \tilde{A}\, \Delta Q + \ldots \\ S &= \bar{S} + \tilde{D}\, \Delta Q + \ldots \end{aligned} \tag{24}$$

where $\Delta Q = Q - \bar{Q}$. The Jacobian matrices $\tilde{A}$ and $\tilde{D}$ are obtained from

$$\tilde{A} = \partial F / \partial Q$$

$$\tilde{D} = \partial S / \partial Q$$

The difference equation (23) becomes

$$\begin{aligned} &\left(\tilde{A}_{i+1} - \tfrac{1}{2}\, \tilde{D}_{i+1}\, \Delta x_i\right) \Delta Q_{i+1} - \left(\tilde{A}_i + \tfrac{1}{2}\, \tilde{D}_i\, \Delta x_i\right) \Delta Q_i \\ &= -\bar{F}_{i+1} + \bar{F}_i + \tfrac{1}{2}\, \Delta x_i\, (\bar{S}_{i+1} + \bar{S}_i) \qquad i = 1,2,3,\ldots,I-1 \end{aligned} \tag{25}$$

and the difference equation for the energy equations for the solid has the special form

$$\sum_{n=1}^{4} \tilde{D}_{4n}\, Q_n = \bar{S}_4 \qquad i = 1,2,\ldots,I \tag{26}$$

The boundary conditions are

At $x = 0$

$$\Delta Q_1 = (Q_1)_{in} - \bar{Q}_1 \quad \text{where } (Q_1)_{in} = \bar{M}\,\epsilon\, p_{in}/R\,T_{in} \tag{27a}$$

At $x = 0$ or L

$$\frac{1}{2}\,\bar{u}^2\,\Delta Q_1 - \bar{u}\,\Delta Q_2 + \Delta Q_3 = \epsilon\, p_*/(\gamma-1) - \bar{Q}_3 + \frac{1}{2}\,\bar{Q}_2^2/\bar{Q}_1 \tag{27b}$$

where p_* is p_{in} or p_{out} at the appropriate boundary.

The difference equations (25) and (26) along with the boundary conditions (27) provide 4I relations which are used to solve for the 4I unknown dependent variables at the I grid points. The difference equations and boundary conditions are written as the following block-tridiagonal system:

$$\begin{aligned} B_1\,W_1 - C_1\,W_2 &= D_1 \\ -A_i\,W_{i-1} + B_i\,W_i - C_i\,W_{i+1} &= D_i \qquad i = 2,3,\ldots,\,I-1 \\ -A_I\,W_{I-1} + B_I\,W_I &= D_I \end{aligned} \tag{28}$$

where

$$W_i = \begin{bmatrix} \Delta Q_1 \\ \Delta Q_2 \\ \Delta Q_3 \\ \Delta Q_4 \end{bmatrix}_i$$

and the governing relations are used in the following manner for the midpoint scheme:

At $i = 1$

Boundary condition equation (27a)
Momentum equation (25) (29a)
Boundary condition equation (27b)
Solid energy equation (26)

At $i = 2, 3, \ldots, I-1$

Continuity equation ($i \rightarrow i+1$ in equation 25)
Momentum equation (25) (29b)
Fluid energy equation (25)
Solid energy equation (26)

At $i = I$

Continuity equation ($i = I-1$ in equation 25)
Boundary condition (27b) (29c)
Fluid energy equation (25)
Solid energy equation (26)

The conventional method for solving equation (1) with an implicit scheme is to use central spatial differences and to use the transient solution to obtain the steady-state result. When this approach is applied to the governing equations (1) with the linearization (24), the difference equations are of the form of equation (28) where the central difference coefficients are:

$$\left.\begin{aligned} A_i &= \theta \tilde{A}_{i-1}/x_T \\ B_i &= \bar{I}/\Delta t - \theta \tilde{D}_i \\ C_i &= -\theta \tilde{A}_{i+1}/x_T \\ D_i &= S_i^n - (F_{i+1} - F_{i-1})^n/x_T \end{aligned}\right. \qquad i = 2,3,\ldots,I-1 \tag{30}$$

and

$$x_T = x_{i+1} - x_{i-1}$$

$$\theta = \begin{cases} 1 & \text{Fully implicit (or steady-state solution)} \\ 1/2 & \text{Trapezoidal scheme} \end{cases}$$

$\bar{I}$ = Unit matrix (zero for steady-state equation)

These difference equations can be used to replace the midpoint difference equations (25) except the relations for $i = 1$ have been loss. Therefore, there is a need to provide a boundary approximation at $i = 1$ and two boundary approximations at $i = I$. The solid energy equation still can be applied at $i = 1$ and I. The foregoing central difference equations (30) for the steady-state can be obtained from equation (25) and equation (25) with i replaced with $i-1$. These two equations are added and divided by x_T to obtain the additive midpoint coefficients.

$$\left.\begin{aligned} A_i &= (\tilde{A}_{i-1} + \tfrac{1}{2}\,\Delta x_{i-1}\,\tilde{D}_{i-1})/x_T \\ B_i &= -\tfrac{1}{2}\,\tilde{D}_i \\ C_i &= -(\tilde{A}_{i+1} - \tfrac{1}{2}\,\Delta x_i\,\tilde{D}_{i+1})/x_T \\ D_i &= \tfrac{1}{2}\left[\Delta x_i (S_{i+1} + S_i)^n + \Delta x_{i-1}(S_i + S_{i-1})^n\right]/x_T \\ &\quad - (F_{i+1} - F_{i-1})^n/x_T \end{aligned}\right\} \quad i = 2,3,\ldots,I-1 \tag{31}$$

The steady-state form of equations (30) becomes equations (31) if the quantities $\tilde{D}_i$ ΔQ_i and S_i are evaluated with the following weighting relation:

$$W_i = \left[\Delta x_i \ (W_{i+1} + W_i) + \Delta x_{i-1} \ (W_i + W_{i-1})\right] / (2x_T) \qquad (32)$$

Since difference equations (28) with the additive midpoint coefficients (31) are just another formulation of the midpoint scheme, the appropriate relations at $i = 1$ and I are the midpoint relations (29a) and (29c) respectively. These same boundary approximations are used with the central difference scheme (30) replacing equations (29b).

The numerical results are obtained for the following conditions:

$$\begin{array}{rl}
\varepsilon = & 0.32 \\
d_p = & 5 \times 10^{-6} \ \mathrm{m} \\
\gamma = & 1.4 \\
p_{in} = & 1.01325 \times 10^{7} \quad \mathrm{N/m^2} \\
p_{out} = & 1.01325 \times 10^{5} \quad \mathrm{N/m^2} \\
T_{in} = & 297.15 \ \mathrm{K} \\
L = & 1 \ \mathrm{cm} \\
\mu = & 1.458 \times 10^{-6} \ T_f^{1.5}/(T_f + 110.4) \quad \mathrm{kg/m\text{-}s}
\end{array}$$

$$\left.\begin{array}{rl}
h = & 18.75 \ \mathrm{J/m^2\text{-}s\text{-}K} \\
c_s = & 880.0 \ \mathrm{J/kg\text{-}K} \\
\rho_s = & 2648.0 \ \mathrm{kg/m^3} \\
\overline{M} = & 28.966 \ \mathrm{kg/(kg\ mol)} \\
R = & 8314.3 \ \mathrm{J/(kg\ mol)(K)}
\end{array}\right\} \text{Not needed for steady-state solution}$$

The numerical solution of the steady-state form of the governing equations is readily obtained with the midpoint scheme (29) and this procedure requires several iterations with rapid convergence. When the central difference scheme (30) with $\theta = 1$ and $\bar{\Upsilon} = 0$ is used, the solution does not converge. This same behavior is observed with the additive midpoint scheme. If a subtractive midpoint scheme is developed from equation (25), then this approach has the same convergence properties of the midpoint scheme. In order to obtain the steady-state solution with the central difference scheme, the transient solution approach is used. With a fully implicit scheme ($\theta = 1$) a steady-state solution is obtained while with the Crank-Nicolson approach ($\theta = 0.5$) the solution tends to have small oscillations. When the transient midpoint scheme is used, the fully implicit scheme ($\theta = 1$) converges to a steady-state while with $\theta = 0.5$ the solution has large oscillations. With more time steps the magnitude of the oscillations can be reduced. The numerical results presented with the transient procedure are for the case of $\theta = 1$.

With the midpoint scheme the numerical solution is obtained without any boundary approximations. The mass flux $\rho u \varepsilon$, which is constant through the porous media, is used to judge the accuracy of the numerical solutions with the exact solution obtained with Richardson extrapolation. The accuracy of the midpoint scheme is illustrated in figure 4 where the number of grid points through the porous media is varied. This method has the expected second-order behavior. The accuracy of the central difference scheme with the second-order midpoint boundary approximations defined by equations (29a) and 29b) has nearly the same accuracy as the midpoint scheme as shown in figure 3.

The influence of boundary approximations with the central difference scheme is investigated by replacing the momentum equation (29a) at the entry with the following first-order difference relations for the momentum equation:

$$\#1: \quad (F_{i+1} - F_i)/\Delta x_i = S_i \qquad i = 1 \tag{33a}$$

$$\#2: \quad (F_{i+1} - F_i)/\Delta x_i = S_{i+1} \qquad i = 1 \tag{33b}$$

The first boundary approximation (33a) actually improves the accuracy of the results but the overall accuracy is not completely second-order for the grid size investigated. The second boundary approximation (33b) is less accurate but the overall accuracy of the scheme has second-order behavior. The use of a first-order boundary approximation of the governing equation with a second-order interior difference scheme still results in a scheme with overall second-order behavior.

DISSIPATIVE MODEL PROBLEM

The importance of boundary condition discretization and boundary or extraneous approximations on the finite-difference solution of a dissipative type differential equation is investigated by considering the model problem

$$\frac{\partial}{\partial \eta}\left(\ell \frac{\partial W}{\partial \eta}\right) - b^2 W = 0 \tag{34}$$

with boundary conditions

At $\eta = 0$

$$\text{Dirichlet} \qquad W_B = 0 \tag{35a}$$

or

$$\text{Neumann} \qquad (\partial W/\partial \eta)_B = 0 \tag{35b}$$

At $\eta = 1$

$$W = 1 \tag{36}$$

The exact solution of this equation is

$$W_E = (e^{\alpha\eta} \pm e^{-\alpha\eta})/(e^{\alpha} \pm e^{-\alpha}) \tag{37}$$

where the plus sign corresponds to the Neumann boundary condition while the negative is for the Dirichlet boundary condition. The parameter $\alpha = b/\sqrt{\ell}$ and for the numerical solutions $b = \ell = 2$. For the Dirichlet problem, the value of W at $\eta = 0.1$ is 0.073327303 and is used to test the accuracy of the numerical solutions. For the Neumann problem the value of W at $\eta = 0$ is 0.45909813 and is used for judging the accuracy of these numerical solutions. These exact solutions for the two types of boundary conditions are given in figure 5.

The numerical discretization of the boundary conditions are approximated with the following relations where h is the grid size and the local truncation is indicated:

Dirichlet (Boundary $\eta = 0$ is located between first and second grid points and the distance from first grid point is fh where $0 \leq f \leq 1$)

First-order:

$$W_1 = W_B + 0(h) \tag{38a}$$

Second-order:

$$W_1 = W_B - f(W_2 - W_1) + 0(h^2) \tag{38b}$$

Neumann

First-order (Boundary $\eta = 0$ at first grid point)

$$(W_2 - W_1)/h = \left(\frac{\partial W}{\partial \eta}\right)_B + 0(h) \tag{39a}$$

Second-order (Boundary midway between first and second grid points)

$$(W_2 - W_1)/h = \left(\frac{\partial W}{\partial \eta}\right)_3 + 0(h^2) \tag{39b}$$

The numerical solutions are obtained with a uniform grid in order to isolate the influence of the boundary condition discretization errors. The derivative in equation (34) is evaluated with a central difference scheme and the equation becomes

$$(W_{j+1} - 2W_j + W_{j-1})/h^2 - \alpha^2 W_j = 0 \tag{40}$$

which has a local truncation error of $0(h^2)$. The resulting difference equations and boundary conditions (38) or (39) are tri-diagonal equations of the form of equation (28).

With the Dirichlet boundary condition $W = 0$ at $\eta = 0$, the numerical solution has been obtained to the model difference equation with the boundary located midway between the first and second grid points. The results for the first-order boundary condition (38a) and the second-order boundary condition (38b) are given in figure 6. A comparison of the first-order solution with the exact solution is given in figure 5. For this problem the first-order boundary condition approximation has a significant adverse influence on the solution which has first-order behavior.

The model problem has been solved with Neumann boundary conditions with a uniform grid. The results of this study are given in figure 7 for the first-order boundary conditions (equations (39a)) and second-order boundary condition (equation (39b)). A comparison of the first-order solution with the exact solution is given in figure 5. With the boundary at the first grid point, a second-order boundary condition can be obtained with the use of the governing equation. A grid point $j = 0$ is introduced beyond the boundary such that $\eta_2 - \eta_1 = \eta_1 - \eta_0 = h$. The derivative boundary condition is written as

$$(W_2 - W_0)/2h = (\partial W/\partial \eta)_B + O(h^2)$$

The governing difference equation (28) is applied at the boundary and for this case becomes

$$-\bar{A}_1 W_0 + \bar{B}_1 W_1 - \bar{C}_1 W_2 = \bar{D}_1$$

where bars have been added to the coefficients. The above equations are combined to eliminate W_0 and the boundary condition is of the form of the first equation of (28) where

$$\begin{aligned} B_1 &= \bar{B}_1 \\ C_1 &= \bar{C}_1 + \bar{A}_1 \\ D_1 &= \bar{D}_1 - 2h\,\bar{A}_1\,(\partial W/\partial \eta)_B \end{aligned}$$

This method gives a second-order boundary condition with the same accuracy of the previous methods.

The foregoing investigation of the influence of boundary condition numerical error can also be investigated analytically. The exact solution of the difference equation (40) is

$$W_j = a\,\sigma_1^{\,j-1} + b\,\sigma_2^{\,j-1} \tag{41}$$

and for the exact Dirichlet boundary condition (35a) becomes

$$W_j = \left(\sigma_1^{\,j-1} - \sigma_2^{\,j-1}\right)/\left(\sigma_1^{\,J-1} - \sigma_2^{\,J-1}\right) \qquad j = 1,2,\ldots,J \tag{42}$$

where

$$\sigma_{1,2} = 1 \pm \alpha h + \frac{1}{2}(\alpha h)^2 \pm \frac{1}{8}(\alpha h)^3 + \ldots$$
$$= e^{\pm\alpha h} \mp \frac{1}{24}(\alpha h)^3 + \ldots$$

The terms in equation (42) are approximated as

$$\sigma_{1,2}{}^{j-1} = e^{\pm\alpha\eta_j}\left(1 \mp \frac{1}{24}\alpha^3 h^2 \eta_j + \ldots\right) \qquad (43)$$

The error of the difference solution is defined as

$$E = (W_j - W_E) \;/\; W_E \qquad (44)$$

The difference solution or global error with the use of equations (37), (42) and (43) in equation (44) becomes

$$E = E_2 h^2 + \ldots \qquad (45)$$

where

$$E_2 = \frac{1}{24}\alpha^3(\coth\alpha - \eta_j \coth\alpha\eta_j)$$

This shows that the central difference scheme with exact Dirichlet boundary conditions results in a second-order global error.

Consider the case where the Dirichlet boundary condition is located between the first and second grid points. The exact solution (37) to this case is

$$W_E = \sinh\alpha\eta/\sinh\alpha \qquad (46)$$

The difference solution of equation (40) with boundary conditions (38) becomes

$$W_j = \phi_j/\phi_J \qquad (47)$$

where

$$\phi_j = (1 - c\sigma_1)\,\sigma_2{}^{j-1} - (1 - c\sigma_2)\,\sigma_1{}^{j-1}$$

$W_1 = CW_2$ C = 0 for boundary condition (38a)

C = −f/(1−f) for boundary condition (38b)

Since $\eta_j = h(j-1) - fh$ and $\sigma_{1,2}$ is given by equation (42), the following is obtained:

$$\sigma_{1,2}^{\;j-1} = e^{\pm\alpha\eta_j} \left[1 \pm f\alpha h + \frac{1}{2}(\alpha f h)^2 \mp \frac{1}{24}\alpha^3 \eta_j h^2 + \ldots\right] \qquad (48)$$

The error as defined by equation (44) becomes with equations (37), (47) and (48) the following:

First-order Boundary Condition (38a)

$$E = f\alpha\,(\coth \alpha\eta_j - \coth \alpha)\,h + \ldots \qquad (49a)$$

Second-order Boundary Condition (38b)

$$E = E_2\,h^2 + \ldots \qquad (49b)$$

Therefore the global accuracy corresponds to the local truncation error of the boundary condition. The errors predicted from equations (49) are the solid lines in figure 6 and are in excellent agreement with the numerical computations indicated with the circles.

If the first-order Neumann boundary condition (39a) is used, the difference solution is

$$W_j = \phi_j/\phi_J \qquad (50)$$

where

$$\phi_j = \lambda_2\,\sigma_1^{\;j-1} - \lambda_1\,\sigma_2^{\;j-1}$$

$$\lambda_{1,2} = (1 - \sigma_{1,2}) = \mp h\,(1 \pm \alpha h + \ldots)$$

With the use of equations (37) and (43), the error for the above difference equation becomes

First-order Boundary Condition (39a)

$$E = \frac{1}{2}\,\alpha\,(\tanh \alpha - \tanh \alpha\eta_j)h + \ldots \qquad (51a)$$

For the second-order Neumann boundary condition (39b), the difference solution is given by equation (47) where C = 1. The use of equations (42) and (48) with $f = 0.5$ gives the error of the difference solution as

Second-order Boundary Condition (39b)

$$E = \frac{1}{24} \alpha^3 (\tanh \alpha - \eta_j \tanh \alpha\eta_j) h^2 + \ldots \tag{51b}$$

The global accuracy corresponds to the local truncation error of the Neumann boundary conditions. The errors predicted from Equations (51) are the solid lines in Figure 7 and are in excellent agreement with the numerical computations indicated with the circles.

In order to investigate the influence of boundary or extraneous approximations, it is assumed that a relation is needed to determine W_2 while W_1 is known from the Dirichlet boundary condition (35a). Extrapolation approximations are considered first where the local truncation error is indicated and obtained from a Taylor's series expansion

First-order: $$W_2 = W_1 + O(h) \tag{52a}$$

Second-order: $$W_2 = W_1 + (W_3 - W_1) / 2 + O(h^2) \tag{52b}$$

The finite-difference solution is given by Equation (50) where

$$\lambda_{1,2} = \sigma_{1,2} = 1 \pm \alpha h + \ldots \tag{53a}$$

and

$$\lambda_{1,2} = \sigma_{1,2} (\sigma_{1,2} - 2) = -1 + (\alpha h)^2 \pm (\alpha h)^3 + \ldots \tag{53b}$$

for the first and second order approximations respectively. The solution error becomes

First-order boundary approximation (52a)

$$E = \alpha (\coth \alpha - \coth \alpha\eta_j) h + \ldots \tag{54a}$$

Second-order, boundary approximation (52b)

$$E = E_2 h^2 + \ldots . \tag{54b}$$

The locally second-order extrapolation approximation results in global second-order accuracy and has the same error as the central difference scheme (45).

Another approach for obtaining a boundary approximation is to difference the governing equation and for this case the result is

$$(W_{j+1} - 2\,W_j + W_{j-1})/h^2 - \alpha^2[\theta W_{j-1} + (1 - \theta)\,W_j] = 0 \qquad (55)$$

where

$$\theta = \begin{cases} 1 & \text{First-order local truncation error} \\ 0 & \text{Second-order local truncation error} \end{cases}$$

If $\theta = 0$, then equation (40) is obtained and a second-order global accuracy results as given by equation (45). If $\theta = 1$, the solution to difference equation (55) is given by equation (42) where

$$\sigma_{1,2} = 1 \pm \alpha h$$

and

$$\sigma_{1,2}^{\,j-1} = e^{\pm\alpha\eta_j}\,(1 - \tfrac{1}{2}\,\alpha^2\eta_j h + \ldots)$$

The difference solution error becomes

$$E = \tfrac{1}{2}\,\alpha^2\,(1 - \eta_j)h + \ldots$$

which shows that the global accuracy is first-order. If the first-order form of Equation (55) is used at $j = 2$, the difference relation (55) becomes

$$W_2 = \tfrac{1}{2}\left[(W_1 + W_3) - (\alpha h)^2\,W_1\right] + O(h^3) \qquad (56)$$

When this approximation is used along with the second-order form of equation (55) at all the remaining grid points, the difference solution error is the same as equation (45) and the global error is second-order. This behavior have been observed previously by Srivastava, Werle and Davis [14] and is the only case where a first-order approximation has not destroyed the second-order global accuracy. Although equation (56) represents the governing equation with a first-order local truncation error, the approximation appears to be third-order when written as equation (56) and is compared to the extrapolation relations (52). This example illustrates the importance of stating whether extrapolation or a difference form of the governing equation is being used to provide the boundary approximation.

SUMMARY OF RESULTS

1. For the quasi-one-dimensional flow in a duct with the interior grid points solved with the MacCormack scheme, the boundary approximations have the following influences on the accuracy of the solution:

a. For boundary approximation difference relations that are inconsistent with the interior scheme, small oscillations near the boundary occur.

b. The midpoint relation gives the most accurate results for the procedures investigated.

c. With first-order extrapolation boundary approximations, the global accuracy is generally reduced to first-order.

2. An interior implicit midpoint difference technique is utilized for solving the compressible one-dimensional flow in a porous material (or quasi-one-dimensional flow with friction). This procedure is consistent with the boundary conditions and does not require any boundary approximations. When spatial central differences are used in the interior implicit scheme, three boundary approximations are required to complete the system of difference equations. The midpoint scheme provides guidance in indicating the appropriate boundary approximations to be employed. If first-order boundary approximations to the governing equations are used, the global accuracy of the solutions still tends to be second-order.

3. Boundary condition discretization accuracy has significant influence on the global accuracy of a dissipative (second derivative) model problem. When a second-order interior difference scheme is used, the use of first-order boundary condition discretization reduces the overall accuracy of the solution to first-order. This result occurs for both Dirichlet and Neumann boundary conditions. A boundary approximation investigation indicates that global second-order accuracy is retained with second-order extrapolation and with the model equation approximated with first-order accuracy.

REFERENCES

1. E. Turkel, "Numerical Methods for Large-Scale, Time-Dependent Partial Differential Equations," Computational Fluid Dynamics Vol. 2, Edited by W. Kollmann, Hemisphere Publishing Corp. (1980).

2. B. Gustafsson, "The Convergence Rate for Difference Approximations to Mixed Initial Boundary Value Problems," Math Comp., Vol. 29, pp 396-406 (1975).

3. G. Skollermo, "Error Analysis of Finite Difference Schemes Applied to Hyperbolic Initial Boundary Value Problems," Math Comp., Vol. 33, pp 11-35 (1979).

4. J. H. Bramble and B. E. Hubbard, "On the Formulation of Finite Difference Analogues of the Dirichlet Problem for Poisson's Equation," Numerishe Mathematik, Vol. 4, pp 313-327 (1962).

5. P. D. Thomas, "Boundary Conditions for Implicit Solutions to the Compressible Navier-Stokes Equations in Finite Computational Domains", AIAA Computational Fluid Dynamics Conference, Paper No. 79-1447, (1979).

6. G. Moretti and M. Pandolfi, "On the Calculation of Subsonic Flows in Ducts", AIAA Journal, Vol. 19, pp. 449-457, (1981).

7. A. H. Shapiro, Compressible Fluid Flow, Vol. II, Ronald Press Company (1954).

8. M. D. Griffin and J. D. Anderson, Jr. "The Application of Boundary Conditions to Time-Dependent Computations for Quasi-One-Dimensional Fluid Flows", Computers and Fluids, Vol. 5, pp. 127-237, (1977).

9. S. Ergun, "Fluid Flow Through Packed Columns", Chemical Engr. Prog., Vol. 48, pp. 89-93, (1952).

10. G. Emanuel and J. P. Jones, "Compressible Flow Through a Porous Plate", Int. J. Heat Mass Transfer, Vol. 11, pp. 827-836, (1968).

11. T. E. W. Schumann, "Heat Transfer: A Liquid Flowing Through a Porous Prism", Jour. Franklin Inst., Vol. 208, pp. 405-416, (1929).

12. F. A. Morrison, "Transient Non-Darcy Gas Flow in a Finite Porous Bed", Jour. of Fluids Engineering, Trans ASME, Vol. 99, pp. 779-781, (1977).

13. S. V. Patankar, Numerical Heat Transfer and Fluid Flow, Hemisphere Publishing Corp. McGraw-Hill Book Company, (1980).

14. B. N. Srivastava, M. J. Werle and R. T. Davis, "A Finite Difference Technique Involving Discontinuous Derivatives", Computers and Fluids, Vol. 7, pp. 69-74, (1979).

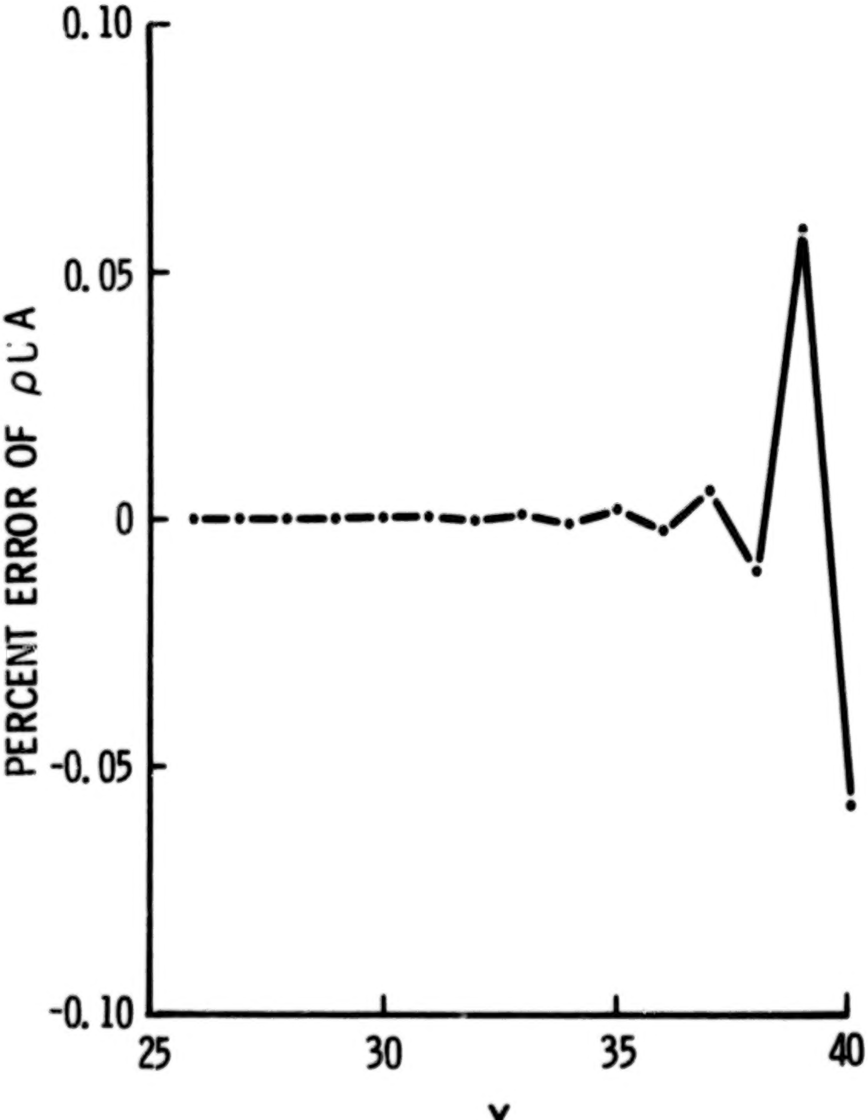

FIG. 1 - INFECTION OF COMPUTATIONAL BOUNDARY RELATION WITH LINEAR EXTRAPOLATION AND SUPERSONIC EXIT FLOW

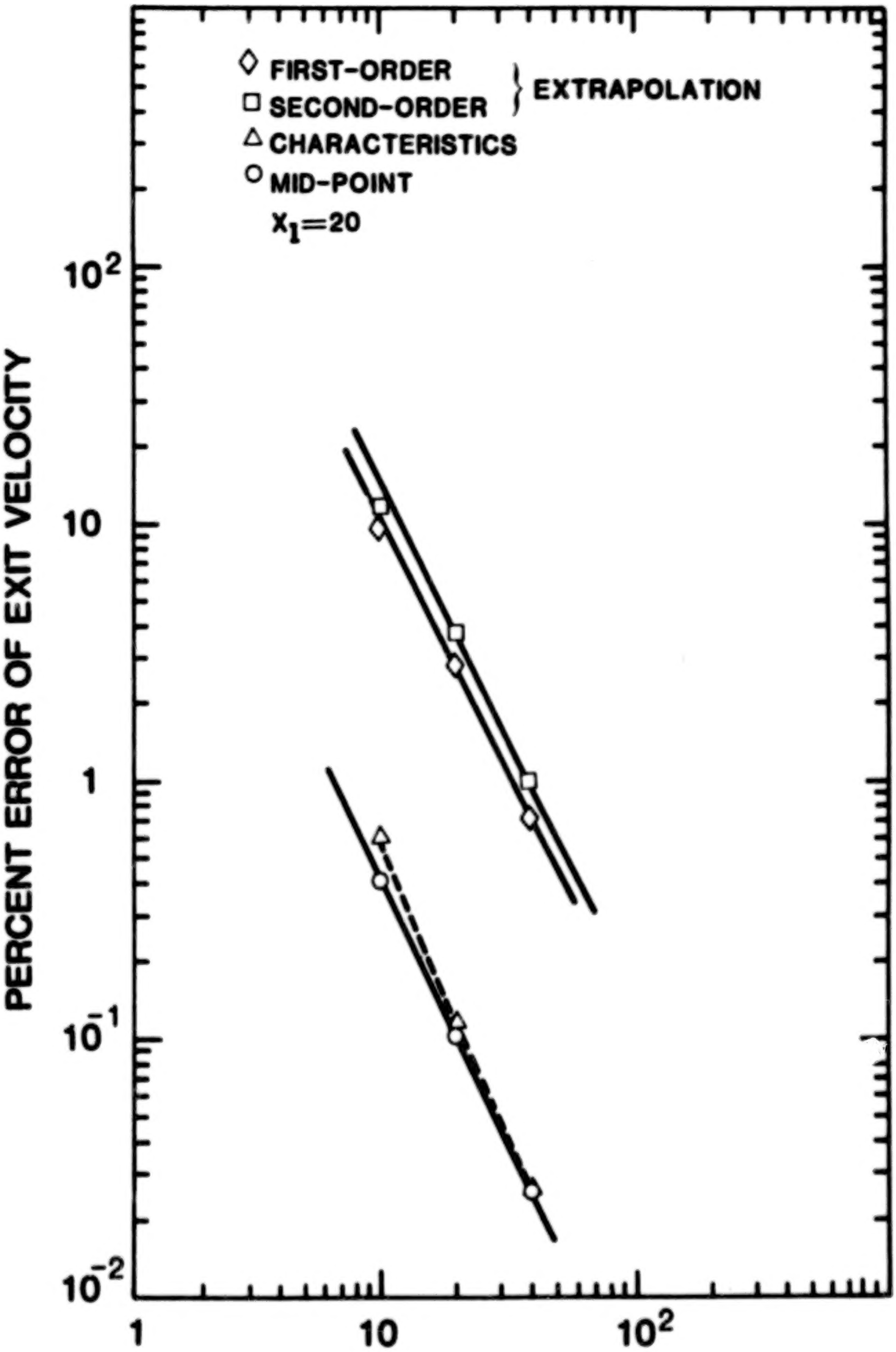

Figure 2. Accuracy of exit velocity with various exit boundary approximations for steady-state, quasi-one-dimensional flow

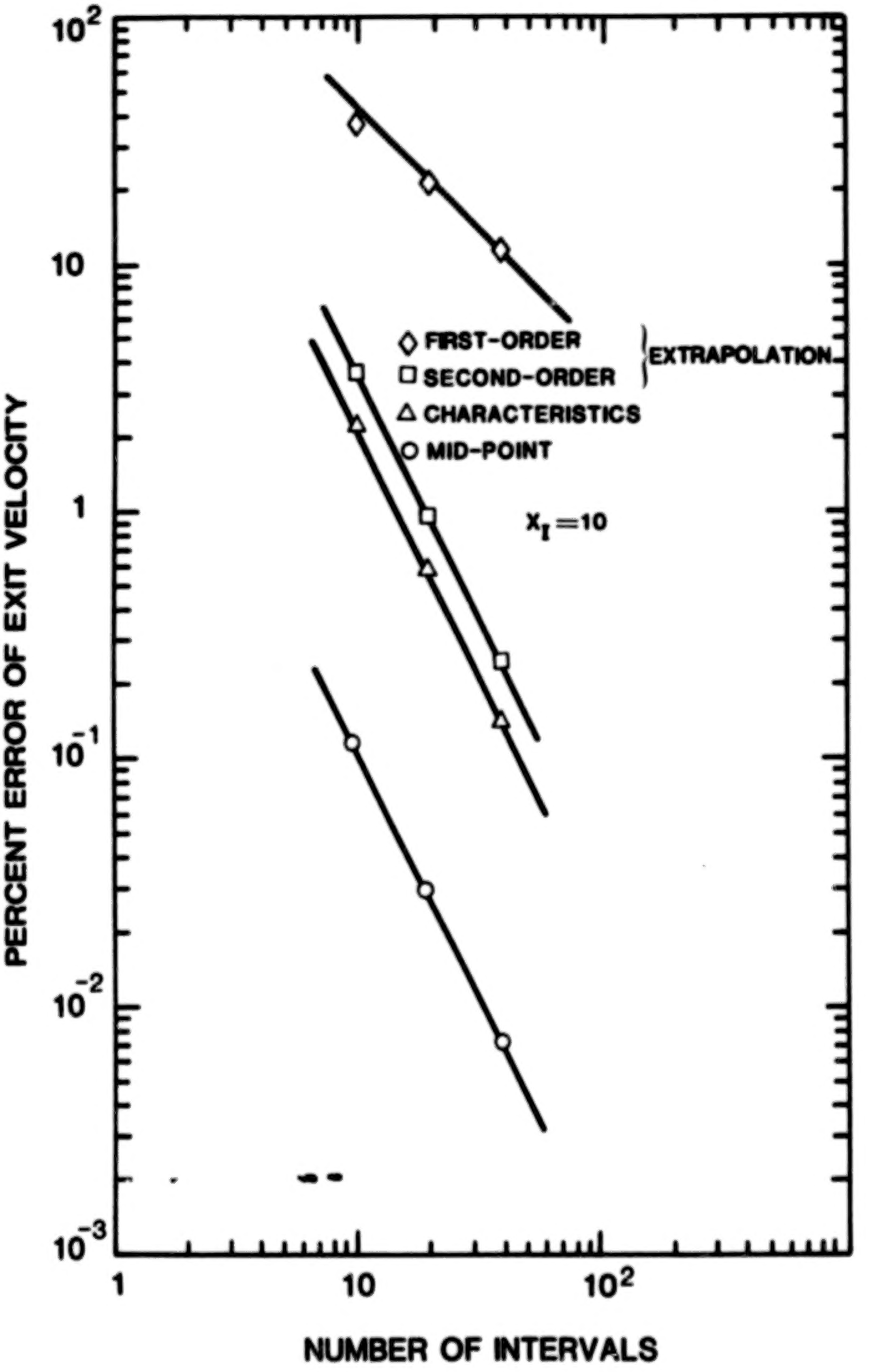

Figure 3. Accuracy of exit velocity with various exit boundary approximations for steady-state, quasi-one-dimensional flow

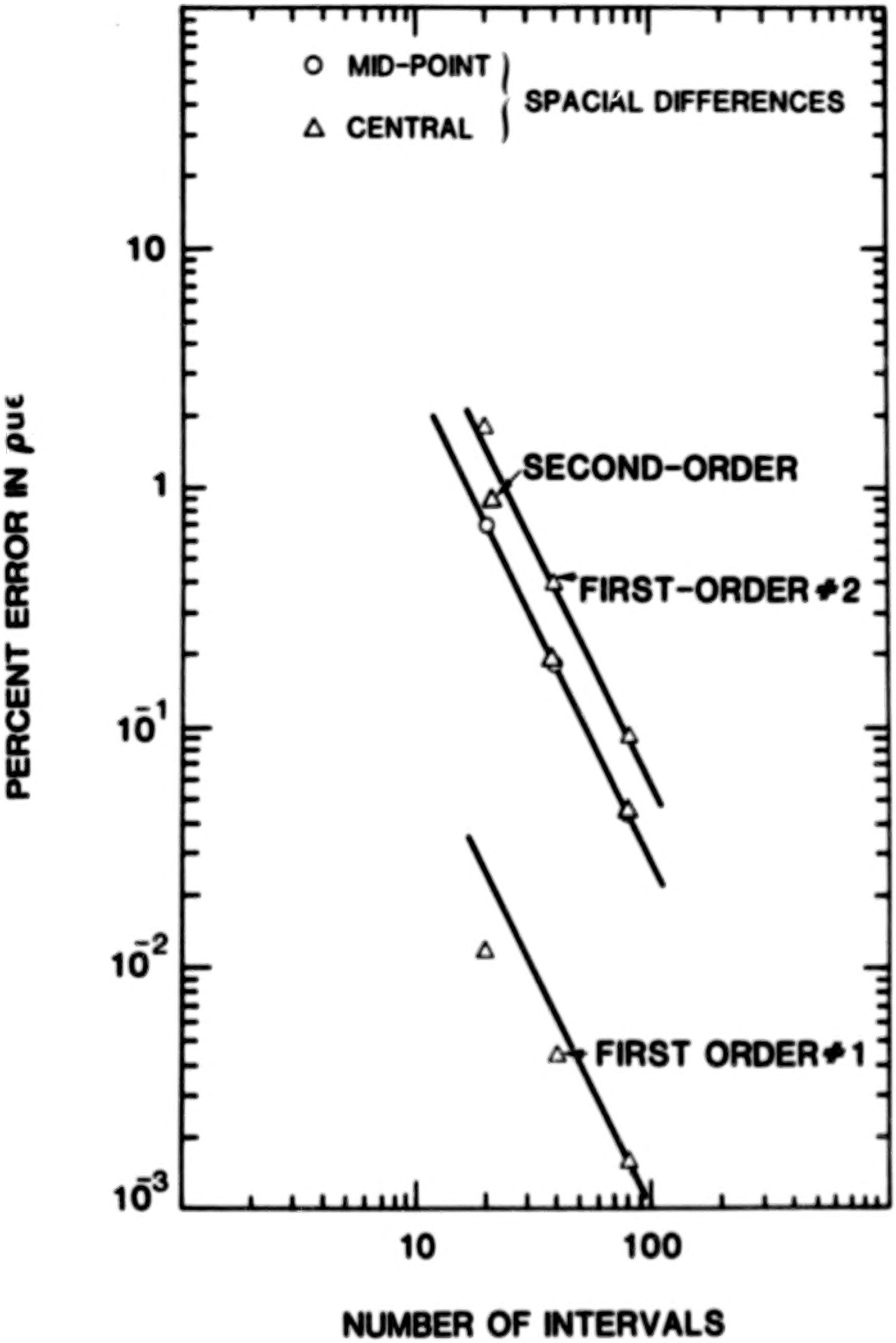

Figure 4. Accuracy of Mass Flux in Porous Media with Several Entry Boundary Approximations.

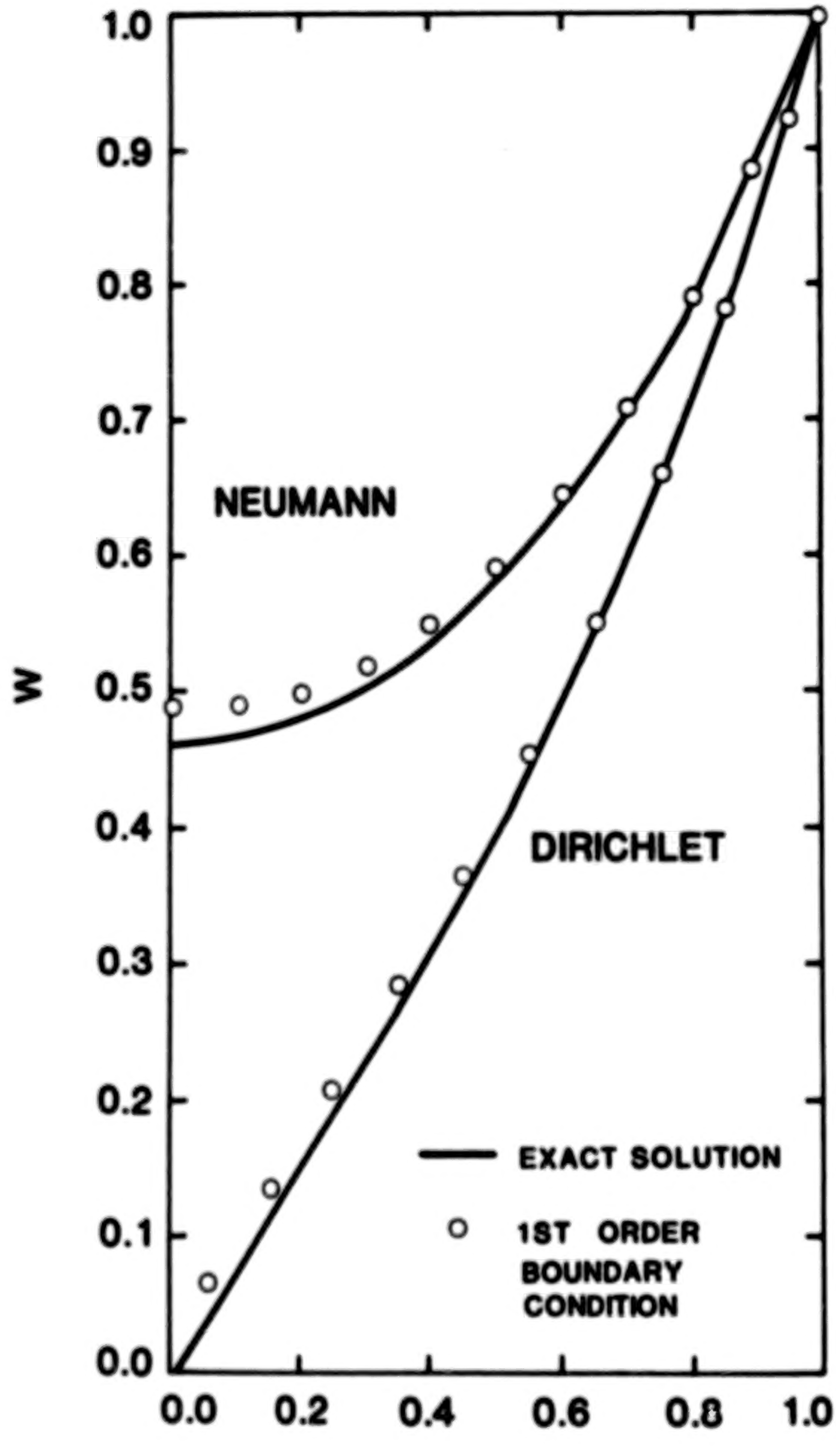

Figure 5. Solution of Dissipative Model Problem.

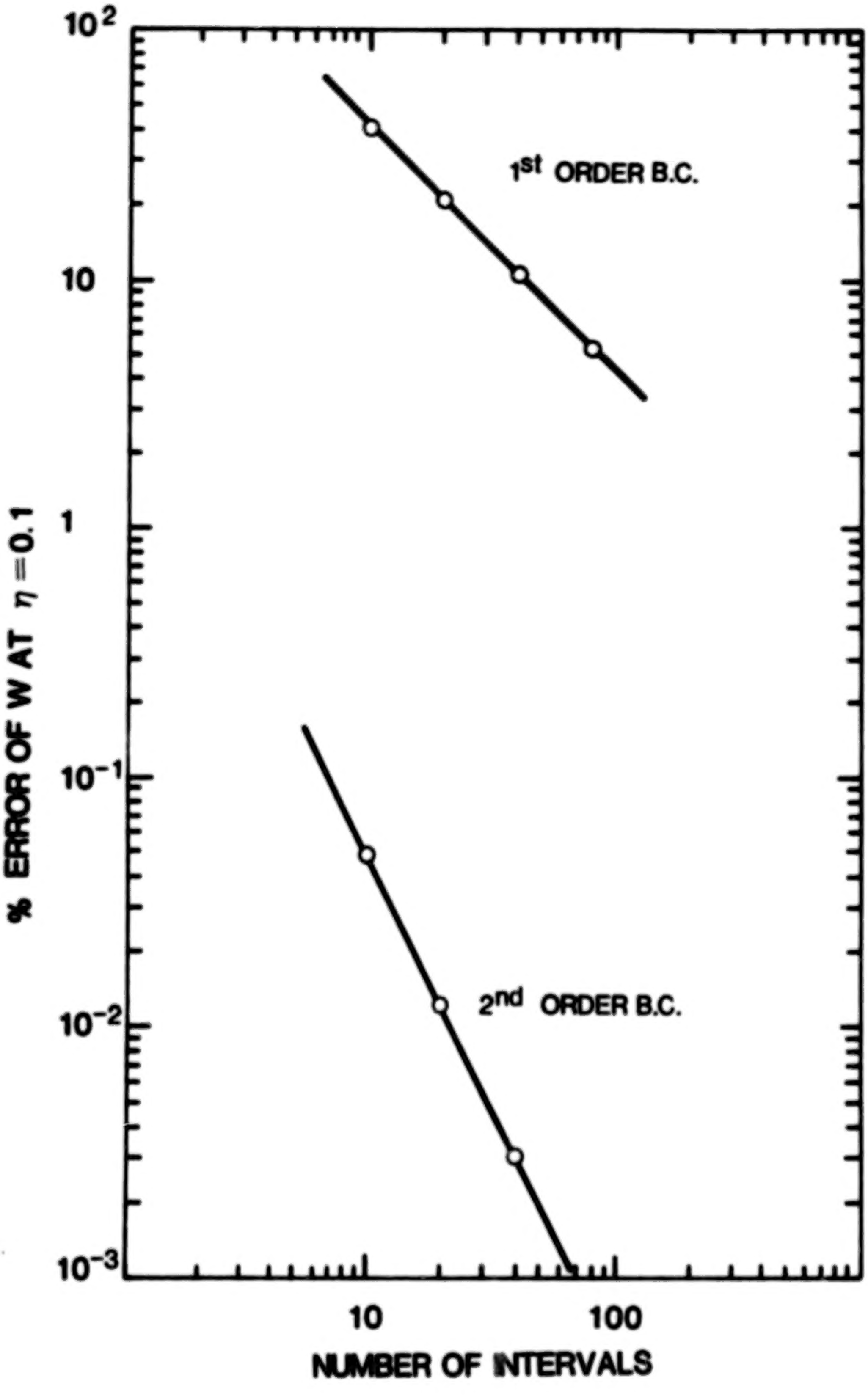

Figure 6. Dirichlet boundary condition for dissipative model problem.

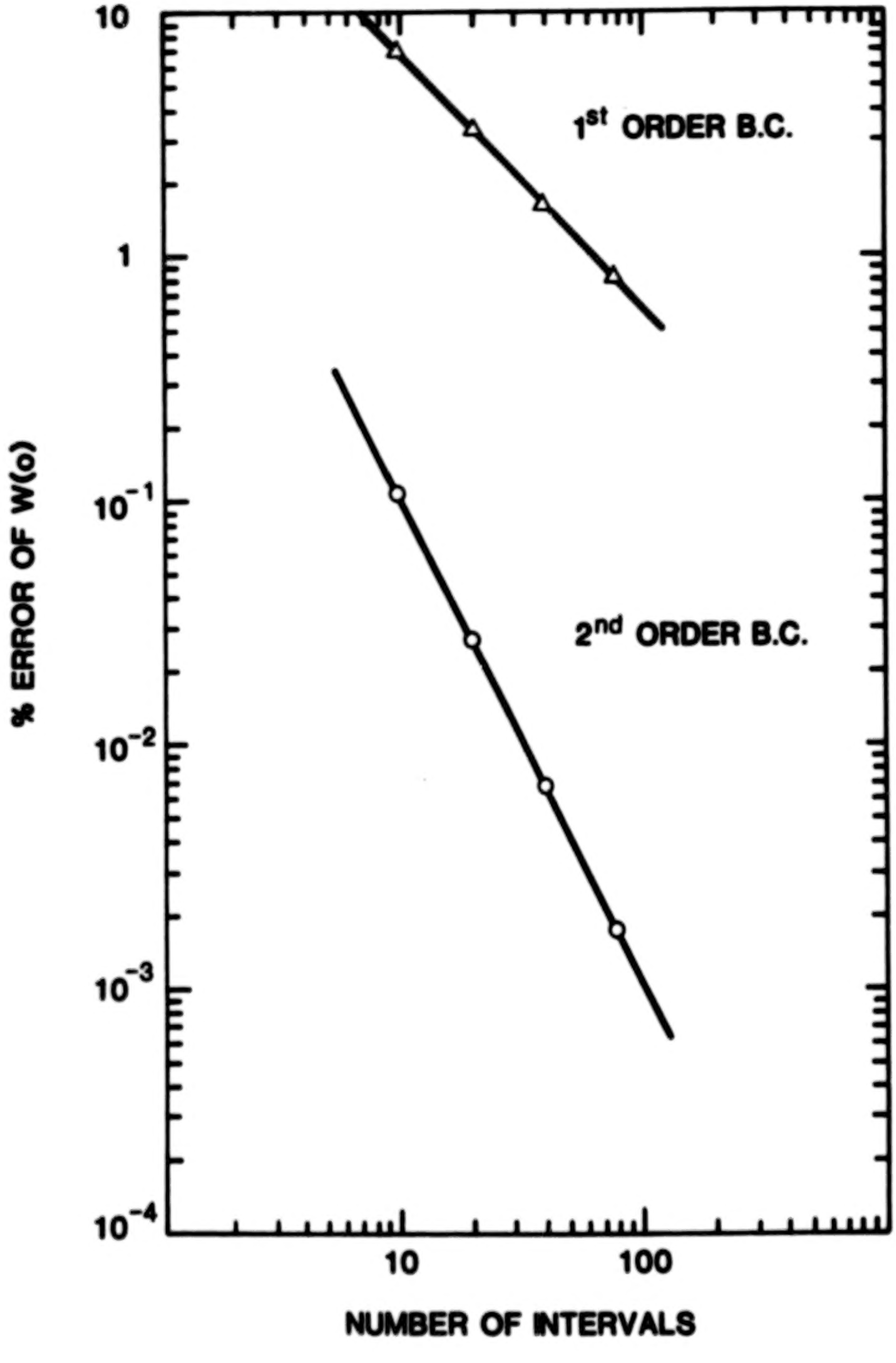

Figure 7 Neumann boundary condition for dissipative model problem.

STABILITY ANALYSIS OF NUMERICAL BOUNDARY CONDITIONS AND IMPLICIT DIFFERENCE APPROXIMATIONS FOR HYPERBOLIC EQUATIONS[1]

R. M. Beam, R. F. Warming, and H. C. Yee
Ames Research Center

ABSTRACT

Implicit, noniterative, finite-difference schemes have recently been developed by several authors for multidimensional systems of nonlinear hyperbolic partial differential equations. When applied to linear model equations with periodic boundary conditions those schemes are unconditionally stable (A-stable). As applied in practice the algorithms often face a severe time-step restriction. A major source of the difficulty is the treatment of the numerical boundary conditions. One conjecture has been that unconditional stability requires implicit numerical boundary conditions. An apparent counter example was the space-time extrapolation considered by Gustafsson, Kreiss, and Sundström. In this paper we examine spatial (implicit) and space-time (explicit) extrapolation using normal mode analysis for a finite and infinite number of spatial mesh intervals. The results indicate that for unconditional stability with a finite number of spatial mesh intervals the numerical boundary conditions must be implicit.

1. INTRODUCTION

The boundary-condition analysis described in this paper was motivated by the application of implicit finite difference algorithms to hyperbolic partial differential equations. As a simple example, consider the quasi-one-dimensional inviscid flow described by the gas-dynamic equations in conservative form:

$$\frac{\partial U}{\partial t} + \frac{\partial F(U)}{\partial x} + H(U) = 0 \tag{1.1}$$

A typical implicit algorithm has the form

$$\left[I + \Delta t \left(\frac{\partial}{\partial x} A^n + D^n\right)\right] \Delta U^n = -\Delta t \left(\frac{\partial F}{\partial x} + H\right)^n \tag{1.2}$$

where $\Delta U^n = U^{n+1} - U^n$, $A = \partial F/\partial U$, $D = \partial H/\partial U$ and $\partial/\partial x$ is approximated by a 3-point central difference operator. Consider the nozzle sketched in Figure 1.1 with purely supersonic flow. For a well-posed problem U is

---

[1] The one-step method results of this paper were presented at the SIAM 1981 National Meeting, Troy, New York, June 8-10, 1981.

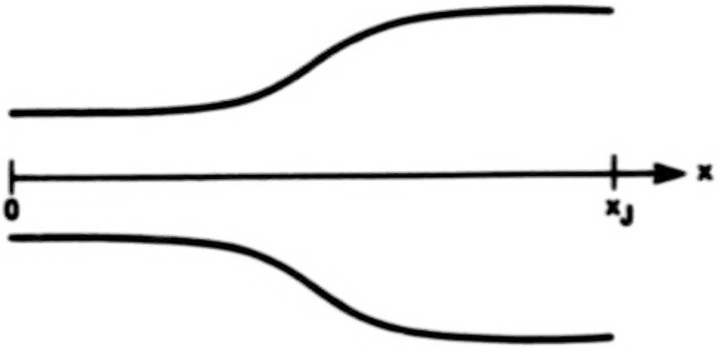

Figure 1.1.- Divergent nozzle (ref. 1).

specified on the inflow boundary ($x = 0$) and nothing is given on the supersonic outflow boundary. Algorithm (1.2) with central spatial differencing requires "numerical" boundary conditions on the right boundary at $x = x_J$. One way of providing the numerical boundary condition is by simply setting

$$\Delta U_J^n = 0 \tag{1.3a}$$

on the right boundary and, after the interior solution is computed (by a block tridiagonal inversion), extrapolating the numerical solution to J

$$U_J^{n+1} = U_{J-1}^{n+1} \tag{1.3b}$$

For the backward Euler temporal differencing used in (1.2) procedure (1.3) is linearly equivalent to using zeroth-order space-time extrapolation

$$U_J^{n+1} = U_{J-1}^n \tag{1.4}$$

as the numerical boundary condition. There are two good reasons for using (1.3), or (1.4), as the numerical boundary scheme: it is extremely simple to implement and the interior scheme (1.2) with either (1.3) or (1.4) is stable for the initial-boundary-value problem according to a (linear) normal mode analysis of Gustafsson, Kreiss, and Sundström (ref. 2).

To test the stability of the scheme (1.2), (1.3) we computed the steady-state solution to the nozzle flow (fig. 1.1) using various CFL numbers. The number of time steps to converge is tabulated in table 1.1. We found the following peculiar results: Let J be the number of spatial intervals. For an odd value of J the scheme is unconditionally stable but if J is even there is a finite stability limit. For even J the stability limit depends on J. In addition, if we replace the zeroth-order extrapolation (1.4) by a linear space-time extrapolation

$$U_J^{n+1} = 2U_{J-1}^n - U_{J-2}^{n-1} \tag{1.5}$$

we obtain similar results but with a lower CFL limit (for the case of J even).

TABLE 1.1.- ZEROTH-ORDER SPACE-TIME
EXTRAPOLATION

19 spatial intervals		20 spatial intervals	
CFL	Number of steps to converge	CFL	Number of steps to converge
1	274	1	283
10	33	5	50
20	48	10	34
30	46	15	52
40	42	20	92
50	56	22	141
60	67	23	199
70	77	24	353
80	84	25	2072
90	90	26	does not converge
10^2	93	27	does not converge
10^3	20		
10^4	15		
10^5	14		
10^6	14		
10^9	14		

The linear stability analysis of Gustafsson, Kreiss, and Sundström (GKS) (ref. 2) for the above problem is based on a theorem due to Kreiss (ref. 3) which relates the stability of the initial-boundary-value problem on a finite interval to the stability of the difference approximation applied to the Cauchy problem and the right- and left-quarter plane problems. From the GKS-analysis it is clear that the results of a quarter-plane problem cannot predict either the stability dependence on the number of mesh intervals (odd or even) or the dependence of the stability limit on the order of the space-time extrapolation.

In this paper we analyze the initial-boundary-value problem on the finite interval with a finite number of mesh points. This leads to a more restrictive definition of stability (than GKS-stability) which we call P-stability.

In section 2 we give the difference approximations for the model scalar hyperbolic equation. We use a central spatial difference approximation and a linear multistep formula for the time integration. The extra numerical boundary condition is approximated by q-th order space or space-time extrapolation. In section 3 we review the definition of A-stability and define GKS-stability and P-stability. In addition, we delineate the normal-mode analysis for a quarter-plane problem.

Section 4 contains the stability analysis and the main results of this paper. We prove three theorems regarding the GKS-stability and P-stability of A-stable linear multistep methods and space or space-time boundary extrapolation. To simplify the proofs we make use of known properties of the stability regions of A-stable linear multistep methods. In the appendix we present a more detailed analysis of the necessary and sufficient P-stability conditions for the class of one-step methods and space-time boundary extrapolation. The results show, for example, that the backward Euler method has a P-stability bound that depends on the number of spatial intervals: for an odd number of spatial intervals it is unconditionally P-stable; for an even number of spatial intervals it is conditionally P-stable with the bound being a function of the number of spatial intervals (fig. 1.2). Our analysis explains the peculiar computational results of table 1.1.

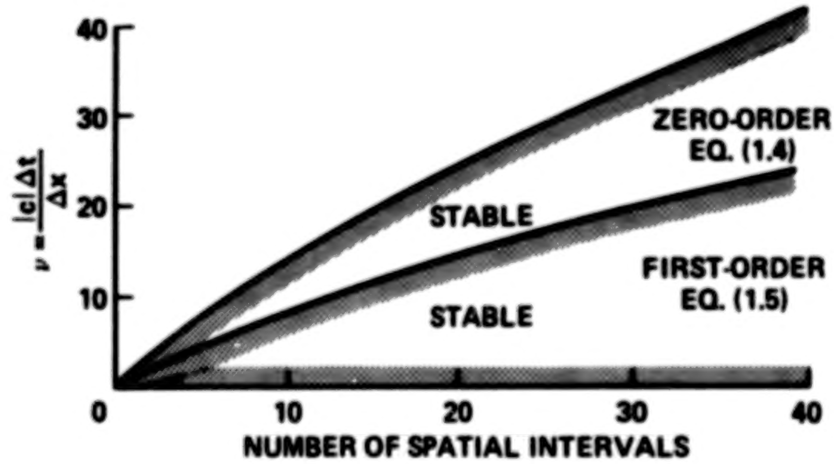

Figure 1.2.- P-stability bound for Euler implicit and space-time extrapolation (even number of spatial intervals).

We give a complete P-stability analysis for the class of all A-stable interior algorithms with all orders of space extrapolation as the numerical boundary condition, for example, zeroth-order space extrapolation

$$U_J^{n+1} = U_{J-1}^{n+1} \tag{1.6}$$

and first-order space extrapolation

$$U_J^{n+1} = 2U_{J-1}^{n+1} - U_{J-2}^{n+1} \tag{1.7}$$

We show that all of these schemes are unconditionally P-stable. As a numerical test, table 1.2 presents results of the nozzle problem when (1.6) is used as the numerical boundary condition.

A more detailed discussion of the implementation of the boundary conditions for the equations of gas dynamics is presented in reference 1.

TABLE 1.2.- ZEROTH-ORDER SPACE EXTRAPOLATION

20 spatial intervals	
CFL	Number of steps to converge
1	295
10	28
20	15
30	11
40	9
50	8
60	7
70	7
80	6
90	6
10^2	6
10^3	4
10^4	4
10^5	4
10^6	4
10^9	4

2. DIFFERENCE APPROXIMATIONS AND BOUNDARY CONDITIONS

In this paper we consider the numerical stability of finite difference approximations for the scalar hyperbolic initial-boundary-value problem

$$u_t - cu_x = 0 , \qquad 0 \leq x \leq \ell , \qquad t \geq 0 \tag{2.1a}$$

where $c > 0$. For a well-posed problem, initial data are given at $t = 0$

$$u(x,0) = f(x) , \qquad 0 \leq x \leq \ell \tag{2.1b}$$

and boundary values are prescribed at $x = \ell$

$$u(\ell,t) = g(t) \tag{2.1c}$$

For the spatial mesh we divide the interval $0 \leq x \leq \ell$ into J equally spaced intervals, $\Delta x = \ell/J$, i.e., $x = j\Delta x$ $(j = 0,1,2,\ldots,J-1,J)$. We consider only the centered three-point spatial difference approximation to $\partial u/\partial x$ in (2.1a), i.e.

$$\frac{du_j}{dt} - c\,\frac{u_{j+1} - u_{j-1}}{2\Delta x} = 0 , \qquad j = 1,2,\ldots,J-1 \tag{2.2}$$

To integrate the first-order system of ordinary differential equations (2.2) we use a linear k-step formula defined by

$$\rho(E)u^n = \Delta t\sigma(E)\frac{du^n}{dt} \tag{2.3}$$

where ρ and σ are the generating polynomials

$$\rho(\zeta) = \sum_{i=0}^{k} \alpha_i\zeta^i , \qquad \sigma(\zeta) = \sum_{i=0}^{k} \beta_i\zeta^i \tag{2.4a,b}$$

and E is the shift operator, that is,

$$Eu^n = u^{n+1} \tag{2.5}$$

In (2.3), u^n is the numerical solution at $t = t^n = n\Delta t$ and Δt is the time step. As an example, the most general consistent two-step formula (i.e., $k = 2$ in (2.4)) can be written as

$$(1 + \xi)u^{n+2} - (1 + 2\xi)u^{n+1} + \xi u^n = \Delta t \left[\theta \frac{du^{n+2}}{dt} + (1 - \theta + \phi) \frac{du^{n+1}}{dt} - \phi \frac{du^n}{dt}\right] \tag{2.6}$$

where (θ,ξ,ϕ) are arbitrary real numbers. The operators $\rho(E)$ and $\sigma(E)$ are

$$\rho(E) = (1 + \xi)E^2 - (1 + 2\xi)E + \xi \tag{2.7a}$$

$$\sigma(E) = \theta E^2 + (1 - \theta + \phi)E - \phi \tag{2.7b}$$

If we apply the linear k-step formula (2.3) to (2.2) we obtain

$$\rho(E)u_j^n = \frac{c\Delta t}{2\Delta x}\sigma(E)(u_{j+1}^n - u_{j-1}^n) , \qquad \begin{array}{l} j = 1,2,\ldots,J-1, \\ n = k,k+1,k+2,\ldots \end{array} \tag{2.8}$$

The values u_J^n are obtained from the prescribed analytical boundary condition (2.1c), i.e.,

$$u_J^n = g(n\Delta t) , \qquad n = 1,2,\ldots \tag{2.9}$$

To complete the computational algorithm we need, in addition to (2.8) and (2.9), a method for computing the values of u_j^n at the boundary $j = 0$, i.e., u_0^n; and a prescription for initial values u_j^n, $n = 0,1,\ldots,k-1$, $j = 1,2,\ldots,J-1$.

For the calculation of the boundary values u_0^n we consider two extrapolation techniques: space extrapolation

$$(F - 1)^q u_j^n = 0 , \qquad j = 0 , \qquad q = 1,2,\ldots \tag{2.10}$$

and space-time extrapolation

$$(FE^{-1} - 1)^q u_j^n = 0 , \quad j = 0 , \quad q = 1,2,... \tag{2.11}$$

where F is the spatial shift operator

$$Fu_j^n = u_{j+1}^n \tag{2.12}$$

and E is the temporal shift operator (2.5). The two lowest degree spatial extrapolations ($q = 1,2$) are simply zeroth- and first-order extrapolation

$$u_0^n = u_1^n \tag{2.13a}$$

$$u_0^n = 2u_1^n - u_2^n \tag{2.13b}$$

or zeroth- and first-order space-time extrapolation

$$u_0^n = u_1^{n-1} \tag{2.14a}$$

$$u_0^n = 2u_1^{n-1} - u_2^{n-2} \tag{2.14b}$$

The initial values u_j^0 are obtained from the analytical initial condition (2.1b), i.e.,

$$u_j^n = f(j\Delta x) , \quad j = 0,1,...,J \tag{2.15}$$

For higher order k-step methods ($k > 1$) we assume that additional levels of initial data are given or they are calculated using an alternate numerical method.

In the following sections we investigate the numerical stability of the algorithm defined by (2.8), (2.9), and (2.10) or (2.11).

3. NUMERICAL STABILITY DEFINITIONS

In this section we first review the definition of A-stable linear multistep methods. Next, we review the normal mode stability analysis of Kreiss (ref. 3) and Gustafsson, Kreiss, and Sundström (ref. 2) and define GKS-stability. Finally we add an additional constraint to the GKS-stability and define what we believe is a stability definition applicable to many practical calculations.

3.1 A-Stability

If the linear k-step formula (2.3) is used to integrate the first-order ordinary differential equation

$$\frac{du}{dt} = f(u,t) , \quad u(0) = u_0$$

one obtains the linear multistep method (LMM)

$$\rho(E)u^n = \Delta t\sigma(E)f^n \tag{3.1}$$

The linear stability of an LMM is analyzed by applying (3.1) to the linear test equation

$$\frac{du}{dt} = \lambda u \tag{3.2}$$

where, in general, λ is a complex constant. The stability region of an LMM consists of the set of all values of $\lambda\Delta t$ for which the characteristic equation

$$\rho(\zeta) - \lambda\Delta t\sigma(\zeta) = 0 \tag{3.3}$$

satisfies the root condition; that is, its roots ζ_ℓ all satisfy $|\zeta_\ell| \leq 1$ and the roots of unit modulus are simple (ref. 4).

An LMM is said to be A-stable (ref. 5) if its stability region contains all of the left half of the complex $\lambda\Delta t$ plane including the imaginary axis. It can be shown (ref. 6) that a linear two-step method, i.e., (2.6), is A-stable if and only if

$$\theta \geq \phi + \frac{1}{2} \tag{3.4a}$$

$$\xi \geq -\frac{1}{2} \tag{3.4b}$$

$$\xi \leq \theta + \phi - \frac{1}{2} \tag{3.4c}$$

In this paper, for the stability analysis, we assume that the temporal difference approximation (2.3) would produce an A-stable LMM. In part of the analysis a stronger stability definition is required.

> An LMM is said to be strongly A-stable if (i) it is A-stable, (ii) its stability boundary locus is tangent to the imaginary axis only at the origin, and (iii) all roots of $\rho(\zeta)$ are inside the unit circle except for the root $\zeta = 1$.

For example, the backward Euler ($\theta = 1$, $\xi = 0$, $\phi = 0$), second-order backward differentiation ($\theta = 1$, $\xi = 1/2$, $\phi = 0$), and Adams type ($\theta = 3/4$, $\xi = 0$, $\theta = -1/4$) methods are strongly A-stable; however, the one-step trapezoidal rule ($\theta = 1/2$, $\xi = 0$, $\phi = 0$) does not satisfy condition (ii) and the two-step trapezoidal ($\theta = 1/2$, $\xi = -1/2$, $\phi = -1/2$) and the Lees type ($\theta = 1/3$, $\xi = -1/2$, $\phi = -1/3$) methods do not satisfy either condition (ii) or (iii).

3.2 GKS-Stability

Kreiss (ref. 3) has shown that the stability of a difference approximation for the initial-boundary-value problem (2.1) is related to the stability of the difference approximation applied to the initial-value, or Cauchy, problem

$$\left.\begin{aligned} u_t - cu_x &= 0\ , \qquad -\infty < x < \infty,\ t \geq 0 \\ u(x,0) &= f(x) \end{aligned}\right\} \tag{3.5a}$$

and to the related quarter-plane problems: the right-quarter-plane problem

$$\left.\begin{aligned} u_t - cu_x &= 0\ , \qquad 0 \leq x < \infty,\ t \geq 0 \\ u(x,0) &= f(x) \end{aligned}\right\} \tag{3.5b}$$

and the left-quarter-plane problem

$$\left.\begin{aligned} u_t - cu_x &= 0\ , \qquad -\infty < x \leq \ell,\ t \geq 0 \\ u(x,0) &= f(x) \\ u(\ell,t) &= g(t) \end{aligned}\right\} \tag{3.5c}$$

Gustafsson, Kreiss, and Sundström (GKS) (ref. 2) developed a normal mode stability theory for general difference approximations to mixed initial-boundary-value problems, e.g., (3.5). For the purposes of this paper we make the following definition:

> A difference scheme for an initial-boundary-value problem on a finite domain is said to be GKS-stable if it is stable (by the von Neumann[2] method) for the Cauchy problem and stable (according to definition 3.3 of reference 2) for the related left and right quarter-plane problems.

3.2.1 Normal mode analysis- In some of the proofs in section 4 we rely on the previous work of Gustafsson and Oliger (ref. 7). In their paper they provide a concise description of the application of the normal mode analysis. We repeat those parts required in the present analysis.

Results obtained by means of the normal-mode analysis are based upon the behavior of the so-called resolvent equations. These are formally derived (for the right-quarter-plane problem) from (2.8) and (2.10), or (2.11), by substituting $u_j^n = z^n v_j$ where z is a complex number. We obtain, respectively

---

[2] For the problems considered here the von Neumann test is necessary and sufficient for the Cauchy problem.

$$\rho(z)v_j = \frac{c\Delta t}{2\Delta x}\,\sigma(z)(v_{j+1} - v_{j-1}) \tag{3.6}$$

and

$$(F - 1)^q v_j = 0 \tag{3.7}$$

or

$$(Fz^{-1} - 1)^q v_j = 0 \tag{3.8}$$

The general solution of (3.6) which is bounded as $j \to \infty$ for $|z| > 1$, can be written in the form

$$v_j = v_0 \kappa^j \tag{3.9}$$

where κ is the root of the characteristic equation

$$\rho(z) = \frac{c\Delta t}{2\Delta x}\,\sigma(z)\left(\kappa - \frac{1}{\kappa}\right) \tag{3.10}$$

such that $|\kappa| < 1$ if $|z| > 1$.

Equation (3.10) is formally obtained from (3.6) by substituting $v_j = \kappa^j$. Only one root of the quadratic in κ, (3.10), has modulus less than one. This is an immediate consequence of the stability of (2.8) for the Cauchy problem (which is assured since the temporal integration scheme is assumed to be A-stable) and justifies (3.9). It is proved in reference 2, Lemma 10.3, and the following sentence, that the approximations are stable for the (right-quarter-plane) initial-boundary-value problem if, and only if, (3.6) with boundary condition (3.7) or (3.8) has no trivial bounded solutions of the form (3.9) for $|z| \geq 1$. (Note that one must include $|z| = 1$.) This is established by substituting (3.9) into (3.7) or (3.8) and showing that $v_0 = 0$. When $|z| = 1$, one or both of the roots of (3.10) may have modulus one. If this is the case, the κ in (3.9) is defined by continuity to be that root which is the limit of the root $\kappa(z')$, $|\kappa(z')| < 1$ for $|z'| > 1$, as $|z'| \to 1$. A nontrivial solution when $|z| > 1$ is said to be an eigensolution and the corresponding z an eigenvalue. A nontrivial solution when $|z| = 1$ is said to be a generalized eigensolution and the corresponding z a generalized eigenvalue.

3.3 P-Stability

The stability analyses that provide GKS-stability bounds are very useful since they are relatively simple for scalar equations (with low order spatial difference approximations) and provide CFL limits that are directly applicable for many calculations which use explicit temporal difference approximations. They also provide a convenient method for eliminating undesirable numerical boundary schemes. However, they fail to provide a sufficient stability condition for some practical calculations with implicit schemes. This is a result of the stability definition 3.3 of reference 2 which allows growing solutions if the mesh interval, Δt or Δx, is not sufficiently small for a fixed value of $\Delta t/\Delta x$. Possible growing solutions for the classical wave equation are discussed in reference 2. Therefore, it is desirable to have a more restrictive stability definition. We incorporate GKS-stability as a necessary condition and make the following definition:

> A difference scheme for an initial-boundary-value problem is said to be P-stable if it is GKS-stable and all eigenvalues of the characteristic equation for a finite number of spatial mesh intervals have modulus less than or equal to unity.

The characteristic equation is obtained by substituting $u_j^n = z^n \kappa^j$ into the difference approximation for the initial-boundary-value problem on the finite domain, e.g., (2.8), and eliminating κ with the homogeneous boundary conditions, e.g., (2.9) with $g = 0$, and (2.10) or (2.11). Note that this characteristic equation, which includes both boundary conditions, differs from the characteristic equation in the GKS normal mode analysis, which includes only one boundary condition (in the analysis of each quarter-plane problem).

4. STABILITY ANALYSIS

In this section we present our principal results. First we consider the space-extrapolation boundary conditions and the general class of all A-stable temporal difference schemes. Next we consider the space-time-extrapolation boundary condition for the more restricted class of strongly A-stable temporal schemes.

4.1 Space-Extrapolation Boundary Scheme

We will prove the following:

Theorem 4.1. Let $\nu = c\Delta t/\Delta x$, $c > 0$. The algorithm (2.8), (2.9) and space-extrapolation boundary scheme (2.10) is P-stable if the polynomials $\rho(E)$ and $\sigma(E)$ correspond to an A-stable LMM.

The GKS-stability for a limited class of two-step LMMs was investigated by Gustafsson and Oliger (ref. 7). The extension to the general class of all A-stable LMMs requires only minor modifications which we consider here. As mentioned previously, the von Neumann stability of the Cauchy problem is assured since the temporal integration scheme is assumed to be A-stable. The GKS analysis of the left-quarter-plane problem is trivial. For the right-quarter-plane problem we substitute (3.9) into the boundary condition (3.7) and find that $v_0 = 0$ unless $\kappa = 1$, which can only happen when $|z| = 1$. Therefore, we need only check for a generalized eigenvalue and the generalization of the Gustafsson and Oliger analysis of the right-quarter-plane problem requires only the following lemma:

Lemma 4.1. Assume the polynomials $\rho(z)$ and $\sigma(z)$ correspond to an A-stable LMM and $\nu > 0$. The equation $\rho(z) = (1/2)\nu\sigma(z)[\kappa - (1/\kappa)]$ has no solutions $|z| = 1 + \delta$, $\kappa = 1 - \varepsilon$ where $\delta > 0$, $\varepsilon > 0$, δ and ε small.

Proof: Let $\kappa = 1 - \varepsilon$, $\varepsilon > 0$. Then $\kappa - (1/\kappa) = -2\varepsilon + O(\varepsilon^2)$. Since $\text{Re}\{\nu[\kappa - (1/\kappa)]\} < 0$ and the polynomials $\rho(z)$, $\sigma(z)$ correspond to an A-stable LMM it follows that $|z| \le 1$, or $\delta \le 0$.

We have proven GKS-stability. To complete the P-stability analysis and the proof of Theorem 4.1 we must prove that the eigenvalues of the characteristic equation have modulus less than or equal to unity. We obtain the characteristic equation by substituting $u_j^n = z^n\kappa^j$ into equation (2.8) and eliminating κ by using the homogeneous boundary conditions (2.9), with $g = 0$, and (2.10). From (2.8) we obtain

$$\rho(z) = \frac{1}{2}\,\nu\sigma(z)\left(\kappa - \frac{1}{\kappa}\right) \tag{4.1}$$

which is a quadratic with two roots κ, $-\kappa^{-1}$. Let

$$u_j^n = z^n\left[a\kappa^j + b\left(-\frac{1}{\kappa}\right)^j\right] \tag{4.2}$$

Boundary condition (2.9) with $g = 0$ leads to

$$0 = a\kappa^J + b\left(-\frac{1}{\kappa}\right)^J$$

or

$$u_j^n = z^n a\left[\kappa^j - (-1)^J\kappa^{2J}\left(-\frac{1}{\kappa}\right)^j\right] \tag{4.3}$$

and the space-extrapolation boundary condition (2.10) gives us an equation for κ, i.e.,

$$(\kappa - 1)^q - (-1)^{J+q}\,\kappa^{2J-q}(\kappa + 1)^q = 0 \tag{4.4}$$

Note that z does not appear explicitly in (4.4).

As a preliminary to the remaining proofs of this section we note the following. The characteristic equation (4.1) can be rewritten as

$$\rho(z) - \lambda\Delta t\sigma(z) = 0 \tag{4.5}$$

where

$$\lambda\Delta t = \frac{\nu}{2}\left(\kappa - \frac{1}{\kappa}\right), \qquad \nu > 0 \tag{4.6}$$

(c.f., (3.3)). An LMM is A-stable if and only if

$$\mathrm{Re}\left[\frac{\rho(z)}{\sigma(z)}\right] = \mathrm{Re}(\lambda\Delta t) \leq 0 \Rightarrow |z| \leq 1 \tag{4.7}$$

or

$$\mathrm{Re}\left(\kappa - \frac{1}{\kappa}\right) \leq 0 \Rightarrow |z| \leq 1 \tag{4.8}$$

where z denotes the roots of the characteristic equation (4.5). Furthermore, from the identity

$$\mathrm{Re}\left(\kappa - \frac{1}{\kappa}\right) = \frac{a(|\kappa|^2 - 1)}{|\kappa|^2} \tag{4.9}$$

where $\kappa = a + ib$, $|\kappa|^2 = a^2 + b^2$, it follows that

$$\left.\begin{array}{l} |\kappa| \leq 1,\ a \geq 0 \\ \text{or} \\ |\kappa| > 1,\ a < 0 \end{array}\right\} \Leftrightarrow \mathrm{Re}\left(\kappa - \frac{1}{\kappa}\right) \leq 0 \tag{4.10}$$

(see the shaded region of fig. 4.1).

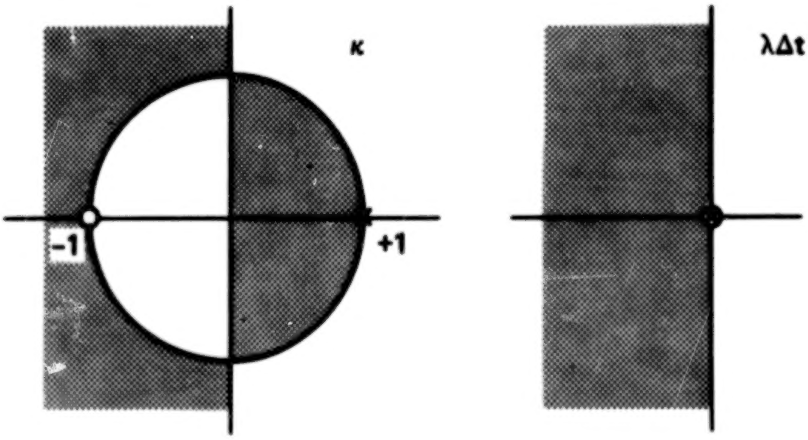

Figure 4.1.- Transformation $\lambda\Delta t = (\nu/2)(\kappa - 1/\kappa)$.

Before we examine the roots of the polynomial[3] (4.4) it is useful to have the following lemma:

Lemma 4.2. Assume the generating polynomials $\rho(z)$ and $\sigma(z)$ correspond to an A-stable LMM and $\nu > 0$. If $|\kappa| \leq 1$ and $\mathrm{Re}(\kappa) \geq 0$ then all roots of the polynomial (4.1) have modulus less than or equal to unity, i.e., $|z| \leq 1$.

Proof: The proof of the lemma follows from (4.10) and (4.8).

---

[3] The characteristic equation would be formally obtained by solving (4.4) for κ and eliminating κ from (4.1) to obtain an equation in z. This procedure is neither practical nor necessary.

If κ is a root of (4.4) then $-\kappa^{-1}$ is also a root; however, each produces the same value of $\kappa - (1/\kappa)$. Therefore we need only consider values of $|\kappa| \leq 1$. To complete the proof of Theorem 4.1 we need only prove:

Lemma 4.3. The polynomial (4.4) has no roots, κ, with $|\kappa| < 1$, $\mathrm{Re}(\kappa) < 0$.

Proof: Rearrange the terms in (4.4)

$$\frac{\kappa^{2J-q}(\kappa + 1)^q}{(\kappa - 1)^q} = (-1)^{J+q} \qquad (4.11)$$

The LHS of (4.11) has $2J - q$ zeros at $\kappa = 0$, q zeros at $\kappa = -1$, and q poles at $\kappa = 1$ as shown in figure 4.2. The modulus of the LHS of (4.11) must equal unity if κ is a root of (4.11), i.e., using the vectors defined in figure 4.2

$$\frac{|r_1|^{2J-q}|r_2|^q}{|r_3|^q} = 1 \qquad (4.12)$$

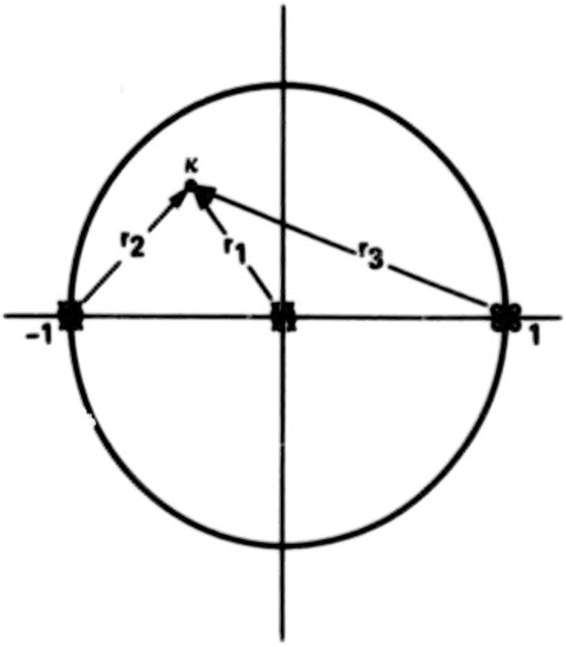

Figure 4.2. κ plane.

If $|\kappa| < 1$, $\mathrm{Re}(\kappa) < 0$ then $|r_1| < 1$, $|r_2| < 1$, and $|r_3| > 1$; therefore κ cannot be a root of (4.4). Consequently, the roots of (4.4) must fall in the shaded region of the κ-plane of figure 4.1, and by (4.10) and (4.8) the eigenvalues of the characteristic equation (4.1) have modulus $|z| \leq 1$.

This completes the proof of Theorem 4.1.

4.2 Space-Time-Extrapolation Boundary Scheme

For these boundary schemes it is convenient to first consider GKS-stability and prove:

Theorem 4.2. Let $\nu = c\Delta t/\Delta x$, $c > 0$. The algorithm (2.8), (2.9) and space-time-extrapolation boundary scheme (2.11) is GKS-stable if the polynomials $\rho(E)$ and $\sigma(E)$ correspond to a strongly A-stable LMM.

Again we present only those modifications of the Gustafsson and Oliger analysis (ref. 3) which are necessary to generalize their results to the class of all strongly A-stable LMMs. We substitute (3.9) into boundary condition (3.8) and find $v_0 = 0$ unless $z = \kappa$ which can only happen when $|z| = 1$. Therefore we need only check for generalized eigenvalues and the modifications can be summarized by the following generalization of Lemma 4.1:

Lemma 4.3. Assume the generating polynomials $\rho(z)$ and $\sigma(z)$ correspond to a strongly A-stable LMM and $\nu > 0$. The equation $\rho(z) = (1/2)\nu\sigma(z)[\kappa - (1/\kappa)]$ has no solutions $|z| = 1 + \delta$, $|\kappa| = 1 - \varepsilon$ where $\delta > 0$, $\varepsilon > 0$, δ and ε small.

Proof: Since $\rho(z)$ and $\sigma(z)$ correspond to a strongly A-stable LMM the stability region ($|z| \leq 1$) includes the entire left half of the complex $\rho(z)/\sigma(z)$ plane plus a region to the right of the imaginary axis except at the origin (fig. 4.3a). All values of $|\kappa| = 1$ lie on the imaginary axis of the $\kappa - (1/\kappa)$ plane and values $|\kappa| = 1 - \varepsilon$ lie near the imaginary axis

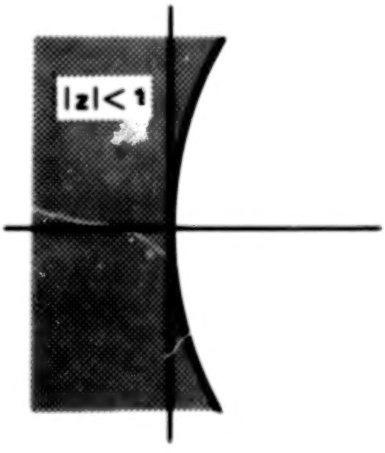

Figure 4.3(a). $\rho(z)/\sigma(z)$ plane.

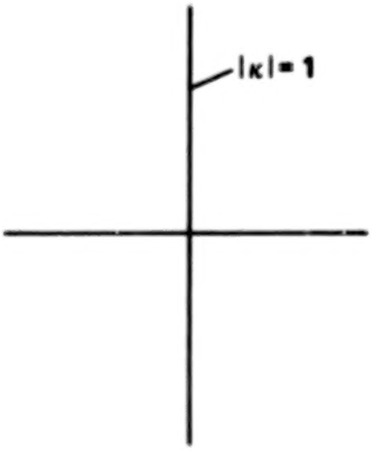

Figure 4.3(b). $\kappa - (1/\kappa)$ plane.

but these values of $\kappa - (1/\kappa)$ correspond to $|z| \leq 1$ (except at the origin) in the $\rho(z)/\sigma(z)$ plane, i.e., $|z| = 1 + \delta$, $\delta \leq 0$. The values $\kappa = \pm 1$ map into the origin of the $\kappa - (1/\kappa)$ plane. Note that $z = 1$ $(\kappa = 1)$ is not a generalized eigenvalue (by lemma 4.1) but we must check $\kappa = -1$. Set $z = \kappa$, i.e., $\rho(z) = (1/2)\nu\sigma(z)[z - (1/z)]$ and then $z = -1$ which implies $\rho(-1) = 0$;

however, -1 is not a root of $\rho(\zeta)$ since $\rho(\zeta)$ corresponds to a strongly A-stable LMM.

This completes the proof of Theorem 4.2.

Next we prove that the space-time-extrapolation boundary scheme leads to a conditional P-stability bound.

Theorem 4.3. Let $\nu = c\Delta t/\Delta x$, $c > 0$. Assume $\rho(E)$ and $\sigma(E)$ correspond to a strongly A-stable LMM. For even values of J the algorithm (2.8), (2.9) and space-time-extrapolation boundary scheme (2.11) has a necessary P-stability condition

$$J \geq q \frac{\ln\left(\frac{1 + \kappa}{1 - 1/\kappa}\right)}{\ln(\kappa^2)} \tag{4.13}$$

where

$$\kappa = \frac{\rho(-1)}{\nu\sigma(-1)} - \sqrt{\left[\frac{\rho(-1)}{\nu\sigma(-1)}\right]^2 + 1} \tag{4.14}$$

Remark: Inequality (4.13) implies a necessary conditional stability bound of the type sketched in figure 4.4.

We proceed as in the case of space extrapolation, i.e., by substitution of u_j^n from (4.3) into boundary condition (2.11) which leads to

$$(\kappa - z)^q - (-1)^{J+q}\,\kappa^{2J}\left(\frac{1}{\kappa} + z\right)^q = 0 \tag{4.15}$$

Note that, in contrast to (4.4) for space extrapolation, z appears explicitly in (4.15). (Again we avoid the formal procedure of finding the characteristic equation which would require solving (4.15) for $\kappa(z)$ and eliminating κ from (4.1).) Note that (4.15) can be rewritten

$$J = \frac{\ln\left[(-1)^J\left(\frac{z - \kappa}{1/\kappa + z}\right)^q\right]}{\ln(\kappa^2)} \tag{4.16}$$

and (4.1) can be rewritten ($\nu \neq 0$, $\sigma(z) \neq 0$)

$$\kappa = \frac{\rho(z)}{\nu\sigma(z)} - \sqrt{\left[\frac{\rho(z)}{\nu\sigma(z)}\right]^2 + 1} \tag{4.17}$$

We seek solutions of (4.16) and (4.17) on the stability boundary, $z = -(1 + \delta)$ as $\delta \to 0$, δ positive and real. Since $\rho(E)$ and $\sigma(E)$ correspond to an A-stable LMM

$$\mathrm{Re}\left[\frac{\rho(z)}{\nu\sigma(z)}\right] \le 0 \Rightarrow |z| \le 1$$

or conversely

$$|z| > 1 \Rightarrow \mathrm{Re}\left[\frac{\rho(z)}{\nu\sigma(z)}\right] > 0$$

Since $z = -(1 + \delta)$ is real and $|z| > 1$ we have

$$\frac{\rho(-1 - \delta)}{\nu\sigma(-1 - \delta)} > 0$$

and from (4.17), as ν goes from 0^+ to ∞, κ increases monotonically from -1^+ to 0, i.e., $-1 < \kappa \le 0$. For even values of J and $z = -1$, (4.16) becomes

$$J = \frac{\ln\left(\frac{1 + \kappa}{-1/\kappa + 1}\right)^q}{\ln(\kappa^2)}$$

and clearly for each value of κ, $-1 < \kappa < 0$, J has a positive real value. From the derivative $d\nu/dJ$ (obtained from equations (4.13) and (4.14)) it is easily shown that $\nu(J)$ is a monotonically increasing function, e.g., figure 4.4. The direction of the inequality (4.13) follows from GKS-stability of the scheme, i.e., for fixed ν no values $|z| > 1$ as $J \to \infty$.

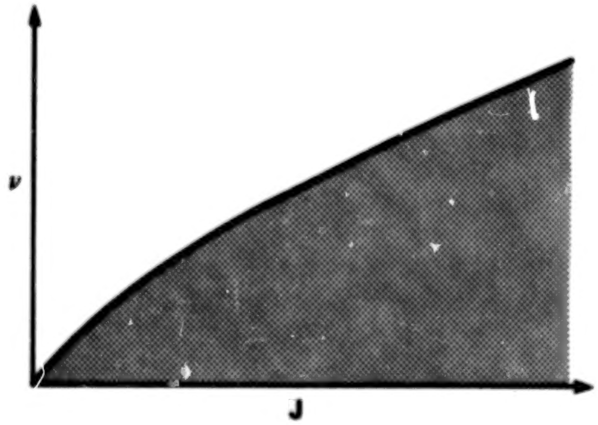

Figure 4.4.- Necessary stability region.

This completes the proof of Theorem 4.3.

Remark: Equations (4.13) and (4.14) provide a necessary P-stability condition. In the appendix we consider necessary and sufficient P-stability conditions for the class of one-step methods.

5. CONCLUDING REMARKS

In the analysis of the scalar hyperbolic initial-boundary-value problem, we have shown that if one combines the implicit space-extrapolation boundary schemes with an unconditionally stable interior scheme the combined scheme is unconditionally stable. However, if one combines the explicit space-time-extrapolation boundary scheme with an unconditionally stable interior scheme the combined scheme will be conditionally stable (if both odd and even numbers of mesh intervals are allowed) and the stability condition will depend on the number of mesh intervals. We have confirmed these results by numerical example for special cases of the quasi-one-dimensional equations of gas dynamics.

APPENDIX

P-STABILITY CONDITIONS FOR ONE-STEP METHODS AND SPACE-TIME-EXTRAPOLATION BOUNDARY SCHEME

In section 4.2 we found a necessary P-stability condition for the general A-stable LMM and space-time-extrapolation boundary scheme (2.11). In this appendix we investigate the necessary and sufficient P-stability conditions for the class of one-step methods.

The class of one-step or θ methods is ($\xi = \phi = 0$ in (2.7) with the temporal index shifted down by one)

$$\rho(E) = E - 1 \tag{A.1a}$$

$$\sigma(E) = \theta E + (1 - \theta) \tag{A.1b}$$

and they are A-stable if and only if (eq. (3.4))

$$\theta \geq \frac{1}{2} \tag{A.2}$$

GKS-Stability Analysis

Before proceeding with the P-stability analysis, it is useful to examine the GKS-stability analysis of the right-quarter-plane problem. From the analysis of the right-quarter-plane problem we have the characteristic equation (see (4.1))

$$(z - 1) = \frac{1}{2} \nu(\theta z + 1 - \theta)\left(\kappa - \frac{1}{\kappa}\right) \tag{A.3}$$

and from the space-time-extrapolation boundary condition (2.11) the condition

$$z = \kappa \tag{A.4}$$

GKS stability requires that there are no nontrivial solutions to (A.3) and (A.4) with $|z| > 1$, $|\kappa| < 1$. Substitution of κ from (A.4) into (A.3) leads to

$$(z - 1) = \frac{1}{2} \nu(\theta z + 1 - \theta)\left(z - \frac{1}{z}\right)$$

or if $z \neq 1$ ($z = +1$ can be shown not to correspond to a generalized eigenvalue, see fig. 4.1)

$$\frac{z}{(z + 1)\left(z + \frac{1 - \theta}{\theta}\right)} = \frac{1}{2} \nu\theta \tag{A.5}$$

The locus of the roots of (A.5) for all $\nu > 0$, $\theta \geq 1/2$ are shown in Figure A1. The arrows indicate the direction of the motion of the roots as the parameter $\nu\theta$ changes from 0 to ∞.

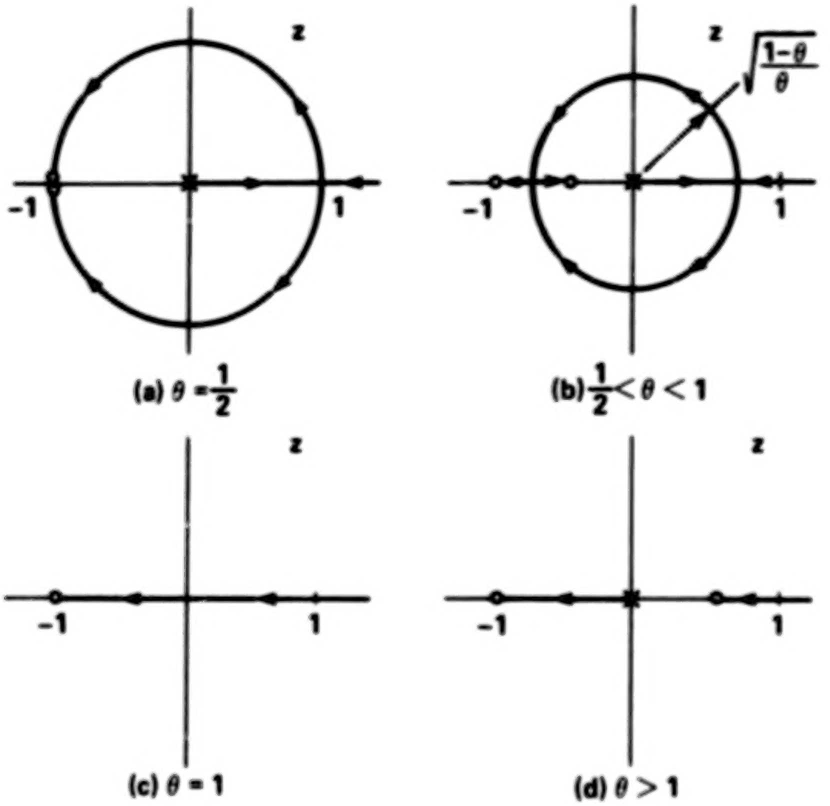

(a) $\theta = \frac{1}{2}$ (b) $\frac{1}{2} < \theta < 1$

(c) $\theta = 1$ (d) $\theta > 1$

Figure A1.- Locus of roots for equation (A.5).

The only possibility of a generalized eigenvalue occurs at the intersection of the root locus and the unit circle, $|z| = 1$. We have already eliminated $z = +1$. Clearly, the only other possibilities are for $\theta = 1/2$ where the locus lies on the unit circle or $z = -1$ for $\theta > 1/2$.

Consider first $\theta = 1/2$. Equation (A.3) becomes

$$\frac{z - 1}{z + 1} = \frac{\nu}{4}\left(\kappa - \frac{1}{\kappa}\right) \tag{A.6}$$

Next, we consider values of κ near $z = \kappa = i$ ($\nu = 2$). Let

$$\kappa = (1 - \varepsilon)e^{i\left(\frac{\pi}{2} + \psi\right)}, \quad \varepsilon > 0 , \quad \psi > 0 \tag{A.7}$$

where ε and ψ are to be considered small. The RHS of (A.6) with κ from (A.7) becomes

$$\frac{1}{2}\left(\kappa - \frac{1}{\kappa}\right) = \frac{1}{2}\left[\frac{(1-\varepsilon)^2 - 1}{1-\varepsilon}\cos\left(\frac{\pi}{2}+\psi\right) + i\,\frac{(1-\varepsilon)^2+1}{1-\varepsilon}\sin\left(\frac{\pi}{2}+\psi\right)\right]$$

For small ψ

$$\mathrm{Re}\left[\frac{1}{2}\left(\kappa - \frac{1}{\kappa}\right)\right] \approx \frac{-2\varepsilon + \varepsilon^2}{2(1-\varepsilon)}\,(-\psi)$$

Thus for ε small ($\varepsilon > 0$, $\psi > 0$)

$$\mathrm{Re}\left[\frac{1}{2}\left(\kappa - \frac{1}{\kappa}\right)\right] \approx \varepsilon\psi > 0 \tag{A.8}$$

Since $\theta = 1/2$ corresponds to an A-stable LMM with none of the right-half plane in its stability region we know that a positive real part of the RHS of (A.6) implies $|z| > 1$. Therefore, $z = \kappa = i$ ($\nu = 2$) represents a generalized eigenvalue. It is easy to show that there is a generalized eigenvalue for all $\nu > 2$ and no generalized eigenvalue for $\nu < 2$. To summarize, if $\theta = 1/2$ the scheme if GKS-stable for $\nu < 2$. (This result is obvious from a comparison of fig. A1a and fig. 4.1.) Note that $\theta = 1/2$ does not correspond to a strongly A-stable LMM and this result does not violate Theorem 4.2.

Next, we consider $\theta > 1/2$, $\nu \to \infty$ (i.e., $z = -1$). Let

$$z = -1 - \delta\ , \qquad \delta > 0 \tag{A.9}$$

and substitute into (A.3)

$$\kappa^2 - \frac{2(2+\delta)}{(\delta\theta + 2\theta - 1)\nu}\,\kappa - 1 = 0 \tag{A.10}$$

For large values of ν

$$\kappa \approx \frac{2+\delta}{(\delta\theta + 2\theta - 1)\nu} \pm \left\{1 + \frac{1}{2}\left[\frac{2+\delta}{(\delta\theta + 2\theta - 1)\nu}\right]^2 + \ldots\right\}$$

We choose the negative sign to ensure $\kappa \to -1$

$$\kappa \approx -1 + \frac{2+\delta}{(\delta\theta + 2\theta - 1)\nu} = -1 + \varepsilon \tag{A.11}$$

where $\varepsilon > 0$ and $\kappa \to -1^+$ as $\nu \to \infty$. We conclude that $z = \kappa = -1$ is a generalized eigenvalue for $\lambda \to \infty$. However, there are no generalized eigenvalues for $\lambda < \infty$ and the scheme is GKS-stable in agreement with Theorem 4.2.

P-Stability Analysis

The necessary P-stability condition of Theorem 4.3, equations (4.13) and (4.14), has (as the asymptotic limit $J \to \infty$) the generalized eigenvalue just considered in the GKS-stability analysis ($z = \kappa = -1$). For the finite values

The solution we obtain is in general one that will exhibit wall penetration, since the normal velocity condition is not satisfied at the solid boundaries. There is, however, one unique distribution of boundary vorticity for which there is no wall penetration. We therefore regard the first solution as tentative and follow it with a second solution in which the proper vorticity values have been placed on the boundary.

Finding the correct vorticity values to place on the boundary involves simultaneous solution of a system of linear agebraic equations that give constant values to the streamfunction at the walls. It is shown here, in the case of the Fourier solution, that a fast and physically meaningful technique, using an influence function, may be used to simply correct initial values present there. The correction represents, for example, the amount of generated vorticity in a time interval of a sequence of solutions and gives insight in the use of suction to modify flow behavior.

We further consider the same procedure in terms of finite differences. We find that through matrix convolution the Fourier convolution may be imitated throughout. This leads to a slightly less accurate solution of local approximation but mimics the fundamental procedure. Comparing this solution to a one step result, using the same local approximation, the solution agrees to within computer roundoff. The one step procedure does not discriminate between slip and no-slip. The normal wall velocity derivative, i.e. the vorticity, of course differs. It appears then that one may justifiably seek out a one step method for faster solution but should use the two step procedure to verify that it is valid for the geometry under consideration.

II. Parallel Flow and the Commonly Used Difference Method

We illustrate the numerical procedures here by considering two dimensional flow between parallel plates. In particular, one may think of plane Poiseuille flow with a characteristic parabolic profile and with a superimposed disturbance so that irregular flow occurs relative to the plates. If the disturbance imposed or naturally occurring has periodicity in the direction of flow, we may readily make use of Fourier series to obtain solutions.

We are interested here only in the solution of Poisson's equation for the streamfunction with vorticity as the "source" term, namely

$$\frac{\partial^2\psi}{\partial x^2} + \frac{\partial^2\psi}{\partial y^2} = -\omega \tag{1}$$

where velocity components in the x and y directions, respectively, are

$$u = \frac{\partial\psi}{\partial y} \text{ and } v = -\frac{\partial\psi}{\partial x}. \tag{2}$$

The boundary conditions at the plates are $u = v = o$, and solutions differ only in that the internal and/or boundary vorticity values differ leading to differing internal flow fields. For example, a developing disturbance of an unstable Poiseuille flow frozen at some instant in time is a typical solution of interest, although it is also of interest to regard changes in boundary vorticity as a generation process occurring over some discrete time interval. In the interior vorticity is modified in time by convection and diffusion[1] (neither considered here), but at the rigid boundaries a timewise change also must occur if both $u = o$ and $v = o$ conditions are to be satisfied. This is to be illustrated in the following.

Intuitively (1) is most simply solved by requiring the normal velocity v at the walls to be zero and thereby, through the second of (2) to have constant values of the streamfunction at the walls.

The usual finite difference expression which is solved simultaneously for all grid points, either directly or iteratively, is

$$\frac{\frac{\psi_1 - \psi_o}{\Delta x} - \frac{\psi_o - \psi_3}{\Delta x}}{\Delta x} + \frac{\frac{\psi_2 - \psi_o}{\Delta y} - \frac{\psi_o - \psi_4}{\Delta y}}{\Delta y} = -\omega_o, \qquad (3)$$

where the grid layout is

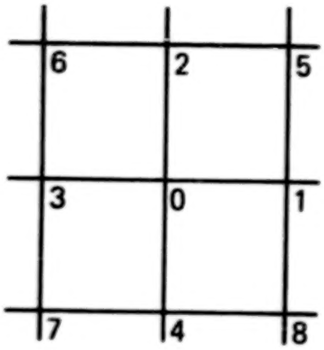

At a rigid plate $\psi_1 = \psi_o = \psi_3$, and we are left with an expression with y dependence only. Consistent with the order of approximation, we assume a local image with oppositely directed flow to satisfy the u = o condition. This leads to $\psi_2 = \psi_4$ and an expression for the boundary vorticity

$$\omega_b = \frac{2(\psi_b - \psi_i)}{\Delta y^2}, \qquad (4)$$

where ψ_i is the nearest internal streamfunction value, ψ_2 or ψ_4.

Much confusion arises at this point because the vorticity at the wall (4) seems to be placed there as an afterthought to solution of the flow field by (3). Particularly confusing is that solution for a free-slip condition would be the same except for (4) replaced with $\omega_b = o$. It must be realized that no-slip and free-slip imply the passage of time, and here time is frozen. There is no contradiction in obtaining solutions the same way since with any past history the flow fields would not be the same. Only at the first instant of an impulsive start would the internal flows coincide.

When considering the above procedure in terms of a discrete Fourier solution, one finds that the local character of (4) can no longer apply. In the Fourier case, all grid information is used, that is, additional mesh points come into play as if, in the finite difference case, we were to first include points 5, 6, 7 and 8, as indicated in the layout, for a better approximation and then consider better and better approximations until we used all mesh points. In the Fourier case then, an analogous procedure, if possible, would not be very satisfying and confidence in its correctness would be low. In the following a different viewpoint applicable to both Fourier solution and finite difference solution is explored.

III. Matrix Convolution

Though the method we consider here had its origin in Fourier solution to our problem, the analogous procedure for finite differences is more readily understood, so we choose to describe it first. We consider the alternative to the above difference procedure; that is, to satisfy the no-slip condition first and then ask what must follow to satisfy non-penetration. We tentatively examine a result satisfying no-slip by employing an image region such that flow relative to a rigid wall is equal and opposite in the image (see Figure 1). This corresponds to a like vorticity field (image with same sign). The boundary values of vorticity may be arbitrary but are generally those of a previous time step in a time dependent calculation. We obtain our tentative result with (3) applied over the entire folded doubly periodic region of grid points M × 2N. Here Hockney's[2] direct method was used, although any other simultaneous solution of (3) will suffice. Figure 2 is a typical first pass solution.

Clearly in the result, wall penetration occurs (Fig. 2) because no reference is made to any uniform values of ψ at the wall. It also is evident that our only lacking feature to precisely defining the flow and getting a correct solution is that the boundary ω's are arbitrary. Thus, if the unique boundary values of vorticity can be found that provide non-penetration, they will be the correct ones for solution of the problem. That is, at each boundary point, we must satisfy an equation

$$\psi_F + \Delta\psi_B = \psi_B \tag{5}$$

where ψ_B is the uniform (constant) value along the boundary and $\Delta\psi_B$ is the change from first pass (ψ_F) values obtained by the image procedure above. The required change in ψ_F, i.e. $\Delta\psi_B$ must be due to the extra boundary vorticity only. Hence if we obtain the corrected values of vorticity to satisfy (5) at each boundary point, then we can again apply (3) to the combined flow and image region to get the final solution.

Since (1) is linear, and because of our simple geometry, we can use an interesting procedure involving an influence matrix derived from the superimposed effects of unit vorticity at boundary points. We obtain the overall solution of a unit vorticity at one point on the boundary in the same manner as the initial pass described above (this result is needed only once in a timewise developing solution). The streamfunction field values for a unit vorticity at the origin is illustrated in Figure 3. Now the boundary streamfunction values resulting from the unit vorticity may be catalogued and the others discarded. A convoluted matrix A may be set up that provides the effects of moving the unit vorticity from point to point along the walls. More explicitly we can write

$$\begin{bmatrix} \Delta\psi_{1,1} \\ \Delta\psi_{1,2} \\ \vdots \\ \Delta\psi_{1,M} \\ --- \\ \Delta\psi_{N,1} \\ \Delta\psi_{N,2} \\ \vdots \\ \Delta\psi_{N,M} \end{bmatrix} = \begin{bmatrix} A_{1,1} & A_{1,2} & \cdots A_{N,M} \\ A_{1,M} & A_{1,1} & \cdots \\ \vdots & & \\ & & \\ & & \\ & & \\ & & \\ & & \\ & & \end{bmatrix} \left[\begin{array}{c} \omega_{1,1} \\ \omega_{1,2} \\ \vdots \\ \omega_{1,M} \\ \hline \omega_{N,1} \\ \omega_{N,2} \\ \vdots \\ \omega_{N,M} \end{array}\right] \tag{6}$$

where the convolution matrix A is generated by slipping elements one notch cyclicly on succeeding rows after the first (accounting for the two walls separately). The corrections to the boundary vorticity then follow by obtaining the inverse of A and solving the matrix equation

$$\Omega = A^{-1}\Delta\Psi \tag{7}$$

When the full boundary vorticity (initial pass plus results of (7)) are used in a final pass, the flow field satisfying both u = o and v = o will emerge (see Figure 4).

The solution here is identical (within roundoff) to the one pass traditional method of the previous section. The matrix method required a doubled grid solved twice. Nevertheless, the confidence level concerning correctness is very high.

IV. Fourier Convolution

In the Fourier method, the convolution takes on a particularly simple form. Though not very physically intuitive it follows from the theory of Fourier transforms.[3] The "wrap-around" procedure illustrated in matrix convolution is effectively automatic in transform space.

Again, we obtain a solution for a folded space, Figure 1, in which the vorticity image is such that the distribution is "even" in the y direction. Because of already existing periodicity in the x direction, no further folding is required there. The tentative result which satisfies the no-slip condition is obtained by taking the discrete Fourier transform of the vorticity distribution with arbitrary vorticity values at j = o and j = n. In transform space we have

$$\psi^{*}_{k\ell} = \frac{\omega^{*}_{k\ell}}{(k\alpha)^2 + (\ell\beta)^2} \tag{8}$$

where * indicates transform and k and ℓ are integers. Further, $\alpha = 2\pi/Lx$ and $\beta = 2\pi/Ly$, where Lx and Ly are the lengths of the folded flow region (Figure 2) in the x and y directions respectively.

We now, in the same manner (Equation(8)) obtain the streamfunction field for a point (unit) vorticity. Again, only the boundary streamfunction values are needed and are set up in a two row sequence of M elements each. Corresponding to the matrix convolution expression (6), we write for any element (m,n)

$$\Delta\psi(m,n) = \sum_{s=1}^{2} \sum_{r=1}^{M} \psi_u(m-r,n-s)\ \omega(r,s) \tag{9}$$

where the ψ_u's are (symbolically) the two row sequence of streamfunction values for a unit vorticity at each point on the boundary. The $\Delta\psi$'s are the corrections we must apply as determined from equation (5) to give constant values of the streamfunction at the boundaries, and the ω's are the unknown corrections to the vorticity to be found. Expression (9) is also referred to as the Green's Function for the boundary (see, for example, reference 4, page 700). m and n of course take on values as r and s respectively, namely M and 2.

The convolution theorem provides for simple treatment of (9) in transform space giving for each element

$$\Delta\psi^{*}(k,\ell) = \psi^{*}_{u}(k,\ell)\ \omega^{*}(k,\ell). \tag{10}$$

Hence in transform space

$$\omega^{*}(k,\ell) = \frac{\Delta\psi^{*}(k,\ell)}{\psi^{*}_{u}(k,\ell)}. \tag{11}$$

The inverse transform then gives the correction to be applied to the vorticity at the walls and reapplication of (8) leads to the final solution.

V. Conclusions

A number of interesting thoughts follow from the above study. Perhaps most important is that the two step approach is very fundamental and rigorous in that the final values of the vorticity are clearly unique in providing the no-penetration condition. Symmetry in the self image and flow field vorticities provides for no-slip. In our test problem, this was easy to achieve. Presumably more general treatment will allow other geometries to be treated similarly, or transformations to convert the geometry to the parallel flow case will allow the present approach to be used.

To appreciate the significance of wall vorticity generation as that amount of vorticity required to provide non-penetration is perhaps a very useful non-traditional view with important consequences. It is a measure of what modifications must be made to flow fields to keep the flow steady by appropriate removal of a local layer of fluid, for example. This is relevant to time dependent calculations where the generated vorticity during a time interval compensates for internal changes.

Of incidental interest in connection with time dependent calculations is that it was found here that Fourier solution of Poisson's equation does not provide dramatically improved accuracy. The accuracy is much more a function of grid resolution in contrast to the dramatic improvement when using Fourier techniques to treat the non-linearity of the Navier-Stokes equations.[5] It is perhaps generally true that in most numerical applications one needs to be concerned mainly with accuracy of local approximation of the non-linear terms.

Finally, for the sake of fast computation of Poisson's equation one should still seek out one pass methods, but it must be shown that they produce corresponding solutions to a two pass calculation.

REFERENCES

1. Fromm, J. E., "Numerical Method for Computing Nonlinear, Time Dependent, Buoyant Circulation of Air in Rooms", IBM J. of Res. and Dev., *15* p. 186, (1971).

2. Hockney, R. W., "The Potential Calculation and Some Applications", *Methods in Computational Physics* (ed. B. Alder) *9*, 135 (Acad. Press 1970).

3. Cooley, J. W., Lewis, P. A. W., Welch, P. D., "The Finite Fourier Transform", IEEE Trans., *AU-17*, No. 2, June (1969).

4. Morse, P. M. and Feshbach, H., *Methods of Theoretical Physics Vol. 1*, McGraw Hill (1953).

5. Gazdag, J., "Numerical Convection Schemes Based on Accurate Computation of Space Derivatives", J. of Comp. Phys., *13*, No. 1, page 100.

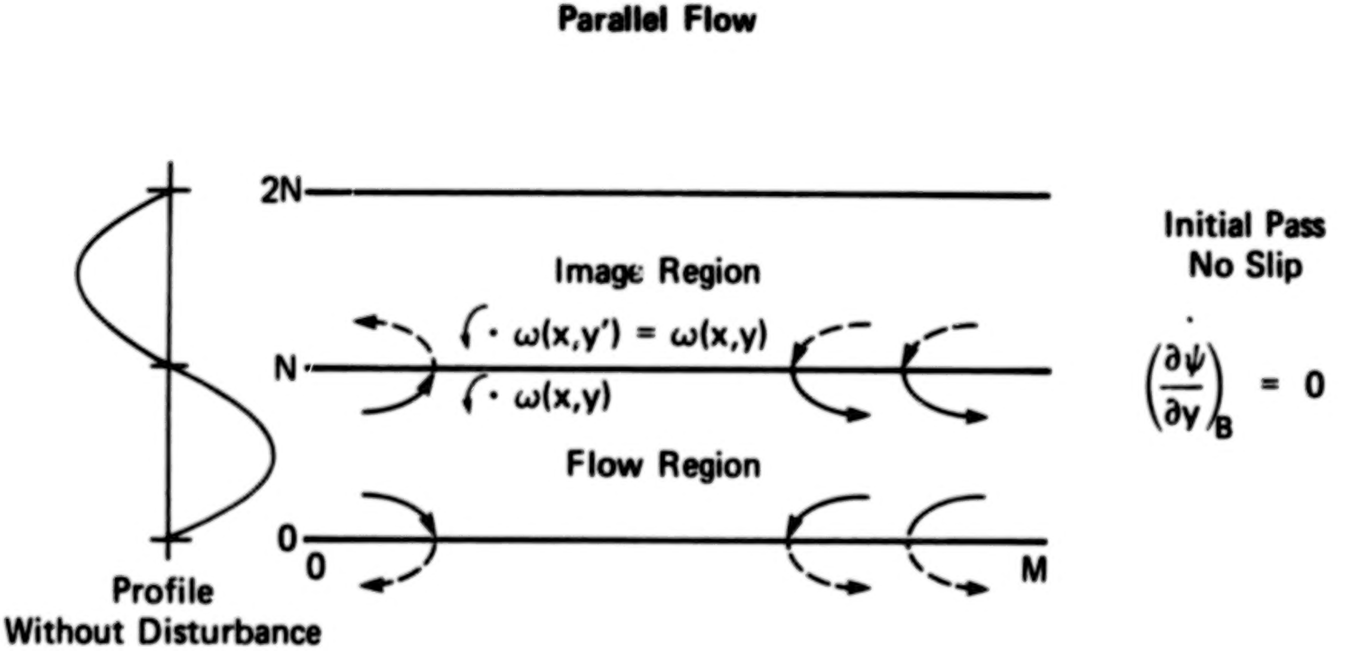
Parallel Flow
2N
Image Region
$\circlearrowleft \cdot\ \omega(x,y') = \omega(x,y)$
N
$\circlearrowleft \cdot\ \omega(x,y)$
Flow Region
0
0
M
Profile
Without Disturbance
Initial Pass
No Slip
$\left(\frac{\partial\psi}{\partial y}\right)_B = 0$

Figure 1: A pictorial representation of the first pass geometry, velocity profile and streamlines for calculation of flow between parallel plates.

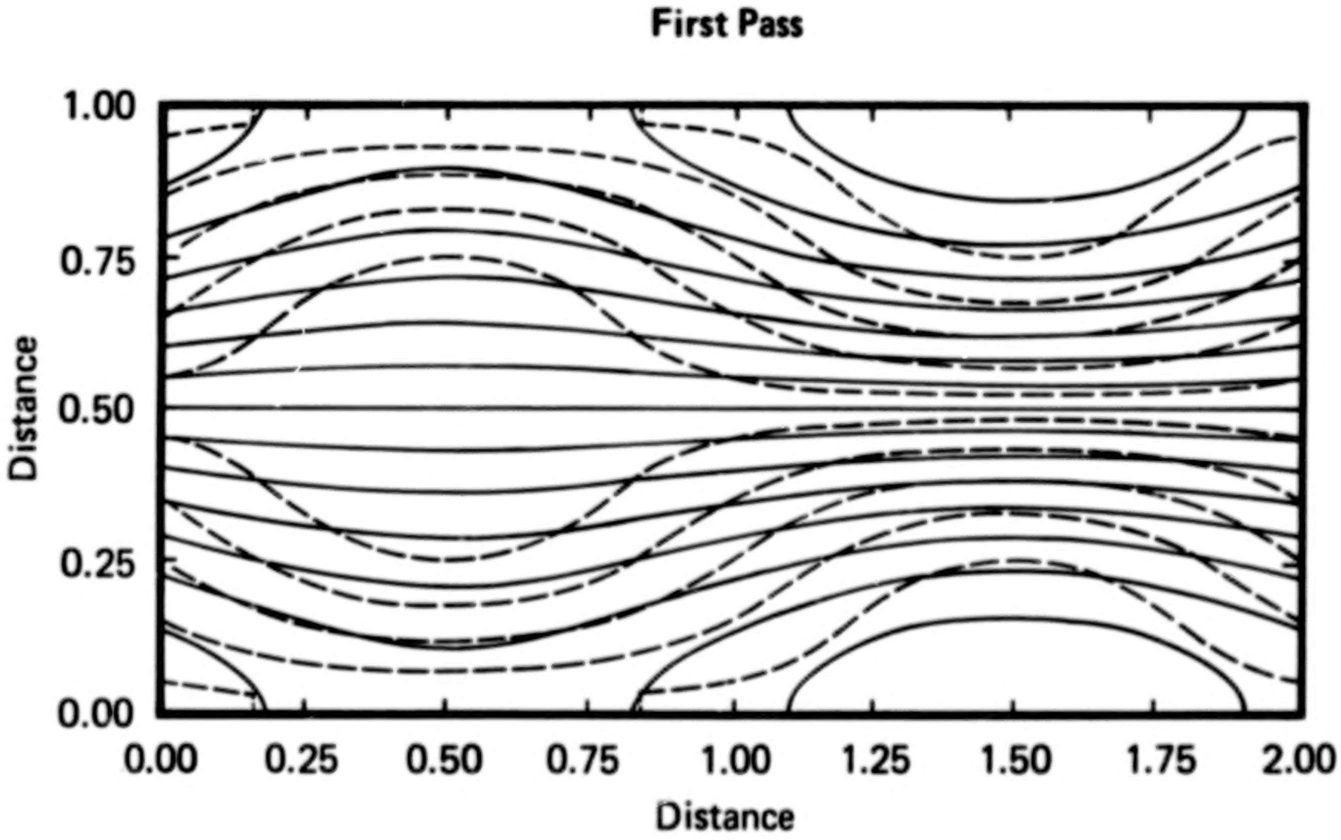

Figure 2: A sample computer result of a first pass solution satisfying no-slip only. Streamlines (solid lines), Vorticity (dashed lines). Arbitrary wall vorticity here takes on next interior values for plotting esthetics.

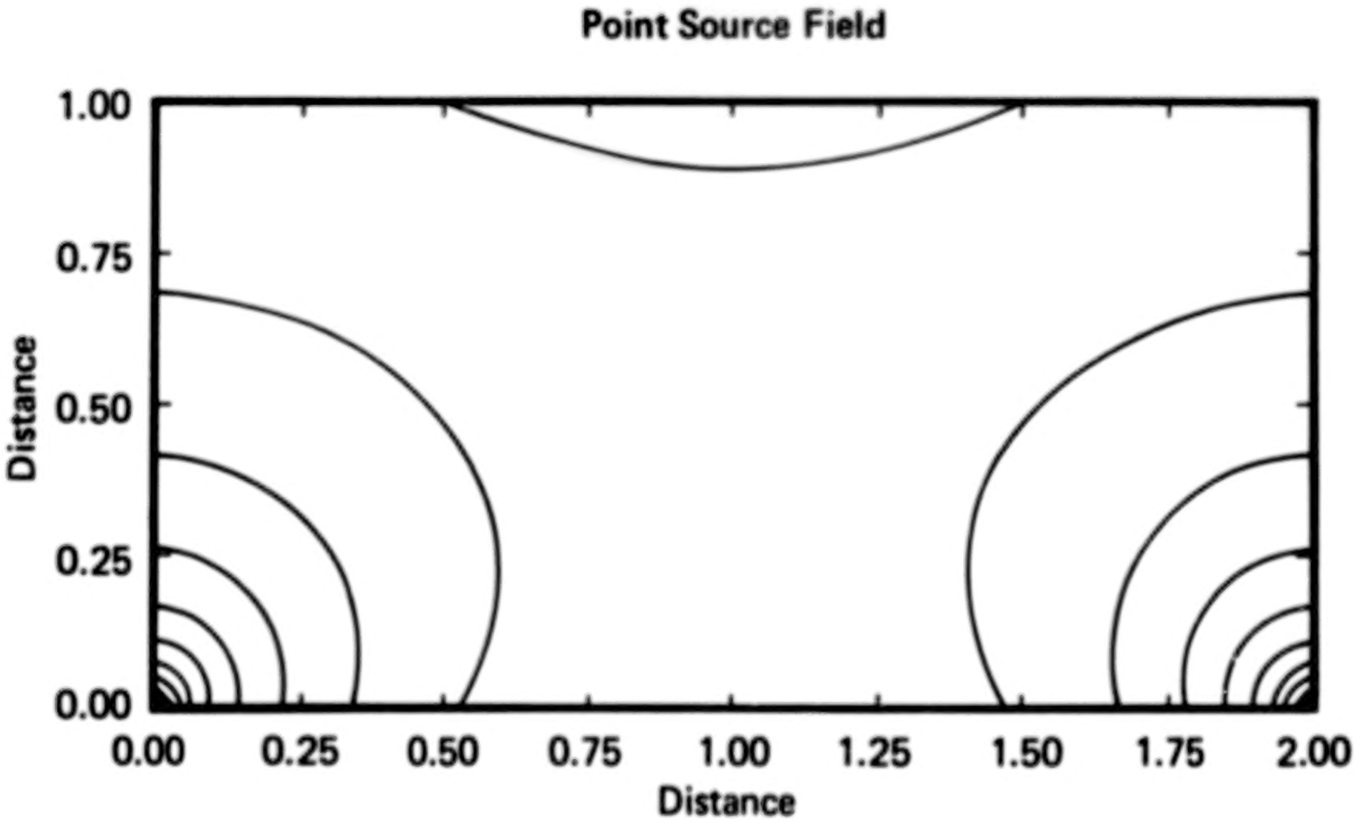

Figure 3. The computer derived point source field or influence function for a unit vorticity at the origin.

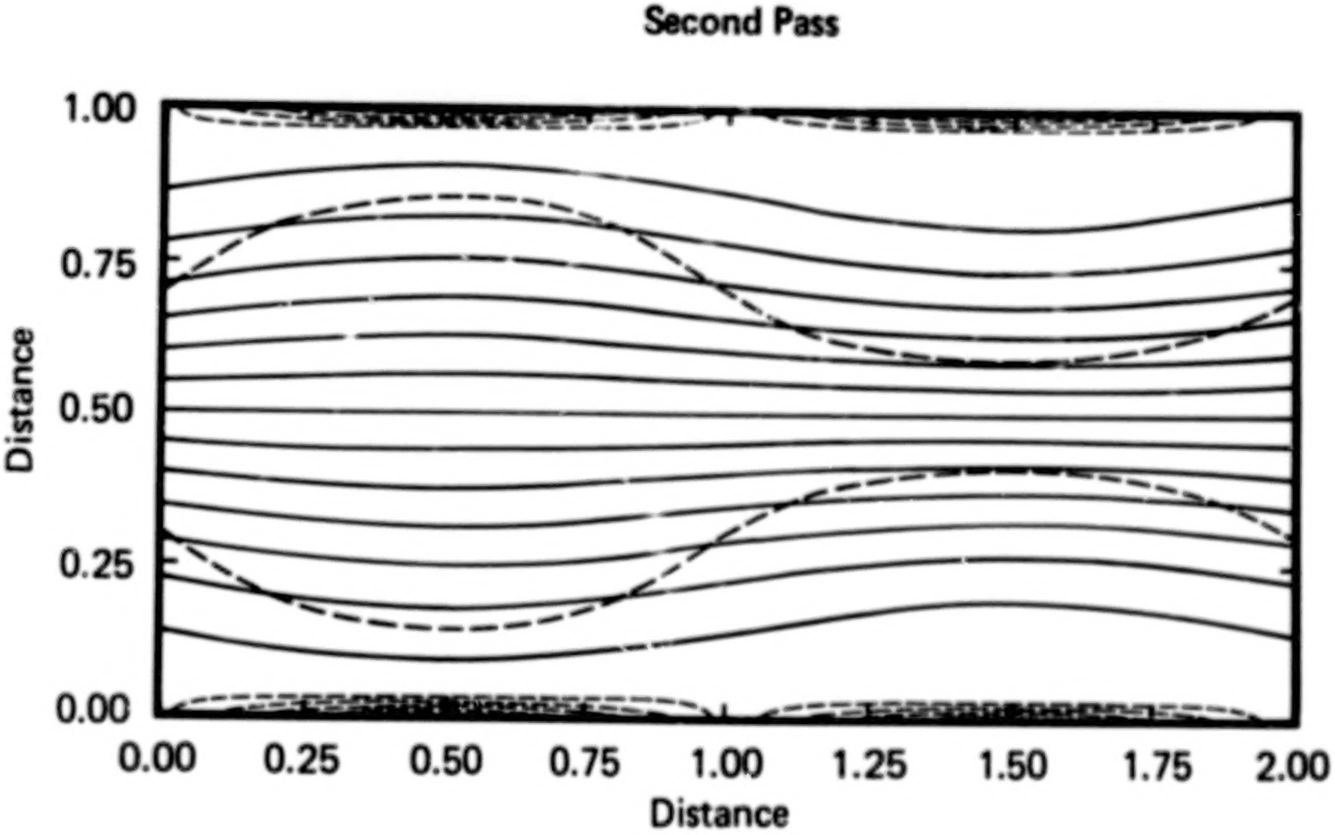

Figure 4. Sample computer solution with same interior vorticity as Figure 2 but now with correct boundary vorticity. Automated plot interval reduces number of interior contours of constant vorticity (dashed lines) because relatively large values occur on boundary.

Blank Page

NUMERICAL TREATMENT OF NON-LINEAR LATENT HEAT BOUNDARY CONDITIONS AT MOVING INTERFACES IN GENUINE TWO-DIMENSIONAL SOLIDIFICATION PROBLEMS

P. M. Beckett
University of Hull, England.

Introduction Two-dimensional solidification problems which do not possess the sort of symmetry that permits only one space variable to be involved (as is the case with freezing spheres or cylinders) are virtually intractable analytically. Moreover numerical methods devoted to such problems are not without difficulties most of which can be traced to the latent heat condition on the interface. The difficulty of setting up a finite difference grid in a region whose shape is changing is commonly overcome by means of some transformation and for the general method of inward solidification. Saitoh (ref. 1) has proposed a method using polar co-ordinates. This approach can be commended in general but for particular geometries alternative co-ordinates can be appropriate; nevertheless whatever the variables or precise nature of the transformation we are led to a non-linear differential equation involving the temperature and the function which defines the shape and position of the interface.

Saitoh recommends the use of A.D.I. methods for the solution of his equations on the grounds of ease of application and economy of computing time. Again his method can be commended in general terms but there are problems for which the method converges very slowly or not at all. Problems in which the boundary conditions are relatively uniform tend to pose less difficulties than those in which there are abrupt changes in wall temperature or heat flux. The purpose of this paper is to propose a method of dealing with the difficult cases, which is equally applicable to the easy cases and which is moreover less time consuming.

The method is based on quazi-linearization of the transformed heat conduction equation and latent heat condition at the interface and an iterative sequence in which these are solved simultaneously. Hitherto A.D.I. methods have been preferred but modern algorithms for solving such large sparse systems [2-4] mean that most of the storage advantage of A.D.I. methods are reduced and the speed of solution can be dramatically improved.

Formulation of Equations Following Saitoh the two-dimensional inward solidification of a region enclosed by a general boundary is formulated in terms of polar co-ordinates r,ϕ; the equation of the boundary is expressed as $r = B(\phi)$ - see fig. 1. At time $t = 0$ the region is either at or above the fusion temperature T_f, while for $t > 0$ a condition is applied at the boundary such that the material solidifies in an inward direction. The position of the solid/liquid interface at a general instant in time is denoted by $r = F(\phi,t)$; so that $F(\phi,0) = B(\phi)$. The problem is that of determining the function $F(\phi,t)$ together with the temperature $T(r,\phi,t)$ in the solidified phase, $F(\phi,t) < r < B(\phi)$, and also the temperature $T^*(r,\phi,t)$ in the molten phase for problems where the initial temperature is higher than T_f.

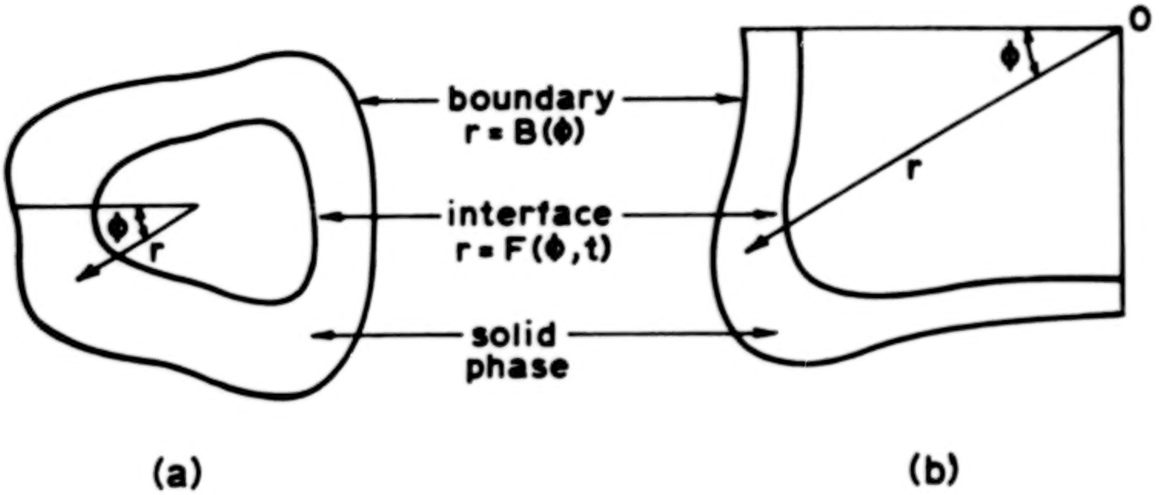

Fig. 1. General configuration: (a) closed region, (b) open region

The temperature distributions T and T* satisfy the heat conduction equation, thus

$$\frac{\partial T}{\partial t} = \kappa \nabla^2 T, \; F(\phi,t) < r < B(\phi) \tag{1}$$

and

$$\frac{\partial T^*}{\partial t} = \kappa^* \nabla^2 T^*, \; 0 < r < F(\phi,t), \tag{2}$$

where κ and κ^* are the thermal diffusivities in the solidified and molten phases. These are supplemented by the conditions that $T = T^* = T_f$ at the interface, by some boundary condition on $r = B(\phi)$ and by the latent heat condition at the interface

$$\rho L \frac{\partial C}{\partial t} = (k^* \underline{\nabla} T^* - k \underline{\nabla} T) . \underline{\nabla} C \tag{3}$$

where $C = r - F(\phi,t)$, L is the coefficient of latent heat, ρ is the density (contraction is neglected), k and k* are the thermal conductivities.

Clearly some thought must be given to the choice of origin of the polar co-ordinates so that it remains in the molten phase. The choice is not always easy and may need to be found by trial and error, indeed for some boundary shapes there may not be a convenient origin and some splitting of the region may be necessary. For open boundaries (Saitoh considers wedge shaped regions) the origin is chosen at the intersection of lines across which there is no heat transfer (so as to obtain simple boundary conditions at the ends of the transformed region).

The problem of integrating over the irregular domains is overcome by introducing the non-dimensional variables

$$\tau = \kappa t/\ell^2, \quad r' = r/\ell, \quad \phi' = \phi/\phi_0, \quad F' = F/\ell, \quad B' = B/\ell, \tag{4}$$

where ℓ is some representative length and ϕ_0 is the angle subtended by the extremeties of the boundary ($\phi_0 = 2\pi$ for a closed boundary), and then making the further transformations

$$\xi = \phi', \qquad \eta = \frac{r' - F'(\phi',t)}{B'(\phi') - F'(\phi',t)}, \quad \eta^* = \frac{r'}{F'(\phi',t)} \tag{5}$$

so the solidified and molten phases are defined by $0 < \xi < 1$, $0 < \eta < 1$ and $0 < \xi < 1$, $0 < \eta^* < 1$ respectively. Saitoh considers only materials which are initially at fusion temperature and hence there is no need to find T^*, the same will be presumed in this paper because the extra phase is a complicating factor only in so far as it adds to the size of the problem - it does not affect the convergence rate.

At the same time a dimensionless temperature $\theta(\xi,\eta,\tau)$ is introduced. The precise definition of θ depends on the form of the boundary condition. When a temperature $T_W(\phi)$ is prescribed on the boundary (or part of the boundary) it is convenient to put

$$\theta = \frac{T - T_W(0)}{T_f - T_W(0)} \tag{6}$$

whereas if a flux or radiation condition is imposed then θ is introduced by

$$\theta = T/T_f. \tag{7}$$

The numerical solution of the equation for $\theta(\xi,\eta,\tau)$ is effected by deducing the solution at time $\tau = \tau_N$ knowing that at τ_{N-1} by implicit differencing so that $\theta_N(\xi,\eta)$ needs to be solved on the unit square $0 < \xi < 1$, $0 < \eta < 1$. The boundary conditions on $\xi = 0$ and $\xi = 1$ are that for open regions derivatives of θ and F' with respect to ξ are zero and for closed regions θ, F' and their derivatives with respect to ξ are the same at $\xi = 0$ and $\xi = 1$.

When dealing with boundaries along which the temperature or flux conditions do not vary very much the solution of the equation for θ_N using simple A.D.I. techniques is usually quite satisfactory. Even sharp corners in the boundary do not pose problems and Saitoh succeeds in solving the inward solidification of rectangles and wedge shaped regions. Saitoh does however restrict himself to problems which have uniform boundary conditions and thereby avoids what seem to be the major difficulties. To assist with directional solidification it is common foundry practice to insert "chills" (which are heat sinks) or "insulating tiles" at or along strategic sections of the inner mould surface. Under such circumstances the variation in the boundary condition is quite abrupt and solution of the equations is usually more difficult. The simple A.D.I. techniques do not always converge and if they do it is commonly only very slowly.

In an attempt to cope with these difficulties the effect of various boundary conditions was considered along a plane wall. Referred to cartesian co-ordinates the wall is defined by $y = 0$, and the location of the interface by $y = E(x,t)$. Non-dimensionalizing similar to the above we put

$$\xi = x/\ell, \quad \eta = y/\ell\,\varepsilon(\xi,\tau), \quad \varepsilon(\xi,\tau) = E(x,t)/\ell$$

and the heat conduction equation yields

$$\begin{aligned}\frac{\partial\theta}{\partial\tau} - \frac{\eta}{\varepsilon}\frac{\partial\varepsilon}{\partial\tau}\frac{\partial\theta}{\partial\eta} &= \frac{\partial^2\theta}{\partial\xi^2} + \frac{2\eta}{\varepsilon}\frac{\partial\varepsilon^2}{\partial\xi}\frac{\partial\theta}{\partial\eta} + \frac{1}{\varepsilon^2}\frac{\partial^2\theta}{\partial\eta^2} \\ &- \frac{\eta}{\varepsilon}\frac{\partial^2\varepsilon}{\partial\xi^2}\frac{\partial\theta}{\partial\eta} - \frac{2\eta}{\varepsilon}\frac{\partial\varepsilon}{\partial\xi}\frac{\partial^2\theta}{\partial\xi\partial\eta} + \frac{\eta}{\varepsilon^2}\frac{\partial\varepsilon^2}{\partial\xi}\frac{\partial^2\theta}{\partial\eta^2} \quad ,\end{aligned} \tag{8}$$

which is solved in the region $\xi_- < \xi < \xi_+$, $0 < \eta < 1$.

The latent heat condition (3) at $\eta = 1$ is transformed to give

$$\beta\,\varepsilon\,\frac{\partial\varepsilon}{\partial\tau} = \left(1 + \frac{\partial\varepsilon^2}{\partial\xi}\right)\left(\frac{\partial\theta}{\partial\eta}\right)_{\eta = 1} \tag{9}$$

The remaining conditions are that $\theta = 1$ when $\eta = 1$ and a boundary condition

$$\theta = g(\xi) \quad \text{or} \quad \frac{\partial\theta}{\partial\eta} = h(\xi) \text{ on } \eta = 0 \tag{10}$$

or a mixture of these.

Finite Difference Representation The Hartree-Wommersley technique - an extension of the split time Crank Nicholson scheme - is used for the temporal differencing. In this the solution at time τ_{N-1} is advanced to that at τ_N by replacing differentials with respect to time by simple differences and all other quantities by averaging between τ_N and τ_{N-1}. Knowing the solution at τ_{N-1} the solution at the next time step is found by solving the following non-linear partial differential equation for $\theta_N(\xi,\eta)$ involving $\varepsilon_N(\xi)$ - $\theta_N(\xi,\eta) = \theta(\xi,\eta,\tau_N)$ etc.

$$\begin{aligned}&\frac{(\varepsilon_N^2 + \varepsilon_{N-1}^2)}{\delta t}\,\theta_N + \left(\eta\,\varepsilon_N\,\frac{d^2\,\varepsilon_N}{d\xi^2} - 2\eta\,\frac{d\varepsilon_N{}^2}{d\xi} + \frac{\eta(\varepsilon_{N-1}^2 - \varepsilon_N{}^2)}{2\delta\tau}\right)\frac{\partial\theta_N}{\partial\eta} \\ &- \varepsilon_N^2\,\frac{\partial^2\theta_N}{\partial\xi^2} + 2\eta\varepsilon_N\,\frac{d\varepsilon_N}{d\xi}\,\frac{\partial^2\theta_N}{\partial\xi\partial\eta} - \left(1 + \eta^2\,\frac{d\varepsilon_N{}^2}{d\xi}\right)\frac{\partial^2\theta_N}{\partial\eta^2}\end{aligned}$$

$$- \left(\frac{\theta_{N-1}}{\delta\tau} + \frac{\eta}{2\delta\tau} \frac{\partial\theta_{N-1}}{\partial\eta}\right)\varepsilon_N{}^2 = \frac{\varepsilon_{N-1}{}^2}{\delta\tau} \theta_{N-1} - \frac{\eta}{2\delta\tau} \varepsilon^2_{N-1} \frac{\partial\theta_{N-1}}{\partial\eta}$$

$$+ \varepsilon^2_{N-1} \frac{\partial^2\theta_{N-1}}{\partial\xi^2} + 2\eta \frac{d\varepsilon_{N-1}{}^2}{d\xi} \frac{\partial\theta_{N-1}}{\partial\eta} - \eta\varepsilon_{N-1} \frac{d^2\varepsilon_{N-1}}{d\xi^2} \frac{\partial\theta_{N-1}}{\partial\eta}$$

$$- 2\eta\, \varepsilon_{N-1} \frac{d\varepsilon_{N-1}}{d\xi} \frac{\partial^2\theta_{N-1}}{\partial\xi\partial\eta} + \left(\eta^2 \frac{d\varepsilon_{N-1}{}^2}{d\xi} + 1\right) \frac{\partial^2\theta_{N-1}}{\partial\eta^2} . \tag{11}$$

The same technique is applied to the latent heat condition which becomes

$$\frac{\beta}{\delta\tau} \varepsilon^2_N - \left(1 + \frac{d\varepsilon_N{}^2}{d\xi}\right) \left(\frac{\partial\theta_N}{\partial\eta}\right)_{\eta = 1}$$

$$= \frac{\beta}{\delta\tau} \varepsilon_{N-1}{}^2 + \left(1 + \frac{d\varepsilon_{N-1}{}^2}{d\xi}\right) \left(\frac{\partial\theta_{N-1}}{\partial\eta}\right)_{\eta = 1}, \tag{12}$$

where $\beta = L/Cp(T_f - T_W(0))$ is the inverse of the Stefan number.

These are discretized over the rectangle $\xi_- \leq \xi \leq \xi_+$, $0 \leq \eta \leq 1$ by taking m divisions in the ξ direction and n in the η direction. There are then m(n-1) interior nodes (ξ_i, η_j), $(i = 1, \ldots m;\ j = 1, \ldots, n-1)$ at which θ_N is to be found and m boundary nodes $(\xi_i, 1)$ for ε_N.

Equation (11) is non-linear because of the presence of θ_N and ε_N but if ε_N is presumed known the equation is a linear elliptic equation for θ_N and this can of course, be solved in a variety of ways. If this is solved exactly there is still an iterative sequence in which having solved (11) for θ_N a new form of ε_N is deduced from (12) and thence another θ_N etc. The convergence of this sequence is one of the problems for non-uniform boundary conditions but that is secondary at the moment to the problem of finding exact solutions of (11). Saitoh and most other workers in the field apply A.D.I. techniques to (11) and include the adjustment to ε_N by solving (12) in the A.D.I. iterations. This procedure involves the solution of n mxm and m (n-1) x (n-1) tridiagonal matrices each iteration and is therefore very simple to apply and it is easy to see why the method is generally favoured. In many cases this is a sound choice of method but when there are sharp temperature gradients it is less satisfactory and considerable benefits accrue from dealing with the sparse matrix equation which can be constructed to give the simultaneous solution of the discretized equations over the entire rectangle. This approach turns out to be convergent when the other is not and moreover can yield solutions more rapidly even when the A.D.I. method does converge.

Dramatic evidence of the power of this approach has been given by Kershaw (ref. 2) who applied iterative methods of solving large sparse systems to laser problems. Kershaw found that his type of approach can be 200 times faster than A.D.I. and is also applicable when A.D.I. fails. Moreover Kershaw states that while A.D.I. methods only apply when there is five point coupling (where the (i,j) point is coupled to the $(i \pm 1,j)$ and $(i,j \pm 1)$ points) the incomplete Choleski-conjugate gradient method, ICCG, is applicable when there is nine point coupling (that is when the points $(i \pm 1, j \pm 1)$ and $(i \pm 1, j \mp 1)$ are also used in the discretization). Kershaw also successfully applied the method to matrices with somewhat random sparsity patterns.

In the case of solidification the difficulty can be traced to the presence of the mixed second order derivative $\frac{\partial^2\theta_N}{\partial\xi\partial\eta}$ in (11). The coefficient of this involves $\frac{d\epsilon_N}{d\xi}$ and if this is small then A.D.I. methods can cope but if it becomes large then such methods are no longer necessarily stable - of course this gradient is significant when there are abrupt changes in the boundary condition. In such situations equation (11) can be solved for known ϵ_N by solving the discretized forms of (11) simultaneously by a method utilizing the sparsity pattern in the resulting matrix of order mn - m. (This matrix has a tridiagonal block structure and each block is tridiagonal.) However there is then still the necessity to iterate between (11) and (12) to obtain compatible θ_N and ϵ_N and it is in this sequence that the extra convergence complications, mentioned earlier, can manifest themselves.

Full Quazi-linearization and simultaneous solution of all equations and boundary conditions The most reliable way of obtaining converged solutions of (11) and (12) has been found to be quazi-linearization of these equations, discretization using simple central differences and an iterative procedure involving the simultaneous solution of the mn linear equations. Quazi-linearization, the name given by Bellman to the extension of Newton's method, replaces any non-linear term by the first order Taylor expansion about the latest approximation to any constituent part. For example the third term in (11) is approximated according to

$$\eta\epsilon_N \frac{d^2\epsilon_N}{d\xi^2}\frac{\partial\theta_N}{\partial\eta} \sim \eta(\bar{\epsilon}_N \frac{d^2\bar{\epsilon}_N}{d\xi^2}\frac{\partial\theta_N}{\partial\eta} + \bar{\epsilon}_N \frac{d^2\epsilon_N}{d\xi^2}\frac{\partial\bar{\theta}_N}{\partial\eta} + \epsilon_N \frac{d^2\bar{\epsilon}_N}{d\xi^2}\frac{\partial\bar{\theta}_N}{\partial\eta}$$

$$- 2\bar{\epsilon}_N \frac{d^2\bar{\epsilon}_N}{d\xi^2} \frac{\partial\bar{\theta}_N}{\partial\eta})$$

where the bar denotes the previous iterate at the time τ_N. Equation (11) thus yields an equation of the type

$$\chi_1\theta_N + \chi_2 \frac{\partial\theta_N}{\partial\eta} + \chi_3 \frac{\partial^2\theta_N}{\partial\xi^2} + \chi_4 \frac{\partial^2\theta_N}{\partial\xi\partial\eta} + \chi_5 \frac{\partial^2\theta_N}{\partial\eta^2}$$

$$+ \chi_6\, \varepsilon_N + \chi_7 \frac{d\varepsilon_N}{d\xi} + \chi_8 \frac{d^2\varepsilon_N}{d\xi^2} = \chi_9, \tag{13}$$

where the coefficients χ_i are dependent upon ε_{N-1}, $\overline{\varepsilon}_N$, θ_{N-1}, $\overline{\theta}_N$, and equation (12) yields

$$\sigma_1\, \varepsilon_N + \sigma_2 \frac{d\varepsilon_N}{d\xi} + \sigma_3 \left(\frac{\partial\theta_N}{\partial\eta}\right)_{\eta=1} = \sigma_4. \tag{14}$$

Using central difference formulae these are discretized to give mn-m linear equations in θ_{ij} and ε_i ($\theta_{ij} = \theta_N(\xi_i,\eta_j)$ and $\varepsilon_i = \varepsilon_N(\xi_i)$) from (13) and m linear equations from (14). The entire set can be written in matrix form as

$$WX = Y, \tag{15}$$

where X is a column vector the transpose of which is given by

$$X^T = (\theta_{11},\ \theta_{21},\ \ldots\ \theta_{m1},\ \theta_{21},\ \ldots\ \theta_{m(n-1)}, \varepsilon_1\ ,\ \ldots\ \varepsilon_m)$$

and W is a matrix with the following block structure

$$W = \left(\begin{array}{cccccccc}
T_{11} & T_{12} & O & . & . & . & . & T_{1m} \\
T_{21} & T_{22} & T_{23} & O & . & . & . & T_{2m} \\
O & T_{32} & T_{33} & T_{33} & O & . & . & T_{3m} \\
. & . & . & . & . & . & . & . \\
. & . & . & . & . & . & . & . \\
O & . & . & . & O & T_{m-1,m-2} & T_{m-1,m-1} & T_{m-1,m} \\
O & . & . & O & D_1 & D_2 & D_3 & T_{mm}
\end{array}\right)$$

in which each block T_{rs} is a tridiagonal matrix and D_p is a diagonal matrix.

This particular form of W is appropriate when the temperature is specified on the entire boundary; if flux or radiation conditions are imposed the temperature at some (or all) points on the boundary must also be determined along with the interior values. In such cases extra elements are included in the vector X and W is enlarged to include linearized forms of the relevant boundary condition. In any event a sparse set of equations can be found which when solved gives a better approximation to the functions at time τ_N. All the advantages of rapid convergence associated with Newton's method are present and if the initial guess at any time is extrapolated from the solution at previous times typically accuracy to six significant figures is possible in 2 or 3 iterations.

Methods of solution of sparse systems The original computations were performed using a set of NAG library routines (ref. 3) on an ICL1904S. Although the matrix changes each iteration its sparsity pattern remains the same and advantage is taken of this by using the first of the routines, FO3AJA, to decompose W into approximate triangular matrices using a pivotal strategy designed to compromise between maintaining sparsity and controlling the loss of accuracy through round-off and for subsequent iterations FO3AKA is used to find the LU decomposition using the same pivotal strategy. The routine FO3AJA contains a parameter in such that when searching a row or column for a pivot any element u times the largest element is excluded. Thus decreasing u biases the algorithm towards maintaining sparsity at the expense of the growth of errors - the value $u = 0.25$ has been found to be satisfactory in test examples. After FO3AJA or FO3AKA the routine FO4APA solves the equation $WX = Y$ by back substitution.

Table 1 shows the typical number of non-zero elements in W for a variety of values of m and n together with the number of non-zero elements in the LU decomposition required to give accuracy $\sim 10^{-12}$. The sizes of these numbers indicates that the routines are an efficient way of solving this type of equation.

TABLE 1 - NUMBER OF ELEMENTS IN LU DECOMPOSITION

m	n	order or W	number of elements in W	number of elements in decomposed form of W
21	5	105	978	1328
41	5	205	1938	2658
21	10	205	2198	2948

These figures relate to the problem of solidification near a plane wall when a temperature distribution in the form of a step function is applied at the wall. In such problems it is necessary to find an approximation to the solution at a small value of τ and work numerically from there. In all these problems one-dimensional solidification from the wall was presumed to obtain the starting solution and the number of iterations was highest in the first few time steps thereafter. The number of iterations using A.D.I. was at least six times the number using the sparse system for an easy problem in which A.D.I. still converged (where the difference between wall and interface temperatures jumps by a factor of 20) but this rose dramatically until A.D.I. failed. Since solution of the sparse system of order mxn takes about four times the solution of n mxm equations using A.D.I. on the face of it there are time savings on even an easy problem. However the coefficients in the sparse matrix representation are more complex than those in the A.D.I. formalization and for such a problem the methods take almost the same total computing time. However when the boundary conditions are more abrupt or more complex there can be substantial time savings using the sparse matrix method.

Moreover there are alternative methods of solving sparse systems of equations which are probably superior and which would make the approach even more appealing. My attention was recently brought to ICCG methods for solving such equations. The method of conjugate gradients was originally conceived as a direct method and lay dormant for two decades until Reid (ref. 4) proposed its use in an iterative scheme; more recently Kershaw (ref. 2) presented a generalization of the Incomplete Choleski-Conjugate Gradient method to arbitrary non singular sparse matrices. Unlike F03AJA which fixes a sparsity pattern on the LU decomposition by ignoring small terms ICCG fixes a sparsity pattern at the outset; if the sparsity pattern for the LU decomposition is the same as that of W the method is denoted as ICCG(0). This reduces the arithmetic labour and if the iterates are used to update the coefficients before each application of the incomplete Choleski step a fast and rapidly convergent algorithm is likely.

Stimulated by the successful convergence on the geometrically simple case of solidification adjacent to a plane wall the method has been applied to more complex configurations. The work was originally stimulated by the need to model the solidification of ingots in the steel industry and the need to solve the solidification in a "coffin" shaped region with boundary conditions representing the insulated and non-insulated parts of the mold. In such problems there is the need to split the domain of integration and the number of coupled equations increases and it is then that simultaneous quasi-linearization seems to be at its most powerful.

Approximate Solutions of Solidification Problems A satisfactory approximate model for one-dimensional solidification utilizes Pohlhausen techniques in which a temperature profile within the solid phase is postulated and the depth of penetration of the interface deduced by integrating the heat conduction equation across the phase. The extension of this concept to 2-dimensional solidification above a plane surface postulates the temperature distribution in the form

$$\theta(x,y,t) = g(x) + (1 - g(x) - S(x,t))\frac{y}{E(x,t)} + \frac{S(x,t)y^2}{E(x,t)^2} \qquad (16)$$

where E(x,t), as before, gives the shape of the interface and S(x,t) is a shape factor for the quadratic temperature profile across the solidified phase. Applying the usual Pohlhausen technique the conduction equation and substituting (16) into the latent heat condition yield the following coupled equations for S(x,t) and E(x,t).

$$\frac{1}{\beta}\left(1+\frac{\partial H}{\partial x}^{2}\right)(1+g-S)+2H\frac{\partial H}{\partial x}\left(\frac{\partial S}{\partial x}-\frac{dg}{dx}\right)$$

$$+2\frac{\partial H}{\partial x}^{2}(1+g-2S)+H\frac{\partial^2 H}{\partial x^2}(S-g-1)=2S, \tag{17}$$

$$H\frac{\partial^2 H}{\partial x^2}-(\beta+1)H\frac{\partial H}{\partial t}-\frac{H}{2}\left(\frac{\partial^2}{\partial x^2}-\frac{\partial}{\partial t}\right)(H(1-g-S/3))$$

$$+1+g+S=0. \tag{18}$$

Again the Hartree-Wommersley scheme is applied to cope with the temporal derivative and there results a pair of coupled non-linear ordinary differential equations at the time $\tau = \tau_N$. In this instance any method which did not solve these simultaneously leads to divergence and solution of the sparse system obtained by quazi-linearizing was found to be the only way forward. It transpires that the model is of limited physical interest but from a numerical standpoint these facts reinforce the belief that solution by means of constructing a large sparse system is worthy of consideration for any problem in which convergence is a problem.

References

1. Saitoh, T., Numerical method for multi-dimensional freezing problems in arbitrary domains, Journ. of Heat Transfer, vol. 100, 1978, pp.294-299.

2. Kershaw, D. S., The Incomplete Choleski-Conjugate Gradient Method for the Iterative Solution of Systems of Linear Equations, Journ. Comp. Phys., vol. 26, 1978, pp. 43-65.

3. Curtis, A. R. and Reid, J. K., Fortran subroutines for the solution of sparse sets of linear equations, U.K.A.E.A. Research Group Report R6844 1971.

4. Reid, J. K., On the method of conjugate gradients for the solution of large sparse systems of linear equations, *in* "Proceedings of the Conference on Large Sparse Systems of Linear Equations", Academic Press, New York 1971.

SHOCK-POINT OPERATORS IN CONSERVATIVE DIFFERENCING

Czeslaw P. Kentzer
Purdue University, Lafayette IN 47907

ABSTRACT

We investigate the conditions under which a finite difference operator, which is designed to approximate the conservative form of the partial differential equations of fluid flow takes on a form of an approximation to the shock jump conditions. Such an operator may be interpreted as an analog of the Rankine-Hugoniot jump operator for rapidly changing solutions while remaining an approximation to the partial differential equations for smooth solutions. This interpretation gives the shock speed and the shock normal as functions of the mesh spacing independently of the solution leading to errors in shock strength and motion. Suggestions are offered concerning modifications of shock-point operators aimed at improving the accuracy of conservative differencing in presence of shock waves.

1. INTRODUCTION

The interest in the use of conservative (divergence) form of the partial differential equations of fluid dynamics for numerical calculations of shocked flows dates back to the pioneering paper of Lax [1]. In [2] Lax has shown that an appropriately defined *weak solution* of conservation law equations satisfies jump conditions derivable from the conservation law form of the p.d.e's. The popular understanding of the results in [1] and [2] is that, 1°, any errors in fluxes cancel at cell boundaries because the same finite difference approximations are used as a rate of outflow at one and as a rate of inflow at the other cell having a common boundary, and, 2°, that, somehow, the *correct* jump conditions, rather than merely their *appropriate form*, are satisfied at discontinuities. The purpose of this paper is to clarify the second point and to suggest the use of known techniques for the purpose of an improvement in the calculations of shock wave motion without taking recourse to shock fitting.

We shall discuss, first, the general balance equations in presence of a singular surface, and then interpret finite difference schemes as approximations to the p.d.e's in regions when the solution is continuous and, simultaneously, as approximations to the jump conditions at surfaces of discontinuity. This interpretation will allow for an examination of the sources of errors in presence of shock waves.

2. GENERAL BALANCE EQUATION

Consider a fixed volume V divided into two volumes V_1 and V_2 separated by a moving surface S(t). Let A_1 and A_2 denote the portions of the surface A of V which form parts of the boundaries of V_1 and V_2. The remaining part of the boundary, common to V_1 and V_2, is S(t). Then the entire boundaries of V_1 and V_2 are $B_1 = A_1 + S(t)$ and $B_2 = A_2 + S(t)$, respectively.

Let $u_n = U\bar{n}$ be the velocity of S(t) along the outward normal to S(t), $\bar{n}$, when S(t) is considered to be a part of the boundary of V_1. The unit normal $\bar{n}$ points from V_1 to V_2. If ψ is any function (property of the fluid per unit mass), which may take different values ψ_1 and ψ_2 on either side of S(t) in V_1 and V_2, respectively, then the rate of increase of ψ inside $V = V_1 + V_2$ plus the flux of ψ across the boundary $A = A_1 + A_2$ of V, equated to the total source of ψ in V, is

$$\iiint\limits_{V_1+V_2} \frac{\partial}{\partial t}(\rho\psi)dV + \iint\limits_{A_1+A_2} \rho\psi\bar{n}\cdot\bar{v}\,dA - \iint\limits_{S} [\rho\psi]U\,dA$$

$$= \iiint\limits_{V_1+V_2} \frac{\partial}{\partial t}(\rho\psi)dV + \iint\limits_{B_1+B_2} \rho\psi\bar{n}\cdot\bar{v}\,dA - \iint\limits_{S} [\rho\psi w_n]dA$$

$$= \iiint\limits_{V_1+V_2} \rho q\,dV \qquad (1)$$

where ρ = mass density, q = source of ψ/mass, $[f] = f_2 - f_1$ = jump in f across S(t), $\bar{v}$ = fluid velocity, $w_n = \bar{v}\cdot\bar{n} - U$ = normal component of fluid velocity relative to S(t).

In presence of a discontinuity one has to consider separately the volumes V_1 and V_2 with their entire boundaries B_1, B_2, respectively, or the combined volume $V = V_1 + V_2$ with the boundary $A = A_1 + A_2$ of V, subtracting in both cases the appropriate terms arising from the presence of S(t), as indicated in Eqn. (1).

If the dependent variables ρ, ψ, $\bar{v}$ are single-valued and continuous in V + B, $\nabla \cdot (\rho\psi\bar{v})$ is piecewise continuous, and the integrals over V_1, V_2 and B_1, B_2 converge, one may use Gauss's Divergence Theorem to obta

$$\frac{\partial}{\partial t} (\rho\psi) + \nabla \cdot (\rho\psi\bar{v}) = q \tag{2}$$

valid in V_1 and V_2 provided that

$$\iint_S [\rho\psi(\bar{v}\cdot\bar{n} - U)]dA = 0 .$$

Thus, on S(t) we must have

$$-U[\rho\psi] + \bar{n} \cdot [\rho\psi\bar{v}] = 0 , \tag{3}$$

and the Rankine-Hugoniot type jump conditions (3) are necessary in order that ψ be conserved.

The general balance equation, allowing for the presence of a persistent singular surface and analogous to Eqn. (1), is discussed by Truesdell and Toupin [3], who, on p. 527 derive the Kotchine's Theorem [4] equivalent to the jump conditions (3). The jump conditions at a surface of discontinuity were derived also by Green and Naghdi [5] as necessary consequences of conservation of energy and invariance conditions under superposed rigid body motions. In summary, in order to define a weak solution of Eqn. (2), the boundary values of ρ, ψ, $\bar{v}$ restricted to the hypersurface S(t) are not arbitrary and satisfy the Rankine-Hugoniot jump conditions (3). Since the surface S(t) is not known in advance, and must be determined as part of the solution of the problem, the equations (2) and (3) describe a multi-dimensional nonlinear free boundary value problem for a system of quasi-linear hyperbolic equations in the case of inviscid gas dynamics, and nonlinear parabolic equations in case of viscous flows. Viscous Rankine-Hugoniot jump conditions in the form of Eqn. (3) are given by Green and Naghdi, [5].

3. FINITE DIFFERENCE APPROXIMATIONS

In regions of space-time where the solution is continuous, the conservative form of a system of p.d.e.'s governing fluid flow is

$$\frac{\partial u}{\partial t} + \nabla \cdot f = 0, \qquad (4)$$

where u is a vector of densities, and f is their flux tensor. Writing Eqn. (4) in the operator form, we have

$$(\partial_t, \nabla)\cdot(u, f)^T = 0. \qquad (5)$$

The jump conditions corresponding to (5) are

$$-U[u] + \bar{n}\cdot[f] = (-U, \bar{n})\cdot[u, f]^T = 0. \qquad (6)$$

We observe here that the conservation principles require that the differential operator (∂_t, ∇), go over into the multiplication operator, $(-U, \bar{n})$ = space-time normal to the singular surface, operating on the difference in the limiting values of the vector $(u, f)^T$ at the two sides of the singular surface.

We investigate now whether a finite difference scheme, which is assumed to be a stable and consistent approximation to Eqn. (5), goes over into a reasonable approximation to the algebraic jump condition (6). That is, if the finite difference approximation to the operator (∂_t, ∇) is $(D_t, D_{\bar{x}})$, we ask under what conditions

$$(D_t, D_{\bar{x}}) \rightarrow \alpha(-U, \bar{n})$$

with α = arbitrary constant.

First, we observe that finite difference approximations to the p.d.e.'s in the conservative form are linear in differences in u and f. For instance, if

$$\frac{1}{\Delta t}(u^{n+1}_{ijk} - u^{n}_{ijk}) + \frac{1}{2\Delta x}(f^{n+\alpha}_{i+1,j,k} - f^{n+\alpha}_{i-1,j,k})$$
$$+ \frac{1}{2\Delta y}(g^{n+\beta}_{i,j+1,k} - g^{n+\beta}_{i,j-1,k}) + \frac{1}{2\Delta z}(h^{n+\gamma}_{i,j,k+1} - h^{n+\gamma}_{i,j,k-1}) = 0 \qquad (7)$$

where $f^{n}_{ijk} = f(n\Delta t, i\Delta x, j\Delta y, k\Delta z)$ with $\alpha, \beta, \gamma = 0$ or 1, depending on a scheme used, approximates Eqn. (4) then, if all the differences in the above are *differences across the shock,* we have

$$\frac{1}{\Delta t}[u] + \bar{N}\cdot[f] = 0,$$

where $\bar{N} = (\frac{1}{2\Delta x}, \frac{1}{2\Delta y}, \frac{1}{2\Delta z})$. The differences (jumps) across the shock should remain finite as the mesh is refined and as $|\bar{N}| \rightarrow \infty$. Therefore, we divide (7) by the magnitude of $\bar{N}$ and introduce a unit normal

$$\bar{n} = \frac{\bar{N}}{|\bar{N}|} = (\frac{\Delta}{\Delta x}, \frac{\Delta}{\Delta y}, \frac{\Delta}{\Delta z}), \quad |\bar{n}| = 1,$$

where

$$\frac{1}{\Delta^2} = \frac{1}{\Delta x^2} + \frac{1}{\Delta y^2} + \frac{1}{\Delta z^2}.$$

Thus we obtain

$$\frac{2\Delta}{\Delta t}[u] + \bar{n}\cdot[f] = (\frac{2\Delta}{\Delta t}, \bar{n})\cdot[u, f]^{T} = 0 \qquad (8)$$

Equation (8) would be an approximation to (6) if:

(a) the points (n+1,i,j,k) and (n,i,j,k), (n+α,i+1,j,k) and (n+α,i-1,j,k), etc., lie, as assumed, on the opposite sides of the shock,

(b) the unit vector $\bar{n}$ points in the direction of the normal to the shock,

(c) $-2\Delta/\Delta t$ is equal to the shock speed, U, measured along the shock normal.

We observe that there exists, at least, a possibility of satisfying approximately the p.d.e.'s and the corresponding jump conditions by choosing correctly the mesh parameters, $\Delta t, \Delta x, \Delta y, \Delta z$, which are at our disposal. In general, however, the approximation to the jump conditions (8) will be in error on the account of:

(a) not all of the finite differences in (7) being taken across the shock,

(b) a possibly incorrect orientation of the shock wave normal, $\bar{n}$,

(c) incorrect shock speed, $-2\Delta/\Delta t$.

All such errors are determined by the mesh or by the numerical scheme employed relative to the expected position of the shock wave. In particular, if all the differences in Eqn. (7) are taken across the shock, then $\bar{n}$ points in the direction of the shortest distance to the convex hull of the computational mesh. If one spatial difference is based on points lying entirely on one side of the shock, then, in the limit as the mesh is being refined, this spatial difference will tend to zero while the remaining spatial differences will tend to a finite, non-zero limit. As a consequence, the corresponding component of the unit vector $\bar{n}$ will vanish in the limit and the jump condition will be applied in a plane parallel to the corresponding coordinate axis. If only one spatial difference is evaluated across the shock, then Eqn. (8) takes the form of jump conditions across a shock aligned with one coordinate plane. The worst situation occurs when at least one spatial difference is taken across the shock, but the temporal difference $(u^{n+1}_{i,j,k} - u^{n}_{i,j,k})$ is not, for then the temporal difference, instead of approaching zero as $t \to 0$, remains finite giving rise to an increment in u^{n}_{ijk} on the order of the jump in the fluxes. This phenomenon leads to the diffusion and dispersion of the shock and was discussed, from a different point of view though, by Lerat and Peyret [6].

4. SHOCK POINT OPERATORS

No numerical experiments are available at this time to substantiate the conjectures as to the possibility of satisfying the p.d.e.'s and the jump conditions accurately by a suitable scheme based on the modification of Eqn. (7). Below are given two suggestions with the hope that they may be readily incorporated into some of the existing algorithms. We remark here that the position, orientation, and speed of the shock could be estimated at a given time level by tracking the shock. With that information available, one should proceed with an attempt at putting Eqn. (7) in the form of the shock jump conditions (8) considering $2\Delta/\Delta t = -U$ and $\bar{n}$ as given. This could be accomplished as follows.

Suggestion (a)

There are many algorithms, both implicit or explicit, and conservative or nonconservative, which place restrictions on spatial difference approximations depending on the characteristic speeds (eigenvalues) of a hyperbolic system. Similar restrictions may be developed based on the location of the shock and the sign of the components of the shock velocity, especially in connection with the flux splitting techniques of Steger and Warming [7] or Reklis and Thomas [8]. The derivatives of the fluxes may be split into derivatives on one side, on the other side, and across the shock, and into derivatives taken at two different time levels (in case of implicit schemes). If the shock normal is known, the weighted differences of flux components taken *across the shock* may be forced to be in a correct proportion to each other so as to satisfy Eqn. (8). The common factor of proportionality could then be adjusted so as to give a desired speed of the shock $U = -2\Delta/\Delta t$. The differences of flux components taken only from one side of the shock will drop out from the jump conditions (8) in the limit. Consequently, differentiation *across the shock*, when skillfully used, could improve capturing of the shock waves and render them thin and without the undesirable "overshoot" or "wiggles." Indiscriminate use of "across the shock" differentiation leads only to a constant generation of errors which depend on the relative position of the shock and the mesh points.

Suggestion (b)

Reklis and Thomas [8] have developed an implicit scheme incorporating flux vector splitting and arbitrary coordinate transformation. Local rotation of coordinates, combined with a change in mesh aspect ratio, could then be used to control the orientation of $\bar{n}$ and the magnitude of Δ and, consequently, also of U. It is particularly important to be able to make Δ arbitrarily small for the case when the shock speed approaches zero, for then $U = -2\Delta/\Delta t \rightarrow 0$ requires $\Delta \rightarrow 0$. We interpret Δ as the shortest distance to the convex hull of the computational module. The condition $\Delta \rightarrow 0$ would dictate a distribution of computational points in planes locally parallel and close to the shock. Data on the new shock-oriented coordinate grid should be obtained by interpolation from the old coordinates, with due attention paid to the domain of dependence and the estimated shock position which determines that domain.

5. SUMMARY

Finite difference schemes in conservation form were interpreted as approximations to the Rankine-Hugoniot jump conditions in situations where shock waves are present and finite differences are taken across the shocks. The analogy of the f.d.e.'s in conservation form to the Rankine-Hugoniot conditions is only formal in as much as the space-time normal, $(-U, \bar{n})$, is not determined as a part of the solution. The information about the space-time normal must be supplied by shock tracking and must be made use of in order that the Rankine-Hugoniot form of the conservative f.d.e.'s approximate the shock jump conditions correctly.

The use of the solution-dependent shock point operators should be distinguished from the straight-forward shock fitting techniques, e.g., as suggested by Kentzer [9], or the post-correction shock fitting method of de Neef and Moretti [10]. The main feature of the present method is that the differentiation across the shock is not avoided; on the contrary, it must be used and must be employed correctly to satisfy conservation principles at a shock wave.

6. REFERENCES

1. Lax, P.D., Solutions of nonlinear hyperbolic equations and their numerical computation, *Comm. Pure Appl. Math.*, 7, 159-193 (1954).

2. Lax, P.D., Hyperbolic systems of conservation laws, II, *Comm. Pure Math.*, 10, 537 (1957).

3. Truesdell, C., and Toupin, R., The classical field theories, C. Singular surfaces and waves, pp. 491-529 in *Handbuch der Physik, Band III/1, Prinzipien der Klassisches Mechanik und Feld Theorie*, S. Flügge, ed., Springer-Verlag (1960).

4. Kotchine, N.E., Sur la théorie des onde de choc dans un fluide, *Rend. Circ. Mat.*, Palermo, 50, 305-344 (1926).

5. Green, A.E., and Naghdi, P.M., On the derivation of discontinuity conditions in continuum mechanics, *Int. J. Engr. Sci.*, 2, 6, 621-624, (1965).

6. Lerat, A., and Peyret, R., Noncentered schemes and shock propagation problems, *Computers and Fluids*, 2, 35-52 (1974).

7. Steger, J.L., and Warming, R.F., Flux vector splitting of the inviscid gasdynamic equations with application to finite difference methods, *NASA Technical Memorandum 78605* (1979).

8. Reklis, R.P., and Thomas, P.D., A shock capturing algorithm for the Navier-Stokes equations, *AIAA Paper No. 81-1021*, AIAA 5-th Comput. Fluid Dyn. Conference, Palo Alto, CA, June 1981.

9. Kentzer, C.P., Discretization of boundary conditions on moving discontinuities, *Lecture Notes in Physics*, 8, 108-113, Springer-Verlag (1971).

10. de Neef, T., and Moretti, G., Shock fitting for everybody, *Computers and Fluids*, 8, 327-334 (1980).

Blank Page

A MESH EMBEDDING APPROACH FOR PREDICTION OF TRANSONIC WING/BODY/STORE FLOW FIELDS*

D. S. Thompson
General Dynamics/Fort Worth Division

SUMMARY

A transonic wing/body/store flow field prediction code has been developed utilizing potential flow and small disturbance theories. The code was developed by extending the Bailey/Ballhaus wing/body flow field prediction code. A mesh embedding approach was utilized to include the store in the computational domain. An evaluation of mesh interface boundary conditions is presented in the text. In addition, comparisons of computed results with experimental data are also presented for two isolated stores.

INTRODUCTION

The aerodynamic design cycle of a military aircraft requires careful attention to detail to achieve the desired aerodynamic characteristics. It is indeed paradoxical to note that even though these aircraft are often used in the operational environment as carriers of a variety of weapon and tank configurations, little consideration is given during the design phase to the performance degradation associated with unfavorable aircraft/store interference effects. These same interference effects can also significantly affect separation characteristics and make accurate delivery of a store to a target difficult. The major reason these important interference effects are neglected during the design phase is that no reliable methodology exists to accurately predict the effect of aircraft/store interference on store carriage and separation. This is especially true in the transonic flow regime. The designer must rely on costly and time-consuming experimental procedures which utilize pseudo-steady wind tunnel grid techniques in conjunction with trajectory codes to obtain the carriage and separation characteristics of an aircraft/store configuration. These procedures are also limited with respect to the ultimate goal of the designer - optimization.

Stahara (Reference 1) has reported development of a predictive method for three-dimensional transonic flow fields about the aircraft and loading distributions on external stores located in the flow field. The theoretical method, designed for rapid calculations,

---

*The research described herein was initiated by Dr. S. P. Shanks while participating in the Industry Research Associate Program sponsored by the NASA Ames Research Center and was continued by the author with partial funding under Contract NAS2-10779.

relies on the classical transonic equivalence rule, which is then extended to account for three-dimensional cross-flow effects. One modification replaces the linear two-dimensional cross-flow solution with a linear three-dimensional solution obtained by panel methods. Another correction employs a three-dimensional non-linear finite-difference solution of the small-disturbance equations. Results presented for the Nielsen generic store are encouraging. However, no attempt was made to simulate a realistic store with fins.

A method for analyzing store separation characteristics has been developed by Deslandes (Reference 2). The problem is simplified by quasi-linearization of the time dependence in the separation dynamics, with a flow-angularity technique employed to evaluate first-order interference effects. The method can use theoretically or experimentally determined flowfield data for the interference calculations. Good correlation with drop model tests is demonstrated for subsonic Mach number with an angle-of-attack variation. High-transonic-Mach-number applicability has not been demonstrated in the literature.

Waskiewicz, DeJongh, and Cenko (Reference 3) presented a method capable of simulating relatively complex store geometries utilizing the higher order panel method code, PANAIR. Relatively good agreement with experimental results was obtained for finned store geometries in close proximity to a flat plate at angle of attack for supersonic Mach numbers. However, due to linear theory limitations, the PANAIR code cannot predict the complex flow phenomena associated with the transonic regime.

Shankar and Malmuth (Reference 4) have developed a method for analyzing aircraft/pylon/store configurations in transonic flow. The method is based on the work done by Ballhaus, Bailey, and Frick (Reference 5) and later refined by Mason, MacKenzie, et al (Reference 6). The modified small disturbance (MSD) equation is solved iteratively using finite difference techniques. The pylon and store are simulated by use of an image point concept. The image point concept avoids excessive storage requirements and lengthened run times due to increased complexity. However, simulation of fins was not demonstrated. The code, with modifications, could be used to simulate horizontal and vertical fins. Simulation of arbitrary angular orientation of fins using this method would be extremely difficult.

As a first step towards simulation of store carriage and separation, a transonic wing/body/store flow field prediction code has been developed utilizing a mesh embedding approach similar to that of Boppe and Stern (Reference 7). The transonic flow field surrounding a wing/body with a finned store in the near field is numerically obtained using potential flow and small disturbance theories. The method is also an extension of the work done by Ballhaus, Bailey, and Frick (Reference 5) and Mason, MacKenzie, et al (Reference 6) for wing/body configurations. The use of potential flow and small disturbance theories does, of course, place limitations on the range of applicability of the code, small angles of attack, etc. However, use of small disturbance theory does allow simulation of relatively complex configurations, since the necessary flow tangency boundary conditions are applied on a mean surface. The mesh embedding approach eliminates the need for a single continuous grid system and allows concentration of coordinate lines in regions where a detailed analysis of the flow field is required. The mesh embedding approach also allows each component of the configuration to use a computational mesh which is suited to its particular surface geometry. The wing/body/store code utilizes three different meshes to discretize the computational domain, a wing fine mesh, a store mesh, and a global crude mesh. The modified small disturbance (MSD) potential equation for transonic flow is iteratively solved on each mesh by successive fine, store, and crude mesh relaxation cycles using finite difference techniques. Dirichlet or Neumann boundary conditions applied at the various mesh interface are updated during the course of each iteration. In addition to prediction of wing/body/store flow fields, the code also has the capability to predict the flow field around an isolated store in transonic flow.

Computed results are presented for two isolated stores as well as results for a wing/body/store configuration. Lifting and non-lifting results are presented for the Nielsen store and the GBU-15. Comparisons with experimental data were made for validation of the isolated store procedure. An F-16/B-61 configuration was chosen for evaluation of mesh interface boundary condition procedures in the wing/body/store code. Results of the boundary condition procedure comparisons are presented for all possible combinations of Dirichlet and Neumann boundary conditions at the mesh interfaces.

COMPUTATIONAL APPROACH

The configuration considered in this analysis is a wing/body with a separated store in the near field as illustrated in Figure 1. Both the aircraft and the store are restricted to small deflections with respect to a uniform freestream. Analysis of the flow field surrounding this configuration was selected as a starting point for development of a more complex computational procedure. The proposed code will be capable of analyzing realistic wing/body/pylon/store configurations with the store in carriage or separated positions. In addition, the configuration illustrated in Figure 1 allows general evaluation of the method without necessitating development of special procedures for strong interference effects such as reflected shocks, etc.

The methods used to numerically obtain the flow field due to the configuration illustrated in Figure 1 are described in the sections that follow. Since the solution of the modified small disturbance (MSD) potential equation for wing/body configurations in transonic flow has been previously well documented in Reference 5 and Reference 6, detailed descriptions will only be made of procedures which specifically pertain to the wing/body/store flow field prediction code.

Embedded Mesh Scheme

Discretization of the wing/body/store flow field illustrated in Figure 1 is accomplished utilizing a mesh embedding approach. Figure 2 illustrates the general embedded mesh system for the wing/body/store configuration under consideration. A planform oriented fine mesh is employed to discretize the region of the flow field surrounding the wing. This fine mesh is embedded in a global Cartesian crude mesh which discretizes the entire computational domain. A cylindrical fine mesh is used to discretize the region of the flow field surrounding the store. Each global iteration of the solution algorithm consists of successive fine, store, and crude mesh relaxations. Details of the transmission of solution information between the three meshes through the appropriate mesh interface is contained in a later section. At present, the cylindrical store mesh is embedded only in the crude mesh which does not allow simulation of wing/body/pylon/store configurations. The cylindrical store mesh may be transformed to a planform oriented mesh using the transformation of Reference 6. This is not imperative and is discussed in more detail in the section reporting the results.

Use of an embedded mesh approach is beneficial for several reasons. Primarily, it eliminates the necessity of having a single continuous grid system to discretize the entire computational domain. That is, coordinate lines are concentrated only in regions where a detailed analysis of the flow field is needed (i.e., regions of high gradients) and mesh points are not "wasted" providing a means of transition from regions of highly concentrated mesh points to sparser regions. Mesh embedding also allows the use of component adaptive meshes or meshes which better represent the surface of the component they surround. In the present study, the cylindrical store mesh is a component adaptive mesh used to improve simulation of the store geometry . In addition, the flow field governing equations can be formulated independently in each mesh system allowing more accurate (more complex) treatment of localized regions of the flow field. Although this feature was not exploited in the present study, it is probable that future research will include utilization of an advanced computational procedure to obtain the store flow field.

The distinctive feature of this method is the use of an additional mesh exclusively for the store. This does, of course, lengthen run times and increase computer storage requirements. However, the advantages of using a cylindrical mesh in terms of configuration simulation more than offset these disadvantages. Most significantly, use of a cylindrical mesh eliminates the need for interpolation at the fin mean surfaces for arbitrary angular fin orientation. Angular coordinate lines can be concentrated near fin positions to allow resolution of gradients normal to the fin surface. In addition, the cylindrical mesh provides a more representative mean surface on which to apply store boundary conditions. Finally, the MSD equation in cylindrical coordinates already contains extra terms describing spanwise (radial) flow. Therefore, only one flow equation is necessary for arbitrary angular orientation of centerline mounted fin. This can be contrasted to the work of Boppe and Stern (Reference 7), where a Cartesian mesh is used and different flow equations are used for wing (x-y plane) and winglet (x-z plane) surfaces.

Governing Equations

The MSD potential equation for transonic flow written in terms of the disturbance velocity potential ϕ is given in conservation form by

$$\left|\left(1-M_\infty^{2}\right)\phi_x - \left(\frac{\gamma+1}{2}\right) M_\infty^{1.75}\,\phi_x^{2} + \underline{\left(1-M_\infty^{2}\right)\phi_y^{2}}\right|_x$$

$$- \underline{\left(1 - \left(\frac{\gamma-1}{2}\right) M_\infty^{2}\right)\left|\phi_y^{2}\right|}_{\,x} + \left|\left(1 - \underline{(\gamma-1)M_\infty^{2}\,\phi_x}\right)\phi_y\right|_y \qquad (1)$$

$$+ \phi_{zz} = 0$$

in the fine and crude meshes. In equation (1), M_∞ is the freestream Mach number, γ is the ratio of specific heats, and x, y, and z denote the axial, spanwise, and vertical Cartesian coordinates. The underlined terms are additions to the classical small disturbance equation which improve resolution of swept shock waves in the x-y plane. Since application of wing and fuselage boundary conditions has been discussed at great length in Reference 5 and Reference 6, no mention of this procedure will be made here except to say that fuselage boundary conditions which have been modified by slender body theory are applied on a prismatic boundary condition support surface (BCSS) in the fine and crude meshes.

Transformation of the MSD equation to cylindrical coordinates is required in the store mesh due to the cylindrical discretization used in this region of the flow field. The formulation used in the store mesh is given by

$$\left|\left(1-M_\infty^2\right)\phi_x - \left(\frac{\gamma+1}{2}\right) M_\infty^{1.75}\phi_x^2 + \underline{\left(1-M_\infty^2\right)\phi_r^2}\right|_x$$

$$- \underline{\left(1-\left(\frac{\gamma-1}{2}\right)M_\infty^2\right)\left|\phi_r^2\right|}_x + \frac{1}{r}\left[\left(1-\underline{(\gamma-1)M_\infty^2\,\phi_x}\right) r\phi_r\right]_r \qquad (2)$$

$$+ \frac{1}{r^2}\phi_{\theta\theta} = 0$$

where x, r, and θ represent the axial, radial, and angular coordinate directions respectively. The underlined terms represent additions to the classical small disturbance equation which improve resolution of swept shockwaves in the x-r plane. The linearized fin and body boundary conditions are given by

$$\frac{1}{r}\phi_\theta = F_x - \alpha\cos\theta + \beta\sin\theta \qquad (3a)$$

and

$$\phi_r = R_x - \alpha\cos\theta - \beta\cos\theta \qquad (3b)$$

respectively, where F_x is the chordwise variation of fin thickness, R_x is the axial variation of body radius, α is the angle of attack, and β is the angle of yaw. It should be noted that equation (3a) and equation (3b) were derived assuming small angles of attack and yaw and that the store body is a body of revolution. The last restriction is not excessive considering the geometry of most current stores.

The MSD equation now must be represented by a finite difference approximation on each of the three meshes. The method of Bailey and Ballhaus (Reference 5) is retained since it represents all aspects of a steady mixed subsonic/supersonic irrotational inviscid flow field. The resulting system of difference equations is solved using a successive-line-over-relaxation (SLOR) algorithm. It should be noted that due to the periodic nature of the store mesh, the matrix generated by the finite difference approximation of equation (2) is periodically tridiagonal. The periodic tridiagonal solver of Steger (Reference 8) is used in the store mesh solution algorithm.

Boundary Conditions

Store body boundary conditions are applied on the surface of a cylinder extending from the upstream to the downstream boundary of the store mesh. This cylinder is denoted as the boundary condition support surface (BCSS). No flow field calculations are performed in the interior of the BCSS. Since the radius of the BCSS is based on an average body radius, the BCSS does not coincide with the body radius at all axial stations as illustrated in Figure 3. It is therefore necessary to modify the body slopes before application on the BCSS. Boppe and Stern (Reference 7) utilize slender body theory to obtain appropriate corrections for both lifting and non-lifting cases. The correction applied to body slopes is based on the equality of source strength and is given by the ratio r_B/r_{BCSS}, where r_B is the true body radius and r_{BCSS} is the radius of the BCSS. The angle of attack correction is based on the equality of doublet strength and is given by the ratio S_B/S_{BCSS}, where S_B is the true body area and S_{BCSS} is the area of the BCSS. Application of the slope and angle of attack corrections to the body boundary condition, equation (3b), yields

$$\phi_r\big|_{BCSS} = \left(\frac{r_B}{r_{BCSS}}\right) R_x - \left(\frac{r_B}{r_{BCSS}}\right)^2 (\alpha\sin\theta + \beta\cos\theta) \tag{4}$$

which is the Neumann boundary condition actually applied on the BCSS. When the solution process is complete, corrections must be applied to the velocities calculated on the computational surface to obtain the true velocities at the body surface. Slender body theory once again provides the necessary correction given by

$$V_B = V_{BCSS} + \left(r_B - r_{BCSS} \right) \frac{d}{dx} \left|\phi_r\big|_{BCSS}\right| \tag{5}$$

where V_B is the true velocity at the body surface and V_{BCSS} is the velocity at the BCSS. Ahead of the body, a zero slope condition is applied on the BCSS. Downstream of the body, equation (4) is used with $R_x = 0$.

The fin upper and lower surface boundary conditions are applied on the appropriate constant θ planes which define the fin surfaces. Since planes of constant θ are concentrated near the angular location of each fin and most fins have small spans, no corrections are applied to the fin boundary conditions. The Kutta condition requirement for each fin is satisfied by applying a jump in potential at each spanwise station on a vortex sheet which extends from the trailing edge of each fin to the downstream boundary. This is analagous to the approach used by the basic wing/body code.

Mesh Interface Boundary Conditions

Information is transmitted between meshes via application of boundary conditions on the various mesh interfaces. In the basic wing/body code, information transmittal occurs at two locations: (1) the outer boundary of the fine mesh and (2) the wing/body surface located in the fine mesh. Dirichlet (potential) boundary conditions interpolated from results of the crude mesh relaxation are applied on the outer boundary of the fine mesh to transmit information about the overall flow field to the fine mesh. Dirichlet boundary conditions interpolated from the results of the fine mesh relaxation are applied on the surface of the wing/body located within the fine mesh to transmit information about the local wing disturbance to the global flow field. Neumann boundary conditions are applied on the portion of the body which extends beyond the fine mesh. In addition, the far field potential based on wing circulation developed by Klunker (Reference 9) is applied on the outer boundaries with the exception of the downstream boundary where a $\phi_x = 0$ condition is applied.

Information transmittal between the store and crude meshes is accomplished in an analagous manner. However, there are two major differences between the procedures: (1) store mesh relaxation results are transmitted to the crude mesh through a rectangular prism enclosing the store denoted as the store flow field support surface (SFFSS) and (2) Dirichlet (potential) or Neumann (velocity) boundary conditions can be applied at each of the store/crude mesh interfaces. Figure 4 illustrates the mesh configuration with the SFFSS included for clarity.

The SFFSS is the surface of a rectangular prism defined in the crude mesh. The SFFSS is initiated upstream of the store and extends to the downstream boundary of the computational domain completely enclosing the store and the associated system of fin vortex sheets. The purpose of the SFFSS is to provide a simple BCSS in the crude mesh on which interpolated results of each store mesh relaxation can be applied as surface boundary conditions for the crude mesh relaxation. Since no crude mesh calculations are performed in the interior of the SFFSS, the store geometry is effectively removed from the crude mesh relaxation allowing arbitrary store orientation within the SFFSS. It is important to note that the front face of the SFFSS is located within store mesh. The location and dimensions of the SFFSS defines the degree of mesh overlap which occurs between the store and crude meshes. Atta (Reference 10) utilized a body fitted coordinate system embedded in a crude Cartesian mesh to discretize the computational domain surrounding a two-dimensional airfoil. The results of Reference 10 show that the degree in which the store and crude meshes overlap determines, in part, the convergence characteristics of the iteration. This topic will be discussed further in the Results section.

Application of Dirichlet boundary conditions on the SFFSS is relatively straightforward. In the case of Neumann boundary conditions, it is necessary to first obtain the velocities relative to the cylindrical store mesh by differencing. These velocities are then interpolated to points on the SFFSS. Finally, the store mesh velocities are transformed to Cartesian velocities and the component normal to the specific SFFSS face is used as a Neumann boundary condition during the upcoming crude mesh relaxation. The boundary conditions, either Dirichlet or Neumann, applied on the SFFSS downstream of the store mesh downstream boundary are obtained by setting $\phi_x = 0$ (Dirichlet) or $\phi_{nx} = 0$ (Neumann) at the downstream boundary of the store mesh and extending the result to the downstream boundary of the computational domain. The SFFSS boundary conditions are updated after each store mesh relaxation.

Boundary conditions applied on the store mesh outer boundary are obtained by interpolation from the results of the crude mesh relaxation. As before, application of Dirichlet boundary conditions is straightforward while application of Neumann boundary conditions is more complex. Cartesian velocities are obtained by differencing the results of the crude mesh relaxation. These Cartesian velocities are then transformed to cylindrical velocities. The Neumann boundary condition applied on the front face of the store mesh is always the velocity component normal to the surface. This is not the case downstream of the store mesh front face. Implementation of a planform oriented mesh transformation of the type described in Reference 6 necessitates application of the velocity component parallel to each ξ line on the store mesh outer boundary as illustrated in Figure 5. If no mesh transformation is performed, the velocity component normal to the outer boundary is used. The boundary conditions applied on the outer boundary of the store mesh are updated after each crude mesh relaxation.

Store Alone Option

The wing/body/store code also has the capability to predict the transonic flow field surrounding an isolated store at small angles of attack and yaw. The store mesh defines the entire computational domain and no other mesh is involved in the solution of the flow field governing equations. The store flow field is obtained in the previous manner with the obvious exception of the boundary conditions applied on the store mesh outer boundary. The boundary conditions applied on the store mesh outer boundary are obtained by a linear superposition of far field potentials representing fin lift and body thickness. The analytic expression for the far field potential due to fin lift is the expression given by Klunker (Reference 9) for a lifting wing modified for cruciform fins of arbitrary angular orientation. The expression for far field potential due to body thickness is given by Krupp and Murman (Reference 11) for an axisymmetric body. The downstream boundary condition is obtained by setting $\phi_x = 0$ at the downstream boundary.

RESULTS

Validation of the isolated store capability was accomplished by direct comparisons between computed results and the experimental data of Stahara and Crissalli (Reference 12) for the Nielsen generic store and Shadow (Reference 13) for the GBU-15. Comparisons with these data allowed an accurate assessment of the validity of the isolated store prediction capability to be made. The F-16/B-61 configuration illustrated in Figure 1 was chosen for evaluation of mesh interface boundary conditions. Unfortunately, it was not possible to make comparisons between results predicted by the wing/body/store code and transonic pressure data due to a lack of experimental data for configurations of this type. Since the store mesh is embedded only in the crude mesh, it was necessary to locate the store so that no mesh overlap occurred between the fine and store meshes. Therefore, it is necessary to locate the store at least one wing chord below the wing/body. No transonic pressure data was found for a wing/body/store configuration of this type.

Comparisons were made only between computed results for the purpose of evaluating the effects of various combinations of boundary conditions applied at the mesh interfaces.

All computations were performed on VAX-11/780 systems. Store alone results were computed on the General Dynamics system requiring 1.5 minutes of CPU time per iteration. All wing/body/store results were computed on the NASA Ames Research Center VAX system requiring 1.87 minutes of CPU time per fine/store/crude iteration. All isolated store solutions presented in the text were stopped after 200 iterations. This represented at least a two order of magnitude decrease from initial values in both the maximum error and residual. Although the values of the error and residual have not been decreased to the defined convergence levels, no significant changes in predicted forces or pressures occur upon continuation of the solution. All computed wing/body/store results are presented at 300 iterations for comparison purposes. It is important to note that these results are also preliminary and not fully converged.

Isolated Store Results

Computation of the Nielsen generic store flow field was performed on a cylindrical store mesh utilizing 118,870 (113 x 30 x 33) points. The mesh outer boundary was located approximately 2 body lengths ahead and behind the store and had a radius of approximately 1 body length. Although these boundaries are located relatively near the body, it was determined that increasing the size of the computational domain beyond these dimensions while maintaining a constant number of radial computational cells had no significant effects on the predicted pressures. Good agreement was obtained between predicted pressures and the experimental data of Reference 12 for the Nielsen generic store at $\alpha = 0^{\circ}$ and $\alpha = 6^{\circ}$ at a freestream Mach number of 0.926 as illustrated in Figure 6. However, it is disheartening to note that the predicted normal force coefficient is significantly lower than the experimental value. In an attempt to alleviate this problem, a far field boundary condition based on body lift was developed by modifying the analytic expression for lifting wings given by Klunker (Reference 9). The total far field potential was obtained by linear superposition of the body lift potential and the far field potential described previously. Application of this outer boundary condition produced no significant change in the computed pressure distributions or forces. In addition, application of a three-dimensional extension of the two-dimensional non-reflecting far field boundary conditions given by Kwak (Reference 14) also produced no significant change in computed pressures or forces. Since implementation of these procedures did not alter the predicted pressures and forces, no additional results are presented. This problem is currently under investigation and implementation of a more accurate formulation of the governing equations in the store mesh is being considered.

Validation of predicted fin pressures proved to be a difficult task primarily due to scarcity of experimental fin pressure data. However, Reference 13 provided sufficient data for comparison with predicted body and fin pressures. Results were computed for the GBU-15 on a cylindrical store mesh utilizing 148,500 (150 x 30 x 33) points. The mesh upstream and downstream boundaries were located approximately 2 body lengths from the store. The outer boundary was located at a radius of 1.5 body lengths from the store.

Good agreement was obtained between predicted pressures and the experimental data of Reference 13 for the GBU-15 at $\alpha = 0^{\circ}$ and a freestream Mach number of 0.8 for both the body and the fins as illustrated by Figure 7 and Figure 8 respectively. Figure 9 and Figure 10 show the good agreement obtained between predicted and experimental results at $\alpha = 6^{\circ}$. Similarly, good agreement was obtained at $\alpha = 0^{\circ}$ and a freestream Mach number of 0.9. Figure 11 shows the good agreement obtained between predicted and experimental body pressures at $\alpha = 6^{\circ}$ and a freestream Mach number of 0.9. However, disagreement between predicted and experimental fin pressures became evident at these conditions as illustrated in Figure 12. It should be noted that all isolated store cases computed to this point did not utilize a planform oriented mesh transformation. In an attempt to improve the fin pressures illustrated in Figure 12, the mesh transformation of Reference 6 was employed. The use of the transformed mesh significantly improved the agreement between predicted and experimental fin pressures as illustrated in Figure 13. However, implementation of the mesh transformation seriously degraded agreement between predicted and experimental body pressures as illustrated in Figure 14. The degradation of body pressures is apparently caused by the deformation of the store mesh outer boundary induced by the mesh transformation. As illustrated in Figure 15, far field boundary conditions applied on the front face of the store mesh are obviously being applied in a region in which they are invalid. The overall agreement with experimental data is decreased by use of the planform mesh transformation of Reference 6. It will be necessary to develop a transformation scheme which does not adversely affect the far field mesh boundaries before improved results can be obtained for both the store and fins.

The normal force coefficients predicted for the GBU-15 were also significantly lower than experimental values. The disagreement was not as severe as with the Nielsen store since the GBU-15 fins produce approximately one-half of the normal force coefficient. However, it is important to note that although the predicted force coefficients are not in agreement with experimental values, the general pressure distributions are very encouraging and continued refinement of the method is expected to improve force predictions.

Wing/Body/Store Results

All F-16/B-61 flow fields were computed at $\alpha_{wb} = \alpha_{s} = 5^{\circ}$ and a freestream Mach number of 0.8. Solutions were also obtained for an isolated F-16 and an isolated B-61 at the same flight conditions to provide data for validation of wing/body/store code predictions. Use of predicted isolated store results for verification of the wing/body/store code was feasible because interference effects were expected to be minimal due to the distance separating the aircraft and the store. Comparisons were performed between predicted results in lieu of a direct correlation with experiemental data due to the previously mentioned shortage of transonic pressure data for configurations of this type. All computations were performed on a fine mesh of 37,800 (63 x 3 x 20) points, a store mesh of 61,248 (64 x 29 x 33) points and a global crude mesh of 10,800 (30 x 18 x 20) points. The number of field points utilized in the store mesh was decreased significantly from the number of points used for analysis of the GBU-15 and Nielsen store configurations. The additional field points utilized in the prior computations were required to perform the detailed analysis necessary for correlation of predicted pressures with experiemental data. Since a detailed analysis of the store flow field was not required for evaluation of the mesh interface boundary conditions, the number of field points utilized in the store mesh was decreased and the accuracy of the store mesh solution degraded somewhat. Isolated F-16 and B-61 solutions were obtained using the meshes described above.

Initially, F-16/B-61 flow field solutions were diverging regardless of the type of boundary conditions applied at the mesh interfaces. The cause of this divergence was determined to be an improper mesh overlap arrangement. The crude mesh had been generated such that the axial cross-section of the SFFSS was a nine-celled square with sides 0.20 body lengths centered about the store mesh longitudinal acts. The SFFSS was initiated 0.25 body lengths upstream of the store. No particular attention had been given to the degree of store/crude mesh overlap during generation of the mesh configuration.

Atta (Reference 10) reported the significance of the degree of mesh overlap on accuracy and convergence characteristics for a two-dimensional embedded mesh configuration. According to Atta, improper arrangement of mesh overlap regions can produce inaccuracy in the solution and decrease rate of convergence. In an attempt to stabilize the F-16/B-61 solution, a second store/crude mesh configuration was generated by extending the optimum two-dimensional mesh overlap criteria of Atta to three-dimensions. The store and crude meshes were generated such that the axial cross-section of the SFFSS was a nine-celled square with sides of 0.5 body lengths centered about the store mesh longitudinal axis. The SFFSS was initiated 0.25 body lengths upstream of the store. The maximum and minimum mesh overlaps were 15% and 25% of the radius of the store mesh outer boundary. Since the three-dimensional mesh overlap criteria were developed by extension of the two-dimensional criteria of Atta, the mesh overlap criteria used here may not represent a three-dimensional optimum. Therefore, further study is necessary to determine the true optimum three-dimensional mesh overlap criteria.

F-16/B-61 results were computed for all possible combinations of mesh interface boundary conditions utilizing the store/crude mesh configuration which satisfies the three-dimensional mesh overlap criteria. Figure 16 shows the relatively good agreement between B-61 fin pressures predicted at two span stations by the wing/body/store and isolated store procedures. This solution was obtained utilizing Dirichlet boundary conditions applied on both the store mesh outer boundary and the SFFSS. This combination of mesh interface boundary conditions is denoted as the Dirichlet/Dirichlet condition (type of boundary condition applied on store mesh outer boundary/type of boundary condition applied on SFFSS). This notation is used hereafter. Good agreement was also obtained for the Neumann/Neumann condition as illustrated in Figure 17. It is interesting to note that when mesh interface boundary conditions were mixed, Dirichlet/Neumann or Neumann/Dirichlet, significant deviation from isolated store results occurred. Figure 18 shows a significant disagreement between pressures predicted at two span stations by the isolated store code and wing/body/store code with the Dirichlet/Neumann condition enforced. In addition, utilization of the Neumann/Dirichlet condition produced a divergent solution after only 80 fine/store/crude iterations. Although experimental pressure data is necessary for a more complete evaluation, it appears that the pressures predicted using the Dirichlet/Neumann condition, shown in Figure 18, are the least promising of the F-16/B-61 results since it was not anticipated that the interference of the parent vehicle would significantly alter the store pressure distributions. Since the influence of the store on the aircraft was negligible, no F-16 results are presented.

Unfortunately, no definite convergence characteristics could be determined from results presented in this paper. All solutions were stopped at 300 iterations for comparison purposes. The only trend which could be ascertained from these results was that the Dirichlet/Dirichlet condition decreased the error and residual more rapidly than the other combinations of mesh interface boundary conditions. These results are only preliminary and a more thorough evaluation of mesh interface boundary conditions will be performed in the next phase of this study utilizing a wing/body/store configuration with the store located within the wing/body fine mesh. Simulation of the complex interference effects associated with a configuration of this type will necessitate use of the optimum mesh interface boundary conditions.

CONCLUDING REMARKS

A numerical method is being developed utilizing potential flow and small disturbance theories for prediction of transonic wing/body/store flow fields. The code also has the capability to predict isolated store flow fields. Use of a mesh embedding scheme to include the store in the wing/body flow field allows simulation of relatively complex store geometries. At arbitrary angular orientation. Good agreement is obtained between predicted fin and body pressures and experimental data for results computed by the isolated store procedure. However, satisfactory agreement has not yet been obtained between predicted forces and experimental data. Direct correlation of results predicted by the wing/body/store code and transonic pressure data is not possible due to a lack of experimental data for configurations of this type. Computed results seem to indicate store mesh outer boundary and the SFFSS should be of the same type (i.e., Dirichlet/Dirichlet; Neumann/Neumann). This result does need to be verified by comparison with experimental pressure data. In addition, the degree of mesh overlap also plays an important role in the convergence of the iteration. It is anticipated that further development and refinement of these procedures will produce a code capable of predicting the flow fields of realistic wing/body/store configurations.

REFERENCES

1. Stahara, S. S., "Study of Transonic Flow Fields About Aircraft: Application to External Stores," AGARD Conference on Subsonic/Transonic Configuration Aerodynamics, CP 285, Paper 8, May 1980, Munich Neubiberg, Germany.

2. Deslandes, R., "Evaluation of Aircraft Interference Effects on External Stores at Subsonic and Transonic Speeds," AGARD Conference on Subsonic/Transonic Configuration Aerodynamics, CP 285, Paper 6, May 1980, Munich Neubiberg, Germany.

3. Waskiewicz, J. D., DeJongh, J., and Cenko, A., "Application of Panel Methods to the Aerodynamic Analysis of Proximity and Mutual Interference Effects on Store Separation at Supersonic Speeds," AIAA-81-1653 presented at the Aircraft Systems and Technology Conference, August 1981.

4. Shankar, V. and Malmuth, N.D., "Computational and Simplified Analytical Treatment of Transonic Wing-Fuselage-Pylon-Store Interactions," AIAA-80-0127 presented at the 18th Aerospace Sciences Meeting, January 1980.

5. Ballhaus, W. F., Bailey, F. R., and Frick, J., "Improved Computational Treatment of Transonic Flow About Swept Wings," Advances in Engineering Sciences, NASA CP-2001, 1976.

6. Mason, W. H., MacKenzie, D. A., Stern, M. A., Ballhaus, W. F., and Frick, J., An Automated Procedure for Computing the Three Dimensional Transonic Flow Over Wing/Body Combinations, Including Viscous Effects, Volume I, Air Force Flight Dynamics Laboratory, TR-77-122, October 1977.

7. Boppe, C. W., and Stern, M. A., "Simulated Transonic Flows For Aircraft with Nacelles, Pylons, and Winglets," AIAA-80-0130 presented at the 18th Aerospace Sciences Meeting, January 1980.

8. Steger, J. L., "Implicit Finite Difference Simulation of Flow About Arbitrary Geometries With Application to Airfoils," AIAA-77-665 presented at the 10th Fluid and Plasmadynamics Conference, June 1977.

9. Klunker, E. B., "Contribution to Methods for Calculating the Flow About Thin Lifting Wings at Transonic Speeds - Analytic Expressions for the Far Field," NASA TN D-6530.

10. Atta, E., "Component-Adaptive Grid Interfacing," AIAA-81-0382 presented at the 19th Aerospace Sciences Meeting, January 1981.

11. Krupp, J. A., and Murman, E. M., "The Numerical Calculation of Steady Transonic Flows Past Thin Lifting Airfoils and Slender Bodies," AIAA-71-566 presented at the 4th Fluid and Plasmadynamics Conference, June 1971.

12. Stahara, S. S. and Crisalli, A. J., Data Report for a Test Program to Study Transonic Flow Fields About Wing-Body/Pylon/Store Combinations, Volumes I - III, AFSOR-TR-79-1070 to 1072, January 1978.

REFERENCES (Continued)

13. Shadow, T. O., Wind Tunnel Tests to Determine the Distributed Loads on a 0.25-Scale GBU-15 (CWW) Model at Transonic Mach Numbers, AEDC-TSR-80-P14, February 1980.

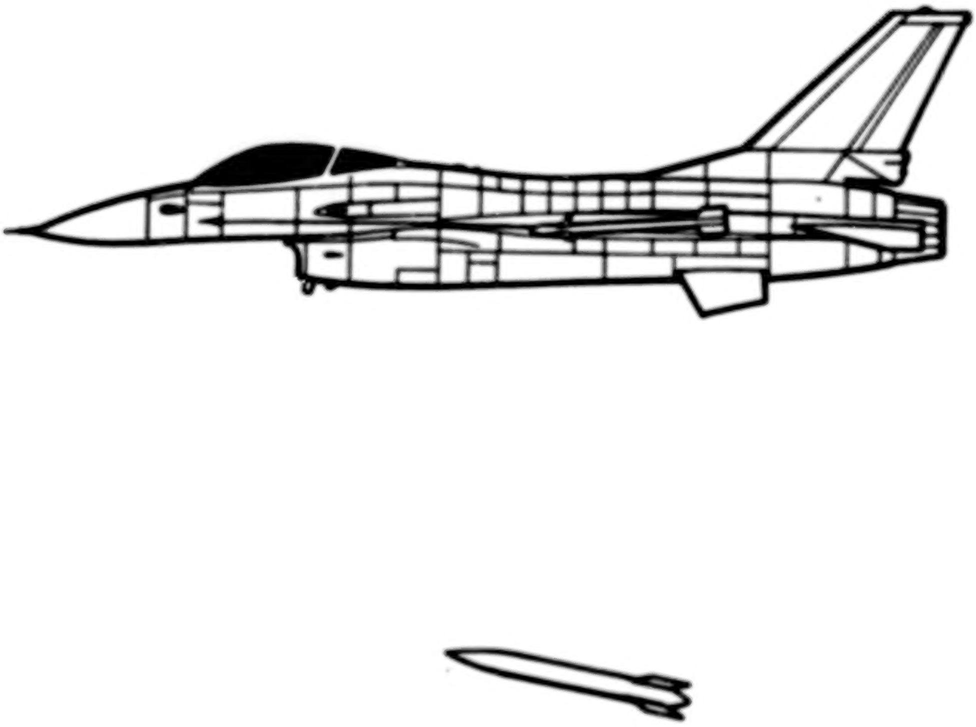

Figure 1.- Analysis of the flow field due to an aircraft with a separated store was accomplished during this study.

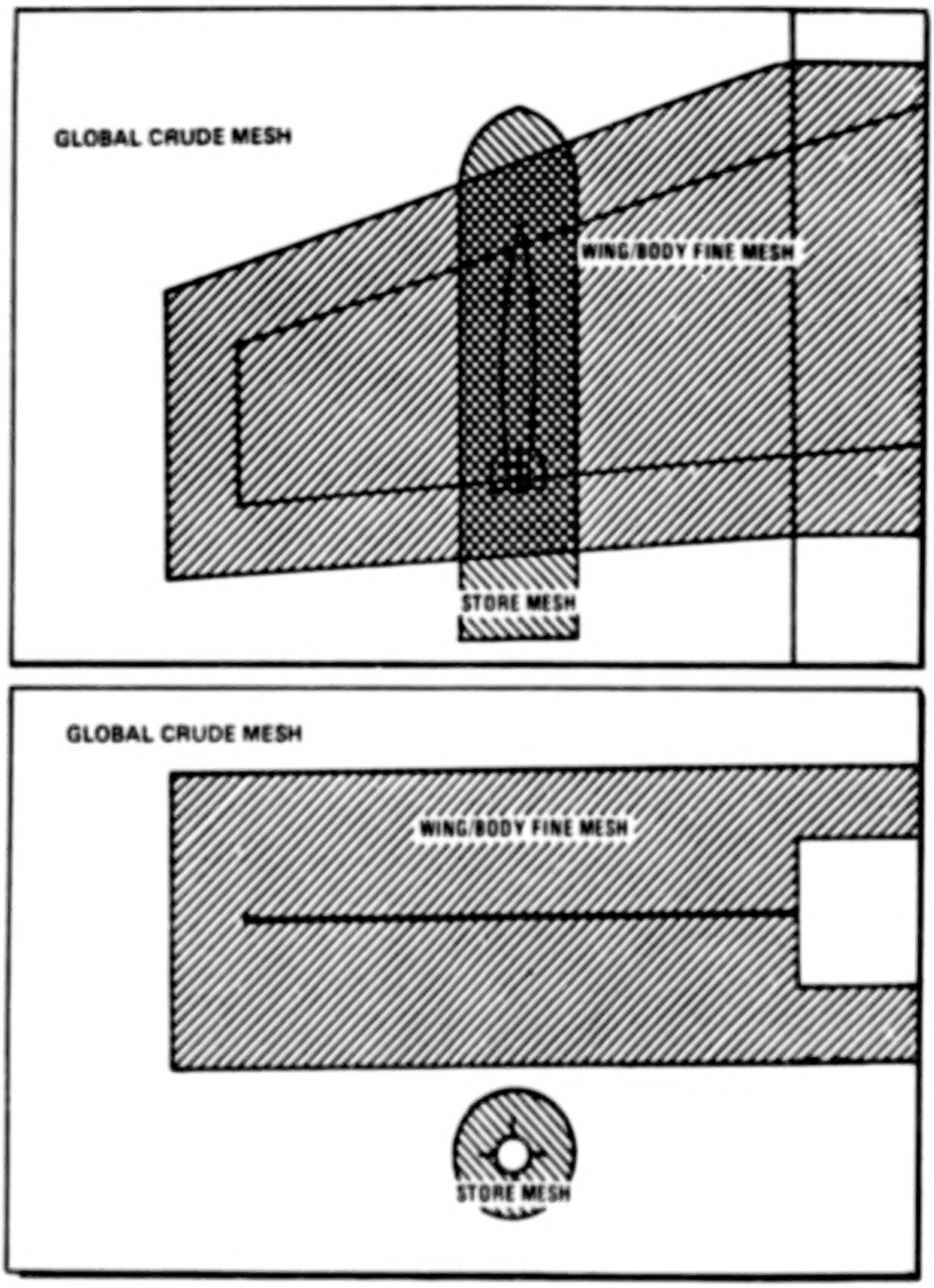
GLOBAL CRUDE MESH
WING/BODY FINE MESH
STORE MESH
GLOBAL CRUDE MESH
WING/BODY FINE MESH
STORE MESH

Figure 2.- Wing/body/store flow field is discretized by three mesh systems.

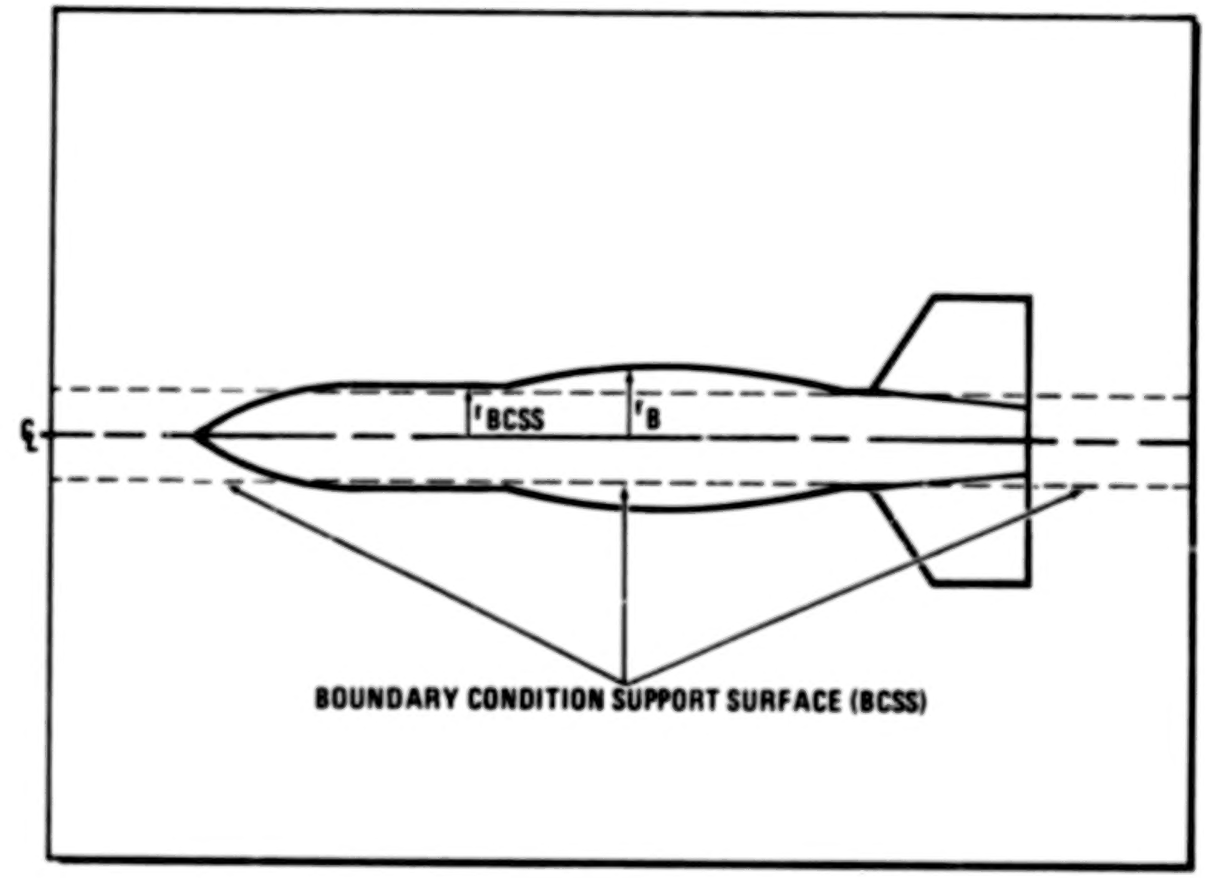
℄
r_{BCSS}
r_B
BOUNDARY CONDITION SUPPORT SURFACE (BCSS)

Figure 3.- Boundary condition support surface (BCSS) does not coincide with the body surface at all axial stations.

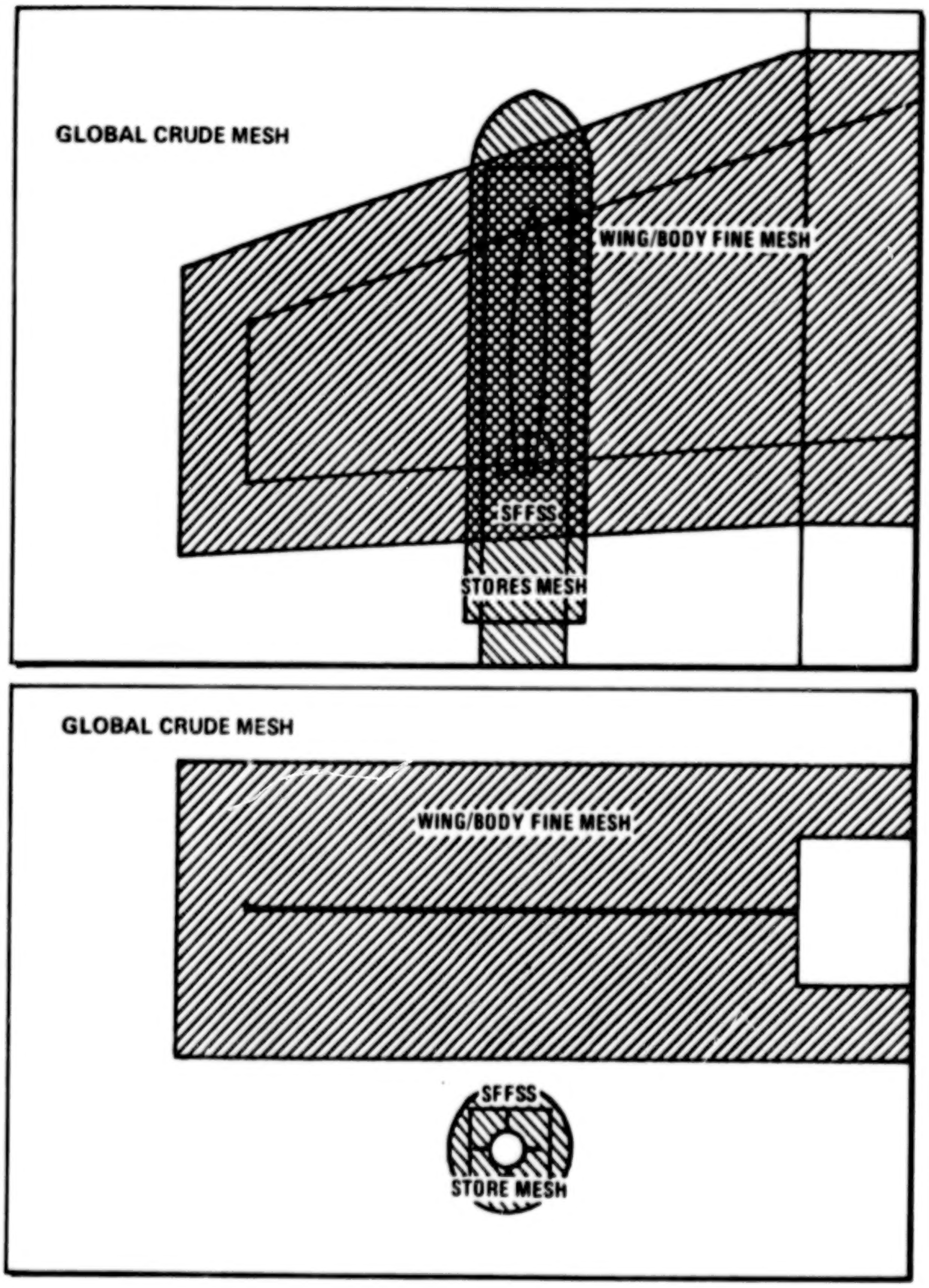
GLOBAL CRUDE MESH
WING/BODY FINE MESH
SFFSS
STORES MESH
GLOBAL CRUDE MESH
WING/BODY FINE MESH
SFFSS
STORE MESH

Figure 4.- Results of the store mesh relaxation are transmitted to the global flow field through the store flow field support surface (SFFSS).

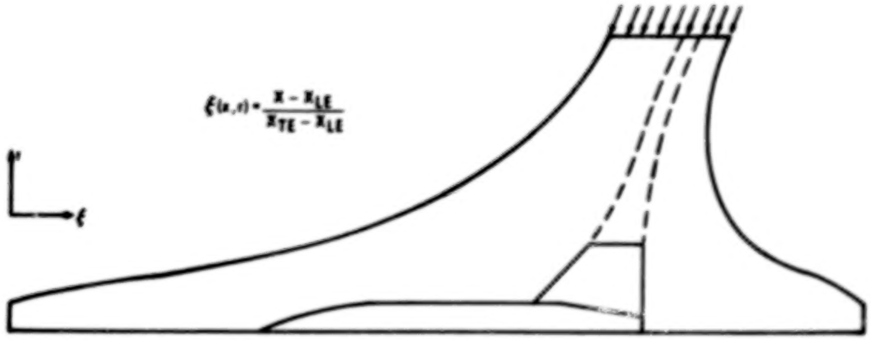

Figure 5.- Velocity component parallel to ξ lines is Neumann boundary condition applied on outer boundary of store mesh downstream of front face.

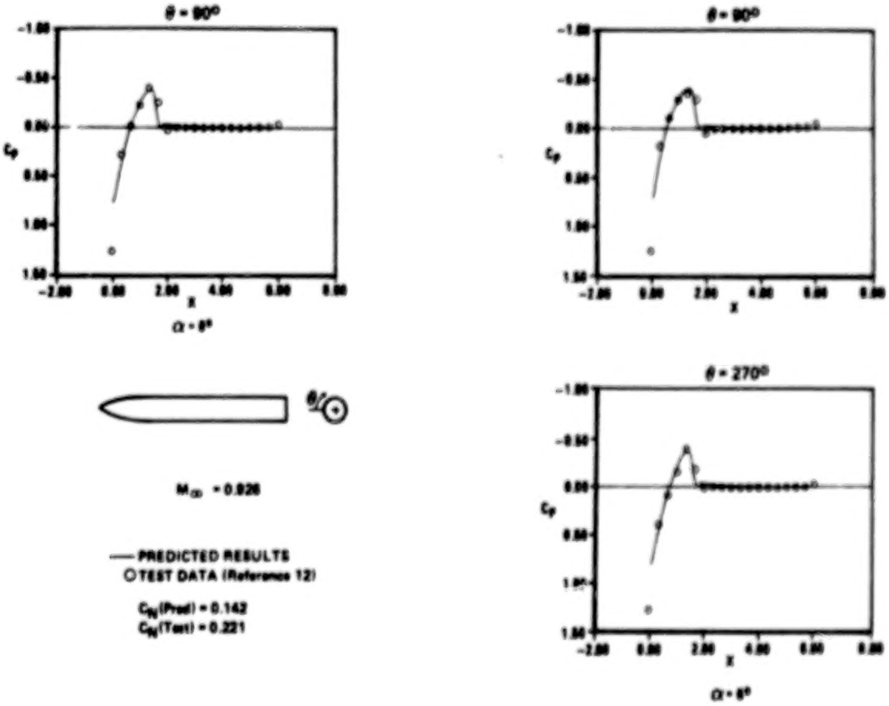

Figure 6.- Predicted pressures show good agreement with Nielsen test data.

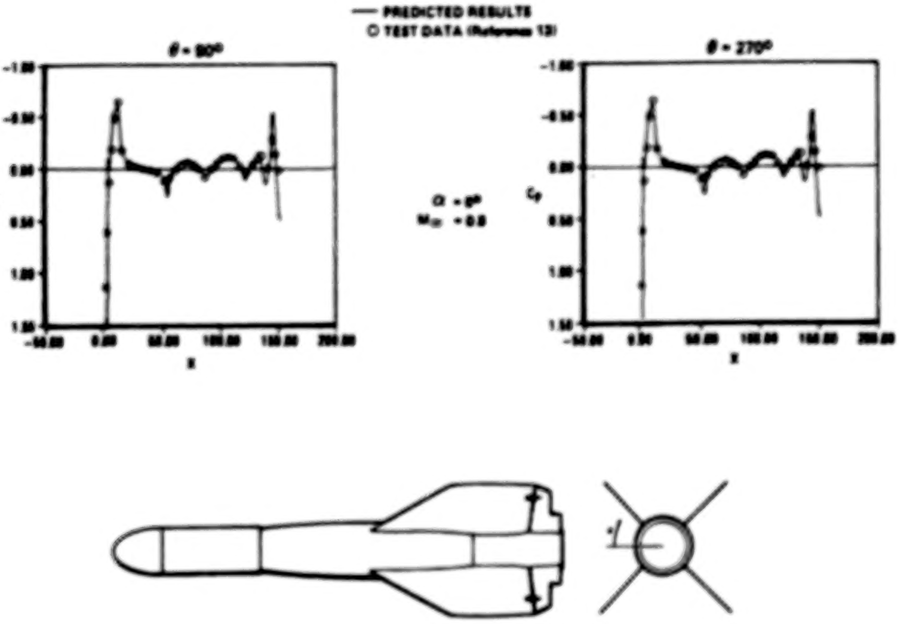

Figure 7.- Predicted GBU-15 body pressures show good agreement with test data at $\alpha = 0^\circ$ and $M_\infty = 0.8$.

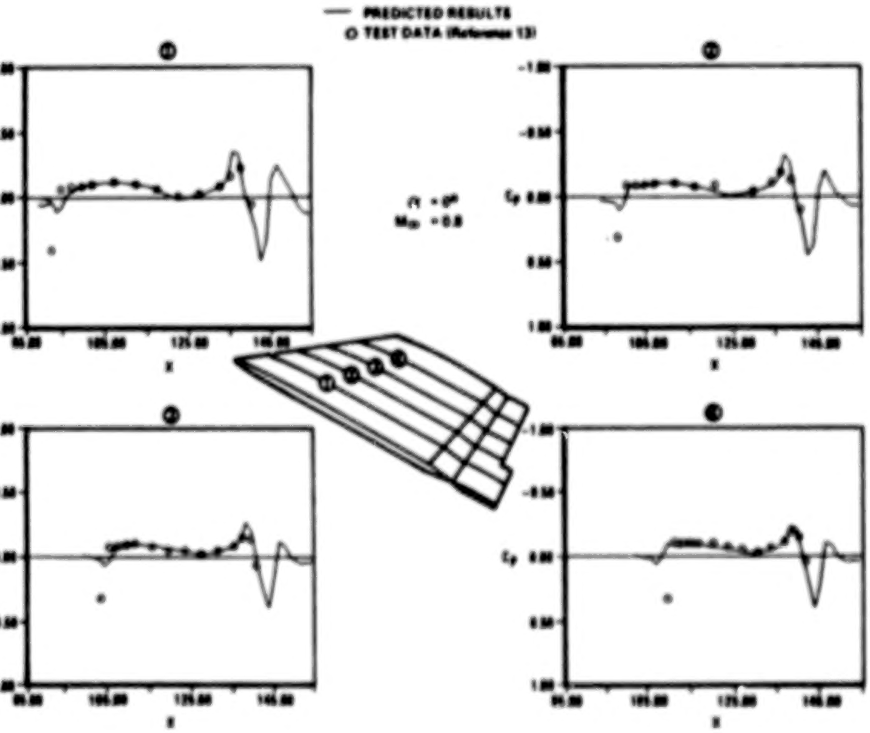

Figure 8.- Predicted GBU-15 fin pressures show good agreement with test data at $\alpha = 0^\circ$ and $M_\infty = 0.8$.

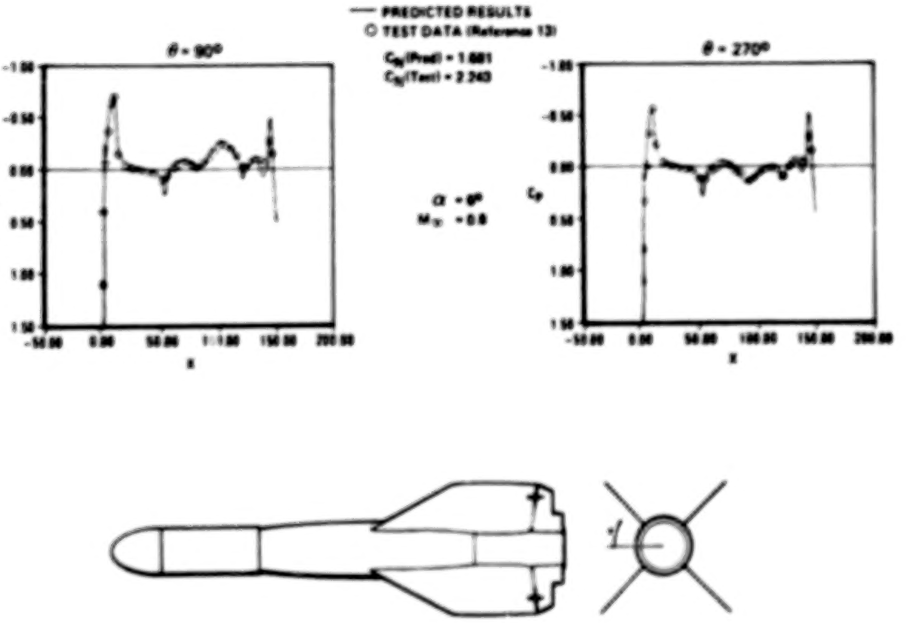

Figure 9.- Predicted GBU-15 body pressures show good agreement with test data at $\alpha = 6^\circ$ and $M_\infty = 0.8$.

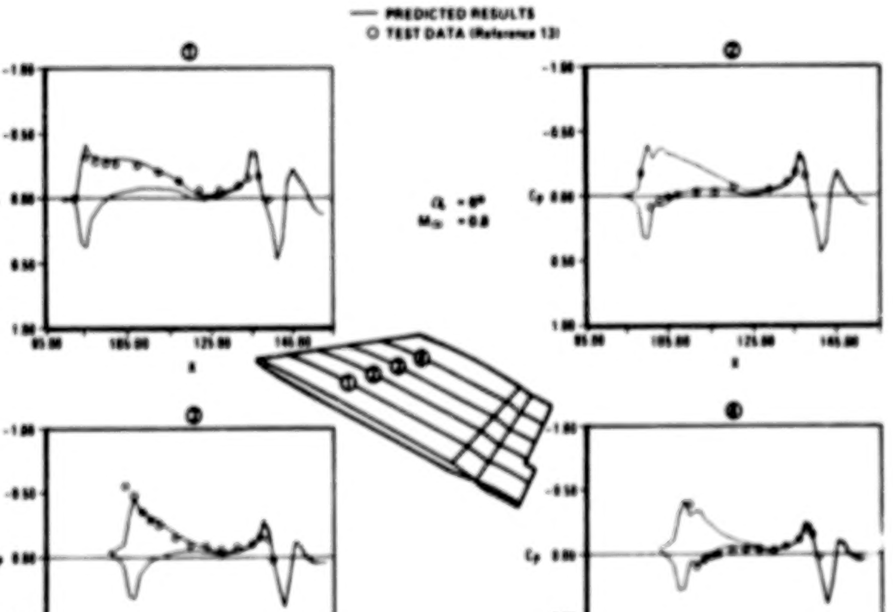

Figure 10.- Predicted GBU-15 fin pressures show good agreement with test data at $\alpha = 6^\circ$ and $M_\infty = 0.8$.

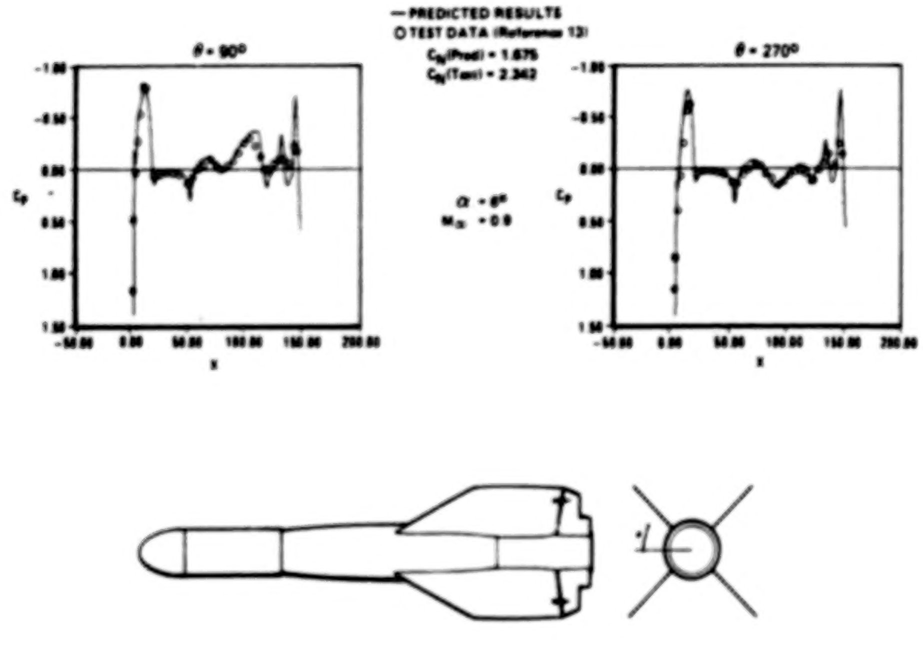

Figure 11.- Predicted GBU-15 body pressures show good agreement with test data at $\alpha = 6^\circ$ and $M_\infty = 0.9$.

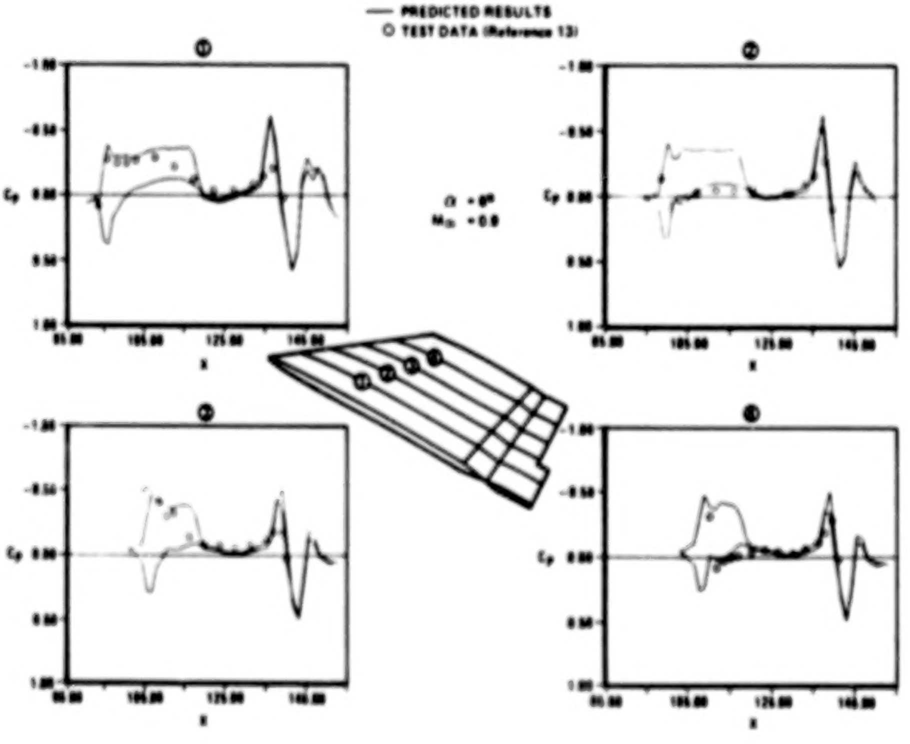

Figure 12.- Agreement between GBU-15 fin pressures and test data is degraded at $\alpha = 6^\circ$ and $M_\infty = 0.9$.

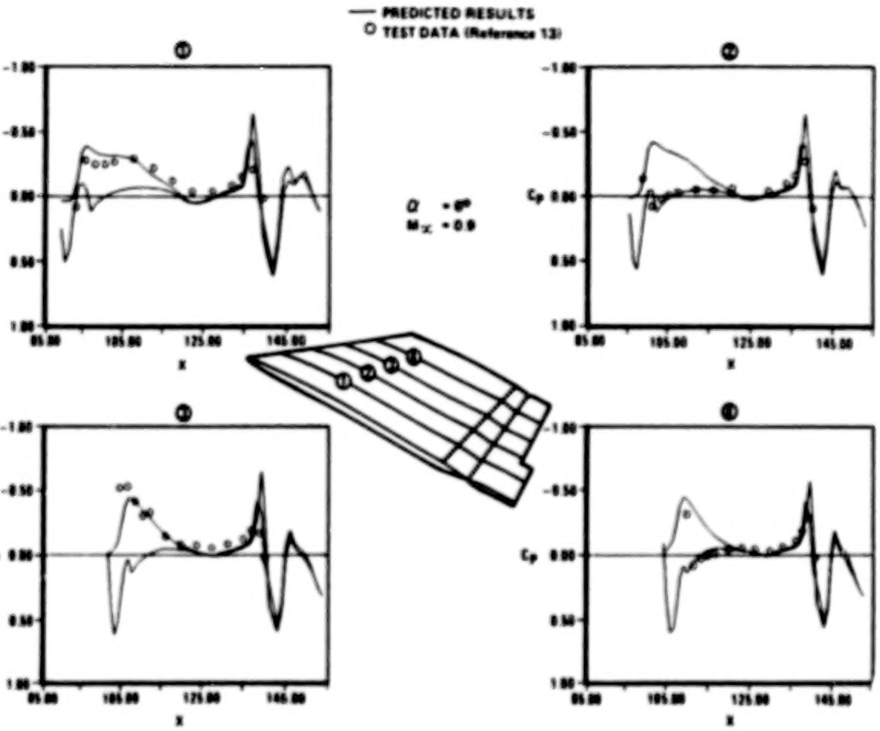

Figure 13.- Use of a planform oriented mesh transformation improves agreement between predicted GBU-15 fin pressures and test data at $\alpha = 6^\circ$ and $M_\infty = 0.9$.

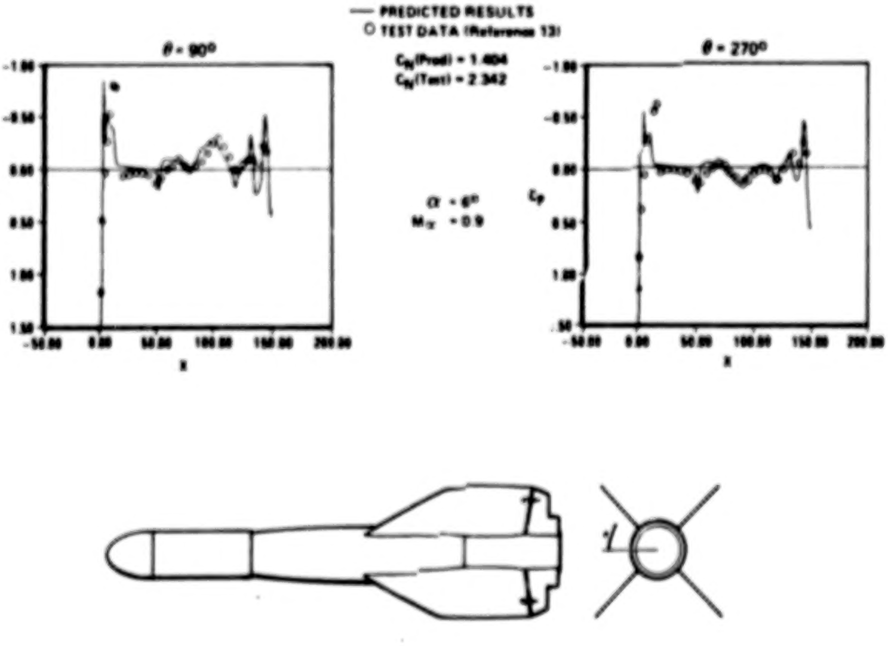

Figure 14.- Agreement between predicted GBU-15 body pressures and test data is significantly degraded when a planform oriented mesh transformation is used.

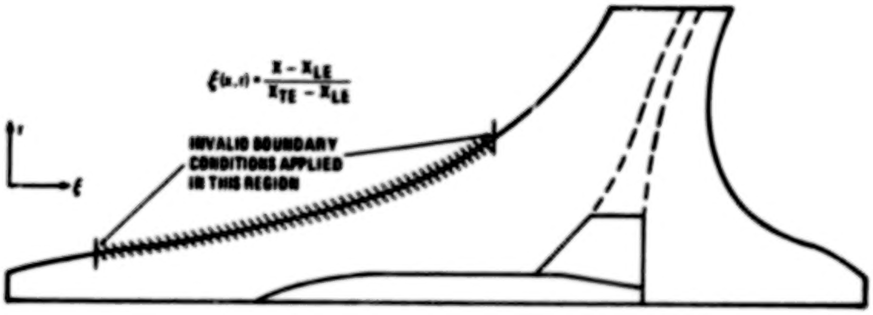
$\xi(x,r) = \frac{X - X_{LE}}{X_{TE} - X_{LE}}$
r
ξ
INVALID BOUNDARY CONDITIONS APPLIED IN THIS REGION

Figure 15.- Distortion of planform oriented mesh forces invalid application of farfield boundary conditions on front face of store mesh.

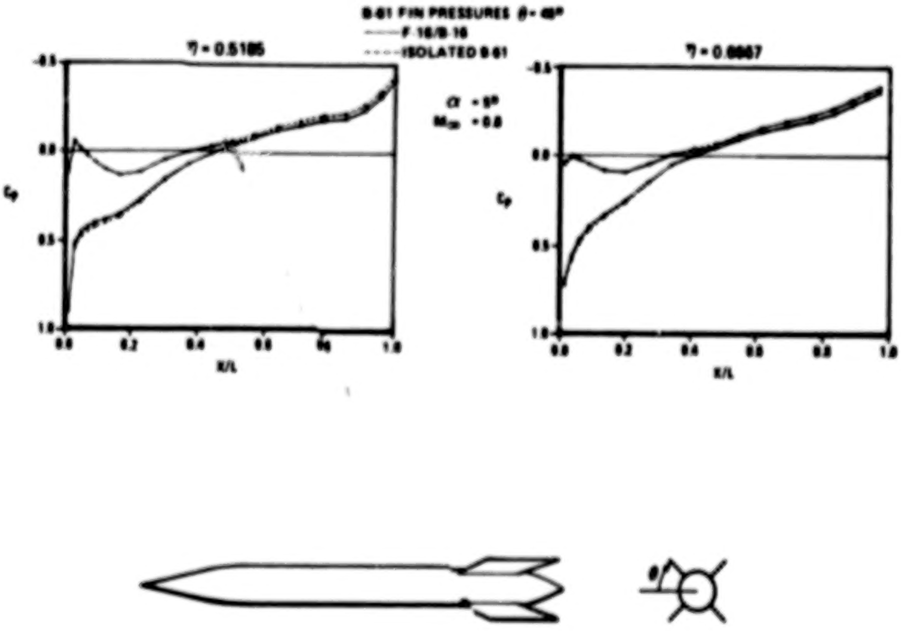

Figure 16.- B-61 fin pressures predicted by wing/body/store code utilizing Dirichlet/Dirichlet condition show good agreement with isolated store results.

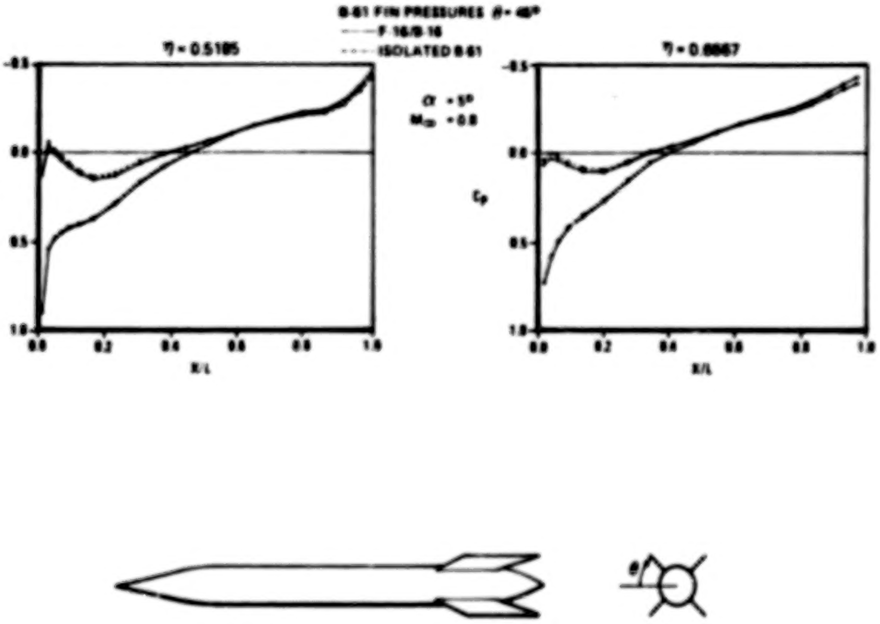

Figure 17.- B-61 fin pressures predicted by wing/body/store code utilizing Neumann/Neumann condition show good agreement with isolated store results.

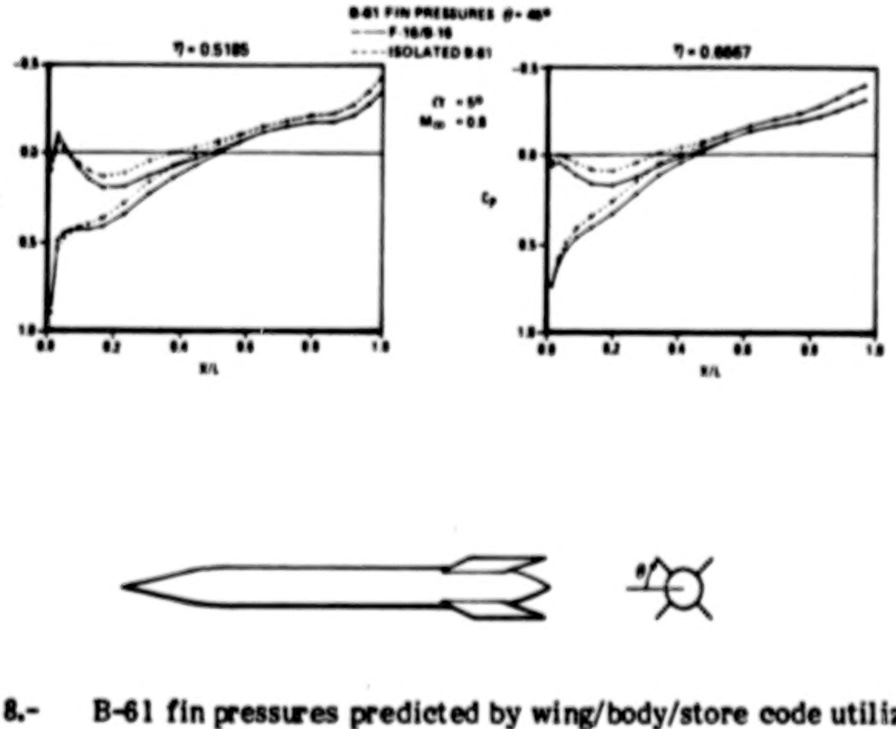

Figure 18.- B-61 fin pressures predicted by wing/body/store code utilizing Dirichlet/Neumann condition deviate from isolated store results.

CONFEREES AT NUMERICAL BOUNDARY CONDITION PROCEDURES AND MULTIGRID METHODS SYMPOSIA

October 19-22, 1981

NASA Ames Research Center, Moffett Field, CA 94035

ABARBANEL, Saul
(Visiting from Tel-Aviv University)
Massachusetts Institute of Technology
Room 33-208
Cambridge, MA 02139
Title: Professor

ABBETT, Michael
Acurex Corporation
485 Clyde Ave., MS 8-8800
Mountain View, CA
Title: Principal Scientist

ABLOW, C. M.
Stanford Research Institute International
Menlo Park, CA 94025
(415) 859-3954
Title: Staff Scientist

AGGARWAL, Hans R.
NASA, Ames Research Center
MS 227-8
Moffett Field, CA 94035
(415) 965-5862
Title: Research Scientist

ALMOSNINO, Dan
NASA, Ames Research Center
Moffett Field, CA 94035
(415) 965-6272
Title: NRC Research Associate

ANDERSON, Chris
University of California Berkeley
& L. B. L.
Mathematics Department
Berkeley, CA 94720
(415) 524-9120 or 486-4851
Title: Graduate Student

ANDERSON, David V.
Lawrence Livermore National Laboratory
L-561, P.O. Box 5509
Livermore, CA 94550
(415) 422-9818
Title: Plasma Physicist

ANDOU, Yasunori
Heat and Fluid Dynamics Department
Research Institute
Ishikawajima-Harima Heavy
Industries Co., Ltd.
1 Shinnakahara, Isogo-Ku
Yokohama 235, JAPAN
Title: Research Engineer

ANDREWS, Alison
NASA, Ames Research Center
MS 202A-14
Moffett Field, CA 94035
(415) 965-6415
Title: Research Scientist

ATTA, Essam
Lockheed Georgia Company
Dept. 72/74, Zone 403
Marietta, GA 30063
(404) 424-2587
Title: Scientist

BAILEY, Harry
NASA, Ames Research Center
MS 202A-1
Moffett Field, CA 94035
(415) 965-5548
Title: Research Scientist

BALAKRISHNAN, A.
NASA, Ames Research Center
MS 229-4
Moffett Field, CA 94035
(415) 965-6198
Title: Research Scientist

BALLHAUS, William F.
NASA, Ames Research Center
MS 200-4
Moffett Field, CA 94035
(415) 965-5065
Title: Director of Astronautics

BARNETT, Mark
University of Cincinnati
Dept. of Aero. Engr. and Appl. Mech.
Rhodes Hall, Mail Drop #70
Cincinnati, OH 45221
(513) 475-6619
Title: Graduate Research Assistant

BARR, P. K.
Sandia National Laboratories
P.O. Box 969
Livermore, CA 94550
(415) 422-2249
Title: Tech. Staff, Thermofluids Div.

BARTON, John
NASA, Ames Research Center
MS 202A-1
Moffett Field, CA 94035
(415) 965-6667
Title: Research Scientist

BATCHELDER, Richard A.
McDonnell Douglas Astronautics Co.
5301 Bolsa Ave.
A03-203-AATA Station 13-3
Huntington Beach, CA 92647
(714) 896-5266
Title: Senior Engineer/Scientist

BAYLISS, Alvin
Courant Institute of Mathematical
Sciences
251 Mercer St.,
New York, NY 10012
(212) 460-7459
Title: Research Scientist

BEAM, R. M.
NASA, Ames Research Center
MS 202A-1
Moffett Field, CA 94035
(415) 965-5895
Title: Research Scientist

BECK, Robin A. S.
Acurex Corporation
485 Clyde Avenue
Mountain View, CA
(415) 964-3200
Title: Staff Engineer

BECKETT, P. M.
Hull University
Department of Applied Mathematics
Hull, ENGLAND
(0482) 46311
Title:

BELL, John B.
Naval Surface Weapons Center
Code R44, Naval Surface Weapons Center
White Oak, MD 20910
(202) 394-1136
Title: Research Mathematician

BENEK, J. A.
CALSPAN Field Services
AEDC Division
Arnold Air Force Station, TN 37388
(615) 455-2611, Ext. 7588
Title:

BERGER, Marsha
Stanford University
Computational Science Department
Stanford, CA 94305
(415) 497-4101
Title:

BERGER, M. H.
Union Carbide Corporation
Nuclear Division
P.O. Box P
Oakridge, TN
FTS 624-7955
Title: Engineer

BLOTTNER, Frederick G.
Sandia National Laboratories
P.O. Box 5800
Albuquerque, NM 87185
(505) 844-8549
Title: Staff Member

BOBER, Lawrence J.
NASA, Lewis Research Center
2100 Brookpark Road
Cleveland, OH 44070
(216) 433-4000, Ext. 5520
Title: Aerospace Engineer

BOERSTOEL, Dr. Ir. J. W.
National Aerospace Laboratory
Amsterdam, THE NETHERLANDS
(020) 5113113
Title: Senior Research Scientist

BOLSTAD, John
Lawrence Berkeley Laboratory
50A2129
Berkeley, CA 94720
FTS 451-6006
Title: Staff Scientist

BORLAND, Christopher
Boeing Military Airplane Company
MS 41-10, P.O. Box 3707
Seattle, WA 98124
(206) 655-5240
Title: Principal Engineer

BRANDEIS, Julius
Lawrence Livermore National Laboratory
P.O. Box 808, L-451
Livermore, CA 94550
(415) 423-0152
Title: Physicist

BRIDGEMAN, John
NASA, Ames Research Center
MS 202A-14
Moffett Field, CA 94035
(415) 965-6415
Title: Research Scientist

BROWN, Jeffrey J.
Boeing Commercial Airplane Company
P.O. Box 3707
Seattle, WA 98124
(206) 237-2519
Title: Senior Specialist Engineer

BUBE, Kenneth P.
University of California Los Angeles
Department of Mathematics
Los Angeles, CA 90024
(213) 825-4314
Title: Assistant Professor

BUNING, Peter
NASA, Ames Research Center
MS 202A-1
Moffett Field, CA 94035
(415) 965-5194
Title: Research Scientist

BUSH, Robert H.
Massachusetts Institute of Technology
Room 37-375
Cambridge, MA 02139
(617) 253-4923
Title:

CARMICHAEL, Ralph
NASA, Ames Research Center
MS 227-2
Moffett Field, CA 94035
(415) 965-6216
Title: Aerospace Engineer

CAUGHEY, David A.
Cornell/Princeton University
D307B E. Quad.
Princeton, New Jersey 08544
(609) 252-5205
Title:

CHAN, Stevens T.
Lawrence Livermore National Laboratory
L-262, P.O. Box 808
Livermore, CA 94550
(415) 422-1822
Title: Physicist

CHANG, I-Chung
NASA, Ames Research Center
MS 227-8
Moffett Field, CA 94035
(415) 965-5656
Title: NRC Research Associate

CHANG, S. S.
Lockheed Missiles & Space Co., Inc.
Dept. 81-11, Bldg. 154
P.O. Box 504
Sunnyvale, CA 94086
(408) 742-2903
Title: Research Specialist

CHAPMAN, G. T.
NASA, Ames Research Center
MS 202A-1
Moffett Field, CA 94035
(415) 965-5654
Title: Senior Staff Scientist

CHAUSSEE, Denny
NASA, Ames Research Center
MS 202A-14
Moffett Field, CA 94035
(415) 965-6415
Title: Research Scientist

CHEN, Hai-chow
Boeing Company
P.O. Box 3707, MS 3N-19
Seattle, WA 98124
(206) 773-8166
Title: Sr. Specialist Engineer

CHEN, Lee T.
McDonnell Douglas Corporation
P.O. Box 516
St. Louis, MO 63141
Title: Research Scientist

CHENG, H. K.
University of Southern California
Department of Aerospace Engineering
Los Angeles, CA
(213) 743-6204
Title: Professor

CHIBA, Zoher
Acurex Corporation
Aerotherm Division
485 Clyde Ave.
Mountain View, CA
(415) 964-3200, Ext. 3127
Title: Staff Engineer

CHILDS, Robert
NASA, Ames Research Center
MS 202A-1
Moffett Field, CA 94035
(415) 965-5361
Title: NRC Research Associate

CHIMA, Rod
NASA, Lewis Research Center
21000 Brookpark Road
Cleveland, OH 44135
Title:

CHIN, Jin H.
Lockheed Missiles & Space Co., Inc.
Dept. 81-11, Bldg. 154
P.O. Box 504
Sunnyvale, CA 94086
(408) 743-2307
Title: Senior Staff Engineer

CHIN, Ray
Lawrence Livermore National Laboratory
Livermore, CA
(415) 422-1284
Title: Physicist

CHOW, Leslie
NASA, Ames Research Center
MS 202A-14
Moffett Field, CA 94035
(415) 965-6415
Title: Research Scientist

CHRUSCIEL, G. T.
Lockheed Missiles & Space Co., Inc.
Dept. 81-11, Bldg. 154
P.O. Box 504
Sunnyvale, CA 94086
(408) 742-5254
Title: Staff Engineer

CHYU, Gil
NASA, Ames Research Center
MS 227-8
Moffett Field, CA 94035
(415) 965-6116
Title: Aerospace Engineer

CLARK, Roger W.
McDonnell Douglas Aircraft Co.
Lakewood Blvd.
Long Beach, CA 90846
(213) 593-6681
Title:

CLINE, Michael C.
Los Alamos National Laboratory
MS-216
Los Alamos, NM 87545
(505) 667-4156
Title:

COAKLEY, T.
NASA, Ames Research Center
MS 229-1
Moffett Field, CA 94035
(415) 965-6200
Title: Research Scientist

COLE, James K.
Sandia Laboratory
P.O. Box 5800
Albuquerque, NM 87185
(505) 887-7506
Title: Division Supervisor

CONCUS, Paul
Lawrence Berkeley Laboratory
Berkeley, CA 94720
(415) 486-5508
Title: Professor

CONTI, Raul
Lockheed Palo Alto Research Laboratory
3251 Hanover Street
Palo Alto, CA 94306
(415) 858-4036
Title: Sr. Staff Scientist

COUGHRAN, Bill
Bell Laboratories
Room 2C-273,
500 Mountain Ave.
Murray Hill, NJ 07974
Title:

COX, Ronald A.
General Dynamics
P.O. Box 748, MZ 2882
Ft. Worth, TX 76101
(817) 732-4811, Ext. 4418
Title: Aerodynamics Engineer

CRISPIN, Yechiel
NASA, Ames Research Center
MS 227-8
Moffett Field, CA 94035
(415) 965-5655
Title: NRC Research Associate

DAVY, W.
NASA, Ames Research Center
MS 229-4
Moffett Field, CA 94035
(415) 965-6198
Title: Research Scientist

DECONINCK, Herman
Department of Fluid Mechanics
Vrije Universiteit
Pleinlaan 2,
1050 Brussels, BELGIUM
Title: Research Assistant

DEIWERT, George
NASA, Ames Research Center
MS 202A-1
Moffett Field, CA 94035
(415) 965-5894
Title: Research Scientist

DENDY, Joel E.
Los Alamos National Laboratory
MS 610
Los Alamos, NM 87545
(505) 662-5772
Title:

DESIDERI, J. A.
NASA, Ames Research Center
MS 202A-1
Moffett Field, CA 94035
(415) 965-5361
Title: NRC Research Associate

DEY, Suhrit K.
NASA, Ames Research Center
MS 202A-1
Moffett Field, CA 94032
(415) 965-6607
Title: NRC Research Associate

DOUGHERTY, F. Carroll
NASA, Ames Research Center
MS 202A-14
Moffett Field, CA 94035
(415) 965-6415
Title: Research Scientist

DWYER, H. A.
Sandia National Laboratories
P.O. Box 969
Livermore, CA 94550
(415) 422-2363
Title: Technical Staff, Thermofluids Div.

EIDELMAN, Shmuel
Naval Postgraduate School
Department of Aeronautics
Monterey, CA 93940
(408) 646-2958
Title: Research Associate

ENGQUIST, Bjorn
University of California Los Angeles
Mathematics Department
405 Hilgard Ave.
Los Angeles, CA 90014
(213) 825-4340
Title: Professor

FERZIER, Joel
Department of Mechanical Engineering
Stanford University
Stanford, CA 94305
(415) 497-3615
Title: Professor

FÖRSTER, Karl M.
Institut fur Aerodynamik and Gasdynamik
Universitat Stuttgart
Pfaffenwalding 21
D-7000 Stuttgart 80
(0711) 784-3405
Title: Prof. Dr.-Ing.

FORESTER, C. K.
Boeing Military Airplane Co.
MS 41-52
Seattle, WA 198124
(206) 655-9086
Title: Specialist Engineer

FRANK, D. R.
Lockheed Missiles & Space Co., Inc.
Dept. 81-11, Bldg. 154,
P.O. Box 504
Sunnyvale, CA 94086
(408) 742-8117
Title: Senior Research Engineer

FUCHS, Laszlo
Department of Gasdynamics
The Royal Institute of Technology
S-100 44
Stockholm, SWEDEN
(08) 787 7577
Title:

FUJII, Kozo
NASA, Ames Research Center
MS 202A-14
Moffett Field, CA 94035
(415) 965-6415
Title: NRC Research Associate

GAZDAG, Jeno
IBM Scientific Center
1530 Page Mill Road
Palo Alto, CA
(415) 955-3145
Title:

GEORGE, Mike
Northrop Corporation
3812/82
1 Northrop Avenue
Hawthorne, CA 90250
(213) 970-4501

GHIA, U.
University of Cincinnati
Department of A.S.E. & A.M.
Mail Loc. 70
Cincinnati, OH 45221
(513) 475-6662
Title: Research Associate Professor

GLOWINSKI, R.
INRIA
78153 Le Chesnay
FRANCE
954 90 20
Title: Professor

GOGINENI, P. R.
Lockheed Missiles & Space Co., Inc.
Dept. 81-11, Bldg. 154
P.O. Box 504
Sunnyvale, CA 94086
(408) 742-0439
Title: Senior Aerodynamic Engineer

GOORJIAN, Peter
NASA, Ames Research Center
MS 202A-14
Moffett Field, CA 94035
(415) 965-6415
Title: Research Scientist

GREEN, M.
NASA, Ames Research Center
MS 229-4
Moffett Field, CA 94035
(415) 965-6198
Title: Research Scientist

GREENBAUM, Anne
Lawrence Livermore National Laboratory
P.O. Box 808
Livermore, CA 94550
(415) 422-4461
Title:

GRESHO, P. M.
Lawrence Livermore Laboratory
L-262, P.O. Box 808
Livermore, CA 94550
(415) 422-1812
Title:

GUSTAFSSON, Bertil
Upsala University
Computer Science Department
Sturegatan 48
Upsala, SWEDEN
018 137738
Title: Professor

GURUSWAMY, P.
Informatics, Inc.
NASA, Ames Research Center
MS 202A-14
Moffett Field, CA 94035
(415) 965-6329
Title: Principal Analyst

HALL, Gerald F.
Texas A&M University
Department of Aerospace Engineering
College Station, TX 77843
(713) 845-1694
Title: Assistant Professor

HALSEY, Douglas
Douglas Aircraft Company
3855 Lakewood Blvd.
Long Beach, CA 90846
(213) 593-6681
Title: Senior Engineer/Scientist

HEDSTROM, Gerald
Lawrence Livermore Laboratory
P.O. Box 808
Livermore, CA 94550
(415) 422-4107
Title:

HESSENIUS, Kristin
NASA, Ames Research Center
MS 202A-14
Moffett Field, CA 94035
(415) 965-6415
Title: Research Scientist

HICKS, Ray
NASA, Ames Research Center
MS 227-8
Moffett Field, CA 94035
(415) 965-6396
Title: Aerospace Engineer

HOFFMAN, Joe
Purdue University
Mechanical Engineering Department
W. Lafayette, IN 42907
(317) 494-1506
Title: Professor

HOLMES, D. Graham
General Electric Company
Corporation Research & Development
Room 377, Bldg. 37
P.O. Box 43
Schenectady, NY 12345
(518) 385-3979
Title:

HOLST, Terry L.
NASA, Ames Research Center
MS 202A-14
Moffett Field, CA 94035
(415) 965-6415
Title: Research Scientist

HOLT, Maurice
University of California
Berkeley, CA 94720
(415) 642-5300
Title: Professor

HORSTMAN, C.
NASA, Ames Research Center
MS 229-1
Moffett Field, CA 94035
(415) 965-5396
Title: Assistant Chief, Experimental
Fluid Dynamics Branch

HUNG, C. M.
NASA, Ames Research Center
MS 202A-1
Moffett Field, CA 94035
(415) 965-6420
Title: Research Scientist

HUYNH, Quyen
SASC
17 Research Drive
Hampton, VA 23666
(804) 827-3171
Title: Staff Scientist

INOUYE, M.
NASA, Ames Research Center
MS 202A-1
Moffett Field, CA 94035
(415) 965-5127
Title: Assistant Chief, Computational Fluid Dynamics Branch

JAMESON, Antony
Princeton University
Mechanical & Aerospace Engineering Department
D 302
Princeton, NJ 08540
(609) 452-5138
Title: Professor

JESPERSON, Dennis
NASA, Ames Research Center
MS 202A-1
Moffett Field, CA 94035
(415) 965-6667
Title: Assistant Professor of Mathematics (on leave from Oregon State University)

JOHNSON, Gary
NASA, Lewis Research Center
21000 Brookpark Road
Cleveland, OH 44135
Title: Research Scientist

KANSA, Edward J.
Lawrence Livermore National Laboratory
P.O. Box 808, L-451
Livermore, CA 94550
(415) 412-0151
Title: Physicist

KENTZER, C. P.
Purdue University
Aeronautics & Astronautics Department
Lafayette, IN 47907
Title: Professor

KERLICK, David
Nielsen Engineering Co.
510 Clyde Avenue
Mountain View, CA 94043
(415) 968-9457
Title: Research Scientist

KERR, Robert
NASA, Ames Research Center
MS 202A-1
Moffett Field, CA 94035
(415) 965-5176
Title: NRC Research Associate

KHOSLA, Prem K.
Department of Aerospace Engineering
University of Cincinnati
ML #70
Cincinnati, OH 45221
(513) 475-6084
Title: Associate Professor

KIM, J.
Stanford University
Department of Mechanical Engineering
Stanford, CA 94305
(415) 497-4264
Title: Assistant Professor

KLOPFER, Goetz
NEAR, Inc.
510 Clyde Ave.
Mountain View, CA
(415) 968-9457
Title: Research Engineer

KNEILE, Karl
Sverdrup Tech., Inc.
MS 500
Arnold Air Force Station, TN
(615) 455-2622, Ext. 7231
Title: Engineering Specialist

KOCKINOS, C. N.
Lockheed Missiles & Space Co., Inc.
P.O. Box 504
Sunnyvale, CA 94086
(408) 742-6027
Title: Staff Scientist

KOPRIVA, David
University of Arizona
Mathematics Bldg.
Tucson, AZ 85721
(602) 626-2276
Title:

KORDULLA, W.
NASA, Ames Research Center
MS 202A-1
Moffett Field, CA 94035
(415) 965-5548
Title: NRC Research Associate

KUTLER, Paul
NASA, Ames Research Center
MS 202A-14
Moffett Field, CA 94035
(415) 965-6032
Title: Chief, Applied Comp.
Aerodynamics Br.

KUWAHARA, Kunio
NASA, Ames Research Center
MS 227-8
Moffett Field, CA 94035
(415) 965-5873
Title: NRC Research Associate

KWAK, Dochan
NASA, Ames Research Center
MS 202A-14
Moffett Field, CA 94035
(415) 965-6415
Title: Research Scientist

LASINSKI, Thomas
NASA, Ames Research Center
MS 202A-14
Moffett Field, CA 94035
(415) 965-6415
Title: Research Scientist

LAWKINS, W. F.
Union Carbide Corp.
Nuclear Division
P.O. Box P
Oakridge, TN
FTS 624-7955
Title: Engineer

LEE, Duk Joo
Stanford University
110F Escondido Village
Stanford, CA 94305
(415) 867-1732
Title: Graduate Student

LEE, H. N.
University of Utah
Salt Lake City, UT 84108
(801) 581-6136
Title: Research Assistant Professor

LEE, Kelly
Acurex Corp./Aerotherm Div.
485 Clyde Avenue
Mountain View, CA 94042
(415) 964-3200, ext. 3109
Title: Staff Engineer

LEE, Ki Dong
Boeing Commercial Airplane Co.
P.O. Box 3707, MS 3N-19
Seattle, WA 98008
(206) 773-8166
Title: Senior Specialist

LEE, Robert L.
Lawrence Livermore National Laboratory
L-262, P.O. Box 808, LLNL
Livermore, CA 94550
(415) 422-1859
Title: Research Scientist

LEONARD, A.
NASA, Ames Research Center
MS 202A-1
Moffett Field, CA 94035
(415) 965-6459
Title: Research Scientist

LEONE, Jr., John M.
Lawrence Livermore National Laboratory
L-262, LLNL
Livermore, CA 94550
(415) 422-6449
Title: Staff Scientist

LE VEQUE, Randy
Stanford University
Computer Science Dept.
Stanford, CA 94305
(415) 497-4101
Title:

LIANG, Shen-Min
Aerospace & Mech. Eng. Dept.
University of Arizona
Tucson, AZ 85721
(602) 626-4424
Title: Graduate Student

LIU, Nan-suey
Scientific Research Associates, Inc.
P.O. Box 498
Glastonbury, CT 06033
(203) 633-8100
Title: Research Scientist

LIU, Yen
Stanford University
P.O. Box 2410
Stanford, CA 94305
(415) 322-7998
Title:

LOMAX, H.
NASA, Ames Research Center
MS 202A-1
Moffett Field, CA 94035
(415) 965-5124
Title: Chief, Computational Fluid Dynamics Branch

LOMBARD, Charles
Pacific Engineering Design Analysis Co.
1150 Fife Street
Palo Alto, CA 94301
Title: President

LONGO, Jose Mario Antonio
FAA-Argentine
Av. Fuerza Aerea Argentina
km 5 1/2
5000 Cordoba, ARGENTINA
(presently with Dornier GmbH
7990 Friedrichshafen, WEST GERMANY)
(005451) 60631
Title: Engineer (Aeronautic Eng.)

LOTTATI, Itzhak
NASA, Ames Research Center
MS 227-8
Moffett Field, CA 94035
(415) 965-6265
Title: NRC Research Associate

LUSTMAN, Liviu R.
SASC
Numerical Methods Branch
NASA Langley Research Center
Hampton, VA 23665
Title: Senior Scientist

MANTEUFFEL, Tom
Los Alamos National Laboratory
MS 265 C-10
Los Alamos, NM 87547
(505) 667-3569
Title: Member Technical Staff

MARK, Andrew
Ballistic Research Laboratory
Aberdeen Proving Ground, MD 21005
(301) 278-5574, ext. 4320
Title: Research Aero. Eng.

MARTIN, E. D.
NASA, Ames Research Center
MS 202A-1
Moffett Field, CA 94035
(415) 965-6587
Title: Research Scientist

MARX, K. D.
Sandia National Laboratories
P.O. Box 969
Livermore, CA 94550
(415) 422-2619
Title: Tech. Staff, Thermofluids Div.

MC CARTHY, Douglas R.
Department of Computer Science
Purdue University
W. Lafayette, IN 47907
(317) 494-6028
Title: Associate Professor

MC CORMICK, Steve
Colorado State University
Dept. of Mathematics
Fort Collins, CO 80523
(303) 491-5763
Title: Professor

MC CROSKEY, W. J.
NASA, Ames Research Center
MS 202A-1
Moffett Field, CA 94035
(415) 965-6428
Title: Senior Staff Scientist

MEHTA, U.
NASA, Ames Research Center
MS 202A-1
Moffett Field, CA 94035
(415) 965-5548
Title: Research Scientist

MENDOZA, Joel
NASA, Ames Research Center
MS 227-8
Moffett Field, CA 94035
(415) 965-6272
Title: Aerospace Engineering Technician

MERRIAM, M.
NASA, Ames Research Center
MS 202A-1
Moffett Field, CA 94035
(415) 965-6417
Title: Research Scientist

MICHELSON, Daniel
U. of California Los Angeles
Mathematics Dept.
Los Angeles, CA 90024
(213) 825-4127
Title: Assistant Professor

MIKAMI, Hisashi
Research Lab. for Nuclear Reactors
Tokyo Institute of Technology
Okayama, Meguro-ku
Tokyo, JAPAN
03-726-1111 Ex. 3064
Title: Professor

MORETTI, Gino
G.M.A.F., Inc.
514 S. Long Beach Avenue
Freeport, NY 11520
Title: President

MORRISON, Harry L.
U.S. Steel Research Laboratory
MS 59
125 Jamison Lane
Monroeville, PA 15146
(412) 372-1212, ext. 2087
Title: Research Scientist

MOSHER, Marianne
NASA, Ames Research Center
MS 247-1
Moffett Field, CA 94035
(415) 965-5044
Title: Aerospace Engineer

MUNCE, Currie
Stanford University
Dept. of Mechanical Engineering
Stanford, CA 94305
(415) 497-3188
Title: Research Assistant

MURDOCK, J. W.
Aerospace Corporation
El Segundo, CA
(213) 648-6103
Title: Staff Engineer

MURMAN, Earll M.
Dept. of Aeronautics and Astronautics
Massachusetts Institute of Technology
Room 33-208
Cambridge, MA 02139
(617) 253-3284
Title: Professor

MURRAY, Al
Acurex Corp.
485 Clyde Avenue
Mountain View, CA 94042
(415) 964-3200, ext. 3156
Title: Staff Engineer

MYERS, Michael
Lockheed Georgia Co.
D 7277 Z 419
Marietta, GA 30063
(404) 424-5280
Title: Dynamics Engineer

NAKAMURA, S.
Ohio State University
206 W. 18th Avenue
Columbus, OH 43210
(614) 422-0127
Title: Professor

NAKAMURA, Yoshiaki
NASA, Ames Research Center
MS 202A-1
Moffett Field, CA 94035
(415) 965-5176
Title: NRC Research Associate

NDEFO, Ejike
Aerospace Corp.
2350 E. El Segundo Blvd.
El Segundo, CA
(213) 648-6359
Title: Mgr., Flow Analysis Section

NEWSOME, Jr., Richard W.
AFWAL/FIMM
Wright-Patterson AFB, OH 45433
(513) 255-7127
Title: Capt., USAF, Aerospace Eng.

NIELSEN, H. L.
San Jose State University
Washington Square
San Jose, CA 95192
(408) 277-2484
Title: Professor

NIETUBICZ, Charles
Aerodynamics Research Branch
Launch and Flight Div.
U.S. Army Ballistic Research Lab.
Aberdeen Proving Ground, MD
(FTS 8-922-3311)
Title:

NIXON, David
Nielsen Engineering & Research, Inc.
510 Clyde Avenue
Mountain View, CA 94043
(415) 968-9457
Title: Research Scientist

NOACK, Ralph W.
Sandia National Laboratory
P.O. Box 5800
Albuquerque, NM
(505) 844-2462
Title: Member Technical Staff

OHRING, Samuel
David W. Taylor Ship R&D Center
Bethesda, MD 20084
(202) 227-1929
Title: Mathematician

OLIGER, Joseph
Stanford University
Computer Science Department
Stanford, CA 94305
(415) 497-3134
Title: Professor

ONO, Kiyoaki
NASA, Ames Research Center
MS 227-8
Moffett Field, CA 94035
(415) 965-5873
Title: NRC Research Associate

OSHER, Stanley
University of California Los Angeles
Department of Mathematics
Los Angeles, CA 90024
(213) 825-1758
Title: Professor

OSKAM, Bastiaan
National Aerospace Lab. (NLR)
Anthony Fokkerweg 2
Amsterdam, THE NETHERLANDS
020-5113113
Title:

OSSWALD, Gary A.
University of Cincinnati
Dept. of A.S.E. & A.M.
Mail Loc. 70
Cincinnati, OH 45221
(513) 475-6096
Title: Research Assistant

O'SULLIVAN, R. J.
Lockheed Missiles & Space Co., Inc.
Dept. 81-11, Bldg. 154
P.O. Box 504
Sunnyvale, CA 94086
(408) 741-3080
Title: Research Specialist

PERRIER, Pierre
Avions Marcel Dassault — Breguet Aviation
Societe Anonyme
78 qvai CARNOT
92210 ST. CLOUD
FRANCE

Peterson, Victor L.
NASA, Ames Research Center
MS 229-3
Moffett Field, CA 94035
(415) 965-5273
Title: Chief, Thermo- and Gas-Dynamics Division

POOL, L. A.
Lockheed Missiles & Space Co., Inc.
Dept. 81-11, Bldg. 154
P.O. Box 504
Sunnyvale, CA 94086
(408) 742-0439
Title: Senior Aerodynamic Engineer

PULLIAM, T.
NASA, Ames Research Center
MS 202A-1
Moffett Field, CA 94035
(415) 965-6417
Title: Research Scientist

RAJ, Predeep
Lockheed-California Co.
Dept. 75-52, Bldg. 63-3
Burbank, CA 91520
(213) 847-7150
Title: Sr. Aerodynamics Eng.

RAKICH, J.
NASA, Ames Research Center
MS 229-1
Moffett Field, CA 94035
(415) 965-6192
Title: Research Scientist

REINHARDT, Walter A.
NASA, Ames Research Center
MS 202A-14
Moffett Field, CA 94035
(415) 965-6447
Title: Assistant Chief, Applied Comp. Aerodyn. Branch

REKLIS, Robert
Lockheed Research Laboratory
Dept. 52-33, Bldg. 255
3251 Hanover St.
Palo Alto, CA 94304
(415) 858-4010
Title:

REYHNER, Theodore A.
Boeing Commercial Airplane Co.
MS 73-07, P.O. Box 3707
Seattle, WA 98124
(206) 237-2519
Title: Principal Engineer

RIZK, Magdi
Flow Research Co.
Kent, WA 98031
(206) 872-8500
Title: Research Scientist

RIZK, Yehia
University of Dayton Research Institute
MS 202A-14
NASA, Ames Research Center
Moffett Field, CA 94035
(415) 965-6329
Title: Research Aerodynamicist

RIZZETTA, Donald P.
Boeing Military Airplane Company
Mail Stop 41-10, P.O. Box 3707
Seattle, WA 98124
(206) 655-5240
Title: Senior Specialist Engineer

ROLOFF, Richard
Lockheed Palo Alto Research Laboratory
3251 Hanover St.
Palo Alto, CA 94304
(415) 858-4011
Title: Assoc. Research Scientist

RUBESIN, M. W.
NASA, Ames Research Center
MS 202A-1
Moffett Field, CA 94035
(415) 965-5235
Title: Senior Staff Scientist

RUDMAN, Stanley
Grumman Aerospace Corp.
MS A08-35
Bethpage, NY 11714
(516) 575-9136
Title: Senior Staff Scientist

RUGE, John W.
Colorado State University
Department of Mathematics
Fort Collins, CO 80523
(303) 491-5265
Title: Instructor

SAHU, J.
U.S. Army Ballistic Research Laboratory
USARRADCOM, Bldg. 120
Aberdeen Proving Ground, MD 21005
(301) 278-3707
Title: Aerospace Engineer

SANDERS, B. R.
Sandia National Laboratories
P.O. Box 969
Livermore, CA 94550
(415) 422-3113
Title: Supervisor, Thermofluids Div.

SCHAFFER, Steve
Colorado State University
Fort Collins, CO 80523
(303) 491-5265
Title: Instructor

SCHIPPERS, H.
National Aerospace Laboratories
Anthony Fokkerweg 2
1059 CM Amsterdam, NETHERLANDS
020-5113113
Title: Doctor

SHANKAR, V.
Rockwell
P.O. Box 1085
Thousand Oaks, CA 91360
(805) 498-4545
Title: Member Technical Staff

SHANKS, Samuel P.
Flow Simulation, Inc.
278 So. Sunnyvale Ave., #204
Sunnyvale, CA 94086
(408) 736-6495
Title: Senior Research Scientist

SHEN, H. S.
Lockheed Missiles & Space Co., Inc.
Dept. 81-11, Bldg. 154
P.O. Box 504
Sunnyvale, CA 94086
(408) 742-3833
Title: Research Engineer

SHIR, C. C.
IBM Research Laboratory
K32-281
5600 Cottle Road
San Jose, CA 95193
(408) 256-7661
Title:

SHMILOVICH, Arvin
Cornell University
Upson Hall 246
Ithaca, NY 14853
(607) 257-5962
Title: Graduate Student

SOLOMON, Jay M.
Naval Surface Weapons Center
White Oak
Silver Spring, MD
(202) 394-2062
Title: Mathematician

SORENSON, Reese L.
NASA, Ames Research Center
MS 202A-14
Moffett Field, CA 94035
(415) 965-6415
Title: Research Scientist

SRINIVASAN, G.
Flow Simulations, Inc.
298 So. Sunnyvale Avenue, Suite 204
Sunnyvale, CA 94086
(408) 736-9364
Title: Senior Research Engineer

STAHARA, Stephen
Nielsen Engineering
510 Clyde Avenue
Mountain View, CA 94042
(415) 968-9457
Title: Dept. Manager

STEGER, Joseph L.
Stanford University
387 B Durand Bldg.
Stanford, CA 94305
(415) 497-1139
Title: Professor

STEINHOFF, John
University of Tennessee Space Inst.
Tullahama, TN 37388
(615) 455-0631, ext. 467
Title: Associate Professor

STELLING, G. S.
Rykswatesstaat, Data Processing Division
Nyvesheldsstract 1
Ryswyks, HOLLAND
070/906620 ext. 445
Title: Project Leader

STRIGBERGER, Jack
Stanford University
Dept. of Aero/Astro
Stanford, CA 94305
(415) 322-4182
Title: Student

STUBBS, Robert
NASA Lewis Research Center
21000 Brookpark Road
Cleveland, OH 44135
Title:

SUBRAMANIAN, N. R.
NASA, Ames Research Center
MS 202A-14
Moffett Field, CA 94035
(415) 965-6329
Title: NRC Research Associate

SWANSON, Charles
NASA Langley Research Center
MS 280
Hampton, VA 23665
(804) 827-2673
Title: Aerospace Engineer

TADMOR, Eitan
California Institute of Technology
Pasadena, CA
(213) 356-4563
Title: Research Instructor

TAYLOR, Thomas D.
The Johns Hopkins University
Applied Physics Laboratory
Johns Hopkins Road
Laurel, MD 20707
(301) 953-7100
Title: Engineer

TEZDUYAR, Tayfun
Stanford University
Room 252, Durand Bldg.
Stanford, CA 94305
(415) 497-2189
Title: Student

THAMES, Frank C.
NASA Langley Research Center
Mail Stop 360
Hampton, VA 23665
(804) 827-2627
Title: Aerospace Technologist

THOMAS, J. W.
Colorado State University
Department of Mathematics
Fort Collins, CO
(303) 491-8652
Title: Professor of Mathematics

THOMAS, P. D.
Lockheed Research Laboratory
3251 Hanover Street
Palo Alto, CA 94304
(415) 858-4026
Title: Staff Scientist

THOMAS, Scott D.
Informatics, Inc.
NASA, Ames Research Center
MS 202A-14
Moffett Field, CA 94035
(415) 965-6329
Title: Research Scientist

THOMPKINS, William T.
Massachusetts Institute of Technology
Bldg. 33, Room 208
Cambridge, MA 02139
(617) 253-2442
Title: Professor

THOMPSON, David S.
General Dynamics/Fort Worth Division
P.O. Box 748
Mail Zone 2882
Fort Worth, TX 76101
(817) 732-4811, ext. 3391/4418
Title: Engineer

TREADWAY, Alex
Sandia National Laboratories
Division 2646
P.O. Box 5800
Albuquerque, NM 87185
(505) 844-6850
Title:

TREFETHEN, Lloyd
Stanford University
Computer Sciences Dept.
Stanford, CA 94305
(415) 497-4102
Title: Graduate Student

TSAI, C-Y
Lockheed Missiles & Space Co., Inc.
Dept. 81-11, Bldg. 154
P.O. Box 504
Sunnyvale, CA 94086
(408) 742-1245
Title: Senior Research Engineer

UPSON, Craig
Lawrence Livermore National Laboratory
P.O. Box 808, L-262
Livermore, CA 94550
Title: Computational Scientist

VAN DALSEM, William R.
NASA, Ames Research Center
MS 202A-14
Moffett Field, CA 94035
(415) 965-6415
Title: Research Scientist

VERHOFF, A.
McDonnell Douglas
P.O. Box 516
St. Louis, MO 63166
(215) 233-6343
Title: Technical Specialist

VERBOOM, G. K.
Delft Hydraulics Laboratory
c/o Public Relations Department
P.O. Box 177
2600 MH
Delft, HOLLAND
(15) 569353
Title:

VIEGAS, J.
NASA, Ames Research Center
MS 229-1
Moffett Field, CA 94035
(415) 965-5950
Title: Research Scientist

VINOKUR, Marcel
NASA, Ames Research Center
MS 202A-1
Moffett Field, CA 94035
(415) 965-6607
Title: Research Scientist, University of
Santa Clara

VON LAVANTE, Ernst
Texas A&M University
Aerospace Department
College Station, TX
(713) 845-1696
Title: Assistant Professor

WANG, H. H.
IBM Palo Alto Scientific Center
1530 Page Mill Road
Palo Alto, CA 94304
(415) 855-3163
Title: Staff Member

WARMING, R. F.
NASA, Ames Research Center
MS 202A-1
Moffett Field, CA 94035
(415) 965-5215
Title: Research Scientist

WATSON, V.
NASA, Ames Research Center
MS 202A-1
Moffett Field, CA 94035
(415) 965-6421
Title: Research Scientist

WEDAN, Bruce
Northrop Corp.
1 Northrop Ave., 3812/82
Hawthorne, CA
(213) 970-4501
Title: Engineer

WHITLOW, Jr., Woodrow
NASA Langley Research Center
MS 341
Hampton, VA 23665
(804) 827-2661
Title: Aerospace Engineer

WIDHOPF, George
Aerospace Corp.
P.O. Box 92597
Los Angeles, CA 90009
(213) 648-5818
Title: Director, Fluid Mechanics Dept.

WONG, James
U.S. Army Research and Technology
Laboratory
Ames Research Center
MS 207-5
Moffett Field, CA 94035
(415) 965-5578
Title: Staff Mathematician

WONG, Yau Shu
ICASE
NASA Langley Research Center
Hampton, VA 23665
(804) 827-2513
Title:

YANG, Joseph
NASA, Ames Research Center
MS 229-4
Moffett Field, CA 94035
(415) 965-6198
Title: Research Scientist

YEE, H. C.
NASA, Ames Research Center
MS 202A-1
Moffett Field, CA 94035
(415) 965-6420
Title: Research Scientist

YEN, Shee-Mang
Coordinated Science Lab.
University of Illinois
2202 W. Springfield
Urbana, IL 61801
(217) 333-6360
Title: Professor

ZALESAK, Steven T.
Naval Research Lab., Code 4780
4555 Overlook Avenue, S.W.
Washington, D.C. 20375
(202) 767-3169
Title: Research Physicist

ZANG, Thomas
College of William & Mary
Dept. of Math. & Comp. Science
Williamsburg, VA 23185
(804) 253-4481
Title: Professor

1. Report No.
NASA CP-2201

2. Government Accession No.

3. Recipient's Catalog No.

4. Title and Subtitle
Numerical Boundary Condition Procedures

5. Report Date
April 1982

6. Performing Organization Code

7. Author(s)

8. Performing Organization Report No.

9. Performing Organization Name and Address
NASA Ames Research Center
Moffett Field, CA 94035

10. Work Unit No.
A-8736

11. Contract or Grant No.

12. Sponsoring Agency Name and Address
National Aeronautics and Space Administration
Washington, DC 20546

13. Type of Report and Period Covered
Conference Publication

14. Sponsoring Agency Code
505-31-11

15. Supplementary Notes
A symposium held at NASA Ames Research Center, October 19-20, 1981
Point of Contact: Paul Kutler, NASA Ames Research Center, Moffett Field, CA 94035, Mail Stop 202A-14, (415) 965-6032, FTS 448-5824

16. Abstract

This Conference Publication is a compilation of three invited and twenty-one contributed papers presented at the Symposium on Numerical Boundary Condition Procedures held at Ames Research Center on October 19-20, 1981. The purpose of the symposium was to provide a forum for the presentation and interchange of recent technical findings in the field of numerical boundary approximations. Topics include numerical procedures for treating inflow and outflow boundaries, steady and unsteady discontinuous surfaces, far field boundaries, and multiblock grids as well as the effects of numerical boundary approximations on stability, accuracy, and convergence rate of the numerical solution. A list of symposium attendees is included.

17. Key Words (Suggested by Author(s))
Computational fluid dynamics
Numerical methods
Boundary conditions
Numerical boundary conditions

18. Distribution Statement
Unclassified - Unlimited

Subject Category 64

19. Security Classif. (of this report)
Unclassified

20. Security Classif. (of this page)
Unclassified

21. No. of Pages
452

22. Price*
A20

*For sale by the National Technical Information Service, Springfield, Virginia 22161

END

7-2-82